INTERNATIONAL COUNCIL FOR BUILDING RESEARCH STUDIES AND DOCUMENTATION

WORKING COMMISSION W18 - TIMBER STRUCTURES

CIB - W18

MEETING TWENTY - EIGHT

COPENHAGEN

DENMARK

APRIL 1995

Lehrstuhl für Ingenieurholzbau und Baukonstruktionen
Universität Karlsruhe
Germany
Compiled by Rainer Görlacher
1995

ISSN 0945-6996

CONTENTS

0 List of Participants

INTERNATIONAL COUNCIL FOR BUILDING RESEARCH STUDIES AND DOCUMENTATION

WORKING COMMISSION W18 - TIMBER STRUCTURES

MEETING TWENTY-EIGHT

COPENHAGEN, DENMARK, 18-21 APRIL 1995

LIST OF PARTICIPANTS

CANADA

J D Barrett	Departement of Wood Science UBC, Vancouver
E Karacabeyli	Forintek Canada Corp., Vancouver
F Lam	Departement of Wood Science UBC, Vancouver
B Madsen	575 Alpine Court, North Vancouver

DENMARK

A Egerup	EURO-TRUSS, København
P Hoffmeyer	Laboratoriet for Bygningsmaterialer DTU, Lyngby
H J Larsen	Danish Building Research Institute, Hørsholm

FINLAND

J Kangas	VTT Building Technology, Espoo
A Ranta-Maunus	VTT Building Technology, Espoo
K Riipola	Tampere University of Technology
T Poutanen	Tampere University of Technology

FRANCE

P Galimard	LRBB, Bordeaux
F Rouger	CTBA, Paris

GERMANY

N Burger	University of Munich
J Ehlbeck	University of Karlsruhe
R Görlacher	University of Karlsruhe
H Kreuzinger	Technical University of Munich
H Werner	University of Karlsruhe

ISRAEL

U Korin	National Building Research Institute, The Technion, Haifa

ITALY

A Ceccotti	University of Florence

JAPAN

M Yasumura	BRI, Tsukuba

NETHERLANDS

H J Blass	Delft University of Technology
J Kuipers	Delft
A D Leijten	Delft University of Technology

NORWAY

P Aune	Norwegian Institute of Wood Technology, Trondheim
E Aasheim	Norwegian Institute of Wood Technology, Oslo
K H Solli	Norwegian Institute of Wood Technology, Oslo

POLAND

L Muszyñski	Agricultural University of Poznan
P Olejniczak	Agricultural University of Poznan

SWEDEN

L Boström	Swedish National Testing and Research Institute, Borås
J Brundin	Swedish Institute for Wood Technology Research, Stockholm
P J Gustafsson	Lund Institute of Technology
T Isaksson	Lund University
C J Johansson	Swedish National Testing and Research Institute, Borås
B Källsner	Swedish Institute for Wood Technology Research, Stockholm
J König	Swedish Institute for Wood Technology Research, Stockholm
S Ohlson	Chalmers University of Technology, Göteborg
H Petersson	Lund Institute of Technology
S Thelandersson	Lund University

SWITZERLAND

E Gehri	ETH, Zürich
A U Meierhofer	EMPA, Dübendorf

UK

T D G Canisius	Building Research Establishment, Watford
V Enjily	Building Research Establishment, Watford
A R Fewell	Building Research Establishment, Watford
H D Mansfield-Williams	Buckinghamshire College, High Wycombe
R F Marsh	London
C J Mettem	TRADA Technology Limited, High Wycombe
J Sunley	Private Consultant

USA

J D Dolan	Brooks Forest Products Center, Blacksburg
R Gupta	Oregon State University

1. Chairman's Introduction

2. Cooperation with other Organisations

3. Strength grading

4. Symbols

5. Timber Joints and Fasteners

6. Eurocode 5

7. Duration of Load

8. Laminated Members

9. Particle and Fibre Building Boards

10. Fracture Mechanics

11. Venue for Next Meeting

12. Close

INTERNATIONAL COUNCIL FOR BUILDING RESEARCH STUDIES AND DOCUMENTATION

WORKING COMMISSION W18 - TIMBER STRUCTURES

MEETING TWENTY-EIGHT

COPENHAGEN, DENMARK, 18-21 APRIL 1995

MINUTES

1. CHAIRMAN'S INTRODUCTION

The Chairman, **H Blass**, welcomed the delegates to the twenty-eighth meeting of CIB-W18A and congratulated **H-J Larsen** on his birthday.

The Chairman thanked SBI for hosting the meeting and then went on to outline changes made to the agenda.

H-J Larsen made the necessary housekeeping announcements.

2. COOPERATION WITH OTHER ORGANISATIONS

a) CIB-W18B

No report was given because **R Leicester** was absent from the meeting.

b) ISO TC165

As **C Stieda** was absent from the meeting a report was given by **E Karacabeyli**. He reported on the last meeting which was held in Quebec City, Canada on 7/8 April 1994, and at which about twenty people attended. The next meeting will be held on 4 October 1995 at CTBA in Paris.

c) RILEM

S Thelandersson gave a brief report saying that the group chaired by C Le Govic on 'Test methods for creep measurements of wooden materials' had folded. He also urged non-German and non-Italian experts to join the group of **W Rug** working on 'Diagnosis and repair of historic load-bearing timber structures'.

S Thelandersson also reported on the COST action on multi-storey buildings and asked those interested to contact him.

d) **CEN**

H-J Larsen reported on progress of the Eurocode and CEN standards saying that Eurocode 5 should be a full EN by the year 2000, and that TC124 had completed eight standards in WG1, six in WG2 and five in WG3, with a further seven in WG2 ready for the enquiry stage.

e) **IABSE**

No report.

f) **IUFRO**

P Hoffmeyer reported that the next meeting would be held in Copenhagen and Lund on 10-14 June 96, and that there would be a world congress in Finland during August 95.

g) **CIB-W85**

S Ohlsson reported that the last meeting was in Sydney, Australia on 24 September 94, and the main topics of discussion were:-

-Serviceability requirements and design principles, and
-Floor vibrations.

There is no date yet fixed for the next meeting, but it would probably be held in Budapest. It is intended to have discussions on holding a workshop.

3 STRENGTH GRADING

Paper 28-5-1 'Grading methods for structural timber' by S Ohlsson.

The paper is critical of a number of the CEN standards, e.g. that EN519 restricted the use of certain principles of operation for grading machines, and that EN384 allowed shear values to be calculated from bending characteristic values. **A Fewell** responded, saying that EN519 was drafted around existing accepted machines but work was going on to change the requirements to make a wider variety of machines acceptable provided a certain level of performance was reached. As regards EN384, **S Ohlsson's** criticisms showed his lack of understanding of the document, the procedures for which were fully discussed by CIB-W18 in Parksville. **B Madsen** advocated the use of proof testing to increase the reliability of machine grading.

Paper 28-5-2 'Modulus of elasticity of structural timber.' by N Burger and P Glos.

H Blass queried the relation between edgewise and flatwise MOE given in the conclusions. **K Riipola** stated that the type of relations used could give negative values of shear modulus. **A Fewell** queried how a G/E ratio of 1:30 could be explained by the two methods of measuring MOE.

Paper 28-6-3 'On the influence of loading head profiles on determined bending strength.' by L Muszynski and R Szukala.

A Leijten asked for the difference between the test methods at the 5% level. **L Muszynski** said the difference was insignificant. **H Blass** said the difference may not affect characteristic values but may affect relations used in grading machine models. He added that the high correlation between bending strength and MOE could be due to the few pieces at the high MOE level.

Paper 28-6-1 'Shear strength of Canadian softwood structural timber.' by F Lam, H Yee and D Barrett

A Fewell asked if different grades had different proportions of the various types of failure, and was told that the lower grades with lower density had more compression perp and bending failures. **E Gehri** said that the shear area was small and compression perp would be significant. **H-J Larsen** doubted the merits of forcing shear failures in the centre span. **C Mettem** asked why shear block tests hadn't been done on graded specimens and suggested we need a better design method rather than a test method. **F Lam** replied that we need both.

Paper 28-6-2 'Shear strength of Douglas fir timber.' by B Madsen.

The paper urged that codes should be corrected for shear to make significant cost savings. **A Meierhofer** asked if the results had been analysed to determine the duration of load effect. **B Madsen** replied that no final conclusions had yet been reached but the in-service loading in this case could be accurately estimated.

Paper 28-6-4 'Length and load configuration effects on bending strength.' by T Isaksson and S Thelandersson

A Fewell commented that as the critical section had been selected by the grading machine only and visual evidence was not taken into account, as required by the CEN standard, he would not expect the results to show a significant difference between the standards. **B Madsen** said that the lack of a length effect may reflect different modes of failure.

4 SYMBOLS

Paper 28-3-1 'Symbols for timber and wood-based materials' by J Kuipers and B Noren

A Leijten queried the number of meanings for the symbol 'T' and the subscripts in figure 1a. **K Riipola** said the units for 'stress intensity factor' and 'energy release rate' should be interchanged. **J Kuipers** said that we should obtain CEN approval before CIB publish this paper, but **H-J Larsen** said there was no need.

5 TIMBER JOINTS AND FASTENERS

Paper 28-7-9 'Axial strength of glued-in bolts' by C-J Johansson, E Serrano and P-J Gustafsson

F Lam said there was a difference in the results for different sizes and asked if it was due to the stressed volume. **C-J Johansson** said he believed it was due to the stress distribution in the bolt. **C Mettem** asked if there were details in the paper of the simplifying assumptions, and was answered yes. **U Meierhofer** queried the influence of

glue-line thickness, and was told that the current paper was the result of a preliminary study, and the effect of glue-line thickness and other effects, such as moisture and drying during curing, would be studied later.

Papers 28-7-1 'Expanded tube joint in locally DP reinforced timber' by A Leijten, P Ragupathy and K Virdi, and 28-7-2 'A strength and stiffness model for the expanded tube joint' by A Leijten

U Meierhofer asked what proportion of the load is transferred by the tube and was told, all of it. **F Lam** asked whether friction played a significant part in the model, and was told that it didn't because it was a very variable factor.

Paper 28-7-3 'Load carrying capacity of steel-to-timber joints with annular ring shanked nails. A comparison with the EC5 design model.' by R Görlacher

Comments from **H-J Larsen, S Thelandersson** and **E Gehri** said that the theory didn't necessarily apply, and the latter added that this was because of the pull-out resistance of the ring shanked nails.

Paper 28-7-4 'Dynamic effects on metal-plate connected wood truss joints.' by S Kent, R Gupta and T Miller

H-J Larsen commented that you wouldn't expect any earthquake effect if the earthquake loads are so much below the static loads.

Paper 28-7-5 'Failure of timber bolted joints subjected to lateral load perpendicular to grain' by M Yasumura and L Daudeville

T D G Canisius queried the correctness of the finite element model.

Paper 28-7-6 'Design procedure for locally reinforced joints with dowel type fasteners' by H Werner

A Leijten commented that designers need other properties, e.g reinforcement thickness, before they can design for these joints, and that the paper only proposes to include in EC5 the load capacities. **S Ohlsson** said there is a need for information on out-of-plane forces. **B Madsen** asked what increases in load capacity were achieved, and was told 2 to 4 times for plywood and 4 to 6 times for densified wood. **E Gehri** said that the assumed system factor was really due to using dowels with higher yield moments than given in EC5. **C Mettem** commented that with more complicated joints, researchers always had the problem of knowing how close were the properties of the components to the assumed characteristic values. **H-J Larsen** said that the individual component values should be used, not the EC5 values. **H Werner** said that he had tested the individual components.

Paper 28-7-7 'Variability and effects of moisture content on the withdrawal characteristics for lumber as opposed to clear wood.' by J Dolan and J Stelmokas

H-J Larsen asked why the title referred to small clears. **J Barrett** asked for clarification of the moisture change factors for nailing in US codes. **S Thelandersson** suggested that only ring shanked nails should be used in hurricane areas.

Paper 28-7-8 'Nail plate capacity in joint line' by A Kevarinmäki and J Kangas

A Egerup asked for a comparison with other plates and was told that the results are similar.

Paper 28-7-10 'Cyclic lateral connection tests conducted on dowels' by J Dolan

A Ceccotti asked if the descending phases in the cyclic load test were important. **J Dolan** replied that they weren't for timber but the test standard was written for other materials.

6 EUROCODE 5

Paper 28-102-1 'Eurocode 5 - Design of timber structures - Part 2: Bridges' by D Bajolet, E Gehri, J König, H Kreuzinger, H-J Larsen, R Mäkipuro and C Mettem

S Ohlsson suggested that durability requirements should be under the ultimate limit state rather than serviceability and that there is a lack of background documents on vibration. He also asked if there are test data supporting the damping information and was told that there are. **H Blass** asked why the information on fasteners was split between 'dowels' and 'others', and was told that information on others was being sought. He also queried the application of a size factor to composite decks, saying that in EC5: Part 1 the size factor applied to tension and bending. **S Thelandersson** queried the use of a system factor and was told that it was to account for the stochastic effect. **B Madsen** asked if reinforcing rods or prestressing had to be encased for protection. He was referred to the durability section but it was said that it may not be adequate. Both **B Madsen** and **H Blass** said that the rules for doweled connectors should be the same in Parts 1 and 2. **E Gehri** explained why different rules were given for the number of effective dowels in multi-dowel joints. **J Barrett** asked if $f_{v,k}$ for glued in rods was the shear strength value given in EN338. He was told that it was.

Paper 28-102-2 'Design of wall diaphagms according to Eurocode 5' by B Källsner

D Dolan said that the tension studs should be anchored to the ground. **H-J Larsen** said that EC5 said that they should. He also commented that EC5 was a mix of elastic and plastic design.

7 DURATION OF LOAD

Paper 28-9-1 'Evaluation of creep behaviour of structural lumber in the natural environment' by R Gupta and R Shen

B Madsen asked if the relative creep and elastic deformation were quantified. He was referred to table 2. **S Thelandersson** queried whether creep was only affected by temperature and not moisture content. **H-J Larsen** agreed, and said that creep should be given as relative creep. **S Thelandersson** asked if the temperature variations also affected the metal brackets supporting the transducers and was told that it had not been checked. **R Gupta** said that the conclusions might well be modified as the tests continued. **U Meierhofer** suggested that there was something wrong with the measurement of relative humidity.

8 LAMINATED MEMBERS

Paper 28-12-1 'Determination of characteristic bending strength of glued laminated timber' by E Gehri

H Blass asked how moment eccentricities were dealt with when testing longer lengths. **E Gehri** said that he measured the deformation on parallel faces and the differences were small for high grades.

Paper 28-12-2 'Size factor of Norwegian glued laminated beams' by E Aasheim and K Solli

H-J Larsen queried whether 5% or mean values should be used for small samples. **E Gehri** reported some Austrian results which complimented the Norwegian results. **L Muszynski** asked for details of the loading heads used as he suspected they may have an effect on the test results.

Paper 28-12-3 'Design of glulam beams with holes' by K Riipola

K Riipola presented the paper and there was no discussion from the meeting.

Paper 28-12-4 'Compression resistance of glued laminated timber' by U Korin

H-J Larsen queried the definition of column length used for the tests. **U Korin** said that the column length was the distance between the support pivots.

9 PARTICLE AND FIBRE BUILDING BOARDS

Paper 28-13-1 'Background information for design rated Oriented Strand Board in CSA standards - Summary of short term test results' by E Karacabeyli, K Lau, C Henderson, F Meakes and W Deacon

S Ohlsson pointed out the importance of the relation between flake size and test specimen size. **E Karacabeyli** said the test specimens were large. **F Lam** asked what testing was required for quality control. **V Enjily** asked what test method was used for planar shear and was told that it was the ASTM method. **R Gupta** queried the property relations for large and small specimens.

Paper 28-13-2 'Torsional stiffness of wood-hardboard composite I-beam' by P Olejniczak

A Fewell asked if there was any experience of torsional failures in use and was told no.

10 FRACTURE MECHANICS

Paper 28-19-1 'Fracture of wood in tension perpendicular to the grain: Numerical simulation by damage mechanics' by L Daudeville, M Yasumura and J-D Lanvin

The paper was presented by **F Rouger. T Canisius, L Boström, H Petersson and J Barrett** then had a discussion that centred around species differences, and differences between initial and plateau crack propagation.

Paper 28-19-2 'A new method of determining fracture energy in forward shear along the grain' by H Mansfield-Williams

No comments were made or questions asked.

Paper 28-19-3 'Fracture design analysis of wooden beams with holes and notches. Finite element analysis based on energy release rate approach' by H Petersson

K Riipola disputed some of the conclusions which may be due to the finite element software. There was then a discussion about the behaviour at initiation of crack growth. **J Barrett** asked if there was agreement with Leicester's early work and was told that that had been done by Gustafsson.

Paper 28-19-4 'Design of timber beams with holes by means of fracture mechanics' by S Aicher, J Schmidt and S Brunold

As the meeting had run out of time the Chairman asked for comments to be given to the authors after the meeting.

11 VENUE FOR NEXT MEETING

The next meeting will be in Bordeaux on 26-31 August 1996, and the following meeting will be in Vancouver, possibly combined with W18B, in the second half of June 1997.

12 CLOSE

The Chairman closed the meeting by thanking all the authors, and our host **H-J Larsen.**

13. List of CIB-W18 Papers, Copenhagen, Denmark 1995

List of CIB-W18 Papers, Copenhagen, Denmark 1995

28-3-1	Symbols for Timber and Wood-Based Materials - J Kuipers and B Noren
28-5-1	Grading Methods for Structural Timber - Principles for Approval - S Ohlsson
28-5-2	Relationship of Moduli of Elasticity in Tension and in Bending of Solid Timber - N Burger and P Glos
28-6-1	Shear Strength of Canadian Softwood Structural Lumber - F Lam, H Yee and J D Barrett
28-6-2	Shear Strength of Douglas Fir Timbers - B Madsen
28-6-3	On the Influence of the Loading Head Profiles on Determined Bending Strength - L Muszyñsky and R Szukala
28-6-4	Effect of Test Standard, Length and Load Configuration on Bending Strength of Structural Timber- T Isaksson and S Thelandersson
28-6-5	Grading Machine Readings and their Use in the Calculation of Moment Configuration Factors - T Canisius, T Isaksson and S Thelandersson
28-6-6	End Conditions for Tension Testing of Solid Timber Perpendicular to Grain - T Canisius
28-7-1	Expanded Tube Joint in Locally DP Reinforced Timber - A J M Leijten, P Ragupathy and K S Virdi
28-7-2	A Strength and Stiffness Model for the Expanded Tube Joint - A J M Leijten
28-7-3	Load-carrying Capacity of Steel-to Timber Joints with Annular Ring Shanked Nails. A Comparison with the EC5 Design Method - R Görlacher
28-7-4	Dynamic Effects on Metal-Plate Connected Wood Truss Joints - S Kent, R Gupta and T Miller
28-7-5	Failure of the Timber Bolted Joints Subjected to Lateral Load Perpendicular to Grain - M Yasumura and L Daudeville

28-7-6	Design Procedure for Locally Reinforced Joints with Dowel-type Fasteners - H Werner
28-7-7	Variability and Effects of Moisture Content on the Withdrawal Characteristics for Lumber as Opposed to Clear Wood - J D Dolan and J W Stelmokas
28-7-8	Nail Plate Capacity in Joint Line - A Kevarinmäki and J Kangas
28-7-9	Axial Strength of Glued-In Bolts - Calculation Model Based on Non-Linear Fracture Mechanics - A Preliminary Study - C J Johansson, E Serrano, P J Gustafsson and B Enquist
28-7-10	Cyclic Lateral Dowel Connection Tests for seismic and Wind Evaluation - J D Dolan
28-9-1	Evaluation of Creep Behavior of Structural Lumber in Natural Environment - R Gupta and R Shen
28-12-1	Determination of Characteristic Bending Strength of Glued Laminated Timber - E Gehri
28-12-2	Size Factor of Norwegian Glued Laminated Beams - E Aasheim and K H Solli
28-12-3	Design of Glulam Beams with Holes - K Riipola
28-12-4	Compression Resistance of Glued Laminated Timber Short Columns- U Korin
28-13-1	Background Information for "Design Rated Oriented Strand Board (OSB)" in CSA Standards - Summary of Short-term Test Results - E Karacabeyli, P Lau, C R Henderson, F V Meakes and W Deacon
28-13-2	Torsional Stiffness of Wood-Hardboard Composed I-Beam - P Olejniczak
28-19-1	Fracture of Wood in Tension Perpendicular to the Grain: Experiment and Numerical Simulation by Damage Mechanics - L Daudeville, M Yasumura and J D Lanvin
28-19-2	A New Method of Determining Fracture Energy in Forward Shear along the Grain - H D Mansfield-Williams

28-19-3 Fracture Design Analysis of Wooden Beams with Holes and Notches. Finite Element Analysis based on Energy Release Rate Approach - H Petersson

28-19-4 Design of Timber Beams with Holes by Means of Fracture Mechanics - S Aicher, J Schmidt and S Brunold

28-102-1 Eurocode 5 - Design of Timber Structures - Part 2: Bridges - D Bajolet, E Gehri, J König, H Kreuzinger, H J Larsen, R Mäkipuro and C Mettem

28-102-2 Racking Strength of Wall Diaphragms - Discussion of the Eurocode 5 Approach - B Källsner

14. Current List of CIB-W18(A) Papers

CURRENT LIST OF CIB-W18(A) PAPERS

Technical papers presented to CIB-W18(A) are identified by a code CIB-W18(A)/a-b-c, where:

a denotes the meeting at which the paper was presented. Meetings are classified in chronological order:

1 Princes Risborough, England; March 1973
2 Copenhagen, Denmark; October 1973
3 Delft, Netherlands; June 1974
4 Paris, France; February 1975
5 Karlsruhe, Federal Republic of Germany; October 1975
6 Aalborg, Denmark; June 1976
7 Stockholm, Sweden; February/March 1977
8 Brussels, Belgium; October 1977
9 Perth, Scotland; June 1978
10 Vancouver, Canada; August 1978
11 Vienna, Austria; March 1979
12 Bordeaux, France; October 1979
13 Otaniemi, Finland; June 1980
14 Warsaw, Poland; May 1981
15 Karlsruhe, Federal Republic of Germany; June 1982
16 Lillehammer, Norway; May/June 1983
17 Rapperswil, Switzerland; May 1984
18 Beit Oren, Israel; June 1985
19 Florence, Italy; September 1986
20 Dublin, Ireland; September 1987
21 Parksville, Canada; September 1988
22 Berlin, German Democratic Republic; September 1989
23 Lisbon, Portugal; September 1990
24 Oxford, United Kingdom; September 1991
25 Åhus, Sweden; August 1992
26 Athens, USA; August 1993
27 Sydney, Australia; July 1994
28 Copenhagen, Denmark, April 1995

b denotes the subject:

1 Limit State Design
2 Timber Columns
3 Symbols
4 Plywood
5 Stress Grading
6 Stresses for Solid Timber
7 Timber Joints and Fasteners
8 Load Sharing
9 Duration of Load
10 Timber Beams
11 Environmental Conditions
12 Laminated Members
13 Particle and Fibre Building Boards
14 Trussed Rafters
15 Structural Stability
16 Fire
17 Statistics and Data Analysis
18 Glued Joints
19 Fracture Mechanics
20 Serviceability
100 CIB Timber Code
101 Loading Codes
102 Structural Design Codes
103 International Standards Organisation
104 Joint Committee on Structural Safety
105 CIB Programme, Policy and Meetings
106 International Union of Forestry Research Organisations

c is simply a number given to the papers in the order in which they appear:

Example: CIB-W18/4-102-5 refers to paper 5 on subject 102 presented at the fourth meeting of W18.

Listed below, by subjects, are all papers that have to date been presented to W18. When appropriate some papers are listed under more than one subject heading.

LIMIT STATE DESIGN

1-1-1	Limit State Design - H J Larsen
1-1-2	The Use of Partial Safety Factors in the New Norwegian Design Code for Timber Structures - O Brynildsen
1-1-3	Swedish Code Revision Concerning Timber Structures - B Noren
1-1-4	Working Stresses Report to British Standards Institution Committee BLCP/17/2
6-1-1	On the Application of the Uncertainty Theoretical Methods for the Definition of the Fundamental Concepts of Structural Safety - K Skov and O Ditlevsen
11-1-1	Safety Design of Timber Structures - H J Larsen
18-1-1	Notes on the Development of a UK Limit States Design Code for Timber - A R Fewell and C B Pierce
18-1-2	Eurocode 5, Timber Structures - H J Larsen
19-1-1	Duration of Load Effects and Reliability Based Design (Single Member) - R O Foschi and Z C Yao
21-102-1	Research Activities Towards a New GDR Timber Design Code Based on Limit States Design - W Rug and M Badstube
22-1-1	Reliability-Theoretical Investigation into Timber Components Proposal for a Supplement of the Design Concept - M Badstube, W Rug and R Plessow
23-1-1	Some Remarks about the Safety of Timber Structures - J Kuipers
23-1-2	Reliability of Wood Structural Elements: A Probabilistic Method to Eurocode 5 Calibration - F Rouger, N Lheritier, P Racher and M Fogli

TIMBER COLUMNS

2-2-1	The Design of Solid Timber Columns - H J Larsen
3-2-1	The Design of Built-Up Timber Columns - H J Larsen
4-2-1	Tests with Centrally Loaded Timber Columns - H J Larsen and S S Pedersen
4-2-2	Lateral-Torsional Buckling of Eccentrically Loaded Timber Columns - B Johansson
5-9-1	Strength of a Wood Column in Combined Compression and Bending with Respect to Creep - B Källsner and B Norén
5-100-1	Design of Solid Timber Columns (First Draft) - H J Larsen
6-100-1	Comments on Document 5-100-1, Design of Solid Timber Columns - H J Larsen and E Theilgaard
6-2-1	Lattice Columns - H J Larsen
6-2-2	A Mathematical Basis for Design Aids for Timber Columns - H J Burgess
6-2-3	Comparison of Larsen and Perry Formulas for Solid Timber Columns - H J Burgess
7-2-1	Lateral Bracing of Timber Struts - J A Simon
8-15-1	Laterally Loaded Timber Columns: Tests and Theory - H J Larsen
17-2-1	Model for Timber Strength under Axial Load and Moment - T Poutanen
18-2-1	Column Design Methods for Timber Engineering - A H Buchanan, K C Johns, B Madsen
19-2-1	Creep Buckling Strength of Timber Beams and Columns - R H Leicester
19-12-2	Strength Model for Glulam Columns - H J Blaß

SYMBOLS

PLYWOOD

9-4-2	The Evaluation of Test Data on the Strength Properties of Plywood - L G Booth
9-4-3	The Sampling of Plywood and the Derivation of Strength Values (Second Draft) - B Norén
9-4-4	On the Use of the CIB/RILEM Plywood Plate Twisting Test: a progress report - L G Booth
10-4-1	Buckling Strength of Plywood - J Dekker, J Kuipers and H Ploos van Amstel
11-4-1	Analysis of Plywood Stressed Skin Panels with Rigid or Semi-Rigid Connections - I Smith
11-4-2	A Comparison of Plywood Modulus of Rigidity Determined by the ASTM and RILEM CIB/3-TT Test Methods - C R Wilson and A V Parasin
11-4-3	Sampling of Plywood for Testing Strength - B Norén
12-4-1	Procedures for Analysis of Plywood Test Data and Determination of Characteristic Values Suitable for Code Presentation - C R Wilson
14-4-1	An Introduction to Performance Standards for Wood-base Panel Products - D H Brown
14-4-2	Proposal for Presenting Data on the Properties of Structural Panels - T Schmidt
16-4-1	Planar Shear Capacity of Plywood in Bending - C K A Stieda
17-4-1	Determination of Panel Shear Strength and Panel Shear Modulus of Beech-Plywood in Structural Sizes - J Ehlbeck and F Colling
17-4-2	Ultimate Strength of Plywood Webs - R H Leicester and L Pham
20-4-1	Considerations of Reliability - Based Design for Structural Composite Products - M R O'Halloran, J A Johnson, E G Elias and T P Cunningham

21-4-1 Modelling for Prediction of Strength of Veneer Having Knots - Y Hirashima

22-4-1 Scientific Research into Plywood and Plywood Building Constructions the Results and Findings of which are Incorporated into Construction Standard Specifications of the USSR - I M Guskov

22-4-2 Evaluation of Characteristic values for Wood-Based Sheet Materials - E G Elias

24-4-1 APA Structural-Use Design Values: An Update to Panel Design Capacities - A L Kuchar, E G Elias, B Yeh and M R O'Halloran

STRESS GRADING

1-5-1 Quality Specifications for Sawn Timber and Precision Timber - Norwegian Standard NS 3080

1-5-2 Specification for Timber Grades for Structural Use - British Standard BS 4978

4-5-1 Draft Proposal for an International Standard for Stress Grading Coniferous Sawn Softwood - ECE Timber Committee

16-5-1 Grading Errors in Practice - B Thunell

16-5-2 On the Effect of Measurement Errors when Grading Structural Timber - L Nordberg and B Thunell

19-5-1 Stress-Grading by ECE Standards of Italian-Grown Douglas-Fir Dimension Lumber from Young Thinnings - L Uzielli

19-5-2 Structural Softwood from Afforestation Regions in Western Norway - R Lackner

21-5-1 Non-Destructive Test by Frequency of Full Size Timber for Grading - T Nakai

22-5-1 Fundamental Vibration Frequency as a Parameter for Grading Sawn Timber - T Nakai, T Tanaka and H Nagao

24-5-1 Influence of Stress Grading System on Length Effect Factors for Lumber Loaded in Compression - A Campos and I Smith

26-5-1 Structural Properties of French Grown Timber According to Various Grading Methods - F Rouger, C De Lafond and A El Quadrani

28-5-1 Grading Methods for Structural Timber - Principles for Approval - S Ohlsson

28-5-2 Relationship of Moduli of Elasticity in Tension and in Bending of Solid Timber - N Burger and P Glos

STRESSES FOR SOLID TIMBER

4-6-1 Derivation of Grade Stresses for Timber in the UK - W T Curry

5-6-1 Standard Methods of Test for Determining some Physical and Mechanical Properties of Timber in Structural Sizes - W T Curry

5-6-2 The Description of Timber Strength Data - J R Tory

5-6-3 Stresses for EC1 and EC2 Stress Grades - J R Tory

6-6-1 Standard Methods of Test for the Determination of some Physical and Mechanical Properties of Timber in Structural Sizes (third draft) - W T Curry

7-6-1 Strength and Long-term Behaviour of Lumber and Glued Laminated Timber under Torsion Loads - K Möhler

9-6-1 Classification of Structural Timber - H J Larsen

9-6-2 Code Rules for Tension Perpendicular to Grain - H J Larsen

9-6-3 Tension at an Angle to the Grain - K Möhler

9-6-4 Consideration of Combined Stresses for Lumber and Glued Laminated Timber - K Möhler

11-6-1	Evaluation of Lumber Properties in the United States - W L Galligan and J H Haskell
11-6-2	Stresses Perpendicular to Grain - K Möhler
11-6-3	Consideration of Combined Stresses for Lumber and Glued Laminated Timber (addition to Paper CIB-W18/9-6-4) - K Möhler
12-6-1	Strength Classifications for Timber Engineering Codes - R H Leicester and W G Keating
12-6-2	Strength Classes for British Standard BS 5268 - J R Tory
13-6-1	Strength Classes for the CIB Code - J R Tory
13-6-2	Consideration of Size Effects and Longitudinal Shear Strength for Uncracked Beams - R O Foschi and J D Barrett
13-6-3	Consideration of Shear Strength on End-Cracked Beams - J D Barrett and R O Foschi
15-6-1	Characteristic Strength Values for the ECE Standard for Timber - J G Sunley
16-6-1	Size Factors for Timber Bending and Tension Stresses - A R Fewell
16-6-2	Strength Classes for International Codes - A R Fewell and J G Sunley
17-6-1	The Determination of Grade Stresses from Characteristic Stresses for BS 5268: Part 2 - A R Fewell
17-6-2	The Determination of Softwood Strength Properties for Grades, Strength Classes and Laminated Timber for BS 5268: Part 2 - A R Fewell
18-6-1	Comment on Papers: 18-6-2 and 18-6-3 - R H Leicester
18-6-2	Configuration Factors for the Bending Strength of Timber - R H Leicester
18-6-3	Notes on Sampling Factors for Characteristic Values - R H Leicester

18-6-4	Size Effects in Timber Explained by a Modified Weakest Link Theory - B Madsen and A H Buchanan
18-6-5	Placement and Selection of Growth Defects in Test Specimens - H Riberholt
18-6-6	Partial Safety-Coefficients for the Load-Carrying Capacity of Timber Structures - B Norén and J-0 Nylander
19-6-1	Effect of Age and/or Load on Timber Strength - J Kuipers
19-6-2	Confidence in Estimates of Characteristic Values - R H Leicester
19-6-3	Fracture Toughness of Wood - Mode I - K Wright and M Fonselius
19-6-4	Fracture Toughness of Pine - Mode II - K Wright
19-6-5	Drying Stresses in Round Timber - A Ranta-Maunus
19-6-6	A Dynamic Method for Determining Elastic Properties of Wood - R Görlacher
20-6-1	A Comparative Investigation of the Engineering Properties of "Whitewoods" Imported to Israel from Various Origins - U Korin
20-6-2	Effects of Yield Class, Tree Section, Forest and Size on Strength of Home Grown Sitka Spruce - V Picardo
20-6-3	Determination of Shear Strength and Strength Perpendicular to Grain - H J Larsen
21-6-1	Draft Australian Standard: Methods for Evaluation of Strength and Stiffness of Graded Timber - R H Leicester
21-6-2	The Determination of Characteristic Strength Values for _Stress Grades of Structural Timber. Part 1 - A R Fewell and P Glos
21-6-3	Shear Strength in Bending of Timber -_U Korin
22-6-1	Size Effects and Property Relationships for Canadian 2-inch Dimension Lumber - J D Barrett and H Griffin

22-6-2	Moisture Content Adjustements for In-Grade Data - J D Barrett and W Lau
22-6-3	A Discussion of Lumber Property Relationships in Eurocode 5 - D W Green and D E Kretschmann
22-6-4	Effect of Wood Preservatives on the Strength Properties of Wood - F Ronai
23-6-1	Timber in Compression Perpendicular to Grain - U Korin
24-6-1	Discussion of the Failure Criterion for Combined Bending and Compression - T A C M van der Put
24-6-3	Effect of Within Member Variability on Bending Strength of Structural Timber - I Czmoch, S Thelandersson and H J Larsen
24-6-4	Protection of Structural Timber Against Fungal Attack Requirements and Testing - K Jaworska, M Rylko and W Nozynski
24-6-5	Derivation of the Characteristic Bending Strength of Solid Timber According to CEN-Document prEN 384 - A J M Leijten
25-6-1	Moment Configuration Factors for Simple Beams- T D G Canisius
25-6-3	Bearing Capacity of Timber - U Korin
25-6-4	On Design Criteria for Tension Perpendicular to Grain - H Petersson
25-6-5	Size Effects in Visually Graded Softwood Structural Lumber - J D Barrett, F Lam and W Lau
26-6-1	Discussion and Proposal of a General Failure Criterion for Wood - T A C M van der Put
27-6-1	Development of the "Critical Bearing": Design Clause in CSA-086.1 - C Lum and E Karacabeyli
27-6-2	Size Effects in Timber: Novelty Never Ends - F Rouger and T Fewell

27-6-3 Comparison of Full-Size Sugi (Cryptomeria japonica D.Don) Structural Performance in Bending of Round Timber, Two Surfaces Sawn Timber and Square Sawn Timber - T Nakai, H Nagao and T Tanaka

28-6-1 Shear Strength of Canadian Softwood Structural Lumber - F Lam, H Yee and J D Barrett

28-6-2 Shear Strength of Douglas Fir Timbers - B Madsen

28-6-3 On the Influence of the Loading Head Profiles on Determined Bending Strength - L Muszyñsky and R Szukala

28-6-4 Effect of Test Standard, Length and Load Configuration on Bending Strength of Structural Timber- T Isaksson and S Thelandersson

28-6-5 Grading Machine Readings and their Use in the Calculation of Moment Configuration Factors - T Canisius, T Isaksson and S Thelandersson

28-6-6 End Conditions for Tension Testing of Solid Timber Perpendicular to Grain - T Canisius

TIMBER JOINTS AND FASTENERS

1-7-1 Mechanical Fasteners and Fastenings in Timber Structures - E G Stern

4-7-1 Proposal for a Basic Test Method for the Evaluation of Structural Timber Joints with Mechanical Fasteners and Connectors
- RILEM 3TT Committee

4-7-2 Test Methods for Wood Fasteners - K Möhler

5-7-1 Influence of Loading Procedure on Strength and Slip-Behaviour in Testing Timber Joints - K Möhler

5-7-2 Recommendations for Testing Methods for Joints with Mechanical Fasteners and Connectors in Load-Bearing Timber Structures
- RILEM 3 TT Committee

5-7-3	CIB-Recommendations for the Evaluation of Results of Tests on Joints with Mechanical Fasteners and Connectors used in Load-Bearing Timber Structures - J Kuipers
6-7-1	Recommendations for Testing Methods for Joints with Mechanical Fasteners and Connectors in Load-Bearing Timber Structures (seventh draft) - RILEM 3 TT Committee
6-7-2	Proposal for Testing Integral Nail Plates as Timber Joints - K Möhler
6-7-3	Rules for Evaluation of Values of Strength and Deformation from Test Results - Mechanical Timber Joints - M Johansen, J Kuipers, B Norén
6-7-4	Comments to Rules for Testing Timber Joints and Derivation of Characteristic Values for Rigidity and Strength - B Norén
7-7-1	Testing of Integral Nail Plates as Timber Joints - K Möhler
7-7-2	Long Duration Tests on Timber Joints - J Kuipers
7-7-3	Tests with Mechanically Jointed Beams with a Varying Spacing of Fasteners - K Möhler
7-100-1	CIB-Timber Code Chapter 5.3 Mechanical Fasteners;CIB-Timber Standard 06 and 07 - H J Larsen
9-7-1	Design of Truss Plate Joints - F J Keenan
9-7-2	Staples - K Möhler
11-7-1	A Draft Proposal for International Standard: ISO Document ISO/TC 165N 38E
12-7-1	Load-Carrying Capacity and Deformation Characteristics of Nailed Joints - J Ehlbeck
12-7-2	Design of Bolted Joints - H J Larsen
12-7-3	Design of Joints with Nail Plates - B Norén

13-7-1	Polish Standard BN-80/7159-04: Parts 00-01-02-03-04-05. "Structures from Wood and Wood-based Materials. Methods of Test and Strength Criteria for Joints with Mechanical Fasteners"
13-7-2	Investigation of the Effect of Number of Nails in a Joint on its Load Carrying Ability - W Nozynski
13-7-3	International Acceptance of Manufacture, Marking and Control of Finger-jointed Structural Timber - B Norén
13-7-4	Design of Joints with Nail Plates - Calculation of Slip - B Norén
13-7-5	Design of Joints with Nail Plates - The Heel Joint - B Källsner
13-7-6	Nail Deflection Data for Design - H J Burgess
13-7-7	Test on Bolted Joints - P Vermeyden
13-7-8	Comments to paper CIB-W18/12-7-3 "Design of Joints with Nail Plates" - B Norén
13-7-9	Strength of Finger Joints - H J Larsen
13-100-4	CIB Structural Timber Design Code. Proposal for Section 6.1.5 Nail Plates - N I Bovim
14-7-1	Design of Joints with Nail Plates (second edition) - B Norén
14-7-2	Method of Testing Nails in Wood (second draft, August 1980) - B Norén
14-7-3	Load-Slip Relationship of Nailed Joints - J Ehlbeck and H J Larsen
14-7-4	Wood Failure in Joints with Nail Plates - B Norén
14-7-5	The Effect of Support Eccentricity on the Design of W- and WW-Trussed with Nail Plate Connectors - B Källsner
14-7-6	Derivation of the Allowable Load in Case of Nail Plate Joints Perpendicular to Grain - K Möhler
14-7-7	Comments on CIB-W18/14-7-1 - T A C M van der Put

15-7-1 Final Recommendation TT-1A: Testing Methods for Joints with Mechanical Fasteners in Load-Bearing Timber Structures. Annex A Punched Metal Plate Fasteners - Joint Committee RILEM/CIB-3TT

16-7-1 Load Carrying Capacity of Dowels - E Gehri

16-7-2 Bolted Timber Joints: A Literature Survey - N Harding

16-7-3 Bolted Timber Joints: Practical Aspects of Construction and Design; a Survey - N Harding

16-7-4 Bolted Timber Joints: Draft Experimental Work Plan - Building Research Association of New Zealand

17-7-1 Mechanical Properties of Nails and their Influence on Mechanical Properties of Nailed Timber Joints Subjected to Lateral Loads - I Smith, L R J Whale, C Anderson and L Held

17-7-2 Notes on the Effective Number of Dowels and Nails in Timber Joints - G Steck

18-7-1 Model Specification for Driven Fasteners for Assembly of Pallets and Related Structures - E G Stern and W B Wallin

18-7-2 The Influence of the Orientation of Mechanical Joints on their Mechanical Properties - I Smith and L R J Whale

18-7-3 Influence of Number of Rows of Fasteners or Connectors upon the Ultimate Capacity of Axially Loaded Timber Joints - I Smith and G Steck

18-7-4 A Detailed Testing Method for Nailplate Joints - J Kangas

18-7-5 Principles for Design Values of Nailplates in Finland - J Kangas

18-7-6 The Strength of Nailplates - N I Bovim and E Aasheim

19-7-1 Behaviour of Nailed and Bolted Joints under Short-Term Lateral Load - Conclusions from Some Recent Research - L R J Whale, I Smith and B O Hilson

19-7-2 Glued Bolts in Glulam - H Riberholt

19-7-3 Effectiveness of Multiple Fastener Joints According to National Codes and Eurocode 5 (Draft) - G Steck

19-7-4 The Prediction of the Long-Term Load Carrying Capacity of Joints in Wood Structures - Y M Ivanov and Y Y Slavic

19-7-5 Slip in Joints under Long-Term Loading - T Feldborg and M Johansen

19-7-6 The Derivation of Design Clauses for Nailed and Bolted Joints in Eurocode 5 - L R J Whale and I Smith

19-7-7 Design of Joints with Nail Plates - Principles - B Norén

19-7-8 Shear Tests for Nail Plates - B Norén

19-7-9 Advances in Technology of Joints for Laminated Timber - Analyses of the Structural Behaviour - M Piazza and G Turrini

19-15-1 Connections Deformability in Timber Structures: A Theoretical Evaluation of its Influence on Seismic Effects - A Ceccotti and A Vignoli

20-7-1 Design of Nailed and Bolted Joints-Proposals for the Revision of Existing Formulae in Draft Eurocode 5 and the CIB Code - L R J Whale, I Smith and H J Larsen

20-7-2 Slip in Joints under Long Term Loading - T Feldborg and M Johansen

20-7-3 Ultimate Properties of Bolted Joints in Glued-Laminated Timber - M Yasumura, T Murota and H Sakai

20-7-4 Modelling the Load-Deformation Behaviour of Connections with Pin-Type Fasteners under Combined Moment, Thrust and Shear Forces - I Smith

21-7-1 Nails under Long-Term Withdrawal Loading - T Feldborg and M Johansen

21-7-2 Glued Bolts in Glulam-Proposals for CIB Code - H Riberholt

21-7-3 Nail Plate Joint Behaviour under Shear Loading - T Poutanen

21-7-4 Design of Joints with Laterally Loaded Dowels. Proposals for Improving the Design Rules in the CIB Code and the Draft Eurocode 5 - J Ehlbeck and H Werner

21-7-5 Axially Loaded Nails: Proposals for a Supplement to the CIB Code - J Ehlbeck and W Siebert

22-7-1 End Grain Connections with Laterally Loaded Steel Bolts A draft proposal for design rules in the CIB Code - J Ehlbeck and M Gerold

22-7-2 Determination of Perpendicular-to-Grain Tensile Stresses in Joints with Dowel-Type Fasteners - A draft proposal for design rules - J Ehlbeck, R Görlacher and H Werner

22-7-3 Design of Double-Shear Joints with Non-Metallic Dowels A proposal for a supplement of the design concept - J Ehlbeck and O Eberhart

22-7-4 The Effect of Load on Strength of Timber Joints at high Working Load Level - A J M Leijten

22-7-5 Plasticity Requirements for Portal Frame Corners - R Gunnewijk and A J M Leijten

22-7-6 Background Information on Design of Glulam Rivet Connections in CSA/CAN3-086.1-M89 - A proposal for a supplement of the design concept - E Karacabeyli and D P Janssens

22-7-7 Mechanical Properties of Joints in Glued-Laminated Beams under Reversed Cyclic Loading - M Yasumura

22-7-8 Strength of Glued Lap Timber Joints - P Glos and H Horstmann

22-7-9 Toothed Rings Type Bistyp 075 at the Joints of Fir Wood - J Kerste

22-7-10 Calculation of Joints and Fastenings as Compared with the International State - K Zimmer and K Lissner

22-7-11 Joints on Glued-in Steel Bars Present Relatively New and Progressive Solution in Terms of Timber Structure Design - G N Zubarev, F A Boitemirov and V M Golovina

22-7-12 The Development of Design Codes for Timber Structures made of Compositive Bars with Plate Joints based on Cyclindrical Nails - Y V Piskunov

22-7-13 Designing of Glued Wood Structures Joints on Glued-in Bars - S B Turkovsky

23-7-1 Proposal for a Design Code for Nail Plates - E Aasheim and K H Solli

23-7-2 Load Distribution in Nailed Joints - H J Blass

24-7-1 Theoretical and Experimental Tension and Shear Capacity of Nail Plate Connections - B Källsner and J Kangas

24-7-2 Testing Method and Determination of Basic Working Loads for Timber Joints with Mechanical Fasteners - Y Hirashima and F Kamiya

24-7-3 Anchorage Capacity of Nail Plate - J Kangas

25-7-2 Softwood and Hardwood Embedding Strength for Dowel type Fasteners - J Ehlbeck and H Werner

25-7-4 A Guide for Application of Quality Indexes for Driven Fasteners Used in Connections in Wood Structures - E G Stern

25-7-5 35 Years of Experience with Certain Types of Connectors and Connector Plates Used for the Assembly of Wood Structures and their Components- E G Stern

25-7-6 Characteristic Strength of Split-ring and Shear-plate Connections - H J Blass, J Ehlbeck and M Schlager

25-7-7 Characteristic Strength of Tooth-plate Connector Joints - H J Blass, J Ehlbeck and M Schlager

25-7-8 Extending Yield Theory to Screw Connections - T E McLain

25-7-9 Determination of k_{def} for Nailed Joints - J W G van de Kuilen

25-7-10 Characteristic Strength of UK Timber Connectors - A V Page and C J Mettem

25-7-11	Multiple-fastener Dowel-type Joints, a Selected Review of Research and Codes - C J Mettem and A V Page
25-7-12	Load Distributions in Multiple-fastener Bolted Joints in European Whitewood Glulam, with Steel Side Plates - C J Mettem and A V Page
26-7-1	Proposed Test Method for Dynamic Properties of Connections Assembled with Mechanical Fasteners - J D Dolan
26-7-2	Validatory Tests and Proposed Design Formulae for the Load-Carrying Capacity of Toothed-Plate Connectored Joints - C J Mettem, A V Page and G Davis
26-7-3	Definitions of Terms and Multi-Language Terminology Pertaining to Metal Connector Plates - E G Stern
26-7-4	Design of Joints Based on in V-Shape Glued-in Rods - J Kangas
26-7-5	Tests on Timber Concrete Composite Structural Elements (TCCs) - A U Meierhofer
27-7-1	Glulam Arch Bridge and Design of it's Moment-Resisting Joints - K Komatsu and S Usuku
27-7-2	Characteristic Load - Carrying Capacity of Joints with Dowel - type Fasteners in Regard to the System Properties - H Werner
27-7-3	Steel Failure Design in Truss Plate Joints - T Poutanen
28-7-1	Expanded Tube Joint in Locally DP Reinforced Timber - A J M Leijten, P Ragupathy and K S Virdi
28-7-2	A Strength and Stiffness Model for the Expanded Tube Joint - A J M Leijten
28-7-3	Load-carrying Capacity of Steel-to Timber Joints with Annular Ring Shanked Nails. A Comparison with the EC5 Design Method - R Görlacher
28-7-4	Dynamic Effects on Metal-Plate Connected Wood Truss Joints - S Kent, R Gupta and T Miller
28-7-5	Failure of the Timber Bolted Joints Subjected to Lateral Load Perpendicular to Grain - M Yasumura and L Daudeville

28-7-6 Design Procedure for Locally Reinforced Joints with Dowel-type Fasteners - H Werner

28-7-7 Variability and Effects of Moisture Content on the Withdrawal Characteristics for Lumber as Opposed to Clear Wood - J D Dolan and J W Stelmokas

28-7-8 Nail Plate Capacity in Joint Line - A Kevarinmäki and J Kangas

28-7-9 Axial Strength of Glued-In Bolts - Calculation Model Based on Non-Linear Fracture Mechanics - A Preliminary Study - C J Johansson, E Serrano, P J Gustafsson and B Enquist

28-7-10 Cyclic Lateral Dowel Connection Tests for seismic and Wind Evaluation - J D Dolan

LOAD SHARING

3-8-1 Load Sharing - An Investigation on the State of Research and Development of Design Criteria - E Levin

4-8-1 A Review of Load-Sharing in Theory and Practice - E Levin

4-8-2 Load Sharing - B Norén

19-8-1 Predicting the Natural Frequencies of Light-Weight Wooden Floors - I Smith and Y H Chui

20-8-1 Proposed Code Requirements for Vibrational Serviceability of Timber Floors - Y H Chui and I Smith

21-8-1 An Addendum to Paper 20-8-1 - Proposed Code Requirements for Vibrational Serviceability of Timber Floors - Y H Chui and I Smith

21-8-2 Floor Vibrational Serviceability and the CIB Model Code - S Ohlsson

22-8-1 Reliability Analysis of Viscoelastic Floors - F Rouger, J D Barrett and R O Foschi

24-8-1 On the Possibility of Applying Neutral Vibrational Serviceability Criteria to Joisted Wood Floors - I Smith and Y H Chui

25-8-1 Analysis of Glulam Semi-rigid Portal Frames under Long-term Load - K Komatsu and N Kawamoto

DURATION OF LOAD

3-9-1 Definitions of Long Term Loading for the Code of Practice - B Norén

4-9-1 Long Term Loading of Trussed Rafters with Different Connection Systems - T Feldborg and M Johansen

5-9-1 Strength of a Wood Column in Combined Compression and Bending with Respect to Creep - B Källsner and B Norén

6-9-1 Long Term Loading for the Code of Practice (Part 2) - B Norén

6-9-2 Long Term Loading - K Möhler

6-9-3 Deflection of Trussed Rafters under Alternating Loading during a Year - T Feldborg and M Johansen

7-6-1 Strength and Long Term Behaviour of Lumber and Glued-Laminated Timber under Torsion Loads - K Möhler

7-9-1 Code Rules Concerning Strength and Loading Time - H J Larsen and E Theilgaard

17-9-1 On the Long-Term Carrying Capacity of Wood Structures - Y M Ivanov and Y Y Slavic

18-9-1 Prediction of Creep Deformations of Joints - J Kuipers

19-9-1 Another Look at Three Duration of Load Models - R O Foschi and Z C Yao

19-9-2 Duration of Load Effects for Spruce Timber with Special Reference to Moisture Influence - A Status Report - P Hoffmeyer

19-9-3 A Model of Deformation and Damage Processes Based on the Reaction Kinetics of Bond Exchange - T A C M van der Put

19-9-4 Non-Linear Creep Superposition - U Korin

19-9-5 Determination of Creep Data for the Component Parts of Stressed-Skin Panels - R Kliger

19-9-6 Creep an Lifetime of Timber Loaded in Tension and Compression - P Glos

19-1-1 Duration of Load Effects and Reliability Based Design (Single Member) - R O Foschi and Z C Yao

19-6-1 Effect of Age and/or Load on Timber Strength - J Kuipers

19-7-4 The Prediction of the Long-Term Load Carrying Capacity of Joints in Wood Structures - Y M Ivanov and Y Y Slavic

19-7-5 Slip in Joints under Long-Term Loading - T Feldborg and M Johansen

20-7-2 Slip in Joints under Long-Term Loading - T Feldborg and M Johansen

22-9-1 Long-Term Tests with Glued Laminated Timber Girders - M Badstube, W Rug and W Schöne

22-9-2 Strength of One-Layer solid and Lengthways Glued Elements of Wood Structures and its Alteration from Sustained Load - L M Kovaltchuk, I N Boitemirova and G B Uspenskaya

24-9-1 Long Term Bending Creep of Wood - T Toratti

24-9-2 Collection of Creep Data of Timber - A Ranta-Maunus

24-9-3 Deformation Modification Factors for Calculating Built-up Wood-Based Structures - I R Kliger

25-9-2 DVM Analysis of Wood. Lifetime, Residual Strength and Quality - L F Nielsen

26-9-1 Long Term Deformations in Wood Based Panels under Natural Climate Conditions. A Comparative Study - S Thelandersson, J Nordh, T Nordh and S Sandahl

28-9-1 Evaluation of Creep Behavior of Structural Lumber in Natural Environment - R Gupta and R Shen

TIMBER BEAMS

4-10-1 The Design of Simple Beams - H J Burgess

4-10-2 Calculation of Timber Beams Subjected to Bending and Normal Force - H J Larsen

5-10-1 The Design of Timber Beams - H J Larsen

9-10-1 The Distribution of Shear Stresses in Timber Beams - F J Keenan

9-10-2 Beams Notched at the Ends - K Möhler

11-10-1 Tapered Timber Beams - H Riberholt

13-6-2 Consideration of Size Effects in Longitudinal Shear Strength for Uncracked Beams - R O Foschi and J D Barrett

13-6-3 Consideration of Shear Strength on End-Cracked Beams - J D Barrett and R O Foschi

18-10-1 Submission to the CIB-W18 Committee on the Design of Ply Web Beams by Consideration of the Type of Stress in the Flanges - J A Baird

18-10-2 Longitudinal Shear Design of Glued Laminated Beams - R O Foschi

19-10-1 Possible Code Approaches to Lateral Buckling in Beams - H J Burgess

19-2-1 Creep Buckling Strength of Timber Beams and Columns - R H Leicester

20-2-1 Lateral Buckling Theory for Rectangular Section Deep Beam-Columns - H J Burgess

20-10-1	Draft Clause for CIB Code for Beams with Initial Imperfections - H J Burgess
20-10-2	Space Joists in Irish Timber - W J Robinson
20-10-3	Composite Structure of Timber Joists and Concrete Slab - T Poutanen
21-10-1	A Study of Strength of Notched Beams - P J Gustafsson
22-10-1	Design of Endnotched Beams - H J Larsen and P J Gustafsson
22-10-2	Dimensions of Wooden Flexural Members under Constant Loads - A Pozgai
22-10-3	Thin-Walled Wood-Based Flanges in Composite Beams - J König
22-10-4	The Calculation of Wooden Bars with flexible Joints in Accordance with the Polish Standart Code and Strict Theoretical Methods - Z Mielczarek
23-10-1	Tension Perpendicular to the Grain at Notches and Joints - T A C M van der Put
23-10-2	Dimensioning of Beams with Cracks, Notches and Holes. An Application of Fracture Mechanics - K Riipola
23-10-3	Size Factors for the Bending and Tension Strength of Structural Timber - J D Barret and A R Fewell
23-12-1	Bending Strength of Glulam Beams, a Design Proposal - J Ehlbeck and F Colling
23-12-3	Glulam Beams, Bending Strength in Relation to the Bending Strength of the Finger Joints - H Riberholt
24-10-1	Shear Strength of Continuous Beams - R H Leicester and F G Young
25-10-1	The Strength of Norwegian Glued Laminated Beams - K Solli, E Aasheim and R H Falk

25-10-2 The Influence of the Elastic Modulus on the Simulated Bending Strength of Hyperstatic Timber Beams - T D G Canisius

27-10-1 Determination of Shear Modulus - R Görlacher and J Kürth

ENVIRONMENTAL CONDITIONS

5-11-1 Climate Grading for the Code of Practice - B Norén

6-11-1 Climate Grading (2) - B Norén

9-11-1 Climate Classes for Timber Design - F J Keenan

19-11-1 Experimental Analysis on Ancient Downgraded Timber Structures - B Leggeri and L Paolini

19-6-5 Drying Stresses in Round Timber - A Ranta-Maunus

22-11-1 Corrosion and Adaptation Factors for Chemically Aggressive Media with Timber Structures - K Erler

LAMINATED MEMBERS

6-12-1 Directives for the Fabrication of Load-Bearing Structures of Glued Timber - A van der Velden and J Kuipers

8-12-1 Testing of Big Glulam Timber Beams - H Kolb and P Frech

8-12-2 Instruction for the Reinforcement of Apertures in Glulam Beams - H Kolb and P Frech

8-12-3 Glulam Standard Part 1: Glued Timber Structures; Requirements for Timber (Second Draft)

9-12-1 Experiments to Provide for Elevated Forces at the Supports of Wooden Beams with Particular Regard to Shearing Stresses and Long-Term Loadings - F Wassipaul and R Lackner

9-12-2	Two Laminated Timber Arch Railway Bridges Built in Perth in 1849 - L G Booth
9-6-4	Consideration of Combined Stresses for Lumber and Glued Laminated Timber - K Möhler
11-6-3	Consideration of Combined Stresses for Lumber and Glued Laminated Timber (addition to Paper CIB-W18/9-6-4) - K Möhler
12-12-1	Glulam Standard Part 2: Glued Timber Structures; Rating (3rd draft)
12-12-2	Glulam Standard Part 3: Glued Timber Structures; Performance (3 rd draft)
13-12-1	Glulam Standard Part 3: Glued Timber Structures; Performance (4th draft)
14-12-1	Proposals for CEI-Bois/CIB-W18 Glulam Standards - H J Larsen
14-12-2	Guidelines for the Manufacturing of Glued Load-Bearing Timber Structures - Stevin Laboratory
14-12-3	Double Tapered Curved Glulam Beams - H Riberholt
14-12-4	Comment on CIB-W18/14-12-3 - E Gehri
18-12-1	Report on European Glulam Control and Production Standard - H Riberholt
18-10-2	Longitudinal Shear Design of Glued Laminated Beams - R O Foschi
19-12-1	Strength of Glued Laminated Timber - J Ehlbeck and F Colling
19-12-2	Strength Model for Glulam Columns - H J Blaß
19-12-3	Influence of Volume and Stress Distribution on the Shear Strength and Tensile Strength Perpendicular to Grain - F Colling
19-12-4	Time-Dependent Behaviour of Glued-Laminated Beams - F Zaupa
21-12-1	Modulus of Rupture of Glulam Beam Composed of Arbitrary Laminae - K Komatsu and N Kawamoto

21-12-2 An Appraisal of the Young's Modulus Values Specified for Glulam in Eurocode 5 - L R J Whale, B O Hilson and P D Rodd

21-12-3 The Strength of Glued Laminated Timber (Glulam): Influence of Lamination Qualities and Strength of Finger Joints - J Ehlbeck and F Colling

21-12-4 Comparison of a Shear Strength Design Method in Eurocode 5 and a More Traditional One - H Riberholt

22-12-1 The Dependence of the Bending Strength on the Glued Laminated Timber Girder Depth - M Badstube, W Rug and W Schöne

22-12-2 Acid Deterioration of Glulam Beams in Buildings from the Early Half of the 1960s - Prelimination summary of the research project; Overhead pictures - B A Hedlund

22-12-3 Experimental Investigation of normal Stress Distribution in Glue Laminated Wooden Arches - Z Mielczarek and W Chanaj

22-12-4 Ultimate Strength of Wooden Beams with Tension Reinforcement as a Function of Random Material Properties - R Candowicz and T Dziuba

23-12-1 Bending Strength of Glulam Beams, a Design Proposal - J Ehlbeck and F Colling

23-12-2 Probability Based Design Method for Glued Laminated Timber - M F Stone

23-12-3 Glulam Beams, Bending Strength in Relation to the Bending Strength of the Finger Joints - H Riberholt

23-12-4 Glued Laminated Timber - Strength Classes and Determination of Characteristic Properties - H Riberholt, J Ehlbeck and A Fewell

24-12-1 Contribution to the Determination of the Bending Strength of Glulam Beams - F Colling, J Ehlbeck and R Görlacher

24-12-2 Influence of Perpendicular-to-Grain Stressed Volume on the Load-Carrying Capacity of Curved and Tapered Glulam Beams - J Ehlbeck and J Kürth

25-12-1 Determination of Characteristic Bending Values of Glued Laminated Timber. EN-Approach and Reality - E Gehri

26-12-1 Norwegian Bending Tests with Glued Laminated Beams-Comparative Calculations with the "Karlsruhe Calculation Model" - E Aasheim, K Solli, F Colling, R H Falk, J Ehlbeck and R Görlacher

26-12-2 Simulation Analysis of Norwegian Spruce Glued-Laminated Timber - R Hernandez and R H Falk

26-12-3 Investigation of Laminating Effects in Glued-Laminated Timber - F Colling and R H Falk

26-12-4 Comparing Design Results for Glulam Beams According to Eurocode 5 and to the French Working Stress Design Code (CB71) - F Rouger

27-12-1 State of the Art Report: Glulam Timber Bridge Design in the U.S. - M A Ritter and T G Williamson

27-12-2 Common Design Practice for Timber Bridges in the United Kingdom - C J Mettem, J P Marcroft and G Davis

27-12-3 Influence of Weak Zones on Stress Distribution in Glulam Beams - E Serrano and H J Larsen

28-12-1 Determination of Characteristic Bending Strength of Glued Laminated Timber - E Gehri

28-12-2 Size Factor of Norwegian Glued Laminated Beams - E Aasheim and K H Solli

28-12-3 Design of Glulam Beams with Holes - K Riipola

28-12-4 Compression Resistance of Glued Laminated Timber Short Columns- U Korin

PARTICLE AND FIBRE BUILDING BOARDS

7-13-1 Fibre Building Boards for CIB Timber Code (First Draft) - O Brynildsen

9-13-1	Determination of the Bearing Strength and the Load-Deformation Characteristics of Particleboard - K Möhler, T Budianto and J Ehlbeck
9-13-2	The Structural Use of Tempered Hardboard - W W L Chan
11-13-1	Tests on Laminated Beams from Hardboard under Short- and Longterm Load - W Nozynski
11-13-2	Determination of Deformation of Special Densified Hardboard under Long-term Load and Varying Temperature and Humidity Conditions - W Halfar
11-13-3	Determination of Deformation of Hardboard under Long-term Load in Changing Climate - W Halfar
14-4-1	An Introduction to Performance Standards for Wood-Base Panel Products - D H Brown
14-4-2	Proposal for Presenting Data on the Properties of Structural Panels - T Schmidt
16-13-1	Effect of Test Piece Size on Panel Bending Properties - P W Post
20-4-1	Considerations of Reliability - Based Design for Structural Composite Products - M R O'Halloran, J A Johnson, E G Elias and T P Cunningham
20-13-1	Classification Systems for Structural Wood-Based Sheet Materials - V C Kearley and A R Abbott
21-13-1	Design Values for Nailed Chipboard - Timber Joints - A R Abbott
25-13-1	Bending Strength and Stiffness of Izopanel Plates - Z Mielczarek
28-13-1	Background Information for "Design Rated Oriented Strand Board (OSB)" in CSA Standards - Summary of Short-term Test Results - E Karacabeyli, P Lau, C R Henderson, F V Meakes and W Deacon
28-13-2	Torsional Stiffness of Wood-Hardboard Composed I-Beam - P Olejniczak

TRUSSED RAFTERS

4-9-1	Long-term Loading of Trussed Rafters with Different Connection Systems - T Feldborg and M Johansen
6-9-3	Deflection of Trussed Rafters under Alternating Loading During a Year - T Feldborg and M Johansen
7-2-1	Lateral Bracing of Timber Struts - J A Simon
9-14-1	Timber Trusses - Code Related Problems - T F Williams
9-7-1	Design of Truss Plate Joints - F J Keenan
10-14-1	Design of Roof Bracing - The State of the Art in South Africa - P A V Bryant and J A Simon
11-14-1	Design of Metal Plate Connected Wood Trusses - A R Egerup
12-14-1	A Simple Design Method for Standard Trusses - A R Egerup
13-14-1	Truss Design Method for CIB Timber Code - A R Egerup
13-14-2	Trussed Rafters, Static Models - H Riberholt
13-14-3	Comparison of 3 Truss Models Designed by Different Assumptions for Slip and E-Modulus - K Möhler
14-14-1	Wood Trussed Rafter Design - T Feldborg and M Johansen
14-14-2	Truss-Plate Modelling in the Analysis of Trusses - R O Foschi
14-14-3	Cantilevered Timber Trusses - A R Egerup
14-7-5	The Effect of Support Eccentricity on the Design of W- and WW-Trusses with Nail Plate Connectors - B Källsner
15-14-1	Guidelines for Static Models of Trussed Rafters - H Riberholt
15-14-2	The Influence of Various Factors on the Accuracy of the Structural Analysis of Timber Roof Trusses - F R P Pienaar

15-14-3 Bracing Calculations for Trussed Rafter Roofs - H J Burgess

15-14-4 The Design of Continuous Members in Timber Trussed Rafters with Punched Metal Connector Plates - P O Reece

15-14-5 A Rafter Design Method Matching U.K. Test Results for Trussed Rafters - H J Burgess

16-14-1 Full-Scale Tests on Timber Fink Trusses Made from Irish Grown Sitka Spruce - V Picardo

17-14-1 Data from Full Scale Tests on Prefabricated Trussed Rafters - V Picardo

17-14-2 Simplified Static Analysis and Dimensioning of Trussed Rafters - H Riberholt

17-14-3 Simplified Calculation Method for W-Trusses - B Källsner

18-14-1 Simplified Calculation Method for W-Trusses (Part 2) - B Källsner

18-14-2 Model for Trussed Rafter Design - T Poutanen

19-14-1 Annex on Simplified Design of W-Trusses - H J Larsen

19-14-2 Simplified Static Analysis and Dimensioning of Trussed Rafters - Part 2 - H Riberholt

19-14-3 Joint Eccentricity in Trussed Rafters - T Poutanen

20-14-1 Some Notes about Testing Nail Plates Subjected to Moment Load - T Poutanen

20-14-2 Moment Distribution in Trussed Rafters - T Poutanen

20-14-3 Practical Design Methods for Trussed Rafters - A R Egerup

22-14-1 Guidelines for Design of Timber Trussed Rafters - H Riberholt

23-14-1 Analyses of Timber Trussed Rafters of the W-Type - H Riberholt

23-14-2 Proposal for Eurocode 5 Text on Timber Trussed Rafters - H Riberholt

24-14-1 Capacity of Support Areas Reinforced with Nail Plates in Trussed Rafters - A Kevarinmäki

25-14-1 Moment Anchorage Capacity of Nail Plates in Shear Tests - A Kevarinmaki and J. Kangas

25-14-2 Design Values of Anchorage Strength of Nail Plate Joints by 2-curve Method and Interpolation - J Kangas and A Kevarinmaki

26-14-1 Test of Nail Plates Subjected to Moment - E Aasheim

26-14-2 Moment Anchorage Capacity of Nail Plates - A Kevarinmäki and J Kangas

26-14-3 Rotational Stiffness of Nail Plates in Moment Anchorage - A Kevarinmäki and J Kangas

26-14-4 Solution of Plastic Moment Anchorage Stress in Nail Plates - A Kevarinmäki

26-14-5 Testing of Metal-Plate-Connected Wood-Truss Joints - R Gupta

26-14-6 Simulated Accidental Events on a Trussed Rafter Roofed Building - C J Mettem and J P Marcroft

STRUCTURAL STABILITY

8-15-1 Laterally Loaded Timber Columns: Tests and Theory - H J Larsen

13-15-1 Timber and Wood-Based Products Structures. Panels for Roof Coverings. Methods of Testing and Strength Assessment Criteria. Polish Standard BN-78/7159-03

16-15-1 Determination of Bracing Structures for Compression Members and Beams - H Brüninghoff

17-15-1 Proposal for Chapter 7.4 Bracing - H Brüninghoff

17-15-2	Seismic Design of Small Wood Framed Houses - K F Hansen
18-15-1	Full-Scale Structures in Glued Laminated Timber, Dynamic Tests: Theoretical and Experimental Studies - A Ceccotti and A Vignoli
18-15-2	Stabilizing Bracings - H Brüninghoff
19-15-1	Connections Deformability in Timber Structures: a Theoretical Evaluation of its Influence on Seismic Effects - A Ceccotti and A Vignoli
19-15-2	The Bracing of Trussed Beams - M H Kessel and J Natterer
19-15-3	Racking Resistance of Wooden Frame Walls with Various Openings - M Yasumura
19-15-4	Some Experiences of Restoration of Timber Structures for Country Buildings - G Cardinale and P Spinelli
19-15-5	Non-Destructive Vibration Tests on Existing Wooden Dwellings - Y Hirashima
20-15-1	Behaviour Factor of Timber Structures in Seismic Zones. - A Ceccotti and A Vignoli
21-15-1	Rectangular Section Deep Beam - Columns with Continuous Lateral Restraint - H J Burgess
21-15-2	Buckling Modes and Permissible Axial Loads for Continuously Braced Columns - H J Burgess
21-15-3	Simple Approaches for Column Bracing Calculations - H J Burgess
21-15-4	Calculations for Discrete Column Restraints - H J Burgess
21-15-5	Behaviour Factor of Timber Structures in Seismic Zones (Part Two) - A Ceccotti and A Vignoli
22-15-1	Suggested Changes in Code Bracing Recommendations for Beams and Columns - H J Burgess

22-15-2	Research and Development of Timber Frame Structures for Agriculture in Poland - S Kus and J Kerste
22-15-3	Ensuring of Three-Dimensional Stiffness of Buildings with Wood Structures - A K Shenghelia
22-15-5	Seismic Behavior of Arched Frames in Timber Construction - M Yasumura
22-15-6	The Robustness of Timber Structures - C J Mettem and J P Marcroft
22-15-7	Influence of Geometrical and Structural Imperfections on the Limit Load of Wood Columns - P Dutko
23-15-1	Calculation of a Wind Girder Loaded also by Discretely Spaced Braces for Roof Members - H J Burgess
23-15-2	Stability Design and Code Rules for Straight Timber Beams - T A C M van der Put
23-15-3	A Brief Description of Formula of Beam-Columns in China Code - S Y Huang
23-15-4	Seismic Behavior of Braced Frames in Timber Construction - M Yasumara
23-15-5	On a Better Evaluation of the Seismic Behavior Factor of Low-Dissipative Timber Structures - A Ceccotti and A Vignoli
23-15-6	Disproportionate Collapse of Timber Structures - C J Mettem and J P Marcroft
23-15-7	Performance of Timber Frame Structures During the Loma Prieta California Earthquake - M R O'Halloran and E G Elias
24-15-2	Discussion About the Description of Timber Beam-Column Formula - S Y Huang
24-15-3	Seismic Behavior of Wood-Framed Shear Walls - M Yasumura
25-15-1	Structural Assessment of Timber Framed Building Systems - U Korin

25-15-3 Mechanical Properties of Wood-framed Shear Walls Subjected to Reversed Cyclic Lateral Loading - M Yasumura

26-15-1 Bracing Requirements to Prevent Lateral Buckling in Trussed Rafters - C J Mettem and P J Moss

26-15-2 Eurocode 8 - Part 1.3 - Chapter 5 - Specific Rules for Timber Buildings in Seismic Regions - K Becker, A Ceccotti, H Charlier, E Katsaragakis, H J Larsen and H Zeitter

26-15-3 Hurricane Andrew - Structural Performance of Buildings in South Florida - M R O'Halloran, E L Keith, J D Rose and T P Cunningham

FIRE

12-16-1 British Standard BS 5268 the Structural Use of Timber: Part 4 Fire Resistance of Timber Structures

13-100-2 CIB Structural Timber Design Code. Chapter 9. Performance in Fire

19-16-1 Simulation of Fire in Tests of Axially Loaded Wood Wall Studs - J König

24-16-1 Modelling the Effective Cross Section of Timber Frame Members Exposed to Fire - J König

25-16-1 The Effect of Density on Charring and Loss of Bending Strength in Fire - J König

25-16-2 Tests on Glued-Laminated Beams in Bending Exposed to Natural Fires - F Bolonius Olesen and J König

26-16-1 Structural Fire Design According to Eurocode 5, Part 1.2 - J König

STATISTICS AND DATA ANALYSIS

24-17-3 Effect of Sampling Size on Accuracy of Characteristic Values of Machine Grades - Y H Chui, R Turner and I Smith

24-17-4 Harmonisation of LSD Codes - R H Leicester

25-17-2 A Body for Confirming the Declaration of Characteristic Values - J Sunley

25-17-3 Moisture Content Adjustment Procedures for Engineering Standards - D W Green and J W Evans

27-17-1 Statistical Control of Timber Strength - R H Leicester and H O Breitinger

GLUED JOINTS

20-18-1 Wood Materials under Combined Mechanical and Hygral Loading - A Martensson and S Thelandersson

20-18-2 Analysis of Generalized Volkersen - Joints in Terms of Linear Fracture Mechanics - P J Gustafsson

20-18-3 The Complete Stress-Slip Curve of Wood-Adhesives in Pure Shear - H Wernersson and P J Gustafsson

22-18-1 Perspective Adhesives and Protective Coatings for Wood Structures - A S Freidin

FRACTURE MECHANICS

21-10-1 A Study of Strength of Notched Beams - P J Gustafsson

22-10-1 Design of Endnotched Beams - H J Larsen and P J Gustafsson

23-10-1 Tension Perpendicular to the Grain at Notches and Joints - T A C M van der Put

23-10-2 Dimensioning of Beams with Cracks, Notches and Holes. An Application of Fracture Mechanics - K Riipola

23-19-1 Determination of the Fracture Energie of Wood for Tension Perpendicular to the Grain - W Rug, M Badstube and W Schöne

23-19-2 The Fracture Energy of Wood in Tension Perpendicular to the Grain. Results from a Joint Testing Project - H J Larsen and P J Gustafsson

23-19-3 Application of Fracture Mechanics to Timber Structures - A Ranta-Maunus

24-19-1 The Fracture Energy of Wood in Tension Perpendicular to the Grain - H J Larsen and P J Gustafsson

28-19-1 Fracture of Wood in Tension Perpendicular to the Grain: Experiment and Numerical Simulation by Damage Mechanics - L Daudeville, M Yasumura and J D Lanvin

28-19-2 A New Method of Determining Fracture Energy in Forward Shear along the Grain - H D Mansfield-Williams

28-19-3 Fracture Design Analysis of Wooden Beams with Holes and Notches. Finite Element Analysis based on Energy Release Rate Approach - H Petersson

28-19-4 Design of Timber Beams with Holes by Means of Fracture Mechanics - S Aicher, J Schmidt and S Brunold

SERVICEABILITY

27-20-1 Codification of Serviceability Criteria - R H Leicester

27-20-2 On the Experimental Determination of Factor k_{def} and Slip Modulus k_{ser} from Short- and Long-Term Tests on a Timber-Concrete Composite (TCC) Beam - S Capretti and A Ceccotti

27-20-3 Serviceability Limit States: A Proposal for Updating Eurocode 5 with Respect to Eurocode 1 - P Racher and F Rouger

27-20-4 Creep Behavior of Timber under External Conditions - C Le Govic, F Rouger, T Toratti and P Morlier

CIB TIMBER CODE

2-100-1 A Framework for the Production of an International Code of Practice for the Structural Use of Timber - W T Curry

5-100-1 Design of Solid Timber Columns (First Draft) - H J Larsen

5-100-2 A Draft Outline of a Code for Timber Structures - L G Booth

6-100-1 Comments on Document 5-100-1; Design of Solid Timber Columns - H J Larsen and E Theilgaard

6-100-2 CIB Timber Code: CIB Timber Standards - H J Larsen and E Theilgaard

7-100-1 CIB Timber Code Chapter 5.3 Mechanical Fasteners; CIB Timber Standard 06 and 07 - H J Larsen

8-100-1 CIB Timber Code - List of Contents (Second Draft) - H J Larsen

9-100-1 The CIB Timber Code (Second Draft)

11-100-1 CIB Structural Timber Design Code (Third Draft)

11-100-2 Comments Received on the CIB Code
a U Saarelainen
b Y M Ivanov
c R H Leicester
d W Nozynski
e W R A Meyer
f P Beckmann; R Marsh
g W R A Meyer
h W R A Meyer

11-100-3 CIB Structural Timber Design Code; Chapter 3 - H J Larsen

12-100-1 Comment on the CIB Code - Sous-Commission Glulam

12-100-2	Comment on the CIB Code - R H Leicester
12-100-3	CIB Structural Timber Design Code (Fourth Draft)
13-100-1	Agreed Changes to CIB Structural Timber Design Code
13-100-2	CIB Structural Timber Design Code. Chapter 9: Performance in Fire
13-100-3a	Comments on CIB Structural Timber Design Code
13-100-3b	Comments on CIB Structural Timber Design Code - W R A Meyer
13-100-3c	Comments on CIB Structural Timber Design Code - British Standards Institution
13-100-4	CIB Structural Timber Design Code. Proposal for Section 6.1.5 Nail Plates - N I Bovim
14-103-2	Comments on the CIB Structural Timber Design Code - R H Leicester
15-103-1	Resolutions of TC 165-meeting in Athens 1981-10-12/13
21-100-1	CIB Structural Timber Design Code. Proposed Changes of Sections on Lateral Instability, Columns and Nails - H J Larsen
22-100-1	Proposal for Including an Updated Design Method for Bearing Stresses in CIB W18 - Structural Timber Design Code - B Madsen
22-100-2	Proposal for Including Size Effects in CIB W18A Timber Design Code - B Madsen
22-100-3	CIB Structural Timber Design Code - Proposed Changes of Section on Thin-Flanged Beams - J König
22-100-4	Modification Factor for "Aggressive Media" - a Proposal for a Supplement to the CIB Model Code - K Erler and W Rug
22-100-5	Timber Design Code in Czechoslovakia and Comparison with CIB Model Code - P Dutko and B Kozelouh

LOADING CODES

4-101-1 Loading Regulations - Nordic Committee for Building Regulations

4-101-2 Comments on the Loading Regulations - Nordic Committee for Building Regulations

STRUCTURAL DESIGN CODES

1-102-1 Survey of Status of Building Codes, Specifications etc., in USA - E G Stern

1-102-2 Australian Codes for Use of Timber in Structures - R H Leicester

1-102-3 Contemporary Concepts for Structural Timber Codes - R H Leicester

1-102-4 Revision of CP 112 - First Draft, July 1972 - British Standards Institution

4-102-1 Comparsion of Codes and Safety Requirements for Timber Structures in EEC Countries - Timber Research and Development Association

4-102-2 Nordic Proposals for Safety Code for Structures and Loading Code for Design of Structures - O A Brynildsen

4-102-3 Proposal for Safety Codes for Load-Carrying Structures - Nordic Committee for Building Regulations

4-102-4 Comments to Proposal for Safety Codes for Load-Carrying Structures - Nordic Committee for Building Regulations

4-102-5 Extract from Norwegian Standard NS 3470 "Timber Structures"

4-102-6 Draft for Revision of CP 112 "The Structural Use of Timber" - W T Curry

8-102-1 Polish Standard PN-73/B-03150: Timber Structures; Statistical Calculations and Designing

8-102-2 The Russian Timber Code: Summary of Contents

9-102-1	Svensk Byggnorm 1975 (2nd Edition); Chapter 27: Timber Construction
11-102-1	Eurocodes - H J Larsen
13-102-1	Program of Standardisation Work Involving Timber Structures and Wood-Based Products in Poland
17-102-1	Safety Principles - H J Larsen and H Riberholt
17-102-2	Partial Coefficients Limit States Design Codes for Structural Timberwork - I Smith
18-102-1	Antiseismic Rules for Timber Structures: an Italian Proposal - G Augusti and A Ceccotti
18-1-2	Eurocode 5, Timber Structures - H J Larsen
19-102-1	Eurocode 5 - Requirements to Timber - Drafting Panel Eurocode 5
19-102-2	Eurocode 5 and CIB Structural Timber Design Code - H J Larsen
19-102-3	Comments on the Format of Eurocode 5 - A R Fewell
19-102-4	New Developments of Limit States Design for the New GDR Timber Design Code - W Rug and M Badstube
19-7-3	Effectiveness of Multiple Fastener Joints According to National Codes and Eurocode 5 (Draft) - G Steck
19-7-6	The Derivation of Design Clauses for Nailed and Bolted Joints in Eurocode 5 - L R J Whale and I Smith
19-14-1	Annex on Simplified Design of W-Trusses - H J Larsen
20-102-1	Development of a GDR Limit States Design Code for Timber Structures - W Rug and M Badstube
21-102-1	Research Activities Towards a New GDR Timber Design Code Based on Limit States Design - W Rug and M Badstube
22-102-1	New GDR Timber Design Code, State and Development - W Rug, M Badstube and W Kofent

22-102-2 Timber Strength Parameters for the New USSR Design Code and its Comparison with International Code - Y Y Slavik, N D Denesh and E B Ryumina

22-102-3 Norwegian Timber Design Code - Extract from a New Version - E Aasheim and K H Solli

23-7-1 Proposal for a Design Code for Nail Plates - E Aasheim and K H Solli

24-102-2 Timber Footbridges: A Comparison Between Static and Dynamic Design Criteria - A Ceccotti and N de Robertis

25-102-1 Latest Development of Eurocode 5 - H J Larsen

25-102-1A Annex to Paper CIB-W18/25-102-1. Eurocode 5 - Design of Notched Beams - H J Larsen, H Riberholt and P J Gustafsson

25-102-2 Control of Deflections in Timber Structures with Reference to Eurocode 5 - A Martensson and S Thelandersson

28-102-1 Eurocode 5 - Design of Timber Structures - Part 2: Bridges - D Bajolet, E Gehri, J König, H Kreuzinger, H J Larsen, R Mäkipuro and C Mettem

28-102-2 Racking Strength of Wall Diaphragms - Discussion of the Eurocode 5 Approach - B Källsner

INTERNATIONAL STANDARDS ORGANISATION

3-103-1 Method for the Preparation of Standards Concerning the Safety of Structures (ISO/DIS 3250) - International Standards Organisation ISO/TC98

4-103-1 A Proposal for Undertaking the Preparation of an International Standard on Timber Structures - International Standards Organisation

5-103-1 Comments on the Report of the Consultion with Member Bodies Concerning ISO/TC/P129 - Timber Structures - Dansk Ingeniorforening

7-103-1 ISO Technical Committees and Membership of ISO/TC 165

8-103-1 Draft Resolutions of ISO/TC 165

12-103-1 ISO/TC 165 Ottawa, September 1979

13-103-1 Report from ISO/TC 165 - A Sorensen

14-103-1 Comments on ISO/TC 165 N52 "Timber Structures; Solid Timber in Structural Sizes; Determination of Some Physical and Mechanical Properties"

14-103-2 Comments on the CIB Structural Timber Design Code - R H Leicester

21-103-1 Concept of a Complete Set of Standards - R H Leicester

JOINT COMMITTEE ON STRUCTURAL SAFETY

3-104-1 International System on Unified Standard Codes of Practice for Structures - Comité Européen du Béton (CEB)

7-104-1 Volume 1: Common Unified Rules for Different Types of Construction and Material - CEB

CIB PROGRAMME, POLICY AND MEETINGS

1-105-1 A Note on International Organisations Active in the Field of Utilisation of Timber - P Sonnemans

5-105-1 The Work and Objectives of CIB-W18-Timber Structures - J G Sunley

10-105-1 The Work of CIB-W18 Timber Structures - J G Sunley

15-105-1 Terms of Reference for Timber - Framed Housing Sub-Group of CIB-W18

19-105-1 Tropical and Hardwood Timbers Structures - R H Leicester

21-105-1 First Conference of CIB-W18B, Tropical and Hardwood Timber Structures Singapore, 26 - 28 October 1987 - R H Leicester

INTERNATIONAL UNION OF FORESTRY RESEARCH ORGANISATIONS

7-106-1 Time and Moisture Effects - CIB W18/IUFRO 55.02-03 Working Party

INTERNATIONAL COUNCIL FOR BUILDING RESEARCH STUDIES AND DOCUMENTATION

WORKING COMMISSION W18 - TIMBER STRUCTURES

SYMBOLS FOR TIMBER AND WOOD-BASED MATERIALS

by

J Kuipers
Delft
The Netherlands
B Noren
Svenska Träforskningsinstitutet, Stockholm
Sweden

MEETING TWENTY - EIGHT

COPENHAGEN

DENMARK

APRIL 1995

SYMBOLS FOR TIMBER AND WOOD-BASED MATERIALS

by

J Kuipers
Delft
The Netherlands
B Noren
Svenska Träforskningsinstitutet, Stockholm
Sweden

INTRODUCTION

In 1976 CIB - W18 - "Timber Structures " published a recommended list of symbols for use in structural design documentation.
Since the publication of this document a large number of standards have been drafted by ISO and CEN both in the structural and non - structural field and it has been considered desirable to bring the 1976 - version up to date.
This revision extends the scope of the earlier document and covers both the structural and non - structural use of all timber and wood - based materials.

This second edition has been drafted after the development of the CEN-document prEN 1438, with the same title as this CIB-document and except for the Introduction and Foreword the content is the same. It has been judged worth while to transform it into this CIB-document to widen its scope from European to world-wide. A first draft of this paper was presented at the CIB - W18 - meeting in Athens , August 1993 , and some comments were received and taken into account. The prEN 1438 was published for the CEN - Enquiry in April 1994 and the comments were received in November 1994, leading to a new draft. It is this draft, which now is brought again in its CIB - format.

prEN 1438 was developed in conjunction with the various CEN - timber committees and is based on the general ISO - recommendations for symbols contained in ISO 3898 " Basis for design of structures - Notations-General symbols ". The ISO standard covers all materials, but is limited to the use in structural design ; it covers only general terms necessary in this field of application and excludes terms relevant to a particular material or to a special technical field.

This paper extends its principles to take into account features which are special to timber and wood-based materials. It has been drafted in three parts.
The first part gives general information and principles.
The second part separates the symbols into specific groups covering geometric properties, directional subscripts, actions, mechanical and physical properties. This part is set up in the same way as the first edition of the CIB - document.
The third part follows the layout of ISO 3898 , so here the symbols are presented as letter types in alphabetical order.

To facilitate communication it is hoped that ISO and CEN timber committees, CIB - W18 research workers and individual publishers will use this information when drafting standards and writing papers, publications or reports.

FOREWORD to the first edition (1976)

CIB Working Commission W18 - Timber Structures - was re-formed in 1973 and is today a recognised authority on all aspects of timber engineering.

The terms of CIB-W18 are :

"To study and highlight the major differences between the relevant national design codes and standards and suggest ways in which in the future developments of these codes and standards might take place in order to minimise or eliminate these differences"

These objectives are being rigorously pursued at the regular meetings of the commission.

Interchange of information is facilitated and duplication of effort is avoided in the field of timber structures by the close links that W18 maintains with other international organisations, including IUFRO , RILEM , CEI , and FEMIB *.
CIB-W18 also provides guidance on matters related to structural timber engineering to ECE ,ISO , EEC , CEN , CEB , and JCSS **.

This paper is the first agreed document to be produced by Working Commission W18. It will be followed by others to cover all aspects of engineered timber structures.

The principal contributors to this paper were :

DR J KUIPERS, Stevin Laboratory , Delft, The Netherlands
DR B NOREN , Svenska Träforskningsinstitutet, Stockholm, Sweden

---

.

IUFRO	International Union of Forestry Research Organisations
RILEM	Réunion International des Laboratoires d'Essais et de Recherches sur les Matériaux et les Constructions
CEI	European Confederation of Woodworking Industries
FEMIB	Féderation Européenne des Syndicats de Fabricants de Menuiseries Industrielles de Batiment

..

ECE	United Nations Economic Commission for Europe
ISO	International Standards Organisation
EEC	European Economic Community
CEN	Commité Européen de Coordination des Normes
JCSS	Joint Committee on Structural Safety
CEB	Commité Européen du Beton

FOREWORD to the second edition (1995)

The drafting group for this second edition was the Task Group 4 "Symbols " of Working Group 1 of CEN/TC175 , consisting of:

Jan Kuipers (chairman)	The Netherlands
Roland Hue	France
Henry H. Knutsson	Denmark
George Nowacki / T. Robson	United Kingdom
Torbjörn Schmidt	Sweden
John Sunley	United Kingdom

SYMBOLS FOR TIMBER AND WOOD-BASED MATERIALS

PART I GENERAL INFORMATION AND PRINCIPLES

I.1 Scope

This document gives a wide range of symbols for use in documents covering solid timber and all wood - based materials. The symbols appear in two separate parts II and III.
Part II separates the symbols into specific groups covering geometric properties, dimensional subscripts, actions, mechanical and physical properties.
Part III follows the layout of ISO 3898 so here the symbols are presented as letter types in alphabetical order.

I.2 Normative references

ISO 3898: 1987 Basis for design of structures-Notations-General symbols.

I.3 Letter types

Both upper case (capital) and lower case (small) Latin and Greek letters appear in Roman (upright) and Italic (sloping) style, as shown in table 1.

Table 1: Letter types

		ROMAN	ITALIC
LATIN	upper case	A, B, C, etc.	*A, B, C, etc.*
	lower case	a, b, c, etc.	*a, b, c, etc.*
GREEK	upper case	A, B, Γ, etc.	*A, B, Γ, etc.*
	lower case	α, β, γ, etc.	*α, β, γ, etc.*

I.4 Principles

I.4.1 The principal use of letters as symbols is as given in ISO 3898, see table 2.

Table 2: Letter guide for the construction of symbols

Type of letter	Dimensions	Usage
Latin upper case	Force, force times length, length to a power other than 1, temperature	1. Actions and action-effects 2. Area, first and second moment of area 3. Elastic moduli (exception to the general rule) 4. Temperature
Latin lower case	Length, quotient of length and time to a power, force per unit length or area, mass, time	1. Actions and action-effects per unit of length or area 2. Linear dimensions (length, width, thickness, etc.) 3. Strengths 4. Velocity, acceleration, frequency 5. Descriptive letters (subscripts) 6. Mass 7. Time
Greek upper case		Reserved for mathematics and for physical quantities excluding geometrical and mechanical quantities
Greek lower case	Dimensions	1. Coefficients and dimensionless ratios 2. Strains 3. Angles 4. Densities (mass density and weight density) (exception to the general rule) 5. Stresses (exception to the general rule)
NOTE: Concepts not included in table 2 should comply with the nearest appropriate category listed.		

I.4.2 For substantive symbols this standard uses
Latin upper case Italic letters,
Latin lower case Italic letters and
Greek lower case Italic letters.
For subscripts this standard uses
Latin and Greek lower case Roman letters.

I.4.3 For subscripts the use of small format letters and numbers is preferred. They shall be printed Roman.

I.4.4 In subscripts a comma followed by a space is used for separation of different digits, letters, symbols or abbreviations. The comma(s) and the space(s) may be omitted where no confusion is expected.

I.4.5 The order of the different parts of a subscript is from basic to evaluated as in $f_{c\,k}$ for the characteristic value of the basic property compressive strength.

I.4.6 Digits shall always be printed Roman

I.4.7 For mechanical properties of timber and wood - based materials used in design of structures the subscript $_k$ is normally used for the 5- percentile values of strength and modulus of elasticity, if this modulus is critical for strength, e.g. in the case of buckling. They are denoted as f_k and E_k respectively.
Where the E-modulus is used to calculate (mean) values of deformation the mean value can be used, denominated E_{mean}.

More precise denominations can be used, eg. f_{05} , or f_{50} , to make clear that a 5-, or a 50-percentile is meant.

I.4.8 Free choice between two symbols for one concept has been avoided as far as possible, e.g.:
only Q (not V) for Variable action and
only V (not Q) for Shear force.

I.4.9 The symbols in this standard are complemented with examples of preferred units to be used. The units given can be replaced by other corresponding units, e.g. N/mm^2 can be changed into kN/m^2, or into MPa.

PART II : SYMBOLS FOR GROUPS OF QUANTITIES

II.1 Geometric properties

II.1.1 *Cross section properties*

	Basic symbol	Derived symbol	Preferred unit
coordinate coordinate (see figure 1a) coordinate	x y z		

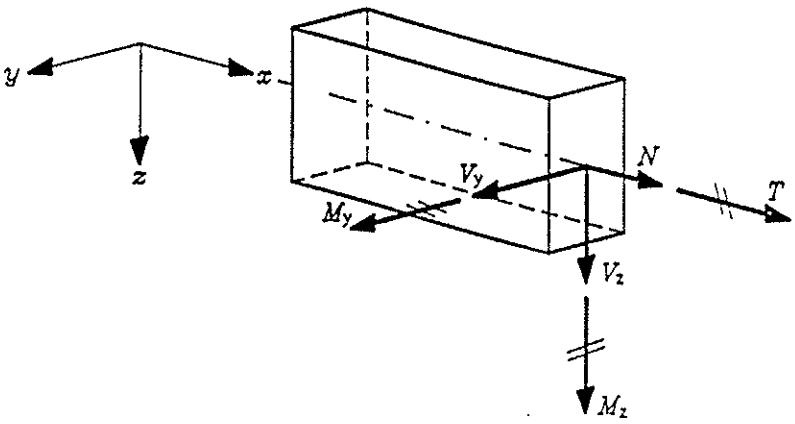

Figure 1a : coordinates

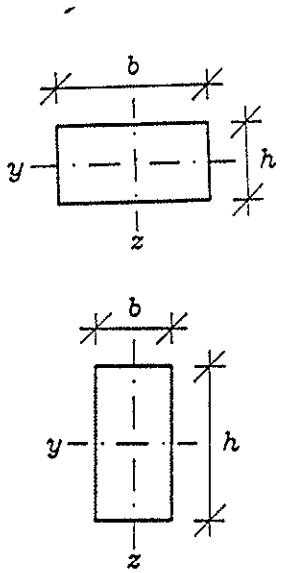

Figure 1b: cross-sectional dimensions

	Basic symbol	Derived symbol	Preferred unit
depth, height (see figure 1b)	h		mm
depth of compression zone		h_c	mm
depth of tension zone		h_t	mm
diameter	d		mm
distance	a		mm
radius	r		mm
radius of gyration	i		mm
thickness	t		mm
thickness (when equal to depth)	h		mm
width	b		mm
tip width of finger joint		b_t	mm
area	A		mm^2
area of flange		A_{fl}	mm^2
area of web		A_{web}	mm^2
area of one wane		A_{wane}	mm^2
first moment of plane area	S		mm^3
section modulus	W		mm^3
second moment of plane area	I		mm^4

II.1.2 *Composed section properties*

number of members or layers	n		
member number	i		
contribution of member i to total			
height		h_i	mm
area		A_i	mm^2
second moment		I_i	mm^4
second moment of area of member i (about its own axis)		$I_{0\,i}$	mm^4
effective second moment of area		I_{ef}	mm^4

II.1.3 *Other geometric properties*

distance	a		mm
length, span	l		mm
critical length (buckling length)		l_{cr}	mm
spacing (distance centre to centre)	s		mm
eccentricity	e		mm
knot diameter ratio		β_d	
knot area ratio		β_a	
volume	V		mm^3

	Basic symbol	Derived symbol	Preferred unit
II.2 Directions			
II.2.1 *General*			
angle between force and grain direction	α		° or rad (no preference)
II.2.2 *Subscripts*			
angle between force and grain direction	α		° or rad ,,
parallel to grain direction	0		° or rad ,,
perpendicular to grain direction	90		°
longitudinal (parallel to the fibre direction)	ℓ		
radial to annual rings	r		
tangential to annual rings	t		
examples			
For shear stress (τ) :			
direction r , in plane perpendicular to ℓ		$\tau_{\ell r}$	
direction z , in plane perpendicular to x		τ_{xz}	
For shear deformation (γ) and rigidity moduli (G) : shear deformation caused by $\tau_{\ell r}$ and $\tau_{r\ell}$		$\gamma_{\ell r}$	

II.2.3 *Special applications*

The symbols l, t, r, or x, y, z can be used for laminated timber or for panels , as in table 3.

Table 3 Symbols for and in relation to laminated wood and wood-based panels.

Laminated wood	Wood - based panels		Symbol
	Plywood , OSB , and similar	Particleboard , fibre board and similar	
Grain direction of laminae	Grain direction of face*) veneer	Machine or longitudinal **) direction	l or x
Perpendicular to grain direction of laminae, parallel to plane of joints	Perpendicular to grain direction of face veneer parallel to glue lines (rolling shear)	Perpendicular to machine or longitudinal direction, parallel to face	t or y
Perpendicular to plane of joints	Perpendicular to face (through thickness)	Perpendicular to face	r or z

*) Not necessarily the main direction

**) May be marked on the panel with the symbol ⟺

	Basic symbol	**Derived symbol**	**Preferred unit**
II.3 Actions, forces, loads			
action, force or load in general	F		N
components of F along the axes		F_x, F_y, F_z	N
maximum load[1)]		F_{max}	N
estimated maximum load [1)]		$F_{max,\ est}$	N
ultimate load [1)]		F_u	N
estimated ultimate load[1)]		$F_{u,\ est}$	N
accidental action	A		N
permanent action	G		N
variable action	Q		N
wind action (load)	W		N

[1)] F_{max} is used for the maximum load reached during a strength test, within the standardised duration , e.g. within a certain deformation as with strength tests on joints.
F_u is used for the load at the end of a standardized strength test.

Basic symbol	Derived symbol	Preferred unit	
normal force, axial force	N		N
prestressing force	P		N
shear force	V		N
moment	M		N mm
Torsional moment (Torque)	T		N mm
reaction force; resultant force	R		N
components of R along the axes		R_x, R_y, R_z	N
horizontal component of force	H		N
vertical component of force, reaction force	V		N
angle between force or stress and grain	α		° or rad
For intensity (force per unit length or area) use lower case letters, for example:			
Distributed permanent action (Dead load)	g		N/mm or N/mm^2
Distributed variable action	q		N/mm or N/mm^2

II.4 Stresses and mechanical properties

II.4.1 *Stresses*

normal stress	σ		N/mm^2
compressive stress		σ_c	N/mm^2
tensile stress		σ_t	N/mm^2
bending stress		σ_m	N/mm^2
shear stress	τ		N/mm^2
strength, general	f		N/mm^2
strength in compression (compressive strength)		f_c	N/mm^2
strength in tension (tensile strength)		f_t	N/mm^2
strength in shear (shear strength)		f_v	N/mm^2
strength in bending (bending strength)		f_m	N/mm^2
embedding strength		f_h	N/mm^2
characteristic value of bending strength		f_{mk}	N/mm^2
characteristic value of shear strength		f_{vk}	N/mm^2
characteristic value of compressive strength parallel to grain		$f_{c,0,k}$	N/mm^2
characteristic value of tensile strength perpendicular to grain		$f_{t,90,k}$	N/mm^2
sample fifth percentile of tensile strength perpendicular to grain		$f_{t,90,05}$	N/mm^2
factor for adjusting f_{05} - values to f_k	k		
if depth differs from test standard		k_h	
if length differs from test standard		k_l	
for number and size of samples		k_s	
for grading method		k_v	
yield moment		M_y	N/mm^2

	Basic symbol	Derived symbol	Preferred unit
II.4.2 *Moduli and coefficients*			
elasticity modulus	E		N/mm^2
apparent elasticity modulus $\frac{E}{1+\varphi}$		E_{app}	N/mm^2
mean value of modulus of elasticity parallel to grain		$E_{0,\,mean}$	N/mm^2
characteristic value of modulus of elasticity parallel to grain		$E_{0,\,k}$	N/mm^2
sample fifth percentile value of modulus of elasticity parallel to grain		$E_{0,\,05}$	N/mm^2
sample fifth percentile value of modulus of elasticity perpendicular to grain		$E_{90,\,05}$	N/mm^2
shear or rigidity modulus	G		N/mm^2
energy release rate	G		$N\ mm^{-3/2}$
flexural rigidity of plates, shells and panels	D		N/mm
racking stiffness of panels	R		N/mm
crack resistance	R		?
displacement modulus	K		N/mm^2
stress intensity factor	K		Nm/m^2
elastic foundation modulus		K_s	N/mm
slip modulus	k		N/mm
Poisson's ratio	ν		
viscosity	η		Ns/m^2
II.4.3 *Rheological properties (subscripts)*			
creep	c		
recovery	r		
permanent (irrecoverable)	ir		
delayed	del		
creep coefficient (function)	φ		
relaxation coefficient		no symbol designated yet	
time	t		
II.5 Strain, deformation and displacement			
strain (including compressive strain)	ε		
displacement, deflection, corresponding to the directions x, y, z in figure 1	u, v, w		mm
rotation	θ		° or rad
shear strain	γ		° or rad

	Basic symbol	Derived symbol	Preferred unit
II.6 Physical properties			
temperature	T		° C or K
relative humidity	ψ		%
moisture content ratio (mass of water to mass of solid)	ω		%
equilibrium moisture content ratio		ω_{ψ}	%
water content ratio (mass of water to mass of water + solid)	ω'		%
density	ρ		kg/m^3
density; mass at ω, volume at ω		ρ_{ω}	kg/m^3
density; mass at $\omega = 0$, volume at ω		$\rho_{0,\,\omega}$	kg/m^3
density; mass at $\omega = 0$, volume at $\omega = 0$		ρ_0	kg/m^3
density; mass at $\omega = 0$, volume at green conditions		$\rho_{0,\,>35}$	kg/m^3
coefficient of swelling (positive) or shrinkage (negative)	β		
II.7 Statistical symbols			
mean value of sample	mean		
median (50 %) value of sample	50		
characteristic value	k		
standard deviation of sample	s		
II.8 Special symbols			
direction of grain (of outer veneer)	⇋		
point of measurement of thickness	⊕		
point of measurement of length	↔		
main direction of wood based panel	⟺		
II.9 Special subscripts			
characteristic value of force (load), strength or deformation (5^{th} or 95^{th} percentile values)	k		
Mean value	mean		
Design value	d		
Ultimate value	u		
Yield value	y		
Critical value	cr		
II.10 Other symbols			
Partial factor	γ		

PART III : SYMBOLS IN ALPHABETICAL ORDER

III.1 Latin upper case - Italic - letters

Note 1: Symbols in the lists, marked with * are corresponding with ISO 3898.

Note 2: Latin upper case Roman letters have not been used in ISO 3898.

Letter(s)	Meaning
A *	area
A	accidental action
D *	flexural rigidity of panels , plates and shells ; also for structural floor decking
E *	longitudinal modulus of elasticity; earthquake action
$E_{0,\,k}$	characteristic value of modulus of elasticity parallel to grain (calculation of critical strength as in buckling)
$E_{90,\,mean}$	mean value of modulus of elasticity perpendicular to grain (calculation of deformations)
F	action in general; force in general
F_{max}	maximum load reached during a strength test, within the standardised duration (e.g. time or deformation) , of the test.
$F_{max,\,est}$	estimated maximum load as above
F_{u}	applied load at a prescribed end of a strength test
$F_{u,\,est}$	estimated applied load at a prescribed end of a strength test
G *	shear modulus; energy release factor; permanent action (dead load); self load
H *	horizontal component of a force
I *	second moment of plane area
K *	any quantity but with a proper dimension in the absence of a specific symbol; displacement modulus; stress intensity factor
K_s	foundation modulus
K_e	elastic foundation modulus
K_{init}	initial foundation modulus
L	(To be avoided for length)
M *	moment in general
M *	bending moment
M_y	yield moment
N *	normal force
O *	(To be avoided as far as possible)
P *	prestressing force; probability (or p, see table 3; ISO 3898)
Q *	variable action (live load)[2)]

[2)] With a subscript if it is necessary to define an imposed load more precisely.

Letter(s)	Meaning
Q_k	characteristic value of variable action/load
R *	resultant force; reaction force; resistance; racking stiffness of panel
S *	first moment of plane area (static moment); action-effect (solicitation); snow action (load)
S_n	snow action (load) where there is a risk of confusion
T *	torsional moment (torque); temperature; period of time; loading time
T_r	recovery time
V *	shear force; volume; vertical component of a force
W *	section modulus; wind action load; impact energy

III.2 Latin lower case - Italic - letters

NOTE: Latin lower case Roman letters have not been used in ISO 3898

Letter(s)	Meaning
a *	distance; acceleration
b *	width
c *	(Void)
d *	diameter; depth (for example foundation)
e *	eccentricity
f *	strength (of a material); frequency
$f_{0,05}$	sample fifth percentile of strength parallel to grain
f_{mk}	characteristic value of bending strength
f_{vk}	characteristic value of shear strength
$f_{c.0,k}$	characteristic value of compressive strength parallel to grain
$f_{t,90,k}$	characteristic value of tensile strength perpendicular to grain
	NOTE: For other strength values the symbols should be built up in the same way.
g *	distributed permanent action (Dead load); acceleration due to gravity
h *	height; depth (of beams); thickness (of plates, shells, panels)
i *	radius of gyration
j *	number of days
k *	coefficient ; factor
k_h	size factor; height factor
l *	span; length of a member; length between two points
m *	bending moment per unit of length or width; mass; average value of a sample
$m(x)$	mean value of the quantity x
n *	normal force per unit of length or width; number of....
o *	(to be avoided)
p *	pressure; probability (or P, see 6.1); pitch

Letter(s)	Meaning
q^*	distributed variable action (live load)[3)]
r^*	radius
s^*	standard deviation of a sample; spacing; distributed snow action (load)
$s(x)$	standard deviation of the quantity x
t^*	time in general; thickness of thin members; thickness of plates, shells, panels; torsional moment per unit of length or width
u	perimeter
u^*, v^*, w^*	components of the displacement of a point
v^*	velocity, speed
w^*	distributed wind action (load)
w_e	elastic deformation
$w_{i,\,mod}$	modified initial deformation
w^*	distributed wind action
x^*, y^*, z^*	coordinates
z^*	lever arm

III.3 Greek lower case letters (Italic)

Letter(s)		Meaning
alpha	α	angle ; ratio. (In timber standards particularly the angle between direction of load/stress and grain)
gamma	γ	safety factor (partial coefficient); shear strain; modification factor
delta	Δ	difference; increment
epsilon	ε	strain
eta	η	viscosity

NOTE: In ISO 3898; eta η , together with xi ξ and zeta ζ are symbols for Relative Coordinates.

kappa	χ	(to be avoided as far as possible)
lambda	λ	slenderness ratio
nu	ν	Poisson's ratio; panel deformation
rho	ρ	mass density
	ρ_k	characteristic value of density
	ρ_{05}	sample fifth percentile of density
sigma	σ	normal stress; standard deviation of population
tau	τ	shear stress
phi	φ	creep function
psi	ψ	relative humidity
omega	ω	angular velocity; moisture content
	ω_n	actual moisture content

[3)] With a subscript if it is necessary to define an imposed load more precisely.

Letter(s)	Meaning
ω_{ref}	reference moisture content
ω_{ψ}	equilibrium moisture content
ω '	water content

III.4 General subscripts; and subscripts formed from abbreviations or other combinations of letters [4]; Latin lower case - Roman - letters [5]

NOTE: Subscripts marked with * have been taken from table 6 of ISO 3898.

NOTE: For subscripts small size lower case letters are preferred.

Letter(s)	Meaning
a *	structural steel
c *	compression in general; concrete
cal *	calculated[6]
cr *	critical
d *	design[7]
def	deformation
dyn *	dynamic
e	elastic; elastic limit[8]
ef *	effective
el *	elastic in general
et	effective test
est *	estimated
ext *	external
f *	beam flange
fat *	fatigue
fin	final
g *	guaranteed
h *	horizontal
i *	initial (in time)
inst	instantaneous
j *	number of days

---

[4]) As far as possible, abbreviations which are not contained in this table should be derived from preferably English words having Latin roots. If there is no risk of confusion, these subscripts may be reduced to one or two letters.

[5]) Other than subscripts for actions and action-effects (see table 7 of ISO 3898) and subscripts formed from abbreviations (see table 8 of ISO 3898) and table 6.5.

[6]) As opposed to "observed".

[7]) This subscript should never be omitted.

[8]) If necessary, a suitable subscript may be added or substituted in order to define the elastic limit more precisely (for example $_{y,0,1}$) etc.

Letter(s)	Meaning
k *	characteristic
l *	longitudinal
m *	average value
max	maximum
min *	minimum
mod	modification
n *	net[9)]
nom *	nominal
nor *	normal
obs *	observed
par *	parallel
per *	perpendicular
red *	reduced
rel *	relative
rep *	representative
ser *	serviceability
st *	static
t *	tension in general[10)]
t *	transversal[11)]
tem *	temperature
ten *	tension
test	test
tim	timber
tor *	torsion
tot	total
u *	ultimate
ult	ultimate, if u would cause confusion
v *	vertical
w *	web
x *, y *, z *	coordinates
y *	yield

NOTE: If there is any other risk of confusion, a complete word may be used as a subscript, written in English , with Latin lower case , Roman letters.

NOTE: From the original table 8 of ISO 3898 a number of frequently used subscripts formed from abbreviations has been taken over, and a number of special interest for timber have been added.

---

[9]) If there is a risk of confusion, "net" should be used.

[10]) If there is a risk of confusion, "ten" should be used .

[11]) If there is a risk of confusion, "tra" should be used .

III.5 Examples of combined subscripts

Letter(s)	Meaning
ck	compression ; characteristic value
mk	bending ; characteristic value
tk	tension ; characteristic value
vk	shear ; characteristic value
c, 0, k	compression ; parallel to grain ; characteristic value
m, 0, k	bending ; parallel to grain ; characteristic value
t, 0, k	tension ; parallel to grain ; characteristic value
c, 90, k	compression perpendicular to grain ; characteristic value
m, 0, k	bending ; perpendicular to grain ; characteristic value
t, 90, k	tension ; perpendicular to grain ; characteristic value
c, 0, 05	compression ; parallel to grain ; sample lower fifth percentile value
m, 0, 05	bending ; parallel to grain ; sample lower fifth percentile value
t, 0, 05	tension ; parallel to grain ; lower fifth percentile value
c, 90, 05	compression ; perpendicular to grain ; sample lower fifth percentile value
c, 90, m	compression ; parallel to grain ; mean value
c, 90, 50	compression ; perpendicular to grain ; sample 50- percentile value

INTERNATIONAL COUNCIL FOR BUILDING RESEARCH STUDIES AND DOCUMENTATION

WORKING COMMISSION W18 - TIMBER STRUCTURES

GRADING METHODS FOR STRUCTURAL TIMBER
PRINCIPLES FOR APPROVAL

by

S Ohlsson
Chalmers University of Technology,
Gothenburg
Sweden

MEETING TWENTY - EIGHT

COPENHAGEN

DENMARK

APRIL 1995

Grading Methods for Structural Timber

- Principles for approval

Paper to be presented at the 28th meeting of working commission CIB-W18 in

Copenhagen 18-20 April 1995 by

Sven Ohlsson, Dynamics in Design, Chalmers University of Technology, S-412 96 Gothenburg

Introduction

Selection of timber has a long tradition. Craftsmen have practised different methods of timber selection for ages. Trees with suitable properties for certain applications in shipbuilding have for instance been identified in the forest, and subsequently logged and used for the intended purpose. Such a procedure may in modern terms be considered as a selection process based on quality criteria and executed by visual inspection. The prerequisite for such a procedure is that the primary parameters representing the required qualities either are directly assessable by eye-sight or are strongly correlated to the appearance of the growing tree.

At the end of the present century of industrialisation, visual inspection is still the dominating method for grading of sawn timber including timber for structural applications. For several reasons, alternative methods for grading of structural timber are being developed. The aim of this paper is to present some aspects on the means for assessing the merits of such methods.

The Grading Process and its Objectives

Initially, the grading process as such should be considered. A typical line of events in the production of a piece of structural timber may be as follows:

- Logs of one or a few species from a limited geographical region are delivered to a sawmill.
- Each log is cut into planks of a limited set of dimensions.
- Each plank is tested (by inspection or by any other method) and as a result of the test it is 'graded', e.i. it is designated to be part of a certain 'strength class'.
- Timber pieces belonging to each combination of dimension and strength class are used for a limited set of purposes such as floor joists, truss members, and others.

It should be observed that the grading procedure is focused on the sawn timber with given dimensions and not the basic material. Additionally, it is noteworthy that the grading process is not based on sample tests, but rather comprises each piece of sawn timber. Both these facts

indicate a combination of wood properties characterised by a large scatter and/or test methods (typically visual inspection) with a low ability to measure (estimate) the properties that should be assured by the process.

The origin of most of the problems associated with grading of structural timber may be found in either of the two following classes:

- The inhomogenities (typically knots) of the material are of the same order of size as the cross sectional dimensions.

- The number of properties that needs to be assured by the grading process is very large. Strength in compression, tension and shear in different directions and corresponding stiffness characteristics as well as ability to enable manufacturing of reliable joints (glued or mechanical) are such essential properties.

The first class of problem is encountered in all materials that include different parts with different properties. The standard test of concrete cubes may serve as an example. The concrete cube sides typically measure 150 mm, while the largest ballast size may be of the order 8 - 16 mm. This would constitute a relation between minimum specimen size and the size of the inhomogeneity of about ten. The inhomogeneities may be considered as rather small and the material may thus be treated as homogenous in the context of a cube test. Structural timber on the other hand is used in cross-sectional dimensions down to 45x70 mm^2, while a knot may well be of a size of the order of, say 30 mm. The corresponding ratio between minimum dimension and size of inhomogeneity can consequently approach values close to unity. Unfortunately, this relation indicates that wood, strictly speaking, cannot be treated as a homogenous material in the context in question.

The second class of problem calls for application of a multitude of test methods within the grading process, which is clearly unrealistic for economical reasons. This is especially so keeping in mind that each and every timber piece is supposed to be tested on an individual basis. The solution applied to this problem so far is that one (or two) properties are estimated by testing (typically by visual inspection or via stress grading machines) and the other properties are implicitly estimated based on the assumption that they are statistically correlated to this tested parameter. Since several of the correlation types relied upon are rather weak, some rather severe problems remain to be solved.

Target Parameters

At present, some of the issues related to grading of structural timber are subjects of an European standardisation process. The standard drafts prEN 338, prEN 384, prEN 518, and prEN 519 are all of concern in this process. The discussion about target parameters and objectives will be carried out in relation to these documents.

The basic document prEN 338 defines a set of strength classes and specifies requirements to be met for a population of timber in order to qualify for being allocated to such a strength class. The overall aim of this draft standard is to provide objective means, by which structural timber can be specified and purchased. This is obviously a very important matter, and such a standard is consequently most welcome. The basic content of this document is a table specifying mini-

mum values for twelve different material type properties for each of fifteen different strength classes. In the following, the discussion is restricted to conifer species, which reduces the number of strength classes to nine. A given 'population' of timber is thus supposed to meet six different requirements on strength, four requirements on stiffness and two requirements on mass density. The requirements on strength and stiffness are primary requirements, which are actually constituted by some structural applications. The requirements on density, however, are probably of a different origin. It is generally accepted that the strength of mechanical joints as well as some other strength properties are strongly correlated to the density of the wood material. The requirement on minimum density may be a substitute requirement on the ability to fabricate strong mechanical joints. Still, however, it is unfortunate if requirements are expressed by use of substitute properties in a document of this fundamental character. There is a need in conjunction with the use of substitute requirements that the real requirements that exist should be mentioned. Nevertheless the set of properties seems to be reasonably chosen in prEN 338 in relation to the wide field of possible application for structural timber.

The nine different requirements on each strength class are expressed as statistically based measures of the *properties of the population* of timber graded to a certain class. This is, however, not done in a strict manner. The characteristic value for the shear strength $f_{v,k}$ is for instance one of these measures. Although it is not clearly stated, one may assume that by characteristic value is understood the lower 5-percentile value. Two main questions are, however, left open:

- Does the 5-percentile refer to the *number* of timber pieces or does it refer to the total *volume* of timber in the population that may have a lower shear strength?

- Which geometrical scale does the shear strength relate to?

The corresponding questions can be put forward in relation to all the other eight specified measures as well, but the shear strength is chosen as an example for the discussion here. The first question is crucial bearing the previous discussion about wood as a non-homogenous material in mind. Each plank in a population may for instance have a weak zone somewhere in its central part, while the *characteristic value for the total volume* of wood may still be very high. If, on the other hand, the characteristic value should be taken as the *fraction of the number* of individuals that doesn't have a lower value for the shear strength than the 5-percentile value anywhere within its volume, then the shear strength will need to be defined in relation to a certain size of the sheared area. The means for verification of shear strength independent of the geometrical scale considered are still not available.

The problems illustrated here stems from what was originally stated about the spatial variability of wood properties in combination with the unwillingness of engineers to abandon the useful theories for structural components made of homogenous elastic materials. It is certainly not the intention of the author to propose that timber structures should not be subject to classical engineering calculations. one idea of this discussion is rather to point out a certain disproportion between real possibilities to estimate structural behaviour including strength and the degree of detailing of certain proposed requirements on grading methods for structural timber.

The authors of prEN 338 have simply stated that if the requirements for a certain strength class on characteristic values for bending strength $f_{m,k}$ and density ρ_k as well as one mean value for Young's modulus parallel to grain $E_{0,mean}$ are met, the population may be allocated to that

class. This means that the fulfilment of the other nine requirements (including that on shear strength) needs no verification. The choice of these three parameters can of course be discussed, but the need to reduce the amount of testing (or other means of verification) is obvious.

Keeping these rather rational and open-minded parts of the draft standard in mind, it seems rather difficult to find a rationale behind the fact that the same document states that grading of structural timber (to meet these requirements) can only be executed according to two specified methods - Visual grading according to prEN 518 or machine grading according to prEN 519.

This very strong restriction on methods acceptable for the grading of structural timber seems even more surprising in the light of the contents of the draft standard prEN 384 denoted 'Structural timber - determination of characteristic values of mechanical properties and density'. This document describes several intricate procedures for the establishment of characteristic values based on non-sufficient or non-existent test data. Among many other things, it *prescribes* the calculation of a characteristic value for the shear strength $f_{v,k}$ to be based on bending test results without shear failures as:

$$f_{v,k} = 0.2(f_{m,k})^{0.8}$$

This would imply that calculation of a characteristic value for the shear strength $f_{v,k}$ based upon shear test results would be in contradiction to the standardized method. This is not acceptable. Such empirical relations, like the one between shear strength and bending stregth, need substantial verification even for use as approximate estimates in order to maintain credibility on behalf of the standardisation body. Unfortunately, this document has a number of shortcomings associated to it, which indicate that it will need further effort to be spent. One such shortcoming is the very scope of the document. Characteristic values are established statistical parameters in the wide field of structural engineering and the procedure to calculate them is hardly an issue for standardisation within the timber engineering area. Furthermore, the present title of the draft standard indicate that characteristic values for, say, tensile strength should be established in different ways for wood and steel. If that is the intention, it will be contrary to the present knowledge of most engineers. Although, the draft standard prEN 384 would deserve a more in-depth evaluation, this is outside the scope of the present paper.

The draft standard prEN 519 is one of two draft standards that are supposed to specify adequate procedures for grading of structural timber to strength classes according to prEN 388. The title of the document 'Structural timber - Grading - Requirements for machine strength graded timber and grading machines' indicates severe problems regarding the objectives. Standards exist for products, materials, test methods and a variety of other objects. One standard, however, usually has one object (or class of objects) which it is supposed to specify. The present draft title announces at least three types of objects; graded timber, a procedure (including a philosophy?) for grading and a type of machine. The first chapter of the draft denoted 'Scope' adds method for assessing the merits of a grading machine as well as operation and quality control to the list of objects for standardisation. It seems that the authors of this draft standard have taken on a task that is too large. A good standard with such a broad scope is simply not achievable.

A possible way forward would be to drop the idea of creating the complex standard EN 519 and to concentrate on drafting two standards denoted 'Requirements on grading procedures

for structural timber' and 'Methods for verification of grading procedures for structural timber' instead. Such a decision would be beneficial in at least two ways. The first aspect is that such standards would have a more clear aim and thus be easier to write. The second aspect is that such a pair of standards may be formulated in a way that stimulates development and competition. The present draft incorporates some sections that are clearly counterproductive in the last sense. The present specification of measurement of strength reducing properties at least every 150 mm along a piece of lumber is clearly of this latter type that tends to conserve existing technology with limited performance. Since this is an important aspect, the subject will be discussed here in some detail.

Strength and Spatial Variation

The concept of machine strength grading has been developed from observed statistical relationships between 'global' edgewise bending strength and bending rigidity calculated from measured edgewise bending deflection of a 'global' character . The relatively strong correlation between these properties ($r^2 \approx 0.6$-0.7) that was found in laboratories initiated the development of grading machines.

A fast and accurate measurement of the edgewise stiffness was, however, not readily achievable. Consequently, flatwise bending and measurement of the associated 'flatwise stiffness' was introduced. A *less strong* (but still useful) *correlation* between edgewise bending strength and *the minimum value* of the flatwise stiffness was found. Today's strength grading machines are thus mostly based on incremental measurements of stiffness in flatwise bending thus estimating the bending strength in edgewise bending relying on a modest statistical correlation between the edgewise bending strength and the minimum value of the Young's modulus calculated from flatwise bending deflections.

Keeping this history of development in mind, it seems not to be rational to disqualify grading methods which are based on global stiffness estimates as the 'indicating' parameter. The present reading of clause 7.1.7 of prEN 519 and other similar texts should be changed accordingly.

To the knowledge of the author, no studies exist proving that the spatial variation of bending rigidity and bending strength along a plank follow each other, see the subsequent section. Further, it is very difficult to measure the bending rigidity with increments as small as 150 mm and it can definitely not be done with acceptable accuracy by use of today's stress grading machines based on bending over a span of 0.9 m or so. Even more important, the bending strength at a given section of a wooden beam is a theoretical property that is non-existent in reality. Timber engineers familiar to testing are well aware that testing of full size structural timber typically results in failures which engage a zone of failure of a length equal to several times the beam depth. This means that a beam failure associated to bending may typically include fractured parts along a distance of half a meter or more. Finally, it is quite often very difficult to judge whether the origin of 'bending' failure was of compressional, tensile or even of shear type.

From another perspective, the idea to prescribe some sort of measurements every 150 mm in order to estimate the bending strength of a 'weakest section' in a mandatory standard seems not to be in harmony with the ideas of the basic standard. In fact, the basic standard prEN 338 specifies twelve different criteria to be met, of which only bending stregth and possibly

Young's modulus are assumed to be directly assessed by prEN 519, while the remaining ten requirements don't have to be verified at all. To demand estimation of spatial variation of these specific parameters based on incremental measurements seems not to be an optimal choice.

It should be a better idea to specify criteria for grading methods, that *aim on the ability to assure some of the required properties for each piece of timber with a given degree of statistical certainty and independently of the procedure* chosen.

Relations between Strength and Stiffness Parameters

The aim of this section is to support some of the statements and suggestions made in the previous section. The material is based on the investigation carried out by Perstorper et al (1994) in which 357 beams of cross sectional dimension 70x290 mm^2 were tested.. The data will be presented in some new formats here in order to shed light on the issues under discussion.

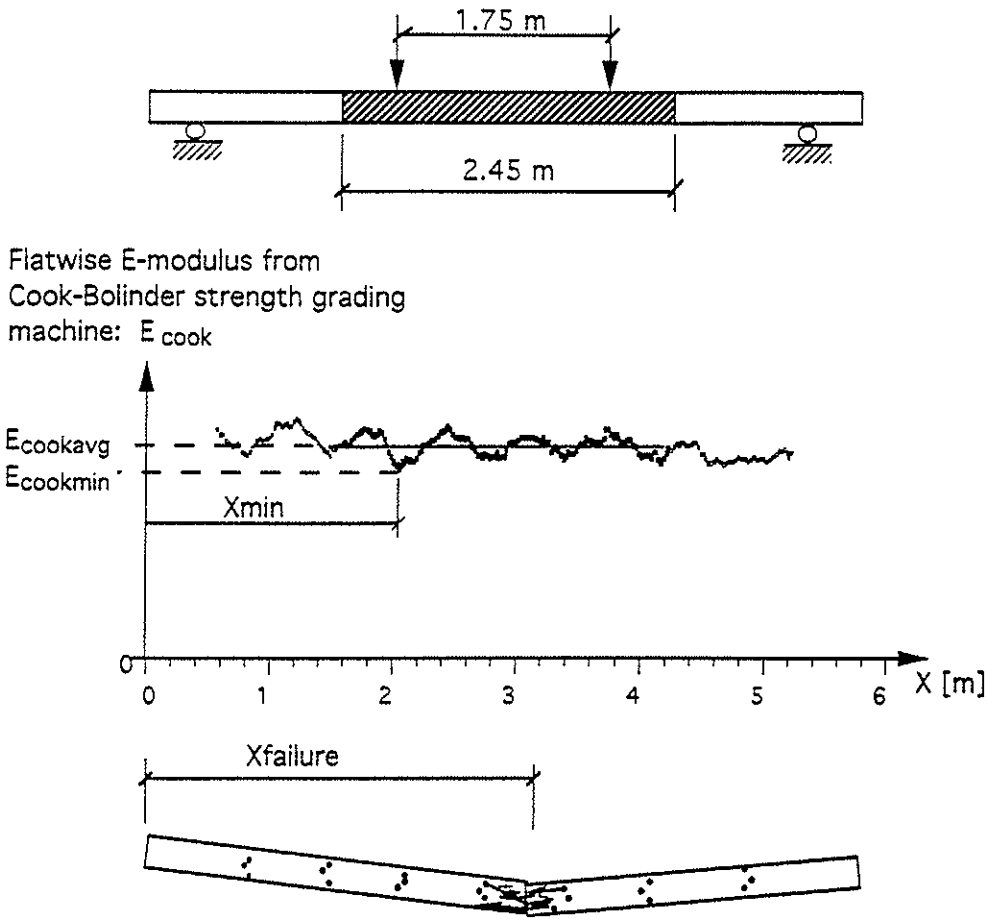

Figure 1. Illustration of test set-up and definition of the co-ordinates X_{min} and $X_{failure}$.

The timber pieces were, among other things, tested in flatwise bending using a strength grading machine of the Cook-Bolinder type and finally tested in edgewise bending to failure. Two parameters describing the co-ordinate X_{min} of the minimum value found for Young's modulus $E_{cook,min}$ and $X_{failure}$ representing the location of the centre of the bending failure are illustrated by Fig. 1.

The relation between the two co-ordinates representing local stiffness minimum in flatwise bending and location of bending failure is shown in Fig. 2. As can be seen from this plot, the

correlation between the two co-ordinates is virtually non-existent. This observation is strongly supporting the suggestion that 'local' stiffness measurements should not be mandatory for a grading method.

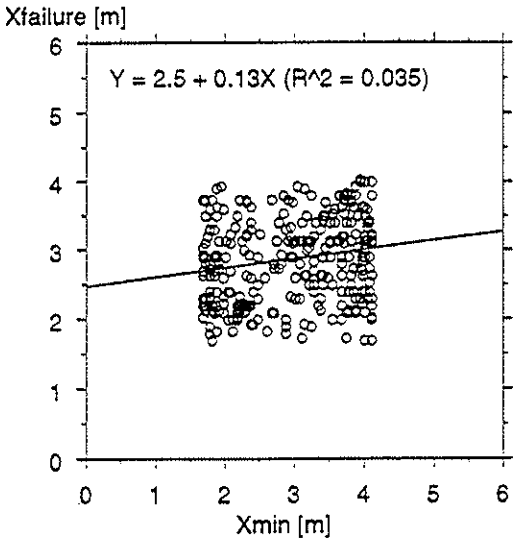

Figure 2. Location of minimum stiffness versus location of failure.

In order to find an alternative perspective for discussion of the relevance of detailed measurement of the longitudinal variation of the stiffness and associated minimum values, two different plots are shown in Figs. 3 and 4.

These graphs show the relation between bending strength and an average type stiffness measure and the longitudinal minimum value previously discussed respectively.

As can be observed when comparing these two graphs, the level of correlation between stiffness and strength is almost the same. This fact further supports the idea that the minimum stiffness has no special merits as the

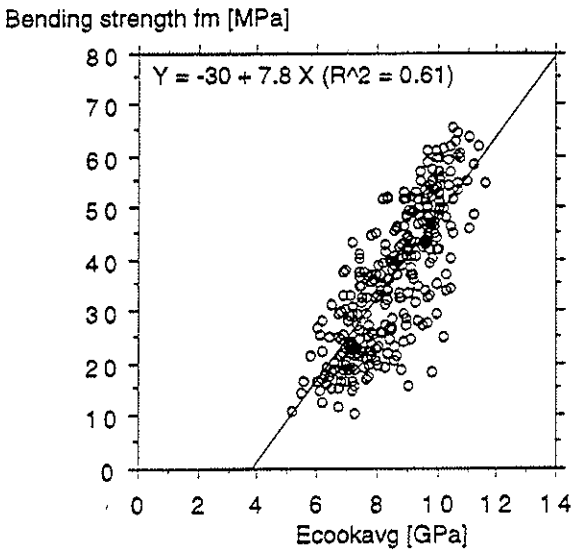

Fig. 3. Bending strength versus average stiffness

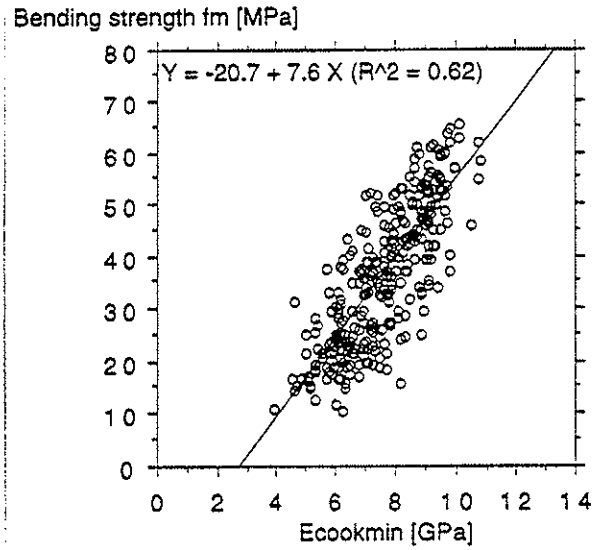

Fig. 4. Bending strength versus minimum stiffness

indicating parameter for bending strength in comparison to stiffness values of an average type.

Concluding Words

Grading of structural timber has been discussed in conjunction with the present European process of standardisation. Attempts to stimulate the development of new grading methods with improved performance require that methods for assessing the merits of such methods are rationally based and free from unnecessary restrictions that may be inherited from present technology for grading machines.

Criteria for grading methods should *aim on the ability to assure some of the required properties for each piece of timber with a given degree of statistical certainty and independently of the procedure* chosen.

The three different contexts in which timber properties are discussed here are:

- Assessment and possibly certification of grading methods
- Industrial grading of structural timber
- Structural use of strength graded timber

It is essential that the level of detail and accuracy in specifications devoted to these different processes are harmonised. At present, this is not the case. Severe economical and legal consequences may result if the standards that are supposed to specify the different procedures are not brought in better harmony. One type of problem that exists in the present versions of the different draft standards is that both the goal and the means to achieve the goal are prescribed. Such 'double' regulation may often be impossible to obey, thus constituting a legal problem.

An example of this type of mistake is that prEN 338 clearly describes the target for a population of timber in a certain strength class, while prEN 519 also attempts to describe suitable means to reach this target. Two kinds of problem are identified here. The first is that prEN 519 is not restricted to describe methods for assessment of the ability of a grading process to meet the targets of prEN 338 but also specifies some aspects of the prospective methods in detail. The second kind of problem stems from a need to minimise the effort needed for assessment. The harmonisation between the different standards should here include a choice of a common set of parameters to be used for verification independent of the grading method.

References

Perstorper, M, Johansson, G & Kliger, R (1994): Konstruktionsvirke från grov gran, delprojekt 2: Hållfasthet och sortering av grova balkar (Structural timber from large diameter spruce logs, part 2: Strength and grading of sawn timber of large cross sectional dimensions). Report S94:9, Steel & Timber Structures, Chalmers University of Technology, Gothenburg.

prEN 338: Structural timber - Strength classes. Final draft, March 1994.

prEN 384: Structural timber - Determination of characteristic values of mechanical properties and density. Final draft, March 1994.

prEN 519: Structural timber - Grading - Requirements for machine strength graded timber and grading machines. Final draft, June 1994.

CIB-W18/28-5-2

INTERNATIONAL COUNCIL FOR BUILDING RESEARCH STUDIES AND DOCUMENTATION

WORKING COMMISSION W18 - TIMBER STRUCTURES

RELATIONSHIP OF MODULI OF ELASTICITY IN TENSION AND IN BENDING OF SOLID TIMBER

by

N Burger
P Glos
University of München
Germany

MEETING TWENTY - EIGHT

COPENHAGEN

DENMARK

APRIL 1995

Relationship of Moduli of Elasticity in Tension and in Bending of Solid Timber

N. Burger and P. Glos
Institute for Wood Research, University of Munich

Abstract

This paper compares moduli of elasticity determined in edgewise and flatwise bending and in tension. It shows that the modulus of elasticity of full-size structural timber in contrast to small clear specimens depends on the type of load (bending, tension) and specimen orientation (edgewise, flatwise bending) as well as on timber quality (grade effect). On average variations amount to approx. 8 to 9%.

So far neither EN 384 nor EN 338 indicate how to deal with these differences when assigning structural timber to a specific strength class on the basis of tests other than bending tests.

1. Introduction

Due to its anatomic structure the behaviour of timber under tension and compression tends to vary. This is evident from the different stress-strain curves shown in Fig. 1. While timber follows the Hookian Law when loaded in tension until failure, showing a largely linear behaviour, the latter becomes non-linear with increasing load in compression.

For timber design standards different design values for tension, compression and bending are in general use. By contrast, the same value is being used for all three kinds of load for modulus of elasticity (E) parallel to grain in solid timber. Similarly, the new European standards use a single modulus of elasticity for all three kinds of load in tension, compression and bending for solid timber.

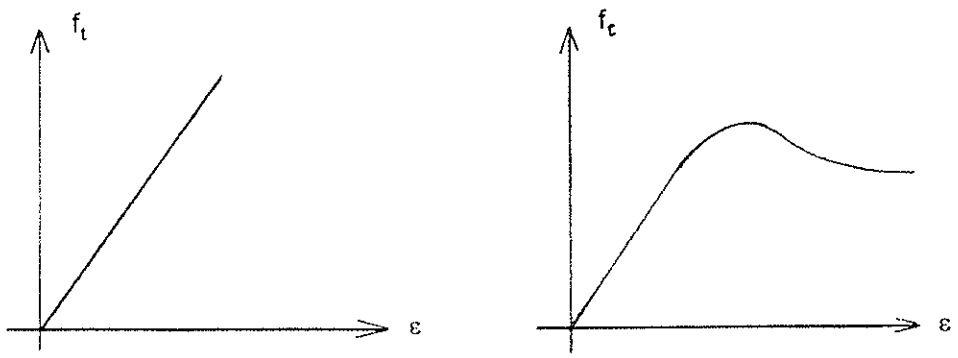

a) Tension b) Compression

Fig. 1. Stress-strain curves for timber (after Glos, 1981)

2. Objectives

To determine characteristic strength and stiffness values for German structural timber graded according to DIN 4074 for the use in Eurocode 5 (EC 5) available test results were evaluated of some 3,500 full-size pieces of structural timber tested in bending, tension and compression according to the specifications of EN 384 "Structural timber - Determination of characteristic values of mechanical properties and density". These tests were carried out in the course of the past 10 years at the Institute for Wood Research and available through the institute's data base. The results were compiled in a research report by Glos and Burger (1994).

For solid timber the European standards define the same value for E in tension, compression and bending. The understanding is that this shall be the modulus of elasticity in bending, to be determined according to EN 408 "Timber Structures - Structural timber and glued laminated timber - determination of some physical and mechanical properties". For the reasons given below the following ratios between E determined under different loading and test conditions and E in bending determined according to EN 408 were investigated (Burger and Glos, 1995):

1. The ratio between E in bending according to EN 408 in edgewise bending and that according to DIN 52186 "Testing of timber - Bending test". The main difference between these two procedures lies in the different gauge lengths for the deflection measurements. According to DIN 52186 the determination of E is done over the full span, while the basis for measurements according to EN 408 is 5 times the specimen depth between the two load points.
2. The ratio between E in bending and in tension determined according to EN 408. With a view to the use of machine strength graded timber for glulam production mainly tension tests were carried out and tensile strength as well as E in tension determined. These results supplied the basis for the settings of machine grades MS 10, MS 13 and MS 17 acc. to DIN 4074.
3. The ratio between E in edgewise bending according to EN 408 and flatwise bending according to DIN 52186. In the past solid timber boards such as glulam laminates were frequently tested in flatwise bending tests. Moreover, within quality assurance procedures for machine graded solid timber flatwise bending tests have to be carried out.

3. Literature on the ratio between moduli of elasticity

Investigations on the ratio between the moduli of elasticity were compiled and described by Conners and Medvecz (1992). These tests were generally carried out with small clear specimens to determine the ratio between the modulus of elasticity in tension and in compression. The ratio E_t/E_c was determined by either using matched samples or bending specimens where the strain at the edges of the compression and tension areas was measured. Results of tests with coniferous timber are given in Table 1.

For the relationship between stiffness values Schneider and Phillips (1991) used the following equation by Behr and Johnston (1985), which led to a good correlation with results on sugar maple and basswood.

$$E_b = \frac{4 \cdot E_t \cdot E_c}{\left(E_t^{0.5} + E_c^{0.5}\right)^2} \qquad (1)$$

Modification of equation (1) leads to the following ratio between the moduli of elasticity in bending and in tension:

$$\frac{E_b}{E_t} = 4 \cdot \left(\left(\frac{E_t}{E_c} \right)^{0.5} + 1 \right)^{-2} \qquad (2)$$

Table 1 thus reflects the values E_b/E_t, calculated from the ratios E_t/E_c.

In the mean ratios E_t/E_c and E_b/E_t are close to 1. However, the values exhibit great variations and show poor consistency as far as ratios are concerned. A more detailed analysis, in particular of what causes these variations, was not possible as no data were available on density, dimensions and gauge lengths used here in determining E.

Investigation	Species	Moisture content	E_t / E_c	E_b/E_t acc. to Eq. (2)
Dietz (1942)	Douglas fir (Pseudotsuga menziesii)	9 24	1.035 1.028	0.966 0.973
Sawada (1958)	Sugi (Cryptomeria japonica)	15 16 16	1.049 0.884 1.107	0.953 1.127 0.901
	Yedo-Spruce (Picea jezoensis)	14	1.030	0.971
	Japan. Redpine (Pinus densiflora)	13	1.056	0.946
Mazur (1965)	Spruce (Picea spp.)	12	0.848	1.171
Sliker (1973)	Douglas fir (Pseudotsuga menziesii)	13	0.976	1.024
	Hemlock (Tsuga heterophylla)	13	0.996	1.004
Bazan (1980)	Spruce und Douglas fir	12	1.06	0.94
Mean value			1.006	0.998

Table 1. Ratios E_t/E_c from literature and calculated values for E_b/E_t for coniferous timber (after Conners and Medvecz, 1992)

4. Results

4.1 Ratio between moduli of elasticity according to EN 408 and DIN 52186 in edgewise bending

To investigate the ratio between E in bending determined according to EN 408 and DIN 52186 almost 1,200 bending tests were evaluated, using solid timber specimens mainly from European spruce and, to a lesser extent, from fir and pine. Specimen dimensions varied from 35 to 116 mm in width and 50 to 274 mm in depth. Both moduli were determined simultaneously in one test run. The mean of ratios $E_{b,EN}/E_{b,DIN}$ for individual specimens was 1.087, i.e. on the average

E determined according to EN 408 was about 9 % higher than that measured according to DIN 52186. The ratio $E_{b,EN}/E_{b,DIN}$ is related to timber quality and increases with higher grades (see Table 2, line 1).

	Total	Grade acc. to DIN 4074		
		S 7	S 10	S 13
$E_{b,EN}/E_{b,DIN}$	1.09	1.08	1.09	1.11
$E_{b,EN}/E_t$	1.09	1.07	1.08	1.11
$E_{b,EN}/E_{b,flat,900}$	1.17	1.17	1.19	1.18

Table 2. Ratios between E in bending and in tension for all specimens and broken down according to grades (mean of ratio values for individual tests). Test values from the data base of the Institute for Wood Research, University of Munich.

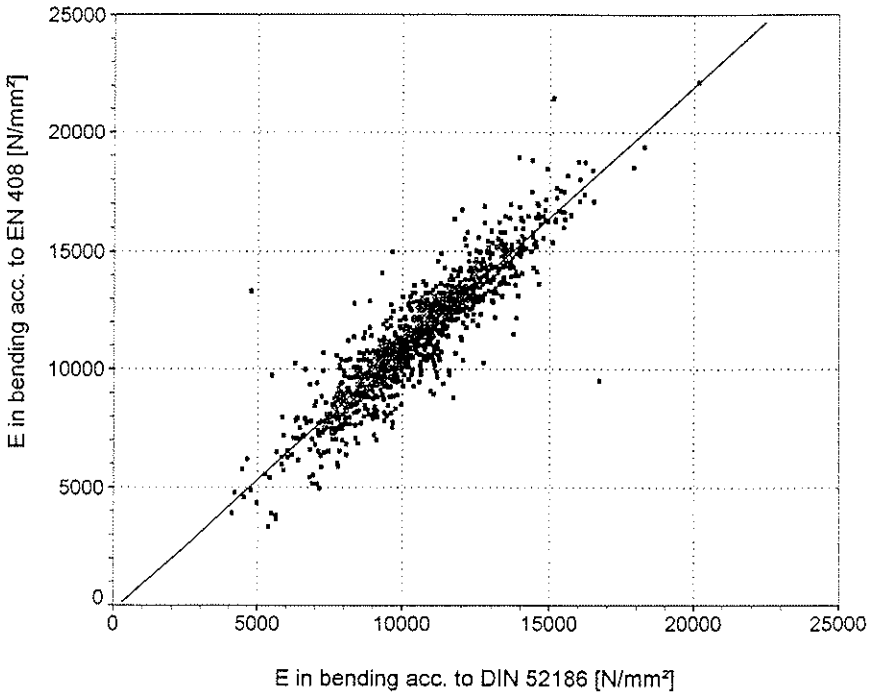

Fig. 2. Relationship between E in bending according to EN 408 and DIN 52186. 1,187 bending tests from the data base of the Institute for Wood Research, University of Munich.

The linear regression equation based on a total of about 1,200 bending tests is as follows:

$$E_{b,EN} = -210 + 1.107 \cdot E_{b,DIN} \qquad (3)$$

The correlation coefficient is r = 0.91. Fig. 2 provides all test data and the regression curve according to equation (3).

The values shown above vary due to different test arrangements. The gauge length for E according to DIN 52186 corresponds to the total specimen span. The deflection measured includes some shear deflection between the load points and the supports, which is usually disregarded when determining E. By contrast, measurements according to EN 408 are carried out

in the shear-free area between the two load points. Moreover, measurements according to DIN 52186 may occasionally include some compression perpendicular to grain deformation at the supports. Assuming a ratio between shear modulus and modulus of elasticity of G/E = 1/30, based on tests by Ehlbeck (1967) (tests using European coniferous timber resulted in mean G/E ratios of 1/22.5 to 1/32.5) and disregarding compression perpendicular to grain deformation, the difference in average values can be explained entirely in terms of shear deflection. DIN 1052, however, specifies a G/E ratio of 1/20, while EN 338 "Structural Timber - Strength classes" assumes a value for G/E of 1/16.

Based on the above test series the G/E ratio of 1/16 according to EN 338 used for the design of timber structures is therefore not considered conservative and needs to be discussed.

The modulus of elasticity $E_{b,EN}$ has a 20 % higher coefficient of variation than that of $E_{b,DIN}$, with about 15 %. This may be allocated to the following:

- The modulus of elasticity according to EN 408 is determined over a smaller span; local defects thus have a greater impact on results, which provides a reasonable explanation for the effect of timber grades on the ratio $E_{b,EN}/E_{b,DIN}$.
- When determining E according to EN 408 measuring inaccuracies have a greater effect on results due to considerably less deformation.

4.2 Ratio between modulus of elasticity in bending and in tension

To determine the relationship between E in bending and in tension two research projects were re-evaluated which had been carried out at the Institute for Wood Research (Glos and Gaede, 1992; Henrici et al. 1992) and in which 147 European spruce specimens dimensioned 50/120 mm (54 specimens) and 60/105 mm (93 specimens) had been tested both for E in bending and in tension according to EN 408, using the same specimen for both test runs.

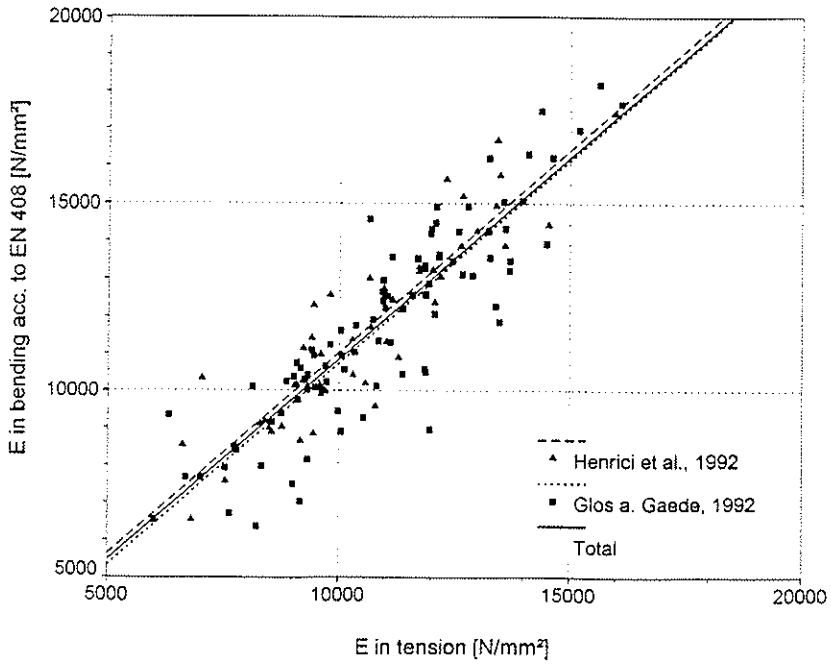

Fig. 3. Ratio between E in bending and in tension according to test results from investigations by Glos and Gaede (1992) and Henrici et al. (1992).

The gauge length for the tests of E in tension was 480 mm, i.e. it was not in agreement with the specified gauge length of 5 times the depth (600 mm and 525 mm respectively).

On average E in bending according to EN 408 lies 9 % above E in tension (see Table 2, line 2). A break-down of test results according to grades again indicates the influence of timber quality. The ratio between E in tension and in bending according to EN 408 is shown in Fig. 3. The two sub-samples give consistent results. Based on all tests the regression equation is as follows:

$$E_{b,EN} = 90 + 1.077 \cdot E_t \qquad (4)$$

The correlation coefficient is r = 0.94

4.3 Ratio between modulus of elasticity in edgewise and flatwise bending according to EN 408 and DIN 52186 respectively

The investigation by Henrici et al. (1992) also dealt with the determination of E in flatwise bending, using the same specimen for all test runs. E was determined in centre point bending (i.e. apparent E), according to the loading method in a bending-type grading machine, with spans of 900 mm, 700 mm and 500 mm (i.e. 15, 11.7, and 8.3 times the depth resp.)

The ratios between edgewise and flatwise bending as well as between different gauge lengths have been compiled in Fig. 4 and Table 3. The linear regression equations are as follows:

900 mm:	$E_{b,EN} = -2330 + 1.417 \cdot E_{b,flat,900}$	r = 0.93	
700 mm:	$E_{b,EN} = -2840 + 1.610 \cdot E_{b,flat,700}$	r = 0.91	(5)
500 mm:	$E_{b,EN} = -4500 + 2.248 \cdot E_{b,flat,500}$	r = 0.88	

Table 3 indicates that the ratios of the moduli of elasticity in flatwise bending are independent of timber quality. With decreasing spans, hence increasing shear forces, the ratios rise steeply. Assuming a ratio of G/E = 1/30 the values given in Table 4 line 2 were obtained. The regression equations (5) are thus modified to give

900 mm:	$E_{b,EN} = -2330 + 1.316 \cdot E_{b,flat,900}$	r = 0.93	
700 mm:	$E_{b,EN} = -2840 + 1.427 \cdot E_{b,flat,700}$	r = 0.91	(6)
500 mm:	$E_{b,EN} = -4500 + 1.799 \cdot E_{b,flat,500}$	r = 0.88	

Even when taking shear deformation into account no consistent values for E were calculated. The variation between E determined in edgewise and in flatwise bending increases with decreasing spans, i.e. with increasing shear forces.

This may be due to the following assumptions made in the simple beam theory:

- Both shear stress and shear angle are not uniformly distributed over the cross-section. However, in practice calculations are based on mean shear stress and mean shear angle. The effect of this simplification is the greater the larger the portion of shear within the total deformation (i.e. with decreasing depth/span ratio, thus with increasing span) and the larger the total deformation itself.
- Timber is not an isotropic material as assumed in the theory.

Furthermore, effects of size on E probably exist. However, this field has not been thoroughly investigated as to effects on E and further research is therefore required.

		Total	Grade acc. to DIN 4074		
			S 7	S 10	S 13
$E_{b,flat}$	$\frac{700}{900}$	0.91	0.91	0.91	0.91
	$\frac{500}{900}$	0.73	0.73	0.73	0.73
	$\frac{500}{700}$	0.80	0.80	0.80	0.80
$E_{b,EN}/E_{b,flat,900}$		1.17	1.17	1.19	1.18
$E_{b,EN}/E_{b,flat,700}$		1.29	1.29	1.31	1.29
$E_{b,EN}/E_{b,flat,500}$		1.61	1.62	1.64	1.61

Table 3. Ratio E in bending $E_{b,flat}$ between different spans in flatwise bending and ratio of edgewise bending according to EN 408 and flatwise bending according to DIN 52186. Test values from the data base of the Institute for Wood Research, University of Munich

		span in flatwise bending		
		900 mm	700 mm	500 mm
consideration of	no	1.17	1.29	1.61
shear deformation	yes	1.08	1.13	1.25

Table 4. Ratio $E_{b,EN}/E_{b,flat}$ for different spans in flatwise bending with and without consideration of shear deformation, assuming G/E = 1/30. Test values from the data base of the Institute for Wood Research, University of Munich.

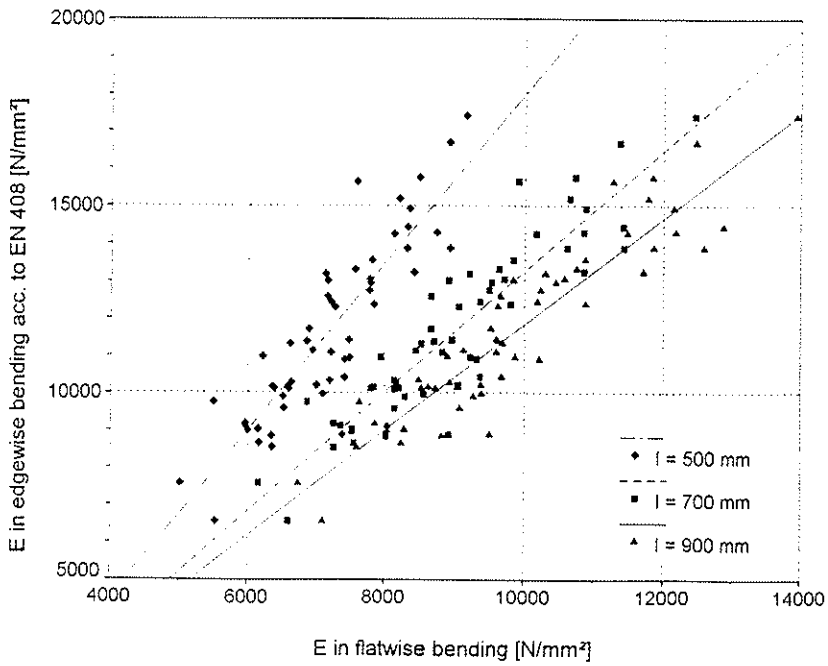

Fig. 4. Relationship between E in flatwise bending with different spans and E in edgewise bending according to EN 408. Test values from the data base of the Institute for Wood Research, University of Munich.

5. Conclusions

Summarizing the results of the investigations the following conclusions can be drawn:

- The modulus of elasticity of structural timber, in contrast to small clear specimens, depends on the type of load (bending, tension) and specimen orientation (edgewise, flatwise bending).
- The difference between E in edgewise bending acc. to EN 408 and DIN 52186 is about 9%. This can be entirely explained by the shear deformation, if a ratio of G/E = 1/30 is assumed.
- The difference between E in edgewise bending and in tension acc. to EN 408 is about 9%. The gauge length for the determination of E in tension was 4·b and 4.6·b respectively as compared to 5·b acc. to EN 408.
- The difference between E in edgewise bending acc. to EN 408 and flatwise bending acc. to DIN 52186 is about 17%. When shear effects are taken into account assuming a ratio of G/E = 1/30 the difference is about 8%.
- The differences between E in edgewise bending acc. to EN 408 and DIN 52186 and between E in bending and in tension depend on timber quality.

The results are in contrast to published results obtained in tests with small clear specimens. This may be due to the different behaviour of structural timber and small clear specimens.

Whether these differences should be taken into account in the design of timber structures needs further discussions in a wider context. At any rate these variations must not be disregarded when allocating structural timber into strength classes according to EN 338 on the basis of tension or flatwise bending tests.

Symbols

E_b	modulus of elasticity in bending
E_t	modulus of elasticity in tension parallel to grain
E_c	modulus of elasticity in compression parallel to grain
$E_{b,EN}$	modulus of elasticity in edgewise bending according to EN 408
$E_{b,DIN}$	modulus of elasticity in edgewise bending according to DIN 52186
$E_{b,flat}$	modulus of elasticity in flatwise bending, loaded in centre point bending
G	shear modulus

INTERNATIONAL COUNCIL FOR BUILDING RESEARCH STUDIES AND DOCUMENTATION

WORKING COMMISSION W18 - TIMBER STRUCTURES

SHEAR STRENGTH OF CANADIAN SOFTWOOD STRUCTURAL LUMBER

by

F Lam

H Yee

J D Barrett

University of British Columbia

Canada

MEETING TWENTY - EIGHT

COPENHAGEN

DENMARK

APRIL 1995

SHEAR STRENGTH OF CANADIAN SOFTWOOD STRUCTURAL LUMBER

by

F. Lam[1], H. Yee[2] and J.D. Barrett[3]

Abstract

An experimental study has been conducted to evaluate the longitudinal shear strength of Canadian softwood structural lumber using a two span five point bending test procedure. Three species groups, Douglas fir, Hem-fir and Spruce-Pine-Fir, have been considered. Approximately 40% of the failures can be attributed to shear failures. Two test configurations have been considered: test span to specimen depth ratios of 6 and 5. American Society for Testing and Materials (ASTM) shear block tests have been conducted to evaluate the shear strength of small clear specimens. Based on the ASTM shear block test results, finite element analyses coupled with Weibull weakest link theory have been used to predict the median shear failure loads. Good agreement between predicted and measured median failure loads have been observed.

Introduction

Longitudinal shear strength of lumber is important because it governs beam designs for cases with small span to depth ratios. Under realistic loading and support conditions, tests results have shown that it is very difficult to obtain pure shear failures in members especially when the members do not have end splits. This observation seems to suggest that longitudinal shear strength design values may be over conservative.

Two distinct failure modes can be observed during shear strength tests of lumber. These failure modes are controlled by: 1) the shear strength of the material when end split or other similar defects are not present and 2) the crack length and mode II fracture toughness (K_C) in members where parallel to grain end split defects exist. To account for these two modes of failures, development of design shear stresses for lumber in North America traditionally followed provisions of ASTM standard D245 (ASTM, 1994b). Small clear straight grain shear block specimens are first tested in shear. The shear block test results are modified by a reduction factor of 4.1 to account for safety and load duration (1.82), and stress concentrations (2.25) due to strength reducing characteristics

[1] Assistant Prof., Dept. of Wood Sci., Univ. of British Columbia, Van., B.C. Canada V6T 1Z4.

[2] Grad. Res. Assistant, Dept. of Wood Sci., Univ. of British Columbia, Van., B.C. Canada V6T 1Z4.

[3] Prof., Dept. of Wood Sci., Univ. of British Columbia, Van., B.C. Canada V6T 1Z4.

in commercial full size material. The effect of end cracks is then considered by the introduction of another factor:

$$S = 1 - \frac{a}{3H} \qquad [1]$$

where S is the strength ratio, a is the crack length and H is the member depth.

The use of ASTM shear block test results to first determine the shear capacity of small clear specimens and then adjusting for natural defects in lumber is somewhat inconsistent with the in-grade philosophy of testing full size members which has been adopted worldwide for the development of characteristics strength properties of structural lumber. The major difficulties associated with testing for the longitudinal shear strength of full size lumber using typical test setup are that the members would usually fail in another failure mode such as bending or compression perpendicular to grain especially in members which do not contain end-splits.

A two span five point bending test procedure, originally developed for the evaluation of the shear strength of composite materials, has been proposed for testing of the shear strength properties of full size lumber. Experimental programs in the U.S. Forest Products Laboratory and CSIRO in Australia have successfully used these test setup to evaluate the shear strength of glued-laminated beams and full size commercial lumber (Leicester and Breitinger 1992, Breitinger *et al.* 1994, Soltis and Rammer 1994). In the U.S. Forest Product Laboratory program a span to depth ratio of 5:1 was used and in the CSIRO test program a span to depth ratio of 6:1 was used.

Past studies, based on the Weibull Weakest Link concept, demonstrated that member shear strength capacities depend strongly on the test configuration, member size, and stressed volume (Foschi and Barrett 1976, 1977a, 1977b, Liu 1980 and 1981). Clear understanding of the measured test results in relation with the different test configurations is necessary before new test procedures can be adapted for standards and conversion of test data into design properties.

In this paper, an experimental study was conducted to evaluate the longitudinal shear strength of three species groups of Canadian softwood structural lumber using a two span five point bending test set up. Two test configurations were considered: test span to specimen depth ratios of 6:1 (6D case) and 5:1 (5D case). A procedure based on finite element (FE) analyses coupled with Weibull weakest link theory (Weibull, 1939) was used to predict the median shear failure loads of the lumber from ASTM shear block test results and to establish the relationships between the full size specimens test results from the two test configurations.

Materials

Three species groups of Canadian softwood dimension lumber were sampled from mills in British Columbia: Douglas-Fir, Hem-Fir, and Spruce-Pine-Fir. Approximately 100 pieces of nominal 38 mm x 185 mm x 3 m lumber were obtained for each species group. The material was kiln dried and confirmed to be select structural grade. After delivery to the laboratory, the specimens were further air dried to an approximate equilibrium moisture content of 12%.

Experimental Methods

Each specimen was tested using the Cook Bolinders AG-SF grading machine to measure its flatwise modulus of elasticity profile along the specimen length. The specimen was fed through the machine lengthwise with the grade stamp end first. As the piece traveled through the test machine, it was deflected on flat under center point loading on a span of 900 mm with a prescribed center point deflection of 4.5 mm. The force required to deform the piece was continuously monitored and converted into flatwise modulus of elasticity estimates. The piece was then rotated 180° about its longitudinal axis and fed through the machine again. The flatwise modulus of elasticity estimates from both passes were averaged to eliminate the effects of bow and surface roughness of the piece on the load measurements.

The material was also tested non-destructively on edge under third point loading with a span to depth ratio of 16:1 to estimate the edgewise modulus of elasticity. The test span was dictated by the original specimen length of 3 m. A yoke device with a linear voltage displacement transducer (LVDT) was attached to the specimen at mid depth to obtain the vertical deformation of the specimen at mid span relative to the loading points. The edgewise modulus of elasticity values were estimated from the measured load deformation relationships. A rate of loading of 32 mm/minute was used.

The two span five point bending test configuration are shown in Figure 1. Finite element analyses were conducted to size the loading and reaction plates aiming to minimize the compression perpendicular to grain failures while allowing proper shear failures to develop within the members. Lengths of the loading and reaction plates are shown in Figure 1. Teflon coated lateral support devices were also installed to eliminate possibility of lateral buckling of the member. The locations of the lateral supports were chosen near the vertical supports such that the possible development of any frictional forces would not impact on the failure mechanism and failure loads.

Specimens were trimmed to the appropriate length for the testing. An overhang, corresponding to the member depth, measured from the center of the end reaction plate was provided at each end of the member. Half of the specimens were tested with a span to depth ratio of 5:1 and the other half with a span to depth ratio of 6:1. Here the specimen depth was taken as the nominal beam depth of 185 mm. The applied load and

movement of the loading head were continuously measured during the test. A yoke device with an LVDT was mounted on the specimen at mid depth under the center of one of the loading plates to measure the relative deformation between the specimen and the end and center supports (see Figure 1). Vertical lines, at an approximate spacing of 30 mm, were drawn on both wide faces of each specimen. Longitudinal shear failures can be readily detected when the lines were broken in shearing mode. Other possible failure modes such as tension perpendicular to grain, compression perpendicular to grain, and bending failures were noted. In some cases failures in the shearing mode were not readily apparent. A rule was adopted such that if failures resulted in cracks or splits which extended within 25 mm of the top and bottom surfaces of the beam, these beams were not considered as failures in shear.

After the full size shear tests, one ASTM shear block specimen was cut from each beam near the failure zone but away from the actual failures and damaged areas. The shear block specimens were tested for the small clear specimen shear strength τ_{ASTM} following the ASTM Standard D143 (ASTM, 1994a).

Analytical Methods

Based on classical engineering mechanics theory and assuming point loads and simple supports, the free body, shear force, and maximum shear stress diagrams for the two span load configuration are shown in Figure 2. The magnitude of the shear forces in the middle spans are 2.2 times the shear forces in the end spans. The maximum shear stress can be estimated as:

$$\tau_{\text{max classical}} = \frac{33\ P}{64\ bd} \qquad [2]$$

where

P = total load,
b = beam width, and
d = beam depth.

Note that the shear stresses calculated from the classical theory is independent of test span to specimen depth ratio.

Finite element analyses, based on eight nodes quadratic isoparametric elements, were performed to evaluate the stress distributions in the two test configurations. Figure 3 shows the finite element mesh chosen for the analyses with symmetry about mid span taken into consideration. The loading are assumed to be uniformly distributed along the loading plates. The supports are assumed to be pins or rollers. The modulus of elasticity values in the x and y directions, modulus of rigidity, and Poisson ratios (v_{xy} and v_{yx}) of the three species used in the finite element analyses are given in Table 1. Here the x and y

directions are taken as the direction parallel and perpendicular to the long axis of the member, respectively. The modulus elasticity values in the x direction were obtained from the mean edgewise modulus of elasticity test results. The other elasticity values were obtained from relationships provided by Goodman and Bodig (1973).

Table 1. Elasticity values used in the finite element analyses.

	Modulus of Elasticity x-direction (MPa)	y-direction (MPa)	Modulus of Rigidity (MPa)	Poisson Ratios ν_{xy}	ν_{yx}
Douglas-Fir	12207	592	756	0.42	0.033
Hem-Fir	9690	507	716	0.42	0.033
Spruce-Pine-Fir	10993	552	738	0.42	0.033

Under an applied load P, the shear stress field can be numerically integrated over the volume following a Gauss quadrature integration scheme (Foschi and Barrett 1976). Foschi and Barrett (1976) also showed that Weibull weakest link theory can be applied to estimate the shear failure load at a probability level of interest if the shear strength associated with an unit volume is known τ^* at the same probability level is known. For the median level, the median shear failure load can be estimated as:

$$P_{0.5} = \frac{P\,\tau^*_{0.5}}{I^{\frac{1}{k}}} \qquad [3]$$

where

I = value of the shear stress field integrated over the volume under an applied load P,
$P_{0.5}$ = median failure load,
$\tau^*_{0.5}$ = median shear strength of a unit volume,
k = Weibull shape parameter = $CV^{-1.085}$, and
CV = coefficient of variation of shear strength.

In general, it is very difficult to experimentally measure the unit volume shear strength directly. Foschi and Barrett (1976) used finite element analysis to relate τ_{ASTM} to τ^* as:

$$\tau^* = \beta_t\, \tau_{ASTM} \qquad [4]$$

where

$$\beta_t = 1.333 + 0.336\,(k - 4) \quad \text{if } 4 \le k \le 8$$
$$\beta_t = 2.678 + 0.251\,(k - 8) \quad \text{if } 8 \le k \le 10$$

So from ASTM shear block test results, failure load associated with a particular test configuration can be evaluated.

Close examination of the stress field generally reveal high stress concentrations at loading and support points. If these locations were considered during the evaluation of I, unrealistic estimation of longitudinal shear strength will result. At these high stress concentration points, one can assume that a combination of local shear and compression perpendicular to grain type failures will occur locally; therefore, the stresses here should be ignored during the integration. In the current analysis, we ignored the shear stresses in some of the elements located in the top and bottom rows during the evaluation of I (see Figure 3). This is consistent with the interpretation of the experimental data base as beam failures within 25 mm of the top and bottom surfaces of the beam were not considered as shear failures.

Results and Discussions

Table 2 shows the summary statistics of the nondestructive modulus of elasticity tests for the entire sample and for the samples groups in the 6D and 5D test cases. It is clear that both sample groups were well matched in terms of modulus of elasticity values. Shown in Figures 4 to 6 are the cumulative distributions of the failure loads for the 5D and 6D test cases for the Douglas-Fir, Hem-Fir, and Spruce-Pine-Fir material, respectively. Here all the failure modes except compression perpendicular to grain failures were included. Figures 7 to 9 show the cumulative distributions of the failure loads corresponding to shear failures for the 5D and 6D test cases for the Douglas-Fir, Hem-Fir, and Spruce-Pine-Fir material, respectively. In the Spruce-Pine-Fir species group there was less shear failures and more compression perpendicular to grain failures compared to other species groups as the compression perpendicular to grain strength of Spruce-Pine-Fir is relatively lower than the other two species groups.

Table 2. Summary statistical results for the nondestructive testing.

	Edgewise modulus of elasticity			Flatwise modulus of elasticity		
	Mean (MPa)	CV (%)	Sample Size	Mean (MPa)	CV (%)	Sample Size
Entire Sample						
Douglas-Fir	12135	15	114	10986	14	114
Hem-Fir	10102	19	115	9789	16	115
Spruce-Pine-Fir	11302	20	128	10039	13	128
6D						
Douglas-Fir	13110	26	54	12498	13	54
Hem-Fir	10195	34	60	9927	13	60
Spruce-Pine-Fir	11014	16	43	10867	12	43
5D						
Douglas-Fir	12438	29	47	12094	16	47
Hem-Fir	11407	33	42	9545	13	42
Spruce-Pine-Fir	10770	18	52	10777	13	52

The median and coefficient of variation of the τ_{ASTM}, the estimated shape parameter k, and the calculated τ^* (Eqn. 4) for the various species are given in Table 3.

Table 3. Clear wood shear strength parameters.

	τ_{ASTM}				
	Median (MPa)	CV (%)	Sample Size	k	τ^* (MPa)
Douglas-Fir	8.989	12.35	100	9.665	27.830
Hem-Fir	8.234	12.87	97	9.243	24.619
Spruce-Pine-Fir	7.666	12.43	92	9.599	23.606

Table 4 shows the predicted and experimental median failure loads from the finite element and Weibull weakest link analyses. Furthermore, based on the median failure loads, median failure stresses can be determined based on classical engineering mechanics approach. Predicted and experimental median failure stresses and the associated prediction errors are also provided in Table 4.

Table 4. Predicted and experimental results.

	Experimental Results		Model Predictions				
			FE and Weibull analysis			Soltis and Rammer	
	Failure Load (kN)	Failure Stress (MPa)	Failure Load (kN)	Failure Stress (MPa)	Error (%)	Failure Stress (MPa)	Error (%)
(6D)							
Douglas-Fir	134.44	9.47	126.78	8.94	-5.7	6.65	-29.9
Hem-Fir	111.70	7.82	104.14	7.29	-6.8	6.08	-22.2
Spruce-Pine-Fir	109.15	7.65	106.35	7.45	-2.6	5.66	-26.0
5D							
Douglas-Fir	122.21	8.61	106.00	7.46	-13.3	6.40	-25.6
Hem-Fir	88.50	6.20	87.41	6.13	-1.2	5.86	-5.5
Spruce-Pine-Fir	95.30	6.70	89.03	6.26	-6.6	5.46	-18.5

Soltis and Rammer (1994) proposed a method to relate τ_{ASTM} to beam shear strength (τ) as follows:

$$\tau = \frac{1.3\, C_f\, \tau_{ASTM}}{A^{0.2}} \qquad [5]$$

where
$C_f = 2$ = concentration factor to adjust τ_{ASTM} to true strength at failure,
A ($inch^2$)= shear area = area of beam subjected to shear forces = length x depth of beam.

The predicted median failure stresses (Eqn. 5) for the three species groups and the 6D and 5D beam cases and the associated prediction errors are shown in Table 4.

Figure 11 compares the two prediction method with measured median failure loads from the various cases. Clearly good agreement can be observed with the finite element and Weibull weakest link approach which tends to under predict the failure stress with an maximum error of 13%. The empirical based approach also tends to under predict the failure stress with a maximum error of 30%.

Conclusions

An experimental study was undertaken to evaluate the longitudinal shear strength of three species groups of Canadian softwood structural lumber using a two span five point bending test procedure. Two test configurations were studied: span to depth ratios of 6:1 and 5:1. Longitudinal shear type failure was achieved in approximately 40% of the test cases. Based on the ASTM shear block test results, finite element analyses coupled with Weibull weakest link theory was used to predict the median shear failure loads. Predicted and measured median failure loads agreed well with an maximum under prediction error of 13%.

References

ASTM. 1994a. Standard methods of testing small clear specimens of timber. ASTM D143. American Society of Testing and Materials. Philadelphia, U.S.A.

ASTM. 1994b. Establishing structural grades and related allowable properties for visually graded lumber. ASTM D245. American Society of Testing and Materials. Philadelphia, U.S.A.

Breitinger H.O., R.H. Leicester, C. Seath and P. Walsh 1994. In-grade wood beam-shear strength. In Proc. of Pacific Timber Engineering Conference. Gold Coast, Australia. July 11-15. 1:642-645.

Foschi, R.O. and J.D. Barrett 1976. Longitudinal shear strength of Douglas-fir. Canadian Journal of Civil Engineering. 3(2):198-208

Foschi, R.O. and J.D. Barrett 1977a. Shear strength of uniformly loaded dimension lumber. Canadian Journal of Civil Engineering. 4(1):85-96

Foschi, R.O. and J.D. Barrett 1977b. Longitudinal shear in wood beams: a design method. Canadian Journal of Civil Engineering. 4(3):363-370

Goodman, J.R. and J. Bodig. 1973. Prediction of Elastic Parameters for Wood. Wood Sci. 5(4): 249-264.

Leicester, R.H. and H.O. Breitinger. 1992. Measurement of beam shear strength. In Proc. of IUFRO S.05.02 Timber Engineering Meeting. Bordeaux, France. August 17-21. 12pp.

Liu, J.Y. 1980. Shear strength of wood beams: a Weibull analysis. Journal of structural division. ASCE. 106(10):2035-2052.

Liu, J.Y. 1981. Shear strength of tapered wood beams. Journal of structural division. ASCE. 107(5):719-731.

Soltis, L.A. and D.R. Rammer. 1994. Shear strength of unchecked glued laminated beams. Forest Products Journal. 44(1):51-57

Weibull, W. 1939. A statistical theory of strength of materials. Swedish Royal Institute of Engineering Research. Report No. 151. Stockholm, Sweden.

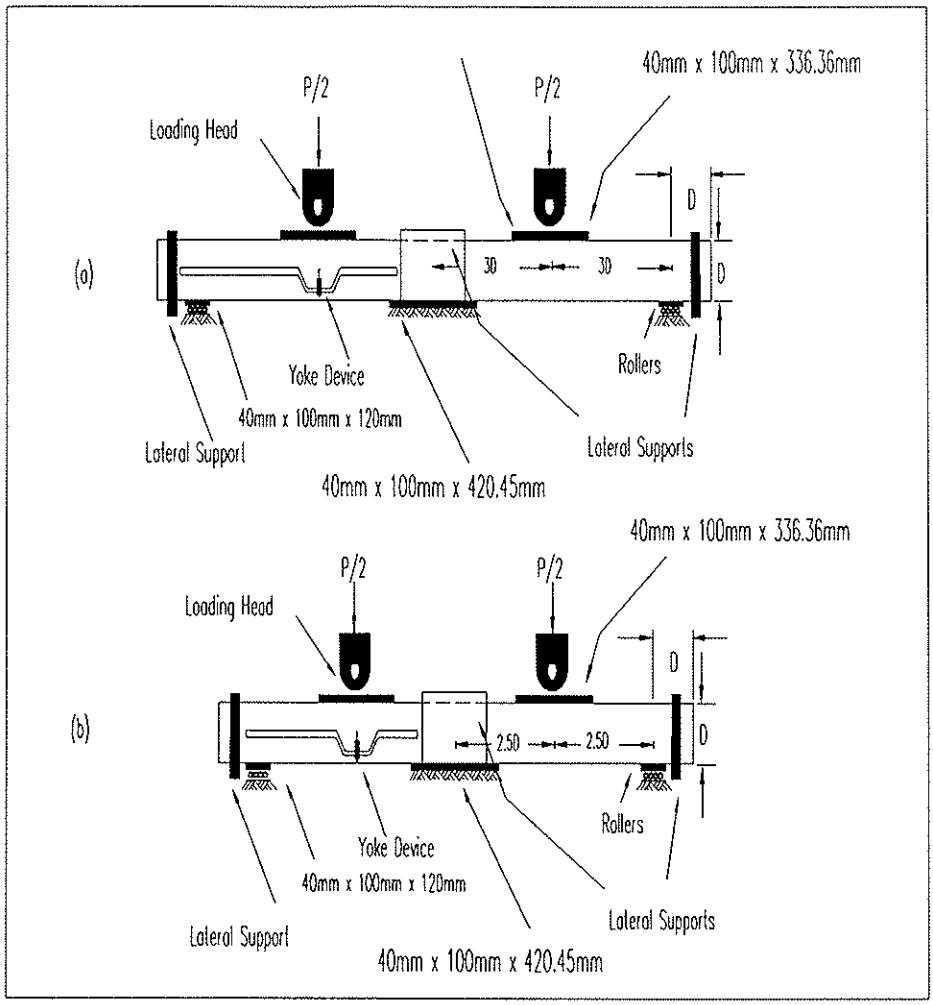

Figure 1. Two span five point loading test configurations for 5D and 6D

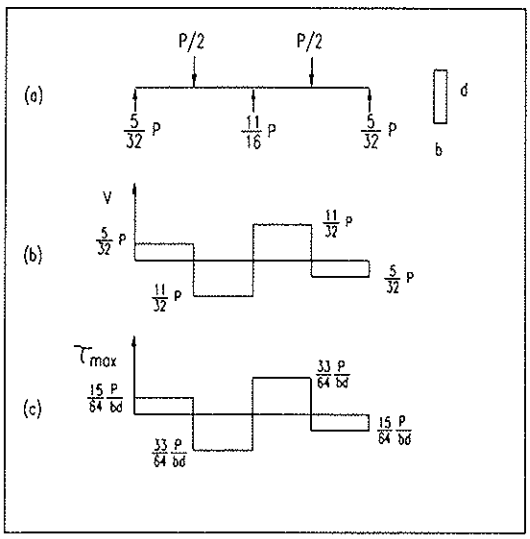

Figure 2. Classical analysis of test system

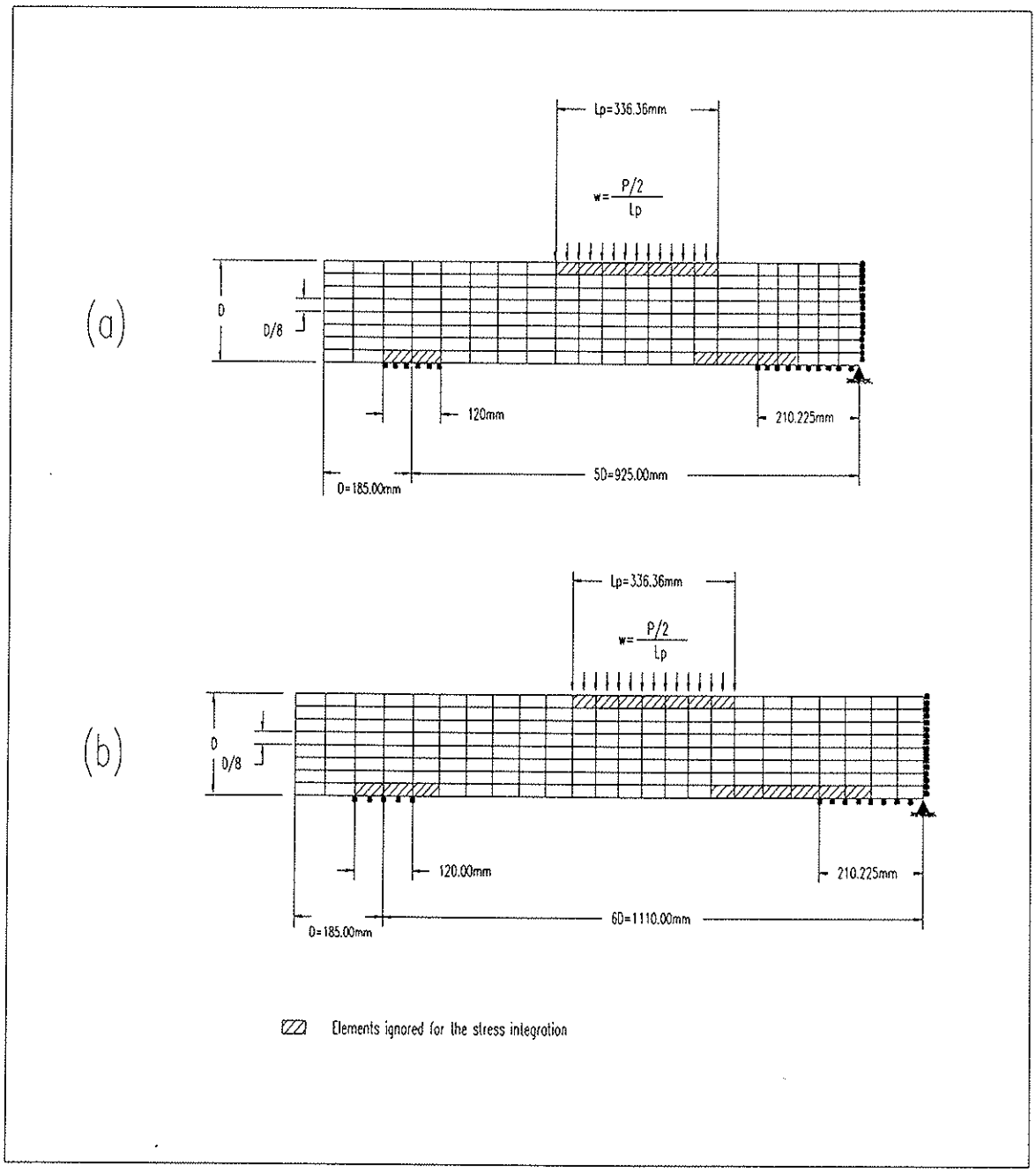

Figure 3. Finite element mesh about the mid span for test configurations 5D and 6D

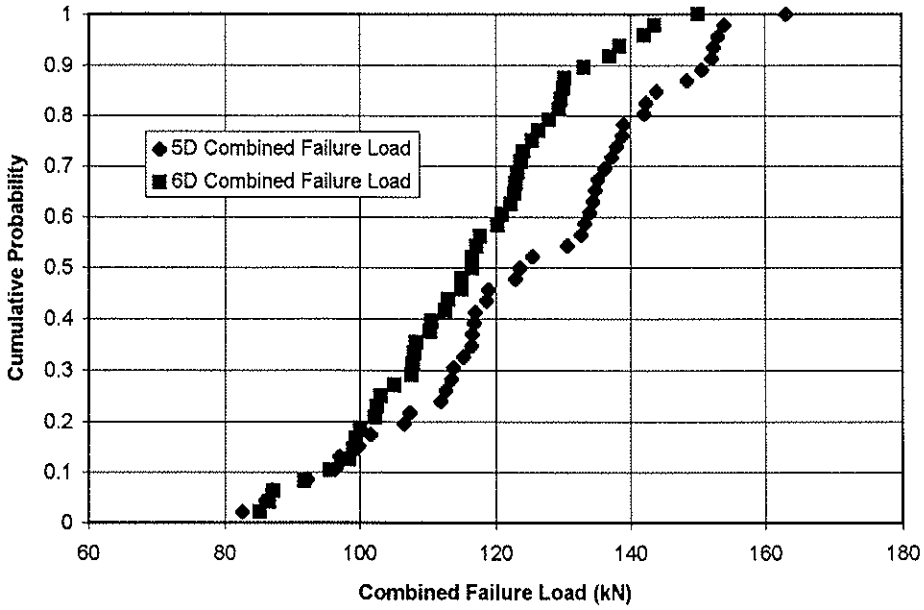

Figure 4. Cumulative probability distributions of failure loads for Douglas-Fir

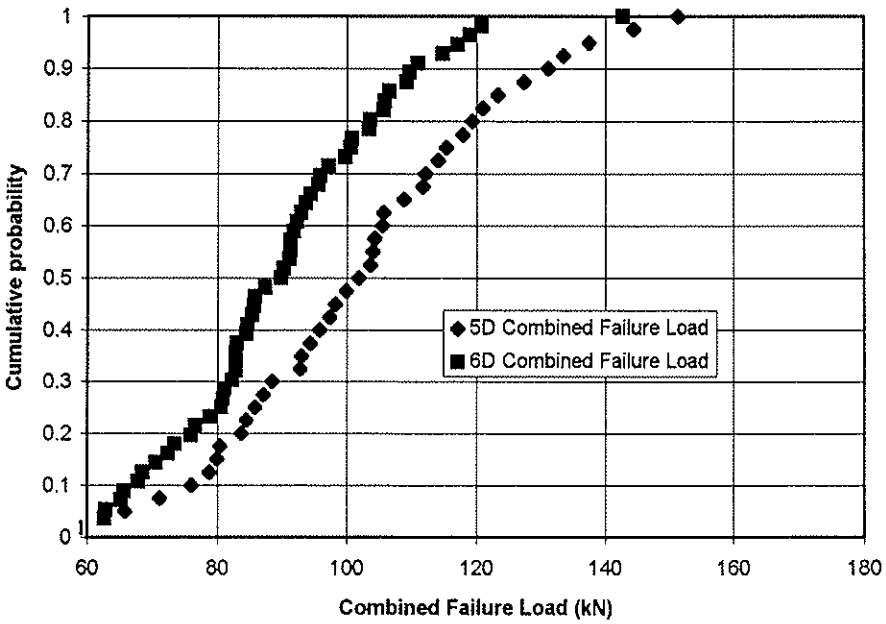

Figure 5. Cumulative probability distributions of failure loads for Hem-Fir

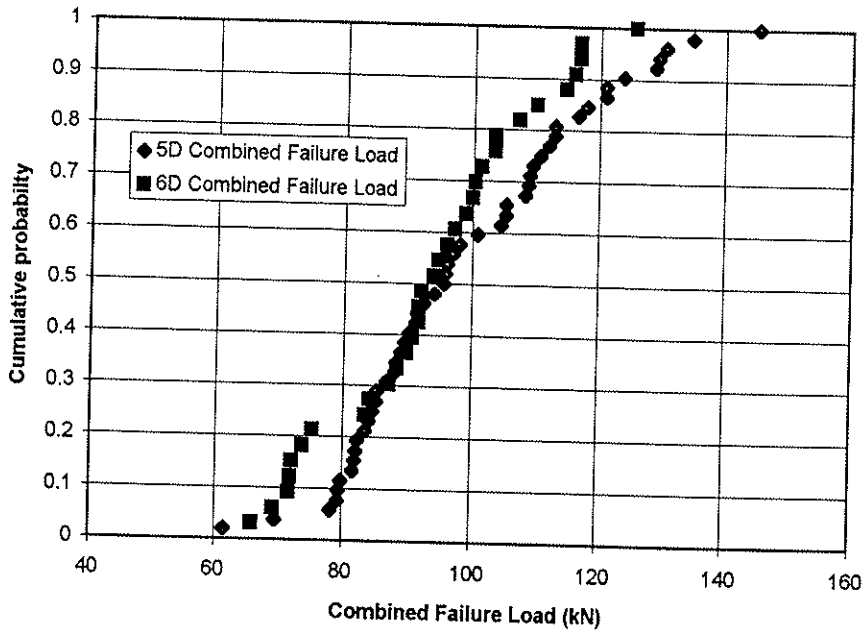

Figure 6. Cumulative probability distributions of failure loads for Spruce-Pine-Fir

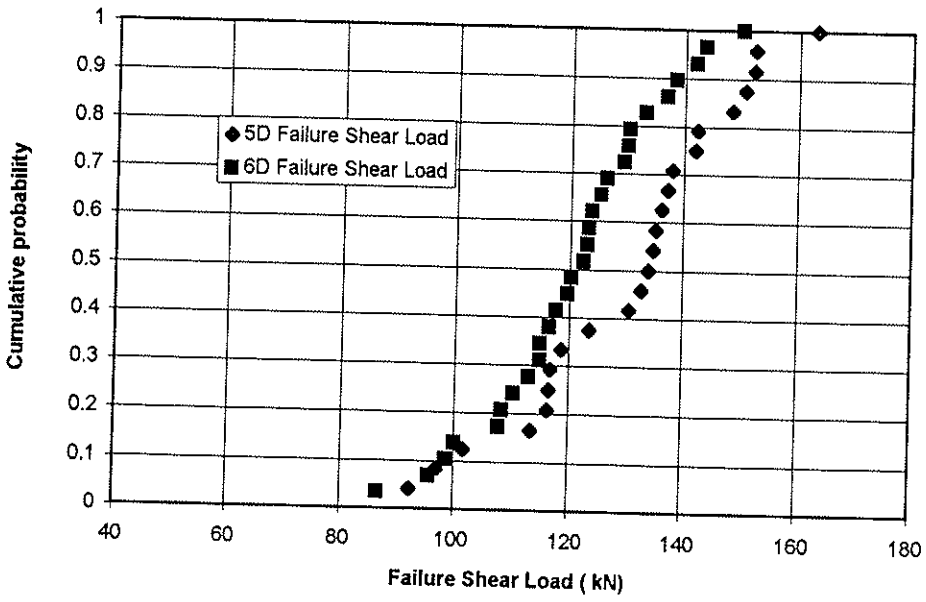

Figure 7. Cumulative probability distributions of failure loads in shear for Douglas Fir

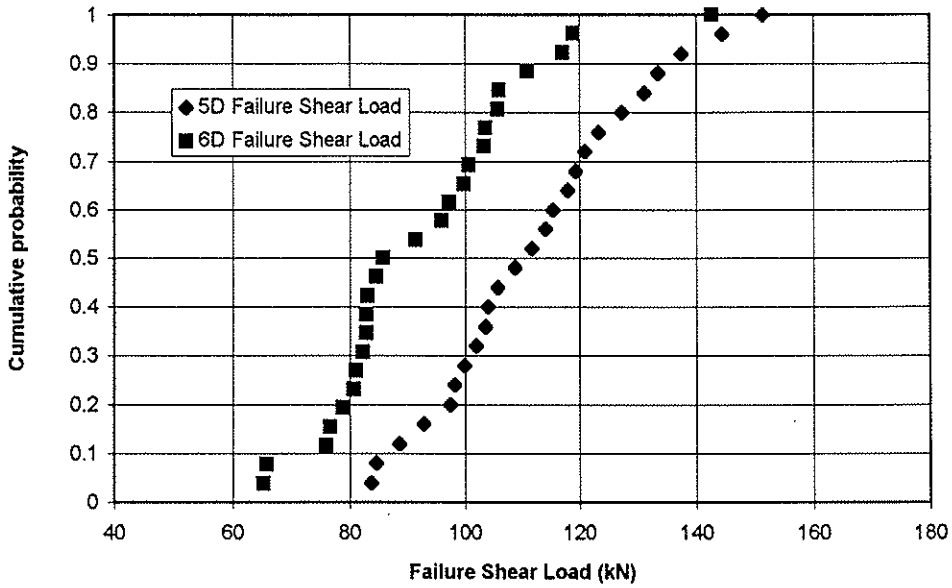

Figure 8. Cumulative probability distributions of failure loads in shear for Hem-Fir

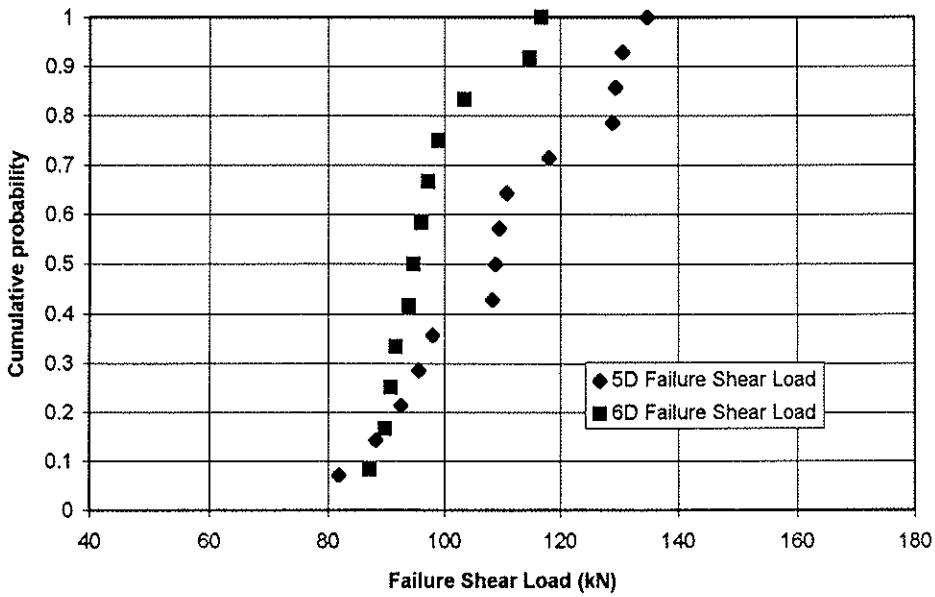

Figure 9. Cumulative probability distributions of failure loads in shear for Spruce-Pine-Fir

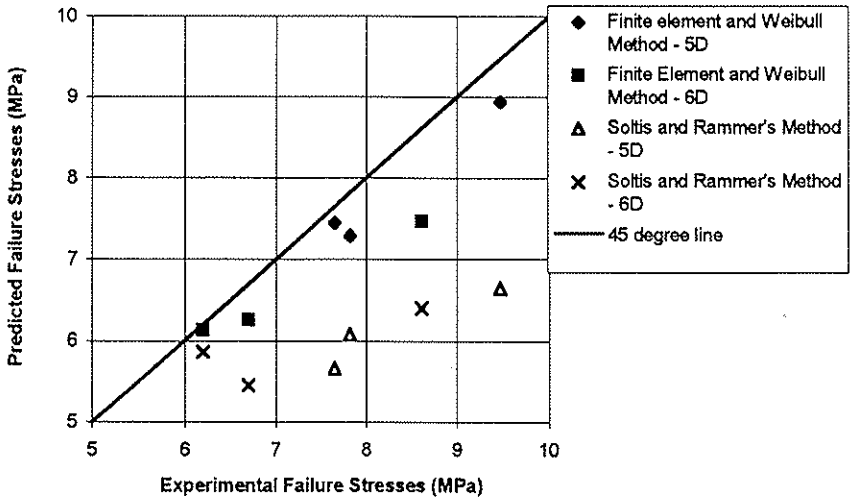

Figure 10. Plot of predicted versus experimental failure stresses

INTERNATIONAL COUNCIL FOR BUILDING RESEARCH STUDIES AND DOCUMENTATION

WORKING COMMISSION W18 - TIMBER STRUCTURES

SHEAR STRENGTH OF DOUGLAS FIR TIMBERS

by

B Madsen
Timber Engineering Ltd., Vancouver
Canada

MEETING TWENTY - EIGHT

COPENHAGEN

DENMARK

APRIL 1995

SHEAR STRENGTH OF DOUGLAS FIR TIMBERS

BY

BORG MADSEN

TIMBER ENGINEERING LTD.

VANCOUVER CANADA

PREAMBLE

This paper serves two purposes:

A)

It demonstrates that the presently used characteristic strengths for shear are unduely conservative.

It suggests that action be taken to change the design requirements for shear in the timber code to requirements which more correctly reflects the structural behavior of the material, such as the "Weakest Link Principle" and "Fracture Mechanics Considerations" proposed by Drs. J.D. Barrett and R.O. Foschi.

It also shows that the shear capacity in many cases can be doubled by providing an overhang equal to the beam depth.

B)

The case described shows that the code committees must be more careful not to demand unnecessarily stringent requirements which act as detriments to the timber industry, often in the form of lost markets.

In evaluating or accepting proposed new design methods, the committee must realistically investigate the relevance of the present code formulations and compare their soundness to that of the proposal.

In the case presented, it would needlessly have cost one Canadian railroad more than $ 200.000.000 to follow the CSA-086 design code because of the code committee's reluctance to accept changes.

INTRODUCTION.

The Canadian Railway's track system contains numerous bridges and associated approach spans. Figure 1 depicts a typical arrangement of the girders and bridge ties.

The bridge ties are commonly 240x290 mm in cross section and 3.66m or 3.96 m in length, thus providing an overhang on each side of the girders of 0.61 m or 0.76 m. The bridge ties that carry the rails are spaced 356 mm or 406 mm and it can safely be assumed that the axle load will be shared equally between 3 adjacent bridge ties.[A. Shakoor Uppal, 1991]

At present the axle loads used are limited to 290 kN. It is possible that this limit will be increased to 356 kN. in the near future throughout the system, and that it may, subsequently, be increased to 445 kN per axle.

A structural shear analysis of the bridge ties using conventional design methods as presented by CSA-086 "Code for Engineering Design in Wood" indicates that a 290 kN load will over-stress the bridge ties in shear to some extent (1.10 MPa. actual stress vs. 0.90 MPa allowable stress), but an increase to 356 kN per axle would create considerable over-stressing in the bridge ties. It is estimated that more than 600,000 bridge ties will be affected by the proposed increase in axle loads.

While this may sound quite foreboding, it should be realized that the strength properties for lumber and timber were established back in 1926 (ASTM - D - 245-26); based upon tests with small defect-free wood specimens. These tests have formed the basis for the North American allowable strength properties for timber until recently (1980's). At that time it was shown that the small clear wood specimens do not lead to reliable estimates of the actual strength of lumber and timber members. Extensive testing with full size structural members was undertaken to establish reliable design stresses for bending, compression parallel to grain, and tension parallel to grain as well as modulus of elasticity [Borg Madsen and Peter C. Nielsen, 1978 & 1979]. Unfortunately, shear strength was not included in the investigation, because shear stresses do not normally govern the design of the type of structural members used in ordinary houses or buildings.

The task now being faced is: TO ESTABLISH THE ACTUAL LOAD CAPACITY IN SHEAR OF BRIDGE TIES and TO INVESTIGATE TO WHAT EXTENT THE SHEAR PROPERTIES ARE CRITICAL FOR THE SPECIFIC LOADING CONFIGURATION USED IN BRIDGES AND THEIR APPROACH SPANS.

INFORMATION ON SHEAR

Over a period of time, three procedures have been used for the calculation of shear stresses. None of them were based on a detailed understanding of timbers structural behavior with regards to shear. The formulae had simply been adopted from studies of the theoretical behaviour of elastic, isotropic and homogeneous materials and applied to timber which is an anisotropic material. Granted, a hefty factor of ignorance was used in the process; which penelizes the use of timber.

It should not be inferred, however, that we today have a full understanding of the failure mechanism of the shear forces, but some new avenues have been developed.

One is the realization that the weakest link principle, at least partially, applies to timber. Drs. R.O. Foschi and J.D. Barrett [1976] employed the idea to explain observations with shear stresses in Glulam beams. The weakest link principle is based upon the notion that materials - all materials, but specifically brittle materials - contain random flaws on the microscopic level, and that the final failure will occur when one of these flaws starts to grow catastrophically when subjected to high stresses. The probability of such an occurrence is a function of the volume of the material and the stress distribution within the material. This work has been included in the Glulam section of the CSA-086-M 89 "Standard for Engineering Design in Wood". However, this is only mandatory for Glulam members containing more than 2.0 cubic metres of material, and is not being used for sawn timber.

In the 1989 version of CSA-086 the treatment of shear stresses in lumber was improved for material 38 mm in thickness by incorporating the effects of splits. (SPLITS: A separation of the wood fibres passing from one face of the member to he opposite face. CHECKS: Separations of the wood fibres that only partly penetrates the member). Splits are of concern from a structural point of view, while checks generally are not a concern.

Using fracture mechanics considerations Drs. J.D.Barrett and R.O. Foschi (I977) investigated a failure mechanism (Mode II Failure) where the material above a split will slide lengthwise relative to the material below the split. This movement will take place when the stresses at the front of the split reaches the value of the critical stress intensity factor. The stress intensity factor is not a stress, but a material property that has the dimension of psi x square root of inches. The upper limit for the shear strength will be the value determined by the volume effect, but it may be diminished by the introduction of splits that may grow according to the fracture mechanics model. Using these more advanced failure concepts, it is possible to determine the shear strength more accurately. However, the theoretical models have still to be verified further by tests in order for us to gain confidence in the models and their applicability to the larger timber sizes. One of the problems is associated with the determination of the length of the split. It is quite easy to obtain the length of a split in 38 mm lumber because the length is large relative to the thickness, but in timber the ratio of length of split to thickness may be close to unity, and it is

not always known, what path the split takes on its way from one face to the other.

OBJECTIVES of TESTING

The aim of the testing was: TO ESTABLISH THE CARRYING CAPACITY IN SHEAR FOR 240x290 mm BRIDGE TIES SUBJECTED TO A LOAD CONFIGURATION EMULATING THAT USED IN EXISTING BRIDGES.

Additionally, this question should be investigated : WHAT EFFECT WILL THE CANTILEVERED OVERHANGING ENDS HAVE ON THE SHEAR STRENGTH OF THE BRIDGE TIES?.

Because we were to establish the weak portion of the strength distribution - not the whole strength distribution - it was possible to use a proof loading approach to the testing regime. Under that system, all the specimens in the sample would be subjected to a proof load of a magnitude that would cause approximately 15% of the specimens to fail. From the strength of the pieces that failed it would be easy to obtain the required strength information on the 5th. percentile level.

MATERIALS

Two hundred new Douglas Fir bridge ties 240x290mm by 3.66m long, pressure preservative treated and drilled so the ties would be ready for normal use, were obtained. These ties were shipped by CN to the Civil Engineering Structures Laboratory at the University of British Columbia. They were typical of today's production. They did have some checking, but very few ties were found with splits and the lengths of these splits were less than half the beam depth. The tests with this material will be referred to as "new ties".

A second shipment consisting of 200 treated bridge ties 240x290 mm by 3.96m long were also delivered to UBC. These ties had seen 30 years of service on bridge spans at the Edson subdivision near Magnolia in Alberta.The purpose of these tests were to compare the strength of the ties after 30 years of service with the strength of the new ties. It was noted that these old ties had fewer checks than the new ties. This was not expected. The sizes of the knots were generally smaller than those in the new ties and they were also more dense in the sense that the old ties had more annual growth rings per inch. The ties had 38mm deep daps 356mm long cut into the edge resting on the girders; many of the ties showed sign of severe damage at the points where the rails had been located. Some deterioration due to rot was also observed in many of the ties; this rot was most frequently found in the tie plate areas. The tests with these ties will be referred to as "old ties".

Twenty untreated ties 240x290mm without holes and without framing were also made available, enabling us to get a feel for the strength difference which may be caused by the treatment process. This group will be referenced as "untreated ties"

TEST SET-UP

The testing set-up had to be arranged in such a manner that the handling of the very heavy bridge ties (about 200kg each) could be done with reasonable ease. A system of rollers transported the ties to the position where the testing would be performed. It was convenient to test the ties up-side down, i.e. the load simulating the axle loads acted up-ward in the test set-up; this enabled easy observation of the tension zone of the failed ties. Two hydraulic cylinders were placed on the floor 1.52m apart representing the axle loads, while two hold-down frames spaced 2.44m apart emulated the girders as shown in Fig.2. The cylinders would lift the bridge tie so it would bear against the hold-down frames and then proceed to apply the desired proof load. Bearing plates 356mm long and 240mm wide were provided to simulate the bearing plates used in the field. The bearing plates were mounted in such a manner that they could rotate as the tie deflected due to the loading. The hold-down frames were flexible in the longitudinal direction so any elongation of the tension zone would not impose additional tension stresses in the bridge tie. A load cell was inserted between the south hold-down frame and the bearing plate. This load cell was in turn connected to a data acquisition system which simultaneously recorded the deflection and the load that caused it. A transducer was used to sense the deflections. One set of readings were obtained every second during the loading cycle. The loads reportet here represent the loads as measured by the load cell, i.e. the loads from one cylinder, so the total load carried by the bridge ties was twice as much.

TESTING PROCEDURE

The test specimen was first placed symmetrically in the test set-up, just as it is in the field. The deflection transducer was attached to the bottom of the tie at the center of the span. The interconnected cylinders were then activated and the bridge tie lifted up against the hold-down frames and the load increased. The current load and the load deformation curve would automatically be shown on the computer screen as the loading progressed.

If the tie failed, the maximum load would be recorded and shown on the screen. The unloading would be commenced. If the bridge tie did not fail, the loading would be terminated at the selected proof load level. For the treated ties this proof load was 220 kN at each load point. The test, therefore, told us that the tie had a total carrying capacity in excess of 220 Kn. The time to reach the proof load level was between two to three minutes. This test was designed to obtain the shear capacity for ties with equal overhang at each end. That load configuration was the most important one, because it did represent the conditions in the field. It is referred to as the "Central Condition".

Before going further, it is appropriate to place the proof load level in relation to the axle loads in question. As mentioned, during the test each tie is loaded with a total load of 100 kips. But, the axle load used in the field is assumed to be shared by three ties, so the 220 Kn proof load is in fact three times the load which the tie will experience from a 220 Kn axle load, or 3.7 times the load created by the 176 kn axle load.

The stresses generated in the 240x290mm cross section by a 50 kips load at each load point are : Bending 29.7MPa and Shear 4.7MPa. according to v=1.5xV/ A.

If the bridge tie, mentioned in the test method described above, did not fail, or if it was deemed possible to conduct a second test with a broken tie, a second test would be conducted. The bridge tie would be shifted so the north end of the tie would be flush with the bearing plate and thus represent the load case with no overhang. The loading procedure described above would be repeated and the collected data kept in the file for the particular specimen. If the tie survived the second test or it was not too badly damaged, a third test was conducted. This time the south end would be placed flush with the bearing plate and the loading regime repeated. In this manner we would obtain strength information on 200 tests with the central location and 400 tests less the broken specimens for the flush end condition. This sequence is illustrated in Fig.3.

The untreated ties were tested in the same manner as the new ties, except that the proof load was increased to 250 kN in order to assure that a sufficient number of failures would develop.

FAILURES

The failures were classified as either shear or bending failures. The bending failure would usually start in the vicinity of a knot located close to the tension edge where local slope of grain existed. The failure would progress toward the centre of the tie and stop. In a few cases the crack would progress all the way to the end of the tie, resulting in a shear failure.

A shear failure was defined as a failure where a step was created on the end surface of the tie. Typical bending and shear failures are shown in Figure 4.

It should be pointed out that we did not observed failures caused by compression perpendicular to the grain.

In Table #2 are shown the number of tests conducted, the number of failures, and the percent of survivors found in the different kinds of materials, separately for bending induced failures and shear induced failures.

The table shows in a quantitative manner that rate of survival is consistently higher for the shear failures than for the bending failures. Also, it is evident that the old ties are weaker than the new ties in bending. Overall 1033 tests were conducted of which 388 failed in bending and 53 in shear; the rest survived the proof load. It should be mentioned that the high number of bending failures came primarily from the old ties.

As mentioned, the old ties had all been dapped where they were to rest on the girders and some ties had been dapped under the rails. These daps caused a re-entrant corner from which point the bending failure would originate resulting in greatly reduced strength. This failure mode can best be characterized as a tension perpendicular to grain failure caused by the stress concentration. Because of this artificially created stress concentration, it becomes very difficult to make a direct comparison between the new and old ties. This practice of dapping the ties was stopped in the CN lines in 1990.

Another cause for the observed strength reduction was the presence of rot. However, it appears that these strength reducing mechanisms, - rot and stress concentrations - while affecting the bending strength, have not affected the shear strength, at least not to the same extent.

Another presentation of the data is shown in Figures 5-8. Here the data is shown as maximum load vs. normalized rank. These graphs places the emphasis on the weak end of the strength distribution.

The data are presented as loads at the load points rather than stresses, in order to show shear and bending on the same graph.

The graphs each represent the data from one of the three types of material (new, untreated, and old). The scales are the same for the three graphs so a direct comparison can be made. The graphs show the points below the 15^{th} percentile laying below the applied proof load level. Each curve is marked

according to the load configuration it depicts: C for central, F for flush, and H for half overhang. The second letter indicates the type of failure that the curve represents; B for bending and S for shear. The curves include lots of bending failures, but relatively few shear failures; which in itself indicates that the ties are stronger in shear than in bending.

In Figure 5, dealing with new ties, it should be noticed that the CB curve is considerably below the CS curve. For the central loading condition - the one we are most interested in - we can see that the 5th percentile in bending capacity is 190 kN, (25.2MPa) while the 5th percentile in shear is in excess of the proof load of 220 kN. (4.7MPa) However, we do not know how much stronger the bridge ties are in shear, because they broke in bending before the shear strength had been reached. When the bridge ties are placed in the flush position we can observe that the shear strength and the bending strength are roughly the same; about 215 kN at the 5th percentile level.

In Figure 6 are shown the results from the 20 specimens tested in the untreated condition. Since the sample size is so small, it is difficult to make very specific statements, but a general idea can be obtained. The proof loading was raised to 250 kN in these tests, but regardless of this only 8 failures were observed below the proof load level and below the 15th percentile. Despite the small sample size, the tests indicate that the shear strength is greater than the bending strength.

Figure 7 shows the normalized rank presentation for the old ties. The first thing to be noticed is that both the CB line and the FB line are located much lower than the lines for the new ties which were shown in Fig.5. Also, the FB-line is lower than CB. Obviously something has happened to the bending strength. It was mentioned earlier that these ties had daps cut into their surfaces. The daps have caused a different failure mode, one associated with tension perpendicular to the grain, the weakest strength property of timber.

Unfortunately these daps make it very difficult to make strength comparisons between new and old ties with regard to the bending strength. We don't know for sure how much of the strength difference is caused by duration of load, deterioration, rot, stress concentration or have some other origin.

This dilemma made it advisable to test some 60 new ties, dapped in the same manner as the old ties, enableling us to estimate what portion of the observed strength reduction was caused by the daps (comparing new ties with daps, with new ties without daps) and also to estimate the effect of the time-dependent bio-degradation (comparing new ties with daps, with old ties with daps.

Figure 8. shows the graph of the new data set, and Table #3 lists the 5th. percentile values obtained from the four different data sets. For the central condition, the stress concentration from the daps causes the bending capacity to decrease to 76% of the un-dapped ties. Furthermore, the old ties with daps have a bending capacity equal to 82% of the new ties with daps.

The shear capacity for the central loading condition is greater than 220 kN, while the shear capacity for the flush condition is about 210 kN for all four data sets, Apparently, the shear capacity is not affected by the stress concentrations nor by the bio-degradation in the same manner as the bending capacity. The difference in the structural behaviour in shear and bending is shown in Figures 9 and 10 where the bending curves are shown together for the central condition, and the shear curves for the flush condition respectively. The bending values are spread out, while the shear values are concentrated and overlapping

With regards to the shear strength, it can be concluded that it does not appear to have been reduced, and that the 5^{th} percentile for the flush condition is about 210 kN. For the central position the shear capacity at the 5^{th} percentile level is in excess of 220 kN. The shear capacity of the bridge ties is more than satisfactory for the load conditions investigated, since the strength divided with the nominal maximum load is in excess of 3.7. For the bending capacity of the 30 year old ties we find that the ratio of 5^{th} percentile strength to nominal maximum load is 115/59=1.95, using an axle load of 80 kips.

This does not appear to be out of line considering that the ties have been in service for more than 30 years.

FINITE ELEMENT ANALYSIS

In order to develop an understanding of the effect the overhanging ends has on the shear strength, it was decided to carry out a finite element analysis. A program developed by Dr. R.O. Foschi [private communication] was available and the analysis was carried out by Mr. Felix Yao, an assistant to Dr. Foschi. The model used emulates the forward shear mode II, which determines at what load a split of a given length will start to grow.

The configurations are shown in Figure 11.

The results from the analyses are presented in Figure 12 to 15. The graph in Figure 12 shows the ultimate load in pounds plotted along the ordinate, while the abscissa is the ratio of the length of the split to the depth of the beam. The points plotted are the loads which can be carried at the instance when the level of the critical stress intensity factor is reached and the split starts to run uncontrolled.

The lower curve represents the case where the beam is flush with the bearing plate. This is the condition normally assumed in shear design; here referred to as the "flush" condition. If the split has a length equal to the beam depth, the split will not grow until the load has reached 80,000# (356 kN), but if the load is increased the beam will fail. If the ratio of split length to beam depth is 1.5 the failure will take place at a load of about 40,000# (178 kN). At a ratio of 2.0 the maximum load is 32.000# (142 kN) and it essentially stays at that level for higher ratios of split length to depth, the shear stress being 3.0 MPa.

In the case where an overhang without splits is present, and it further is assumed that a split in the beam has been created as before, starting at the end of the bearing plate and extending toward the centre of the beam, there will be two split fronts as indicated in Figure 11. One will travel towards the centre, the other will move towards the free end of the beam. Catastrophic failure will not occur until the split has grown to a point where the capacity of both split fronts has been exhausted.

The middle curve marked "interior" in Figure 12 describes the carrying capacity of the interior split front. It can be seen that for a length of split to depth ratio of 1.0 the capacity 93000# (414 kN) is somewhat larger than for the flush case. This happens because the exterior split front prevents the interior split from growing and thereby help carrying some load. The capacity of the external split is shown by the top curve marked "exterior". At a/h equal to 1.5 the interior split will start to grow when the load reaches 50,000 # (222 kN), but due to the shape of the curve, the growth of the split will stop at a/h equal to 2.5 (see dotted line) because enough load has been shifted to the exterior split which still have some strength left. Where the interior and the exterior curves cross each other is the point at which the shear capacity has been exhausted and catastrophic growth of the split will commence. Because the shear capacity cannot exceed the intersection point, the shear capacity will have the form shown in Figure 13 with crosses. It shows us that the failure will not take place until the split has reach a length of 3.2 times the beam depth, and that the shear capacity is about 65,000# (290 kN) or approximately twice that of the flush condition.

The computer program was used to run a series of combinations of the above parameters, and the shear capacity can now be calculated as the product of the critical stress intensity factor K_{2crit} and an adjustment factor, F, obtained from the computer runs. Figure 14 shows values of the adjustment factor F versus a/h. The curves are similar to the curves in Figure 12. In Figure 15 is shown an example of a family of curves of the values of F when the length of the overhang is changed. It should be noticed that the strength increases as the overhang is increased, but only up to one beam depth. Overhangs larger than the beam depth do not enhance the shear capacity.

Rather than presenting the results as graphs, it may in this case be better to prepare a table for the values of F. To obtain the shear capacity the selected value of the critical stress intensity factor should be multiplied by the appropriate value of F in Table #4. The value of K_{2crit} depends on the species and which percentile the designer wishes to use. From Table #4 it can be perceived that a plateau exist in most of the cases corresponding to the flat portion in Figure 13. To cover the same information in graphs would require a multitude of figures.

The information in Table #4 is based upon the fracture mechanics failure mode. The other failure mode mentioned previously- that of the volume effect caused by the weakest link concept- relates to un-split material and provides an upper limit for the shear capacity. It can be calculated using the information presented in Table #5.

For Douglas Fir the un-split shear strength of a unit volume (1 inch^3) is equal to 1580 psi.(10.9 MPa) at the 5th percentile level. The volume V to be used in the formula is half the volume of the tie. (P is half of the total load placed on the tie). The value of k is 5.5. This carrying capacity should be checked and compared with the capacity obtained from the fracture mechanics model and the lowest value used in the design.

The one important parameter governing the shear capacity is the length of split existing or developing with time in the structural member. This concept may appear disconcerting to some engineers, because they will not normally know the length of the split at the time they design the structural member. Nor will the engineer be accustom to consider a split as a prime material property. It will undoubtedly take some time to get used to, but this test and others have proven that the length of split is an important characteristic in order correctly to calculate the shear capacity of timber members. The engineer will have to make sure that sufficient overhang is provided, so even with time, a split will not develop that will weaken the member.

It should be noticed that providing an overhang equal to the beam depth will in some cases double the shear capacity. It should also be observed that even a small overhang (e/h = 0.1 or 0.25) will increase the shear capacity and that e greater h will not provide much improvement. Figures 17 and 18 show sketches of the cases mentioned in Table #4 and may help the reader to visualize the relationship between the different parameters. To get a feel for the capacity of the un-split material relative to the capacity of material containing a split, the capacities from the two formulae shown in Tables #4 and #5 can be postulated to be equal and the ratio of the shear factors F and F_u can be found. The volume which enter the formula for un-split material is raised to the 0.18 power and the ratio is, therefore, not very sensitive to the volume. As an approximation it is found that the ratio is equal to 0.3. When the values in Fig. 17 are more than 50, the design is controlled by the un-split material (capacity shown in a circle); for values less than 50, the split will govern. For the cases in Fig.18 the boundary between the two formulae is 39. It should also be noted that the splits have to be large in order for them to be governing. Splits of that size are rare occurrences.

In the preceding remarks, references were made to the bending capacity and the shear capacity. More specifically these references were made to the characteristic value i.e. the short term strength at the 5th. percentile level. This characteristic strength has to be modified further in order fot us to arrive at a suitable design stress or design resistance. If Working Stresses are to be used the characteristic strength should be divided by a factor in the range of 1.9-2.1 which is commonly used for the other strength properties for wood such as bending , compression, etc. For shear, the factor used in deriving at the Working Stress for the building code was 4.1, but this large factor was applied because the shear stress was obtained from tests with small shear blocks. In our case, where the shear strength is derived from testing of large realistic specimens, there is no need to use a greater factor of safety than that used for the other strength properties. Recommend that a factor for shear of 2.0 be used.

The real shear failure mode takes place in the weakest direction, which is parallel to the grain. The above described analysis method for shear more accurately reflects timber's behaviour in shear and will lead to some structures becoming more economical. Very few structural members will be governed by shear in the future.

The question may be asked: how well did the computer model predict the shear capacity obtained from the tests?

The test conducted with the new ties - using the flush condition - showed that 9% of the specimens failed in shear at loads less than the 50 kips proof load. The computer program was used to generate the cumulative probability of failure versus split length to beam depth ratio (a/h) as shown in Fig. 16. At 9% the length of the split was predicted to be 1.35h. Using linear interpretation for the value 1.35 for a/h in the column for e/h = 0 and s/h = 1.0 in Table #4, we find that F is equal to 50.4, which multiplied with the $K_{2\ crit}$ value for the 5^{th} percentile of 1054 psi, results in a shear capacity of 52.1 kips. This is to be compared with the 50.0 kips from the tests and can be considered to be an acceptable verification of the model proposed by Dr. Foschi.

The case of the bridge ties is unique in several respects, one of them being that it is relatively easy to evaluate the cost of applying the present code requirements to the problem. The code requirements clearly lead to the conclusion that the bridge ties will have to be replaced with larger ties in order to cope with the increased loads.

The cost of replacing a tie is well known to be in the neighbourhood of $ 300 to $ 350. However, in this case the replacement tie is larger which makes the replacement process more difficult, especially as the replacement has to take place between trains. A cost of $ 400.00 per tie would be a realistic in-place cost.

As mentioned, the number of ties to be replaced is in excess of 600,000 which places the total cost between 200 and 300 Million Dollars.

This expenditure would not be needed if the code in this case would reflect the structural behaviour of the material rather than some grossly outdated assumptions.

The responsibilities on the members of the committee are great and a fine line between safety and economics has to be negotiated. Unfortunately that was not done in this aspect of the code.

SUMMARY OF PAPER

- For the load configuration with a cantilever at each end (Fig #1) the bridge ties predominantly failed due to bending. Only 6 shear failures out of a potential 904 were observed. The 5th. percentile could not be established, due to lack of failures, but the 0.7 percentile level would appear to be greater than 4.7 MPa.

- For the flush condition, 47 shear failures were found amongst 557 tests. The 5th. percentile was 4.5 MPa.

- It was demonstrated that the cantilever portion pays a major role in increasing the shear capacity.

- When the ties were dapped they lost 24% of their original bending capacity.

- The old dapped ties had -after 30 years service- a bending capacity 18% less than the new dapped ties.

- A computer program based upon the fracture mechanics Mode II failure criterion was able to predict the test results for the condition to within 4%.

- A design method was proposed based upon the computer analysis conducted by Dr. R.O. Foschi.

- The characteristic shear stress for Douglas Fir was found to be 4.5 MPa. for the flush condition. (In the Canadian code this value is multiplied by 0.8 i.e. 3.6 MPa. to allow for Duration of Load. The comparable shear value in the code for Glulam is 2.0 MPa. and for timber 1.2 MPa.)

TABLE #1

TRADITIONAL SHEAR STRESSES

	CSA-086 - 1984		CSA-086 - 1970		CSA-086 - 1989	
AXLE LOAD	stress in ties	allowable stress	stress in ties	allowable stress	stress in ties	allowable stress
66 kips	1.10 (159)	0.90 (130)	0.77 (112)	0.99 (144)	0.81 (118)	1.20 (179)
80 kips	1.32 (192)		0.94 (136)		0.99 (143)	
100 kips	1.66 (240)		1.17 (170)		1.24 (179)	

allowable stresses in MPa (psi in brackets)

TABLE #2

SURVIVAL RATES

POSITION:	central		flush		½overhang	
FAILURE MODE:	bending	shear	bending	shear	bending	shear
UN-FRAMED TIES (n=20)						
# failures	7	1	1	3		
# tests	20	20	26	26		
% survivors	65	95	96	88		
% failures	35	5	4	12		
loaded to 56 kips						
NEW UNDAPPED TIES (n=200)						
# failures	32	2	21	30		
# tests	184	184	315	315		
% survivors	83	99	93	90		
% failures	17	1	7	10		
loaded to 50 kips						
NEW DAPPED TIES (n=60)						
# failures	34	0	43	8		
# tests	60	60	83	83		
% survivors	43	100	48	90		
% failures	57	0	52	10		
loaded to 50 kips						
OLD DAPPED TIES (n=200)						
# failures	149	3	88	6	13	0
# tests	188	188	133	133	24	24
% survivors	21	98	34	95	46	100
% failures	79	2	66	5	54	0
loaded to 50 kips						

TABLE #3

5th PERCENTILE STRENGTH VALUES

Imperial units

	sample size	proof load [kips]	BENDING				SHEAR			
			CAPACITY [kips]		STRESS [psi]		CAPACITY [kips]		STRESS [psi]	
			CB	FB	CB	FB	CS	FS	CS	FS
Un-framed ties	20	56	46.0	>54.6	3954	>4693	>55.5	46.3	>762	636
New undapped ties	200	50	42.7	49.0	3680	4212	>49.5	47.9	>686	658
New dapped ties	60	50	32.4	26.0	2785	2235	>49.5	47.2	>686	648
Old dapped ties	200	50	26.5	25.4	2278	2183	>49.5	47.7	>686	655

Comments:

> : *greater than*
CAPACITY : *load in load points*
STRESS (SHEAR) : $v = \frac{1.5 \times V}{A}$

CB : *central location bending*
CS : *central location shear*
FB : *flush location bending*
FS : *flush location shear*

SI units

	sample size	proof load [kN]	BENDING				SHEAR			
			CAPACITY [kN]		STRESS [MPa]		CAPACITY [kN]		STRESS [MPa]	
			CB	FB	CB	FB	CS	FS	CS	FS
Un-framed ties	20	250	205	>243	27.3	>32.4	>247	206	>5.3	4.4
New undapped ties	200	220	190	218	25.3	29.0	>220	213	>4.7	4.5
New dapped ties	60	220	144	116	19.2	15.4	>220	210	>4.7	4.5
Old dapped ties	200	220	118	113	15.7	15.1	>220	212	>4.7	4.5

TABLE 4: VALUES OF SHEAR FACTOR F

$$P = F \cdot K_{IIcr}$$

P = Shear Capacity (lbs).
K_{IIcr} = Critical Stress Intensity Factor for Shear ($psi\sqrt{in}$) (for actual values, see below).
F = Shear Factor.

p/h	s/h	a/h	$e/h = 0.0$	$e/h = 0.10$	$e/h = 0.25$	$e/h = 0.50$	$e/h \geq 1.00$
1.5	1.0	1.0	77	87	88	88	88
		1.5	39	47	50	58	62
		2.0	35	42	50	58	62
		2.5	35	38	50	58	62
		3.0	35	31	44	58	62
		3.5	31	25	36	47	55
	0.5	1.0	50	61	62	63	63
		1.5	33	44	51	56	60
		2.0	31	41	51	56	60
		2.5	31	29	42	53	60
		3.0	33	25	36	47	55
		3.5	34	22	31	40	46
3.0	1.0	1.5	72	76	76	76	75
		2.0	45	49	49	49	49
		2.5	29	34	35	35	35
		3.0	25	32	32	32	32
		3.5	22	30	31	31	31
	0.5	1.5	86	93	92	90	89
		2.0	50	55	55	56	56
		2.5	31	37	38	39	39
		3.0	23	32	32	32	32
		3.5	15	21	22	22	22

Douglas Fir	$K_{IIcr}(0.5) = 1611.31$	$K_{IIcr}(0.05) = 1054.13$
Hemlock Fir	$K_{IIcr}(0.5) = 1659.79$	$K_{IIcr}(0.05) = 976.79$
S-P-F	$K_{IIcr}(0.5) = 1202.53$	$K_{IIcr}(0.05) = 706.16$

TABLE 5: VALUES OF UNSPLIT FACTOR F_u

$$P = F_u \cdot \frac{\tilde{u}}{V^{1/k}}$$

P = Shear Capacity (lbs).
F_u = Shear Factor for Unsplit Material (see below).
t_u = Shear Strength of Unsplit Unit Volume (in^3).
V = Volume of half the Bridge Tie.
k = 5.5

p/h	s/h	$e/h = 0.0$	$e/h = 1.0$	$e/h = 3.0$
1.5	1.0	152	158	167
	0.5	137	142	151
3.0	1.0	116	119	125
	0.5	111	114	120

Douglas Fir	$t_u(0.5) = 2526psi$	$t_u(0.05) = 1578psi$
Hemlock Fir	$t_u(0.5) = 1872psi$	$t_u(0.05) = 1169psi$
S-P-F	$t_u(0.5) = 1778psi$	$t_u(0.05) = 1110psi$

TABLE #6

DISTRIBUTION OF WHEEL LOADS FOR DIFFERENT SPACINGS

Modulus of Elasticity (psi)

Etie	1.80E+06
Erail	2.90E+07

Moment of Inertia (in^4)

Rail	Irail
85#	29.49
100#	48.90
115#	65.60
132#	88.20

Rail Gage: 59"
Girder Spacing: 8.00' (96")

	Tie			% of Wheel Load on Ties		
Rail	Width	Depth	Spacing	R1	R2	R3
85#	10"	12"	14"	34.30%	25.38%	10.63%
85#	10"	12"	28"	53.32%	24.94%	1.94%
85#	10"	12"	42"	69.45%	19.18%	-3.08%
100#	10"	12"	14"	30.72%	23.99%	11.67%
100#	10"	12"	28"	47.59%	26.07%	4.64%
100#	10"	12"	42"	62.53%	22.09%	-1.51%
115#	10"	12"	14"	28.67%	23.01%	12.15%
115#	10"	12"	28"	44.65%	26.40%	6.11%
115#	10"	12"	42"	58.60%	23.45%	-0.21%
132#	10"	12"	14"	26.65%	21.94%	12.55%
132#	10"	12"	28"	41.95%	26.52%	7.44%
132#	10"	12"	42"	54.81%	24.56%	1.29%

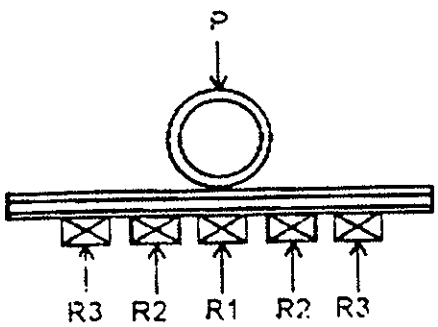

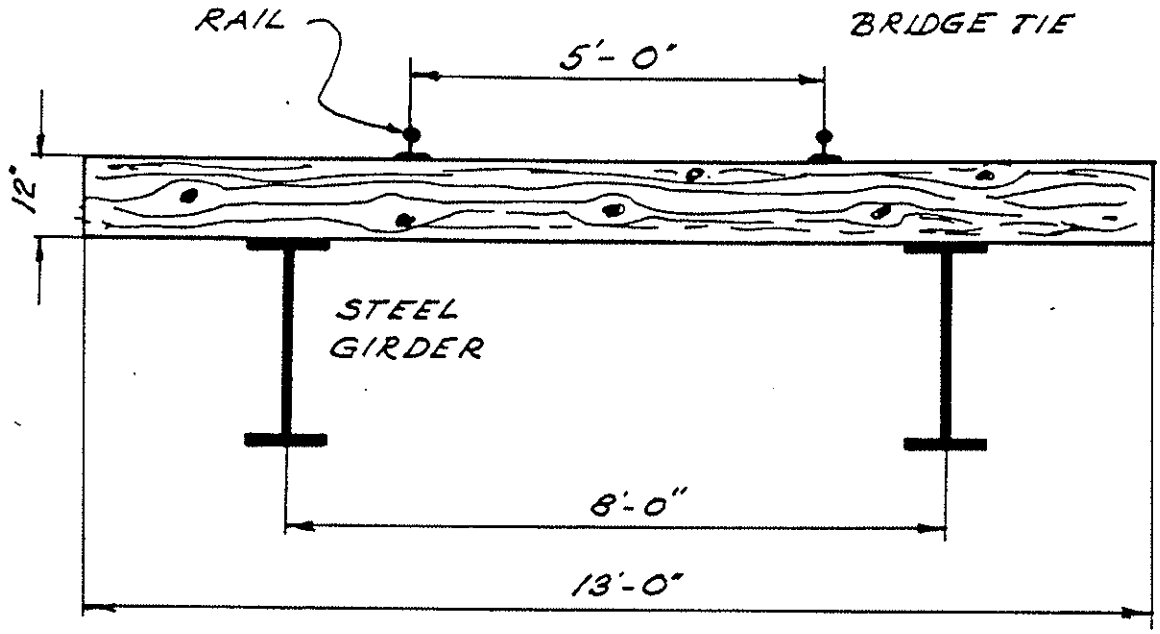

CROSS SECTION

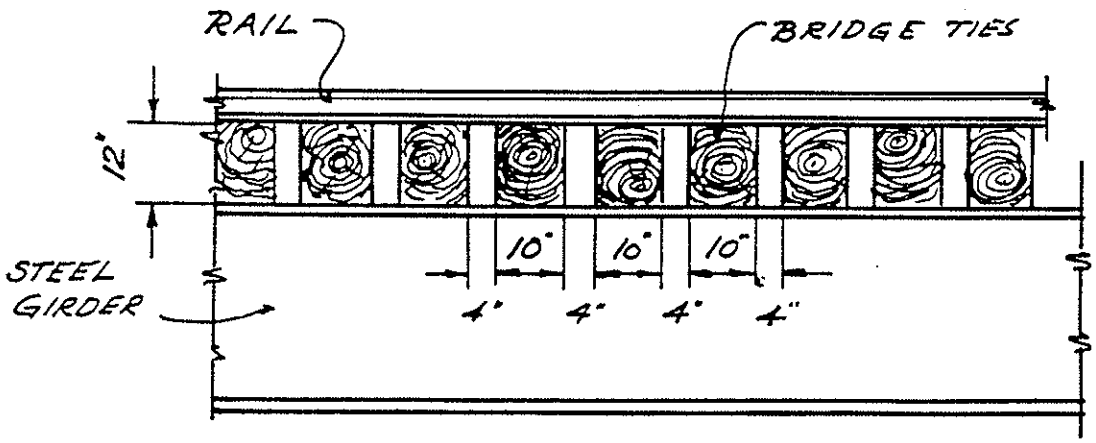

LONGITUDENAL SECTION

FIGURE 1 : Typical Layout of Bridge Ties.

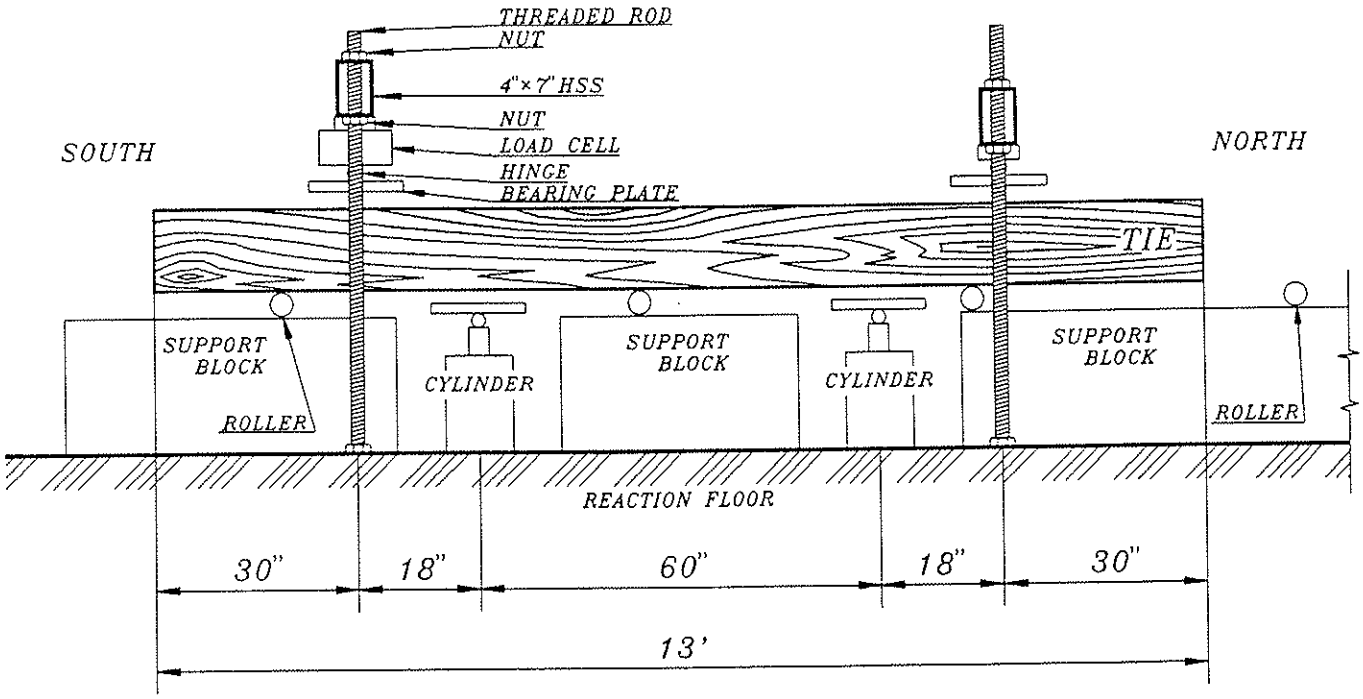

SIDE VIEW

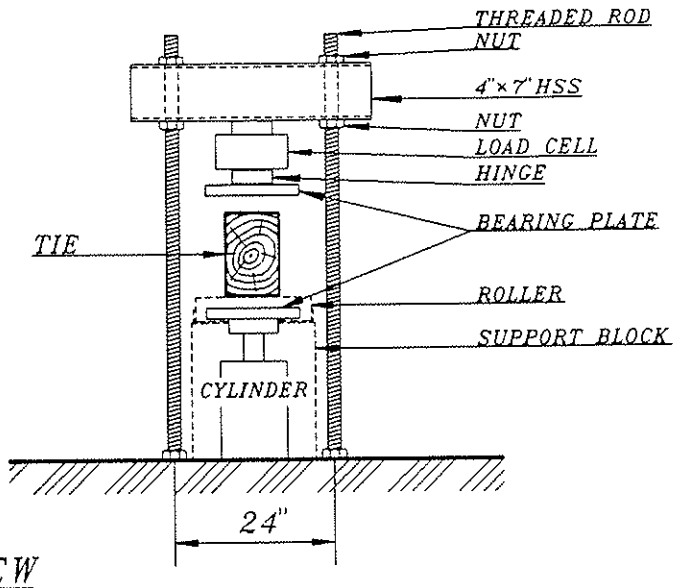

END VIEW

FIG.2. SCHEMATIC OF TESTING SET-UP.

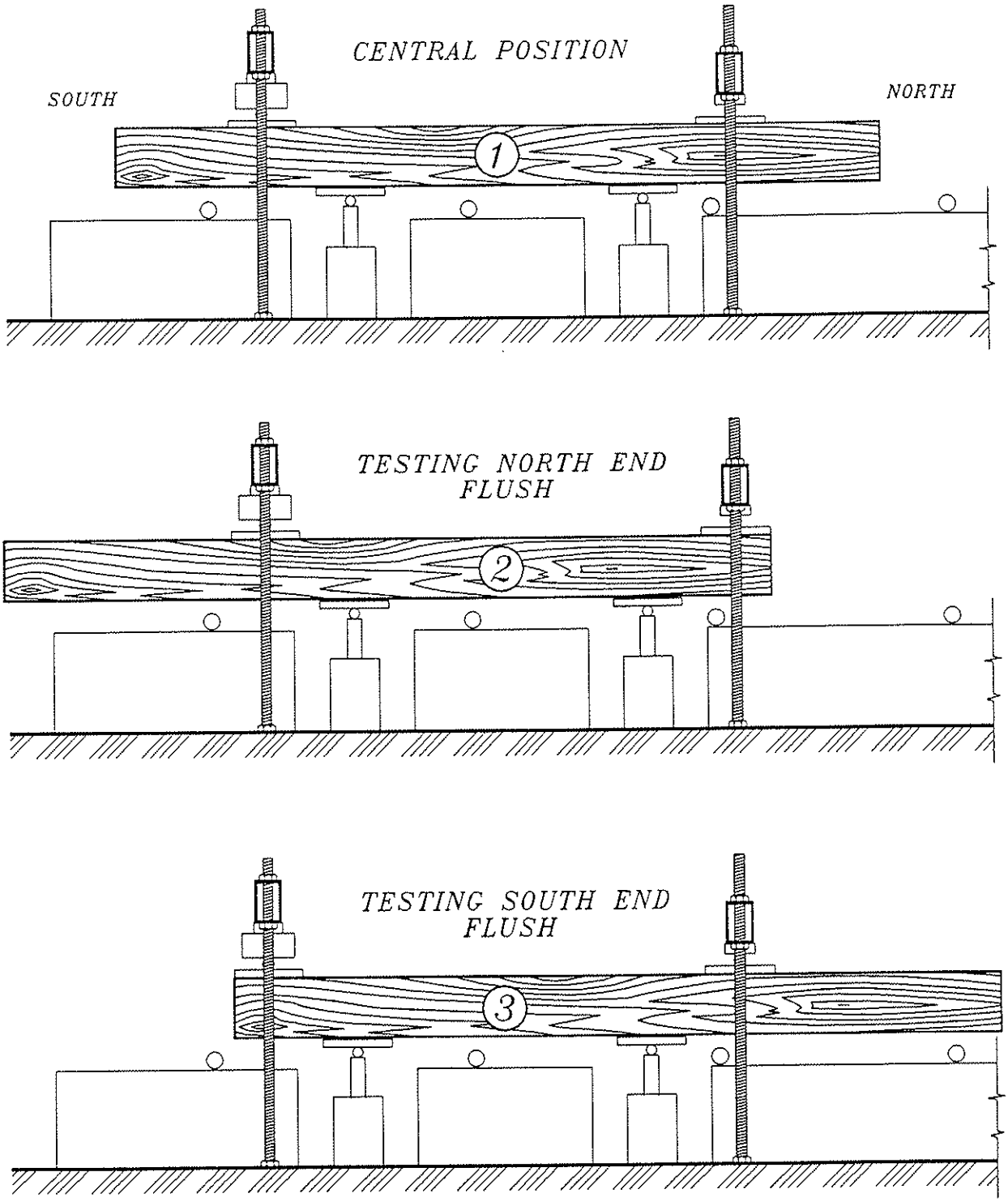

FIG.3. SEQUENCE OF TESTING

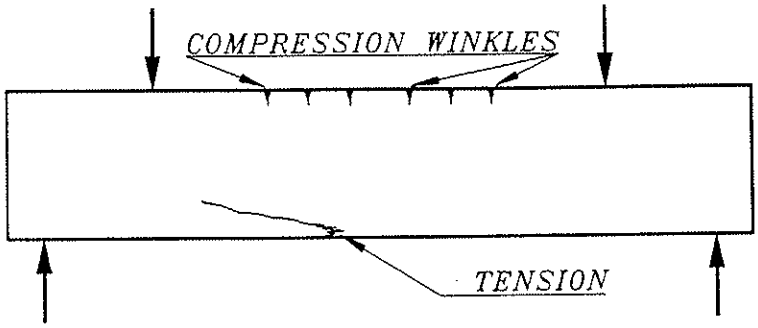

TYPICAL BENDING FAILURES

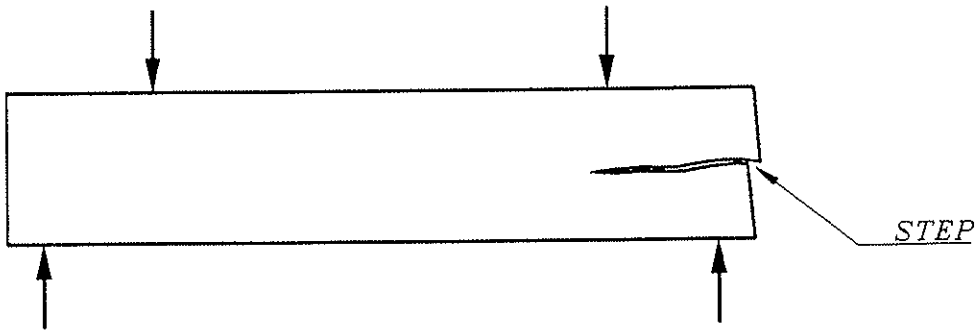

TYPICAL SHEAR FAILURE

FIG.4. TYPICAL FAILURE MODES

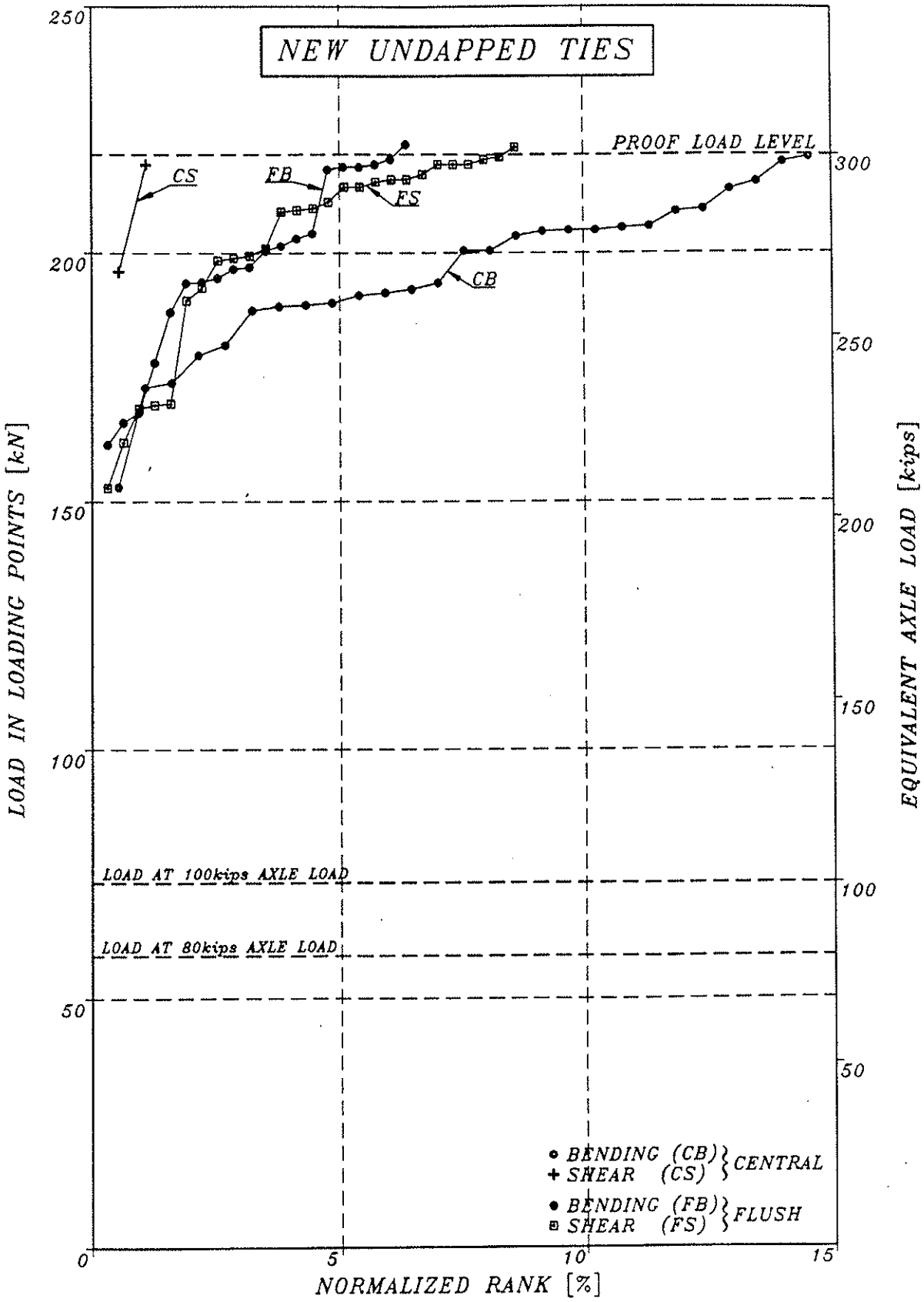

FIG.5. NEW TIES; CAPACITY vs. NORMALIZED RANK

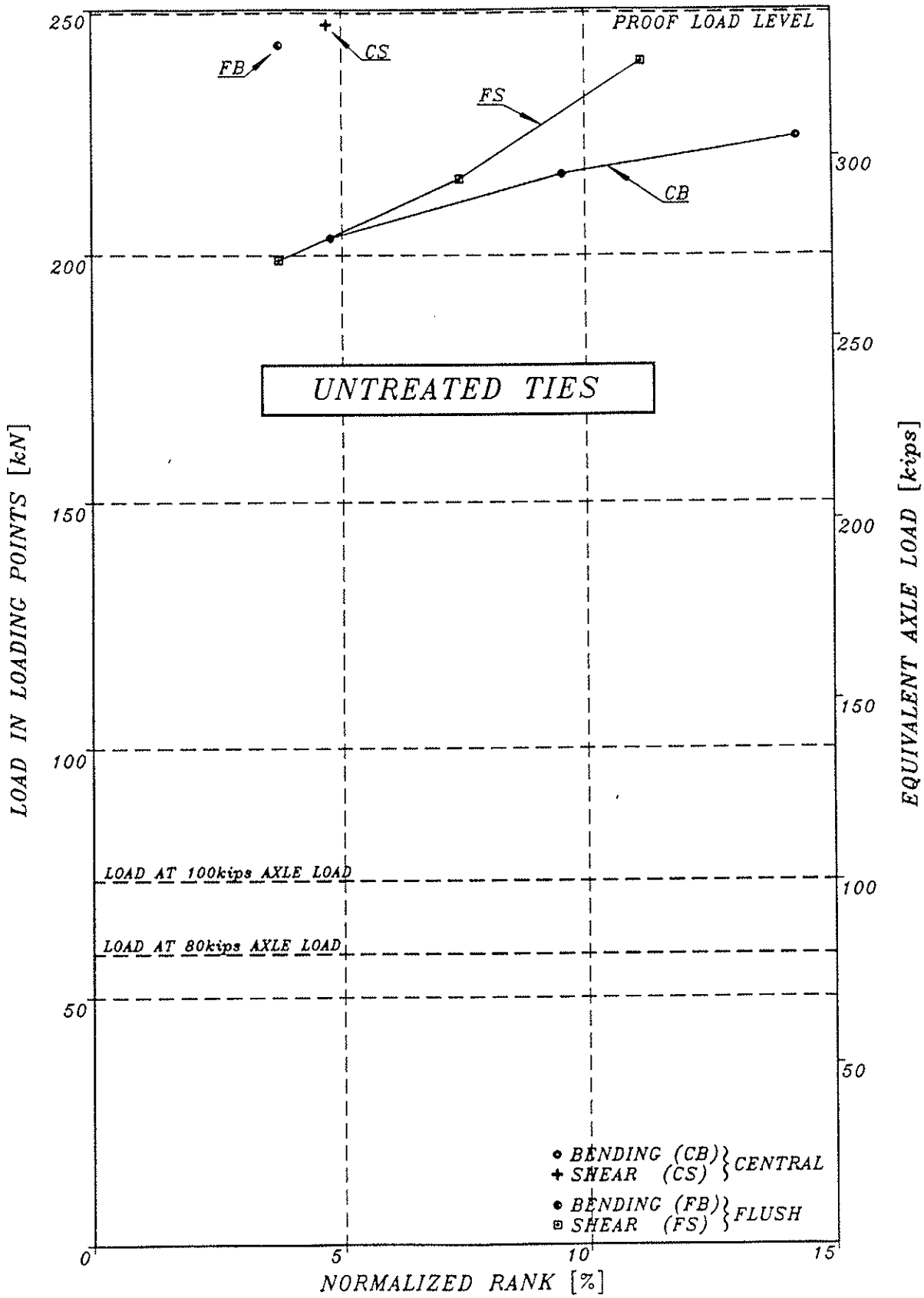

FIG.6. UN-TREATED TIES; CAPACITY vs. NORMALIZED RANK

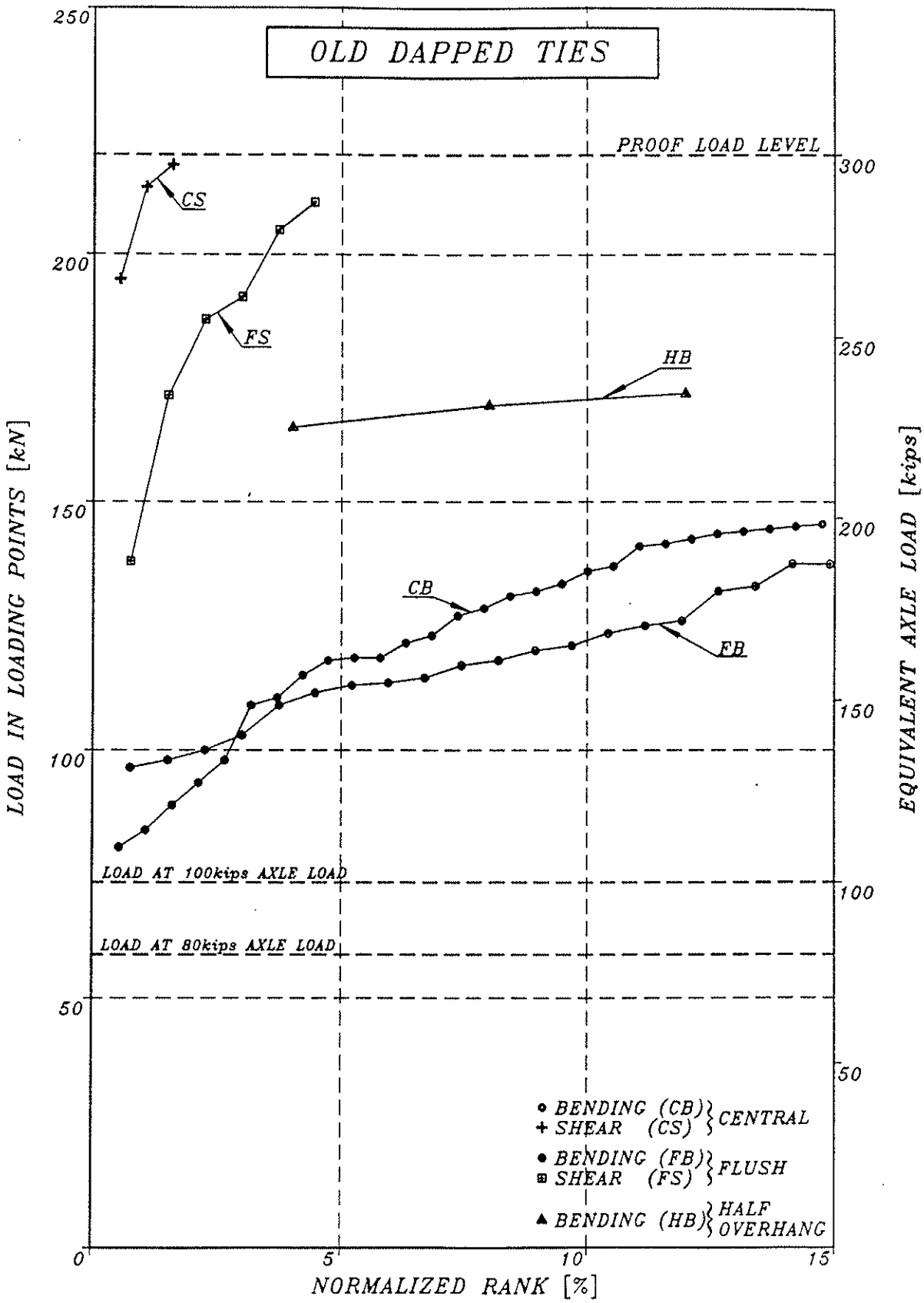

FIG.7. OLD TIES; CAPACITY vs. NORMALIZED RANK

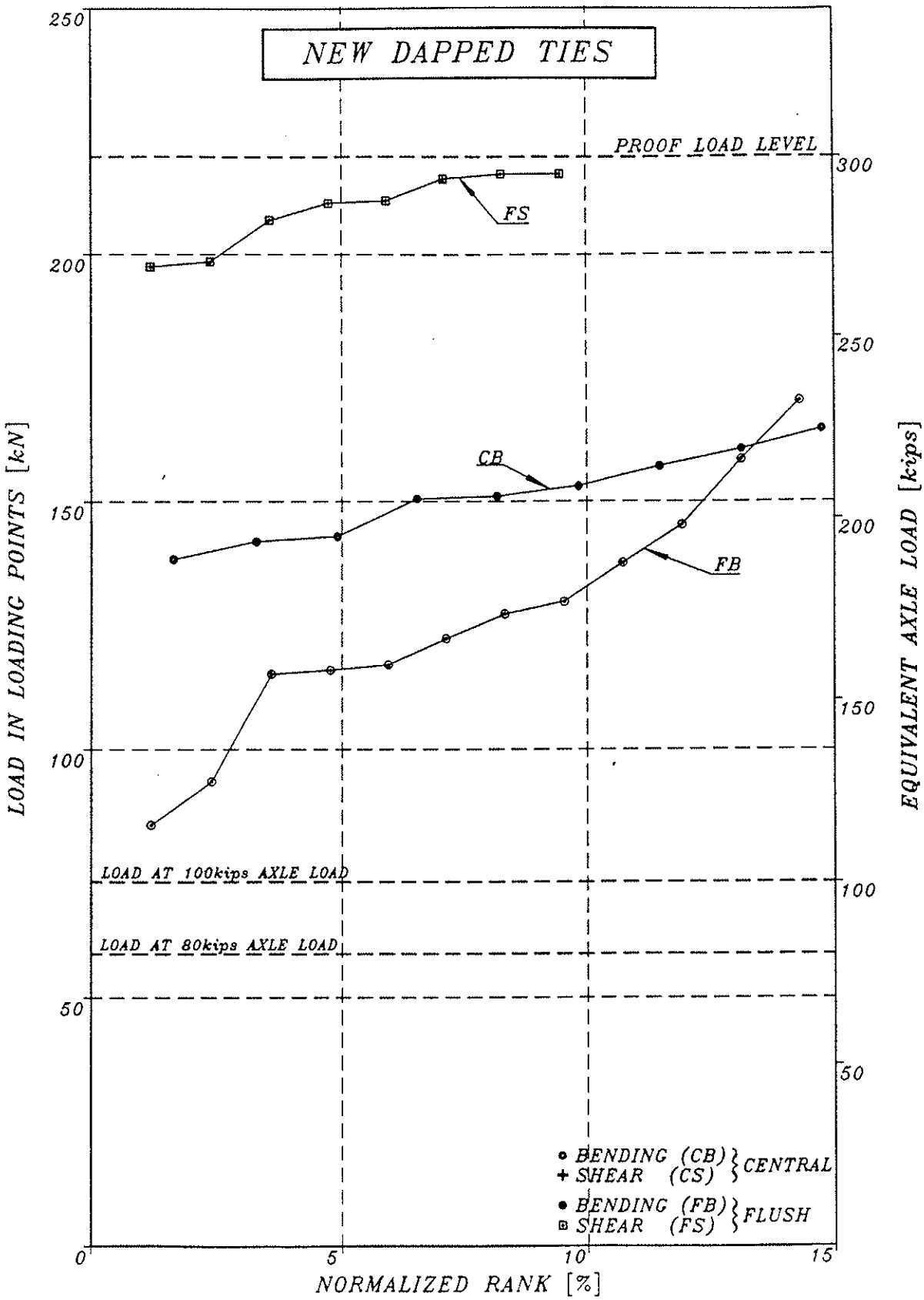

FIG.8. NEW DAPPED TIES: CAPACITY vs. NORMALIZED RANK

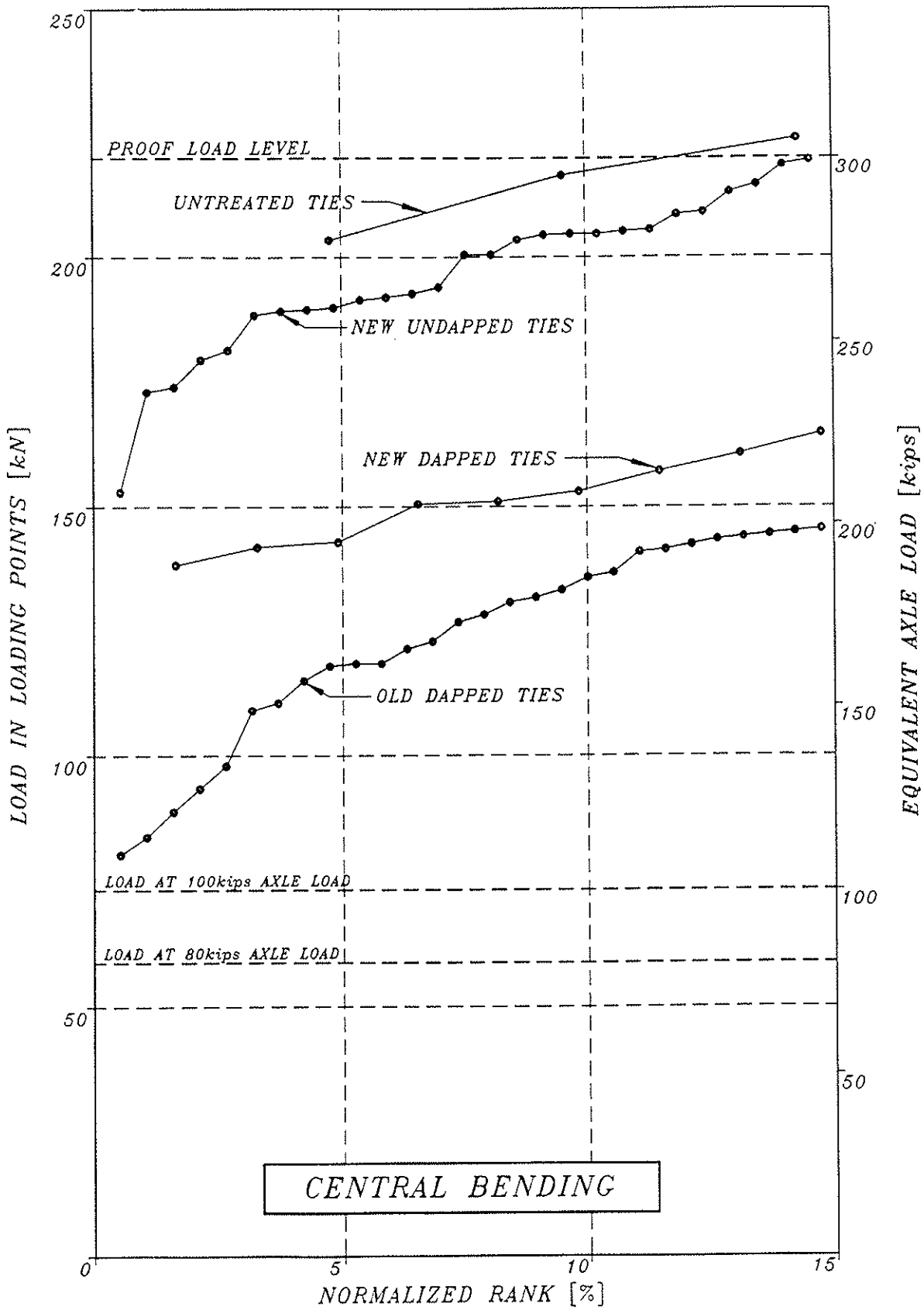

FIG.9. COMBINED BENDING DATA

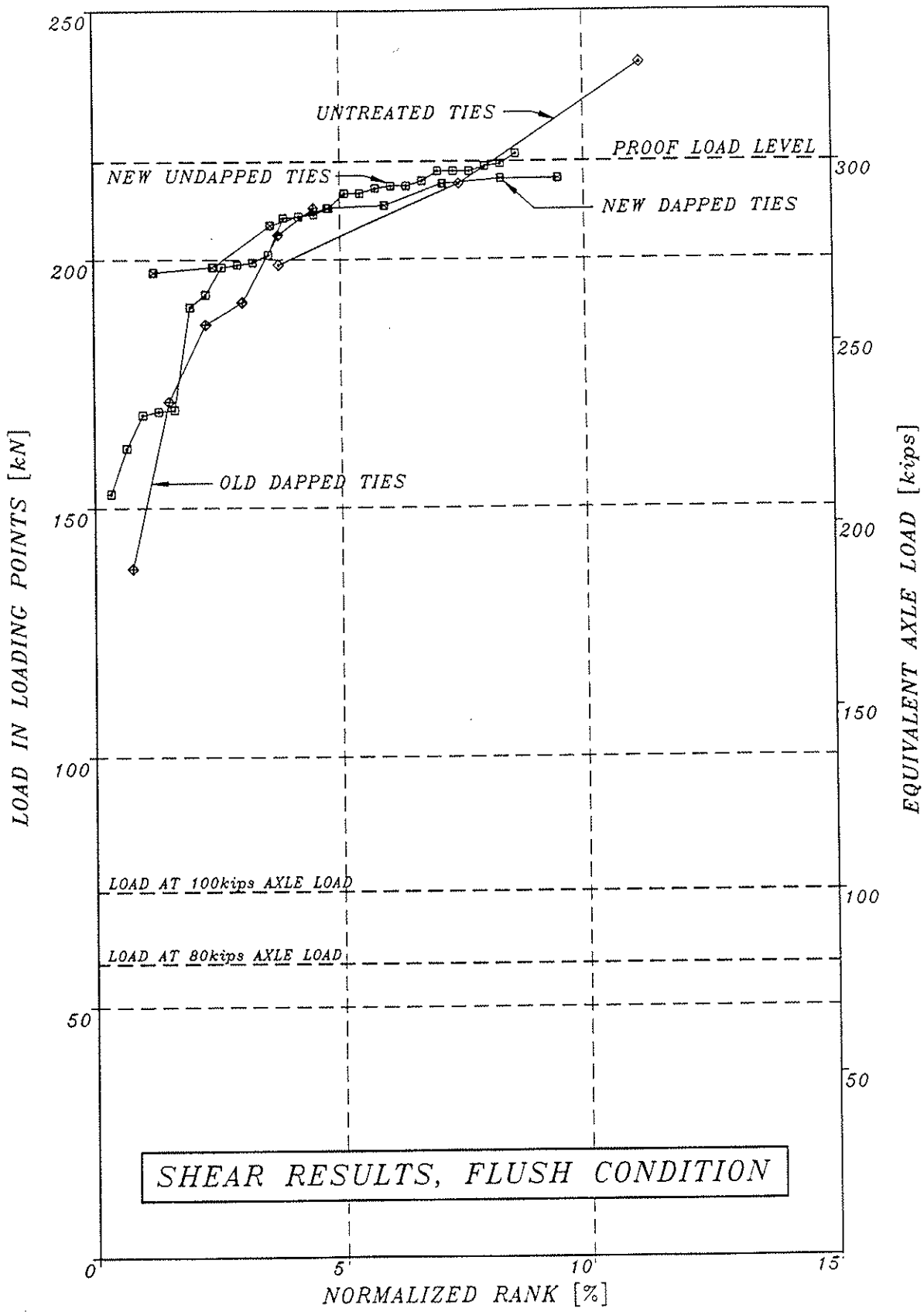

FIG.10. COMBINED SHEAR DATA

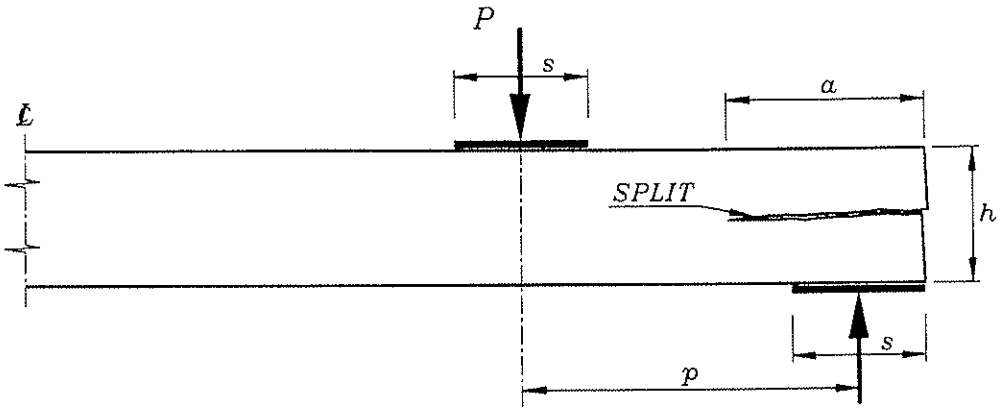

FLUSH END

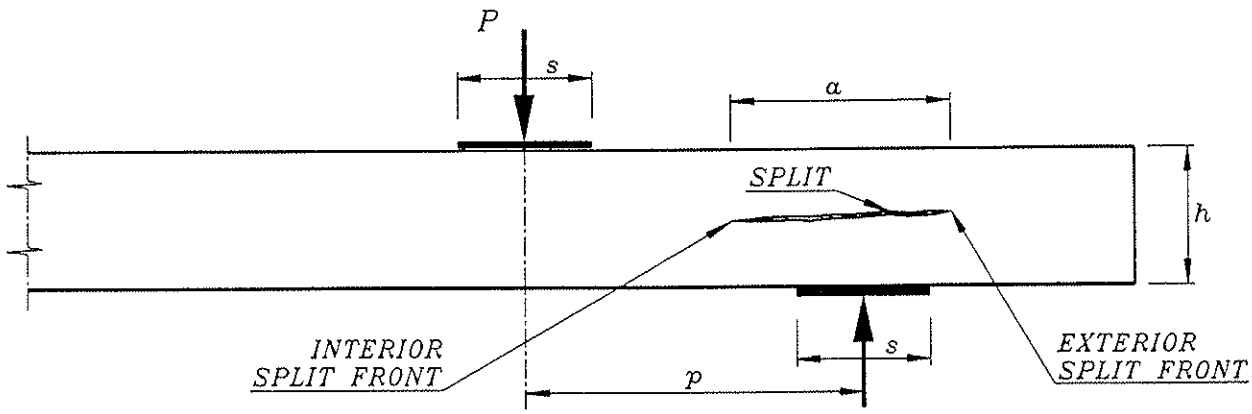

OVERHANGING ENDS

FIG. 11. LOADING CONDITIONS FOR BRIDGE TIES

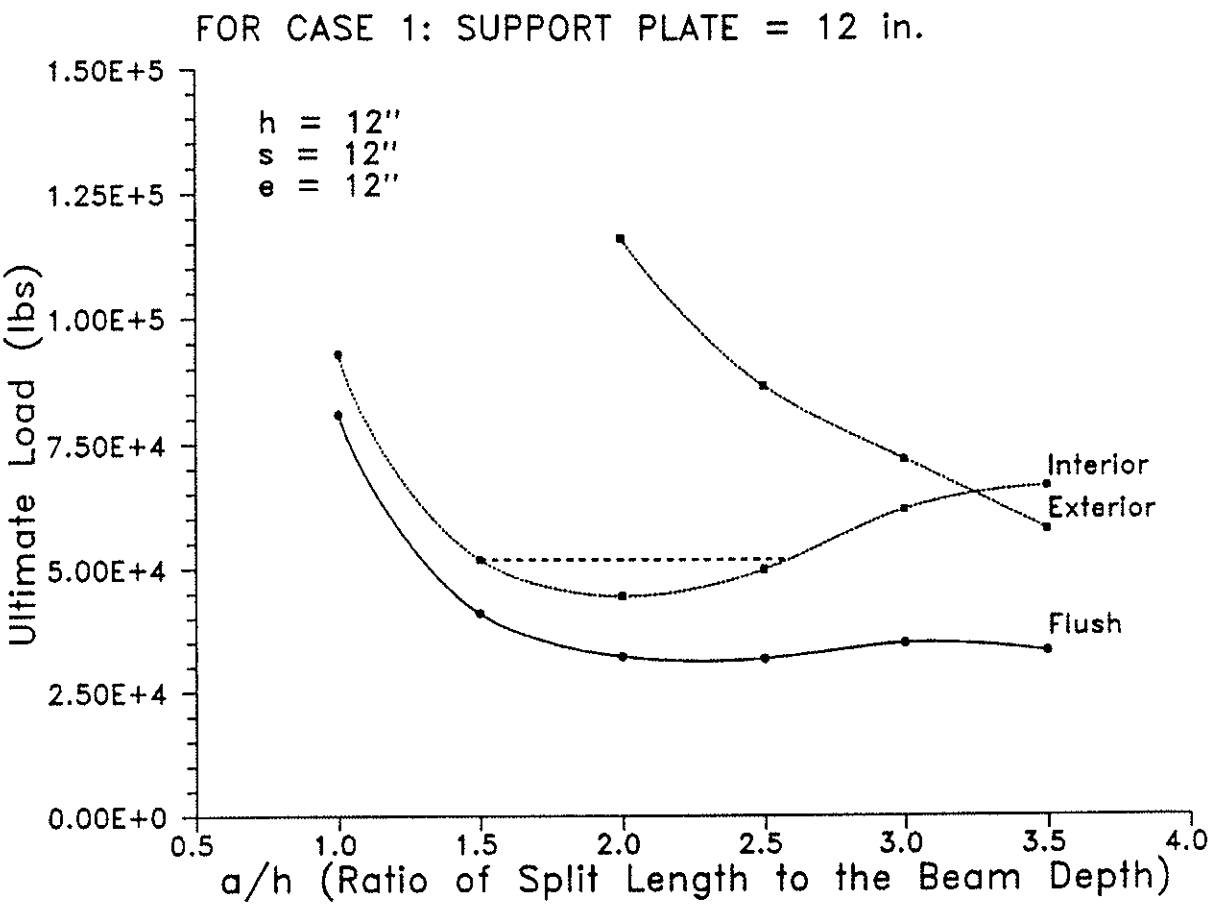

FIGURE 12

SHEAR CAPACITY vs LENGTH OF SPLIT

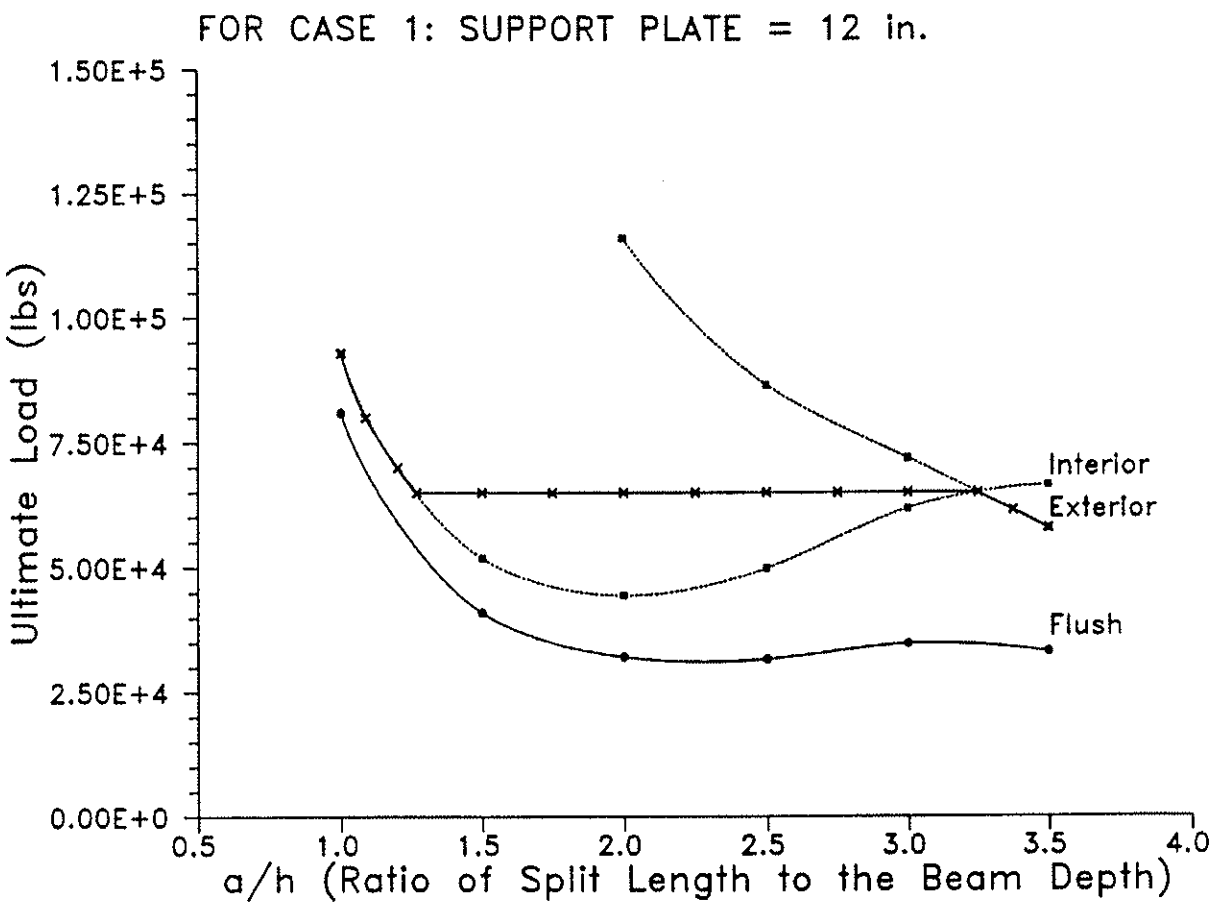

FIGURE 13

DESIGH CAPACITY vs a/h RATIO

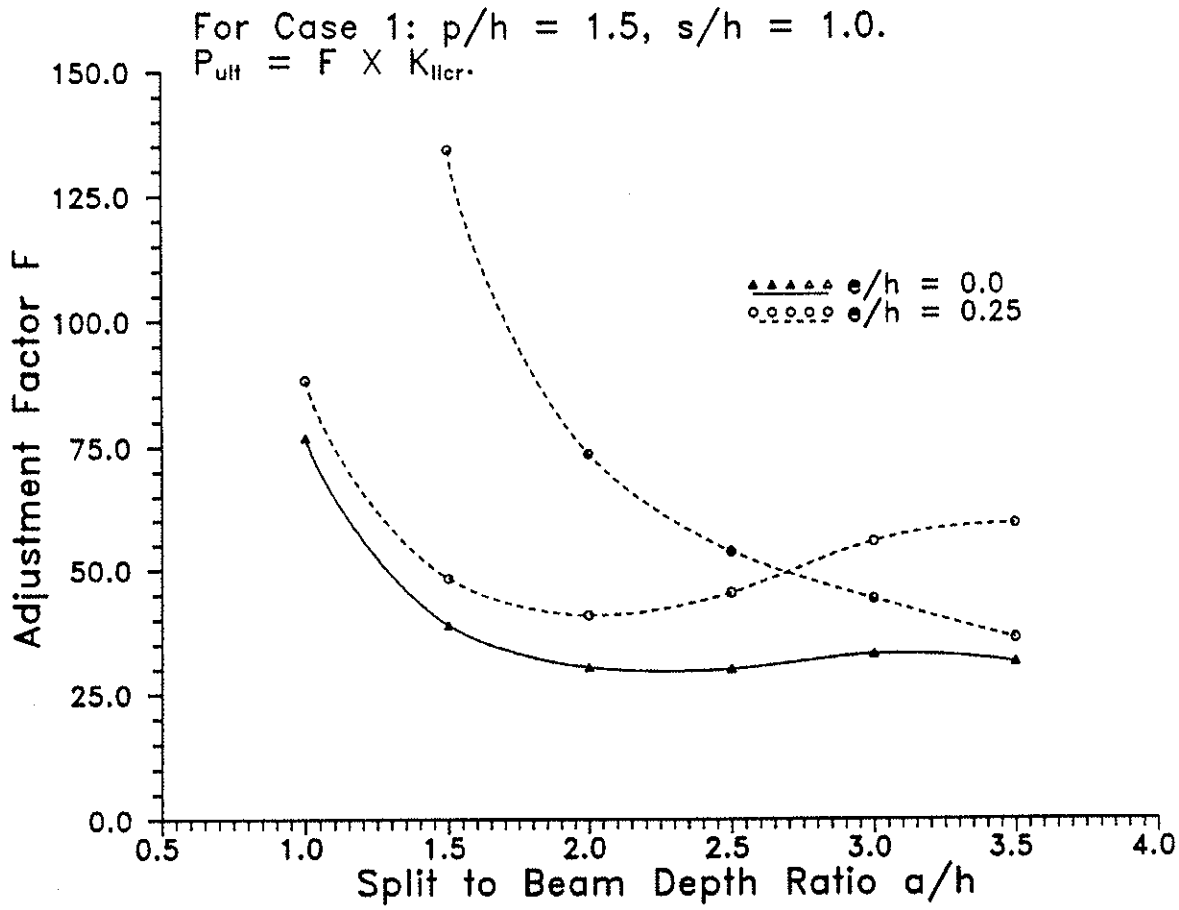

FIGURE 14

ADJUSTMENT FACTOR F vs a/h RATIO

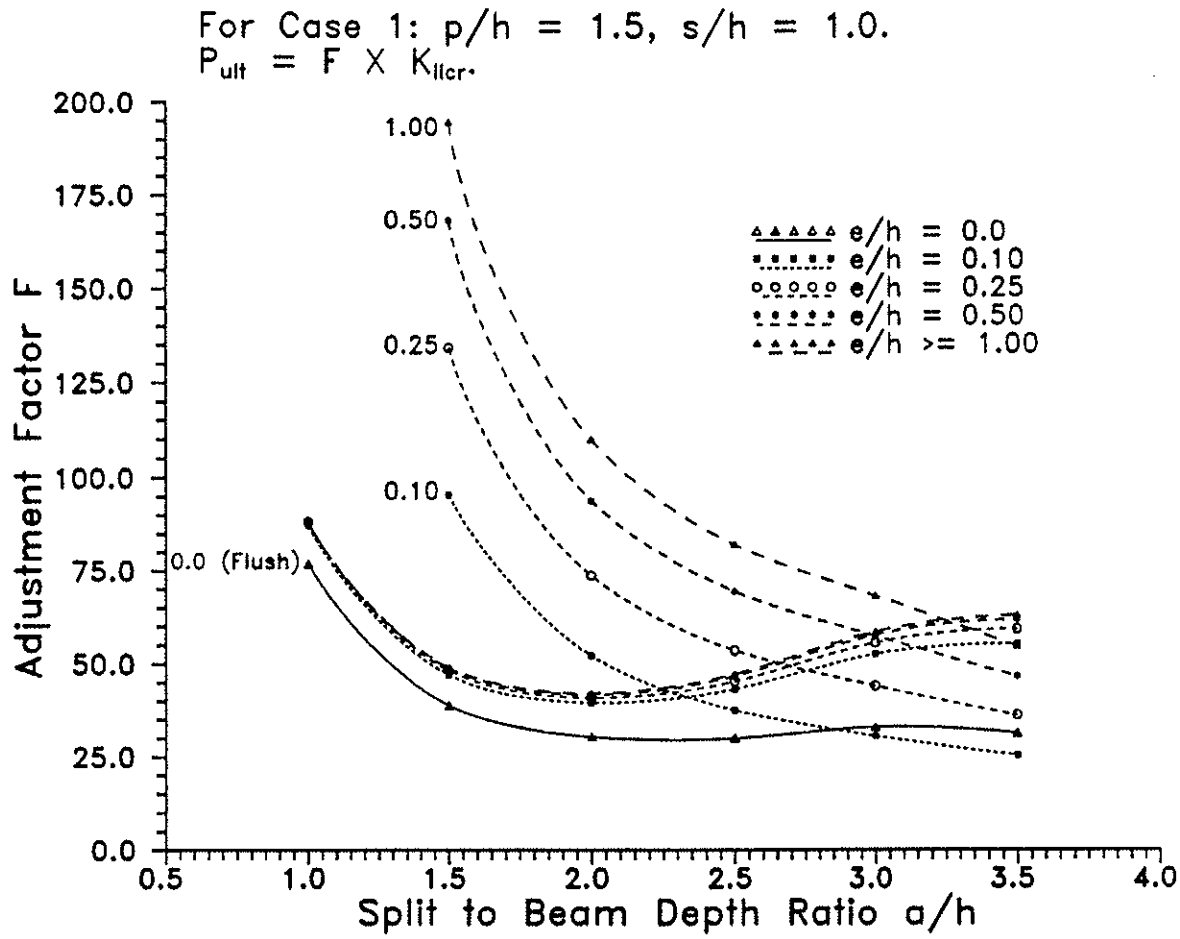

FIGURE 15

FAMILY OF ADJUSTMENT FACTORS vs a/h RATIO

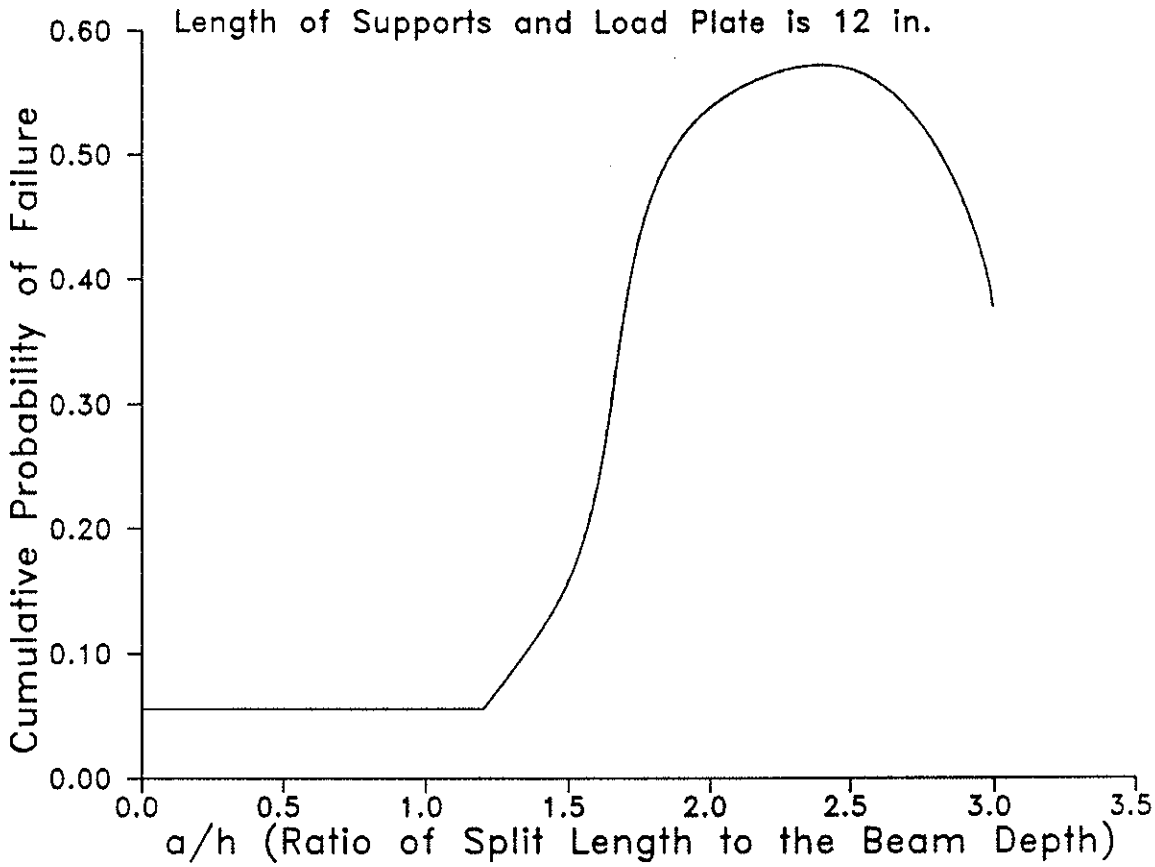

FIGURE 16

CUMULATIVE PROBABILITY OF FAILURE vs a/h RATIO

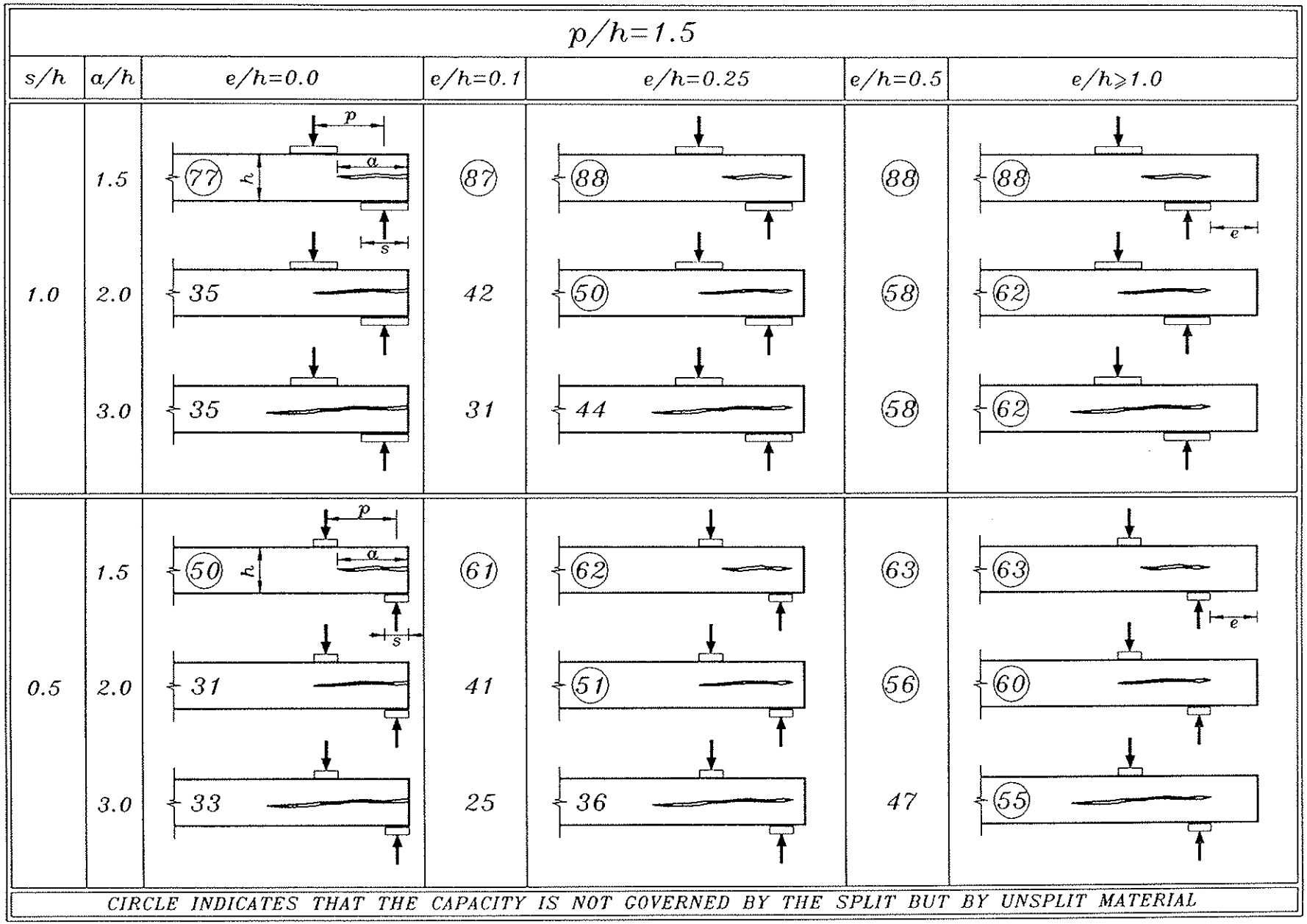

FIG. 17. RELATIONSHIP BETWEEN LENGTH OF SPLIT, LENGTH OF OVERHANG, LENGTH OF BEARING PLATE, AND CAPACITY FOR p/h=1.5

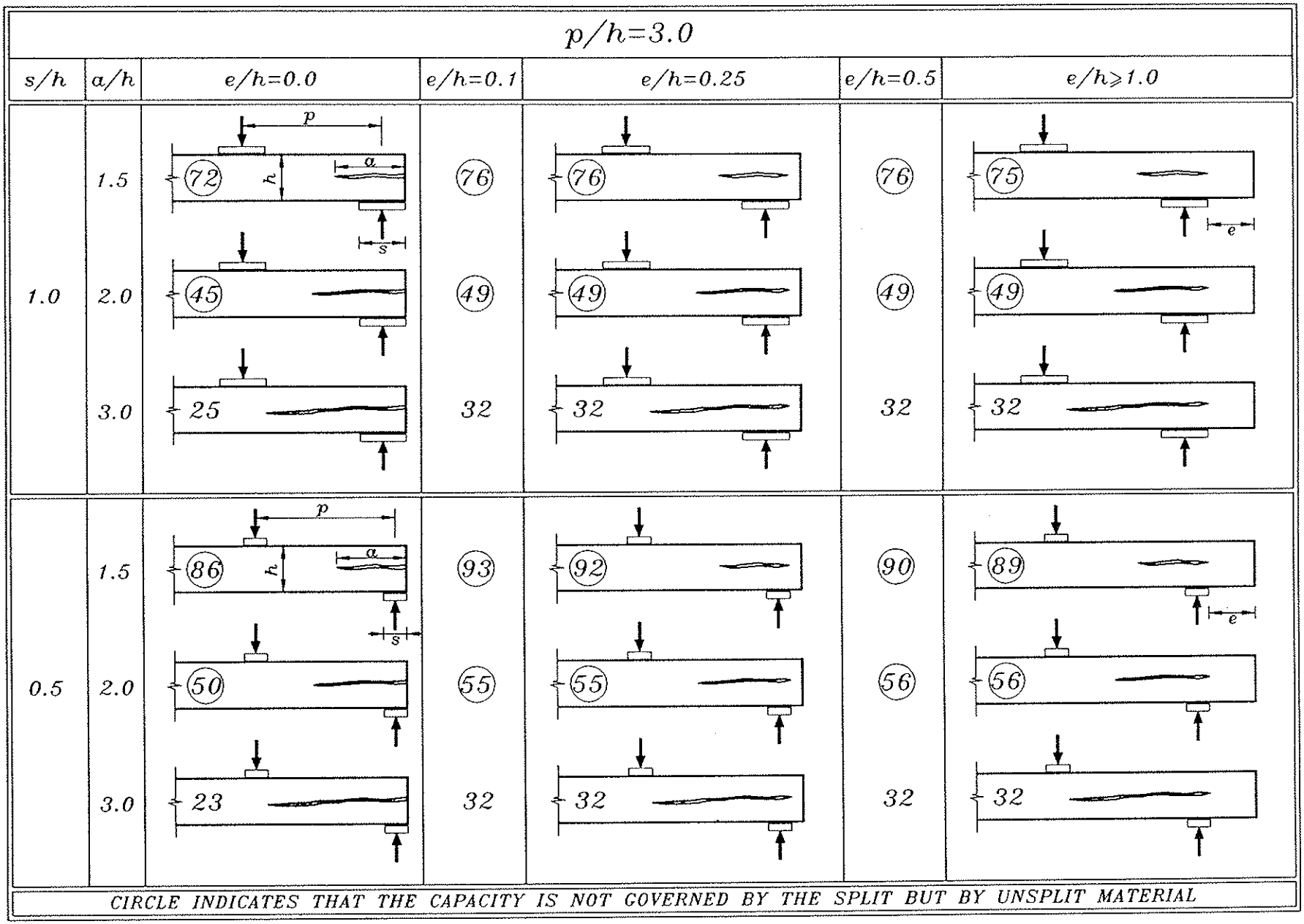

FIG. 18. RELATIONSHIP BETWEEN LENGTH OF SPLIT, LENGTH OF OVERHANG, LENGTH OF BEARING PLATE, AND CAPACITY FOR p/h=3.0

CIB-W18/28-6-3

INTERNATIONAL COUNCIL FOR BUILDING RESEARCH STUDIES AND DOCUMENTATION

WORKING COMMISSION W18 - TIMBER STRUCTURES

ON THE INFLUENCE OF THE LOADING HEAD PROFILES ON DETERMINED BENDING STRENGTH

by

Ł Muszyński
Agricultural University of Poznan
R Szukala
Institute of Wood Technology, Poznan
Poland

MEETING TWENTY - EIGHT

COPENHAGEN

DENMARK

APRIL 1995

ON THE INFLUENCE OF LOADING HEAD PROFILES ON DETERMINED BENDING STRENGTH

L.Muszyński*, R.Szukała**

**Dept. of Engineering Mechanics & Thermal Techniques, Agricultural University of Poznań, POLAND*

***Institute of Wood Technology, Poznań, POLAND*

ABSTRACT

Since most of the wide spread standards for the bending test on timber in structural sizes assume the elementary bending theory consequently they neglect the influence of the stress concentrations induced in the load application zones. Analytical solutions as well as the finite element simulations of contact problems report the stress concentration to be significant (esp. for orthotropic material like wood) and it's magnitude dependant on loading force distribution. Therefore the assumption neglecting the stress concentration influence on determined bending strength is valid on condition that either standards require such a loading head profiles that minimizes the stress concentration magnitude or the influence is believed to be of secondary meaning when compared with influence of wood structure irregularities (like presence of knots or grain slope). Standards however usually do not specify precise requirements for the load heads profiles. Moreover, a preliminary test results presented in the paper show a significant difference between the bending strength determined using loading heads of different profiles (both allowed by most standards). The test results will be discussed during the presentation.

INTRODUCTION

Since most of the wide spread standards for the bending test on timber in structural sizes assume the elementary bending theory consequently they neglect the influence of the stress concentrations induced in the load application zones. In the same time a little attention is paid to the load application conditions. Usually standards require the specimens "*to be supported on rollers, or by other devices which achieve an acceptable free support condition*" and allowe "*small plates to be inserted between the specimen and the loading heads and supports to minimize local indentation*" (ISO 8375-1985 E). Some of them precise that the plate shall not be longer than a half of the specimen depth (DIN EN 408) or require the minimal loading head radius (roller or other cyllindrical shaped that provide propper supporting conditions) to be no less than 1.5 times the specimen height (PN - 84/D-04153). An exception was a German standard DIN 52-186 where rectangular hardwood bars with rounded edges of length equal to the specimen height were required.

This reflects rather common conviction that load application conditions have a secondary and limited influence on the bending tests when compared with usually considered and frequently discussed - as the climate conditions, size effects, natural nonhomogenity of wood (in that number presence of knots, grain slope and other defects and 'anomalia').

Some experiments however, contradict the coviction. According to data presented by Perstorper (1994) 21.7% of total number (323) of 70 x 290 x 2900 mm^3 specimens tested in bending failed in load application zones of 30cm (app. one specimen depth) and the fraction increases to one third when the 50cm zones are considered (Fig.1). In the same time fraction of pieces failed between the zones was 63.8% or 54.8% respectively.

Also in other bending tests (conducted in Poland) closer examination of the broken specimen surface in place where the roller (of radius 1.5 specimen depth) is applied shows not only a permanent dent but quite often also a characteristic compression failure in

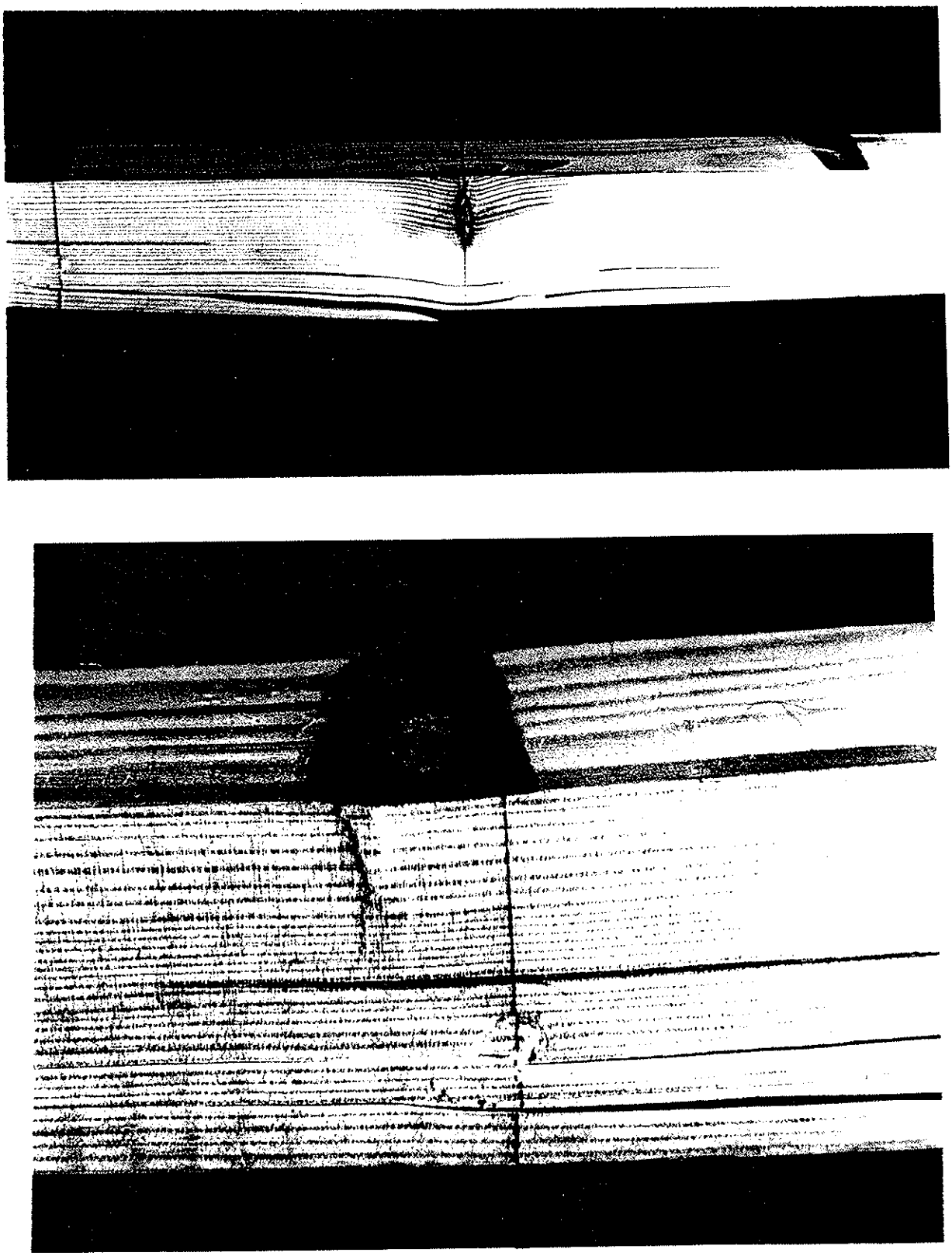

Fig.2 Examples of the longitudinal compression failure in the bottom of transverse dent left by loading head of roller type.

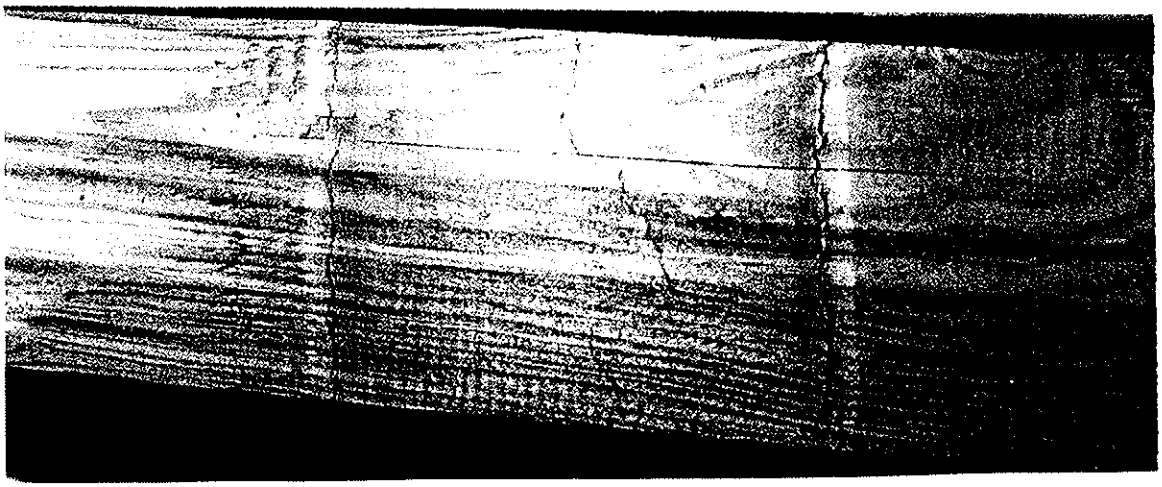

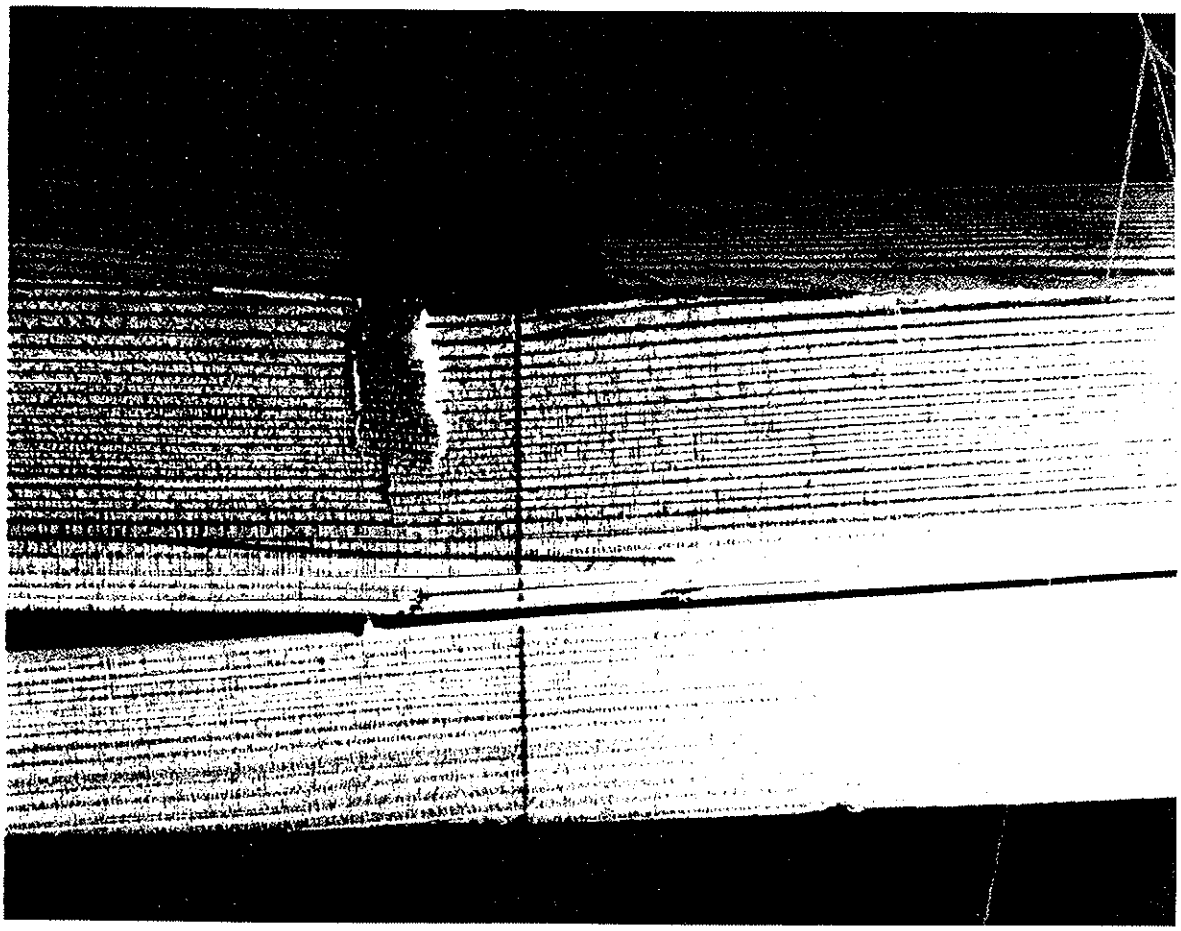

Fig.3 Examples of the longitudinal compression failure in the bottom of transverse dent left by loading head of roller type.

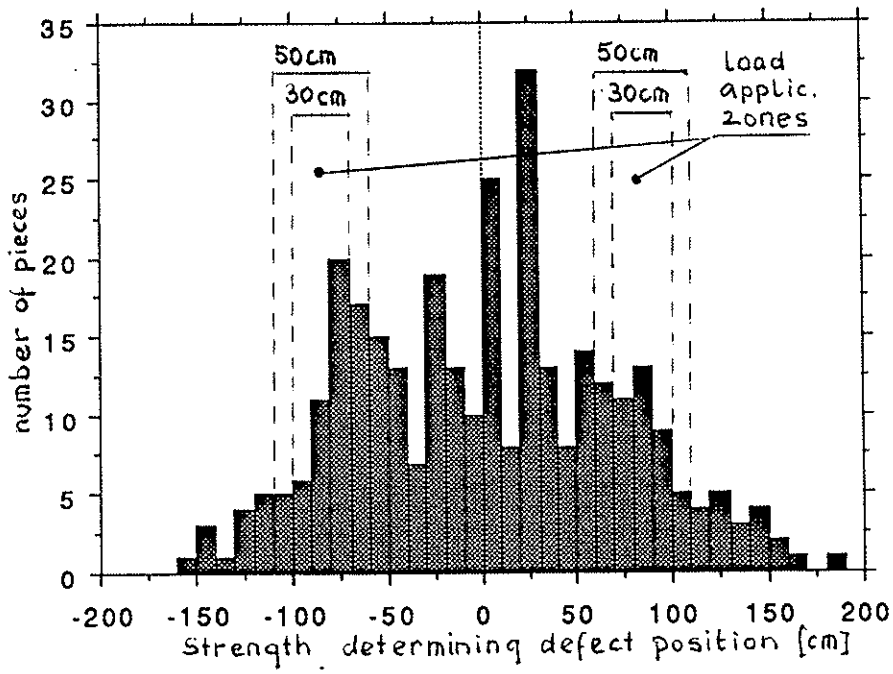

Fig.1 Strength determining defect position for 323 beams of 70 x 290 x 2900 mm³ (Perstorper 1994).

direction parallel to grain in the dent bottom - even when the specimen finally breaks in the tension side...(Fig.2 and 3). This observation is in general agreement with plane stress analysis for the contact zone which indicates not only presence of perpendicular to grain compression stresses under the loading head but also a strong compression stress concentration in longitudinal direction which coincides with maximum compression stresses assumed by elementary bending theory (Timoschenko, Goodier 1962). The main elastic stress components of bending and transverse compression superposition in terms of longitudinal and transverse direction is presented in Fig.4.

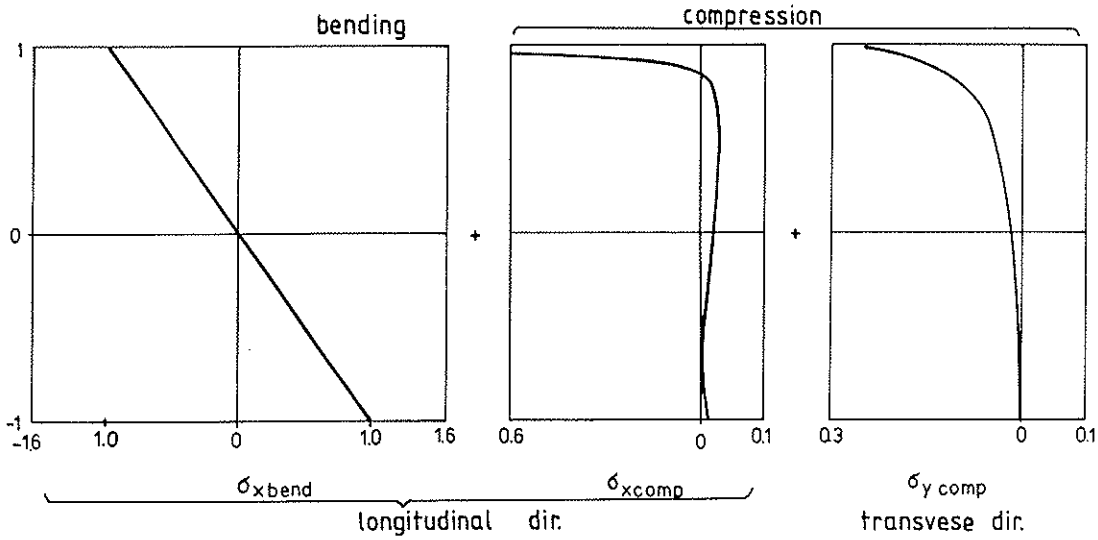

Fig.4 Load application zone cross section: plane stress components (without shear) in longitudinal and transverse direction

Proportion of the components depend on different aspects of contact condition:

$\sigma_{y\,comp} / \sigma_{x\,comp}$ ratio is governed by material elastic compliance matrix (for softwood it is approximately 0.33 to 0.42), while the load distribution influence is not significant;

$\sigma_{x\,comp} / \sigma_{x\,bend}$ ratio is governed by contact area magnitude and contact pressure distribution, loading head rigidity and bending test geometry (transverse load to moment ratio). Fig.5 presents elastic contact pressure distributions under loading heads of different profiles.

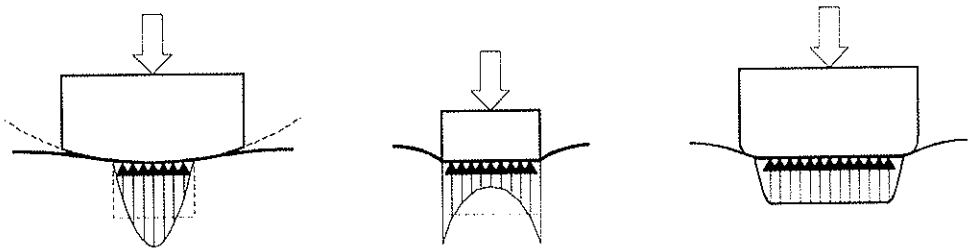

Fig.5 Elastic contact pressure under loading heads of different profiles.

Approximate values of $\sigma_{x\,bend} : \sigma_{x\,comp} : \sigma_{y\,comp}$ proportion obtained from finite element analysis for the same loading level for different transverse pressure distributions standing for different contact conditions are given in Table 1 (α = *average-contact-width / specimen-depth* is contact area ratio at given load level).

Table 1. Simulated proportion of plane stress component under loadings of different distribution (Muszyński 1994).

loading head profile simulated	contact area ratio	stress component ratio		
	α	sx bend	sx comp	sy comp
concentrated force	~ 0	100	91	30
rigid roller (R=1.5h)	0.2*	100	63	25
elastic bar	0.8	100	11	3

*the value was determined using Hertz formula for isotropic elastic body ($E = E_T$) - Hertz formula for orthotropic bodies (developed by Mozharovski 1990) and the experimental formulae (proposed by Zieleśkiewicz 1990) for the simmilar loading case give values of α between 0.033 and 0.1.

Above proportion holds for elastic strain range. However, as the transverse compression strength is one of the weakest wood parameters in real bending tests the transverse compression yielding under rollers (or loading heads of cyllindrical profiles) begins while the nominal bending stress reaches 20 to 68% of it's ultimate value - depending on assumed elastic contact area ratio and proportion of longitudinal to transverse compression strength (Fig.6). Then the contac area increases significantly. That's why the contact area ratio measured on beams undergoing destructive tests reaches 0.3 or even 0.6 when excessive plastic deformation takes place. It is difficult to evaluate the influence of perpendicular to grain yielding on the bending strength analytically but it should be seriously taken into account as the palstic deformation zone coincides with the

maximum compression stress induced by bending and increased by the longitudinal compression stress component induced by transverse loading. Simillar problem is with prediction when the two components would induce longitudinal compression yielding. Nevertheless, the rough analysis above suggests that for severe contact conditions the plastic deformation would appear significantly earlier than the elementary beam theory assumes and the contact area ratio to be one of the key strength determining factor for loading heads of roller type. On the other hand elastic hartwood bar proposed by DIN EN 52 186 give constant - load invariant - contact area of α=0.8 and is believed to induce uniform distribution of contact pressure.

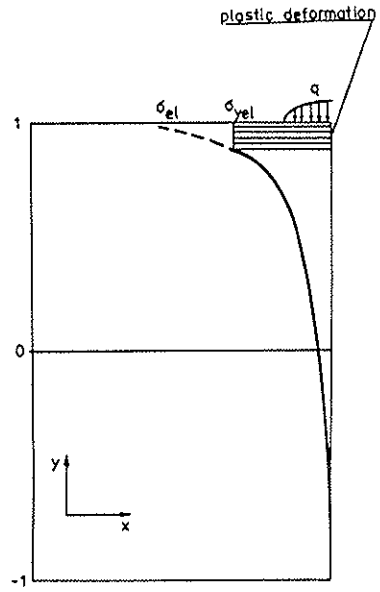

Fig.6 Tranverse compression yielding under load application zone.

The question is then - how much does the loading head profile affect the bending test results when other strength influencing factors are present.

EXPERIMENT

A simple experiment was conducted in order to investigate the actual influence of the stress concentration in load application zone on the tests results. Pine and spruce knoty timber with of different sizes used in the experiments were formerly subjected to series of non destructive tests connected with machine stress grading verification.

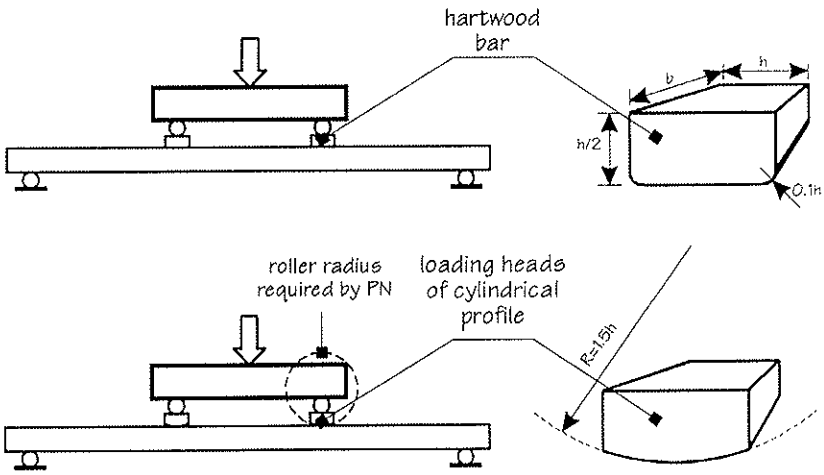

Fig.8 Bending tests scheme and the loading heads profiles used in the experiment

A sample of 67 pine and 26 spruce timber of different sizes was divided into two groups of similar number of pieces in each size.

The density and Modulus of Elasticity MOE distributions in the two groups didn't

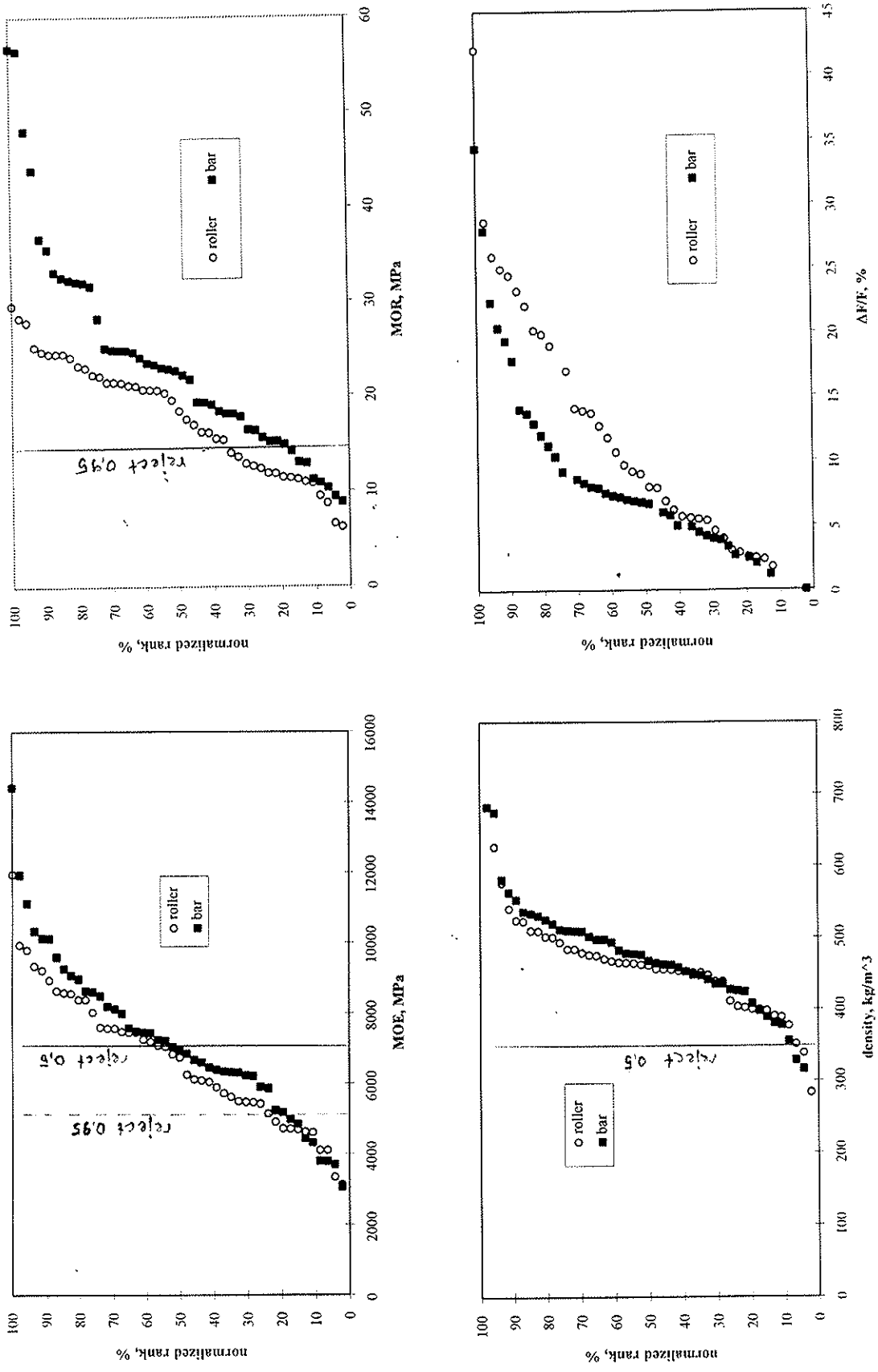

Fig. 7. Distribution curves for two groups of specimens being tested: a) MOE, b) density, c) MOR and d) ΔF/F

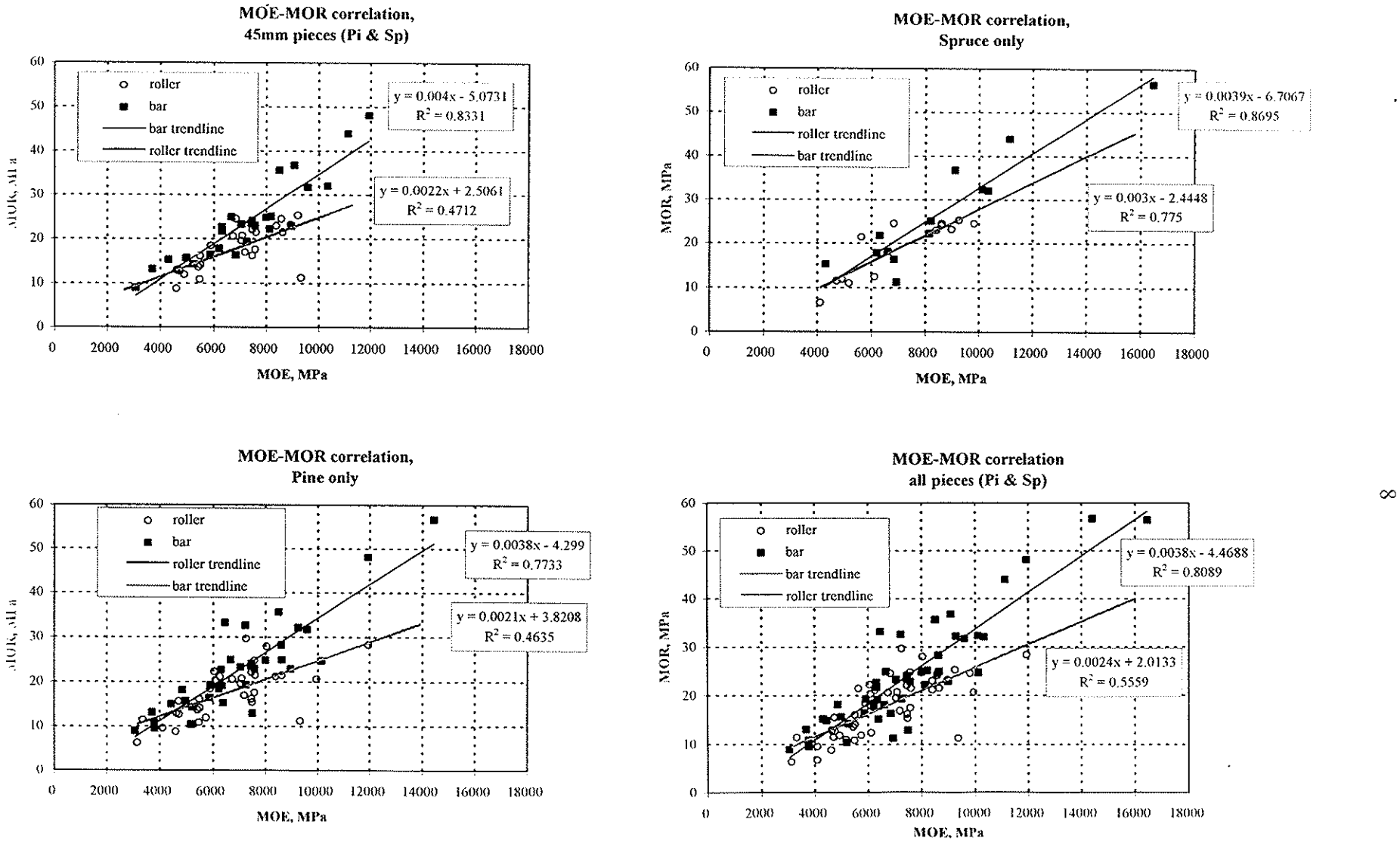

Fig. 9. MOE-MOR correlation trendlines for two groups of specimen being tested.

differ significantly (Fig.7a, b). Consequently they were supposed to have similar strength distributions.

Then (MOR) in bending was tested where the same bending scheme satisfying the free support condition and two different loading head profiles were used. One group was tested using the loading heads of cylindrical shaped profile (called 'roller') satisfying Polish Standard PN - 84/D-04153, the second group was tested using rectangular bars of hardwood (called 'bar') satisfying the German Standard DIN 52 186 - both satisfying the quoted ISO requirements (Fig.8). Modulus of Rupture (MOR) for specimens of different size were recalculated using correction factor K_h taken from DIN EN 348/1990:

$$R_{200} = R_x / K_h, \qquad K_h = (200/h)^{0.2}.$$

The resulting MOR distribution curves for the two groups (Fig.7c) differ significantly beginning at 10% level (under the reject limit) and keep almost constant distance - at least 2MPa (one class interval). At 75% level they split drammatically.

The difference is even more evident when we look at MOE-MOR correlations for the two specimen groups. MOR of pieces tested with 'rollers' are significantly underestimated. Similar difference show samples of pine and spruce timber considered separately as well as pieces of dominating sizes (Fig.9). In all cases the determination factor is much weaker for the 'roller' group. The only possible explanation of the difference is the influence load applicaton conditions.

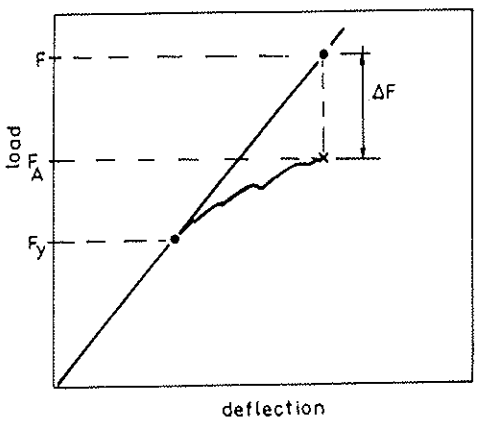

Fig.10 Concept of force reduction factor.

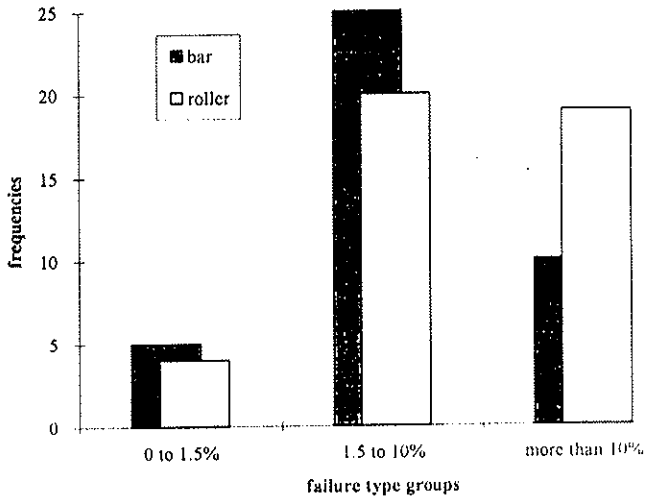

Fig.11 Number of pieces undergoing different failure types.

The longitudinal compression yielding was observed as increased deflection or reduction of force on force-deflection diagrams level since the yield limit is achieved. The magnitude of the reduction for pieces of the two specimen groups was expressed (quantified) in terms of Force Reduction Factor (FRF) - ΔF/F (Fig.10) and divided into three groups of bending failure modes with respect to ΔF/F value acording to criteria proposed by Perstorper (1994). Number of pieces ascribed to groups of less than 1.5%, 1.5% to 10% and more than 10% is presented in Fig.11. Since the yielding behaviour during bending tests is usually ascribed to stronger pieces of clear wood (Buchanan 1990, Malhotra, Bazan 1980, Perstorper 1994) the possible explanation of the fact that number of pieces from the weaker ('roller') group undergoing the third failure case is twice the number of pieces from the stronger ('bar') group - is that higher longitudinal stress concentration under roller makes specimens from the 'roller' group yield earlier. The same conclusion comes from Fig.7d. The ΔF/F dstribution curves of pieces from both groups split at 50% level.

CONCLUSIONS

It appears from the experiment results that the bending strength obtained in tests with loading heads of roller type, that are allowed by most standards, is significantly underestimated and the MOE-MOR correlation much worse when compared with tests where rectangular hardwood bars were applied.

From the statement the conclusion follows that the contact conditions under the loading heads of different profiles significantly influence the static bending tests' results and consequently affect the MOE-MOR correlation which is basic for most strength grading systems and is widely used for a number of non-destructive grading methods callibration. It follows also that the contact conditions in load application zones may be considerabely improved by applying propper loading heads profiles and materials.

The conclusion may be also of interest for other bending strength vs other non-destructive-parameter correlations reliability and comparability and is of special importance right now - while the new standards for strength grades is discussed.

At present, bending tests results published by different laboratories without some loading heads description may be confusing and difficult to compare. Those of them obtained using loading heads of severe contact conditions (like rollers - esp. of smaller diameter) should be seriously revised as they represent wooden element capacity for a case of load with some aspects of bending rather than the bending strength of wood as structural material property.

REFERENCES

Buchanan, A.H. 1990. Bending strength of lumber. *J. of Struct. Engineering, vol.116, No. 5: 1213-1229.*

Malhotra, S.K., Bazan, I.M.M. 1980. Ultimate bending strength theory. *Wood Science 13(1): 50-63.*

Mozharovski, V.V. 1990. The influence of friction between cyllindrical indentor and the composite coating on the contact conditions. (in Russian), *Friction and Wear 11(6): 1014-1024.*

Perstorper, M., Johansson, G., Kliger, R. 1994. Hallfasthet och sortering av grova balkar. *Chalmers Technical University Pub. S.94:4. Goeteborg, 1994.*

Muszyński L. 1994: Stress concentrations in wooden specimen during the bending test. *Holzforschung und Holzverwertung. 49(1): 12-13.*

Timoschenko S., Goodier J.N. - 1962: Theory of Elasticity. (Polish edition), *Warszawa, p.327-331.*

Zieleśkiewicz, Z., Malus, A. 1990. Determination of the magnitude of the cyllindrical loading head contact area on specimen surface during bending tests. (in Polish). *Wood Technology Institute Report No. 6.5.150.2.2.1, Poznań: pp.20.*

DIN 52 186/1978 Testing of wood, bending test.

DIN EN 408/1990 Timber structures - Solid timber and glued laminated timber - Determination of some physical and mechanical properties for structural purposes: German version prEN 408: 1990.

ISO 8375-1985 (E) Solid timber in structural sizes - Determination of some physical and mechanical properties.

PN-84/D-04 153 Wood. Determination of ultimate strength in static bending.

INTERNATIONAL COUNCIL FOR BUILDING RESEARCH STUDIES AND DOCUMENTATION

WORKING COMMISSION W18 - TIMBER STRUCTURES

EFFECT OF TEST STANDARD, LENGTH AND LOAD CONFIGURATION ON BENDING STRENGTH OF STRUCTURAL TIMBER

by

T Isaksson

S Thelandersson

Lund University

Sweden

MEETING TWENTY - EIGHT

COPENHAGEN

DENMARK

APRIL 1995

Effect of test standard, length and load configuration on bending strength of structural timber

Tord Isaksson, M. Sc., Research Assistant

Sven Thelandersson, Professor

Department of Structural Engineering, Lund University
Sweden

Abstract

The within member variability of bending strength in structural timber has been investigated in an experimental study of 133 boards from Norway spruce (Picea Abies). For each board the bending strength was determined in 4-7 of the weakest sections along the length. The choice of test sections was based on knot measurements and readings from two different types of machine grading.

The results from the experimental investigation are used to compare three different standards (European, North American and Australian) for determining characteristic bending strength as well as to study length and load configuration effects on bending strength. These studies were made by direct simulation from the test data on one and the same sample, which makes this investigation unique compared to other studies of these problems.

It was found that the difference between the three test standards is very small for the tested material. In a statistical sense no significant difference could be found although the methods of selection of test section are quite different between the standards. On the other hand, the results from the simulated tests according to all three standards were significantly higher than the strength of the weakest section within the boards both for the 50th and the 5th percentile values of the distributions.

The simulations also showed very small length effects for the sample investigated. The difference in strength distributions for lengths of 2.2 m and 4.2 m was not statistically significant, although both the mean and the 5th percentile for the longer beams were slightly lower than for the shorter ones.

The effect of load configuration was found to be statistically significant, however, when comparing beams of equal length loaded with constant moment, uniformly distributed load and point load at mid-span.

Introduction

Structural timber displays a considerable strength variability within members, which makes it difficult to evaluate its reliability and to design timber members in a rational way. Engineering design methods for timber are based on elementary theory of structures assuming homogeneous material. In reality, the strength is highly variable along a timber board, implying that the real strength depends on length, load configuration and other factors which are not considered in elementary engineering design. Such effects may be accounted for by introducing correction factors, which is also done to some extent in some codes.

As one example, the results from testing to determine characteristic strength of timber can be expected to depend on the strategy used to select the test specimens and that part of a timber board to be placed in the region where the largest stresses occur during testing. This strategy is quite different in the European, American and Australian standards (Barrett & Lam 1994).

Similarly, the length of a timber beam affects the apparent strength since the probability that a weak section is located within the beam increases with increasing length. This has been shown in many investigations, see e.g. reviews in Madsen, 1992 and Barrett & Fewell, 1990.

Furthermore, the apparent strength of a timber beam will also depend on the nature of the moment distribution along the beam. For instance, a beam with a point load at mid-span can be expected to have an apparent strength which is higher than a beam of the same length loaded with constant moment along the length. This has also been confirmed by several investigations, see e.g. Madsen 1992. For cases with narrow moment peaks, the load configuration effect may be very significant, since the probability of occurrence of the weakest section at the location of high moment is small (Czmoch et al 1991).

To study such effects, the within member variability of bending strength in structural timber has been investigated in an experimental study of 133 boards from Norway spruce (Picea Abies). For each board the bending strength was determined in 4 up to 7 of the weakest sections along the board length of 5.1 m to 5.4 m. The choice of test sections was based on knot measurements and readings from two different types of machine grading, Cook Bolinder stress grader and the so called Finnograder, which is based on non-contact measurements. *Figure 1* shows the results from knot measurements (CWAR=1-KAR) and readings from the Cook Bolinder machine along one of the boards in the sample. The measured bending strength in five sections along the board is also shown in the figure. The test method and the method of selection of test sections are described in detail in Isaksson & Thelandersson 1994a and in Isaksson et al 1994b.

The data obtained from these tests can be used to simulate different testing standards for characteristic strength and to investigate length and load configuration effects. These simulations can be performed on only one sample avoiding the statistical errors associated with comparisons between different test samples. In the present paper, however, there is one important limiting assumption valid for all simulations: All failures are assumed to occur in one of those 4-7 weak sections actually tested and nowhere else.

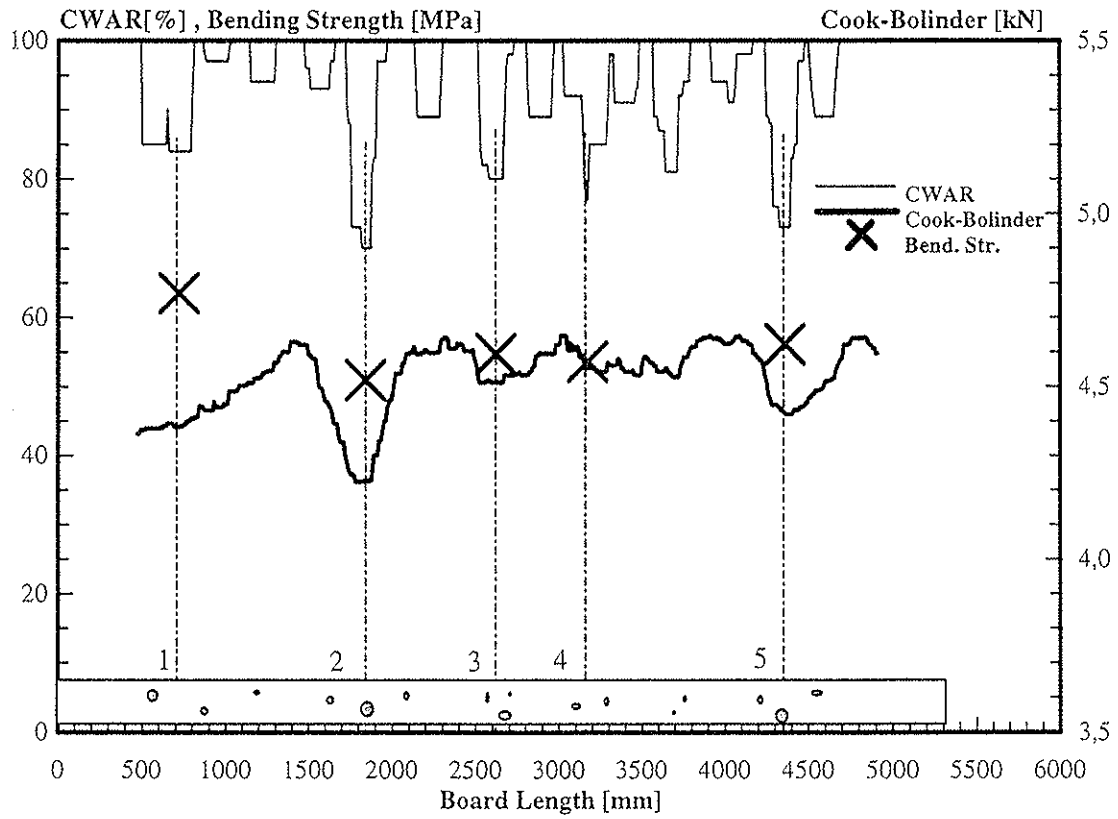

Figure 1. Knot measurements (CWAR=1-KAR), machine stress grading results (Cook-Bolinder) and the tested bending strength in 5 sections.

Three standards to determine the characteristic bending strength

The following three test standards for determination of the characteristic bending strength of structural timber are considered in this paper:

European standard EN 408 and EN 384

The standard EN 408, based on the ISO 8375, specifies laboratory methods for the determination of some physical and mechanical properties of timber in structural sizes. A symmetrical two point loading over a span of 18 times the depth is used for the determination of bending strength. Lateral restraint shall be used to prevent buckling. Maximum load is to be reached within (300±120) s.

The definition of characteristic bending strength and other mechanical properties including density is described in EN 384. The position of the critical section (position at which failure is expected to occur), selected by using visual or machine stress grading, is to be located inside the inner load points. The tension edge shall be selected at random and the reference moisture content shall be consistent with 20°C and 65 % relative humidity. This corresponds to a moisture content of approximately 12 %. Bending strength not tested under these condi-

tions shall be adjusted for at the characteristic level. The depth of the board shall be adjusted to 150 mm.

American Society for Testing and Materials D 4761-88 and D 1990-91

The North American test standard for mechanical properties of lumber and wood-base structural material, ASTM D 4761-88, also expresses the span as a multiple of the test specimen depth. However, the spans range from 17 times the depth to 21 times the depth. In this investigation the span was set to be 17 times the depth. The specimen is loaded by two concentrated forces at the third points of the span and lateral support shall be used if necessary. The tension edge is chosen randomly. Time to failure should be approximately 60 s, not less than 10 s and not more than 10 min.

ASTM D1990-91 is the North American standard practice for establishing allowable properties of visually-graded dimension lumber from In-Grade tests of full-size specimens. In this case the critical zone (containing the maximum strength reducing defect MSRD) shall be randomly located between the supports. The characteristic value is estimated (preferably non-parametrically) after having adjusted the data to the reference conditions (23°C, 15 % moisture content and dimensions of the cross section 38 by 184 mm).

Australia/New Zealand Standards AS/NZ 4063:1992

This standard prescribes a completely random location of the test section using a uniform distribution to choose location for the test specimen. The test set-up is identical with the ISO 8375, the span is 18 times the depth of the board and two concentrated forces at the third points. Characteristic conditions are 20±3 °C and a relative humidity of 65±5 %. The choice of edge to be stressed in tension shall be selected at random.

Procedures common for the three test standards used in the simulation study

Since the purpose with the simulation study in this paper is to detect any significant differences between the procedure for selecting the test specimen in the three test standards, the conditioning (temperature, moisture content and cross section) of the specimens is the same in all three cases. All the comparative simulations are performed on data from the same sample, where the temperature ranged from 18 to 21 °C and the moisture content between 11.6 to 16.6 % with an average of 13.7 %. The nominal cross section is 45 by 145 mm and the actual dimensions varies between 42.2 and 44.1 and 136.7 and 143.4 respectively with averages 43.3 and 141.0.

The effect of rate of testing (0.20 mm/s with a time to failure between 130 and 450 s), selection of tension edge (random), load and support conditions and differences between samples is also eliminated by using simulation on one sample. Four lateral supports were used, one at each support and one at each point load.

For the above reasons, no correction of the tested bending strength values has been carried out.

All statistical test are performed with a confidence level of 95 %.

Comparison of simulated and tested EN standard

The test procedure when determining bending strength in several weak sections within a board (group A) may influence the strength (Isaksson, Thelandersson, 1994), e.g. due to effects from clamping the board in the vicinity of the test section. To detect any differences between the test procedure used and the standard test procedure, a simulation study on group A was made and compared with the results from a matched control sample (group B) tested according to EN 408 and EN 384. The samples were matched with respect to the lowest Cook-Bolinder reading within a board. The cumulative distribution functions for the bending strength obtained in this comparison are shown in *figure 4.* Test for normality is summarised in *table 1* and goodness-of-fit test is shown in *table 2. Figure 2* and *3* shows normal and Weibull plots for the two tests.

	simulation (group A)	control (group B)
chi-square goodness-of-fit statistic	0.681>0.05	0.805>0.05
Shapiro-Wilk's W statistic	0.167>0.05	0.178>0.05
Z-score for skewness	0.593>0.05	0.938>0.05

Table 1. Tests for normality. A p value less than 0.05 indicates lack of fit to the normal distribution implying that there is less than one chance out of 20 that the sample could have been drawn from a normal distribution. The Z-score shows if the data are symmetrically distributed. If so, the data are likely to be normally distributed.

	simulation (group A)	control (group B)
Estimated Kolmogorov-Smirnov statistic	0.687>0.05	0.888>0.05

Table 2. Goodness-of-fit test. The estimated Kolmogorov-Smirnov statistic is significant if p is higher than 0.05. This is a non-parametric method to test the overall goodness-of-fit between the distribution of the data and in this case the normal distribution.

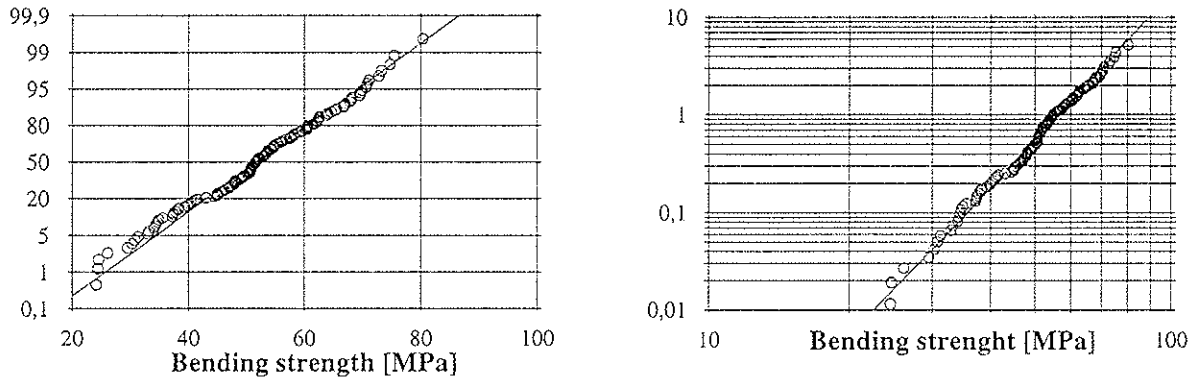

Figure 2. Normal and Weibull plot for simulation (group A).

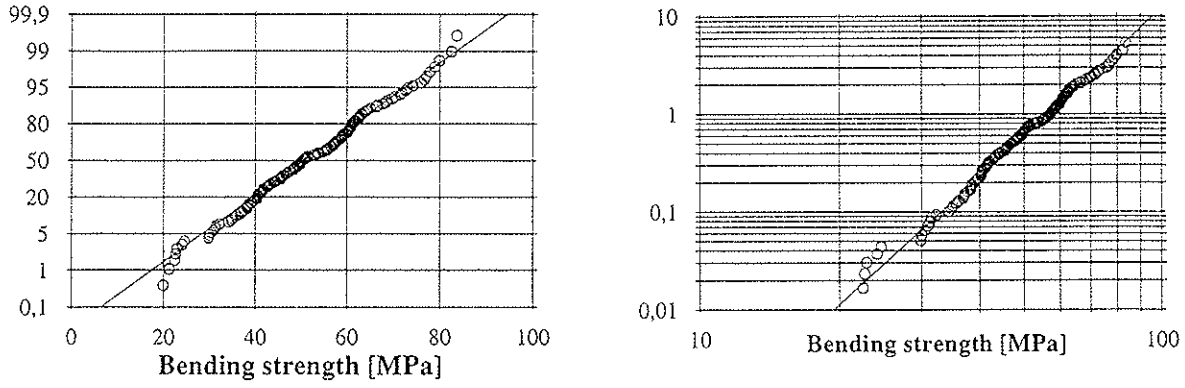

Figure 3. Normal and Weibull plot for control (group B)

The tests do not reveal any serious evidence against the normal distribution fitting the data. Using the normal distribution, a two sample comparison of the two groups can be made. *Table 3* shows a summary of the statistics.

	simulation (group A)	**control (group B)**
Number of observations	133	152
Average	51.77	51.25
Median	51.8	50.45
Variance	142.03	187.08
Standard deviation	11.92	13.68
Minimum	24.2	20.0
Maximum	80.4	83.7
Coeff. of variation	23.02	26.69

Table 3. Summary statistics Control / simulation.

	simulation (group A)	**control (group B)**
95 % confidence interval for means	(49.73, 53.81)	(49.09, 53.44)
95 % confidence interval for differences between means assuming:		
-equal variances		(-3.53, 2.49)
-unequal variances		(-3.50, 2.46)
mean (simulation) not equal mean (control) assuming:		p=
-equal variances		0.74 >0.05
-unequal variances		0.73 >0.05
mean (simulation) > mean (control) assuming:		p=
-equal variances		0.63 >0.05
-unequal variances		0.63 >0.05
mean (simulation) < mean (control) assuming:		p=
-equal variances		0.37 >0.05
-unequal variances		0.36 >0.05

Table 4. Comparison of means. If any of the p values is less than 0.05 it would imply a rejection of the null hypothesis.

To test the null hypothesis that there is no difference between the two test arrangements, we compare the means, i.e. the null hypothesis is that the means are equal. *Table 4* summarises this test and the conclusion is ($p > 0.05$) that there is no significant difference between the two test arrangements. This is a great advantage since a difference would imply that the results from group A must be adjusted in some appropriate way.

A similar test on comparison of standard deviations results in a non-rejection of the hypothesis that the deviations are equal.

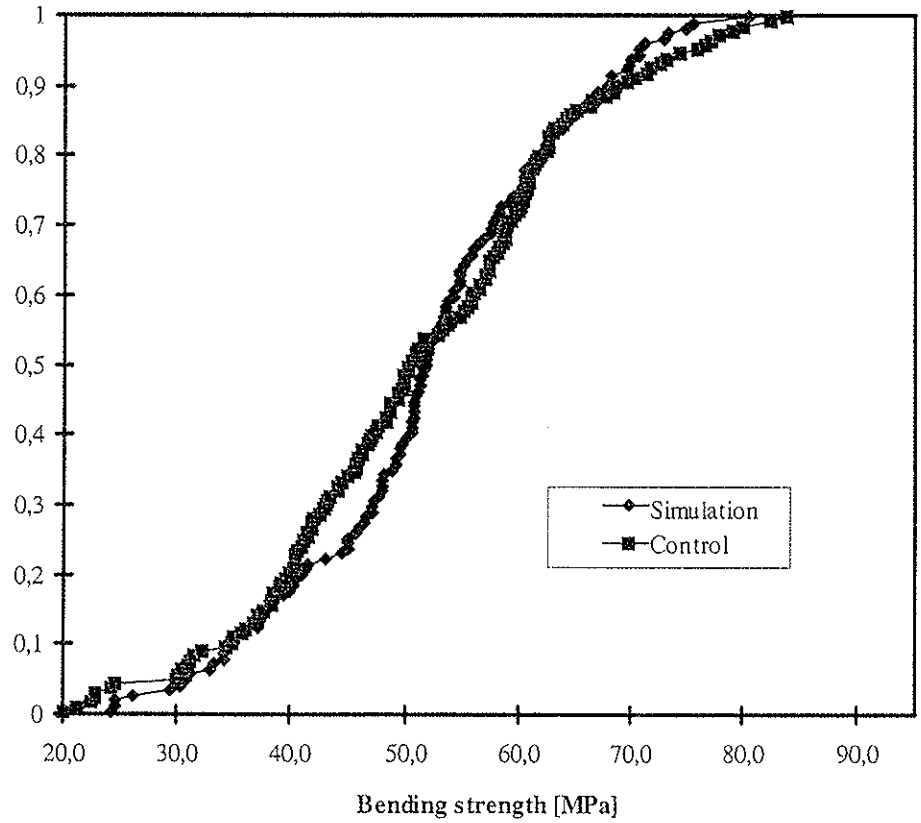

Figure 4. Distribution function for simulated test (A) and the control group (B).

Comparison of simulation results from three test standards

The critical section (grade determining defect), referred to in the European and North American test standard, to be tested is in this investigation chosen on the basis of a machine stress grader, the Cook-Bolinder. The section with the lowest Cook-Bolinder reading (force necessary to give the board a specified flatwise deflection) is selected as the critical section. If it is impossible to test that section, because it is located near the end of the board, the section with the next lowest reading is chosen. This may be the case for the European standard since the section here shall be located inside the inner load points. In simulations according to the ASTM standard, the critical section is placed randomly between the supports using a rectangular distributed distance to test section. The same distribution is used when assigning a distance to the section to be tested according to AS/NZ standard. The results from the simulations are shown in *figure 5*.

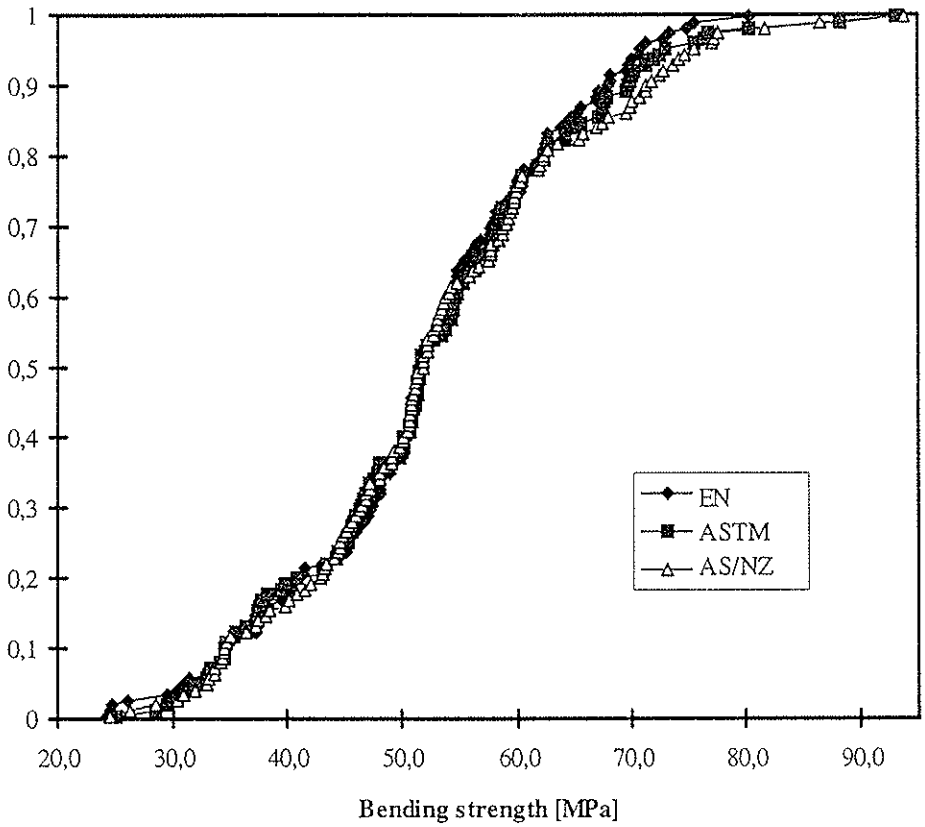

Figure 5. The cumulative distribution function for bending strength simulated according to EN, ASTM and AS/NZ standards.

When testing the hypothesis for no differences between the test standards it is desirable to know that the distribution function for the bending strength is approximately normally distributed. One way to check this is, as was done in the previous section for the EN results, to draw a normal probability plot. This is done for the two remaining tests in *figures 6* and *7*. The figures do not reveal any significant evidence against the assumption of normally distributed bending strength. Also shown is the analogue test for the assumption of Weibull distributed bending strength. The Weibull distribution does not fit any better to a straight line. *Table 5* summarises different tests for normality. If the p value is less than 0.05 the values are significant and the data can not be considered as normally distributed. As shown, the normality test for ASTM is not significant for the chi-square test, but the two other tests indicate significance for the normal distribution. The Goodness-of-fit test is summarised in *table 6*. In spite of this indication of lack of fit for ASTM, the assumption of normally distributed bending strength is used for all three test standards and a summary statistics is shown in *table 7*.

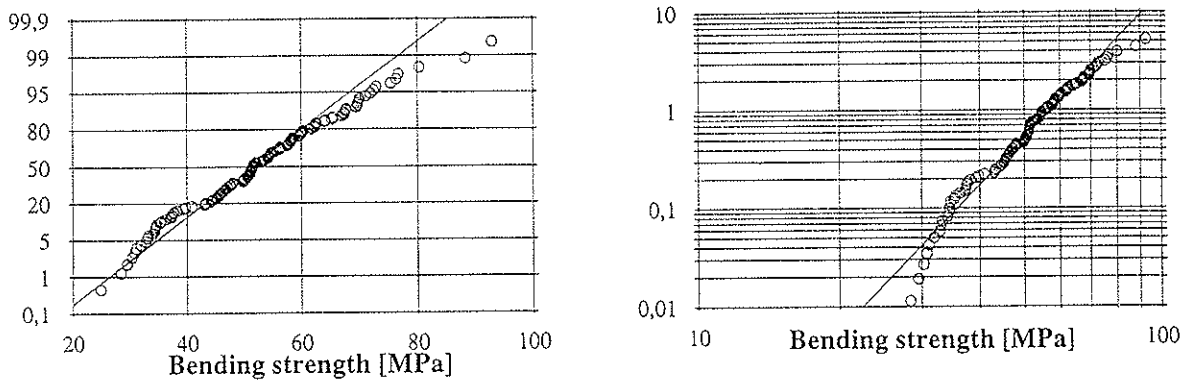

Figure 6. Normal and Weibull plot for ASTM.

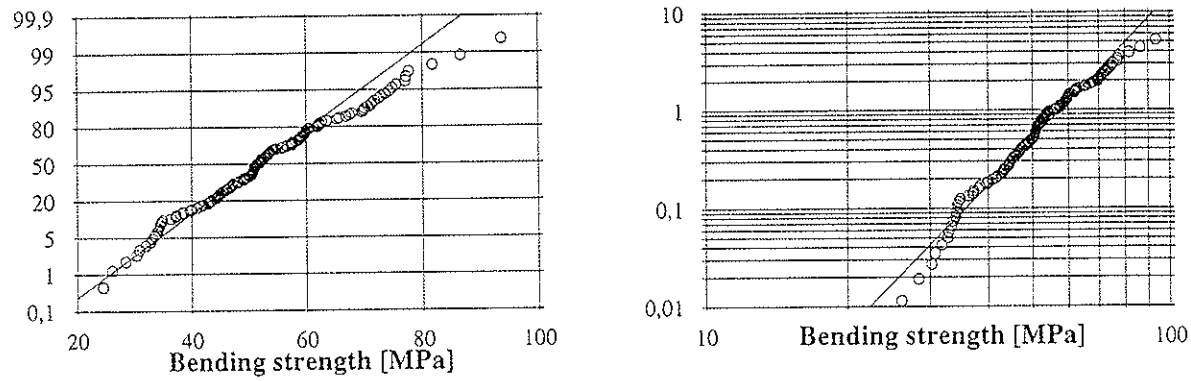

Figure 7. Normal and Weibull plot for AS/NZ.

	EN	ASTM	AS/NZ
chi-square goodness-of-fit statistic	0.68 >0.05	0.02 <0.05 n.s	0.198 >0.05
Shapiro-Wilk's W statistic	0.167 >0.05	0.284 >0.05	0.262 >0.05
Z-score for skewness	0.593 >0.05	0.302 >0.05	0.244 >0.05

Table 5. Tests for normality. A p value less than 0.05 indicates lack of fit to the normal distribution, implying that there is less than one chance out of 20 that the sample could have been drawn from a normal distribution. The Z-score shows if the data are symmetrically distributed. If so, the data are likely to be normally distributed.

	EN	ASTM	AS/NZ
Estimated Kolmogorov-Smirnov statistic	0.687 >0.05	0.893 >0.05	0.443 >0.05

Table 6. Goodness-of-fit test. The estimated Kolmogorov-Smirnov statistic is significant if p is higher than 0.05. This is a non-parametric method to test the overall goodness-of-fit between the distribution of the data, in this case the normal distribution.

	EN	ASTM	AS/NZ
Number of observations	133	133	133
Average	51.77	52.44	52.84
Median	51.8	51.6	51.8
Variance	142.03	164.49	173.69
Standard deviation	11.92	12.83	13.18
Minimum	24.2	24.9	24.5
Maximum	80.4	93.0	93.7
Coeff. of variation	23.02	24.46	24.94

Table 7. Summary statistics for the three test standards.

Now then, is there any difference between the standards. A three sample comparison is carried out. An analysis of variance reveals no significant difference in means and a multiple range test and the non-parametric Kruskal-Wallis test confirms. The variances are also significantly equal.

In *table 8* the test standards are compared at different percentiles. The non-parametric characteristic bending strength is more or less 30 MPa for all three standards, and there does not seem to be any reason for not accepting the result from above that there is **no significant difference** between them. The table also includes the percentiles for the lowest bending strength value within a board, which does not necessarily coincide with the lowest Cook-Bolinder reading. This value is significantly lower than for example the EN.

Percentile [%]	EN	ASTM	AS/NZ	Weakest
1	24.5	28.4	26.1	23.0
5	30.8	31.9	32.8	26.1
10	34.6	34.5	34.4	33.2
25	45.1	45.2	44.6	38.3
50	51.8	51.6	51.8	45.6
75	60.3	59.9	59.9	51.6
90	67.9	69.8	71.3	56.5
95	70.8	73.0	75.5	61.9
99	75.5	88.4	86.6	68.7

Table 8. Percentiles for the three standards and the weakest section.

Length effect

The second simulation performed on the material is a study of length effect for structural timber. So far only a uniform bending moment has been used, other load combinations like uniform load and point loads will be studied later on. *Figure 8* shows the load and length combinations studied. Three different lengths were used, 2200, 3200 and 4200 mm. The two shorter boards were taken randomly from the longer one. The cumulative distribution functions are shown in *figure 9*. They seem to follow each other fairly well, at least at the lower tail. A summary of the statistics is found in *table 9*.

An analysis of variance results in a non-significant difference in means, the same is valid for the variances. A non-parametric Kruskal-Wallis test con-

firms the hypothesis of equal means as well as a multiple range test (Tukey HSD).

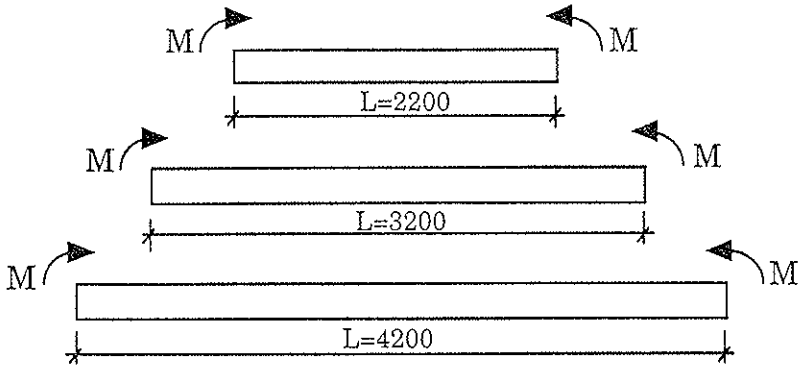

Figure 8 Length effect

	L=2200	L=3200	L=4200
Number of observations	132	132	132
Average μ_R	49.78	47.77	46.69
Median	50.70	48.00	47.35
Variance	143.78	125.87	120.77
Standard deviation σ_R	11.99	11.22	10.99
Minimum	19.9	19.9	19.9
Maximum	77.1	73.6	73.6
Coeff. of variation	24.09	23.48	23.53

Table 9. Summary statistics length effect.

The length effect, assuming Weibull distributed strength, may be expressed as equation 1 shows (Madsen 1992).

$$\frac{f_D}{f_R} = \left(\frac{L_R}{L_D}\right)^k \tag{1}$$

where index R refers to the reference length and strength and D to the one of interest.

Madsen (1992) uses the exponent k=0.2. The 5 and 50 % bending strengths are shown in *table 10*. In *table 11* the exponent k calculated form the test results, is presented.

Length [mm]	Bending strength 5 %	Bending strength 50 %
2200	30.3	50.7
3200	30.3	48.0
4200	26.1	47.35

Table 10. 5th and 50th percentile bending strength values for three lengths.

	5 %	50 %
L_{2200}/L_{3200}	0	0.146
L_{2200}/L_{4200}	0.231	0.106

Table 11. Exponent k at the 5th and 50th percentile.

There is too few observations at the 5th percentile to draw any conclusions, but at the 50th percentile k is somewhere between 0.10 and 0.15, which indicates a slightly smaller length effect than reported by Madsen.

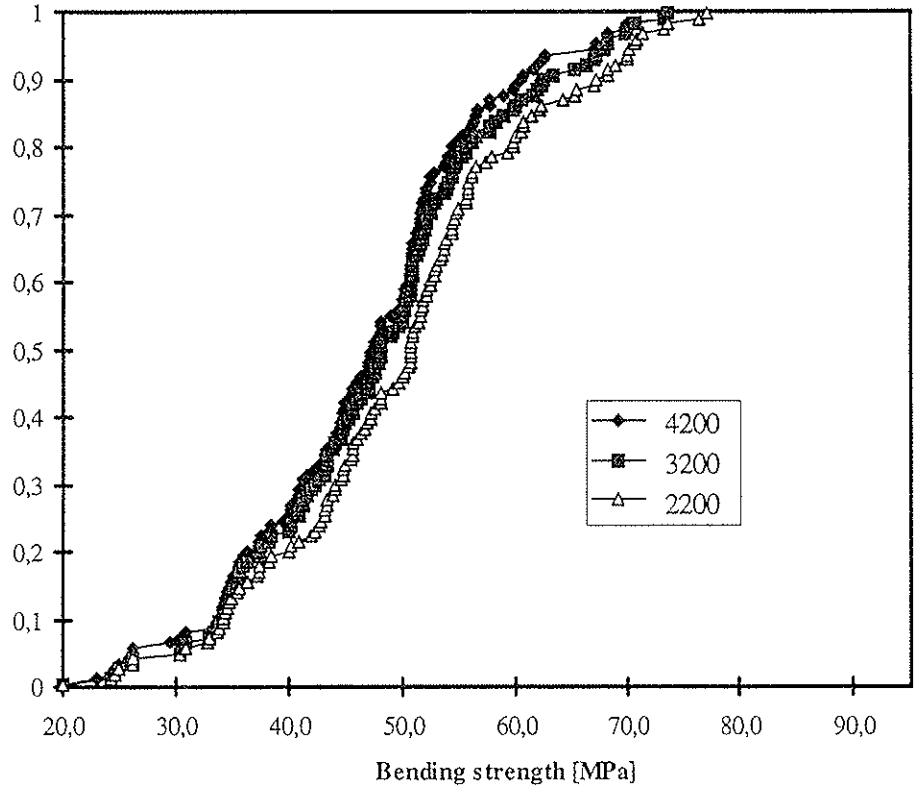

Figure 9. Cumulative distribution function for length effect with uniform moment.

Moment configuration effect

The third and last simulation performed in this paper deals with moment configuration effects. *Figure 10* shows the moment configurations and *figure 11* the cumulative distribution function for the three moment configurations. *Table 12* summarises the statistics.

An analysis of variance results in a significant difference in means. The same conclusion is drawn from a multiple range test denoting significant differences. The hypothesis of equal variances can not be rejected. Finally, the non-parametric Kruskal-Wallis test as well as a multiple range test (LSD) shows significant differences in means. *Table 13* shows the bending strength for the three moment configurations at the 5th and 50th percentile.

The increase in strength when comparing uniformly distributed load and a point load at mid span with a uniform moment at the 5th percentile level is 18 % and 29 % respectively. The corresponding values at the 50th percentile are 8 % and 14 %.

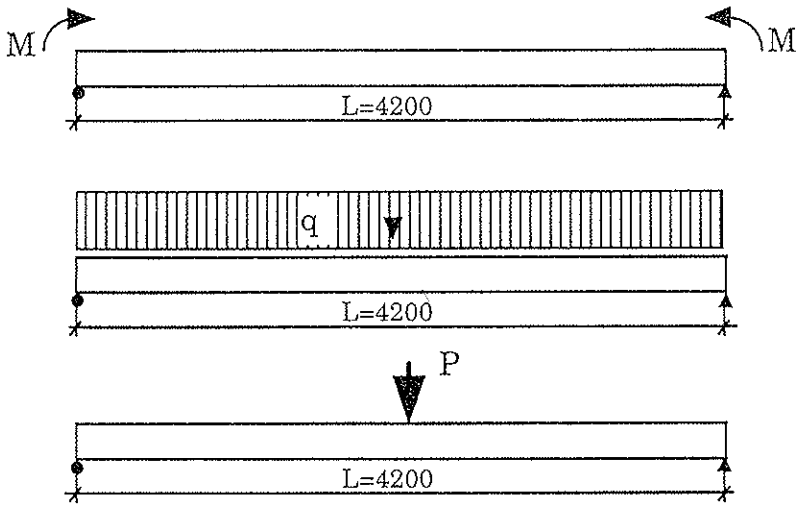

Figure 10. Moment configurations

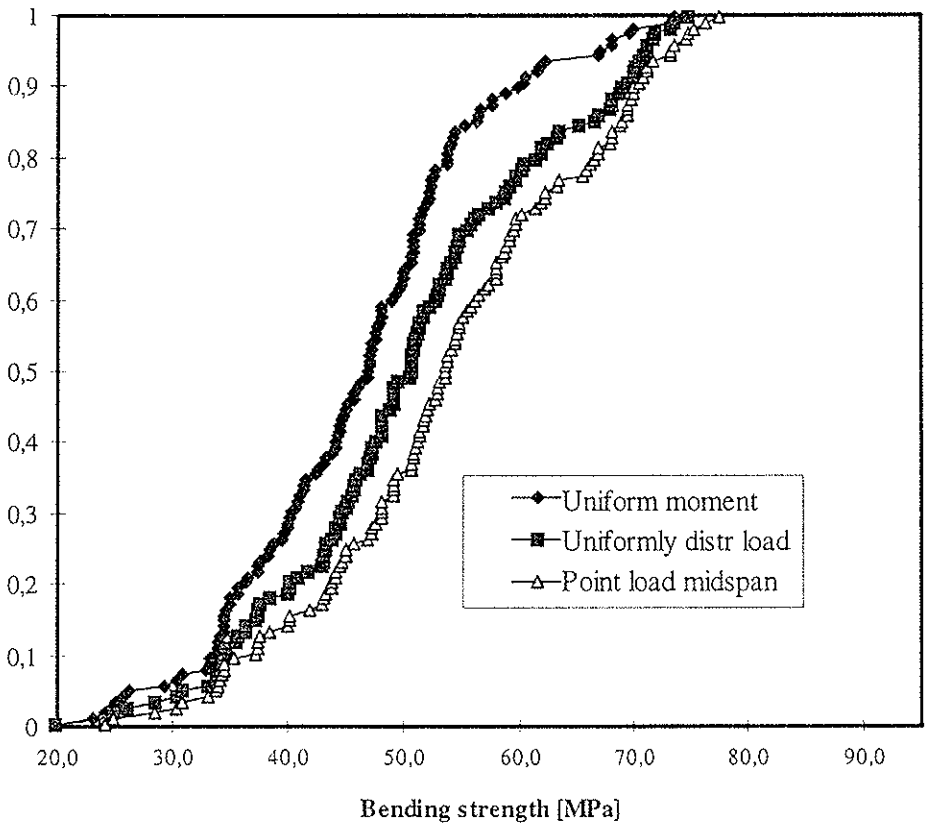

Figure 11. Cumulative distribution function moment configuration effects

	Uniform moment	Uniformly distr. load	Point load at mid span
Number of observations	131	131	131
Average	46.05	50.57	53.74
Median	46.9	50.6	53.6
Variance	117.24	147.92	151.37
Standard deviation	10.83	12.16	12.30
Minimum	19.9	19.9	24.2
Maximum	77.1	74.8	73.6
Coeff. of variation	23.51	24.05	22.90

Table 12. Summary statistics for moment configuration effects.

	Bending strength 5 %	Bending strength 50 %
Uniform moment	26.1	46.9
Uniformly distr. load	30.9	50.6
Point load mid span	33.7	53.6

Table 13. 5th and 50th percentile bending strength values for three moment configurations .

Discussion

Simulations were carried out with the intention to detect differences when using different test standards in the determination of bending strength in structural timber. The test standards used in this investigation, the European EN 408 and 384, North American ASTM D 4761-88 and 1990-91 and Australia/New Zealand AS/NZ 4063:1992 did not result in any statistically significant difference in the resulting bending strengths. The investigation was made on timber with a fairly high bending strength and the strength in the weak sections of the boards does not show any strong variation within boards. Thus one will mostly place fairly similar weak sections between the inner loads irrespective of which standard is used to test bending strength. This may not be the case when testing timber with a much stronger variation of bending strength within boards and if the distance between defects is larger than for the material used in this investigation.

All three test standards gave strengths which were significantly larger than the measured minimum strength within the board. This is surprising since for the EN standard, it is expected that a critical section selected on the basis of visual grading or machine grading, shall be placed in the region with maximum moment. The explanation for this is firstly that the section with minimum strength can not be found with great precision using machine stress grading results, and secondly that in cases where the weakest section is near the end of the board it can not be tested due to geometrical constraints.

Another interesting result from this investigation is that the length effect is very weak; it is not statistically significant. The reason for this might again be that the variability between weak sections within each board seems to be small

compared with the variability between the boards. This will be analysed in more detail later. From these results, it may be concluded that length effects can very well be ignored in practical design, at least for this type of timber. This conclusion is further supported by the fact that any correction factor for length (size) should be calibrated to preserve the reliability index rather than the 5th percentile level. As shown by Canisius, 1994 this will lead to even smaller correction factors for length and load configuration than given by comparing 5th percentiles.

In contrast to the results from the studies of length effect a significant influence of load configuration was found. The reason for this is probably that the distances between the weak sections (or defects) used in the present simulation is rather large, which tends to give a rather large magnification of the apparent strength in many cases. A more detailed modelling may reveal that failure can sometimes occur in other sections than those considered in the present analysis. This may lead to a modification of the above conclusions regarding load configuration effects.

Conclusions

The following main conclusions can be drawn from the investigation reported in this paper:

1 A reliable method of testing the same timber board in several sections along the length has been developed, see Isaksson et al 1994.

2 The test method was used to determine the bending strength in 4-7 sections in a sample of 133 boards of structural timber from Norway spruce.

3 These data were used to simulate length effects and load configuration effects as well as comparisons of different test standards (EN, ASTM and AS/NZ) on one and the same sample. In this way, statistical errors associated with lack of matching between samples can be eliminated.

4 The difference between the test standards was found to be very small for the tested material. In a statistical sense no significant difference could be found, although the methods of selection of test section is quite different between the standards.

5 The results from the simulated tests according to all three standards were significantly higher than the strength of the weakest section within the board both for 50th and the 5th percentile of the sample.

6 The simulations showed very small length effects for the sample investigated. No significant difference could be shown between lengths of 2.2 m and 4.2 m, although both the mean and the 5th percentile for the longer beams were slightly smaller than for the shorter ones.

7 The effect of load configuration was found to be statistically significant, however, when comparing by simulation beams of equal length loaded with constant moment, uniformly distributed load and point load at mid-span.

8 The results indicate that the widely used Weibull concept used to describe length and load configuration effects has limited validity. The reason for this is that the Weibull theory assumes uniformly distributed defects with random properties over the volume of the body

References

AS/NZ 4063:1992. Timber-Stress graded. In-grade strength and stiffness evaluation. Standards Australia/Standards New Zealand. Sydney, Australia.

ASTM D 1990-91. Standard Practice for Establishing Allowable Properties for Visually-graded Dimension Lumber for In-grade Tests of Full-Size Specimens. ASTM Annual Book of Standards. Philadelphia.

ASTM D 4761-88. Standard Test Methods for Mechanical Properties of Lumber and Wood-Base Structural Material. ASTM Annual Book of Standards. Philadelphia.

Barrett, J.D. and Fewell, A.R., 1990. Size factors for the bending and tension strength of structural timber. CIB/W18A - Timber structures. Paper 23-10-3. Lisbon, Portugal.

Barrett, J.D. and Lam, F., 1994. Factors affecting the strength of structural timber. Proc., Pacific Timber Eng. Conf., Gold Coast, Australia, Vol. 3, pp 69-77.

Canisius, T.D.G., 1994. Reliability-based configuration factors for timber beams, J. of Structural Safety, 16, pp. 215-226.

Czmoch, I., Thelandersson, S. and Larsen, H.J., 1991. Effect of within member variability on bending strength of structural timber. CIB/W18A - Timber structures. Paper 24-6-3, Oxford, United Kingdom.

Isaksson, T., Thelandersson, S. and Möller-Pedersen, T., 1994. Within member variability of bending strength of timber, Proc., Pacific Timber Eng. Conf., Gold Coast, Australia, Vol. 1 pp. 634-641.

Isaksson, T., Thelandersson, S., 1994. Within member variability of bending strength of timber. First European symposium on non-destructive evaluation of wood. Hungary 1994.

ISO 8375. Solid timber in structural sizes - Determination of some physical and mechanical properties. International Standards Organisation, Switzerland.

Lindgren, G., Rychlik, I., 1994. Tillförlitlighet och säkerhet. Statistiska metoder och tekniker, del I, II, III och IV. Institutionen för matematisk statistik, Lunds Tekniska Högskola, Lunds Universitet. (Swedish)

Madsen, B., 1992. Structural behaviour of timber. Timber engineering LTD, Vancouver Canada.

Montgomery, D. C., 1991. Design and analysis of experiments. Wiley & Sons.

EN 408. Timber structures -Structural timber and glued laminated timber - Determination of some physical and mechanical properties. Final draft March 1994.

EN 384. Structural Timber - Determination of characteristic values of mechanical properties and density. Amended draft September 1991.

Statgraphics plus, version 1. 1994. User manual. Manugistics Inc. USA.

Thoft-Christensen, P., Baker, J.B., 1982. Structural reliability theory and its applications. Springer-Verlag.

CIB-W18/28-6-5

INTERNATIONAL COUNCIL FOR BUILDING RESEARCH STUDIES AND DOCUMENTATION

WORKING COMMISSION W18 - TIMBER STRUCTURES

GRADING MACHINE READINGS AND THEIR USE IN THE CALCULATION OF MOMENT CONFIGURATION FACTORS

by

T Canisius
Building Research Establishment
The United Kingdom
T Isaksson
S Thelandersson
Lund University
Sweden

MEETING TWENTY - EIGHT

COPENHAGEN

DENMARK

APRIL 1995

Grading machine readings and their use in the calculation of moment configuration factors

T. D. G. Canisius
Timber Structures Section, Building Research Establishment,
Bucknal's Lane, Garston, Watford WD2 7JR, U.K.

T. Isaksson and S. Thelandersson
Department of Structural Engineering, Lund University,
PO Box 118, S-221 00, Lund, Sweden

Abstract

The Lund University is currently involved in a project for the determination of along-member variation of timber beam strengths. This paper present some preliminary results obtained through simulation based on the results from this project and grading machine readings for the beams to be simulated. This study is only a test of the method used for the simulation of beam strengths. The considered method seems to provide good prospects in predicting strengths of beams when grading machine readings are available.

1 Introduction

The determination of the variation of properties along timber beams is a topic which has interested many researchers. If this information is available, then timber structures can be made more efficient, and thus more economical. It will also make it possible to determine reliability levels of structures more accurately.

An important benefit of information on the along-beam variation of flexural properties is the possible introduction of moment configuration factors into the limit state design procedure. This strength conversion factor will help to narrow the difference between reliability levels of different structures and also improve the efficiency of these structures. Such a possibility is present because the European method of beam strength determination, and the resulting design of beams, are based on the strength of the weakest cross section in a beam. This effectively implies the coincidence of the weakest beam section and the maximum bending moment, without exception. However, it is not a deterministic situation and the probability of such coincidence between the weakest section and the maximum bending moment in a beam depends also on the type of bending moment diagram. If this probabilistic phenomenon is neglected, the reliabilities of beams designed according to the above principle will not be the same under different bending moment profiles. In addition, this results in the uneconomical design of structures, especially where the higher bending moments are localised into limited regions. Figure 1 presents a possible hypothetical idealisation of bending strengths along a beam. Figure 2 shows how the 'strength' of a beam, in terms of the maximum possible bending moment in the beam, can be different under two forms of loading. It is this aspect of design which is intended to be addressed by Moment Configuration Factors(MCFs).

Due to the importance of the above phenomenon, many researchers have undertaken work on the lengthwise variation of bending strength and moment configuration factors. References [1] to [11] in the bibliography are some examples of reported related work. Although these studies have resulted in improved understanding of the moment configuration factors, there still remains a great need to obtain relevant data which can be applied to designs with a certain amount of confidence.

1.1 Moment configuration factor

Consider the beam shown in Figure 2. Let the maximum bending moment that can be applied to it under the non-uniform moment profile be M_1. Also, let the maximum uniform bending moment that can be applied be M_2. That is, under the given non-uniform and uniform bending moment profiles, the strengths of the beam are M_1 and M_2, respectively. Then, for this beam, the moment configuration factor (MCF) for the given non-uniform moment

$$\text{MCF} = \frac{M_1}{M_2} \quad . \tag{1}$$

However, it is not a moment configuration factor based on a single beam which is needed in design, but one which considers the total population or representative sample of beams.

1.1.1 Some previous conclusions

In the determination and use of MCFs, several previous conclusions need to be kept in mind. In previous work by the first author[7], it has been found that moment configuration factors can be sensitive to the parameters assumed for the used strength model. It has been also observed that in the case of indeterminate beams, the randomness of the elasticity modulus itself can significantly affect the moment configuration factors[6].

An important discovery was that the definition of moment configuration factors as the ratio of the characteristic strengths under given forms of bending moments could lead to a larger reduction in safety than anticipated[9]. It was shown that this can be avoided by defining MCFs in terms of an equal reliability criterion. The reason for the difference in characteristic strength and reliability based factors was the possible non-constant scaling of different fractiles during the conversion of one strength distribution into another under a different moment configuration[8]. When using a reliability-based criterion

it is necessary to know not only the characteristic values of strengths under different moment configurations, but also at least the lower tails of the strength distributions.

All research work so far has shown not only the relevance of MCFs, but also the need to have reasonably accurate data on the flexural property variations along the beams.

1.2 Current attempts at determining beam strength variations

The importance of having reliable information on the length-wise variation of flexural properties of beams has recently given rise to two independent projects to determine such data[10, 11]. The former project seems to provide good prospects for moment configuration factor studies as it attempts to correlate directly measured strengths to the easily obtained grading machine readings. The present study is an attempt at using the currently available limited data from this exercise to determine moment configuration factors.

1.3 Scope

This study is based on the limited data currently available as a result of the programme of work at Lund University mentioned above[10]. Grading machine readings from 133 beams and the strength results determined from direct tests at weak sections (see Section 2) are expected to be used in the complete study. Only preliminary results based on 19 beams are reported here.

In this study, with the use of Cook-Bolinder grading machine readings, the strengths of beams under various bending moment configurations will be determined. Then, they will be compared with the beam strengths determined through direct strength measurements at weak sections. A similar comparison is made with respect to the moment configuration factors.

The bending moment configurations used are uniform bending moment and those in a simply supported beam due to a uniformly distributed load and due to a central concentrated load. A beam span of 4200mm is considered.

2 Weak section strength-Grading machine reading correlation: Lund study

This section provides a summary of the results from the Lund University tests used in this study. As this programme of work is well documented in [10], only the briefest and essential information are given here.

The currently available strength data are with respect to weak sections of beams as predicted by significant depressions in the Cook-Bolinder grading machine reading profiles. The sample of beams consisted of 133 beams of nominal cross section $45\times145\text{mm}^2$ and lengths of between 5.1 and 5.4m. The grading machine readings for all these beams were obtained, and at least four weak sections of each beam were directly tested for strength.

The grading machine readings at the weak sections were converted to a modulus of elasticity (MOE) value E using the following formula.

$$E = 840 + 1.21\frac{PL^3}{48I\delta} \tag{2}$$

where P is the grading machine reading in Newtons, δ is the grading machine deflection setting, I is the second moment of area of the beam cross-section, and L is the grading machine span. All the the dimensions of the above variable are in mm, and the unit of E is MPa.

Regression analyses were carried out between the determined MOE values and the directly measured strengths of the weak sections. The results are shown in Figures 3 and 4. Figure 3 shows the regression results when all measured strength data were used against the corresponding grading machine readings, while for Figure 4 only the weakest section strength of each

beam and the corresponding machine reading were considered. The regression equations are as follows.

$$S = 0.0048E - 13.47 \quad \text{(all weak sections)} \quad (3)$$

$$S = 0.0035E - 3.880 \quad \text{(weakest sections)} \quad (4)$$

3 Method of beam strength simulation

The simulation of lengthwise variation of beam strengths is carried out as follows. First it is assumed that a defectless region of the beam will be of infinite strength. This is a shortcoming of the currently available strengths as there is no information available with respect to clear areas. However, the importance of such regions should lie with bending moment configurations having high intensity localised peaks, and not with the currently considered ones. This aspect will get addressed in the future through the currently progressing test work on the strengths of clear sections.

The strength reductions in the above infinite-strength beam is assumed to occur at each cross-section with defects as may be spotted from the grading machine data profile. Then, based on a regression equation (Equation 3 or 4) and Equation 2, a mean strength value is determined for the particular section. Then a random strength value is determined using an assumed normal distribution with the determined mean strength and a given coefficient of variation(COV). The COV of the strength is assumed to be independent of the MOE value and the determined mean strength of the section. A zero COV is the case of using the mean strength value provide by the regression equation itself. In the presently reported work, only the regression results obtained by considering all tested weak sections (Figure 3 and Equation 3) have been used.

The above determined strength can be assumed either to be localised in a cross-section of infinitesimal width or can be considered to spread to a region

of finite length. The importance of the assumption used will depend on two aspects, *viz.* the bending moment profile and the width of the region of reduced strength when compared to the total beam length. It is reasonable to argue that the consideration of a finite width of strength reduction is more important when the beam span is short or when the bending moment profile has high intensity localised peaks, as occurs over the supports of continuous beams. Thus, although it does not seem to be important to the problems considered here, it was decided to study the effects of different assumptions. The following describes the model used for this purpose.

3.1 Spread of influence of a weak section

At a weak section, let a strength reduction ratio R be defined as

$$R = \frac{S}{S_m} \tag{5}$$

where S is the weak section strength and S_m is the clear section strength. Here a 'weak section' refers to the beam cross-section which had a local minimum of the grading machine reading. Although the adjoining cross sections may be considered to have strengths less than that of clear wood, and hence to be 'weaker' sections, those are not referred to by the above term.

In order to determine the width of influence of a weak section, *i.e.* the finite width of strength reduction, the following assumptions are made.

1. The width of influence (l) is directly proportional to a multiple n of the beam depth D, *i.e.*

   $$l \propto nD$$

   This indicates that a defect, which is as large as to reduce the strength of a deep beam, will have its influence spread over a wide distance.

2. The width of influence is inversely proportional to a power k of the strength reduction ratio R; *i.e.*

$$l \propto R^{-k} \quad (k \geq 1)$$

If used, a k value of zero will imply the independence of l from R.

3. The reduced strength (RS_m) of the weak section reaches the clear section strength S_m at a distance of l on each side of it. This variation of strength reduction has a parabolic form shown in Figure 5.

These assumptions are necessitated by the fact that no information on these aspects exists at present. The first two assumptions gives the distance of influence l as

$$l = \frac{nD}{R^k} \tag{6}$$

The present study will consider n and k values of 0, 1 and 2. The n value of zero is a case of no spread of influence.

As the clear section strength S_m is not available at present, it is not possible to find the strength reduction ratio R and, hence, the strength profile in the vicinity. Because of this, until the clear strength data are available, it was decided to use an approximation to R using grading machine data. In this way, the new strength reduction ratio $(\tilde{R})$ is obtained as the ratio between the weak section machine reading (G) and the maximum machine reading for the beam (G_m). That is,

$$\tilde{R} = \frac{G}{G_m} \tag{7}$$

The effect of this approximation can be values of $\tilde{R}$ which are possibly always smaller than R. This is because the clear strength of wood can be expected to be more than what may be reflected by the maximum machine reading which provides only a weighted average of MOE within the 900mm machine span.

Now, considering the above approximation on R, and given the weak section strength S, the clear section strength S_m can be approximated by

$$\tilde{S}_m \approx \frac{S}{\tilde{R}} \quad . \tag{8}$$

However, due to the aforementioned possible difference in the sizes of R and $\tilde{R}$, this value of clear section strength can be much smaller than the real strength. Hence, $\tilde{S}_m$ is not used as a substitute for the infinite strength mentioned above, and it is used only as the value of strength at the extremes of the regions of influence of the weak section. This is shown in Figure 5b where, beyond the $2l$ wide region centred at the weak section, beam strength switches back to infinity.

Using the above assumptions and considerations, the strength $S(y)$ at any position within the region of influence, at a distance y from the weak section, can be found as

$$S(y) = \tilde{r}(y)\tilde{S}_m = S\frac{\tilde{r}(y)}{\tilde{R}} = \bar{R}(y)S \quad , \tag{9}$$

where $\bar{R}$ is given by

$$\bar{R} = \frac{(1-\tilde{R})}{n^2 D^2}(\tilde{R}^k)^2 y^2 + \tilde{R}. \tag{10}$$

3.2 Beam simulation procedure

The following is a summary of the beam simulation procedure used to generate along-member variation of beam strength.

1. Plot the grading machine reading against the distance along the beam.

2. Determine the positions and the readings at the valleys (depicting weak sections) in the graph, but independently of any other information on the beam. (To have this independence, this part of the work was carried out by the first author at BRE.)

3. Using Equation 2 determine the modulus of elasticity (MOE).

4. Using the MOE value and Equation 3, predict the mean strength of each weak section.

5. Generate a random strength value from an assumed normal distribution with an assumed coefficient of variation and the above mean strength. (In this exercise COV values of 0.0, 0.1 and 0.2 were used.)

6. Obtain the approximate strength reduction ratio $\tilde{R}$, using the grading machine readings.

7. Using Equations 7,9 and 10, obtain the strengths in the region adjoining the weak section.

4 Analysis of beams

On having simulated the cross sectional strength profile of a beam, to obtain the beam strength values it is necessary to analyse the it under the relevant bending moment diagrams. Here the 'strength' of a beam under a given moment profile is determined in terms of the bending moment at the position of maximum moment when the beam fails at any position along it(see Figure 2). This bending moment can then be converted to a bending stress.

In the present case of statically determinate beams with simple bending moment profiles, this analysis can be carried out with a simple computer program into which the required bending moment profiles have been programmed. If this option is used then, whenever a new problem is to be considered, the new moment profile will need to be computer coded anew. This is a laborious process and can give possible errors in compute coding. Besides, such a program will become difficult for complicated statically indeterminate beams, and cannot be used when the variation of elasticity modulus

need to be considered. However, the use of a finite element program eliminates all these problems and shortcomings. Once the finite element model is available, beam strength analysis for any beam (within the program's class of structures and analysis) can be carried out quite conveniently. Changes in loading patterns, boundary conditions, supports, etc. can be accommodated without additional programming through the data input procedure. Hence, it was decided to implement a finite element analysis at this initial stage itself.

The used finite element program is based on the simple 2-noded cubic beam element. It carries out linear elastic analysis only. This program was augmented with strength determination and allocation routines so that the generated strengths can be input to the finite element analysis routines.

The generated strengths of weak sections and their adjoining areas were used to find the strength of each finite element. If the regions of influence of weak sections overlapped, then from among the contributions of each of them, only the least value was used as the strength of the particular cross section(Figure 6). Within each finite element, the strength was assumed to be constant. The details of the finite element program and the associated strength determination routines are available in its users' manual[12].

5 Results

In the following, most of the results to be dealt with refer to a COV value of zero. The results, especially for the higher COV values will become relevant only once the complete set of beams are simulated and analysed statistically.

The present results are based on analyses which used 70 finite elements to discretise the complete beam. A comparison of beam strength results obtained with 70 and 140 finite element discretisations for the central concentrated load case showed that the maximum error was less than 1.5% of the value for the latter for all n and k combinations. Thus, the concentrated load

case being the most critical with respect to discretisation, 70 finite elements were considered sufficient for the current analyses.

5.1 Effect of width of defect influence

Figures 7 to 9 show the generated strengths for the concentrated load case under different strength COVs and parameters (n, k) for defect influence widths. In the case of random generation of strength, for each COV case the number generator was re-initialised to make a given beam have the same standardised random value at a given defect, whatever the values of other variables n and k were.

From the above Figures it can be seen that the increase of the width of influence through higher values of n and k has resulted in a slight reduction in the beam strengths. This can be explained by the fact that the influence of defects will spread to the positions of higher bending moments when those parameters increase in value. The observed variations are similar for all the three cases of COV considered.

The corresponding graph for the uniformly distributed load case and a COV of zero is shown in Figure 10. In this case the variations due to the increase of defect influence width are not significant for most of the beams. This is because the slope of the bending moment diagram in the area of high bending moment (*i.e.* near the mid-span) is small, thus making the increase of defect influence width not much relevant to failure. Similar patterns were observed for the other two COV values considered.

Figure 11 shows the bending strengths under a uniform moment for the strength COV of zero. Contrary to what may be expected for a constant bending moment profile, the spread of defect influence has resulted in decreases of beam strengths. This is the result of some of the actual beams that went through the grading machine being much longer than the beam span considered here. In such a case, a defect which occurred just outside of

the beam span was able to affect the strength of the beam if its finite width of influence extended into the considered span.

5.2 Comparison of generated strength with measured strength

Figures 12 to 14 show comparisons of generated beam strengths under different COV with the actual measured beam strengths. The measured beam strengths have been determined for beams, in each of which, at least four cross sections were tested. No spread of defect influence was considered for the simulated beam strengths used in these comparisons.

In all three cases, the generated strengths are generally similar to the measured values. The effect of the increase of the coefficient of variation has been to make the generated and actual strengths, depending on the beam, either more dissimilar or more similar to each other. Hence an actual comparison can be made only after considering all the 133 beams and a statistical analysis.

5.3 Moment configuration factors

The moment configurations calculated for the individual beams are shown in Figures 15 and 16 for the concentrated load and uniformly distributed load cases, respectively. The width of defect influence is again considered as zero.

It can be observed that the MCFs calculated with measured strengths generally tend to be higher than those obtained from the simulation. This is more pronounced for the concentrated load case. This phenomenon may possibly be attributed to the limited number of sections used in the determination of the 'real' or measured beam strengths and the consequent MCFs. But, again, firm conclusions can be made only after the analysis of all the beams in the sample.

6 Discussion

The limited results presented in this paper showed that beam strengths can depend on the distance to which the reduction in strength due to a defect may extend. The importance of this phenomenon depends on the nature of the bending moment diagram, with those having higher slopes being influenced more. It can be reasonably argued that the width of defect influence is more important with respect to bending moment diagrams where high intensity localised peaks occur, and for short beams. It was also observed that the width of defect influence may affect uniform bending moment cases if the influence of a defect outside of the span is to spread to within the span.

It was seen that presence of a strength COV can result in different beam strengths than when only the regression equation is used. Hence, considering that the regression equation itself is an 'average' curve, it may be important to consider the COV in the simulation of beam strengths. Its importance for MCF studies will lie more on the way it influences the lower tails of the determined beam strength distributions.

The differences in the predicted and measured strengths need to be accepted as a part of the present limited nature of the analysis. However, the prediction of reasonable strengths and the generally conservative nature of predicted MCFs have shown the usefulness and the importance of the current attempt at predicting the along-member variation of beam strengths using grading machine readings. It can be expected that improvements to the procedure, including the measurement of strengths in clear wood regions, would help in predicting strengths more accurately.

There are several improvements to be made to the simulation procedure itself. At present the manual procedure for obtaining grading machine readings corresponding to non-major defects involves some subjectivity. Hence, there is a need to make this procedure more objective. If objective criteria can be developed, then the procedure may be automated to be carried

out in a computer, thus saving a considerable amount of time. It needs to be additionally studied as to how the above subjectivity may influence the generated strengths.

Currently, the width of influence of a weak section is considered to depend on the grading machine reading, instead of the generated strengths. Thus, at present, the strength COV does not influence the width of influence. However, this problem will not arise when the clear area wood strengths become available.

7 Conclusions

The following conclusions can be made from the limited analyses carried out so far with respect to beam strengths.

- The present project on the determination of along-member beam strengths seems to provide good prospects for the calculation of moment configuration factors(MCFs).
- It is desirable to gather information on the way and the extent to which the strength reductions due to defects may spread along a beam.
- It is advisable to have information on the possible strength coefficients of variation (COVs) with respect to the regression analysis predictions.
- It is necessary to study the effect of the possible subjectivity of manually selected defect positions on the generated strength results. This subjectivity occurs for beams with many smaller close depressions in the graph of force *vs.* the beam length.
- The determination of valleys in the grading machine readings, which may correspond to defects, need to be automated. For this purpose objective criteria need to be developed.

- Firmer conclusions can be made only when the strength predictions of all the 133 beams are simulated and a statistical analysis of results is carried out.

References

[1] Riberholt, H. and Madsen, P.H.; *Strength distribution of timber structures. Measured variation of cross sectional strengths of lumber*, Struct. Res. Lab., Tech. University of Denmark, Rept. R114, 1979.

[2] Riberholt, H.; *Safety of timber structures*, Struct. Research Lab., Tech. University of Denmark, June 1979.

[3] Czmoch, I., Thelanderson, S. and Larsen, H.J.; *Effect of within member variability on bending strength of structural timber*, Proc. Intl. Council for Building Research Studies and Documentation, Working Commission W18A, Meeting 24, Oxford, UK, Sept. 1991.

[4] Madsen, B.; *Structural behaviour of timber*, Timber Engineering Ltd., North Vancouver, BC, Canada, 1992.

[5] T.D.G. Canisius, *Moment Configuration Factors for Simple Beams*, Proc., Int'l Council for Building Research Studies and Documentation, Working Commission W18A,Meeting 26, Ahus, Sweden. August 1992.

[6] T.D.G. Canisius, *Effect of the Elasticity Modulus on the Simulated Bending Strength of Hyperstatic Timber Beams*, Proc., Int'l Council for Building Research Studies and Documentation, Working Commission W18A,Meeting 26, Ahus, Sweden. August 1992.

[7] Canisius, T.D.G.; *Reliability-based moment configuration factors: a parametric study*, BRE Clinet Report, Proj GD263, Garston, UK, August 1993.

[8] Canisius, T.D.G.; *Variation of moment configuration factors with the strength quantile* BRE Internal Report, Proj GD263, Garston, UK, March 1994.

[9] Canisius, T.D.G.; *Reliability-based configuration factors for timber beams*, Structual Safety, **16**, pp. 215-226, 1994.

[10] Isaksson, T., Thelandersson, S., and Moller-Pederson, T.; *Within member variability of bending strength of timber*, Proc., Pacific Timber Eng. Conf., Gold Coast, Australia, pp.634-641, July 1994.

[11] Kallsner, B. and Ditlevsen, O.; *Lengthwise bending strength of variation of structural timber*, Proc., IUFRO Timber engineering meeting, Sydney, Australia, July, 1994.

[12] Canisius, T.D.G.; Manual for beam simulation program BEAMSIM, BRE, Garston, April 1995.

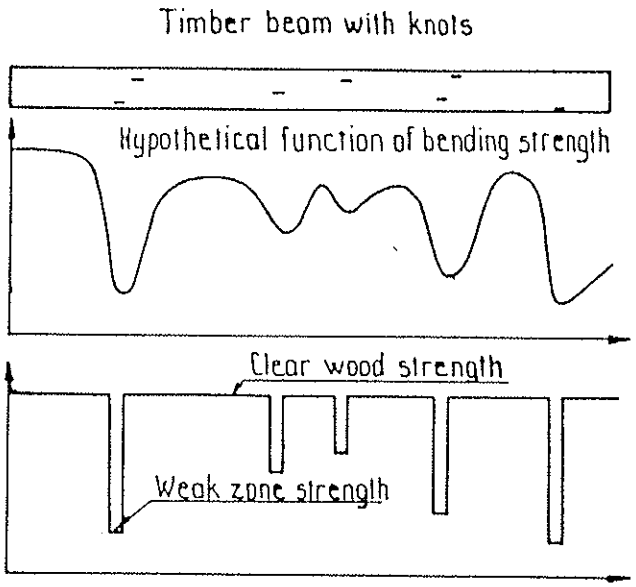

Figure 1: Modelling of lengthwise variation of bending strength

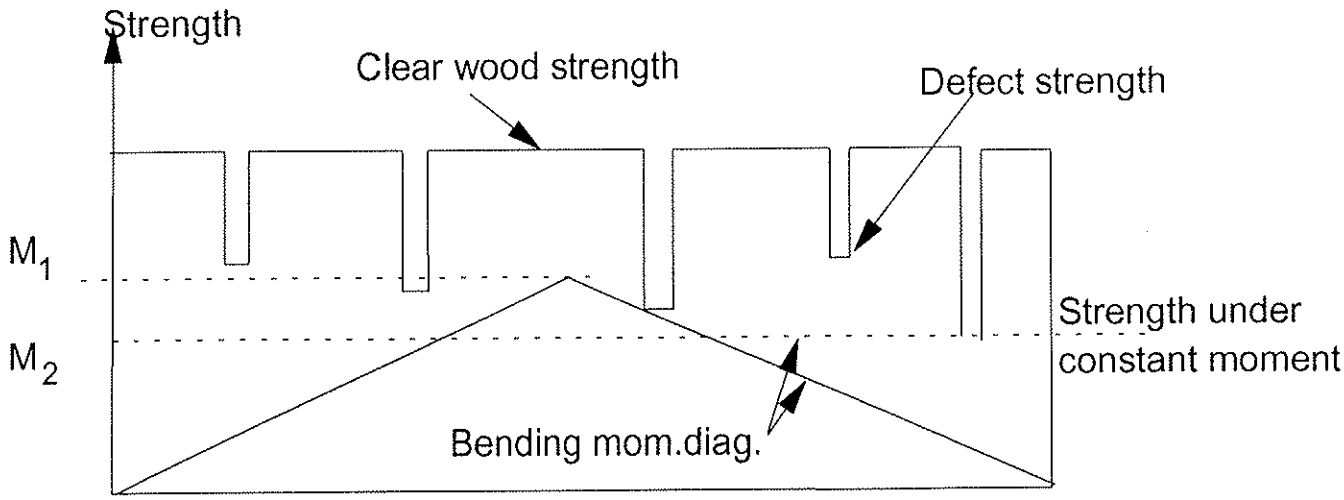

Figure 2: Differences in bending strength due to moment configuration

Figure 3

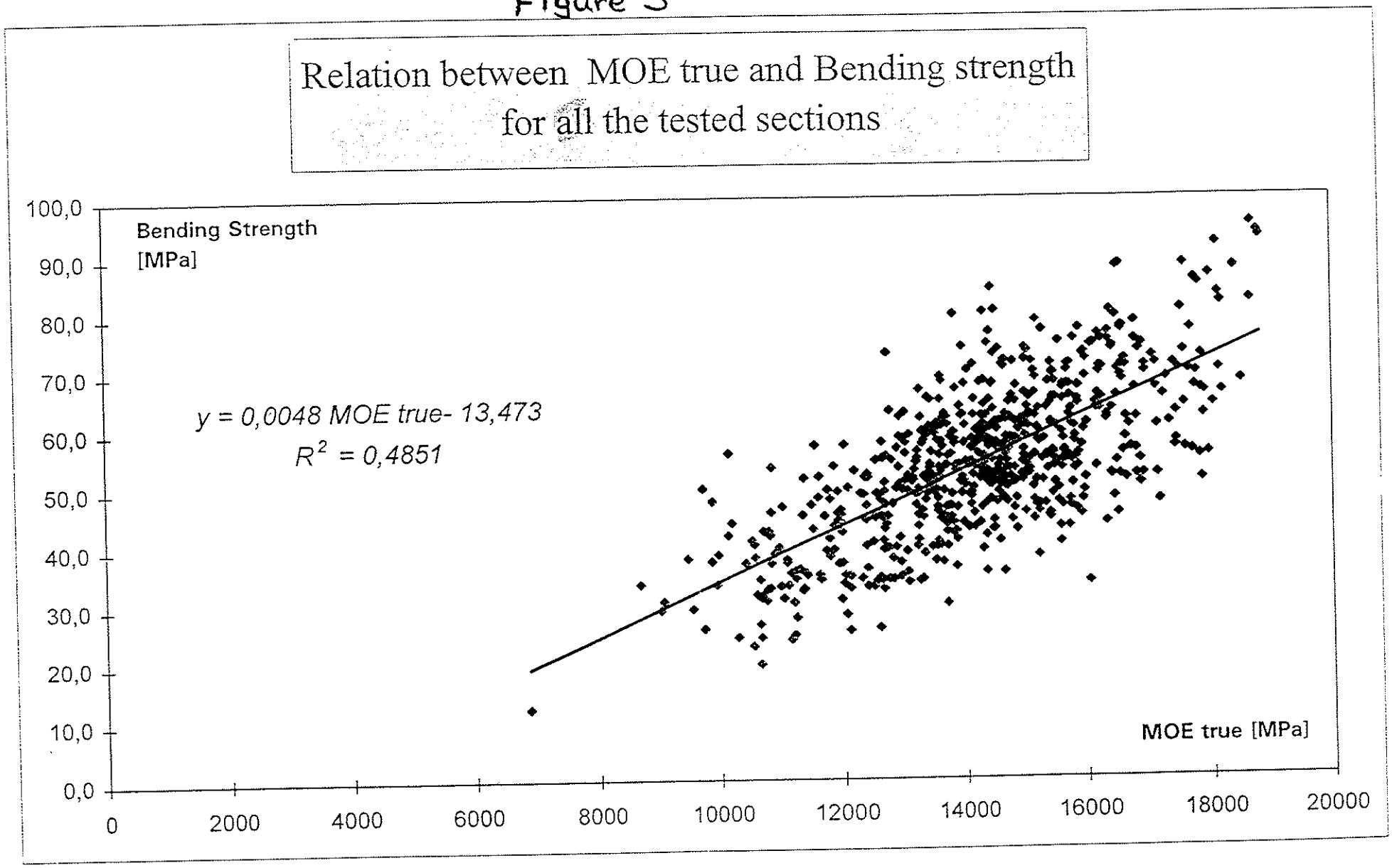
Relation between MOE true and Bending strength for all the tested sections
Bending Strength [MPa]
y = 0,0048 MOE true- 13,473
R² = 0,4851
MOE true [MPa]
100,0
90,0
80,0
70,0
60,0
50,0
40,0
30,0
20,0
10,0
0,0
0
2000
4000
6000
8000
10000
12000
14000
16000
18000
20000

Figure 4

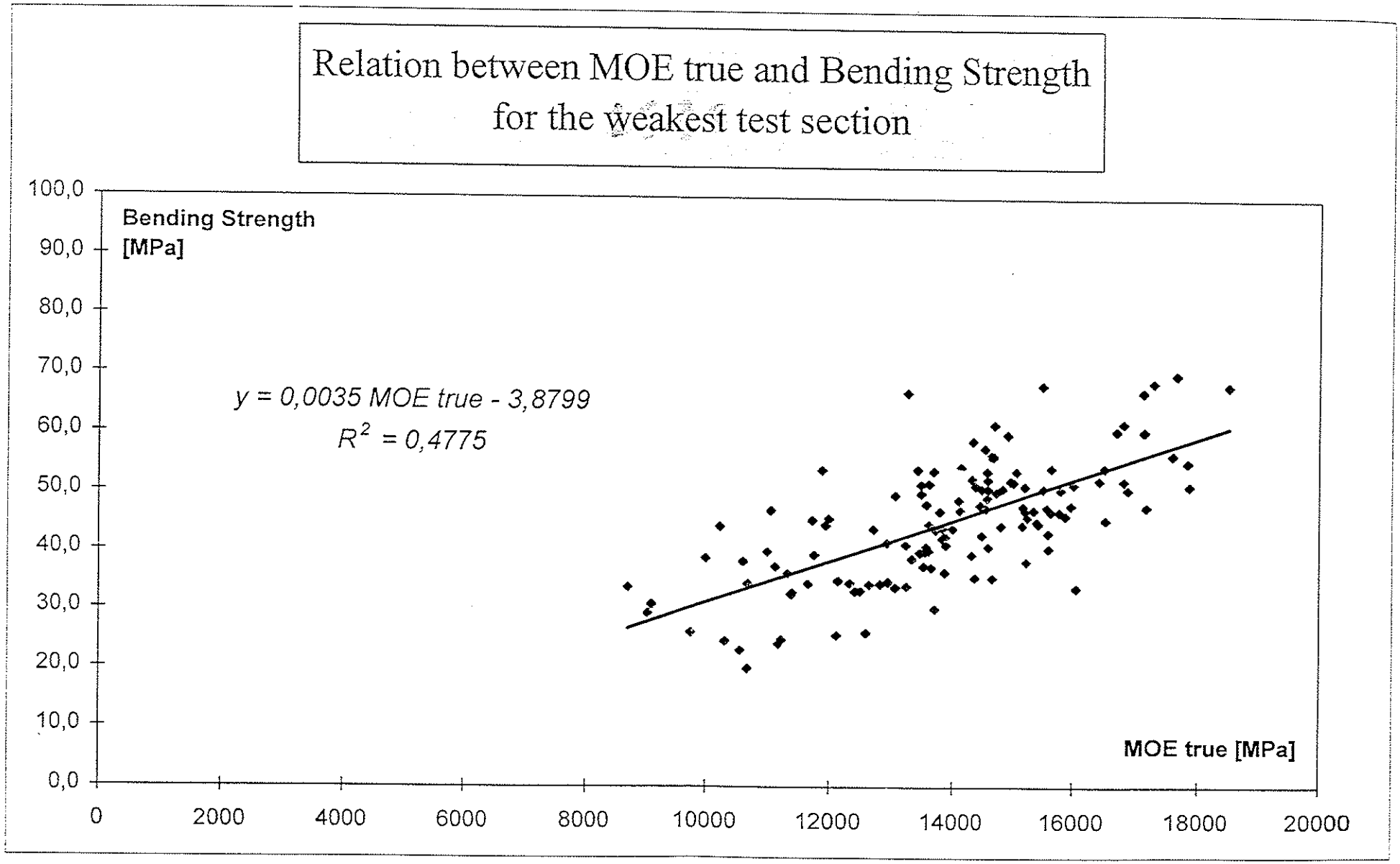
Relation between MOE true and Bending Strength
for the weakest test section
Bending Strength
[MPa]
y = 0,0035 MOE true - 3,8799
R² = 0,4775
MOE true [MPa]
100,0
90,0
80,0
70,0
60,0
50,0
40,0
30,0
20,0
10,0
0,0
0
2000
4000
6000
8000
10000
12000
14000
16000
18000
20000

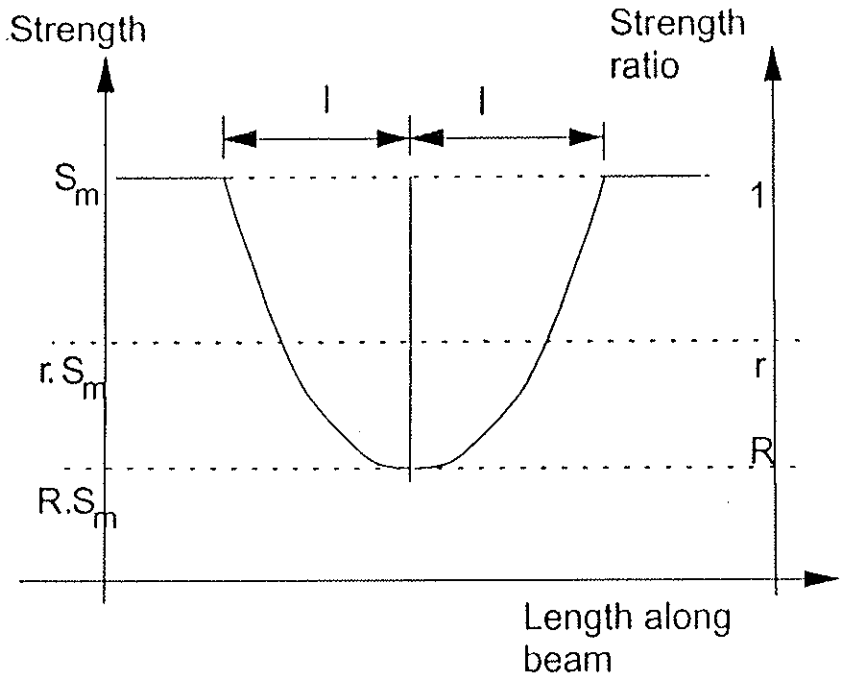

a)

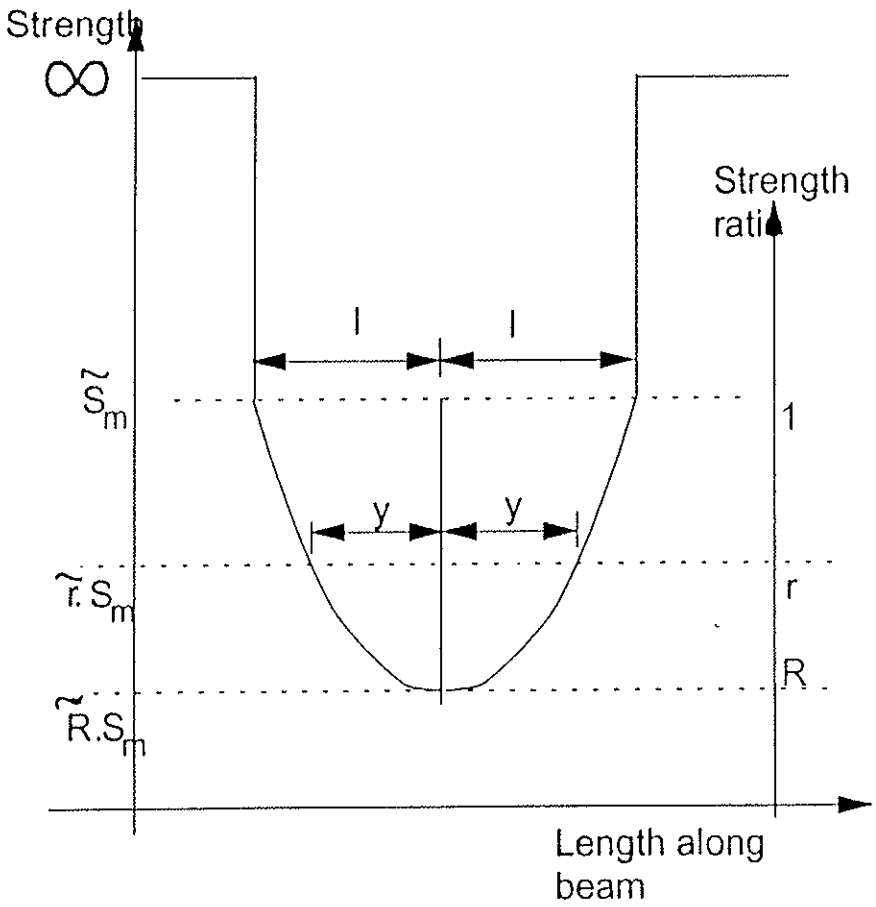

b)

Fig. 5: Strength in the vicinity of a defect:
a) Assumed b) Approximated

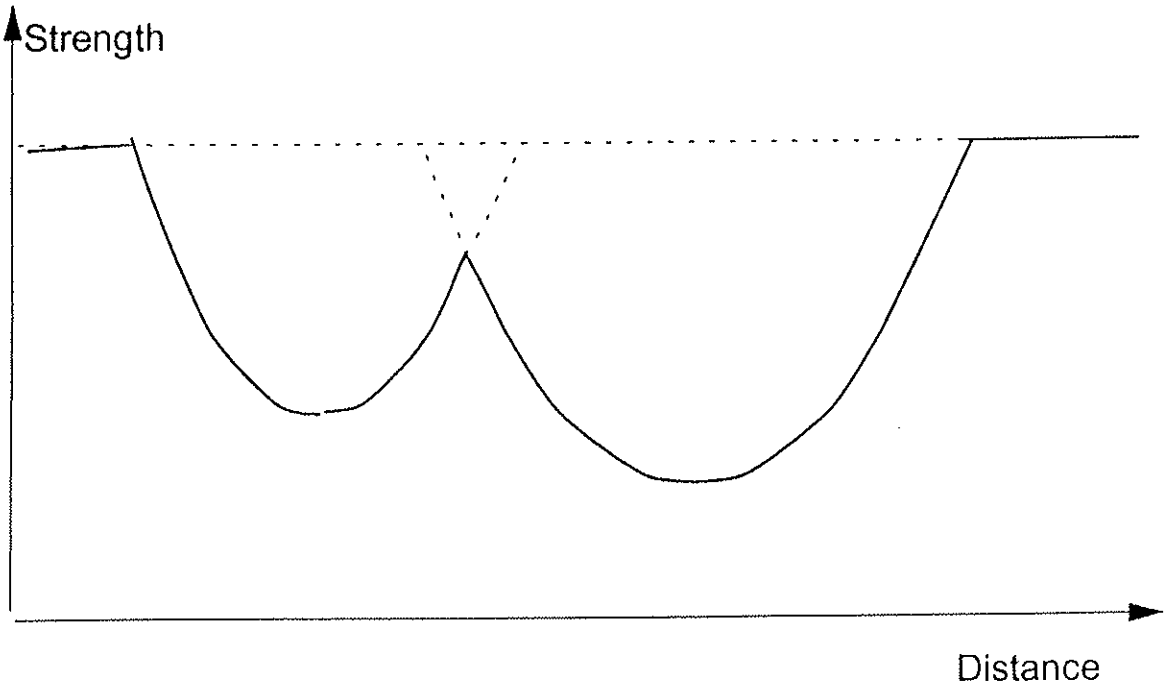

Figure 6: Strengths at sections with overlap of regions of defect influence

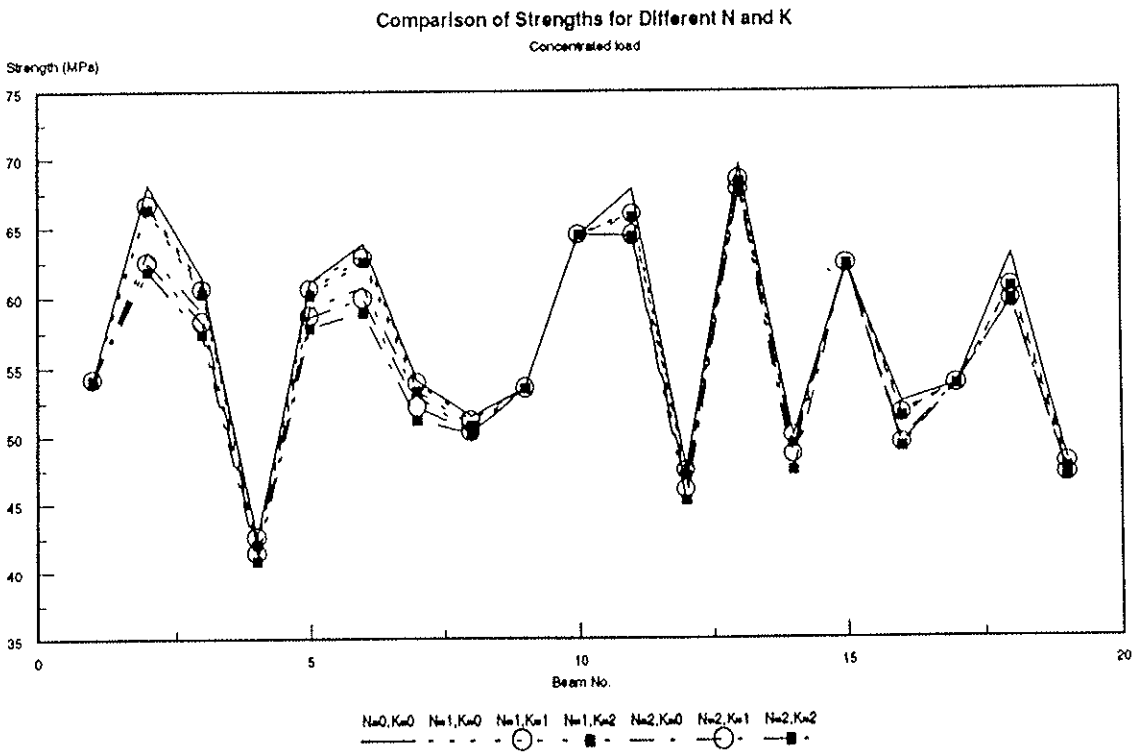

Figure 7

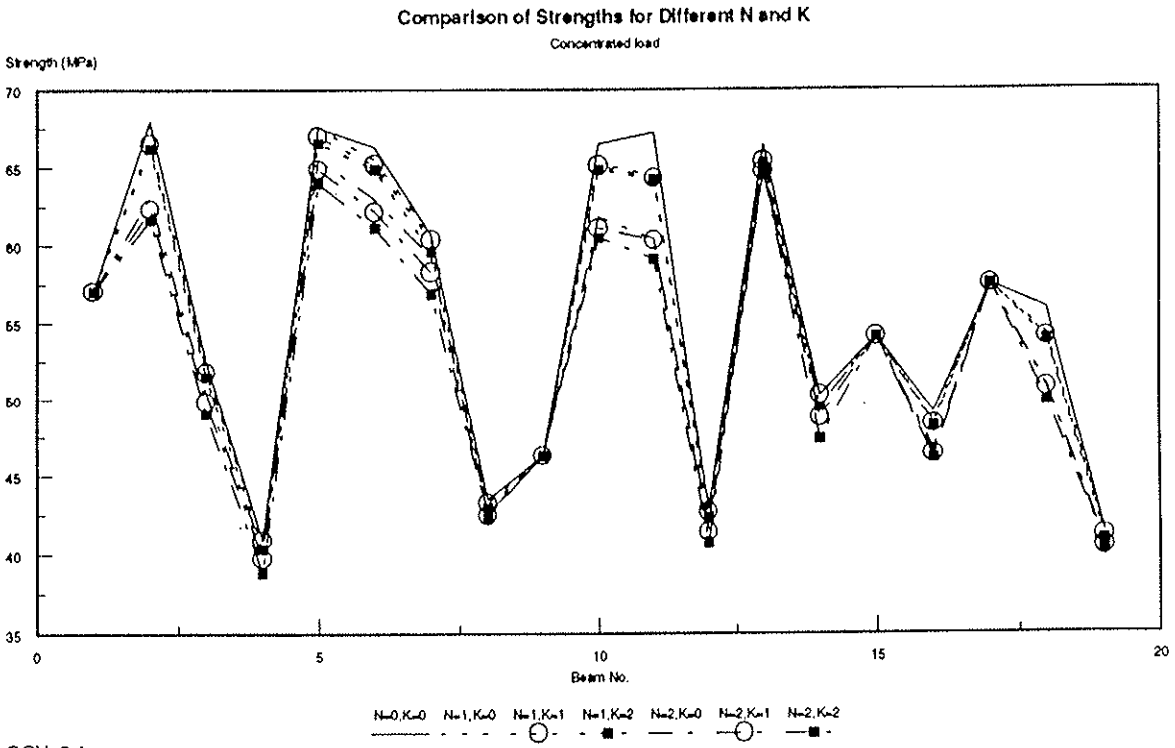

COV=0.1

Figure 8

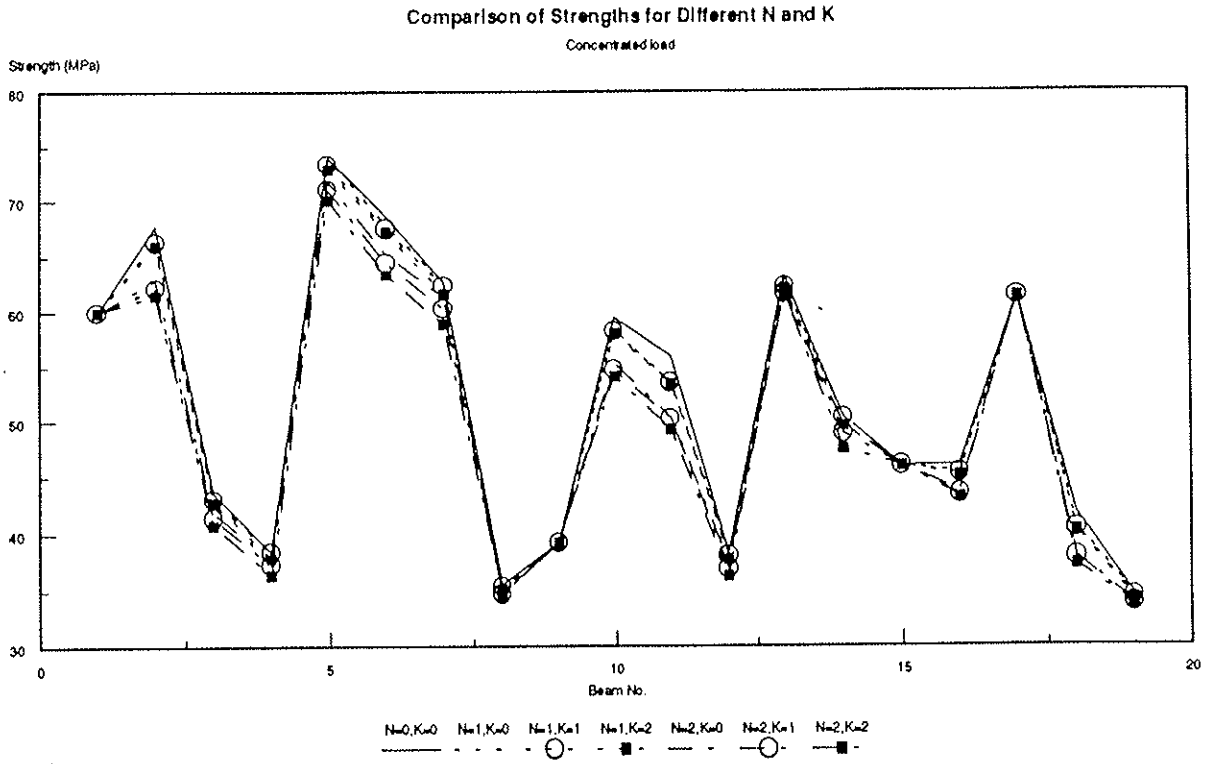

COV=0.2

Figure 9

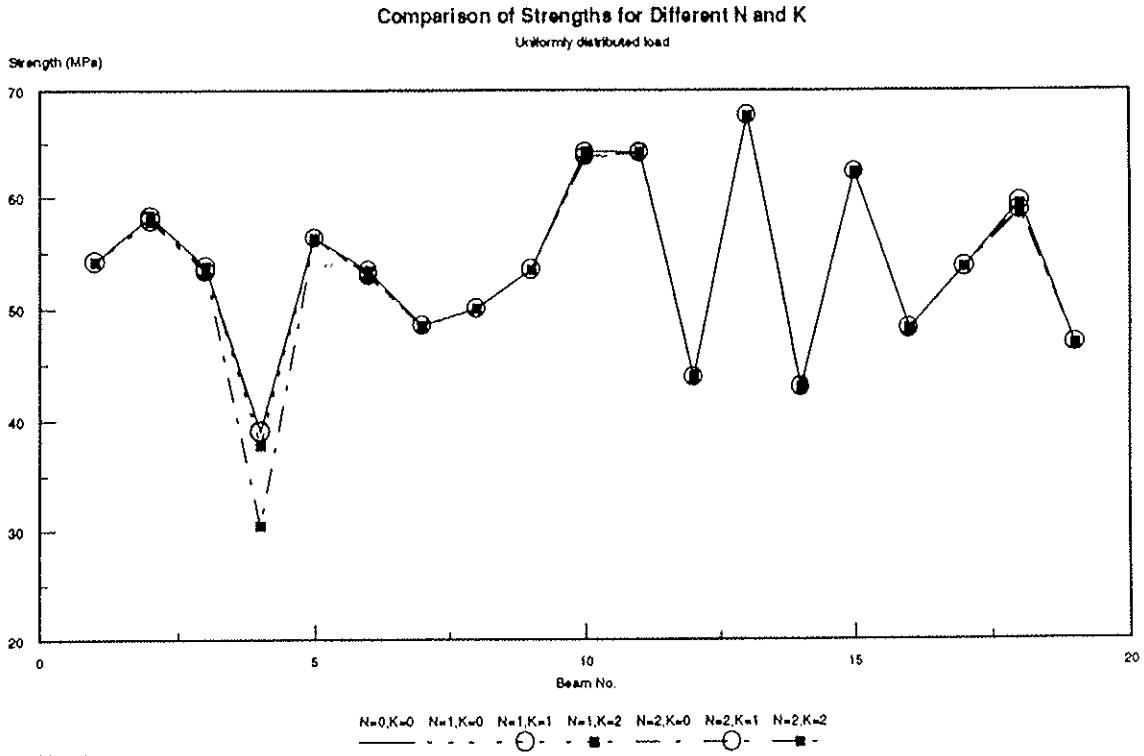

COV=0.0

Figure 10

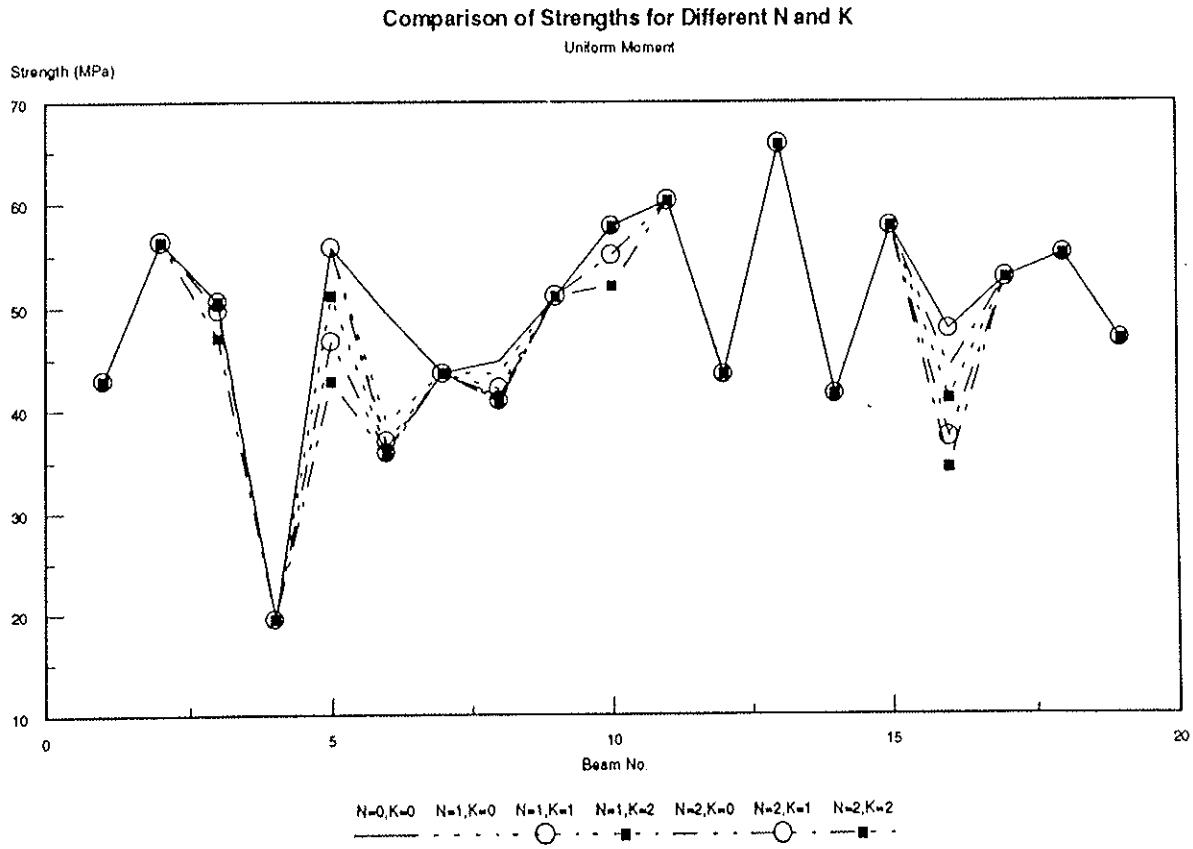

COV=0.0

Figure 11

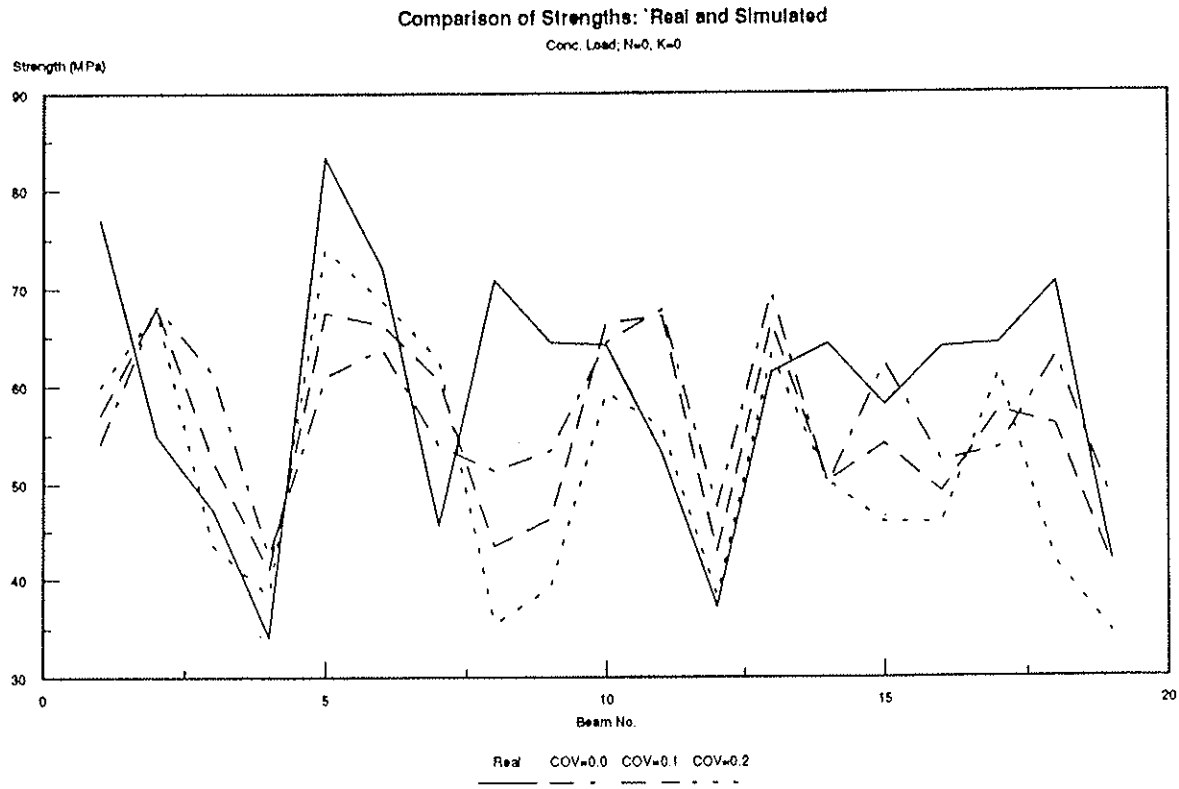

Figure 12

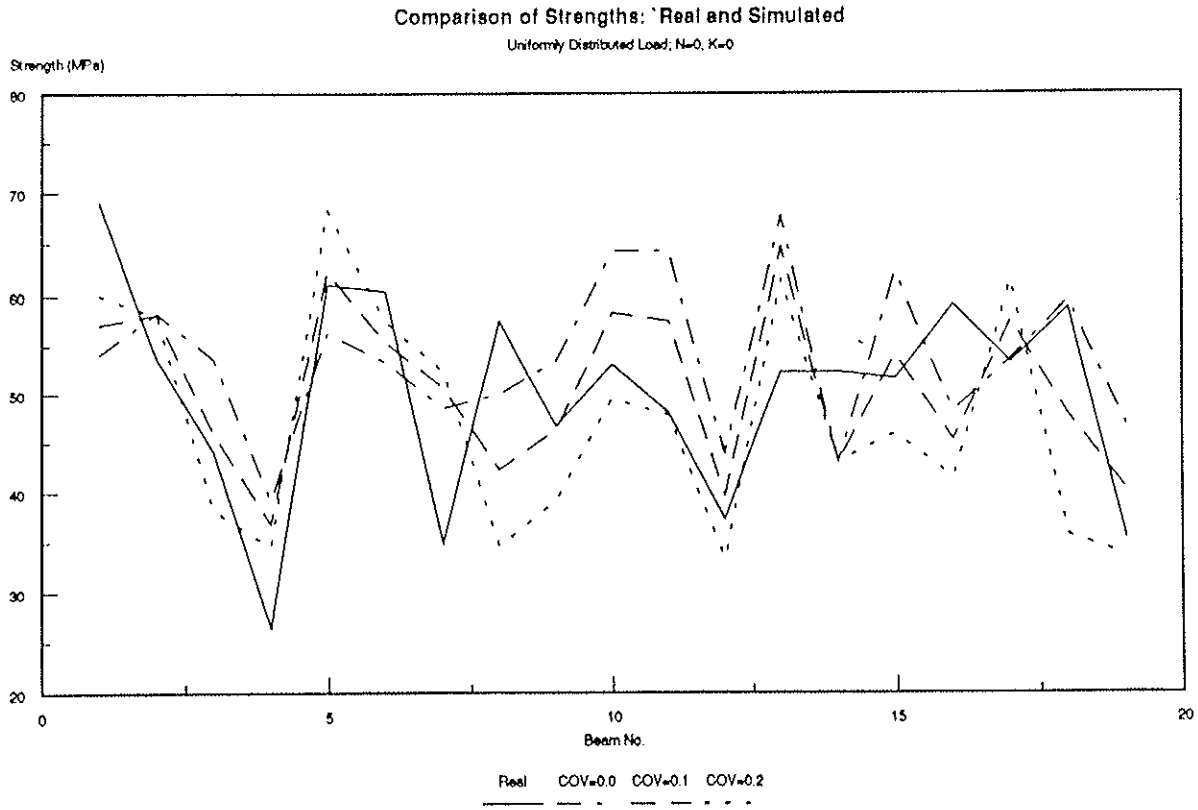

Figure 13

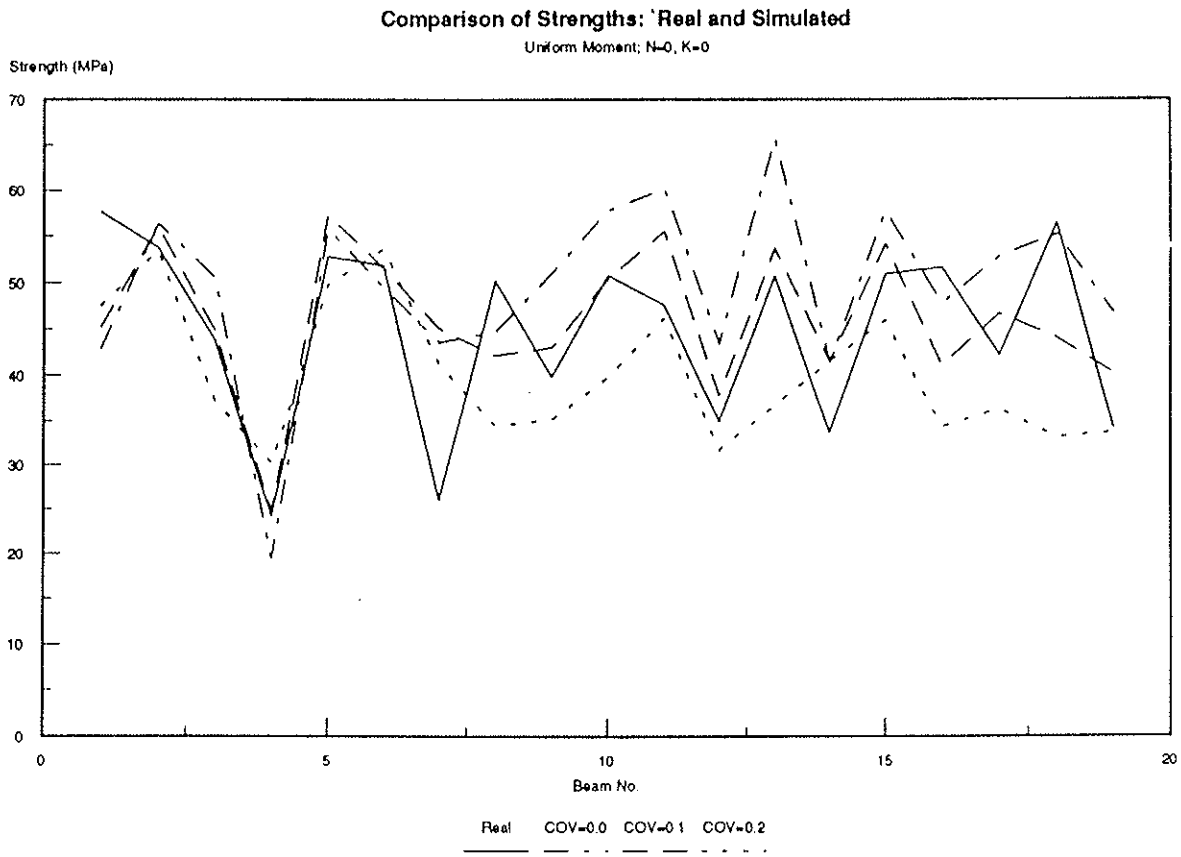

Figure 14

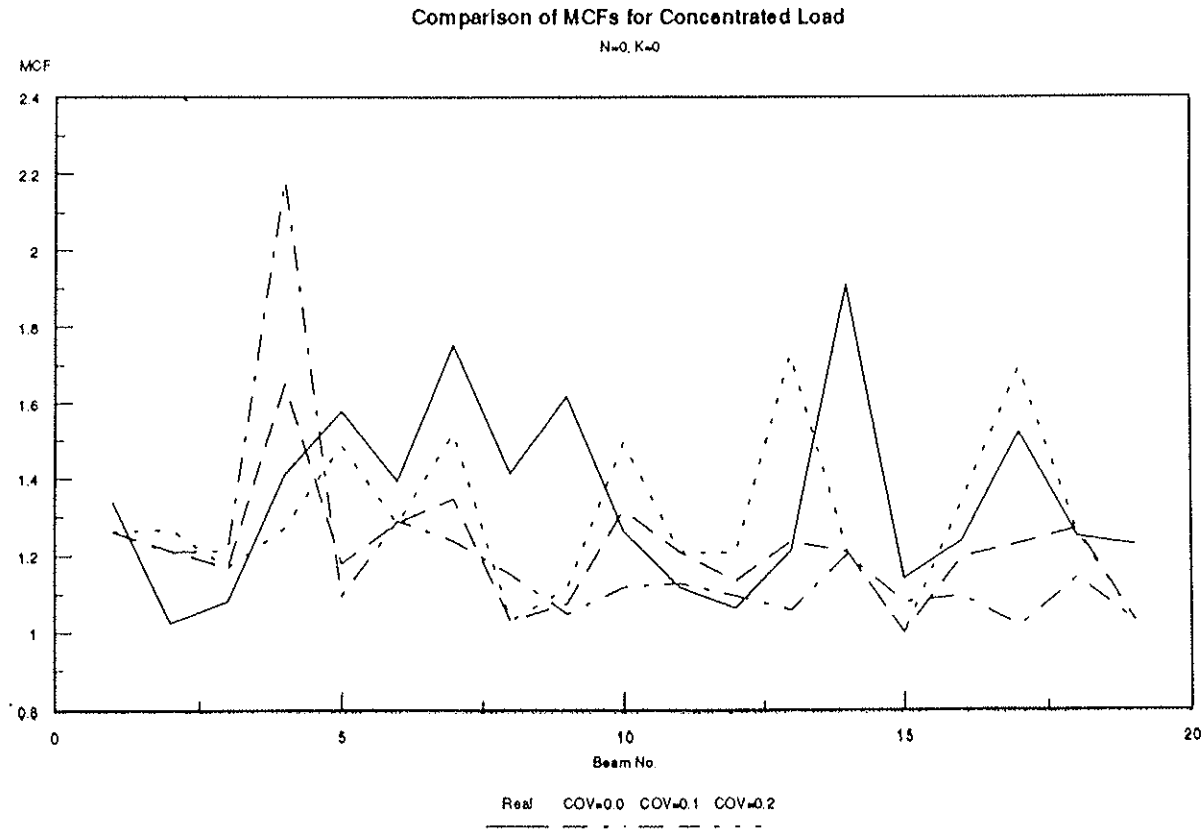

Figure 15

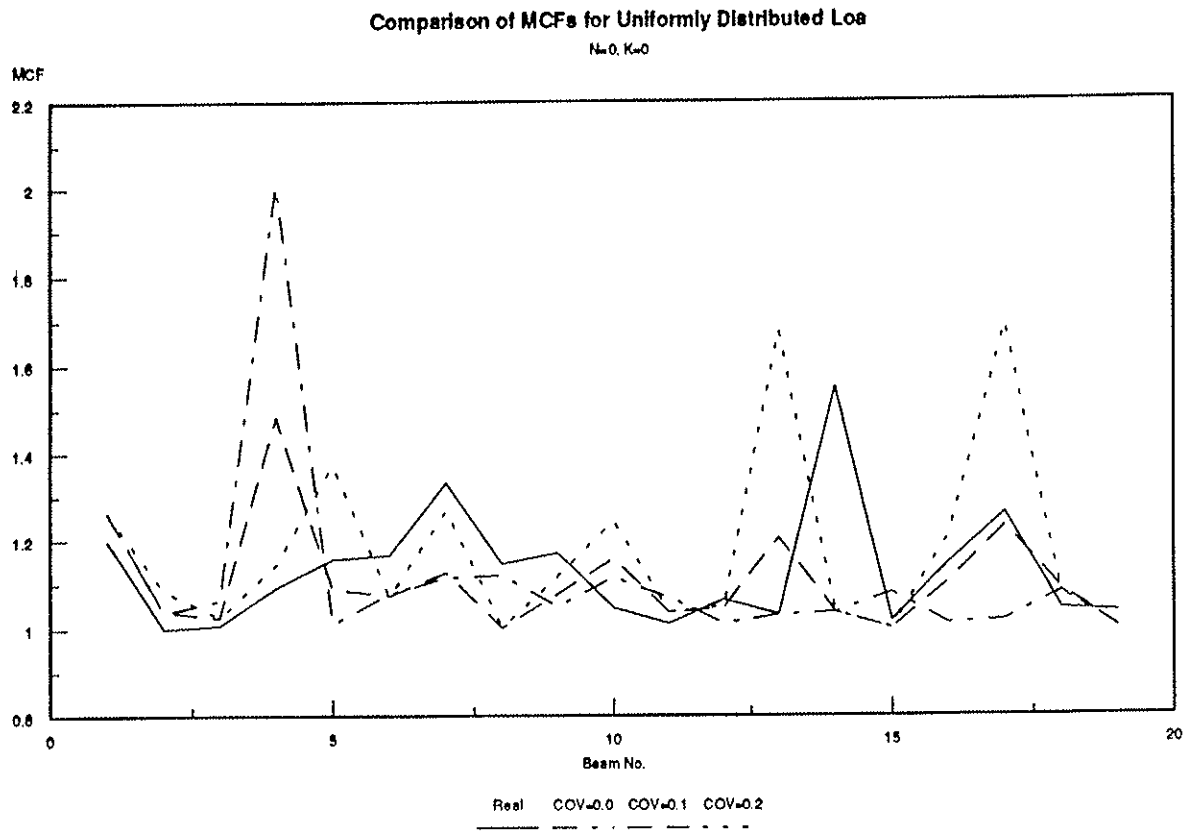
Comparison of MCFs for Uniformly Distributed Loa
N=0, K=0
MCF
2.2
2
1.8
1.6
1.4
1.2
1
0.8
0
5
10
15
20
Beam No.
Real
COV=0.0
COV=0.1
COV=0.2

Figure 16

CIB-W18/28-6-6

INTERNATIONAL COUNCIL FOR BUILDING RESEARCH STUDIES AND DOCUMENTATION

WORKING COMMISSION W18 - TIMBER STRUCTURES

END CONDITIONS FOR TENSION TESTING OF SOLID TIMBER PERPENDICULAR TO GRAIN

by

T Canisius
Building Research Establishment
The United Kingdom

MEETING TWENTY - EIGHT

COPENHAGEN

DENMARK

APRIL 1995

End conditions for tension testing of solid timber perpendicular to grain

Tantirimudalige D. G. Canisius
Timber Structures Section,
Building Research Establishment,
Bucknal's Lane, Garston, Watford WD2 7JR, U.K.

Abstract

It is specified in the draft CEN Standard prEN1193[1] that for tension tests perpendicular to grain of solid timber, the platens be pinned with the pin axis parallel to the grain direction. This is in contrast to the requirement to have 'clamped' ends for the testing of glulam specimens. In this paper, the reason for this difference in requirements is explained with a finite element stress analysis.

1 Introduction

Timber tensile strength perpendicular to grain is required for several design situations. Although this tensile failure is a fracture phenomenon which may be handled more vigorously through fracture mechanics criteria (for example, see [2]), simple strength tests are used in the design of structures.

The tests for obtaining the tensile strength and stiffness (Young's modulus) perpendicular to grain in both solid and glulam timber are specified in the draft CEN Standard prEN1193[1]. There, it is specified that tests with glulam timber be carried out with specimens whose ends are essentially under 'clamped' conditions. Here a 'clamped' condition refers to one which restrains the platen against rotation and lateral movement, thus allowing

only a uniform movement in the axial direction of the specimen. In the case of solid timber, it is specified in the draft Standard that the tests be carried out with pinned end conditions, with the pin-axis parallel to the grain direction. It is this difference in requirements for glulam and solid timber which is explained in this paper.

1.1 The proposed CEN test method

Traditionally tension test specimens for structural materials were 'necked' at their central portions. The reason for such narrowing down was to facilitate failure in a predictable region possessing a close-to-uniform stress distribution. In contrast, if a specimen is of uniform cross section then, due to stress concentrations, there would be a higher tendency for failure to occur at a support. This is especially relevant for brittle materials where no stress re-distribution can occur.

The above traditional approach to testing of small specimens has not formed the basis for the tests specified in prEN1193 which is concerned with medium and large size specimens. The idea of using uniform cross-sectional specimens in such larger sizes is to make failure occur possibly at a naturally weaker position of the specimen, instead of at a position pre-determined by the test method. Such a condition is especially important because of the inhomogeneous nature of timber, size-dependency of its strength, its polar orthotropy centred on the pith position, and the occurrence of defects which need not be small.

The original drafts of prEN1193 specified that 'clamped' ends be used for both glulam and solid timber specimens. This is a very practical condition with respect to glulam specimens which may need to be tested in larger sizes (for example, $250\times100\times400\text{mm}^3$), with pinned conditions being possibly impractical for them. Consequently, it would have been natural to extend this criterion also to the testing of solid timber specimens which, however, are

smaller, *viz.* $70\times45\times180\text{mm}^3$, than the glulam specimens.

During work carried out at the Building Research Establishment to evaluate the solid timber test with clamped end conditions, it was found that a considerably larger proportion of specimen failures occurred at or very close to the specimen ends[3]. This was observed both with and without parallel to grain timber end pieces connected to the specimen, as allowed for by the proposed Standard. But, when the specimen ends were connected to pinned platens, the occurrence of such undesirable failures became much lesser than that with the previous clamped end conditions. Hence, it was proposed, and later accepted by the Standard's Committee, that pinned end conditions shall be used for perpendicular to grain tension test specimens of solid timber.

1.2 Scope

A major contributing factor to the above observed difference in behaviour under the two types of specimen end conditions will be explained in this paper. Finite element stress analyses are used for this purpose. The two specimen ring configurations considered are shown in Figure 1.

This study was carried out with several simplifying assumptions, with the following being the significant ones.

1. The specimens are perfect with respect to ring geometry. No cracks or defects exist in the specimens.

2. The specimens are homogeneous with respect to a polar coordinate system based on the tree pith (see Figure 2). That is, there is no variation of properties either radially (due to late/early wood or heart/sap wood or defects) or tangentially (due to defects).

3. The wood is specially orthotropic with the principal material directions based on the polar coordinate system referred to above.

4. The specimens and the platens are under plane stress conditions.

Further assumptions will be either mentioned or implied in the appropriate sections.

2 Numerical modelling and analysis

The finite element model and the method of analysis are described in the following sections. The analyses were carried out in a '486DX' personal computer.

2.1 Finite element model

The numerical analysis was carried out with a slightly modified version of the FEM finite element program of Foschi, Barrett and Lau[4]. The following modifications were carried out to its original version provided by Prof. Ricardo Foschi of the University of British Columbia.

1. Conversion to run in a personal computer. In order to overcome memory problems, major arrays were made to be written into random access binary scratch files. (This, of course, reduced program speed).

2. Introduction of automatic generation of principal material directions (radial and tangential directions) of each finite element, given the location of the pith.

3. Inclusion of calculation of reactions at displacement restraints.

The basis of the FEM program is the standard orthotropic eight-noded isoparametric quadrilateral finite element. Both plane stress and plane strain analyses, of which the former was considered to be more relevant to the present study, are allowed by the program. Further details of the FEM program can be had from its original users' manual[4] and its current modified version[5].

2.2 Finite element discretisation

Figure 2 shows a typical discretisation used in the finite element analyses reported here. The symmetry about the 'horizontal' geometric centre line (C-C) of the specimens made it possible to analyse only one half of each problem. The boundary conditions to be used along this centre line to account for such symmetry are given in Figure 2. These conditions are zero vertical displacements (v) and free horizontal displacements (u) - with zero horizontal nodal forces - at the nodes along the specimen centre line C-C.

Although the finite element discretisation could have also been in a ring-wise manner, it was carried out here with rectangular elements in a rectangular grid. The latter was easier to use because of the easier fitting of the specimen shape and the fact that the node and element generation routines in the computer code dealt with straight lines only.

Two levels of discretisation, *viz.* coarser and finer, were used in the analyses. The results presented here are from the finer discretisation which had 30 elements in the 45mm width direction and 45 elements in the 90mm height direction(Figure 2). The coarser discretisation, with 15 and 26 elements in the width and height directions, respectively, was used to obtain information on the sufficiency of the finer discretisation for the present study.

As required by the FEM program, the principal material directions, *viz.* the radial and tangential directions, of each finite element were assumed to be constant within it and to be equal to that at its geometric centre. The effect of this approximation becomes negligible as the fineness of the discretisation increases. Although the current discretisation was found to be not yet sufficient to provide smooth tangential stresses at the specimen edges, no further discretisation was attempted as this exercise is a comparison of results for different end conditions under identical discretisations. Besides, due to stress concentrations, finite continuous discretisation cannot be expected to reach convergence at the specimen edges near the platen.

E_R	E_T	G_{RT}	ν_{RT}	ν_{TR}
$1000\,\mathrm{N/mm^2}$	$625\,\mathrm{N/mm^2}$	$230\,\mathrm{N/mm^2}$	0.470	0.294

Table 1: Specially orthotropic properties for softwood.

2.3 Material properties

Based on values reported in [6], properties as given in Table 1 were assumed for the softwood specimens. In this Table, E is the Young's modulus, G is the shear modulus, ν is the Poisson ratio, and R and T are the radial and tangential directions, respectively. For the platen, which was assumed to be of mild steel, the Young's modulus was 2×10^5MPa and the Poisson ratio was 0.3.

2.4 Application of load and displacement boundary conditions

In the case of pinned specimens a load of 1kN was applied at the provided pin at the position A shown in Figure 2. Moderate variations of this position (even away from the specimen with an additional attachment shown in the Figure) were observed to *not* provide any significant variations in the studied stress regimes.

For the clamped condition, the load was applied through a 1mm uniform vertical displacement of the platen. This was implemented by applying this displacement to the nodes I, A and J in Figure 2. Additionally, these nodal points were restrained against horizontal displacements. On having applied the uniform displacement, the actual stresses were obtained by scaling the determined stresses with the total applied load to reflect a total load of 1kN. The total applied load was the sum of the vertical forces at the nodes I,A

and J.

2.5 Analysis details

Only linear elastic analyses were carried out in this study. Choleski decomposition was used for the solution of matrix equations. The stress sampling was at the Gauss numerical integration points in the elements. The used 3×3 numerical integration provided a maximum of nine stress samples in each finite element. No averaging of the stresses was carried out. The sampled (and presented) results were in terms of the radial and tangential stresses in the elements.

3 Results

A comparison of some radial and tangential stresses obtained under clamped and pinned platen conditions is presented in the following. It will be seen that certain stresses near the specimen edges somewhat zig-zag, indicating a possible lack of convergence (which, however, is impossible to achieve as the stresses tend to infinity there). However, under such condition either the specimen mid-point stress or the average of the stresses can be taken as a good reflection of the appropriate stress. Hence, the comparisons for discussion will be carried out with respect to the stress values at the centre lines of the extreme finite elements. But, for completeness, results at the extreme integration points also are presented.

3.1 Comparison of coarser and finer discretisations

Figure 3 is an example comparison of stresses in Specimen 1 under the pinned condition when analysed with both coarser and finer discretisations mentioned above. The stresses have been sampled along different horizontal lines at the heights given in the Figure. These horizontal lines where stresses

were sampled correspond to the top-most and middle integration points in the top-most wood finite elements under the respective discretisations.

While the results for the coarser discretisation zig-zags, the finer discretisation has smoother curves. In addition, the results at element centre lines in the coarser discretisation are similar to the results for the finer discretisation. This indicates a sufficiency of the discretisation for the purpose of the comparisons required in this study. These trends were observed also in the comparisons made under the clamped condition. In the case of the tangential stresses for the pinned condition, the coarser results zig-zagged more than what could be seen in Figure 3 for radial stresses. But, the element midpoint stresses followed a smoother curve similar to the one with the finer discretisation.

3.2 Specimen 1 under pinned and clamped conditions

This is the specimen with its pith at its left-edge at the coordinate (x=0,y=0).

3.2.1 Radial stresses

Figure 4 shows a comparison of the radial stresses in the clamped and pinned specimens, along the top-most integration point level (line L-L in Figure 2) which was at a height of 89.775mm from the symmetric centre line. In terms of the distance from the platen, this line of integration points was only 0.025mm away. At the left side, *i.e.* the pith side, the stresses in the clamped specimen are higher than those in the pinned specimen. This is reversed in the right-hand side. The highest stress occurs in the left-side, and it is on this side that the highest difference between pinned and clamped conditions can be observed.

At the left most integration point, the clamped specimen stress is approximately 21% higher than the pinned specimen stress. At the centre line of the left-most element this difference is 20.3% of the pinned specimen stress. On

the right-hand side, *i.e.* on the side away from the pith, at the right-most and element centre integration points, respectively, the pinned condition stresses are higher than the clamped condition stresses by 7.5% and 8.8% of the latter,

In this case, the maximum stress under pinned conditions is only slightly less than the clamped value, *viz.* 5.36MPa compared to 5.65MPa, respectively. However, the higher difference of the stresses at the two sides makes the clamped condition to be, generally, under a more critical radial stress regime than the pinned condition.

3.2.2 Tangential stresses

A pattern of differences similar to that for radial stresses can be seen also with respect to the tangential stresses shown in Figure 5. At the left-most integration point, the clamped specimen stress is greater than the pinned specimen stress by 19.6% of the latter. At the centre line of the left-most finite element this difference is 18.2%.

Consider the case of the stresses at the right-hand side of the specimen, near the x=45mm line. Here, at the right-most and middle integration points, respectively, of the extreme element the pinned condition stresses are greater than the clamped condition stresses by 9.6% and 15% of the latter.

As can be seen from the results, on the left side of the specimen, the clamped condition is clearly in a more critical stress regime than the pinned condition. On the right side of the specimen, although the pinned condition stresses are higher than the clamped condition ones, the level of the former is similar to its values at the left hand side of the specimen, thus making it less critical.

3.3 Specimen 2

Figures 6 and 8 show the radial and tangential stresses, respectively, in Specimen 2 under the two types of platen conditions. In this specimen the pith is outside of it, on the 'left' side at a coordinate of (x=-45.0,y=0.0). As can be observed, the differences in stresses under the two conditions are not as large as that for the previous specimen. At the previously considered stress sampling positions near the specimen edges, the differences in clamped and pinned condition stresses are always less than 10% of the respective smaller values.

4 Discussion

The above presented results were with respect to two specimen geometries which were not symmetric about their vertical centre lines.

In the case of Specimen 1, the respective stresses under the clamped and pinned platen conditions had significant differences of the order of 20% of each other. These differences were such that, the higher stresses under the clamped condition were more severe than when the stresses under the pinned condition were higher. Thus, during testing of such a specimen, it could be expected that more clamped specimens would fail near the supports than pinned specimens. This makes it advisable to use pinned conditions for tests of specimens with similar geometry.

The reason for less severity of the stresses in the pinned condition can be attributed to flexibility provided by the platen to accommodate the non-uniform deformation of the specimen. This can be seen from Figure ?? which shows the displacement at the points S and T (see Figure 2) of the specimen-platen interface.

In the case of Specimen 2, of which the pith was outside of it at a distance of 45mm from its end, the differences in stresses under the two conditions

were not significant. The reason for this can be the larger radii of the rings in the specimen. Due to these larger radii, the directions of which do not change within this specimen as much as they did within Specimen 1, the former deforms more uniformly than the latter.

When cross-sections available for testing of European softwoods are considered, those providing specimens similar to Specimen 1 are more common than those similar to Specimen 2. This is because the latter has to come from larger trees. Also common are specimens in which the piths occur within them. As the pith move towards the centre of the specimen, the differences between clamped and pinned conditions will become smaller because the specimens again tend towards vertical symmetry. Considering that the pinned conditions can only reduce the stress concentrations in all these specimens, it is important to choose it for the testing of solid timber.

It needs to be noted that due to the differences in the stress distributions within the specimens under different end conditions, the failure stress for a given specimen, when failing away from the platen, need not be the same under the two end conditions.

Glulam specimens, which are manufactured with laminations having different ring geometries, can be considered to possess vertically symmetry about the specimen centre line in an overall manner. This is because different laminations tend to cancel the asymmetric effects of each other, thus making the stress regimes possibly be similar under both pinned and clamped conditions. Hence, there is no necessity to have pinned conditions for the testing of glulam specimens.

5 Conclusions

Based on the results of analyses presented in this paper, the following conclusions can be made.

- For tension testing perpendicular to grain in solid timber, it is preferable to have pinned end conditions than 'clamped' conditions. Such a choice results in a reduction in stress-concentration related failures at or near the specimen ends.

- In the case of glulam specimens, no significant difference can be expected between results from pinned and clamped end conditions. This is because of their effective vertically symmetric *overall* nature.

References

[1] CEN prEN1193: Timber structures - Test methods - Structural timber and glued laminated timber - *Determination of additional physical and mechanical properties*, Draft, 1994.

[2] Petersson, H.; *Fracture design criteria for wood in tension and shear*, Proc. Pacific Timber Engineering Conference, Gold Coast, Australia, pp. 232-239, July, 1994.

[3] Canisius, T.D.G.; *Comments on draft standard prEN1193*, BRE, December 1993.

[4] Foschi, R.O., Barrett, D.J. and Lau, K.; *FEM Finite Element Program*, Users' manual, Western Forest Products Laboratory, Vancouver, Canada.

[5] Canisius, T.D.G.; *FEM2, Modified FEM Program*, Users' manual, BRE, Garston, January 1995.

[6] Bodig, J. and Jayne, B.A.; *Mechanics of wood and wood composites*, Van Nostrand-Reinhold, New York, USA, 1982.

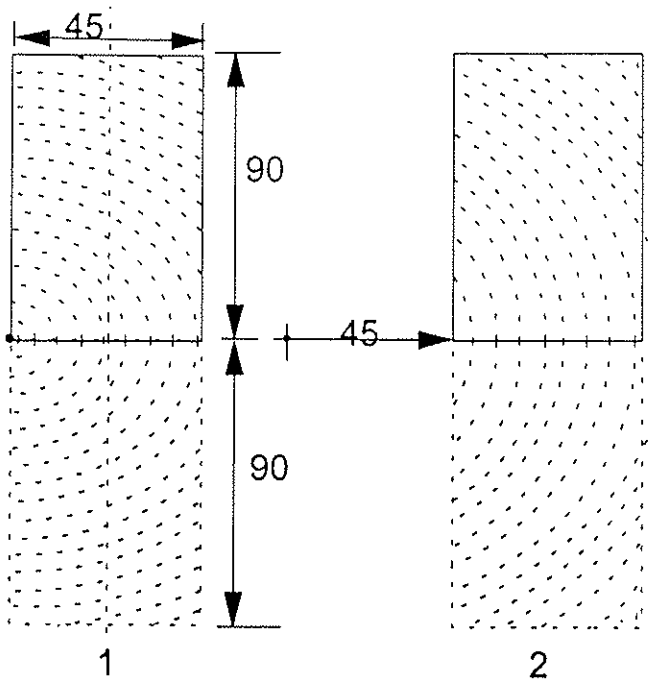

Figure 1: Analysed Specimens

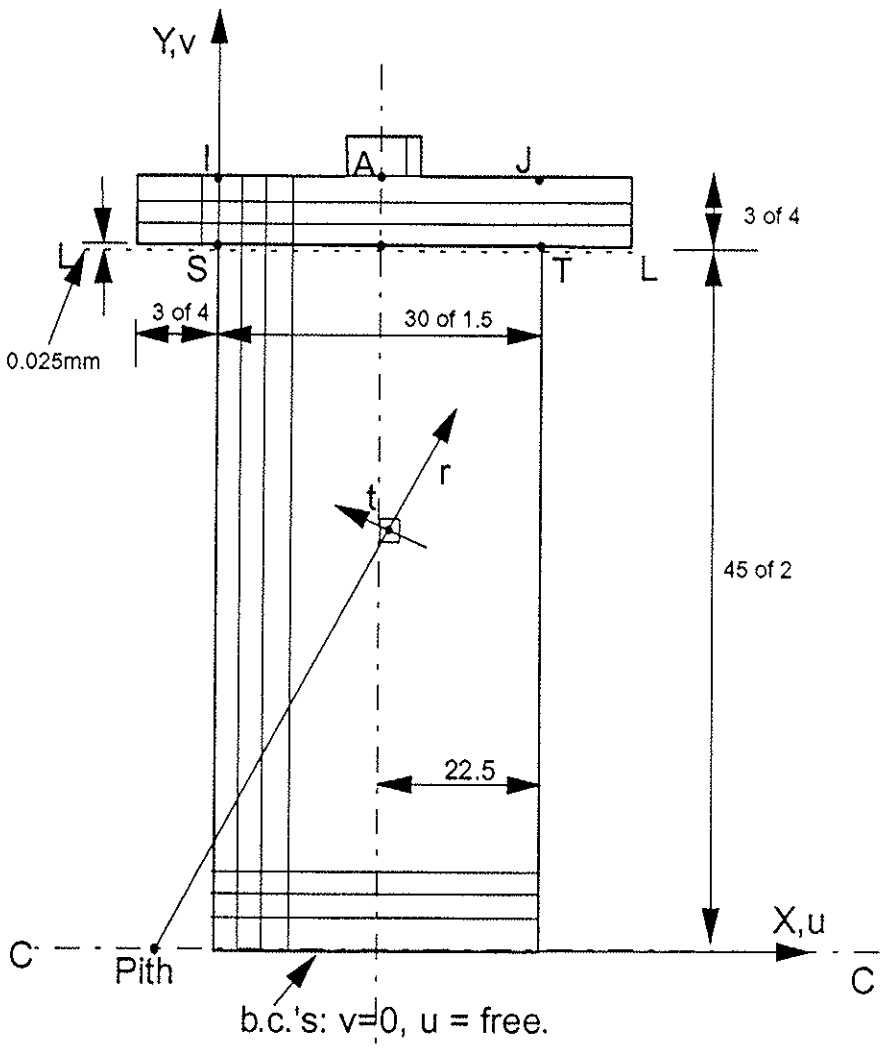

Figure 2: Finite element discretisation and modelling of specimen

Figure 3

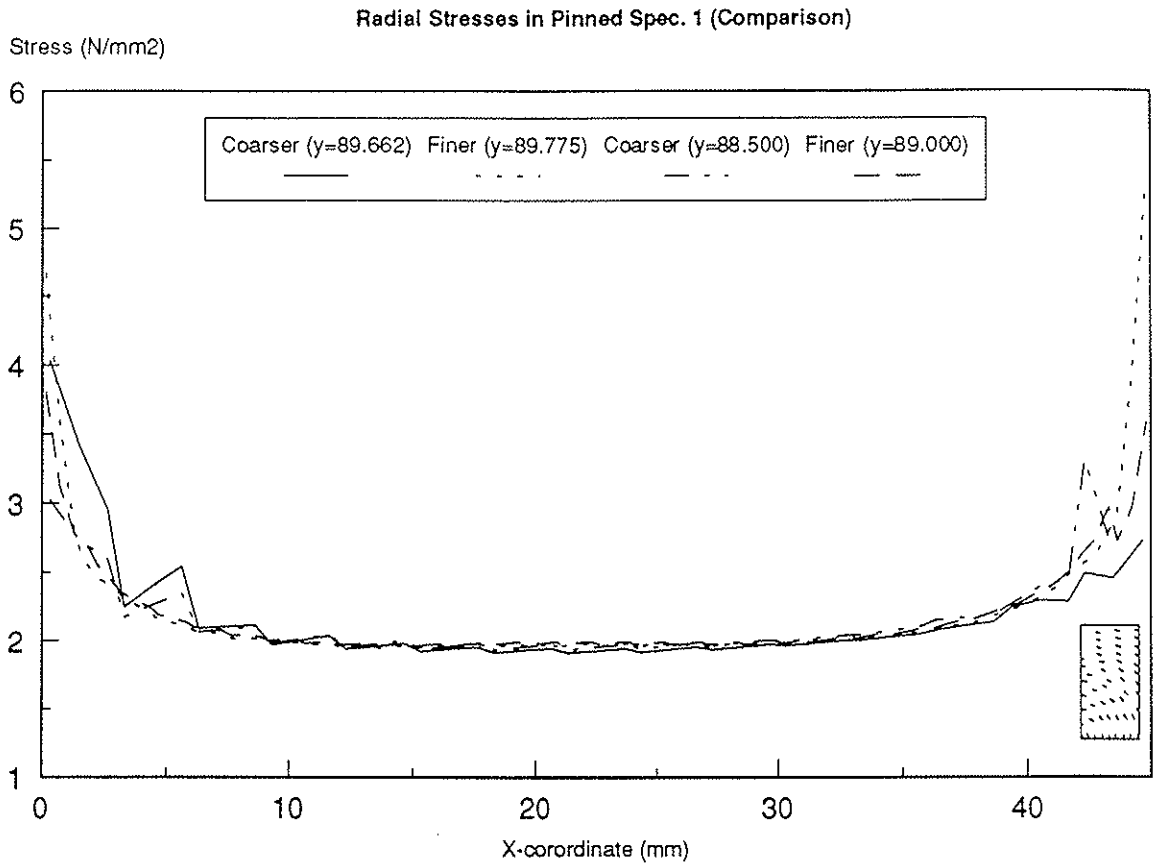

Figure 4

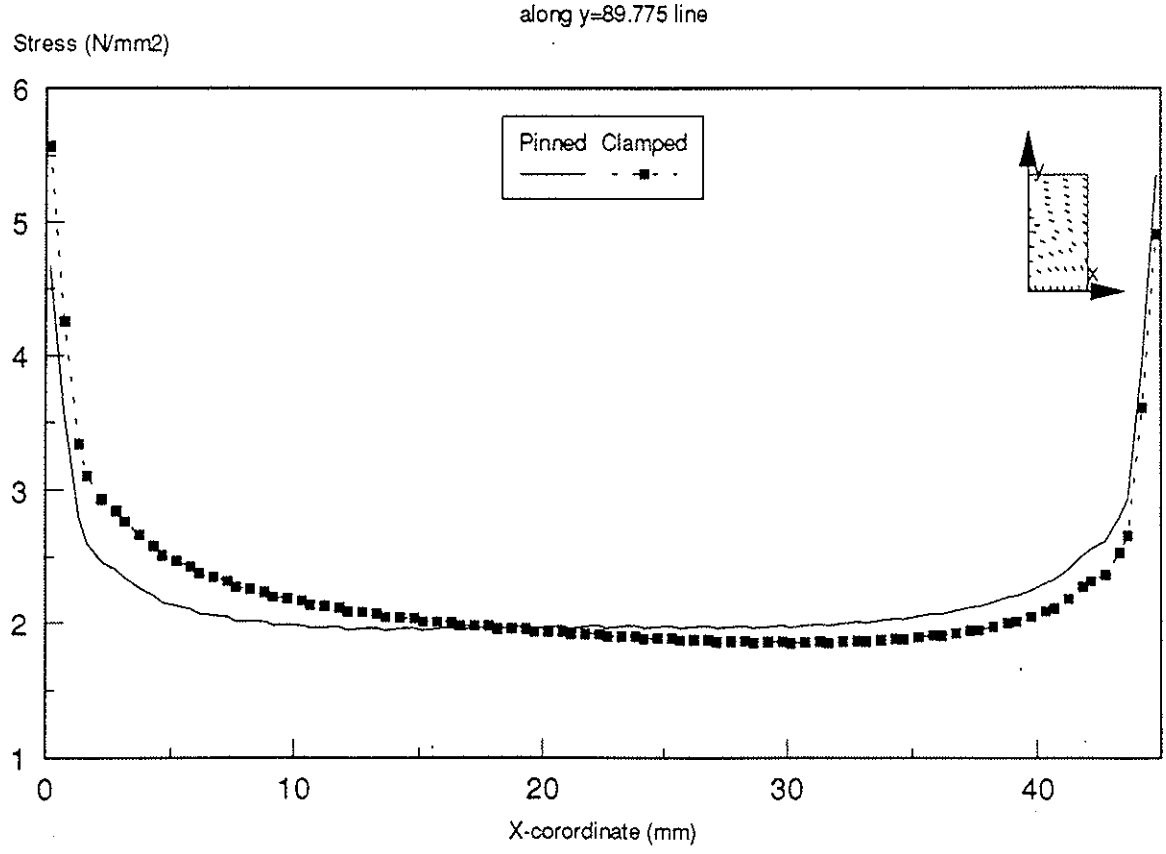

Figure 5

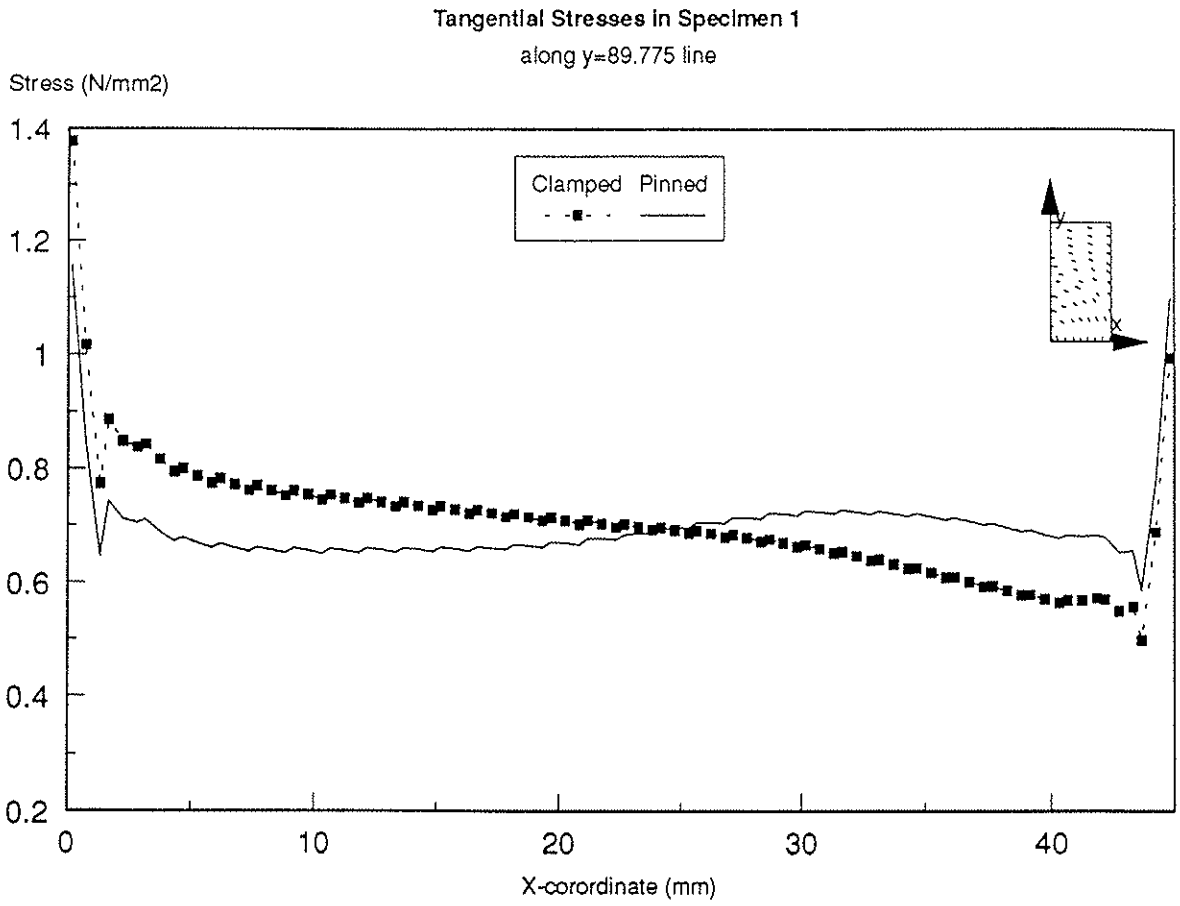

Figure 6

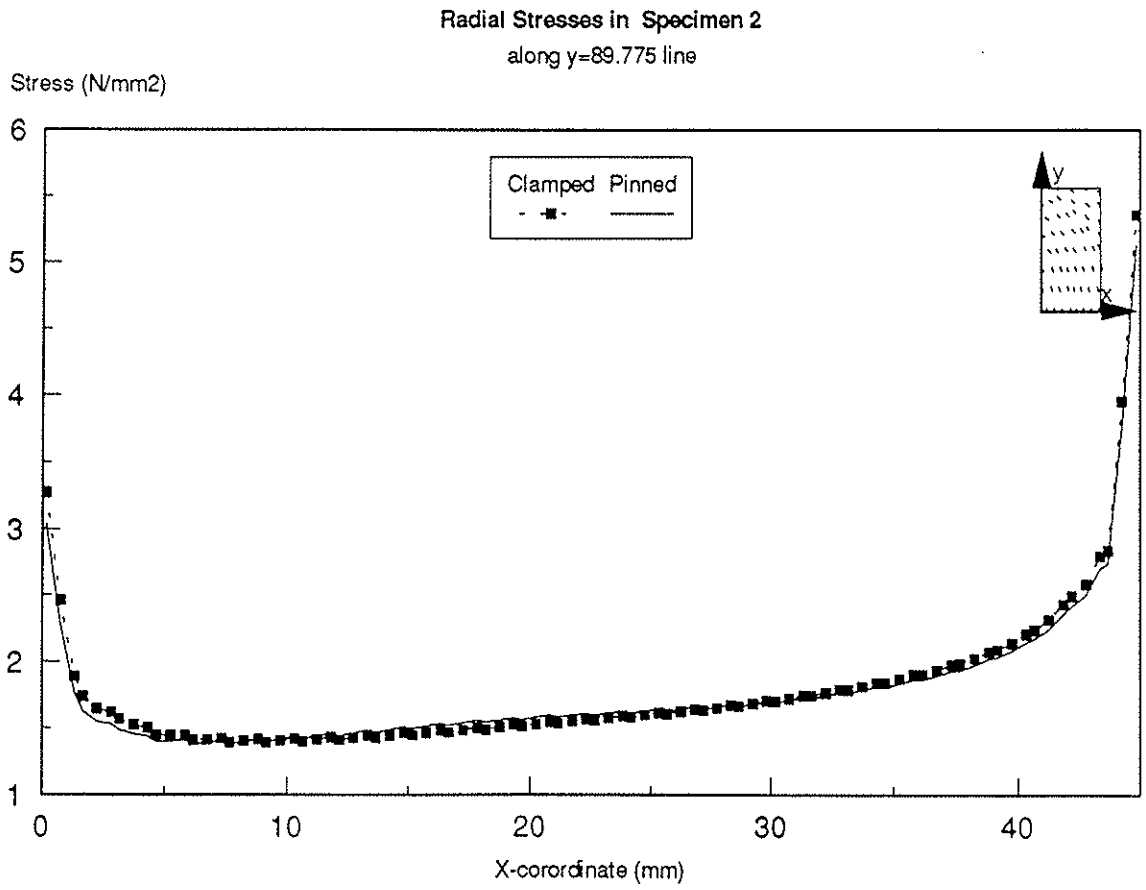

Figure 7

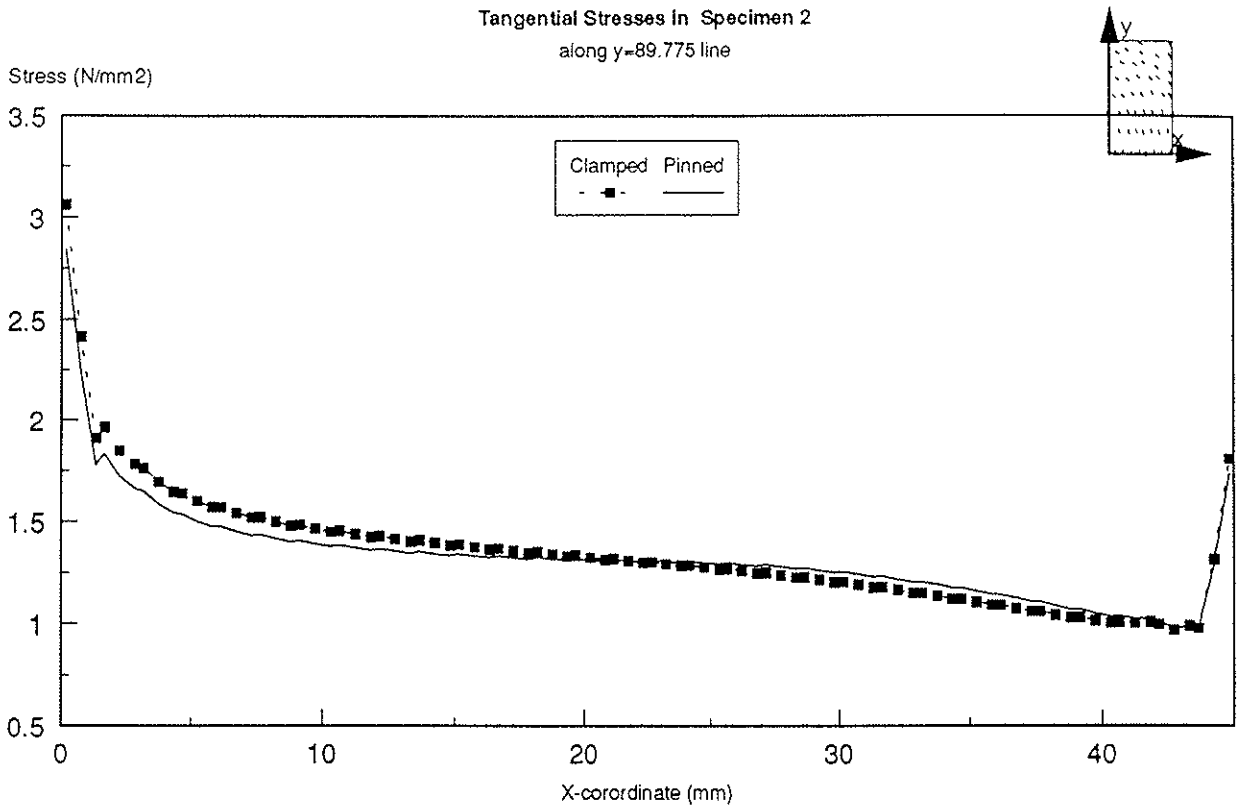

Figure 8

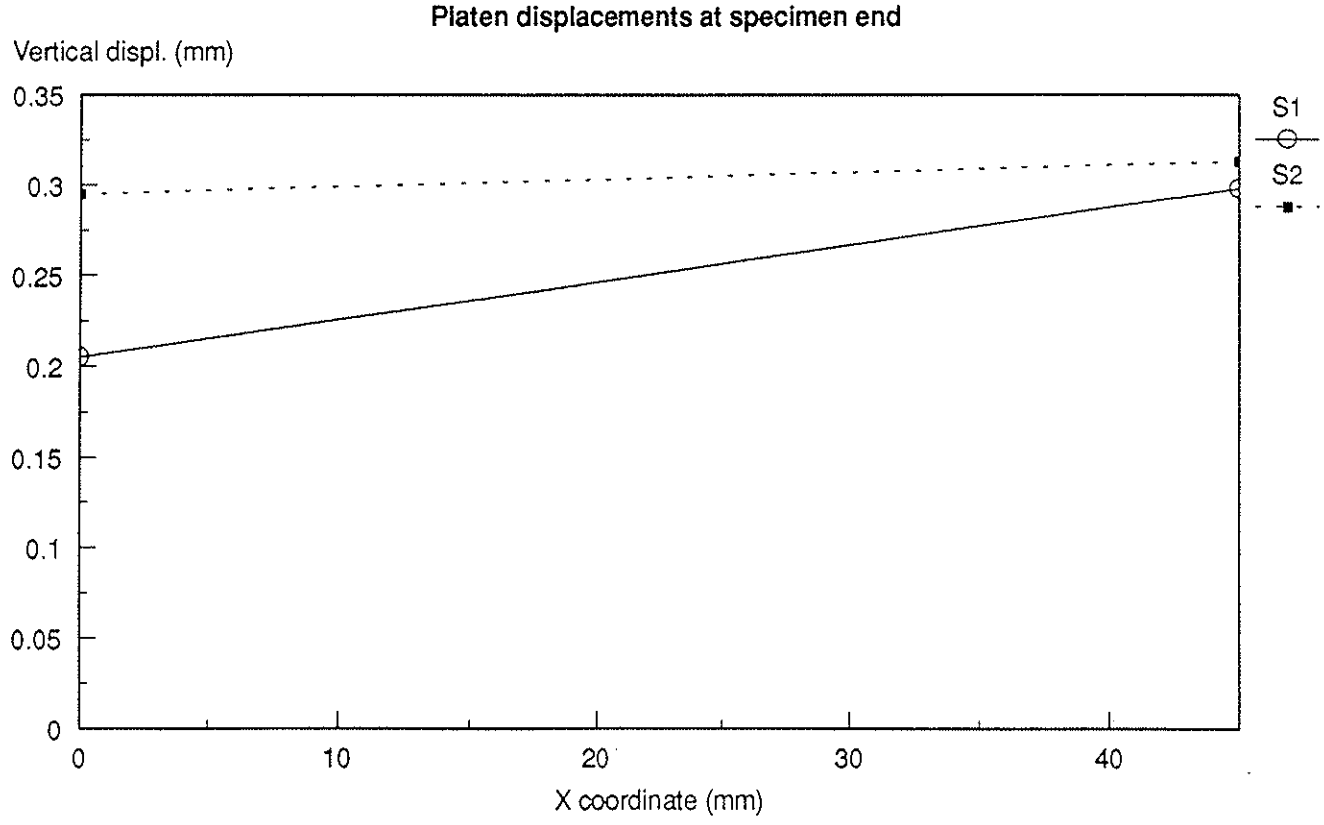

INTERNATIONAL COUNCIL FOR BUILDING RESEARCH STUDIES AND DOCUMENTATION

WORKING COMMISSION W18 - TIMBER STRUCTURES

EXPANDED TUBE JOINT IN LOCALLY DP REINFORCED TIMBER

by

A J M Leijten
Delft University of Technology
The Netherlands

P Ragupathy
K S Virdi
City University London
The United Kingdom

MEETING TWENTY - EIGHT

COPENHAGEN

DENMARK

APRIL 1995

EXPANDED TUBE JOINT IN LOCALLY DP REINFORCED TIMBER

by Ad.J.M. Leijten (1), P. Ragupathy (2) and K.S. Virdi (2)

dedicated to HANS JØRGEN LARSEN

SUMMARY

A revolutionary timber joint is presented with a new type of prestressing connector. The timber is locally reinforced with dp *(densified plywood)*. The high strength and stiffness capacity of the joint is combined with excellent ductile properties. This enables structural timber to be applied much more efficiently than with traditional joints. It is shown that timber savings of up to 30% can be realized.

1 INTRODUCTION

In many cases the efficient use of timber for structutal application is hindered by the low strength, stiffness and ductility of timber joints. Although in essence the timber joints with mechanical fasteners like bolts and dowels behave in a ductile manner the unpredictable occurrence of shear or splitting cracks does not allow designers to take any plasticity or non–linear behaviour into account. In order to develop the full strength and to prevent premature cracks, spacing requirements are prescribed in timber design codes. In its turn this will lead to larger timber dimensions then necessary. For this reason the capacity of timber joints will hardly be higher than 40% to 60% of the bending and tension strength capacity respectively. The discrepancy between the stiffness of joints and timber member is even larger. The application of plastic theory in structural timber design with traditional joints is again hindered because of the unreliable cracking. Investigations aimed at improving the reliability of strength, stiffness and ductility of joints have been a research topic at the Delft University of Technology for many years. Within a EC and industry funded research project, inwhich many well known European Institutes participated, a dvw reinforced joint developed at the TU–Delft was investigated.

2 REINFORCED JOINTS WITH DENSIFIED PLYWOOD

It was Robert Stoeckhart, who first patented the densification of solid wood in Leipzig, Germany, in 1886. Finally in 1922 the Austrian Pfleumer brothers found a more effective method by trial and error. Since then this material is commercially available mainly in Europe. The main thought behind the densification is that the mechanical properties change proportionally with density. In a nutshell, the densification is described as follows. Solid wood or stacks of veneers are heated up to 145°C and compressed, perpendicular to the grain, to 20 MPa. This forces the outer cell wall to become plasticized, allowing the cell to drift and move within the conglomerate of cells so as to close all veins. For poplar, this process is indicated in figure 1. When the fibres are settled, a rapid temperature drop will freeze this situation. Only immersion in water for a long time will activate the material memory. The maximum density obtained is about 1380 kg/m^3. Although many wood species can be densified, the highest mechanical properties are obtained with beech. Tension and compression strength values of maximum 300 MPa can be achieved [1]. For practical application a minimum density is usually specified. As densified plywood (dp) consists of cross–layered veneer sheets,

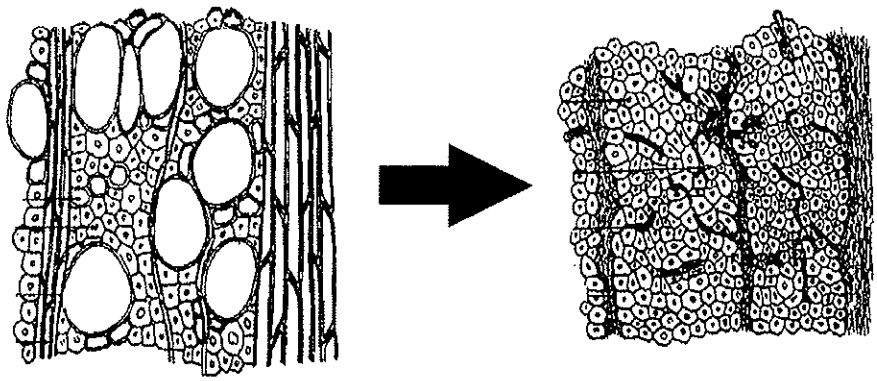

Figure 1: Poplar before and after densification.

(1) Timber Structures, Faculty of Civil Eng., Delft University of Technology, P.O. Box 5048, Delft.
(2) Structures Research Centre, City University, London EC1V 0HB, United Kingdom.

mechanical properties are less grain direction dependent than for wood. No special precautions are required to glue this material to the timber.
The dp is locally glued to the surface of the timber members to prevent splitting at places where the fasteners introduce high concentrated loads. The embedding or bearing strength of the dvw is about 130 MPa compared to 20–25 MPa for spruce [1].

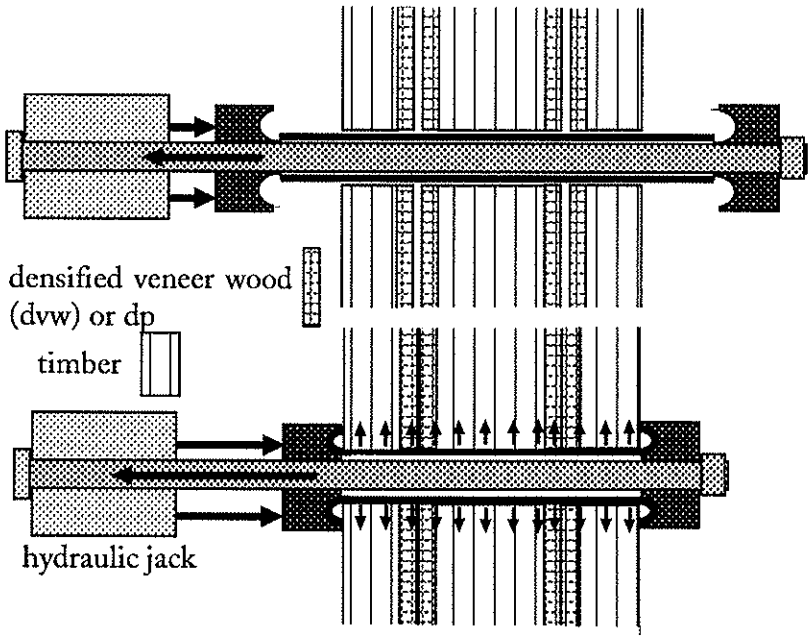

3 THE EXPANDED TUBE DOWEL

One of the major problems in timber joints with mechanical fasteners is to eliminate the clearance space. Although tight fitting holes lead to a reduced clearance, the fasteners are in that case hard to drive in. When the holes are slightly unequally spaced, splitting can already be initiated at this stage. Therefore, very precise drilling equipment is required. To overcome this, there are efforts to drill wide holes and to use injection resin as in steel structures [2]. However, this method is rather expensive while quality control is difficult and doubtful.
To solve all these problems, an innovative new idea was developed and tested. Why not fit in a tube as dowel type fastener in "wide" holes and expand the tube by pressing the tube ends together? A central rod prevents any inward movement of the tube. The clearance is completely vanished. Due to this expansion procedure, the hole diameter is enlarged leading to prestressed densified plywood and timber. This prestressing lead to an increased stiffness at the initial loading as well. On the other hand, the physics of a tube allows very large plastic deformations. The tube material is very cheap; galvanized welded gaspipe Fe360 (according to DIN 2440/ ISO 65). Diameters of 17.2 to 33.7 mm are tested.
The holes drilled are 18 and 35 respectively. Details about some design and production requirements are available in Table 6. There are no patents that hinder the application commercially.

4 TEST RESULTS

All test results obtained during the research project are gathered in [1]. They cover a wide range of investigations such as for instance the embedding strength and stiffness results of dvw.
To show only one example of the

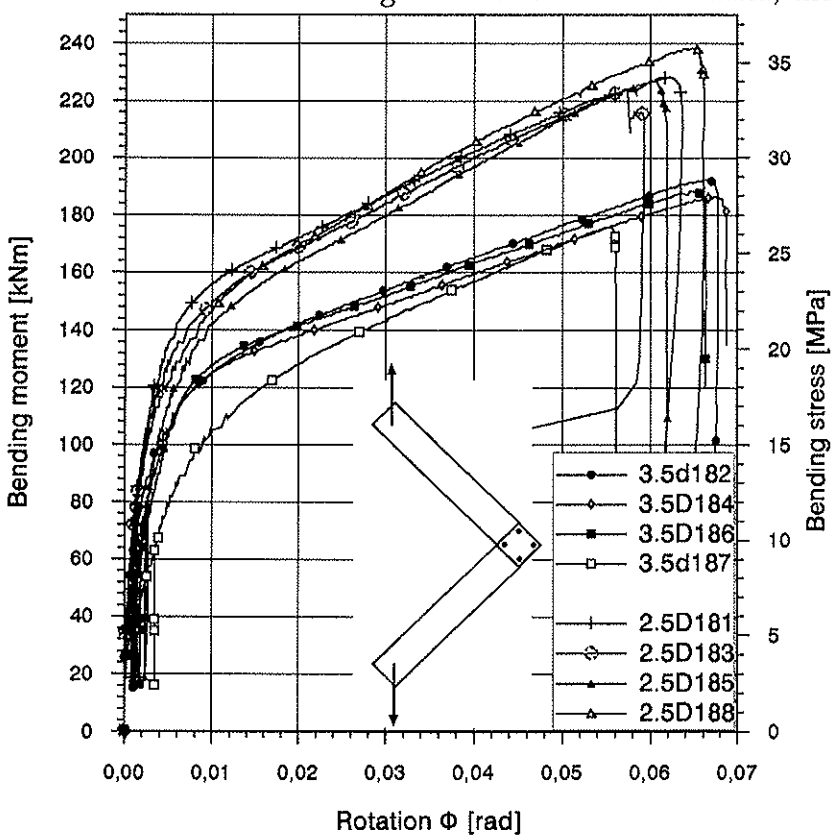

Figure 3: Moment–rotation relation of two tests series expanded tube joints, taken from [1]. Right axis show timber bending stress

high strength and stiffness capacity of the joint, the results on portal frame corners are presented in figure 3.
The moment–rotation characteristics of two test series are given. The only difference is, the spacing of the fasteners. Each joint has four 35 mm diameter tube–dowels at the corner and the dvw thickness is 18 mm density 1300 kg/m^3. At the right hand side of the graph the bending stress in the glued laminated members of 600x110 mm is given as well (char. bending strength 30 MPa). The data of test 3.5d187 should not be considered as the joint was tested twice due a computer break down. All tests ended because of the limited stroke length of the jack (200 mm) without any timber failure. The limitations regarding save end and edge distance as well as other minimum requirements, were based on other tests [1].

Traditional joints with dowels

Diam		*Mmax.*	*Rot.max.*
[mm]	*number*	*[kNm]*	*[rad]*
15 mm	*22*	*31.3*	*0.0036*
16 mm	*16*	*33.6*	*0.0040*
20 mm	*13*	*38.3*	*0.0045*

Table 1: Moment rotation data

5 FRAME DESIGN EXAMPLES I

In what follows, the application of expanded tube joints, is indicated in a single storey and three–storey timber frame. The main objective is to determine the potential improvements in design that could be achieved by using the reinforced joints, especially in terms of the timber (cost) saving ability and the question of rotation capacity required at the ultimate limit state. Not only a computer analyses is presented also a simple graphical moment–rotation figure is very illustrative, see chapter 8.

5.1 Program SWANSA

The structural design analysis was carried out using the computer program *SWANSA*, which takes into account material and geometrical nonlinearities, together with nonlinear semi–rigid behaviour of connections. The background theory is explained in more detail in [3][4]. The structural analysis is initiated with assumed cross–sectional geometry and connection characteristics, for combinations of dead, imposed and wind loads at ultimate (ULS) and serviceability limit state (SLS) conditions.

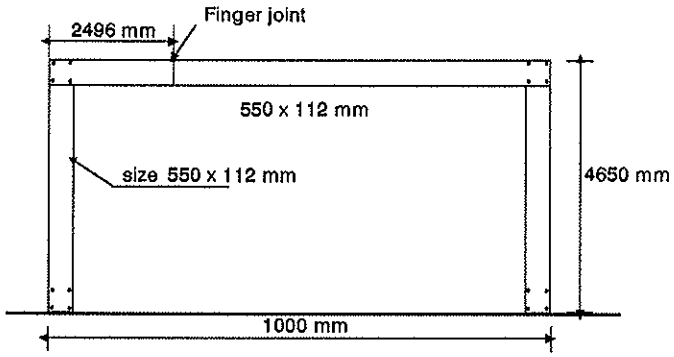

Figure 4: Structure 1

5.2 Geometry of the structures

The portal frame (Structure 1) considered in this analysis is idealised as shown in figure 4. In the structure as built, the frame consists of two 56 x 550 mm deep members and a single column. For purposes of present analysis, the beam is idealised as a single member of size 112 x 550 mm. The beam is connected to either column using four tube–dowels of 35 mm diameter set in a square pattern in the connection zone. The columns which are also of uniform cross–section are fixed to the foundation, using a connection detail similar to the beam to column connection at the top of the column. The spacing of the frames is taken as 5 m. In Structure 2, the joints are simular to Structure 1, except the beams are 120 x 550 mm and the span and hight are changed.

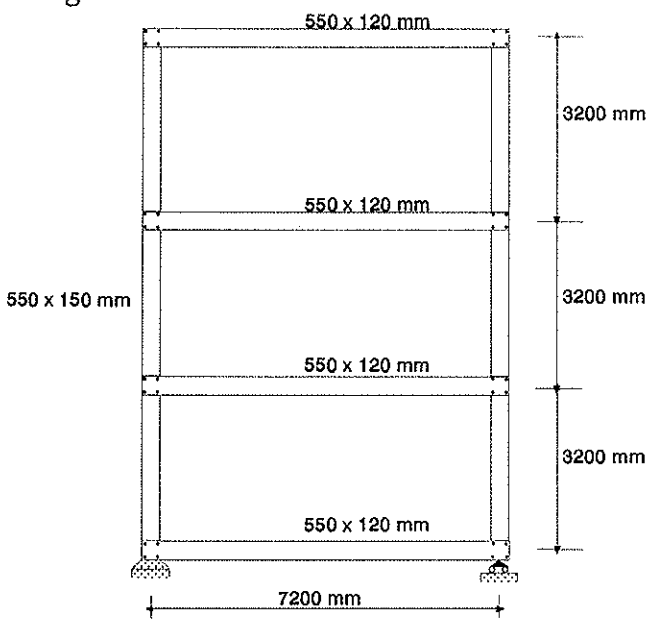

Figure 5: Structure 2

5.3 Material Properties

The structures are made of glued laminated timber of strength class GL30, with a characteristic bending strength of 30 MPa. The design bending strength is 21.2 MPa, according to Eurocode 5. The modulus of elasticity is 12000 MPa for SLS and 6800 MPa for the ULS calculation (see also ch. 8.3).

5.4 Moment rotation characteristic of the connection

For the calculations with the traditional joints, the stiffness and strength values are used in accordance with EC5. Dowels ranging from 12 to 20 mm in diameter were chosen. The moment rotation characteristic of the traditional joints is linear elastic. The design moment and rotation capacity is given in Table 1. The moment–rotation relations of the reinforced joint, required in the frame analysis with semi–rigid joints, can be derived with Table 6 values. The moment capacity of the beams is 121 kNm for Structure 1 and 130 kNm for Structure 2.

6 LOADING AND LOADING COMBINATIONS

The Permanent load, Variable load and Wind load used in the calculations for both structures are shown in Table 2. The structures were analysed for five load combinations, factored in accordance with Eurocode 1 clauses on the combination of actions, as shown in Table 3 below.

Load type	*Structure 1*	*Structure 2*
Permanent load (DL)	*1.5 kN/m*	*9.36 kN/m*
Variable load (LL)	*2.5 kN/m*	*6.00 kN/m*
Wind load (WL)	*12.9 kN/m*	*1.704 kN/m*

Table 2: Loading

Load Combination	*Limit State*	*Combination Formulae*
1	*Ultimate*	*DLx1.1 + LLx1.5*
2	*Ultimate*	*DLx1.1 + LLx1.5 +WLx1.5x0.6*
3	*Ultimate*	*DLx1.1 + LLx1.5x0.7 +WLx1.5*
4	*Serviceability*	*DLx1.0 + LLx1.0*
5	*Serviceability*	*DLx1.0 + LLx1.0 +WLx1.0*

Table 3: Load Combination factores Eurocode 1

In the ultimate limit state calculations, the load factor on live load is varied, while the other load factors are kept constant. The maximum value of the live load factor obtained from the computations is compared with the code specified load factor. The serviceability calculations are made for the specified load factors. The principal objective of serviceability calculations is to check for limiting deflections. When the live load factor is substantially more than the value of 1.5 required for the ultimate limit state, substantial safety margins are available. For these cases the beam sizes have been reduced until comparable safety margins are obtained as with traditional design.

7 RESULTS

In all three ULS load combinations (1–3), the computations indicate failure at the beam midspan for Structures 1 and top storey beam of Structure 2, when the extreme fibre stress reaches the maximum design value of 21.2 MPa. In Table 4a, 4b and 5 the maximum load factors on live load for Structures 1 and 2 are presented for ULS design as well as for the serviceability limit conditions (SLS).

STRUCTURE 1							
Traditional design U.L.S.				Reinforced design U.L.S.			
Member sizes	*num. of dowels*	*Load Comb.*	*LL factor*	*Member sizes*	*num. of dowels*	*Load Comb.*	*L.L. factor*
550x112 mm	*13 of 20 mm*	*1*	*2.38*	*550x112 mm*	*4 tubes 35mm*	*1*	*5.85*
"	*16 of 16 mm*	*1*	*2.00*	*"*	*"*	*2*	*6.78*
"	*22 of 12 mm*	*1*	*1.82*	*"*	*"*	*3*	*9.52*
				500x100mm	*"*	*1*	*5.42*
				480x100mm	*"*	*1*	*4.68*
				450x100mm	*"*	*1*	*3.94*
				400x90 mm	*"*	*1*	*2.69*

Table 4a: Overview of Live Load factors for Structure 1, ULS.

Reinforced design SLS

Member sizes	*num.of dowels*	*Load Comb.*	*Vertical defl.*	*Vert.defl. limit*	*Load Comb.*	*Lateral defl.*	*Lat.defl.limit*
550x112 mm	*4 tubes 35mm*	*4*	*8.23mm*	*30mm*	*5*	*5.7mm*	*8.75mm*
500x100mm	"				*5*	*8.0mm*	*8.75mm*
480x100mm	"				*5*	*10.0mm*	*8.75mm*
Vertical deflection limit is 0.003xspan; Lateral deflection limit is h/500							

Table 4b: Overview of Live Load factors for Structure 1, SLS.

STRUCTURE 2							
Reinforced design ULS							
sizes	*num. of dowels*	*Load Comb.*	*LL factor*				
550x120 mm	*4 tubes 35mm*	*1*	*3.99*				
550x120 mm	"	*2*	*3.92*				
550x120 mm	"	*3*	*5.51*				
Reinforced design SLS							
sizes	*num,of dowels*	*Load Comb.*	*Vertical defl.*	*Vert.defl. limit*	*Load Comb.*	*Lateral. defl.*	*Lat.defl. limit*
550x120 mm	*4 tubes 35mm*	*4*	*11mm*	*21mm*	*5*	*14.7mm*	*19.2mm*
500x100mm	"	–	–	–	*5*	*20.9mm*	*19.2mm*

Table 5: Overview of Live Load factors for Structure 2.

The maximum value of the joint rotation obtained anywhere in the structures is 0.025 radians. The maximum rotation in Structure 2 is about 10% higher than that for Structure 1, but is again well within the maximum rotation deduced from tests for this type of joint. Without any reduction of safety the dimensions of the timber beams can be reduced from 550x120mm in the traditional design to even 480 x 120mm for the expanded tube joint. About 30% of timber is saved. When the production costs of a traditional joint balance costs of the expanded tube joint there is certainly an commercial interest.

8 FRAME DESIGN EXAMPLE II: SIMPLE DESIGN BY HAND

The calculations of the previous chapter are based on a computer analyses. What the influence is of all the parameters that affect the structural performence are however invisible. The use of a very simple hand made diagram enables us to visualize the influence of all important parameters. Therefore, again a portal frame is analysed but now using the moment–rotation graph and the beam–line theory. The method of analyses presented in this chapter has been elaborated in CIB–W18 paper 22–7–5: Berlin 1989 [5]. The portal frame and its dimensions is presented in figure 6.

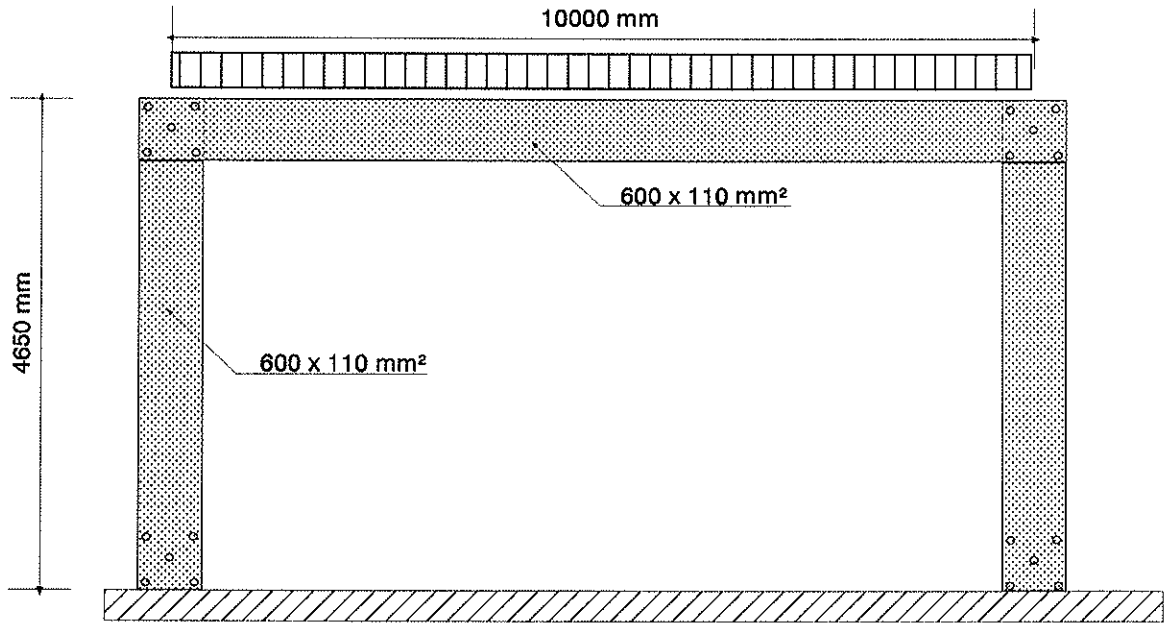

Figure 6: Portal framed with dvw reinforced joints with expanding 35mm tubes.

TUBE quality	nominal diameter [inches]	out-to-out measure [mm]	thickness of wall [mm]	washer galvanized diameter [mm]	washer thickness [mm]	washer central hole [mm]	hole drilled [mm]
gaspipes	3/8"	17.2	2.35	50	3	19	18.0
DIN 2440/	1/2"	21.3	2.65	75	3	24	22.0
ISO 65	3/4"	26.9	2.65	85	4	30	28.0
galvenized	1"	33.7	3.25	95	4	37	35.0
single							
tube	dvw density	Yield		regression	parameters	load-slip	curve
expanded	>1300 kg/m³	strength/	stiffness	F=(a-b)* x/(1+((a-b)*x/c) ^ d) ^ (1/d)+b*x			
diameter	thickness	shear plane	at 0.4Fmax	a	b	c	d
[mm]	[mm]	[kN]	[kN/mm]	[kN/mm]	[kN/mm]	[kN]	[-]
18.0	12	35	30	43	.91	26.6	1.62
22.0	14	55	53	80	1.64	32.2	1.80
28.0	16	70	58				
35.0	18	95	65	125	1.48	63.4	1.32
combinations							
tubes							
17.2+13.5	12	42	55	80	0.75	40.0	1.15
21.3+17.2	14	66	71	140	0.36	63.6	0.92
26.5+21.3	16	85	75				
33.7+26.5	18	115	80	130	1.42	108	0.816
Spacing	parallel	perpendicular	loaded end	unloaded end	loaded edge	unloaded edge	
exp.Tube size	a_1	a_2	a_3t	a_3c	a_4t	a_4c	
[mm]	3.5d	5d	3.5d*cosα≥2.5d	2.5d	3.5d*cosα≥2.5d	2.5d	
18	63mm	90mm	" ≥45mm	45mm	" ≥45mm	45mm	
22	77mm	110mm	" ≥55mm	55mm	" ≥55mm	55mm	
28	98mm	140mm	" ≥70mm	70mm	" ≥70mm	70mm	
35	122mm	175mm	" ≥88mm	88mm	" ≥88mm	88mm	

Tabel 6: strength and stiffness capacity and spacing requirements

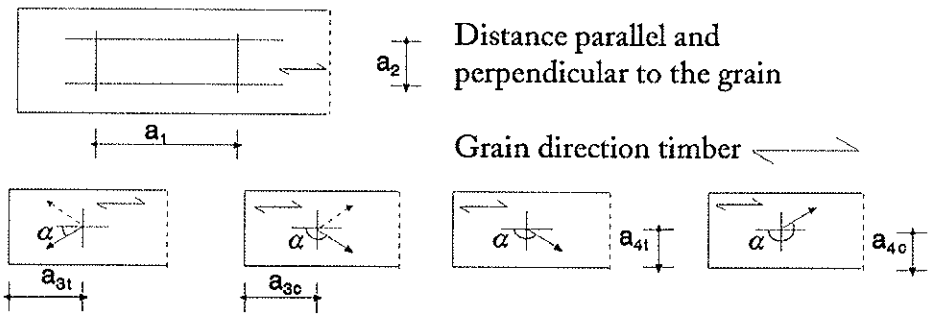

Loaded end $-90^0 \geq \alpha \geq 90^0$ | Unloaded end $90^0 \geq \alpha \geq -90^0$ | Loaded edge $0^0 \geq \alpha \geq 180^0$ | Unloaded edge $180^0 \geq \alpha \geq 360^0$

8.1 Design parameters of the timber and joints:

Member sizes: Glued laminated strength class GL 30

600 x 110 mm middle member

600 x 55mm double side member

Design bending strength timber: $f_{md} = k_{mod}/\gamma_M = 30 \times 0.9/1.3 = 21$ MPa (EC5)

Design shear strength $f_{v,d} = 3.9 \times k_{mod}/\gamma_M = 3.9 \times 0.9 / 1.3 = 2.73$ MPa

Design moment capacity of the timber members:

$M_d = W \times f_{m,d} = 1/6 \times 110 \times 600^2 \times 21 = 138.6$ kNm

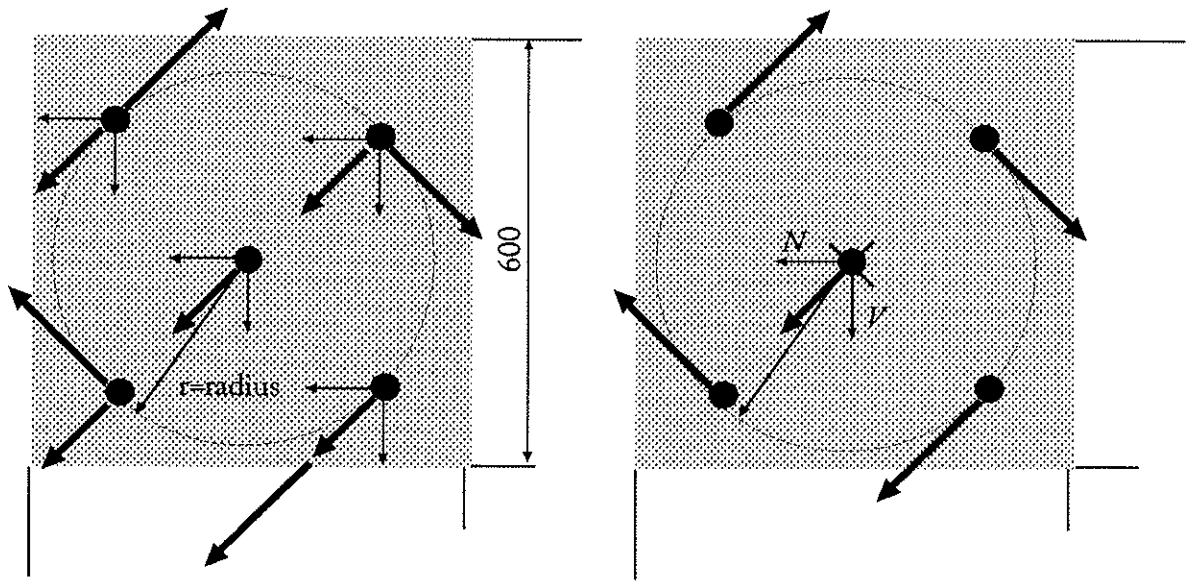

Elastic approximation

Plastic approximation

Figure7: Left; Traditional load distribution according to elastic theory
Right; A failure mechanism and load distribution according to plastic theory

Tubes 35 mm diameter; dvw thickness 18 mm, density 1300 kg/m^3
Radius of fastener pattern:
$r = (600/2 - 2.5d)2^{1/2} = (300 - 2.5 \times 35)\text{x}1.414 = 300.5$ mm

Design strength tube 35 mm diameter:

$F_{max} = 95$ kN per shear plane per fastener, Table 6

$F_{max,d} = 95 \times k_{mod}/\gamma_M = 65.8$ kN (Eurocode 5)

Design capacity for combined normal (N) and shear load (V) only:

$R_d = 2 \times 65.8 = 132$ kN/ tube

Design moment joint capacity:

$M_{y,d} = F_{max,d} \times 2 \times n \times r = 65.8 \times 2 \times 4 \times 0.301 = 158.1$ kNm > bending capacity timber(138.6)
Bending moment capacity of member is 87.5 % of the joint capacity

The plastic approximation of load take up is easier to handle than the elastic one, as shown in figure 7. For the plastic case the shear and normal force are assumed to be carried by the central tube while the others take care of the bending moment. The validity of this assumption has to be verified later.

8.2 Rotation capacity joint

Now two rotations will be calculated, one associated with the design moment capacity of the joint (158 kNm) and the second associated with the rotation of the joint for which the timber near the joint reach its bending strength capacity (138.6 kNm).
The load–slip relationship is given by Richard's/Jaspart model [1]:

$$F = \frac{(a-b)\,\delta}{\{\,1+[\,\frac{(a-b)\,\delta}{c}\,]^{d}\,\}^{1/d}} + b\,\delta$$

inwhich:

F is the load per shear plane per fastener
a the initial stiffness
b the post yield stiffness
c is the transition of elastic to plastic or elastic–plastic bending moment
d a curve fitting parameter
δ is the slip or displacement

With the values of the parameters a,b, c and d taken from Table 6 and substituted in the formula above, it is found:

Design moment capacity of the joint is reached for:
$M_{joint,d}$ = 158.4 kNm ——>F = 65.8 kN obtained for a slip of 4.1 mm —> rotation joint θ = 0.0136 rad.

Design bending capacity of the timber beam near joint reached:
$M_{m,d}$ = 138.6 kNm ——>F = 57.6 kN obtained for a slip of 1.71 mm —> rotation joint θ = 0.0057 rad.

Check of the glueline moment capacity (two gluelines/member):
M_{glu} =2 (600^3 x $f_{v,d}$)/6 = 144 kNm > 138.6 kNm = timber bending capacity but smaller than $M_{joint,d}$

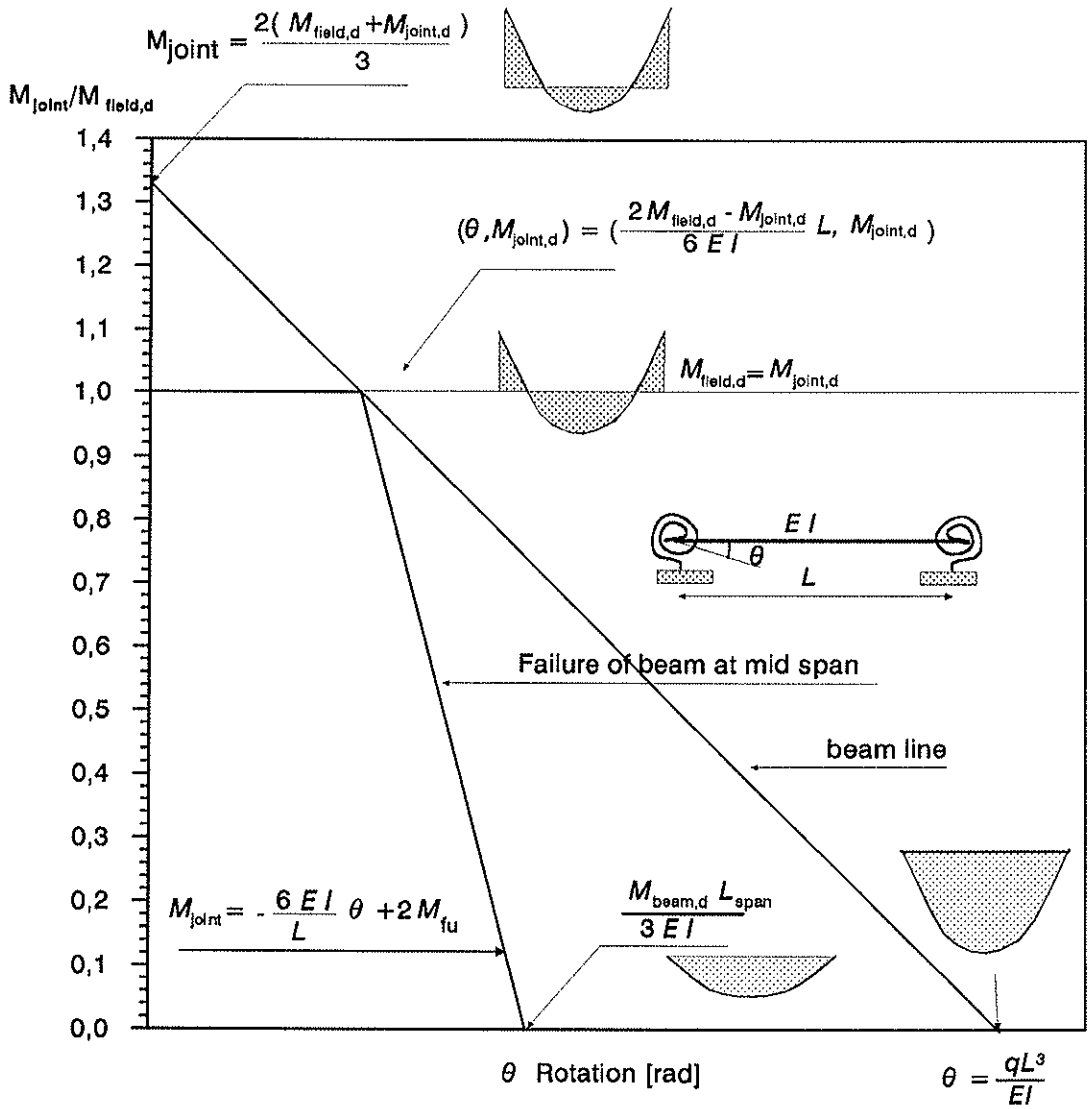

Figure 8: Normalized moment rotation graph

8.3 Influence of stiffness in the structural behaviour: the graphical method

The method of analyses given now, has been elaborated in CIB–W18 paper 22–7–5: Berlin 1989 [5]. The starting point is a moment–rotation graph where not only the non–linear behaviour of the rotation spring is projected but also structural properties of the timber beam are taken into account. In order to show the effect of the reinforcement a comparison of a traditional joint with dowels is made. The analyses will show the performance of both joints and indicate the type of failure at the ultimate limit state. Schematically the beam is drawn in the middle of the graph, figure 8, with two rotation springs at the supports. The rotation springs not only represent the rotation characteristic of the joint but also incorporate the total rotation stiffness of the structural elements connected to the joints. The left axis is normalized by dividing the moment of the joint by the design bending capacity of the beam.

In our case the design bending capacity of the member is 138 kNm and for the joint 158 kNm. However, the timber just outside the joint limits the maximum bending moment on this location. When the rotation springs are considered infinite stiff the maximum equally distributed q–load may force a total bending moment of 138+138=276 kNm. Normalized, dividing this values by the design bending capacity of the timber, 276/138=2.0 set out on the vertical axis of fig.8 (this value is not shown). When the rotation joint is infinite stiff, the total bending moment (1/8 qL^2=276 kNm) is divided between both support and mid span, in two well known parts, 2/3 (=184 kNm) and 1/3 (=92 kNm) respectively. Normalized again, this lead to 184/138=1.33 and 92/138=0.67. Only the 1.33 is set out on the vertical axis of fig.8 (the 0.67 value should be added to the 1.33 value).
On the other hand, when for this particular q–load the rotation springs might be considered as hinges, the rotation at the support is $\theta = qL^3/(24EI)$. This gives a point on the horizontal axis at the right bottom corner. The line which connect these two points is the so–called beam–line, and corresponds to only *one particular* q–load. The change in bending moment distribution among support and mid span along this beam–line is clearly indicated. The only item which is now introduced is the moment–rotation characteristic of the spring. Where this curve intersects the beam–line it shows the ratio between the bending moment at mid span and at the support (for this particular q–load). For lower q–values, additional lower parallel beam–lines can be drawn.
In our case the bending moment at the support (joint) may never exceed a value of 1.0. At the intersection with the beam–line an ideal situation is found. Both bending moment at mid–span and support are equal. It also means that when the moment–rotation charachteristic intersect this point an ideal situation occurs.
Now a very important second limit state is introducted. Suppose the moment–rotation curve of the spring indeed intersect this ideal location on the beam–line. However, due to creep of the joint the stiffness will decrease (constant q–load). What happens now is that the intersection with the beam–line occurs for higher rotation values. But what is more important to realize is that the bending moment at mid–span exceeds the design capacity because going down the beam–line means the bending moment at mid–span grows. A second boundary line can now be drawn which shows the situation where the bending moment at mid–span stays constant while the bending moment at the support decreases. This line runs steeper than the beam line and is shown in figure 8. So the intersection of the moment–rotation curve with this line indicates failure at mid–span. The only, most important curve still missing in fig.8, is the moment–rotation curve.

In figure 9 all elements are brought together. The moment–rotation curve of the rotation spring incorporates the rotation stiffness of the joints as well as the contribution of the column stiffness as indicated. Actually, both springs can be considered as a system of rotation spring in series. According to the method of split–rigidities it follows:

$$\frac{1}{k_s} = \frac{1}{k_{column}} + \frac{1}{k_{spring}}$$

where:

k_{column} = $4EI/L$ if at the column base the joint is very stiff, if it is a hinge k_{column}= $3EI/L$

k_{spring} = actual stiffness of moment joint; linear or non–linear

k_s = the stiffness of the rotation spring (system stiffness)

What value for the modulus of elasticity is substituted, the mean or lower 5% needs some consideration. For concrete and steel design these questions are not considered as the scatter of the modulus of elasticity is rather small(?) For timber, the difference is substantial (12,000MPa or the lower 5%–value 9638 Mpa, coeff. of var. 12%). To use only 5% lower values in the whole analysis is unrealistic. Here probabilistic design methods can give more answers. In our case a lower 5% E–value is applied for the column stiffness while for the calculation of the beam line the average E–value is used.

The ultimate limit state is reached where the moment–rotation curve intersects the boundary line for failure at mid–span, as shown in fig.9. Failure is expected at mid–span when the bending moment of the joint is about 0.88 x 138.6 kNm = 122 kNm. The graph also shows the influence of the column stiffness which is assumed linear elastic. Increasing the stiffness of the column improves the load bearing capacity of the structure, as the intersection of the moment–rotation curve goes up.

Near the origin the moment–rotation curve of a traditional joint with 13 dowels of 20 mm in a circular pattern is drawn as well. The bending moment capacity is 38 kNm. The stiffness is determined on the bases Eurcode 5 regulations. This code specifies a stiffness at ultimate limite state which is 2/3 of the elastic stiffness. Both linear elastic curves are shown. A lack of plasticity is the trouble maker here. As

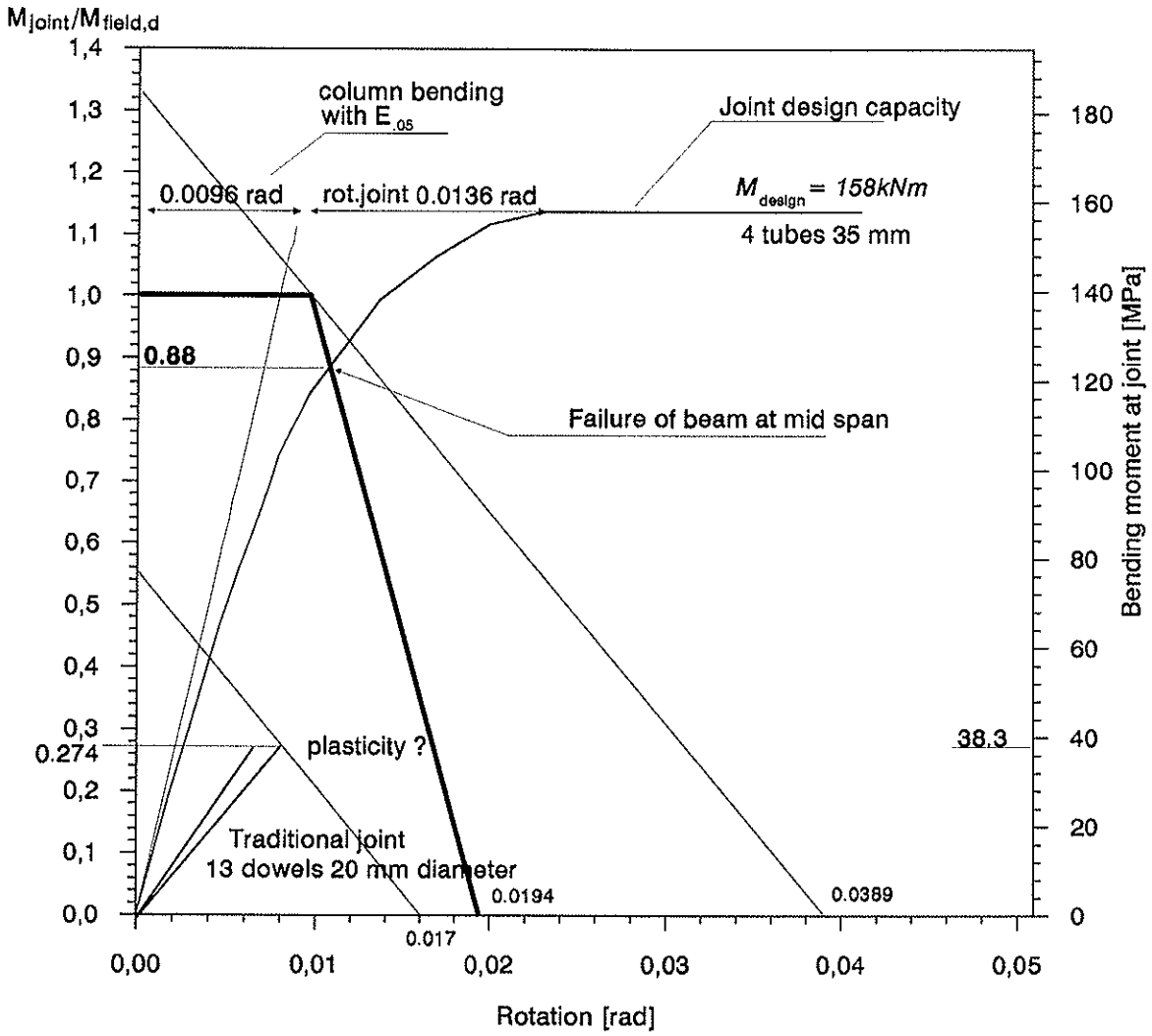

Figure 9: Moment–rotation curve plotted for traditional joints and dp reinforced joints

crack initiation is unpredictable no plasticity is considered for this design. The joint always fails first while the timber at mid span is used very ineffectively. The beam–line associated with the point of failure as shown in fig.9, intersect the vertical axis at a value of 0.55 which stands for a bending moment at the support of 0.55x138 = 76 kNm. The bending moment at mid–span is half this value, so the total design bending moment is 76x1.5=114 kNm= 1/8 qL^2 Of course it is possible to assume the joints as hinged at the ultimate limit which allows the beam to rotate more at the support until the design bending moment capacity at mid span is reached.
The difference in load bearing capacity between the expanded tube joint and the traditional joint is calculated as follows:

Total bending moment
A) dp reinforced joint: $M_{joint} + M_{field}$ = 122 + 138.6 = 260 kNm = 1/8 qL^2 q_{max} = 20.8 kN/m
B) traditional joint: $M_{joint} + M_{field}$ = 114 kNm = 1/8 qL^2 q_{max} = 9.1 kN/m
C) joints assumed as hinged: $M_{joint} + M_{field}$ = 0 + 138 = 138 kNm = 1/8 qL^2 q_{max} = 11.1 kN/m

For vertical loads the load bearing capacity of the structure with reinforced jointis is therefore 2.3 to 1.9 times higher than the other options. Notice the difference between B) and C) due to the lack of rotation capacity of the traditional joint. Another option instead of allowing higher loads is to decrease the timber dimensions. Saving up to 30% are expected.

The shear force at ultimate limite state is (10/2 x 20.8) = 104 kN
The shear stress: 3/2 x 104,000/(600 x 110)= 2.3 MPa < $f_{v,d}$ = 2.7 Mpa

8.4 Seviceability limit state
The deflections at mid span are calculated for a load equal to 40% of the ultimate limit state.
For the dp reinforced joints the servicability load:
q_{ser} = 0.4 x 20.8 = 8.32 kN/m (1/8 qL^2=104 kNm)
with figure 9 for M_{joint}/M_{field} =0.4 —> $M_{joint,ser}$ = 56 kNm, $M_{field,ser}$ = 48 kNm
(almost ideal situation)
In the same way for the traditional design:
q_{ser} = 0.4 x 9.1 = 3.64 kN/m ——> $M_{joint,ser}$ = 15.3 kNm, $M_{field,ser}$ = 30.3 kNm

Deflection at mid span:

$$\delta = \frac{5\,q\,L^4}{384\,EI} - \frac{M_{joint}\,L^2}{8\,EI}$$

reinforced option: δ = 45.6 – 29.4 =16 mm
traditional option: δ = 19.9 – 8.0 = 12 mm
Deflection limit: 0.003 x 10.000 = 30 mm
Both designs are well within the deflection limitation.

8.5 Simple design
In the previous chapter the non–linearity of the moment–rotation curve was taken into account. It is much easier to calculate with an ideal linear elastic–plastic behaviour of the joint. In Table 6 the stiffness at 40% of the maximum strength is given which is only for serviceability checks. The slip of the joint associated with this strength level was calculated with Richards/Jaspart model (4.10 mm). The "design rotation" is calculated as 0.0136 rad. This value determines the end of the linear elastic branch. The design strength is now considered as the beginning of the (ideal) plastic branch.
In short for the reinforced joint:
–design strength per shear plane per tube = 65.8 kN for a slip of 4.10 mm

–design bending moment is 2 x 4 x 65.8 x .3005 = 158.1 kNm
rotation = 4.1/300.5=0.0136 rad (radius pattern = 300.5 mm)
The rotation due to the bending of the column for the design moment is:
$\theta = M_{joint} L /(4E_{.05} I) = 158\ 10^6\ 4650/(4*1.908\ 10^{13}) = 0.0096$ rad
Total rotation 0.096+0.0136 = 0.0232 rad

The elastic–plastic behaviour is plotted in the moment–rotation graph including the column bending stiffness, see figure 10. Failure is expected at mid span for $M_{joint}/M_{field} = 0.65$.
So $M_{joint} = 0.65 \times 158 = 103$ kNm
$M_{joint} + M_{field} = 103 + 139 = 242$ kNm = $1/8\ qL^2$ $q_{max} = 19.4$ kN/m
The more accurate method with the non–linear moment rotation graph showed $q_{max} = 20.8$ kN/m. The difference in load bearing capacity is 7%.
This approach is simple and safe. For convience, the stiffness values for the elastic branch are given in Table 8.

8.6 Design according to Eurocode 3
As Eurocode 5 does not contain any regulations regarding the design with semi–rigid joints Eurocode 3 (design of steel structures), Annex J, is considered now.
Eurocode 3 gives two diagrams to classify joints according to their stiffness (pinned, semi–rigid, rigid); one for braced (non sway) and one for un–braced (sway) frames. For brached frames Eurocode 3 states that a joint might be regarded as rigid if:

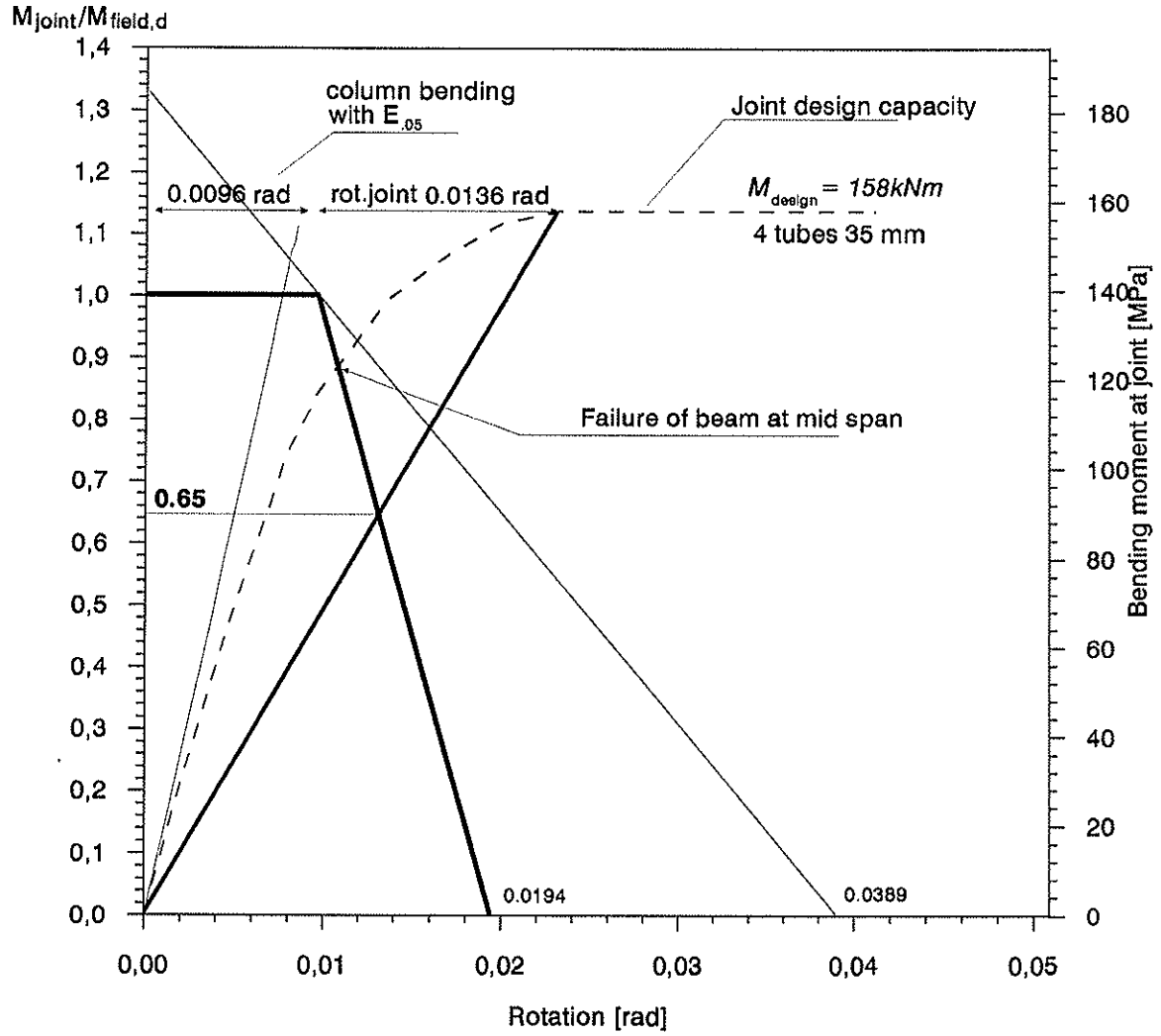

Figure 10: Moment–rotation graph for linear elastic approach: simple design

$$K_s \geq \frac{8\,EI}{L}$$

were:

K_s is the stiffness of the rotation spring (joint + timber elements)

EI is the bending stiffness of the member

L is the span

In unbraced frames the factore 8 is changed to 24.

The background for these rules is that the load bearing capacity of the frame does not drop more than 5% compared to the assumption of an infinite stiff joint ($K_s = \infty$). It also means that when the actual stiffness is different from the one assumed in the pre-calculation this will cause no significant influence in the bearing capacity of the frame.

In the previous chapter it is shown that for the serviceability limit state (SLS) the bending moments at mid-span and joint are about the same. This indicates a factor of 5 for SLS [5]. For the ULS this value is of course lower which means that the requirement mentioned above is not met. This factor is calculated as follows:

$$\frac{1}{K_s} = \frac{1}{k_{column}} + \frac{1}{k_{spring}}$$

where:

$k_{column} = 4EI/L$ if at the column base the joint is very stiff; if it is a hinge $k_{column} = 3EI/L$

k_{spring} = actual stiffness of moment joint linear or non-linear

K_s = the stiffness of the rotation spring (system stiffness)

$k_{column} = M/\theta = 158\ 10^6 / 0.0096 = 1.64\ 10^{10}$ Nmm

$k_{spring} = R^2\, K_{tube}\, n = 300.5^2\ (2 \times 16.2 \times 10^3) \times 4 = 1.17\ 10^{10}$ Nmm

$K_s = 0.68\ 10^{10}$ Nmm $< 8\ (2.376\ 10^{13})/10000 = 1.90\ 10^{10}$ Nmm

or $K_s = 0.358\ EI/L$. So the joint can't be considered as infinite stiff.

In case of other joints and pattern configurations these regulations might become relevant.

8.7 Final remark

In the beginning of this calculation example, the load distribution between the dowels of the joint was based on the occurrence of a plastic failure mechanism, figure 7. The assumed load distribution is only allowed when this failure mechanism really occurs. In this example it is shown that this assumption is not longer valid. Full yielding of the joint does not occur. Apparently at mid-span the timber fails before the yield moment is reached. For statically determined structures however, this failure mechanisme and associated load distribution is valid because exceeding rotation does not influence the moment distribution.

	F yield	F design	slip	Stiffness
tube	strength	strength	Fdesign	ULS
diameter	[kN]	[kN]	[mm]	[kN/mm]
18	35	24.5	1.5	16.3
22	55	38.5	4.0	9.6
28	70	49.0		
35	95	66.5	4.1	16.2

Table 8: Simple design values for ULS calculation (ideal elastic-plastic behaviour)

9 CONCLUSIONS

It has been shown that the application of the joint instead of the traditional joints with dowels opens new frontiers in structural timber design. The bending capacity of traditional timber joints is limited to about 40% of the bending capacity of the timber members. The dp reinforced joint is able to increase this percentage to 100%. Combined with the semi-rigid behaviour of this new innovative joint, timber structures can be designed much more efficiently. The most important aspect of the expanded tube joint is the high stiffness combined with a high strength capacity. It is shown that a graphical design method for non-sway statically indetermined portal frames provide an exellent method of comparing the structural efficiency of traditional and reinforced joints and also clearly shows what properties are of major influence in the structural performance. Application of this innovative joint lead to timber savings of up to 30%. However, the bending capacity of the timber is now the governing factor in ULS design and no longer the joint.

ACKNOWLEDGEMENT

The authors wish to acknowledge the industrial partners, Lignostone (dvw) in Ter Apel (NL) and De Groot Vroomshoop (NL) and the Firm Holzbau (I) as well as the European Commission for their financial support of this research project within the R&D programe FOREST. The results used were obtained in collaboration with the following research laboratories, University of Brighton (GB), University of Florence (I), LNEC Lisbon (P), Tech. University Karlsruhe (D) and City University London (GB). Furthermore, I want to express my gratitude to Jan Kuipers for taking a great interest in careful reading of this paper as well as making proposals for editorial changes.

REFERENCES

1. LEIJTEN A.J.M. et al, Physical and mechanical properties of densified veneer wood for structural applications, FOREST-project, Stevin report EC4-1994, Faculty of Civil Engineering, University of Technology Delft, the Netherlands.
2. RODD P. D. et al, Prediction of embedment characteristics for laterally resin injected bolts in timber, proceedings of the 1991 International Timber Engineering Conference, Volume 3, September 1991, London.
3. RAGUPATHY P., Analysis of precast concrete subframes with semi-rigid joints, PhD Thesis, Structures Research Centre, Department of Civil Engineering, City University, London, 1994
4. VIRDI K.S. and RAGUPATHY P., Analysis of precast concrete subframes with semi-rigid joints, COST C1 Workshop, October 1992, Published by the Commission of the European Communities.
5. GUNNEWIJK R.J.J./ LEIJTEN A.J.M., " Plasticity requirements for portal frame corners", Paper 22-7-5, Proceedings of CIB-W18, meeting twenty-two, Berlin, september 1989.

CIB-W18/28-7-2

INTERNATIONAL COUNCIL FOR BUILDING RESEARCH STUDIES AND DOCUMENTATION

WORKING COMMISSION W18 - TIMBER STRUCTURES

A STRENGTH AND STIFFNESS MODEL FOR THE EXPANDED TUBE JOINT

by

A J M Leijten
Delft University of Technology
The Netherlands

MEETING TWENTY - EIGHT

COPENHAGEN

DENMARK

APRIL 1995

A STRENGTH AND STIFFNESS MODEL FOR THE EXPANDED TUBE JOINT

by Ad. J.M. Leijten,
TU–Delft, the Netherlands

dedicated to: HANS JØRGEN LARSEN

Introduction

Within the framework of the R&D program "FOREST" of the EC, experiments were performed to assess structural properties of densified plywood (dp) as well as the mechanical properties of densified plywood (dp) reinforced timber joints with expanded tube fasteners. A summary of the results is given in the final FOREST–report [1].
This report deals with a proposal for a strength and stiffness model of the joint.

1 Theory of beams on a elastic foundation

In short, densified plywood (dp) is glued to the timber members as a local reinforcement to prevent cracking/splitting due to high concentrated loads of dowel type fasteners.
The stiffness model presented is based on the theory of finite beams on elastic foundation first proposed by Winkler in 1867. The basic solutions for beams with finite length were given by Hetényi [2] in 1946. This theory is applied to model the stiffness of a dp reinforced joint with expanded tube fasteners which prestress the joint.

It the past this theory has been more or less successful in trying to predict the stiffness of timber joints with mechanical fasteners. In the case of dp reinforced joints the dowel runs through various materials. At the shear plane high density dvw (1100–1350 kg/m^3) is glued to the timber (Spruce).
One of the conditions for applying this theory is a tight–fit of the fastener (no clearance) as to obtain full elastic bearing in positive and negative deflection. With traditional fasteners this condition is not always easy to fullfill. The expansion procedure removes this barrier.

For joining the timber elements of the dp reinforced joints expanded tubes are used. The holes drilled are larger than the tube diameter (1 to 2 mm). By expanding the diameter of the tube the clearance is removed (see other CIB–W18 paper of this meeting). The diameter of the tube after expansion is such that considerable radial stresses are introduced without cracking the timber or densified plywood. In this way the timber joint is prestressed. Prestressing also has the advantages to improve the stiffness of the joint.

1.1 The differential equation of the elastic supported beam.

A more extensive treatment of this item can be find in Hetényi [2]. In short the mathematical backgroud is presented as follows:
The beam (dowel) considered is assumed to rest on a linear elastic medium. This means that when the beam is loaded continous reaction forces (stresses) will appear along the length of the beam. The "spring" constant of the supporting medium is called the foundation modulus and is characterized by a force distributed over a unit area, which will cause a deflection equal to unity: k_{fon} [N/mm^3] is called the foundation modulus. Further assumptions are a uniform cross–section of the beam and and constant width b. A unit

deflection will cause a reaction $b\ k_{fun} = k$. The beam width is therefore included in the parameter k. Consequently a deflection y will cause a reaction of $y\ b\ k_{fun}$ or $y\ k$.
The differential equation derived is as follows

$$EI\frac{dy^4}{dx^4} = -ky + q$$

Along the unloaded parts of the beam $q = 0$.
The solution of this equation finally results in expressions for deflections, moments, etc. with:

$$\lambda = \left[\frac{k}{4EI}\right]^{1/2}$$

The parameter λ reflects the flexural rigidity of the beam and the elasticity of the supporting medium. Therefore this parameter is also called the characteristic of the system. Since the dimension is length^{-1} the term $1/\lambda$ is usually referred to as the characteristic length. The quantity λl is a quantity which reflects the relative stiffness of the beam on the elastic foundation. For long beams with long parts being unloaded the solutions of the differential equation are simpler as the effect of the loading dies out. A method to classify the beams using this parameter is given in [2] as follows:

I	Short beams; $\lambda l < \pi/4$
II	Beams of medium length: $\pi/4 < \lambda l < \pi$
III	Long beams: $\lambda l > \pi$ (infinite length)

In [2] general and particular solutions for various elementary loading situations are given for beams with finite length. Using the method of superposition almost any loading case can be described as a combination of these elementary solutions. These solutions will be applied in finding the solution for the problem of beams on foundations with varying stiffness.

1.2 Theory of beams on a varying elastic foundation

In case the elastic supported beam (dowel) passes media with different foundation moduli the beam can be split into parts with constant foundation values. For every single piece the differential equation given previously holds. The end constrains are formulated for each beam part forcing the deflection and slope to be equal, which allows the pieces to be connected again. This method leads to a linair system of equations.

The next part of this chapter will be devoted to this method. The problem is to find a solution for an elastic beam (the dowel type fastener) passing high density dvw and normal density timber as shown in figure 1. In figure 2 the approach of splitting the beam into several parts with a constant elastic foundation modulus is illustrated. For every beam the boundary conditions can be formulated as follows:

beam part *I* and *II*:	$y_{B\,I} = y_{A\,II}$	$\theta_{B\,I} = \theta_{A\,II}$
beam part *II* and *III*:	$y_{B\,II} = y_{A\,III}$	$\theta_{B\,II} = \theta_{A\,III}$
beam part *III* and *IV*:	$y_{B\,III} = y_{A\,IV}$	$\theta_{A\,III} = \theta_{B\,IV}$

where the first indices indicates the left or the right end of the beam part and the second

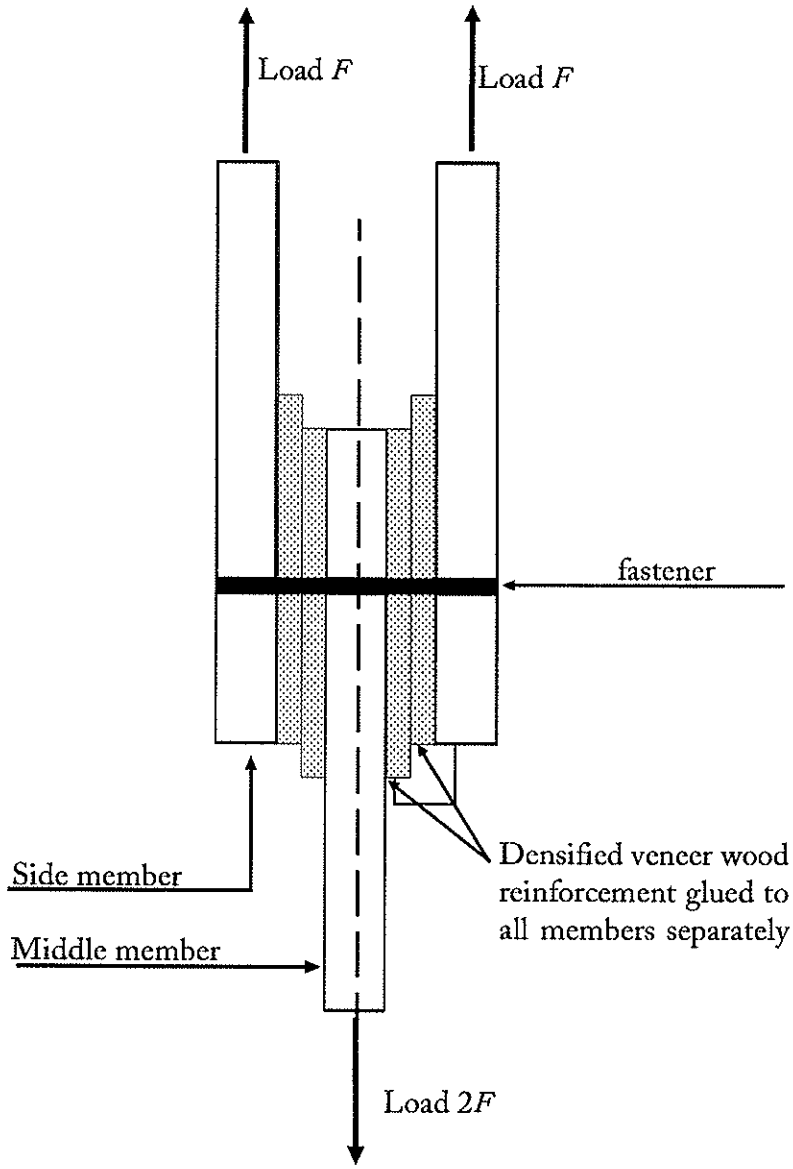

Fig. 1: Three member joint with densified veneer wood (dvw) reinforcement.

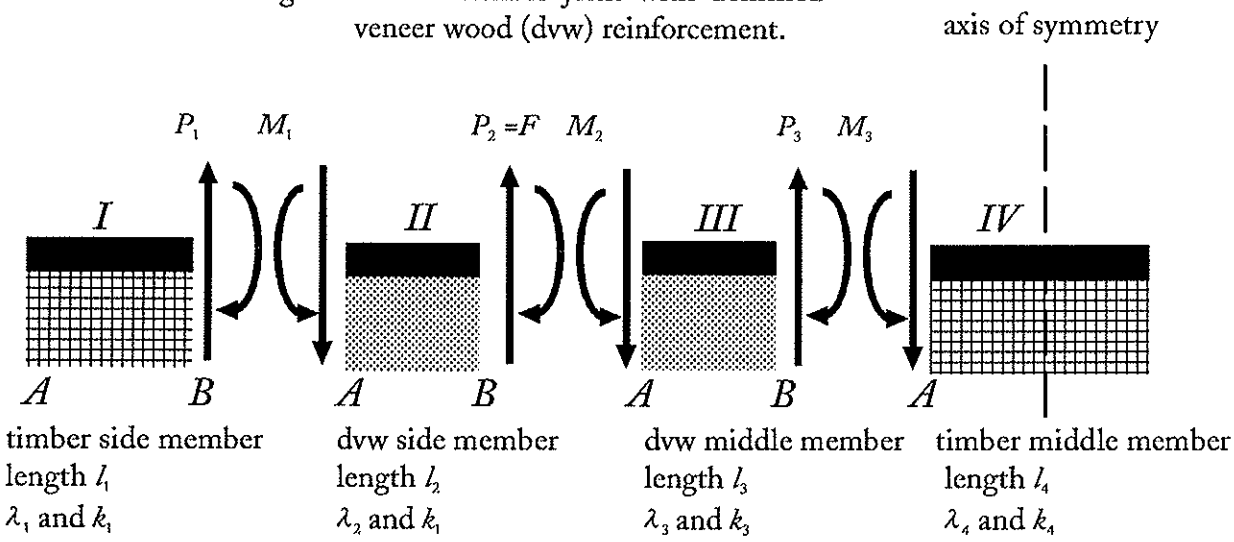

Fig. 2:Analyses of beam (dowel type fastener) on varying elastic foundation

reflects the number of the beam part, see figure 2. The number of equations formulated above is six as well as the unknown parameters, P1; M1; P2; M2; P3; M3; which are the shear forces and bending moments at the beam ends. Formulations of deflection and the slope of at the beam ends are required. Below the principle of superposition is applied to combine the solutions of the elementary loading cases.

1.3 Elementary loading cases on finite beams

Solutions of the differential equation, taken from [2].
In the formulas, wherever the symbol λ is used, it denotes $(k/EI)^{1/2}$, where $k = bk_0$: with k_0 is the modulus of the foundation in N/mm^3; and b is the constant width of the beam; EI is the flexural rigidity of the beam.

Beams with free ends

a. Equal concentrated forces at both ends

Deflection at the end points:

$$y_A = y_B = \frac{2P\lambda}{k}\,\frac{\mathrm{Cosh}\,\lambda l + \cos\lambda l}{\mathrm{Sinh}\,\lambda l + \sin\lambda l}$$

Deflection in the middle:

$$y_C = \frac{4P\lambda}{k}\,\mathrm{Cosh}\,\frac{\lambda l}{2}\cos\frac{\lambda l}{2}$$

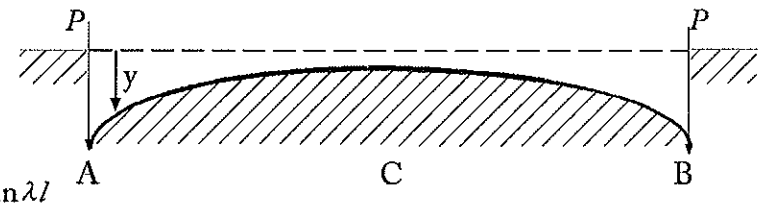

Slope at the end points:

$$\theta_A = -\theta_B = -\frac{2P\lambda}{k}\,\frac{\mathrm{Sinh}\,\lambda l - \sin\lambda l}{\mathrm{Sinh}\,\lambda l + \sin\lambda l}$$

b. Equal Concencentrated moments at both ends

Deflection at the end points:

$$y_A = y_B = -\frac{2M\lambda^2}{k}\,\frac{\mathrm{Sinh}\,\lambda l - \sin\lambda l}{\mathrm{Sinh}\,\lambda l + \sin\lambda l}$$

Slope at the end points:

$$\theta_A = -\theta_B = \frac{4M\lambda^3}{k}\,\frac{\mathrm{Cosh}\,\lambda l - \cos\lambda l}{\mathrm{Sinh}\,\lambda l + \sin\lambda l}$$

c. Concentrated force at one end

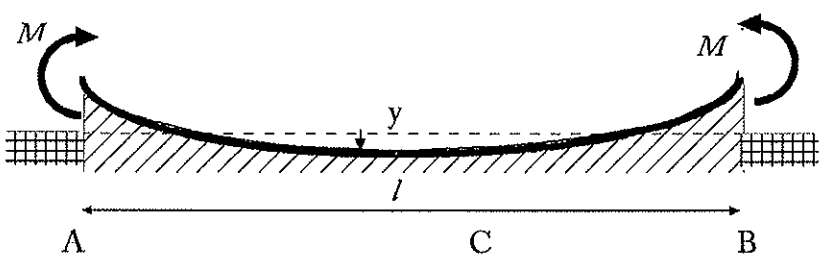

Deflections at the end points:

$$y_A = \frac{2P\lambda}{k}\,\frac{\mathrm{Sinh}\lambda l\ \mathrm{Cosh}\lambda l - \sin\lambda l\cos\lambda l}{\mathrm{Sinh}^2\lambda l - \sin^2\lambda l}$$

$$y_B = \frac{2P\lambda}{k}\,\frac{\mathrm{Sinh}\lambda l\ \cos\lambda l - \sin\lambda l\ \mathrm{Cosh}\lambda l}{\mathrm{Sinh}^2\lambda l - \sin^2\lambda l}$$

Slope at the end points:

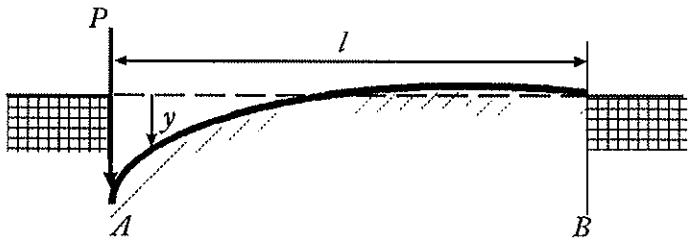

$$\theta_A = -\frac{2P\lambda^2}{k}\,\frac{\mathrm{Sinh}^2\lambda l + \sin^2\lambda l}{\mathrm{Sinh}^2\lambda l - \sin^2\lambda l}$$

$$\theta_A = -\frac{4P\lambda^2}{k}\,\frac{\mathrm{Sinh}\lambda l\ \sin\lambda l}{\mathrm{Sinh}^2\lambda l - \sin^2\lambda l}$$

d. Concentrated moment on one end

Deflections at the end points:

$$y_A = -\frac{2M\lambda^2}{k}\,\frac{\mathrm{Sinh}^2\lambda l + \sin^2\lambda l}{\mathrm{Sinh}^2\lambda l - \sin^2\lambda l}$$

$$y_B = \frac{4M\lambda^2}{k}\,\frac{\mathrm{Sinh}\lambda l\ \sin\lambda l}{\mathrm{Sinh}^2\lambda l - \sin^2\lambda l}$$

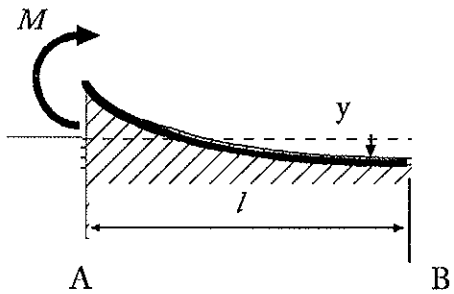

Slope at the end points:

$$\theta_A = \frac{4M\lambda^3}{k}\,\frac{\mathrm{Sinh}\lambda l\ \mathrm{Cosh}\lambda l + \sin\lambda l\cos\lambda l}{\mathrm{Sinh}^2\lambda l - \sin^2\lambda l}$$

$$\theta_A = \frac{4M\lambda^3}{k}\,\frac{\mathrm{Sinh}\lambda l\cos\lambda l + \sin\lambda l\,\mathrm{Cosh}\lambda l}{\mathrm{Sinh}^2\lambda l - \sin^2\lambda l}$$

1.4 Solution of the system

Because the analyses is focussed to find the stiffness of the joint the value of the shear force P_2 is set to unity ($P_2 = F = 1$) and the deflection caused by this unit load determines the stiffness. One should bear in mind that stiffness values always are given per shear plane. Therefore the joint of figure 1 should be loaded with 2 times a unit load to obtain the stiffness per shear plane of one unit load.

The determination of the stiffness per shear plane.
For every beam *I* to *IV*, figure 2, the equations of the elementary loading cases of the previous chapter are combined to obtain the actual loading.

Beam part *I*

$$y_{A\,I} = -\frac{2P_1\lambda_1}{k_1}E_1 - \frac{4P_1\lambda_1^2}{k_1}G_1$$

$$y_{B\,I} = -\frac{2P_1\lambda_1}{k_1}D_1 + \frac{2M_1\lambda_1^2}{k_1}F_1$$

$$\theta_{A\,I} = -\frac{4P_1\lambda_1^2}{k_1}G_1 + \frac{4M_1\lambda_1^3}{k_1}I_1$$

$$\theta_{B\,I} = -\frac{2P_1\lambda_1^2}{k_1}F_1 + \frac{4M_1\lambda_1^3}{k_1}H_1$$

Beam part *II*

$$y_{A\,II} = +\frac{2P_1\lambda_2}{k_2}D_2 + \frac{2M_1\lambda_2^2}{k_2}F_2 - \frac{4M_2\lambda_2^2}{k_2}G_2 - \frac{2F\lambda_2}{k_2}E_2$$

$$y_{B\,II} = +\frac{2P_1\lambda_2}{k_2}E_2 - \frac{4M_1\lambda_2^2}{k_2}G_2 + \frac{2M_2\lambda_2^2}{k_2}F_2 - \frac{2F\lambda_2}{k_2}D_2$$

$$\theta_{A\,II} = -\frac{2P_1\lambda_2^2}{k_2}F_2 - \frac{4M_1\lambda_2^3}{k_2}H_2 + \frac{4M_2\lambda_2^3}{k_2}I_2 - \frac{4F\lambda_2^2}{k_2}G_2$$

$$\theta_{B\,II} = -\frac{4P_1\lambda_2^2}{k_2}G_2 - \frac{4M_1\lambda_2^3}{k_2}I_2 + \frac{4M_2\lambda_2^3}{k_2}H_2 - \frac{2F\lambda_2^2}{k_2}F_2$$

Beam part *III*

$$y_{A\,III} = -\frac{2P_3\lambda_3}{k_3}E_3 - \frac{4M_3\lambda_3^2}{k_3}G_3 + \frac{2M_2\lambda_3^2}{k_3}F_3 + \frac{2F\lambda_3}{k_3}D_3$$

$$y_{B\,III} = -\frac{2P_3\lambda_3}{k_3}D_3 + \frac{2M_3\lambda_3^2}{k_3}F_3 - \frac{4M_2\lambda_3^2}{k_3}G_3 + \frac{2F\lambda_3}{k_3}E_3$$

$$\theta_{A\,III} = -\frac{4P_3\lambda_3^2}{k_3}G_3 + \frac{4M_3\lambda_3^3}{k_3}I_3 - \frac{4M_2\lambda_3^3}{k_3}H_3 - \frac{2F\lambda_3^2}{k_3}F_3$$

$$\theta_{B\,III} = -\frac{2P_3\lambda_3^2}{k_3}F_3 + \frac{4M_3\lambda_3^3}{k_3}H_3 - \frac{4M_2\lambda_3^3}{k_3}I_3 - \frac{4F\lambda_3^2}{k_3}G_3$$

Beam part *IV*

$$y_{A\,IV} = +\frac{2P_3\lambda_4}{k_4}A_4 + \frac{2M_3\lambda_4^2}{k_4}B_4$$

$$\theta_{A\,IV} = -\frac{2P_3\lambda_4^2}{k_4}B_4 - \frac{4M_3\lambda_3^3}{k_4}C_4$$

Where:

Where:

$$A_i = \frac{\text{Cosh}\,\lambda_i l_i + \cos\lambda_i l_i}{\text{Sinh}\,\lambda_i l_i + \sin\lambda_i l_i}$$

$$B_i = \frac{\text{Sinh}\,\lambda_i l_i - \sin\lambda_i l_i}{\text{Sinh}\,\lambda_i l_i + \sin\lambda_i l_i}$$

$$C_i = \frac{\text{Cosh}\,\lambda_i l_i - \cos\lambda_i l_i}{\text{Sinh}\,\lambda_i l_i + \sin\lambda_i l_i}$$

$$D_i = \frac{\text{Sinh}\,\lambda_i l_i\ \text{Cosh}\,\lambda_i l_i - \sin\lambda_i l_i\ \cos\lambda_i l_i}{\text{Sinh}^2\,\lambda_i l_i - \sin^2\lambda_i l_i}$$

$$E_i = \frac{\text{Sinh}\,\lambda_i l_i\ \cos\lambda_i l_i - \sin\lambda_i l_i\ \text{Cosh}\,\lambda_i l_i}{\text{Sinh}^2\,\lambda_i l_i - \sin^2\lambda_i l_i}$$

$$F_i = \frac{\text{Sinh}^2\lambda_i l_i + \sin^2\lambda_i l_i}{\text{Sinh}^2\lambda_i l_i - \sin^2\lambda_i l_i}$$

$$G_i = \frac{\text{Sinh}\lambda_i l_i\ \sin\lambda_i l_i}{\text{Sinh}^2\lambda_i l_i - \sin^2\lambda_i l_i}$$

$$H_i = \frac{\text{Sinh}\,\lambda_i l_i\ \text{Cosh}\,\lambda_i l_i + \sin\lambda_i l_i\ \cos\lambda_i l_i}{\text{Sinh}^2\,\lambda_i l_i - \sin^2\lambda_i l_i}$$

$$I_i = \frac{\text{Sinh}\,\lambda_i l_i\ \cos\lambda_i l_i + \sin\lambda_i l_i\ \text{Cosh}\,\lambda_i l_i}{\text{Sinh}^2\,\lambda_i l_i - \sin^2\lambda_i l_i}$$

and i = 1, 2, 3 or 4 corresponds with the beam parts *I, II, III* or *IV*.

Above expressions are now used for substitution in the boundary conditions. This will lead to a five by five matrix of linear equations in which the unknown parameters are P_1 P_3 M_1 M_2 and M_3. Since P_2 equals F, which is set to unity, expressions containing F are situated at the right hand side to form a one by five matrix. Once again the boundary conditions are:

$$\theta_{B\,I} = \theta_{A\,II}$$
$$y_{B\,I} = y_{A\,II}$$
$$\theta_{B\,II} = \theta_{A\,III}$$
$$y_{B\,II} = y_{A\,III}$$
$$\theta_{B\,III} = \theta_{A\,IV}$$
$$y_{B\,III} = y_{A\,IV}$$

$$\begin{bmatrix} a & 0 & b & c & 0 \\ e & 0 & f & g & 0 \\ i & j & k & l & m \\ 0 & p & 0 & q & r \\ 0 & t & 0 & u & v \end{bmatrix} \begin{bmatrix} P_1 \\ P_3 \\ M_1 \\ M_2 \\ M_3 \end{bmatrix} = \begin{bmatrix} d \\ h \\ n \\ s \\ w \end{bmatrix} F$$

where:

$$a = -\frac{2\lambda_1^2}{k_1} F_1 + \frac{2\lambda_2^2}{k_2} F_2$$

$$b = -\frac{4\lambda_1^3}{k_1} H_1 + \frac{4\lambda_2^3}{k_2} H_2$$

$$c = -\frac{4\lambda_2^3}{k_2} H_2$$

$$d = -\frac{4\lambda_2^2}{k_2} G_2$$

$$e = -\frac{2\lambda_1}{k_1} D_1 - \frac{2\lambda_2}{k_2} D_2$$

$$f = +\frac{2\lambda_1^2}{k_1} F_1 - \frac{2\lambda_2^2}{k_2} F_2$$

$$g = +\frac{4\lambda_2^2}{k_2} G_2$$

$$h = -\frac{2\lambda_2}{k_2} E_2$$

$$i = -\frac{4\lambda_2^2}{k_2} G_2$$

$$j = +\frac{4\lambda_3^2}{k_3} G_3$$

$$k = -\frac{4\lambda_2^3}{k_2} I_2$$

$$l = +\frac{4\lambda_2^3}{k_1} H_2 + \frac{4\lambda_3^3}{k_3} H_3$$

$$m = -\frac{4\lambda_3^3}{k_2} I_3$$

$$n = +\frac{2\lambda_2^2}{k_2} F_2 - \frac{2\lambda_3^2}{k_3} F_3$$

$$p = -\frac{2\lambda_3^2}{k_3} F_3 + \frac{2\lambda_4^2}{k_4} B_4$$

$$q = -\frac{4\lambda_3^3}{k_3} I_3$$

$$r = +\frac{4\lambda_3^3}{k_3} H_3 + \frac{4\lambda_4^3}{k_4} C_4$$

$$s = +\frac{4\lambda_2^2}{k_3} G_3$$

$$t = -\frac{2\lambda_3}{k_3} D_3 - \frac{2\lambda_4}{k_4} A_4$$

$$u = -\frac{4\lambda_2^2}{k_3} G_3$$

$$v = -\frac{2\lambda_3^2}{k_3} F_3 - \frac{2\lambda_4^2}{k_4} B_4$$

$$w = -\frac{2\lambda_3}{k_3} E_3$$

In the above expressions four different foundation moduli are assumed. However, in our particular case it may be assumed that $\lambda_1 = \lambda_4$ and $\lambda_2 = \lambda_3$ disregarding the density differences between the seperate dvw and timber parts. It is important that the dp density and foundation modulus are correlated. It will be shown later that density variations will not have a dominant effect.

Solving the linear system by standard numerical procedures lead to values of the shear forces and bending moments at the interfaces of the beam parts (beam ends). The next step is to

determine the deflection and the slope at the interfaces by substitution of the derived values of shear forces and bending moments in each separate beam part.
The total deflection of the joint caused by the unity force F is the right end deflection of beam part *II* ($y_{B\,II}$) plus the deflection at the left of beam part *III* ($y_{A\,III}$), see figure 3. The stiffness is now taken as the reciprocal value of the total deflection.

With this procedure the thickness of the dvw as well as the timber member thickness can be varied, in order to analyse the sensitivity of the solution for a given variation of the parameter. Also the influence of foundation moduli variations can be analysed.

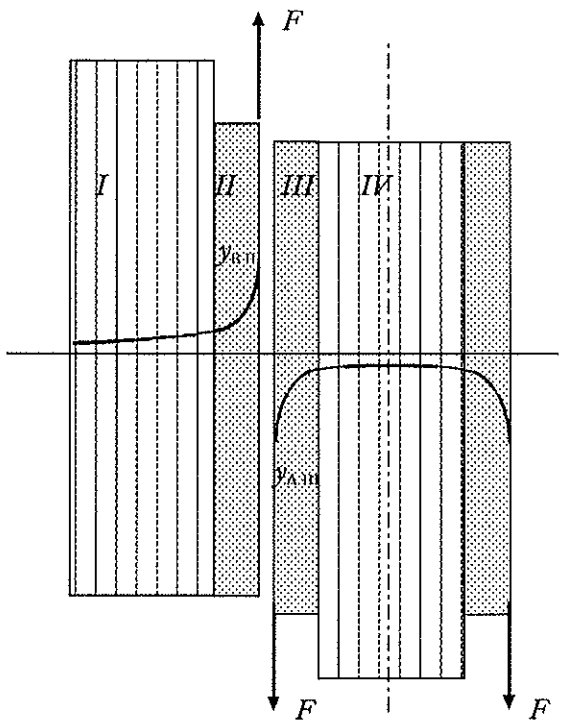

Fig. 3: Exaggerated deflection of the dowel in side and middle member

1.5 Simple method

A simplified method could perhaps be adopted with almost the same stiffness determining accuracy, published by Kuenzi [3] in 1951.

He gave a design method for the determination of the slip of a traditional timber joint with dowels or bolts. The dowel was considered as a beam on an elastic foundation which is the same starting point as the analyses in the previous chapter. There are various methods to make use of his analyses. When it is justified to disregard the timber of the joint for the stiffness analysis, layers *I* and *IV* of figure 3, the particular solution of Keuenzi is direct applicable. Without solving a set of linear equations the solution is obtained directly by:

$$\frac{1}{2K} = L_1 + L_2 - \frac{(J_1 - J_2)^2}{2(K_1 + K_2)}$$

where:

K is the stiffness per shear plane per fastener

$$L_1 = \lambda_i / k_i A_i \quad \text{and} \quad A_i = \frac{\text{Cosh}\,\lambda_i l_i + \cos \lambda_i l_i}{\text{Sinh}\,\lambda_i l_i + \sin \lambda_i l_i} \quad \text{with i = 1 (middle member)}$$

$$L_2 = l_i / k_i D_i \quad \text{and} \quad D_i = \frac{\text{Sinh}\,\lambda_i l_i\ \text{Cosh}\,\lambda_i l_i - \sin \lambda_i l_i\ \cos \lambda_i l_i}{\text{Sinh}^2 \lambda_i l_i - \sin^2 \lambda_i l_i} \quad \text{with i = 2 (side member)}$$

$$J_1 = l_i / k_i B_i \quad \text{and} \quad B_i = \frac{\text{Sinh}\,\lambda_i l_i - \sin \lambda_i l_i}{\text{Sinh}\,\lambda_i l_i + \sin \lambda_i l_i} \quad \text{with i = 1}$$

$$J_2 = l_i / k_i F_i \quad \text{and} \quad F_i = \frac{\text{Sinh}^2 \lambda_i l_i + \sin^2 \lambda_i l_i}{\text{Sinh}^2 \lambda_i l_i - \sin^2 \lambda_i l_i} \quad \text{with i = 2}$$

$$K_1 = l_i / k_i C_i \quad \text{and} \quad C_i = \frac{\text{Cosh}\,\lambda_i l_i - \cos \lambda_i l_i}{\text{Sinh}\,\lambda_i l_i + \sin \lambda_i l_i} \text{ with i = 1}$$

$$K_2 = l_i / k_i H_i \quad \text{and} \quad H_i = \frac{\text{Sinh}\,\lambda_i l_i \ \text{Cosh}\,\lambda_i l_i + \sin \lambda_i l_i \ \cos \lambda_i l_i}{\text{Sinh}^2 \lambda_i l_i - \sin^2 \lambda_i l_i} \text{ with i = 2}$$

Both models are compared in chapter 2 .

1.6 Foundation modulus of densified veneer wood.

To apply the model foundation moduli values are required. The parameters of influence have been evaluated and analysed in [7]. Of major importance is the density of the dvw and the type of test, embedding compression or tension. The embedding test procedure according to prEN 383, given in figure 4, lead to three types of stiffness and therefore three foundation values. The foundation modulus associated with the stiffness k_s is used in this analyses. In figure 5 the foundation modulus data versus the dvw density is given for the tension and compression tests separately, Rodd[4].

It is intented not to use dvw material with lower densities than 1250 kg/m^3 (density classification). The influence of the scatter is taken into account by substitution of the mean, average and upper value of k_s in the model. The lower value of k_{mod} is 180 N/mm^3 while for the mean and upper value 215 and 240 N/mm^3 is substituted.

1.7 Effect of the prestressing

The foundation moduli values of fig.5 are based on embedding tests with "tight" fitting dowels. Now the effect of the tube expansion or prestressing will be considered.

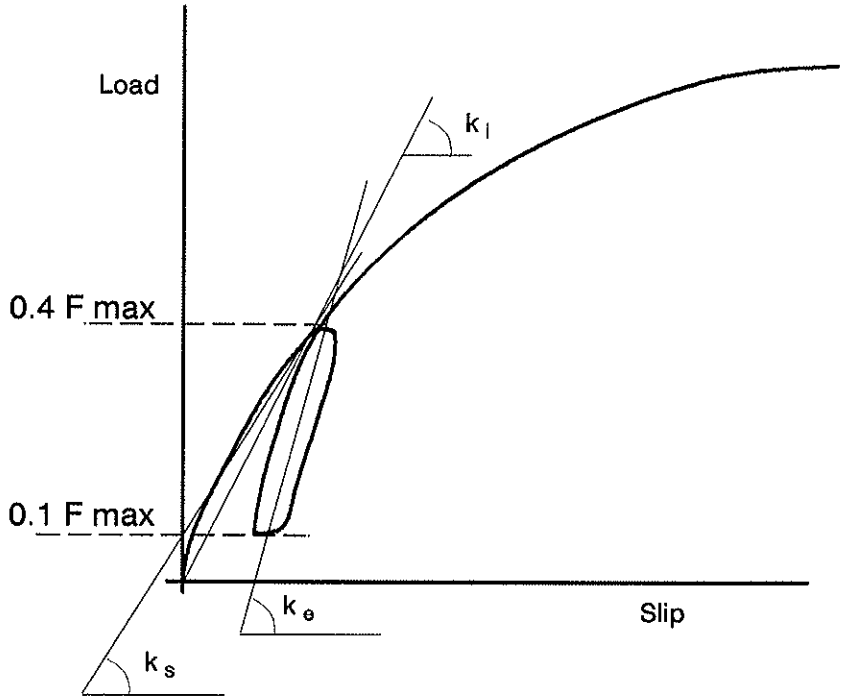

Fig. 4: Loading procedure according to prEN 383 embedding tests:
foundation moduli based on three stiffness values k_i, k_s and k_e

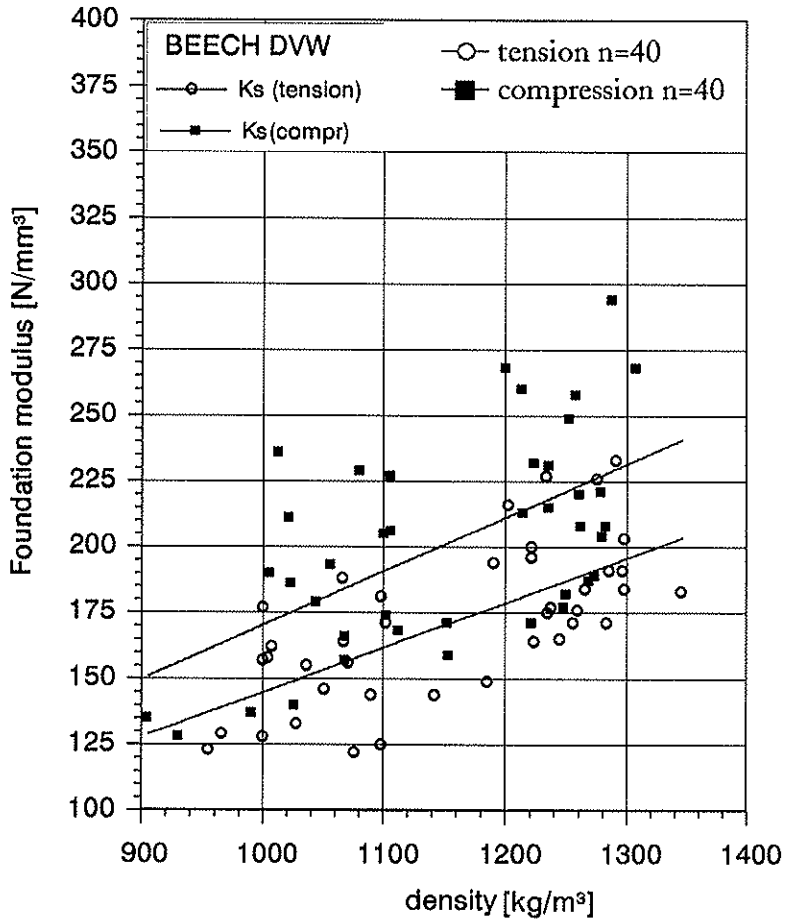

Fig. 5: The foundation modulus of beech dvw in compression and tension by Rodd [4].

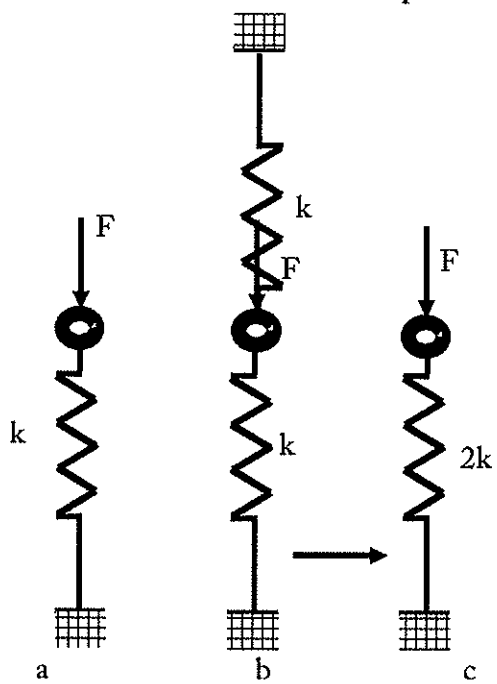

Fig. 6: Foundation modulus in case of

a) embedding tests using a "tight" fitting dowel
b) expanded dowel (prestressed hole)
c) case b) represented by one spring

Due to the expansion procedure the diameter of the pre-drilled hole is increased. This means that radial compression stresses are introduced around the hole both in the dvw and timber. Rough measurements have shown that holes originally 35 mm increased up to 40 mm in the timber and 35.2 mm in the dvw. For the smaller 18 mm holes the diameter in the dvw increased to 18.2 mm and the timber up to 22 mm. In this case the material in "all" directions contribute to the elastic bearing stiffness. The dvw material as well as the timber is prestressed. The foundation modulus is in this case twice as high as in the "tight" fitting dowel tests. In figure 6 this effect is shown.
It means that in the stiffness analyses the foundation modulus is be doubled. To what extend this prestressing effect will disappear due to relaxation of the dvw is not yet investigated. However, the elastic compression stresses imposed by the expanding procedure in the steel tube might counter balance this phenomenen to a certain extend?

2. Application of the theory

The model, outlined in chapter 1.4 was used to analyse the influence of the dvw density and timber thickness. The dvw layers where taken of equal density and thickness at all times while the (Spruce) timber side members were always half the timber middle member thickness. Although initially intended for solid dowels, the model is only modified for tube dowels in that sence that the second moment of plane area of a tube is substituted. It is assumed that in the initial loading stage the behaviour of a tube or solid dowel is the same. Typical tube like deformations are assumed not to occur at this stage.

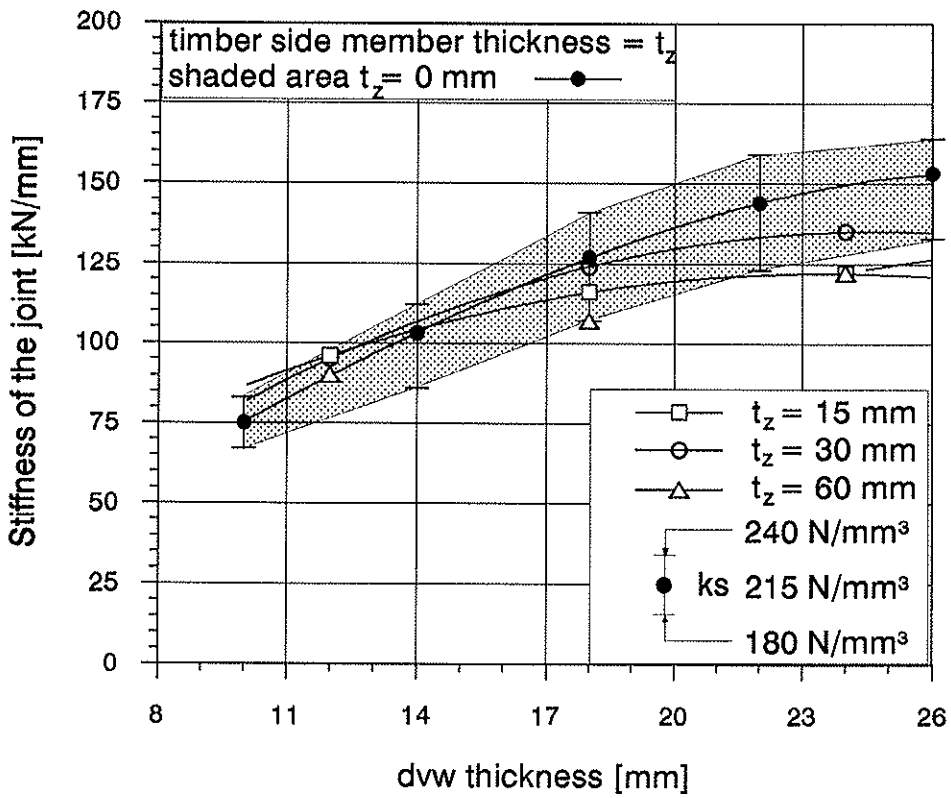

Fig 7.: Model prediction of stiffness of the joint. The curves show the effect of the timber member thickness for 35 mm expanded tube dowel.

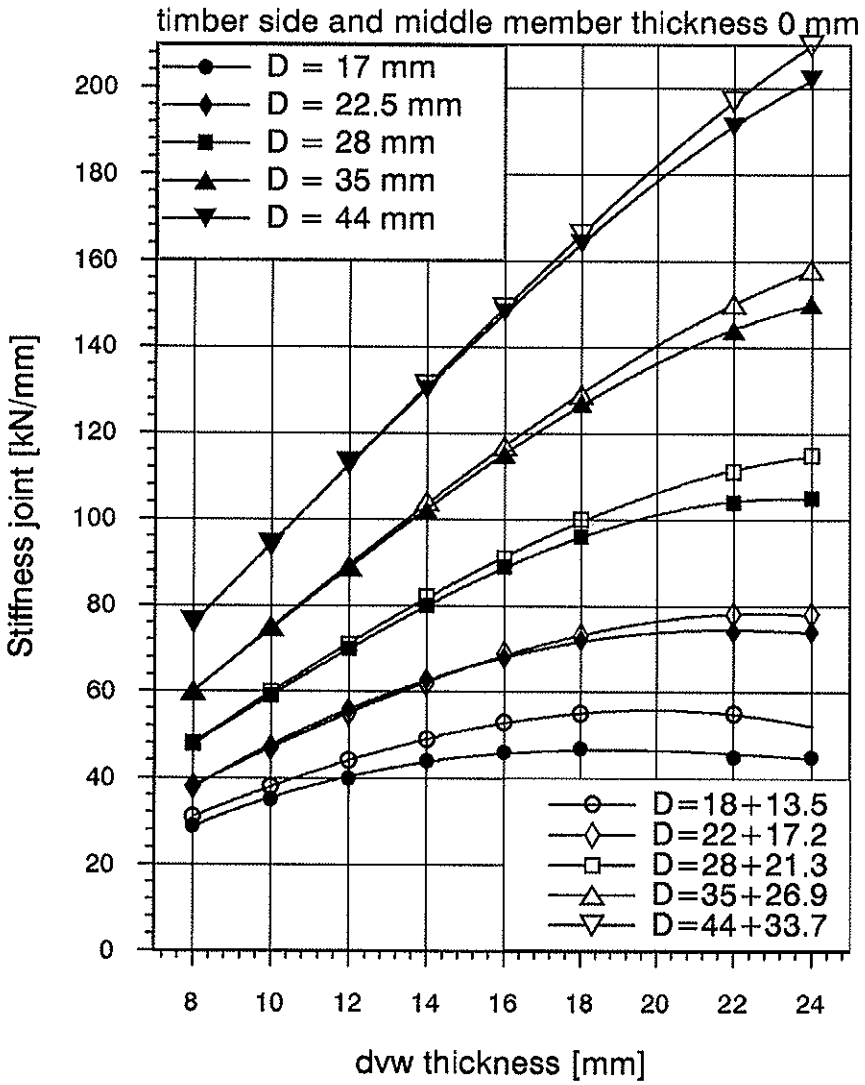

Fig.8: Model prediction of stiffness for single and double expanded tube dowel (D in [mm]).

In figure 7 the results are graphically presented for the 35 mm expanded tube dowel. The influence of the foundation modulus variation is shown by the shaded area. In this case the timber member thickness is zero. The effect of increasing the thickness of the timber side and middle member is indicated. As for 35 mm tube dowels a practical dvw thickness is about 15 to 18 mm it will be clear that the influence of the timber thickness is small and can be neglected. This means that Kuenzi's model can be accepted as being sufficiently accurate. This model is able to predict more.

There is an option to increase the wall thickness of the tube by expanding a second tube inside the first one. The tube dowels of 35 and 28 mm can be combined to obtain a total wall thickness of 5.90 mm. The stiffening effect is small, figure 8 (zero timber member thickness). The curve for the small tube sizes tend to drop for large dvw thicknesses. This is due to the increased slenderness of the dowel and the role of the slenderness in the deformations due to the bending moment caused by the excentricity of the forces in side and middle member.

Results of the stiffness model

– The model indicates a minor influence of the timber thickness. For practical sizes up to

90 and 180 mm for side and middle member respectively, the joint stiffness will not be reduced by more than about 10% compared to very thin timber members.
- Also the variation of the foundation modulus from 180 to 240 N/mm^3 hardly affects the stiffness of the joint by more than about 10%.
- Evidently, the prestressing is of major importance to increase the foundation modulus a factor of two.
- The model shows that increasing the wall thickness of the tube hardly affects the stiffness of the joint.

3. Comparsion of the stiffness model with test data

3.1 The test data

Tests carried out by Ehlbeck & Werner [9], Leijten [10,11,13] as well as by Rodd [12] are considered. In all cases joints with two tube diameters 18 and 35 mm were tested. The wall tickness of the tubes is 2.35 and 3.25 mm (ISO 65/ DIN 2440 gaspipes) respectively . The tension joints were carried out by Werner while Rodd and Leijten focussed on four point bending and moment transmitting joints, figure 9.

3.2 Models to represent the load–slip curve

The models described in literature can be classified in four main categories:
A: Curve fitting
B: Simplified analytical models
C: Mechanical models
D: Finite element models

Although purely empirical the advantage of the curve fitting models (A) is the capacity to represent any shape of load–slip curve with great accuracy. These models have the inability

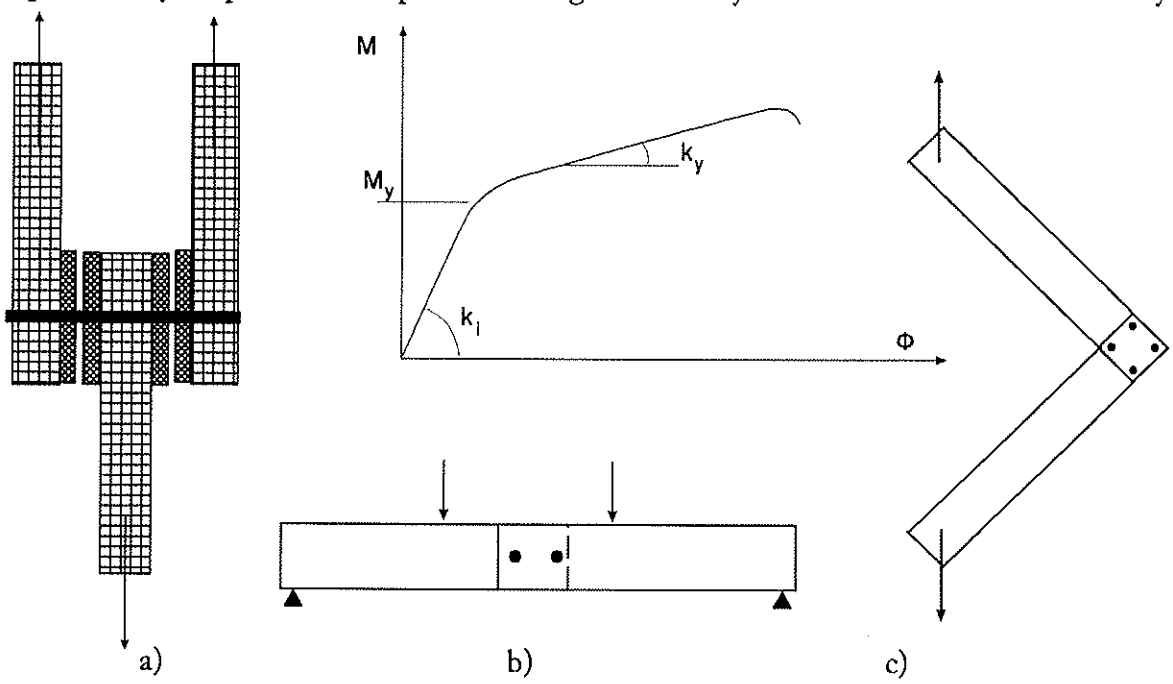

Fig. 9.: Test specimens of Werner a) , Rodd b) and Leijten c)

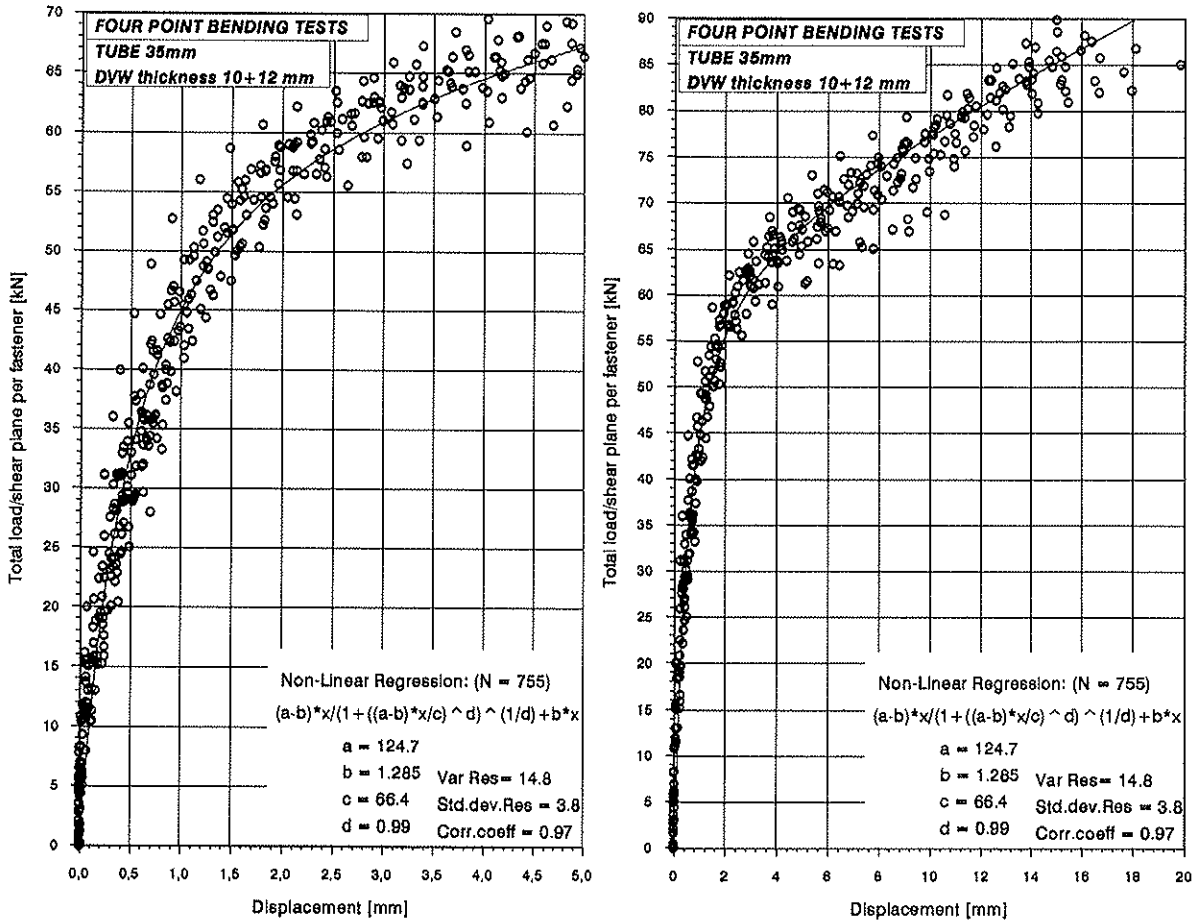

Fig.10: Regression of load – slip curves of four point bending tests

to recognize that, depending on the geometrical and material parameters, the behaviour as well as the contribution of each component to the overall joint response may change significantly. The simplified analytical models (B) can be defined as to reflect the main characteristic values of the load–slip or moment–rotation curves such as initial and post yield stiffness, plastic and ultimate load or moment. For the mechanical and finite element models (C and D) it is required to have knowledge about the behaviour of all components of the joint represented as a set of rigid or deformable elements.

For the joints considered in this report the simplified analytical model of Richard/Jaspar is considered. The model represented below is to be applied for moment–rotation curve fitting:

$$M = \frac{(k_i - k_y)\,\phi}{\{1 + [\frac{(k_i - k_y)\,\phi}{M_y}]^C\}^{1/C}} + k_y \phi$$

inwhich:

M_y is the transition bending moment

k_i the initial stiffness

k_y the post yield stiffness

ϕ is the rotation

C a curve fitting parameter

The parameters of this regression model can of course easily be replaced to describe the load–slip curve instead of a moment–rotation curve.

To show how small the experimental scatter is as well as the ability to describe load deformation curves, two graphs are presented in fig. 10. The first shows in detail the load–slip curve near the origin while the latter shows the whole load–slip curve. As can be

Comparison of regression equation parameters of Jaspar's–model $F = (k_i - k_y).\delta/(1+((k_i-k_y).\delta/M_y)\text{^}C)\text{^}(1/C)+k_y.\delta$						
	Joints with tubes 35 mm			Joints with 18 mm tubes		
Test type	Tension	Moment	Four point bending	Tension	Moment	Four point bending
dvw thickness [mm]	12/18	18	18/14	14/18	10/12	12
k_i [kN/mm]	145.2	125.8	124.7	15.93	30.80	29.84
k_y [kN/mm]	1.58	1.63	1.285	0.696	1.402	0.882
M_y [kN]	60.06	67.6	66.4	24.07	22.35	27.97
C	1.386	1.017	0.99	2.834	3.85	2.05

Table 1: Curve–fitting parameters of Richard–Jaspar model

observed the data clearly indicate the existence of some friction in the beginning . Therefore the data very near to the vertical axis is disregarded in the curve fitting procedure. In Table 1 a review of the curve fitting parameters is given. Regarding the initial stiffness parameter k_i , Table 1 shows both moment and four point bending test series have very simular values which deviate from the tension test; there is no certainty what this caused. When the curves associated with these parameters are plotted like in fig. 11 for the 35 mm tube specimens, the differences are small. The lower post yield stiffness of the tension joints can be explained as during the last stage of loading the side members tend to separate from the middle member creating an increasing gap.

3.2 Comparison

Now this data is compared with the model predictions (Kuenzi's–model). Therefore fig. 12 and 13 are presented. As the dp density is of influence, the total density range of dvw 900 to 1350 kg/m^3 is divided into three classes. Because the dp density is not recorded in all tests, all data irrespective of the dp density class are jointed in these figures.

To show the dependency of the stiffness with the dvw density, fig. 14 is presented. Of all data only a part could be used as only the dvw density of the four point bending and moment joints is recorded. Regression lines indicate the general tendency. Two dotted lines for each tube size shows the model predictions on the bases of the two (embedding tests) foundation moduli. The bottom one derived from embedding tests in tension and top one based on embedding compression tests, see also fig. 5. For the joints with the 18 mm tube, the model fit the experimental data quite well. On the other hand for the joints with 35 mm tubes, the model is somewhat optimistic for low dvw density values but the deviation is small.
Although the test data is still limited, there appears to be a good correlation with the model predictions.

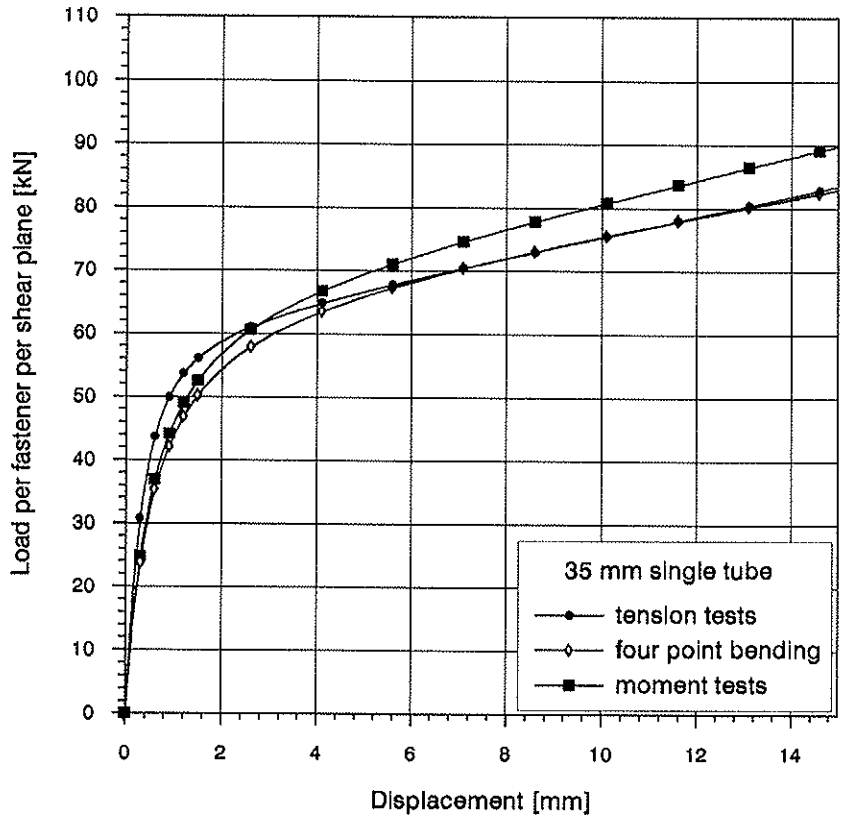

Fig.11: Comparison of regression curves of tension, four point bending and moment tests.

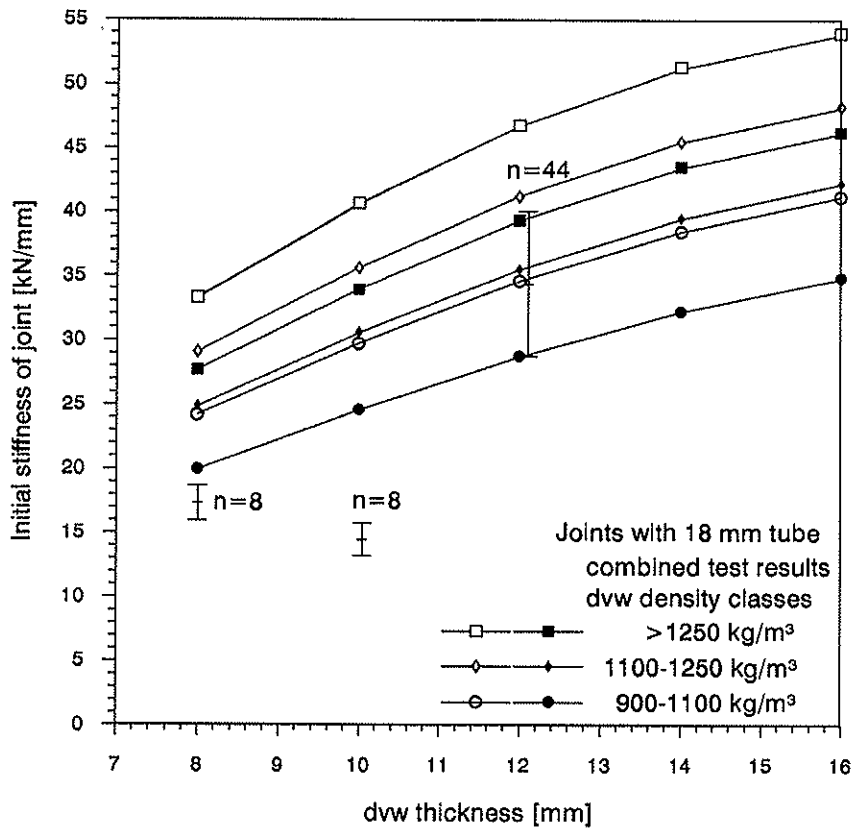

Fig.12: Model prediction and test data combined for joints with 18mm tubes

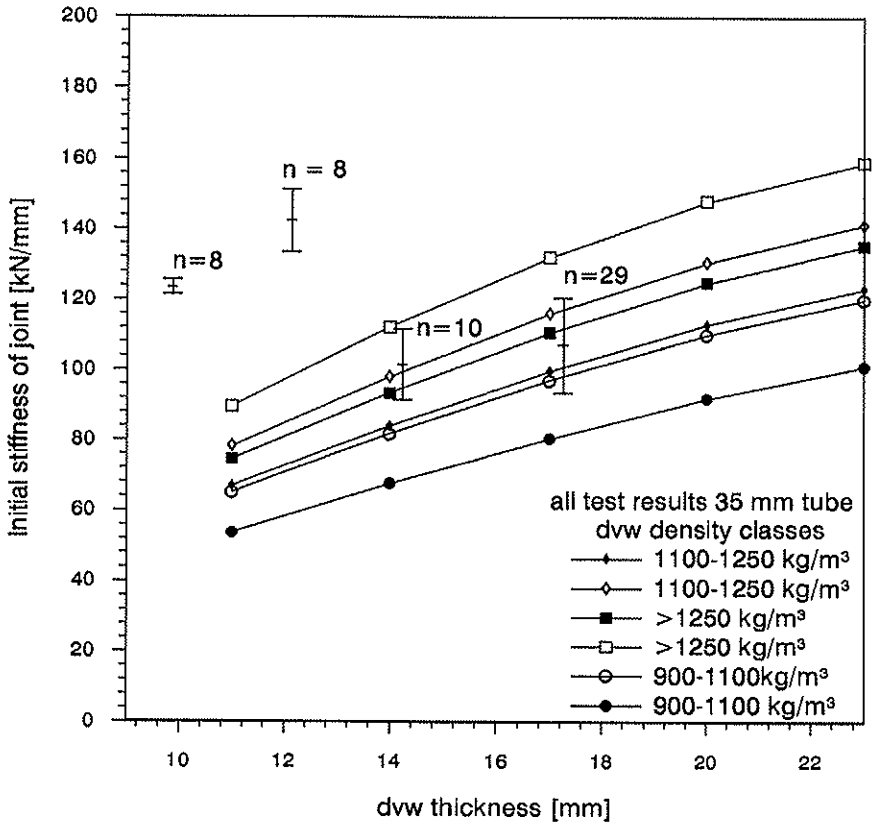

Fig.13: Model prediction and test data combined for joints with 35mm tubes

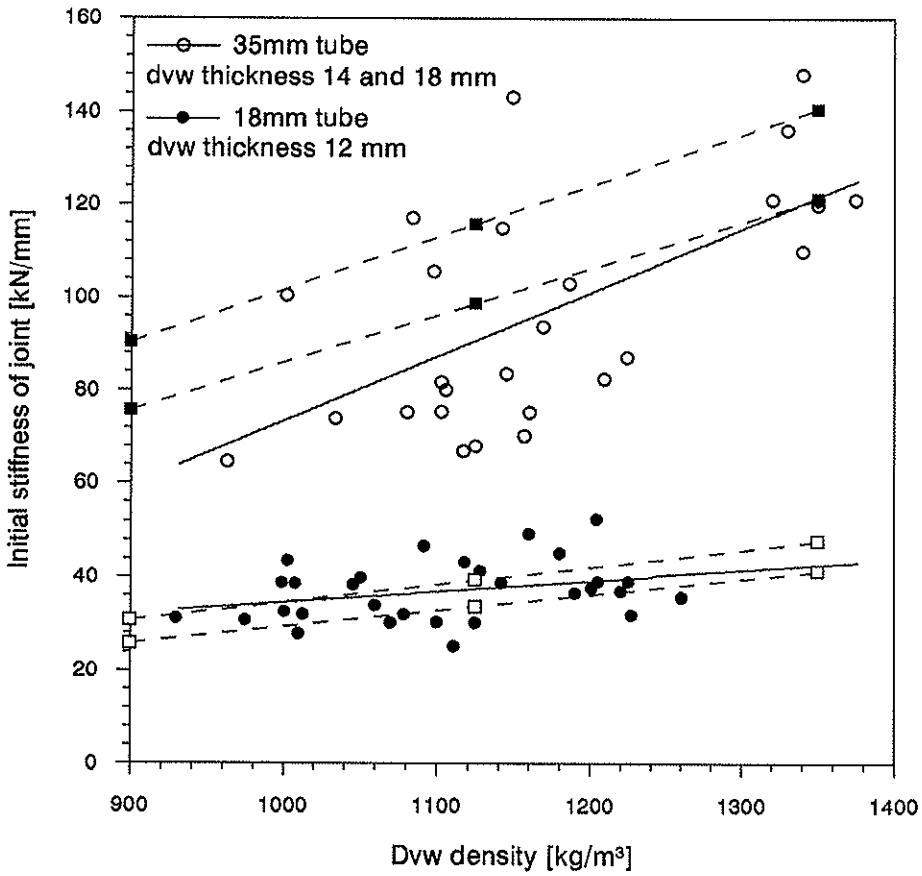

Figure 14: Influence of dvw density related to the initial stiffness of the joint;
– For one tube diameter, the dotted top line is the model prediction based on embedding compression test; the dotted bottom line based on embedding tension test

4. Strength model

For the cases where no premature timber or dvw failure occurred, due to a proper choice of end/edge distance or dvw density and thickness, ideal yielding is observed. In many of these tests no failure occurred at all, despite very large slip displacements or 30 to 40 mm. The timber between the washer and the dvw is squeezed during the tests as the dvw has to make room for the tube to curve. A strength model as shown in fig. 16 is set up. The plastic regions of the tube are considered as hinges. The bending moments which develop in the tube are neglected. There are actually three possible failure modes:

- A: the tube fails in tension
- B: the tube is pulled out of the washers
- C: the embedding strength is reached.

Type A: A number of tension tests are performed to obtain information regarding the yield strength of the tube material. For the 18 and 35 mm tube a yield strength of 35 kN and 105 kN is recorded, which compares very well with the yield load of 18 mm tube joints, fig.15 (right axis). However, the joints with 35 mm tubes and timber members of Spruce usually showed lower values, 95 to 100 kN instead of 105 kN. However, some test results with Maritime pine gave yield strength values of 120 kN.

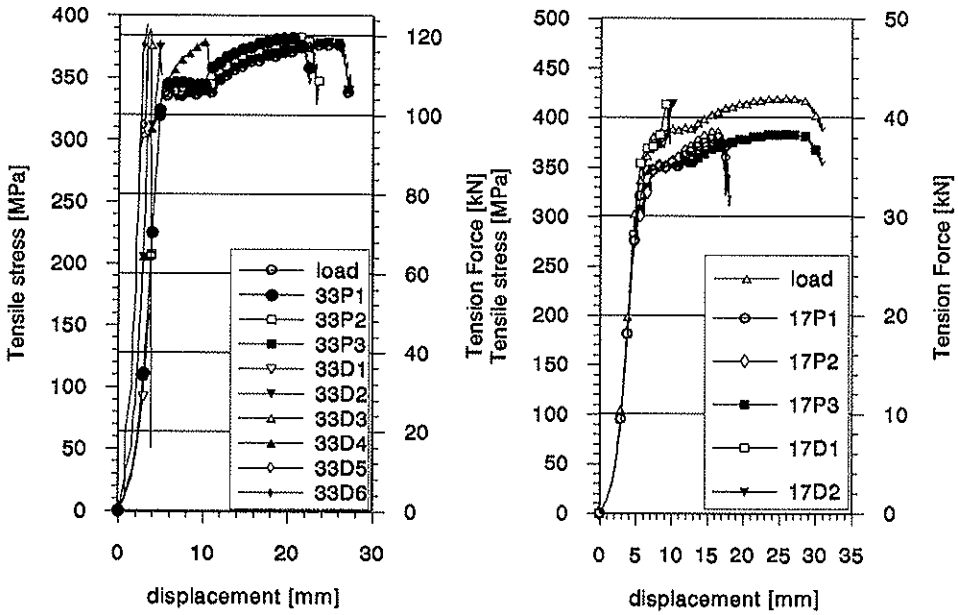

Fig.15: Tension tests results of 35 mm (left) and 18 mm tubes (right)

Type B: This failure mode only occurred for the joints with Maritime Pine. Apparently when the compression perpendicular to the grain is high the anchorage forces tend to concentrate on one edge of the tube while for Spruce the material fails much easier and behaves like a plastic bearing for the washer. In this respect the thickness of the washer is also of importance.

Type C: When it is assumed that the embedding strength of the timber increases proportional with density and the embedding strength of both materials govern the mean maximum load, a very simple approach might be considered, fig.16:

$$F_{max} = (t_t f_{h,t} + t_{dvw} f_{h,dvw}) D$$

were:

t_t thickness of the timber member [mm]

t_{dvw} dvw thickness [mm]

$f_{h,t}$ timber embedding strength [MPa]

$f_{h,dvw}$ is the dvw embedding strength [MPa]

D is the tube diameter [mm]

This approach implies no difference in ultimate load between a solid dowel of 18 mm (failure mode I) and a tube of 18 mm.

The input of the dvw embedding strength is based on tests by Werner [4] and Rodd [5]. The regression formula derived in [8] for the mean dvw embedding strength versus dvw density is:

$f_{h,dvw} = -43.24 + 0.141\ \rho_{dvw}$

with:

ρ_{dvw} the dvw density in [kg/m^3](beech dvw)

The contribution of the embedding strength of the timber member is relatively small but is taken into account. For this purpos the Eurocode5 formulas for the embedding strength is used:

$f_{h,t} = 0.082(1-0.01\ D)\ \rho_t$

were:

ρ_t is the mean timber density [kg/m^3]

(Spruce mean density was 430 kg/m^3)

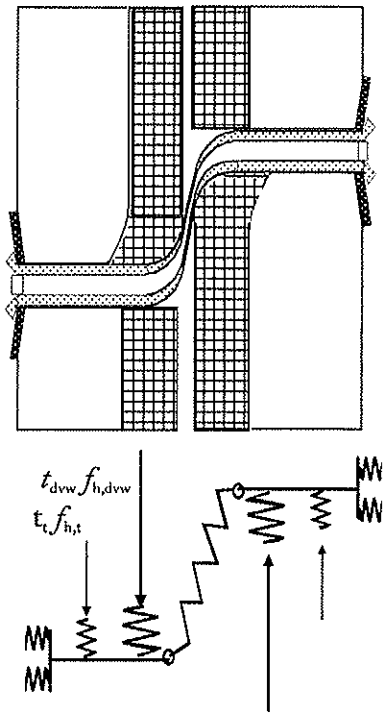

Fig.16: Strength model

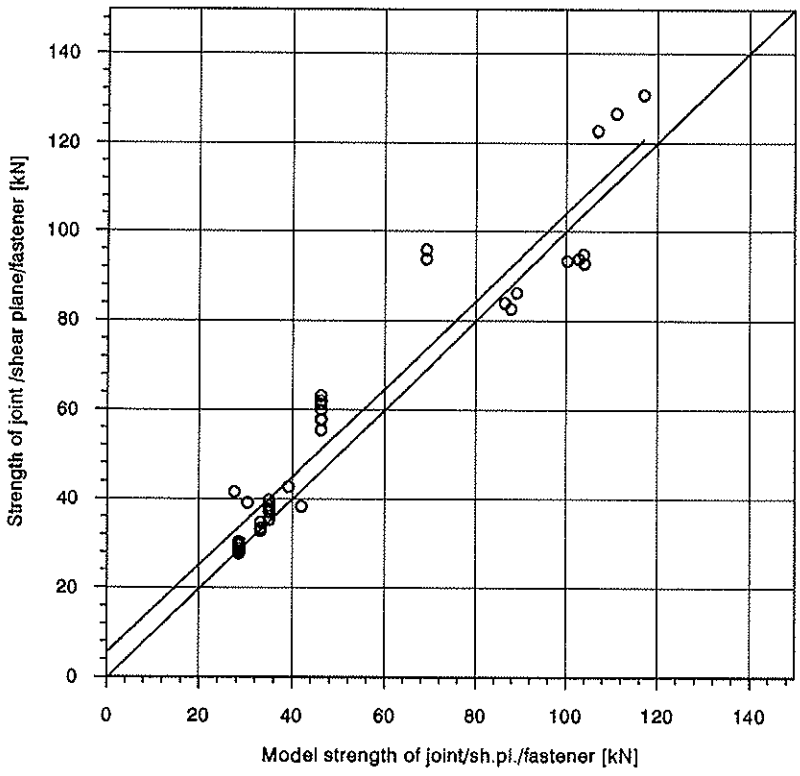

Fig.16: Strength model prediction versus test data

In fig. 17 the strength model predictions are plotted versus the test data. In the ideal situation all data should be on this line. The test data to be selected for this comparison is very limited as only those joints with sufficient slip show a ideal plastic behaviour; 15 mm for the 18mm tube and 20 mm for the 35 mm tube. Also tests results with 22 mm tubes are included. The left line is a linear regression line on the bases of the data points which corresponds very well with the prediction line. The result of this very simple model is not bad.

5. Conclusions

A model to predict the strength and stiffness of dvw reinforced joints with expanded tubes is presented. The stiffness model based on the linear elastic supported beam theory (Winkler/ Kuenzi) is in good agreement with the test results.
The stiffness model predicts that:

- strength and stiffness are governed by the densified plywood; the contribution of the timber can be neglected
- increasing the wall thickness of the tubes hardly affect the initial stiffness,
- the initial stiffness of the joint is correlated with the dvw density.

A strength model based on the yield strength of the tube on one hand and on the embedding strength of the materials on the other hand fit the test results well. Verification of the validity of this model requires more tests.

6. Literature

[1] Leijten, A.J.M., et al," Physical and mechanical properties of densified veneer wood (dvw) for structural applications, Final report FOREST, august 1994.

[2] Hetényi,M. " Beams on elastic foundation", University of Michigan Press, Ann Abor, 1974

[3] Kuenzi, E.W. " Theoretical design of a nailed or bolted joint under lateral load", D1951, Forest Product Laboratory, Madison, Wisconsin, U.S.A., March 1955

[4] Rodd, P.,"Embedding strength of densified veneer wood with dowel–type fasteners", Report of FOREST–project, University of Brighton, Faculty of Engineering and Environmental Studies, Structural Timber Research Unit, 1993.

[5] Ehlbeck and Werner,H," Embedding strength of densified veneer wood for dowel–type fasteners", Report of FOREST–project, University Fridericiana Karlsruhe, Department of Timber Engineering, 1992.

[6] Leijten, A.J.M."Analysis of variation of embedding tests with 17mm dowels", University of Technology Delft, Dep. of Civil Eng., Stevin Report 25.4–94–06/HA–59, January 1994.

[7] Leijten, A.J.M."Analysis of variation of embedding tests with 35mm dowels", University of Technology Delft, Dep. of Civil Eng., Stevin Report 25.4–94–07/HA–60, January 1994.

[8] Leijten, A.J.M."Analysis of embedding tests with 17mm and 35mm dowels", University of Technology Delft, Dep. of Civil Eng., Stevin Report 25.4–94–08/HA–61, February 1994.

[9] Ehlbeck and Werner,H," Densified veneer wood reinforced joints with dowel–type fasteners loaded in tension", Report of FOREST–project, University Fridericiana Karlsruhe, Department of Timber Engineering, 1994.

[10] Leijten, A.J.M."Analysis of tension tests; dvw reinforced joints connected with 18 mm expanded tubes", University of Technology Delft, Dep. of Civil Eng., Stevin Report 25.4–94–09/HV–28, February 1994.

[11] Leijten, A.J.M."Analysis of tension tests; dvw reinforced joints connected with 35 mm expanded tubes", University of Technology Delft, Dep. of Civil Eng., Stevin Report 25.4–94–10/HV–29, March 1994.

[12] Rodd, P. D. ,"Four point bending tests on three member joints", Report of FOREST–project, University of Brighton, Faculty of Engineering and Environmental Studies, Structural Timber Research Unit, 1994.

[13] Leijten, A.J.M."Tests on locally dvw reinforced moment joints with 35 mm and 18 mm tube–dowels", University of Technology Delft, Dep. of Civil Eng., Stevin Report 25.4–94–12/TRV–23, June 1994.

INTERNATIONAL COUNCIL FOR BUILDING RESEARCH STUDIES AND DOCUMENTATION

WORKING COMMISSION W18 - TIMBER STRUCTURES

LOAD-CARRYING CAPACITY OF STEEL-TO-TIMBER JOINTS WITH ANNULAR RINGED SHANK NAILS

A COMPARISON WITH THE EC5 DESIGN METHOD

by

R Görlacher
University of Karlsruhe
Germany

MEETING TWENTY - EIGHT

COPENHAGEN

DENMARK

APRIL 1995

Load-carrying capacity of steel-to-timber joints with annular ringed shank nails

A comparison with the EC5 design method

Rainer Görlacher

University of Karlsruhe, Germany

1 Introduction

For designing a nailed steel-to-timber joint EC5 provides design equations for thin and thick steel plates. For thin steel plates (i.e. for $t < 0{,}5\,d$ where t is the plate thickness and d is the nail diameter) the plate will be unable to provide the rotational resistance to develop a plastic hinge in the fastener. If the steel plate is thick enough ($t > d$) a plastic hinge in the fastener between the steel and the timber will occur. These assumptions are valid for dowels or round wire nails but may be different for ringed shank nails.

Test results with steel-to-timber joints nailed with ringed shank nails with fillet heads have proved that the EC 5 design equations for thick steel plates lead to a safe design situation even if the steel plates have a thickness of not more than half the nail diameter.

2 Design of nailed steel-to-timber joints according to EC5

2.1 EC 5 rules

The design load-carrying capacity per nail for single shear steel-to-timber joints should, for a thin steel plate (i.e. for $t \le 0{,}5d$ where t is the thickness), be taken as the smaller value found from the following formulae:

$$R_d = \min \begin{cases} (\sqrt{2}-1) f_{h,1,d}\, t_1\, d \\ 1{,}1 \sqrt{2 M_{y,d}\, f_{h,1,d}\, d} \end{cases} \qquad (1\text{ a,b})$$

For a thick steel plate (i.e. for $t \ge d$), the design load-carrying capacity should be taken as the smaller value found from the following formulae:

$$R_d = \min.\begin{cases} 1{,}1 f_{h,1,d} t_1 d\left[\sqrt{2+\dfrac{4M_{y,d}}{f_{h,1,d} d t_1^{\,2}}}-1\right] \\ 1{,}5\sqrt{2M_{y,d} f_{h,1,d} d} \end{cases} \qquad (1\text{ c,d})$$

For $0{,}5d < t < d$ linear interpolation is permitted.

The symbols are defined as follows:

t_1	timber thickness or penetration
$f_{h,1,d}$	design value of the embedding strength in t_1
d	nail diameter
$M_{y,d}$	design value of the nail yield moment

The design values of the embedding strengths, $f_{h,1,d}$ should be calculated:

$$f_{h,1,d} = \frac{k_{mod,1} f_{h,1,k}}{\gamma_M} \qquad (2)$$

k_{mod} is given according to the load-duration and the service classes. γ_M is equal to 1,3 for ultimate limit states (fundamental combinations).

The design value of the nail yield moment $M_{y,d}$ should be calculated:

$$M_{y,d} = \frac{M_{y,k}}{\gamma_M} \qquad (3)$$

with $\gamma_M = 1{,}1$.

The following characteristic embedding strength values should be used for nails up to 8 *mm*, for all angles to the grain:

- without predrilled holes $f_{h,k} = 0{,}082\ \rho_k d^{-0,3}\ N/mm^2$ (4)
- with predrilled holes $f_{h,k} = 0{,}082(1\text{-}0{,}01d)\ \rho_k\ N/mm^2$ (5)

with ρ_k in kg/m^3 and d in *mm*.

For common smooth steel wire nails with a minimum tensile strength of the 600 N/mm^2, the following characteristic values for the yield moment should be used:

$$M_{y,k} = 180\, d^{\,2,6} \qquad (6)$$

For annular ringed shank and helically threaded nails the yield moment should be determined according to EN 409.

Failure modes according to equations 1a,b,c,d are shown in Figure 1.

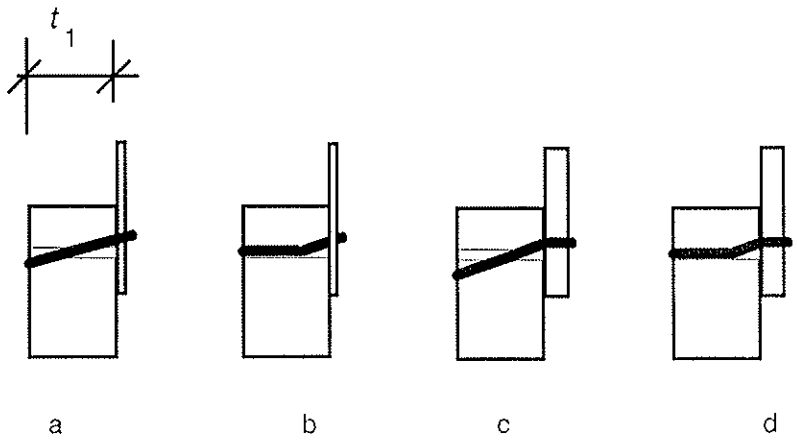

Figure 1 Failure modes for nailed steel-to-timber joints (single shear)

2.2 Discussion

The design procedure in EC 5 assumes, that a thin plate will be unable to provide the rotational resistance to develop a plastic hinge in the fastener (failure mode a and b). Thick plates will provide a rotational resistance so failure mode c and d will occur with significant higher load-carrying capacities of the joint.

In Germany the commonly used 4 *mm* ringed shank nails for nailing joist hangers and framing anchors with a plate thickness of 2 *mm* have a special shape of the head (fillet heads). So it is possible that these nails are clamped even into a thin plate developing a plastic hinge. This results in higher load-carrying capacities.

3 Test results

To check the assumption (thick - thin plate) for determining the load-carrying capacity of nailed steel-to-timber joints with ringed shank nails as used in Germany test results were evaluated. These tests were performed for gaining German Technical Approvals (VERSUCHSANSTALT, 1978-1984) with test specimens type I as well as a research project (EHLBECK und GÖRLACHER 1982) with test specimens type II.

Test specimens are shown in Figure 2 and 3.

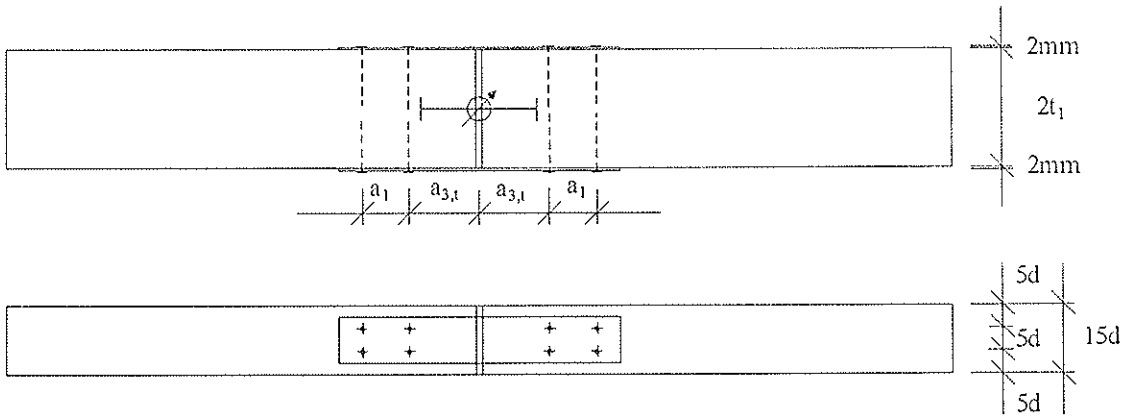

Figure 2 Test specimen type I ($a_1/a_{3,t}$ = 10d/15d for all diameters)

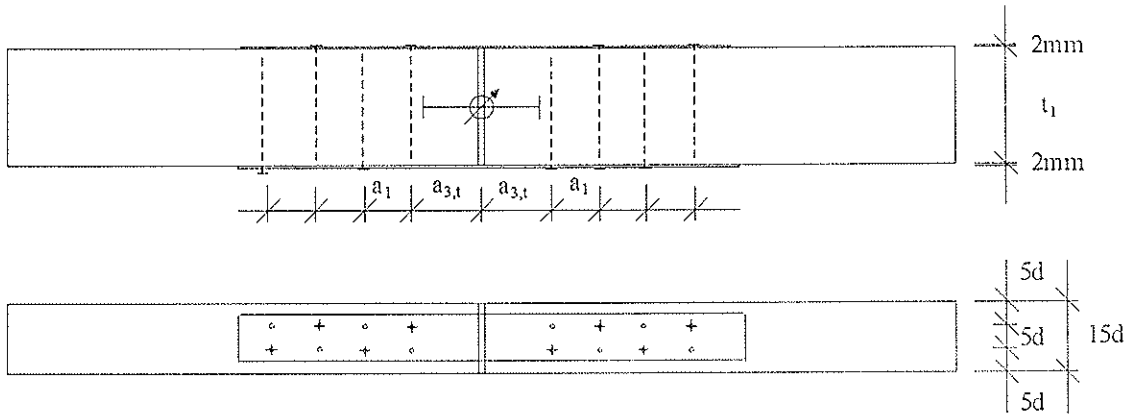

Figure 3 Test specimen type II ($a_1/a_{3,t}$ = 10d/15d for d ≤ 4 mm and $a_1/a_{3,t}$ = 12d/20d for d = 6 mm)

For each test specimen the load-carrying capacity R was calculated using equations 1c,d for thick plates with the following values

- individual density of each specimen or mean density of one test series
- embedding strength according to equation (4)
- yield moment according to equation (6). (This equation is used in Germany also for annular ringed shank nails and is in good agreement with test results according to EN 409)
- k_{mod} = 1 and γ_M = 1

For the tests from EHLBECK und GÖRLACHER 1982 Figure 4 shows the correlation between the ratio of the test value R_{test} and the calculated load-carrying capacity R_{cal}

according to equation 1c,d and the ratio of the penetration depth of the nails and the nail diameter.

A regression line was determined excluding the test values achieved with t_1/d = 24,5 because in this case the nail heads were pulled off, i.e. another failure mode was decisive.

For the minimum penetration depth according to EC 5 of $6d$ the regression line results in a value of R_{test} / R_{cal} = 1,4.

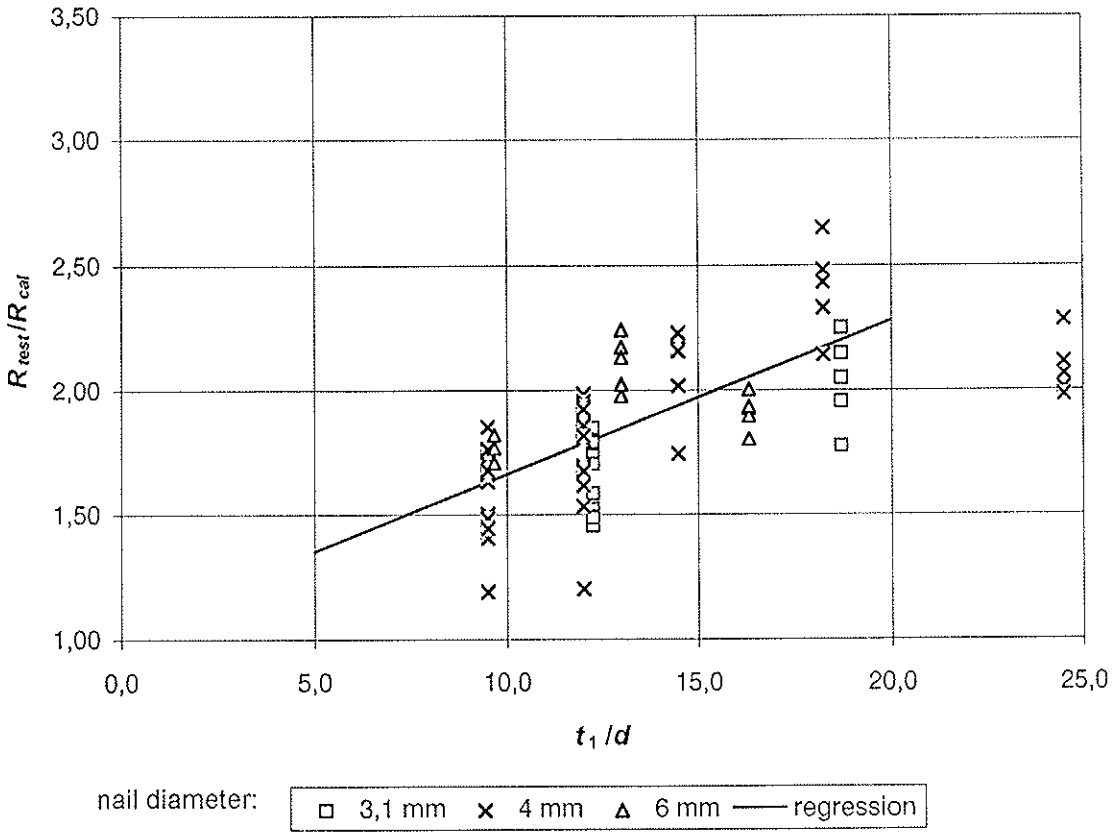

Figure 4 Correlation of the ratio of the test value R_{test} and the calculated load-carrying capacity R_{cal} according to equation 1c,d and the ratio of the penetration depth t_1 of the nails and the nail diameter d. From EHLBECK und GÖRLACHER, 1992

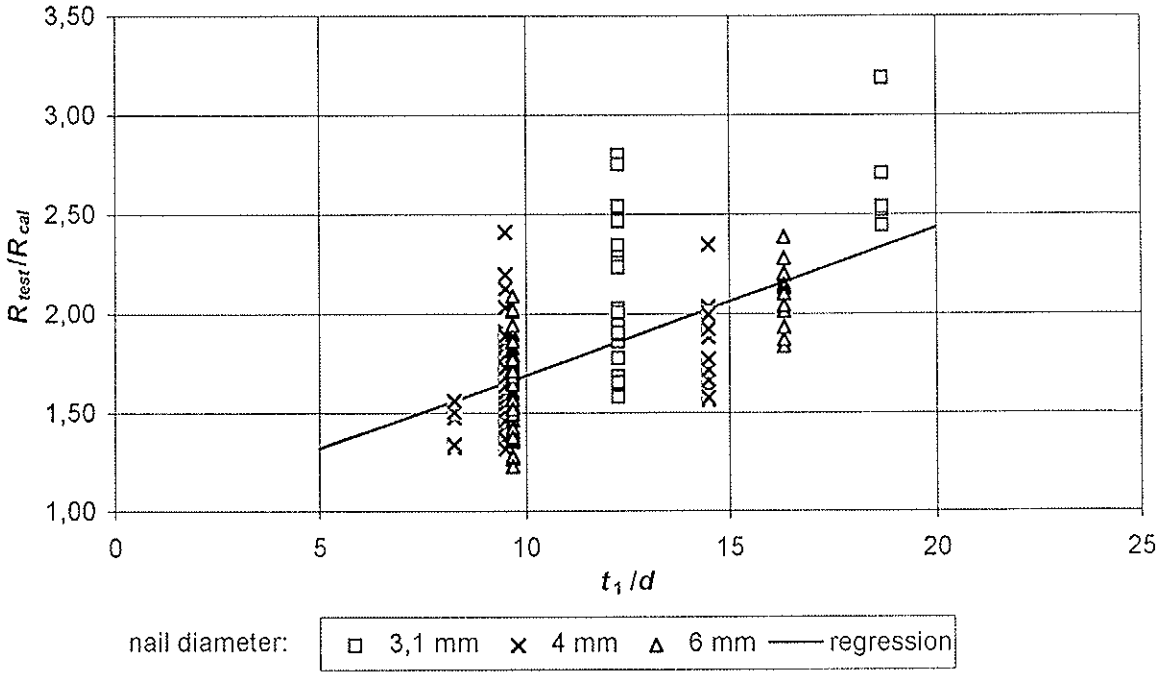

Figure 5 Correlation of the ratio of the test value R_{test} and the calculated load-carrying capacity R_{cal} according to equation 1c,d and the ratio of the penetration depth t_1 of the nails and the nail diameter d. From different test reports VERSUCHSANSTALT, 1978-1984

The evaluation of other test values (VERSUCHSANSTALT 1978-1984)is shown in Figure 5. The regression line is nearly identical with the regression line in Figure 4, but it is evident, that the scattering around the regression line is higher. This has mainly two reasons:

- In the test reports only the mean density of the timber of one test series was given while in the research report the density of each individual test specimen was determined. This has obviously an influence on the accuracy of the prediction of the embedding strength.
- In EHLBECK and GÖRLACHER 1982 all tests were performed with nails of one producer while the tests of the VERSUCHSANSTALT were performed with nails of 10 different producers. The quality of the wire depends on the producer's resources and has an evident influence on the yield moment of the nail. The evaluation of the test data was, however, performed with a constant yield moment according to equation (6).

Figure 4 and 5 show that the EC 5 design equations for thick steel plates lead to a safe design situation for ringed shank nails even if the steel plates have only a thickness of half the nail diameter. Furthermore, the tests show an increase of the load-carrying capacity for penetration depths between $6d$ and $20d$. This can be explained by the beneficial effects of the annular ringed shank.

4 Comparative tests

Finally, some comparative tests were performed in order to determine the load-carrying capacity of nailed-to-timber joints with annular ringed shank nails with fillet heads (5 test specimens) and smooth round wire nails (5 test specimens). The holes in the steel plate were predrilled with a diameter of 4,0 *mm* (smooth nails) and with 4,5 *mm* (ringed shank nails). The test specimens are shown in Figure 6.

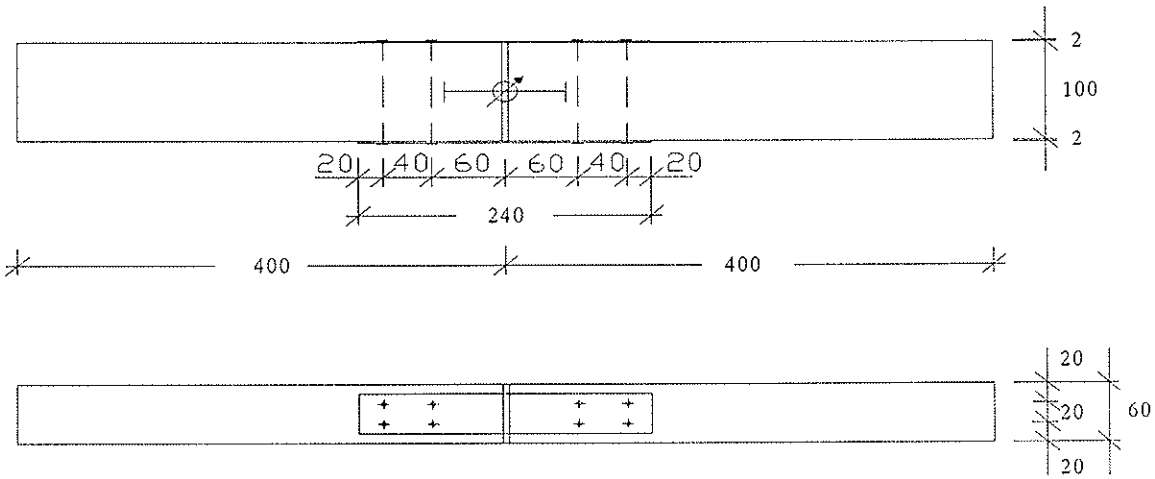

Figure 6 Test specimens for comparative tension shear tests (Dimensions in *mm*)

The yield moment was determined according to DIN EN 409. The results are listed in Table 1.

	nail 4,0 x 50 *mm* (annular ringed)	nail 4,0 x 50 *mm* (smooth round)
single values in *Nm*	6,10 5,90 5,65 6,20 6,60 6,80 6,20 6,55 6,10 6,70	7,40 7,60 7,50 7,30 7,60 7,40 7,80 7,60 7,10 7,70
mean value	6,28	7,50
standard deviation	0,371	0,205
coeff. of variation	5,9%	2,7%

Table 1 Yield moment according to DIN EN 409

The mean density of the timber was 425 kg/m^3 ,ranging from 410 kg/m^3 to 435 kg/m^3.

Tests were performed according to EN 26 981. The maximum load of the smooth nails was reached by slowly pulling the nails out of the timber. Tests with annular ringed shank nails showed still an increasing load after a deformation of 15 mm (opening of the joint's gap). However, the maximum load was defined at a deformation of 15 mm.

The results are given in Table 2. This table also shows the calculated load-carrying capacity according to equations (1a,b,c,d) assuming a mean yield moment according to Table 1, a mean density of 425 kg/m^3 and k_{mod} = 1 and γ_M = 1:

	R_{test} (per nail) (kN)	R_{cal} Eq. (1a) (kN)	R_{cal} Eq. (1b) (kN)	R_{cal} Eq. (1c) (kN)	R_{cal} Eq. (1d) (kN)	ratio $R_{test}/R_{cal,min}$ (-)
smooth-	1,66	1,83	**1,29**			1,29
round	1,76	1,83	**1,29**			1,36
nail	1,84	1,83	**1,29**			1,42
	1,91	1,83	**1,29**			1,48
	1,76	1,83	**1,29**			1,36
annular	2,73			2,21	**1,61**	1,69
ringed	2,73			2,21	**1,61**	1,69
shank	2,71			2,21	**1,61**	1,68
nail	2,69			2,21	**1,61**	1,67
	2,54			2,21	**1,61**	1,57

Table 2 Test results and calculated values

Table 2 leads to the following conclusions:

- for smooth round nails the failure mode b (see Figure 1) occurs, while for annular ringed shank nails the failure mode d occurs. The deformation of the tested nails confirms the respective failure modes (see Figure 7). The smooth nail only shows one plastic hinge whereas the ringed shank nail shows a second plastic hinge under the nail head. This plastic hinge is developed under large deformations, because first of all the fillet head has to be pulled into the hole of the steel plate before the rotational resistance becomes effective. The annular ringed shank prevents the early pull out of the nail.

- For smooth round nails the load-carrying capacity can be determined according to the EC 5 rules for thin plates while for annular ringed shank nails with fillet heads the rules for thick plates lead to a safe design situation.
- The ratio of the load-carrying capacity and the calculated values are higher for ringed shank nails than for smooth nails. This means that there is an additional load increasing effect by the ringed shank. This effect depends on the nail length. To separate these two effects some more systematic tests are desirable.
- Proposal for an additional design rule in EC 5, clause 6.3.1.4: If a special shape of the nail head (e.g. fillet head) is able to clamp the nail into a thin steel plate causing a plastic hinge the rules for thick plates apply

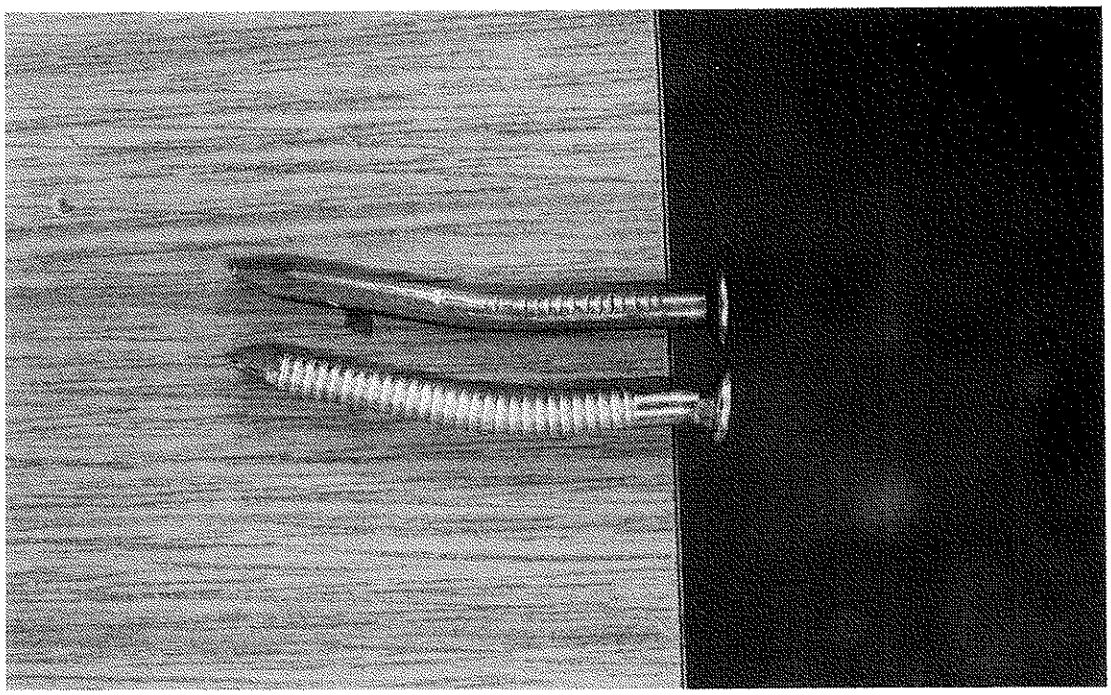

Figure 7 Deformation of smooth round nails and annular ringed shank

References

EHLBECK, J., GÖRLACHER, R. (1982)

Mindestnagelabstände bei Stahlblech-Holz-Nagelung. Forschungsbericht der Versuchsanstalt für Stahl, Holz und Steine, Abt. Ingenieurholzbau, Universität Karlsruhe (1982)

VERSUCHSANSTALT (1987-1984)

Test reports of the Versuchsanstalt für Stahl, Holz und Steine (unpublished), Universität Karlsruhe

CIB-W18/28-7-4

INTERNATIONAL COUNCIL FOR BUILDING RESEARCH STUDIES AND DOCUMENTATION

WORKING COMMISSION W18 - TIMBER STRUCTURES

DYNAMIC EFFECTS ON METAL-PLATE CONNECTED WOOD TRUSS JOINTS

by

S Kent

R Gupta

T Miller

Oregon State University

USA

MEETING TWENTY - EIGHT

COPENHAGEN

DENMARK

APRIL 1995

ABSTRACT

The objectives of this research were to examine the behavior of actual Metal-Plate-Connected (MPC) tension-splice wood truss joints under realistic seismic loads and to develop dynamic characteristics using a proposed standard Sequential Phased Displacement (SPD) method. Strength and stiffness of tension-splice joints after being subjected to the seismic and SPD loadings were compared to those from a control group of tension-splice joints failed under a static ramp load. A 30-ft span MPC Fink truss, composed of nominal 2x4-in Douglas-fir, was modeled using a linear finite element program to simulate the time-history response of the tension-splice joint to accelerations from the Northridge earthquake. A ramp load of 780-lbs/min was applied to ten actual joints until the estimated dead load force of 900-lbs was reached. The earthquake forces, determined from the finite element model, were then applied to a group of ten joints for a duration of 30-seconds, followed by a continuation of the ramp load until the joints failed. The fully reversed SPD loading was also applied to a set of joints until the compressive limit of the loading apparatus was reached. The load was then removed before the initiation of a static ramp load of 780-lbs/min, which was applied until failure of the joints. A statistical comparison revealed that the earthquake and SPD loadings did not significantly reduce the mean strength of the tension-splice joints. The SPD loading did, however, significantly degrade the stiffness, whereas, the earthquake loading did not.

INTRODUCTION

Metal-plate-connected (MPC) wood trusses have widespread use in residential homes, apartments, commercial, and light industrial applications. One advantage of the system is the relative ease in fabrication and low cost of creating complex roof geometries. This engineered product, although exposed to dynamic loadings from wind and earthquakes, is designed based predominately on the response to static loads. The prevalence of these units in construction has not resulted in a widespread understanding of their behavior in service, especially under seismic forces. Significant advances have been made in the area of modeling the earthquake response of timber shear walls and roof diaphragms in recent years, but research on connection response to seismic forces has largely been ignored. The connections are primary factors controlling the response of the structural assembly. Therefore, results from connections tests will continue to be significant in understanding the behavior of buildings during earthquakes.

This paper will characterize structural behavior and failure modes of MPC joints under dynamic loading conditions. This study will also indicate if the ultimate capacity of MPC joints is affected by dynamic forces (simulated earthquake and SPD). Because wood structures rely on the mechanical connections to dissipate energy when subject to earthquake or wind loads, this is a necessary first step towards predicting truss joint behavior and subsequently predicting the behavior of a truss and system of trusses.

The objectives of this research are as follows:

1. Evaluate the behavior of MPC tension-splice joint under realistic earthquake loads.

2. Determine the response of MPC tension-splice joints to the Sequential Phased Displacement (SPD) method proposed by Dolan (1993).

Future research will investigate the dynamic effects on MPC heel joints by subjecting a group of heel joints to a simulated earthquake time-history and the SPD loading. Also, a hysteresis analysis of the tension-splice joint and the heel joint under the SPD method will be conducted.

LITERATURE REVIEW

The structural performance of MPC joints has received extensive research attention in the last 20 years, but most of the research has focused on the performance of tensile joints under static axial loads only. The evaluation of the performance of MPC joints under seismic forces has received no attention. There is currently only one standard for the evaluation of the structural behavior (ultimate capacity, failure modes, etc.) of MPC joints. It makes recommendations for testing the tensile joint under static axial loads only (ASTM 1990). These evaluations are inadequate for even non-earthquake type loadings, because actual joints (having different configurations) experience different loading (cyclic, combined, reversed) conditions in-service.

Only a few studies on the fatigue properties of MPC joints were found (Sletteland 1977, Tokuda et al 1979, Hayashi et al 1980, Tokuda 1980, Dagher et al 1992). In all of these studies, only the tensile joint was tested under repeated axial loads. In MPC wood trusses, other joints are also critical in the overall behavior of the truss. Evaluations from these studies are inadequate to determine behavior of MPC joints during earthquake loadings. Behavior of the joints during an earthquake must be considered in determining safe design loads and for predicting service life of the joints for trusses constructed in many parts of the U.S. In response to the demand for a standard to assess dynamic properties of wood connections, Dolan (1993) proposed a pseudodynamic SPD loading. The purpose of the SPD loading is to provide a consistent method for the evaluation of dynamic properties such as equivalent viscous damping ratio, ductility, and cyclic stiffness.

EXPERIMENTAL PROCEDURE

Apparatus

A horizontal testing frame, developed by Gupta and Gebremedhin (1990), shown in Figure 1, which allows for a versatile range of joint configurations, and an 11,000-lb capacity hydraulic actuator were used to apply the loads to the joints. The hydraulic actuator was positioned on the frame to minimize loading eccentricities. Two linearly variable differential transducers (LVDTs) were placed on either side of the tension-splice joint to measure the relative displacement between the two wood members. Axial force

was measured by a load cell (25,000-lb capacity) which was placed between the hydraulic actuator and one end of the joint.

Joint Fabrication

Joints were fabricated from machine stress rated Douglas-fir (1800f_b-1.6E) lumber which was conditioned in a standard room to an equilibrium moisture content of approximately 14%. The tension-splice joints were connected using 3x4-in metal plates which were pressed into the wood using a hydraulic press at a maximum pressure of 1100-psi. After construction, the joints were placed into the standard room again for a minimum of seven days before testing to allow stress relaxation of the wood fibers near the connection, as recommended by Arbek (1979).

Test Procedures

Groups of ten specimens were tested under different loading conditions including a seismic time-history determined from a linear finite element model based on a historic accelerogram, and a Sequential Phased Displacement loading (SPD) as proposed by Dolan (1993). Static tests were also conducted on a group of tension splice joints to serve as the control.

Static Tests

A linearly increasing ramp load of 780-lbs/min, controlled through a load-feedback loop, was applied to the joints to cause failure in 9 to 10-min. A time-averaging algorithm, with an incremental duration of 0.5-seconds, was used to smooth the voltage output from the load cell and the LVDTs.

Finite Element Modeling and Earthquake Simulation

A 30-ft span Fink truss, composed of nominal 2x4-in Douglas-fir, was modeled using a linear finite element program (SAP90) to estimate the response of the tension-splice joint to ground accelerations from the Northridge earthquake which occurred in California on January 17, 1994. Horizontal and vertical acceleration data were obtained from STA #24538 in Santa Monica, 24-km from the epicenter.

The model is composed of linear truss elements connected by pinned joints, and supported by horizontal and vertical springs connected to the heel joints. The supporting springs simulate both the vertical stiffness and the out-of-plane stiffness of the bearing walls. The stiffness of the supporting springs was varied to determine the sensitivity of the truss member forces due to a variety of support conditions. A modal damping coefficient of 10% is used for the bearing walls (Leiva 1994).

During the literature survey, no information was found for the out-of-plane stiffness of walls applicable to this situation and an in-depth finite element analysis was beyond the scope of this research. Also, this out-of-plane stiffness varies depending on a variety of factors such as the length of the bearing wall, wall height, position of the truss

along the wall, type of construction, etc. The approach was to estimate the maximum possible out-of-plane support stiffness and then incrementally reduce that stiffness in the finite element model to search for the worst-case response.

When compared to the trusses placed near the center of the bearing wall, it was assumed that the trusses placed nearest the end wall (wall running parallel to the trusses) would have the largest horizontal spring stiffness. Experimental values obtained by Leiva (1994) on timber framed shear walls suggest that 16 kips/in was representative of the racking stiffness of a 30-ft long by 8-ft high wall. Once this maximum stiffness was established, the value was incrementally reduced in the finite element model.

Investigation of the effect of vertical spring stiffness on the time history response of the model was also conducted. It was found that the model was not particularly sensitive to changes in the vertical spring stiffness.

The final model included a horizontal spring stiffness equal to 10% of the reference value, which corresponded to a spring stiffness of 1.6-kips/in on either side of the truss. This horizontal spring stiffness maximized the model response in terms of the largest tensile force experienced in the tension splice joint during the time history record. The vertical spring stiffness selected for the final analysis was the equivalent of an 8-ft long 2x6-in Douglas-fir stud, which corresponded to approximately 140-kips/in. Axial stiffness of the studs was defined as K=AE/L where A=8.25-in^2, E=1.6x10^6-psi, and L=96-in.

Figure 2 is a graphical representation of the finite element model. The variables K1 and K2 are stiffness' of the horizontal and vertical linear springs, respectively. The model is almost completely symmetrical with the exception of the tension-splice joint located in the bottom chord. This joint is placed 2-ft off center to model actual Fink truss construction. Pinned joints, which have no rotational restraint, are represented as dark circles. Masses from the roof system and the truss members are lumped at the joints (nodes) for the dynamic analysis.

The 90 DEG (azimuth) horizontal component and the vertical component of the Northridge earthquake, which had maximum accelerations of 866-cm/sec and 228-cm/sec, respectively, were analyzed separately to obtain the time-history response of the force at the tension-splice joint. The two components were then superimposed to obtain the combined response shown in Figure 3.

A group of ten tension-splice joints was subjected to the force-time-history shown in Figure 3, to simulate the effects of an historic earthquake. A ramp load of 780-lbs/min was first applied to the joints until the estimated dead load force of 900-lbs was reached. The earthquake forces were then applied for a duration of 30-seconds followed by a continuation of the ramp load until the joints failed. It should be noted that the earthquake force-time-history alone was not sufficient to fail the joints.

Sequential Phased Displacement

A test method proposed by Dolan (1993), with loading time-history shown in Figure 4, known as the Sequential Phased Displacement (SPD) method will be used to determine the dynamic properties of MPC tension-splice joints such as damping ratio, cyclic stiffness, and ductility ratio. The loading function combines fully reversed stabilized

cyclic displacements preceding degradation cycles. The stabilized and degradation cycles gradually increase until failure of the connection occurs.

SPD cycles are defined in terms of the yield point for a particular joint. Because of the nonlinear load-deflection curves of MPC joints, a yield displacement of 0.005-in, corresponding to the displacement at one third of the average ultimate load (2430-lbs) from the control group, is used to scale the SPD cycles.

During some SPD tests, the compressive load limit for the hydraulic actuator of approximately 10,500-lbs was reached before failure occurred in the joints. On average, this occurred after about 120-cycles. The compressive stiffness of the MPC tension-splice joints increased dramatically as the gap between the two wood members closed. Therefore, as the SPD test progressed, a much higher compressive force than tensile force was required to obtain the same magnitude deflection. Because of this, the actuator compressive force limit was reached before some of the joints could fail in tension. Therefore, it was decided to fail the joints under a ramp load of 780-lbs/min to determine how the abbreviated SPD loading affected the strength and stiffness of the MPC tension-splice joints. For those joints that did not reach the maximum capacity of the hydraulic actuator by 120-cycles, the test was manually stopped at this point so that all the joints would be subjected to the same number of cycles.

TEST RESULTS

Table 1 displays the results for the three loading conditions applied to the MPC tension-splice joints. Note that COV for the groups are very similar.

Static Tests

The mean strength for the static load control group was 7280-lbs with a coefficient of variation (COV) of 6%. Because of the nonlinear shape of the load-deflection curves (Figure 5), the stiffness was defined at one third of the mean strength, which is often used as the allowable design load for tension-splice joints. To calculate the stiffness (secant stiffness), the load at one-third of the mean strength (2430-lbs) was divided by the corresponding deflection for each joint. The mean stiffness for the control group was 4.45×10^5-lbs/in with a COV of 15%.

Historic Earthquake Simulation

Analysis of the data suggest that the tension-splice joints did not degrade in strength or stiffness when subjected to the Northridge earthquake time-history used in the simulation. The mean strength and stiffness of the joints when subjected to the earthquake forces in addition to the ramp load, were 7570-lbs with a COV of 7% and 3.99×10^5-lbs/in with a COV of 9.6%, respectively, where the stiffness was defined as in the static tests.

A statistical comparison of these results (using a t-test) with those from the joints failed under the static ramp load alone suggested that the null hypothesis that the earthquake time-history did not degrade the stiffness of the tension-splice joints could not

be rejected at the 5.0% level of significance (one sided p-value of 7.1%). Also, the null hypothesis that the mean ultimate strengths were the same could not be rejected at the 5.0% level of significance (one sided p-value of 89%).

The "random" nature of the earthquake loads causes some loading control difficulties. First, the frequency components over 10-Hz are largely filtered out by the testing apparatus. It can be assumed that there is very little energy in the high frequency component (that over 10-Hz) of the time-history, when compared to the low frequency components (that under 10-Hz). Therefore, the passive filtering by the hydraulic system would not significantly change the results. Second, a small time lag occurs between the signal and the response. Figure 6 displays how the testing apparatus responds to the time-history input during the most dynamic portion. The dashed line represents the desired response predicted for the tension splice joint from the finite element model. The solid line represents the actual forces applied to the tension-splice joints. The time lag between signal and response is of no consequence to the results; however, it does make the interpretation of Figure 6 difficult.

Sequential Phased Displacement

Figure 7 displays the force-time-history applied to the joints during the SPD loading. Note that the compression forces tend to be much larger than the tension forces for any given cycle. This can be attributed to closure of the gap between the two members of the joint which dramatically increases the compressive stiffness of the tension-splice joint.

The statistical analysis indicated that the SPD loading did not significantly reduce the mean strength of the tension-splice joints; however, a stiffness degradation of approximately 50% occurred as a result of the SPD loading (one sided p-value=1.4×10^{-7}). The dominate failure mode of the MPC tension-splice joint, after being subjected to the SPD loading and failed under a static ramp load, was tooth withdraw.

Some control difficulties were also encountered during the SPD tests. The difference between the maximum tensile force and the maximum compressive force in each cycle, for example, could approach as much as 14,000-lbs. This difference required a loading rate of 28,000-lbs/sec, which appeared to be near the maximum capabilities of the hydraulic system. Also, the deflection feed-back loop was controlled by LVDTs which had an approximate resolution of ±0.0007-inches. A higher resolution would be preferred to tighten the control of the deflection feed-back loop when working with stiff connections.

CONCLUSIONS

The conclusions of this research on MPC tension-splice joints are summarized as follows:

1. The short term dynamic loads examined in this test regime did not significantly affect the strength of the MPC tension-splice joints. The SPD loading caused a stiffness

degradation of approximately 50% in the tension-splice joints; however, no statistically significant stiffness degradation occurred as a result of the Northridge earthquake time-history.

2. The 11,000-lbs capacity hydraulic testing system is not capable of failing the MPC tension-splice joints under the SPD loading. Also, because of the high stiffness, a high resolution deflection recording system is required to maintain adequate control during the deflection-controlled SPD cycles.

ACKNOWLEDGMENTS

This research is funded by the U.S. Department of Agriculture National Research Initiative Competitive Grants Program.

We express our appreciation to Frank Lumber Company, Inc. and Alpine Engineered Products, Inc. for their generous donation of the materials used in this research.

BIBLIOGRAPHY

American Society for Testing and Materials. 1990. Standard Methods of Testing Mechanical Fasteners in Wood. ASTM D1761-77, Vol. 04.09.

Arbek, T. 1979. 'The Effect of Time on Strength of Truss Plate Joints."B. Sc. F. Thesis. Dept. of Civil Engineering, Carleton University. Ottawa, Canada.

Dagher, H. J., Caccese, V., Hsu, Y., Wolfe, R. and Ritter, M. 1992. 'Fatigue Strength of Metal Plate Connector Plates." Paper Abstract, Submitted for 1992 Structures Congress.

Dolan, J. D. (1993). 'Proposed Test Method for Dynamic Properties of Connections Assembled with Mechanical Fasteners." Paper prepared for presentation at the 26th Meeting of CIB W18, Athens, Georgia.

Gupta, R., Gebremedhin, K. G. (1990). 'Destructive Testing of Metal-Plate-Connected Wood Truss Joints." *J. Struct. Engrg.*, ASCE, 116(7), 1971-1982.

Hayashi, T., Sasaki, H., Masuda, M. (1980). 'Fatigue Properties for Wood Butt Joints with Metal Plate Connectors." *Forest Products Journal*, 30(2), 49-54.

Leiva, L. (1994). 'Racking Behaviour of Timber-Framed Shear Walls." Paper prepared for presentation at the Pacific Timber Engineering Conference, Gold Coast Australia.

Polensek, A., Schimel, B. D. (1988). "Analysis of Nonlinear Connection Systems in Wood Dwellings." Journal of Computing in Civil Engineering, 2(4), 365-379.

SAP90-A Series of Computer Programs for the Finite Element Analysis of Structures - Structural Analysis Users Manual, Computers and Structures, Inc., Berkeley, California, 1990.

Sletteland, N. T., Pratt, G. L., and Schuler, R. T. 1977. 'Fatigue life of Metal Plate Connector Plates." ASAE Paper No. 77-4037.

Tokuda, M., Takeshita, M., and Sugiyama, H. 1979. 'The Behaviors of Metal Plate Connector Joins Subjected to Repetitive Tension Force. J. Japan Wood Res. Soc., 25(6): 408-413.

Table 1: Summary of Test Results

Load History on Tension-Splice Joint	Static Ramp Load Only	Earthquake Time-History and Static Ramp Load	SPD Loading and Static Ramp Load
Average Ultimate Load (lbs)	7280	7560	7228
Coefficient of Variation (%)	5	6	7
Average Stiffness (lbs/in)	4.45×10^5	3.99×10^5	1.95×10^5
Coefficient of Variation (%)	15	15	12
Sample Size	9	10	9

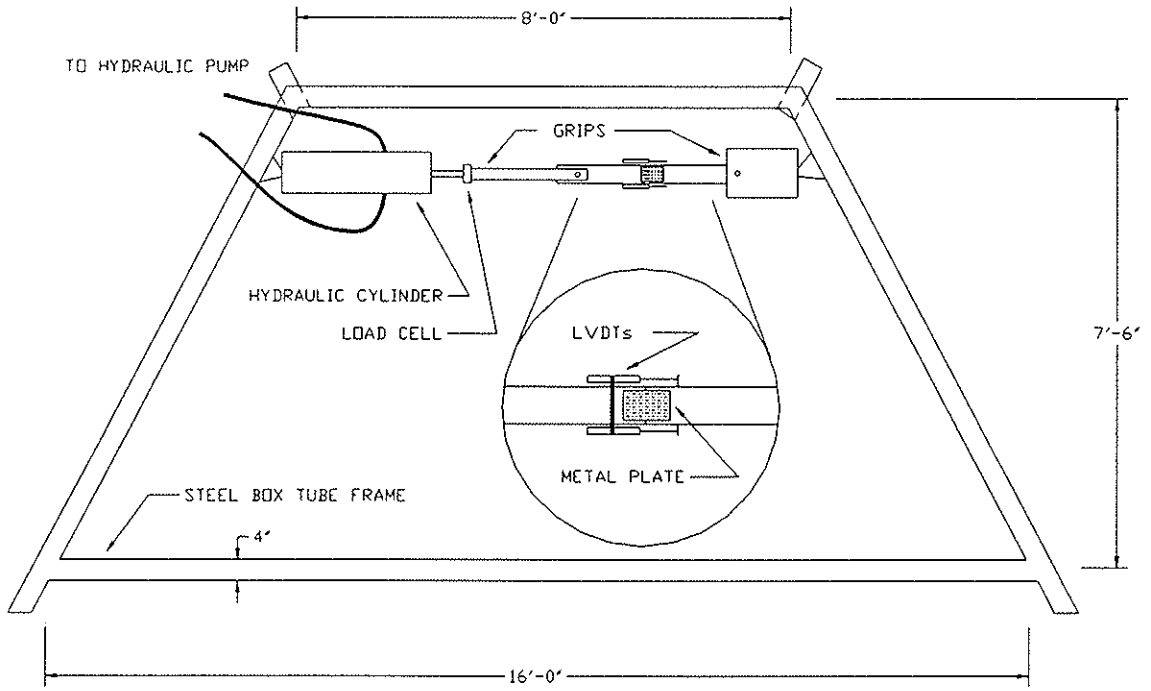

Figure 1: Test Setup

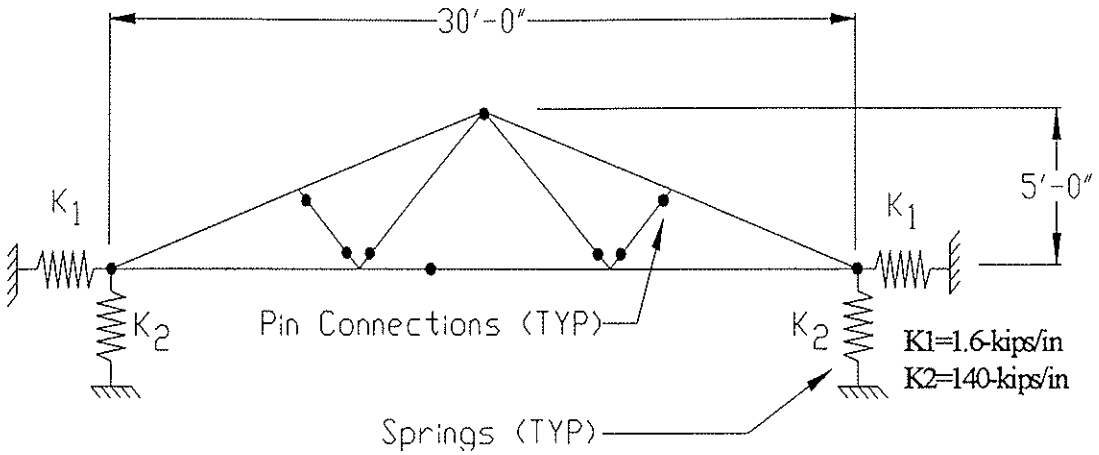

Figure 2: Finite Element Model

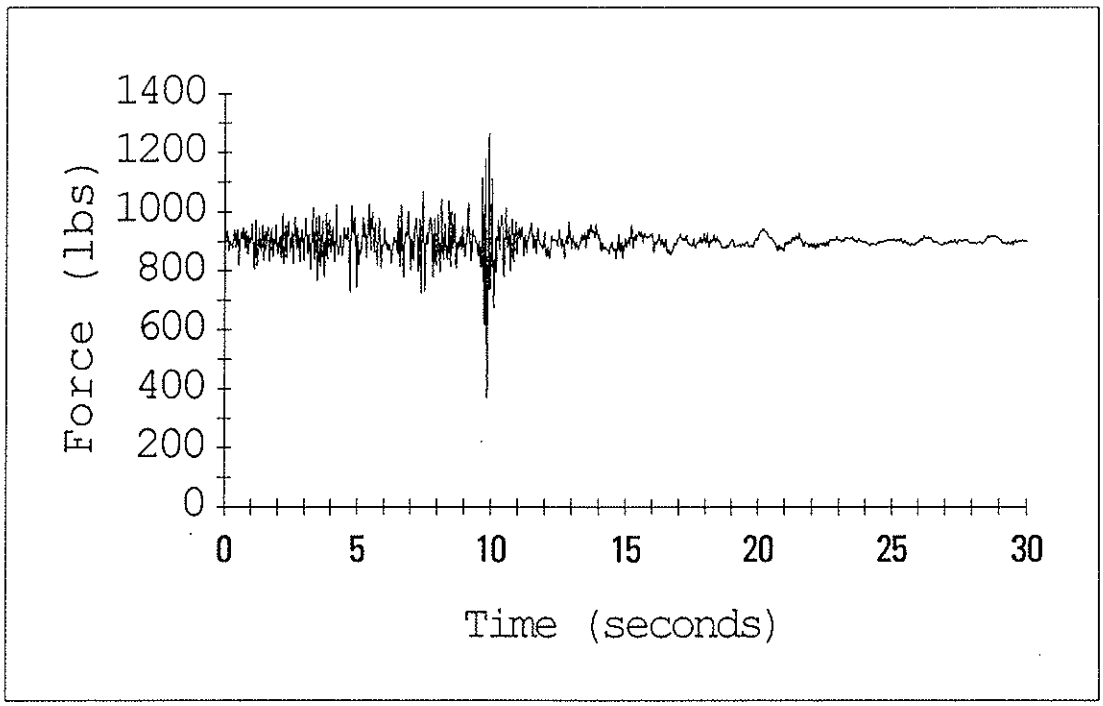

Figure 3: Combined Response of the Tension-Splice Joint to Horizontal and Vertical Motions of the Northridge Earthquake.

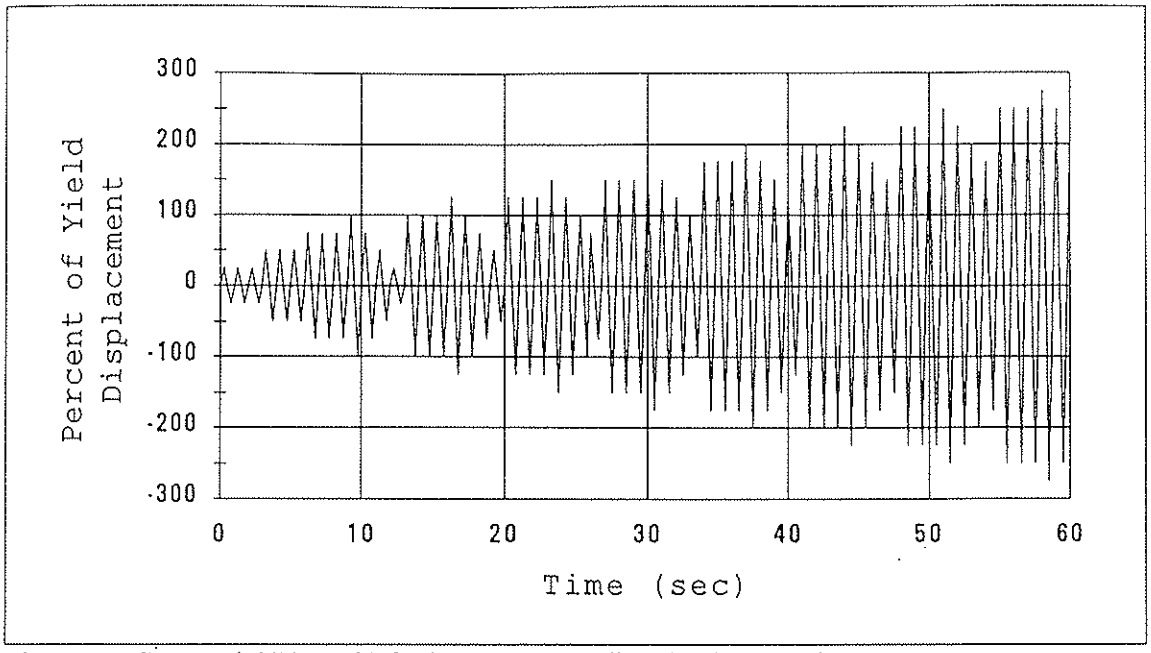

Figure 4: Sequential Phased Displacement Loading (Dolan 1993).

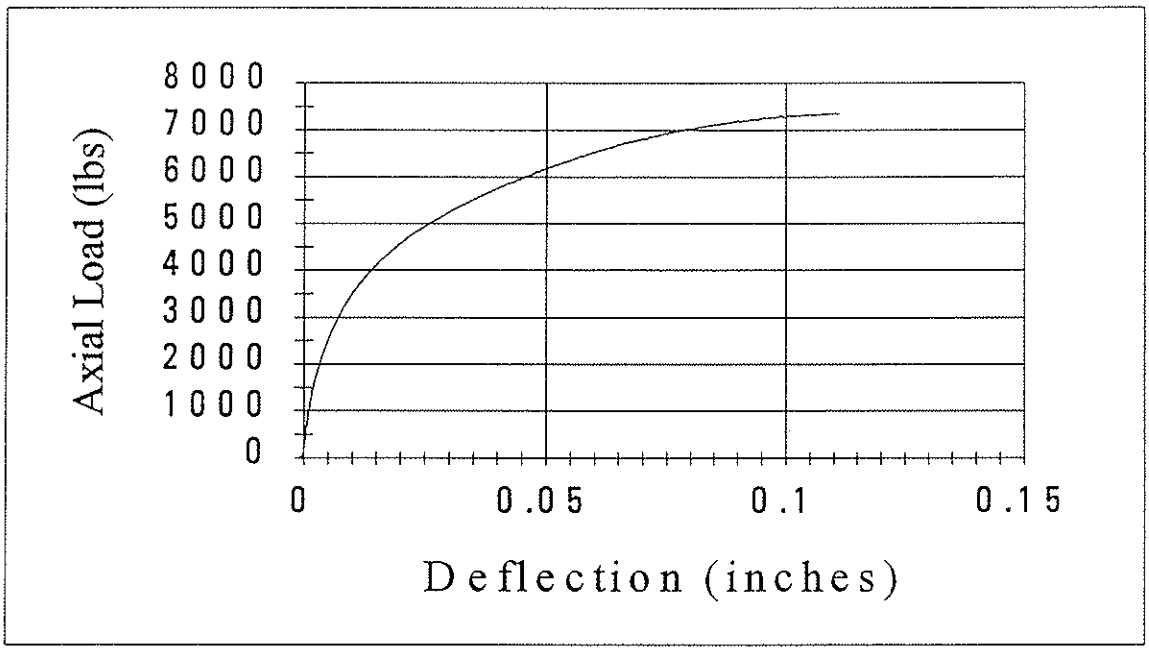

Figure 5: Typical Load-Deflection Curve for Tension-Splice-Joint Under Static Ramp Load.

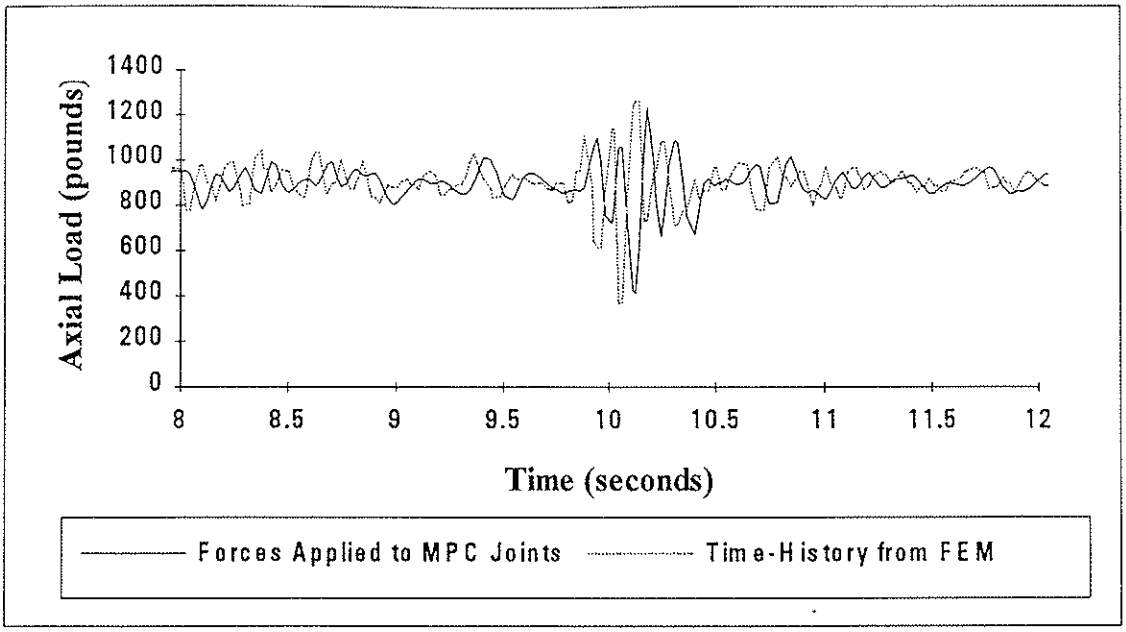

Figure 6: Earthquake Force Time-History Showing Predicted Forces and Actual Forces Applied to the Tension-Splice Joints.

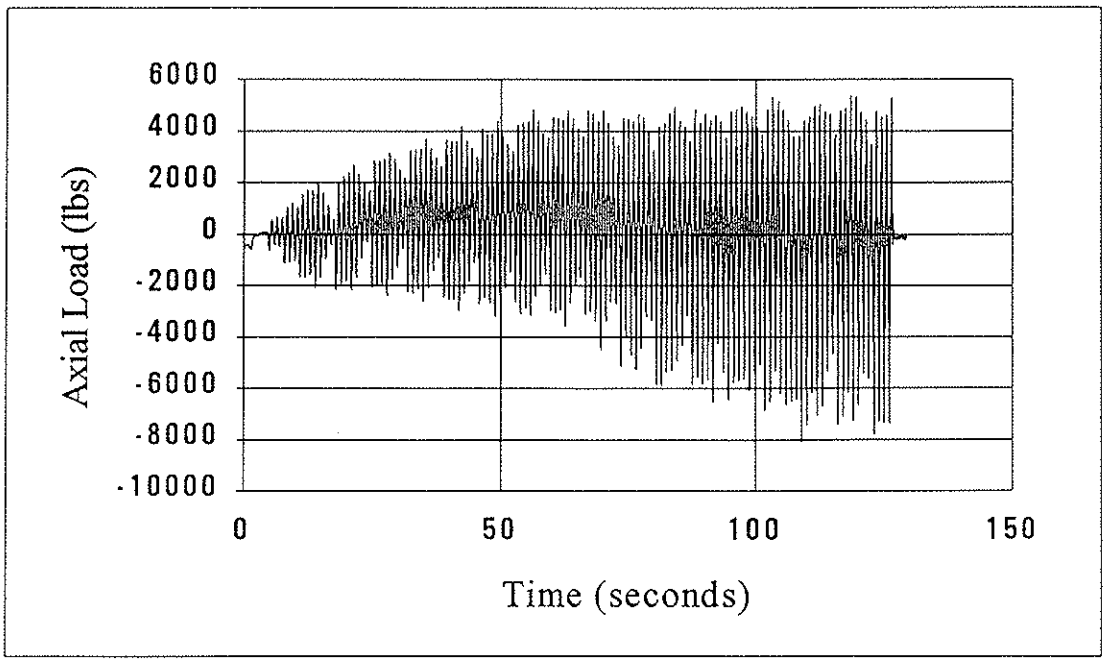

Figure 7: Typical Force Response During SPD Loading on Tension-Splice Joint

INTERNATIONAL COUNCIL FOR BUILDING RESEARCH STUDIES AND DOCUMENTATION

WORKING COMMISSION W18 - TIMBER STRUCTURES

FAILURE OF TIMBER BOLTED JOINTS SUBJECTED TO LATERAL LOAD PERPENDICULAR TO GRAIN

by

M Yasumura

Building Research Institute, Tsukuba

Japan

L Daudeville

Laboratoire de Mécanique et Technologie ENS de Cachan, Cachan

France

MEETING TWENTY - EIGHT

COPENHAGEN

DENMARK

APRIL 1995

Failure of Timber Bolted Joints subjected to Lateral Load Perpendicular to Grain

Motoi YASUMURA[1] and Laurent DAUDEVILLE[2]

1. INTRODUCTION

The failure of timber bolted joints subjected to the lateral force perpendicular to the grain is generally caused by the splitting of wood which initiates at the boundary of bolt hole and propagates parallel to the grain of wood. This failure shows often the brittle failure which should be avoided in the design of timber structures. The current design methods of dowel type joints based on Johansen's yield theory does not take into account of this failure mode as it is based only on the embedding of a bolt into wood and the yielding of a bolt. Although a number of studies have been conducted concerning the mechanical joints, few studies have been carried out on the failure of joints due to the splitting or shear failure of wood. The purpose of this study is to develop the method to predict the ultimate properties of bolted or dowel type joint subjected to the lateral force perpendicular to the grain.

The analysis of the failure process is complicated if we consider the combined factors such as the embedding of bolt into wood, the deformation of bolt, the plasticity of wood in local area, etc. In this study, we simplify the problem by considering the elastic plane stress state with transversal isotropy, and separating the problem of the crack initiation from that of the crack propagation.

Whitney and Nuismer[1] propose a simplified stress fracture criterion based on the actual stress distribution near a hole or notch for composite materials. Applying this approach to a bolted joint, it is assumed that the initiation of a crack occurs when the average elastic stress perpendicular to the grain over a characteristic distance from the boundary of the hole exceeds the tensile strength of the material.

Crack propagation is analyzed by use of classical linear elastic fracture mechanics(LEFM). We combined LEFM with a Griffith criterion based on the critical energy release rate G_{Ic}. The energy release rate is computed with respect to the crack length by the compliance method. Both the initiation and propagation were studied with the finite element method(FEM).

Two experiments were conducted on the bolted and dowel type joints in B.R.I.(Japan) and L.M.T.(France) in order to validate the numerical simulation.

---

[1] Building Research Institute, Tsukuba, Japan

[2] Laboratoire de Mécanique et Technologie, Cachan, France

2. EXPERIMENT

2.1 Specimen

B.R.I. specimens consisted of the glued laminated wood of Spruce and 12mm thick steel side plates placed on both sides of wooden member, and connected with steel bolts of 16 and 20mm in diameter(d). The glued laminated wood was produced of the laminae of 30mm in thickness of the average density of 0.44. The quality of steel used for side plates and bolts was SS400. The bolt hole of wooden member was equal to or slightly larger than the bolt diameter, and the clearance of bolt hole in steel members was 1mm. The thickness of specimens was 4d, 8d and 10d, and the width was 800mm. The edge distance(e_1) varied from 4d to 10d. The outline of specimens is described in Table 1(a).

L.M.T. specimens consisted of the glued laminated wood of "Sapin-Epicea", steel side plates and a dowel. The diameter of dowels was 12, 16 and 20mm, and the thickness of member was 3d. e_1 varied 4d, 8d and 12d. The end distace(e_1) was 7d and 25d. Bolt hole was finished to give the perfect contact with a dowel. The average density of wood was 0.46. The outline of the specimen is described in Table 1(b).

2.2 Test method

(a)B.R.I. test:

Three specimens of each type were subjected to the lateral loading as shown in Fig.1(a). The quasi-static tensile load was applied to the steel side plates by hydraulic jack, and the slips between steel side plates and wooden member were measured with four electric displacement transducers. Nuts were attached to the joints without tightening. The lateral load was increased monotonously until one of the joints failed.

(b)L.M.T. test:

Two to five specimens of each type were subjected to the lateral loading as shown in Fig.1(b). The displacement of the hydraulic jack was controlled in 0.0225mm/sec except for two specimens of A1. For these two specimens, the displacement was controlled in 0.18mm/sec as recommended in Eurocode 5. CD gages were attached near the boundary of bolt hole to detect the crack initiation, and the crack length was measured in the specimen with e_1=25d.

3. MODELING

The following hypothesis were supposed to model the joints.

(1) The plane stress state was assumed.
(2) The contact between a bolt hole and bolt was assumed perfect, and the clearance between them was neglected.
(3) The friction between a bolt hole and bolt was neglected.
(4) A bolt was assumed to be perfectly rigid.
(5) The wooden material was assumed to be elastic and brittle in failure, and transversely isotropic.
(6) The Young's modulus of spruce was assumed to be 15000MPa in the longitudinal direction and 600MPa in the transversal direction considering the average value between T and R direction. The modulus of rigidity and Poisson's ratio were assumed to be 700MPa and 0.5, respectively[3].

Tested joints were modeled as shown in Fig.2. Right half of

the specimen was modeled by considering the symmetry. Fig.3 shows the boundary condition. A bolt hole was blocked in radial direction, and 1mm of displacement was forced at the lower boundary. CASTEM2000 was used for the calculation.

The crack initiation can be estimated by use of the average stress criterion[1][2]. As the principal stress at the end of bolt hole is the tensile stress perpendicular to the grain (σyy), and we can neglect the stress parallel to the grain (σxx) and shear stress (σxy), the criterion for the crack initiation is expressed by the following equation;

$$\frac{1}{l_c}\int_0^{l_c} \sigma_{yy}(P_c)\,dx = f_t \qquad (1)$$

where, lc : Characteristic distance
Pc : Splitting load
ft : Tensile strength of wood perpendicular to the grain

The characteristic distance is dependent upon the characteristics of materials, and can be obtained from the lateral loading test of joints. This approach is less sensible to the fineness of finite elements than the maximum critical stress method.

Once the existence of a small crack is assumed, the LEFM is applicable to analyze the crack propagation by calculating G defined as follows;

$$G = -\frac{1}{b}\frac{\partial W}{\partial A} \qquad (2)$$

where, W: Potential energy
A: Crack length
b: Specimen width

The criterion for the crack propagation is expressed as follows;

$$G(P,A) = G_{Ic} \qquad (3)$$

The crack propagation is unstable when the following criterion is met;

$$\frac{\partial G}{\partial A}(A) \geq 0 \qquad (4)$$

This approach is related to the global structure and less sensible to the fineness of finite elements in local area than the stress analysis. G_{I_c} is obtained by comparing G in critical crack length with the maximum load in lateral loading test of joints.

4.RESULTS AND DISCUSSION

4.1 Crack initiation

Fig.4 shows the distribution of the stress perpendicular to grain(σyy) along the X-axis. The stress(σyy) decreased rapidly with the increase of the distance from the bolt hole. It was shown that the maximum tensile stress near the boundary of the hole calculated from the linear finite model was much higher than the tensile strength perpendicular to the grain of wood, and that the non linear effects such as plasticity or damage in local small area should be considered. By comparing the computed stress distribution and the splitting load of L.M.T. test, we obtained[4][5];

$$lc=2.84mm \text{ for } ft=4.76MPa.$$

Table 2 compares the splitting load calculated from the average stress criterion with the maximum load in B.R.I. test. The splitting load was 170 to 180kN/m for the specimen with 16mm bolt and 200 to 213kN/m for that with 20mm bolt, and varied little regardless of the edge distance. The splitting load was approximately 10 and 33% smaller than the maximum load when the edge distance was 4d and 10d, respectively. This trend indicates that the crack initiates at the critical load, and then the load increases with the propagation of crack until the crack becomes unstable. The increase of the maximum load after the crack initiation was higher as the edge distance was larger.

4.3 Crack propagation

We assumed that a crack initiates at the right border of the bolt hole and propagates rightly parallel to the grain. The crack propagation was modeled by two connected lines which were separated by the crack propagation as shown in Fig.5.

G was obtained by calculating the compliance of the structure from the following equation.

$$\frac{G}{P^2} = \frac{1}{2b}\frac{\partial C}{\partial A} = \frac{1}{2b}\frac{1}{\Delta A}\left(\frac{1}{k_1}-\frac{1}{k_2}\right) \qquad (5)$$

$$\Delta A = A_1 - A_2,\ \Delta A \ll 1$$

where, ki : Stiffness of structure in state (i)
A : Crack length

Figs.6 and 7 show the relation between the energy release rate divided by the load square($G/(P/b)^2$) and the crack length(A). In case the edge distance was 4d, $G/(P/b)^2$ decreased with the increase of the crack length, and it turned to increase at a critical point with the crack length of approximately 2.5d. In

case the edge distance was 7d and 10d, it decreased until the crack length attained 5 to 6d, and remained almost constant.

Figs.8 and 9 show G_{Ic} obtained from the comparison of the numerical analysis with the experimental results. The average value of G_{Ic} was 190N/m in B.R.I. test and 194N/m in L.M.T. test. These values were very close to that obtained from CIB-type test conducted in C.T.B.A.(Paris)[9].

Figs. 10 to 13 show the comparison of the calculated maximum load and the experimental results in B.R.I and L.M.T. test. Figs. 10 to 12 show that the maximum load increases with the increase of the edge distance when the end distance is sufficiently large, but there was almost no increase of the maximum load according to the increase of edge distance when e_1 was 7d. Fig.13 shows that the maximum load increased proportionally as the diameter of bolt increased. Although the experimental results scattered a lot in the specimen with 16mm diameter bolt, the calculated values showed comparatively good agreement with the experimental results, and it showed especially good agreement in the specimen with 12mm and 20mm diameter bolt. These results indicate that the LEFM shall be a useful tool to predict the load-bearing capacity of a bolted joint subjected to a force perpendicular to the grain.

5. CONCLUSION

To summarize the above-mentioned results, the following conclusions were drawn.

1. The splitting load of a bolted joint was almost constant regardless of the edge distance, while the maximum load increased with the increase of the edge distance.
2. It was found that a joint did not fail just after the initiation of crack, but the load increased with the propagation of crack if the end distance was sufficiently large.
3. G_{Ic} obtained from the LEFM model and the lateral loading test was approximately 190N/m both in B.R.I. and L.M.T. test, which was very close to G_{Ic} obtained from CIB-type test.
4. The maximum load obtained from LEFM model showed comparatively good agreements with the experimental results for different edge distance and bolt diameter. This indicates that the LEFM provides good approximation to predict the load-bearing capacity of bolted joint subjected to a force perpendicular to the grain.

REFERENCES

1) Whitney J.M.; Nuismer R.J.: Journal of Composite Materials, 8,253-265(1974)
2) Masuda M.: Proceedings of the 1990 International Timber Engineering Conference,1,28-33(1990)
3) Guitard D.:"Mecanique du materiau bois et composites", Cepadues-Editions(1987)
4) Bengougam A.;Dubois F.:"Simulation de la rupture d'un assemblage en bois boulonne", Memoire de D.E.A. de l'E.N.S. de Cachan(1994)
5) Daudeville L.;Yasumura M.:"Failure analysis of timber bolted joints by fracture mechanics", Materials and Structures, RILEM (to be published)
6) Architectural Institute of Japan: "Standard for Structural Calculation of Timber Structures",169-173(1988)
7) Johansen K.W.: Inter. Assoc. of Bridge and Structural Engineering, 9,249-262(1949)
8) Yasumura M.: Proceedings of International Workshop on Wood Connectors, Forest Products Society, 114-121(1993)
9) Daudeville L.;Yasumura M.;Lanvin J.D.:"Fracture of Wood in Tension Perpendicular to the Grain:Numerical Simulation by Damage Mechanics, Proceedings of 27th CIB-W18,(1995)

Table 1. Outline of specimen

(a) B.R.I. specimen

Specimen	Bolt diameter (d)(mm)	Member thickness (b)	End distance (e_1)	Edge distance (e_2)
B16-4-4	16	4d	25d	4d
B16-8-4	16	8d	25d	4d
B16-10-4	16	10d	25d	4d
B16-4-7	16	4d	25d	7d
B16-8-7	16	8d	25d	7d
B16-10-7	16	10d	25d	7d
16-5-8.75	16	5d	25d	8.75d
B16-4-10	16	4d	25d	10d
B16-8-10	16	8d	25d	10d
B16-10-10	16	10d	25d	10d
B20-4-4	20	4d	20d	4d
B20-8-4	20	8d	20d	4d
B20-4-7	20	4d	20d	7d
B20-8-7	20	8d	20d	7d
B20-4-10	20	4d	20d	10d
B20-8-10	20	8d	20d	10d

(b) L.M.T. specimen

Specimen	Bolt diameter (d)(mm)	Member thickness (b)	End distance (e_1)	Edge distance (e_2)
A1	12	3d	7d	4d
A2	12	3d	7d	8d
A3	12	3d	7d	12d
B1	16	3d	7d	4d
B2	20	3d	7d	4d
C1	12	3d	25d	4d
C2	12	3d	25d	8d
C3	12	3d	25d	12d

Table 2. Comparison of the calculated crack initiation load(Pc) with the maximum load(Pm) in B.R.I. test

Bolt diameter d(mm)	Edge distance (e_1)	Pc/ft' (m)	Pc (kN/m)	Pm (kN/m)	ratio
16	4d	0.03569	169.9	195.4	0.88
	7d	0.03731	177.6	287.1	0.62
	8.75d	0.03772	179.6	265.1	0.68
	10d	0.03793	180.6	271.1	0.67
20	4d	0.04218	200.8	219.8	0.91
	7d	0.04408	209.8	251.8	0.83
	10d	0.04475	213.0	311.9	0.68

Note: ft: Tensile strength of spruce perpendicular to grain (4.76MPa)

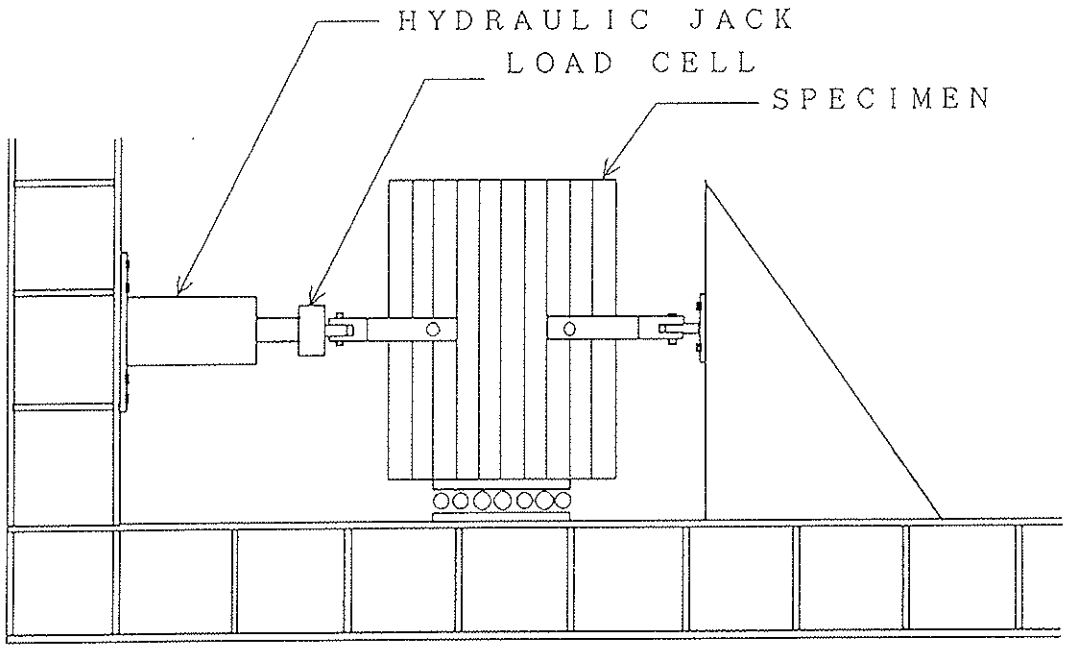

(a) B. R. I. Test

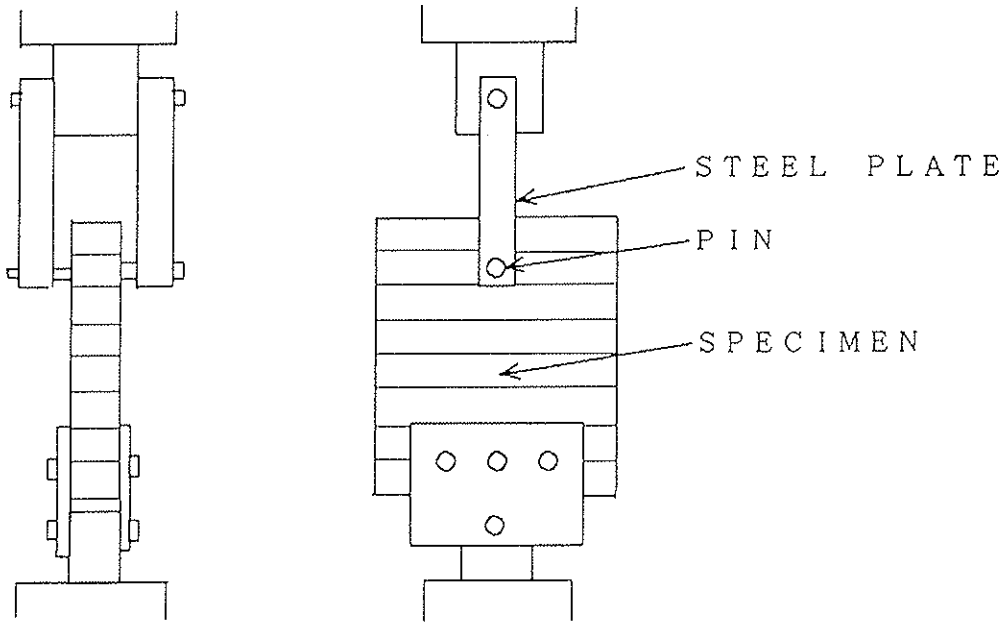

(b) L. M. T. Test

Fig.1 Test apparatus

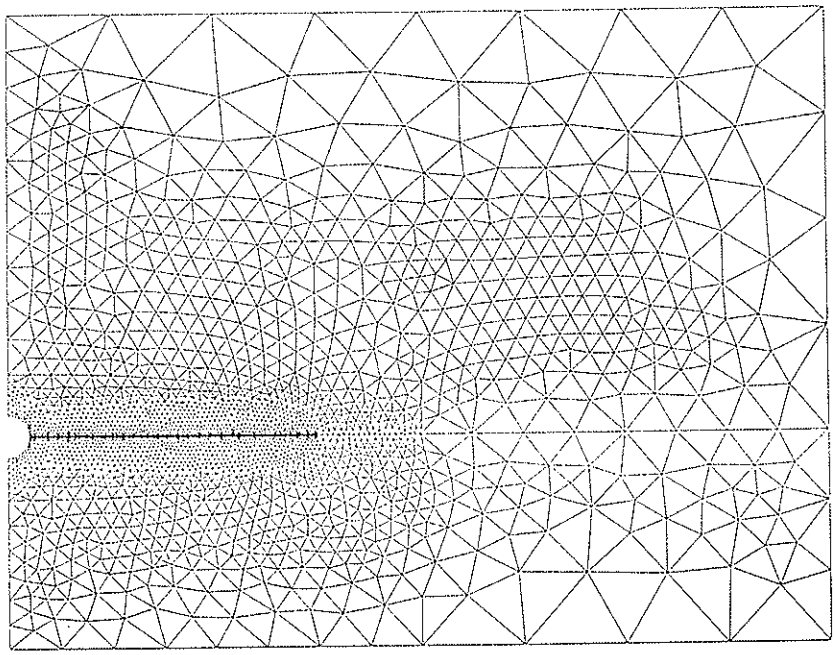

Fig.2 Finite element model for crack propagation

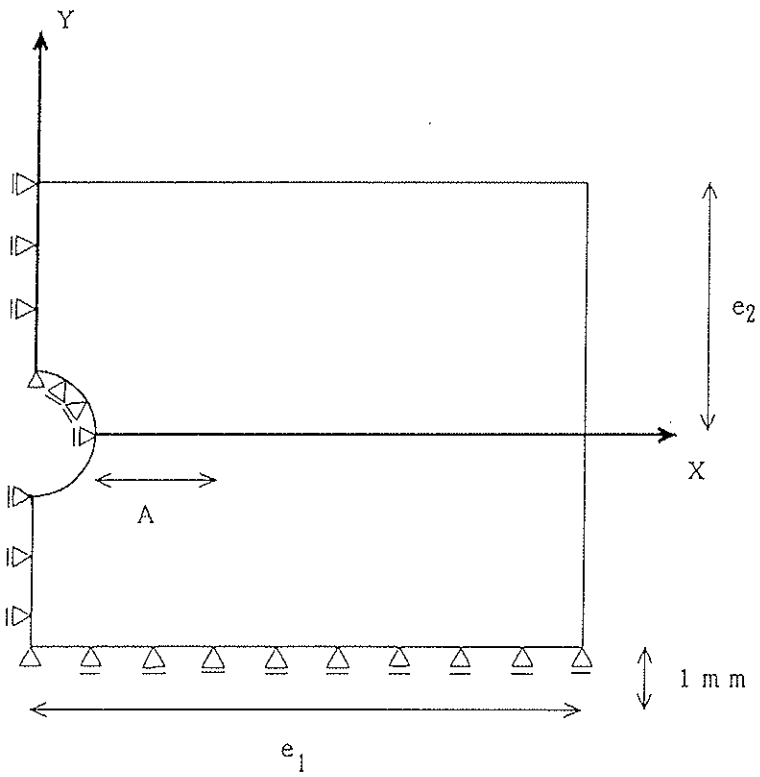

Fig.3 Boundary condition

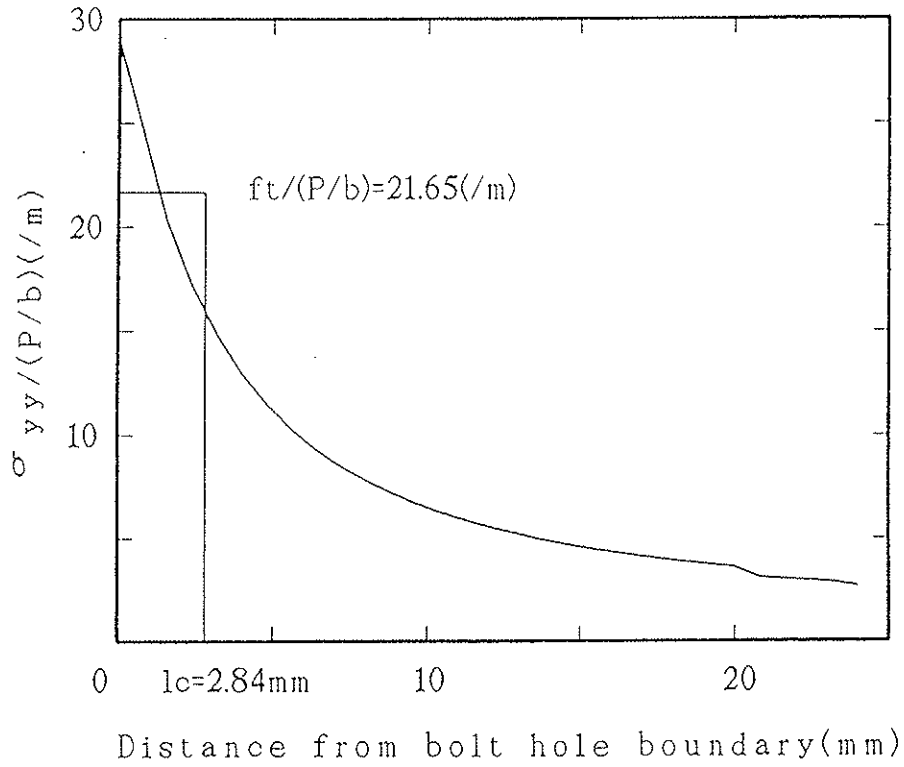

Fig.4 Stress perpendicular to grain and distance from a bolt hole

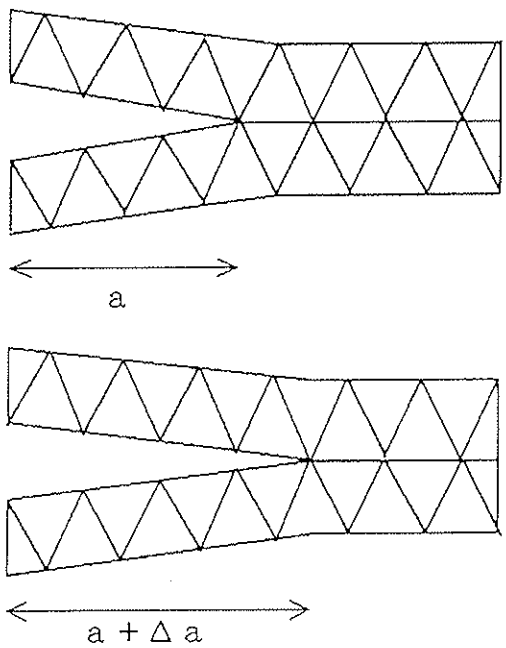

Fig.5 Modeling of propagation of a crack by two separate lines

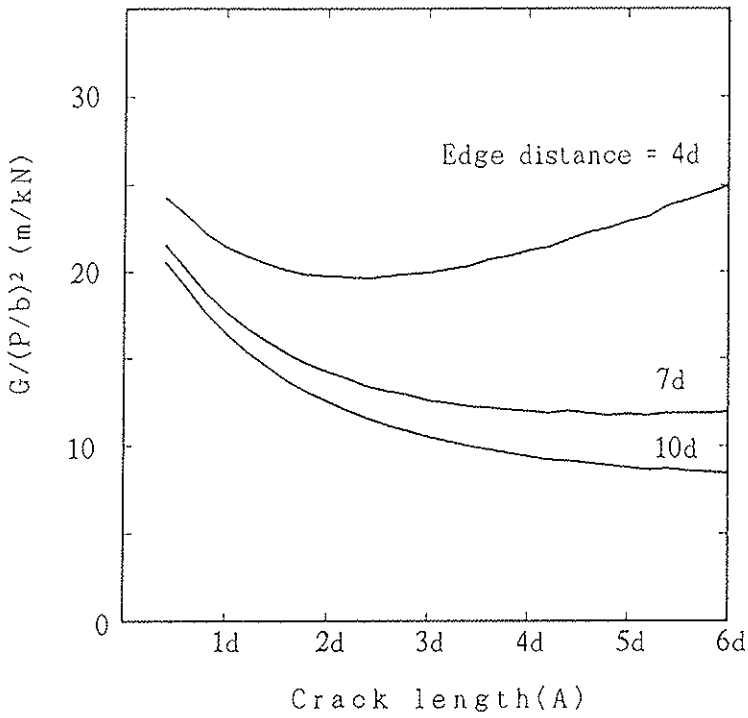

Fig.6 G/(P/b)² and crack length(A)(d=16mm).

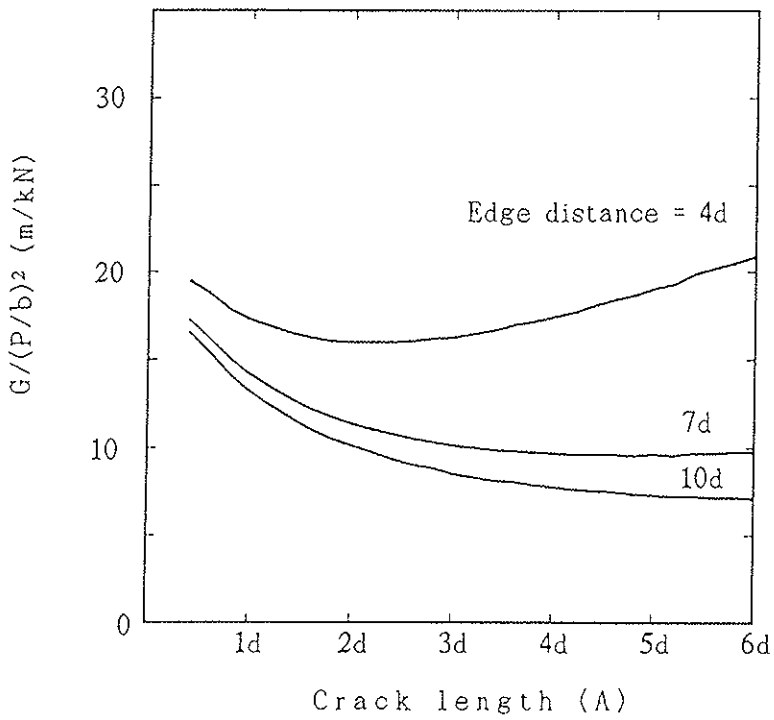

Fig.7 G/(P/b)² and crack length(A)(d=20mm).

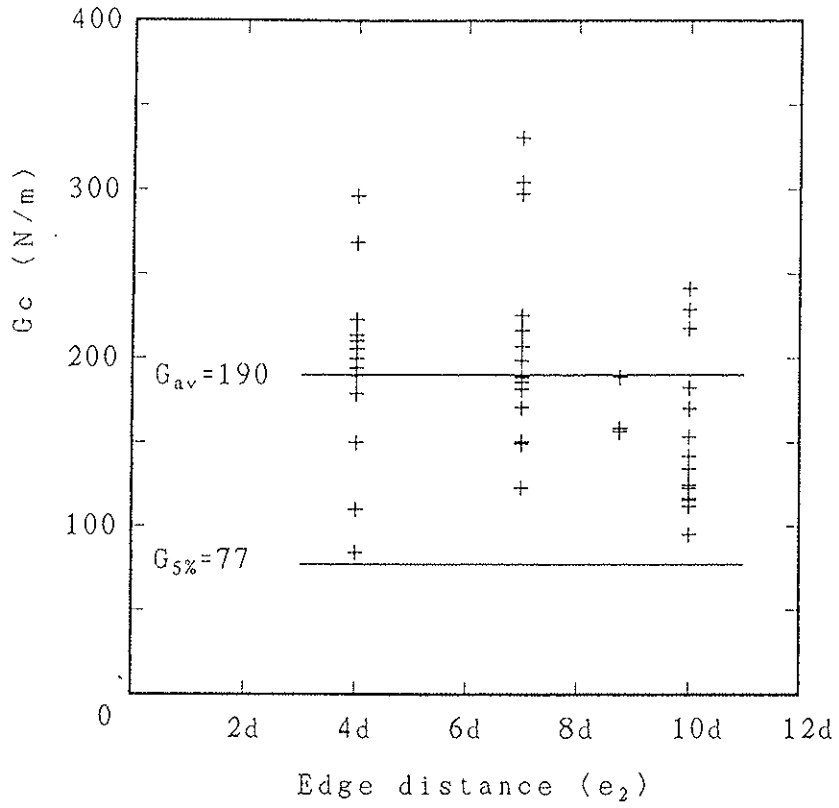

Fig.8 G_{Ic} obtained from B.R.I. test.

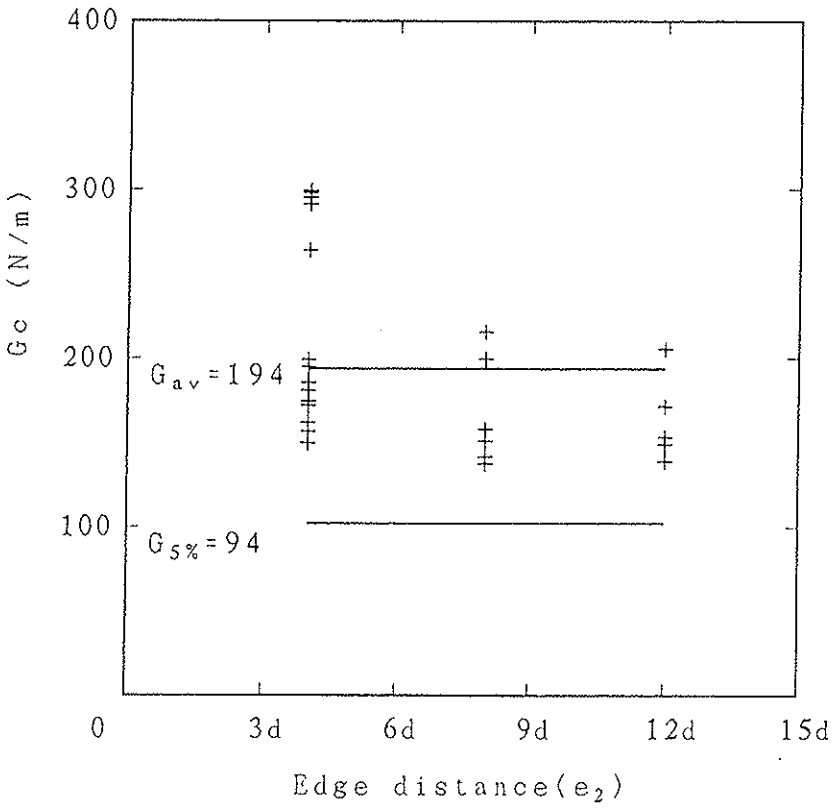

Fig.9 G_{Ic} obtained from L.M.T. test.

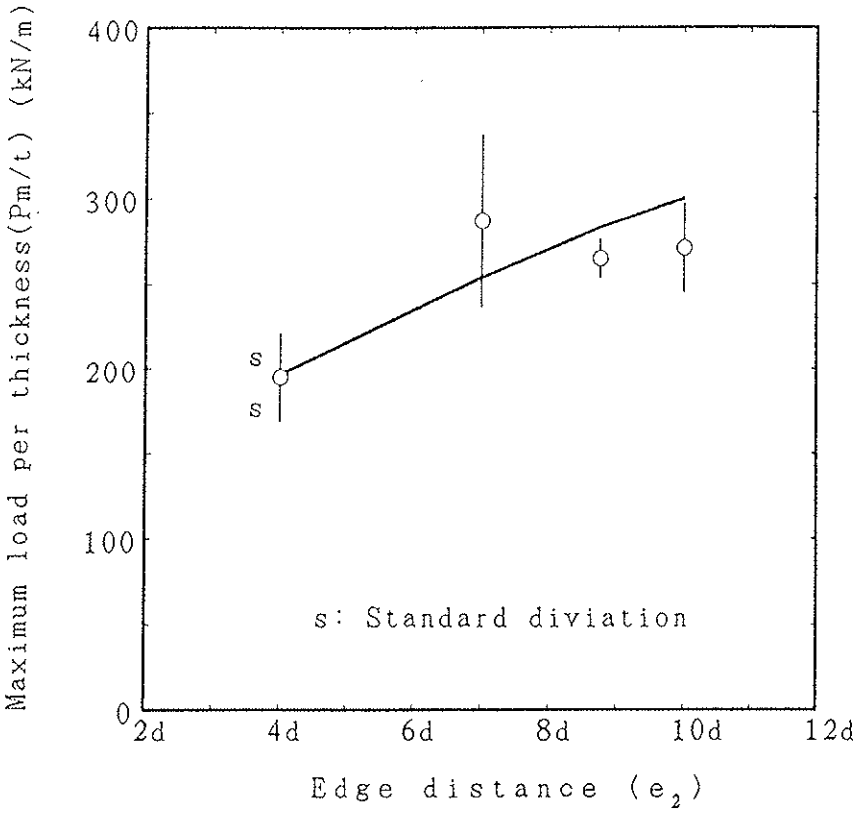

Fig.10 Maximum load and e_2(d=16mm).

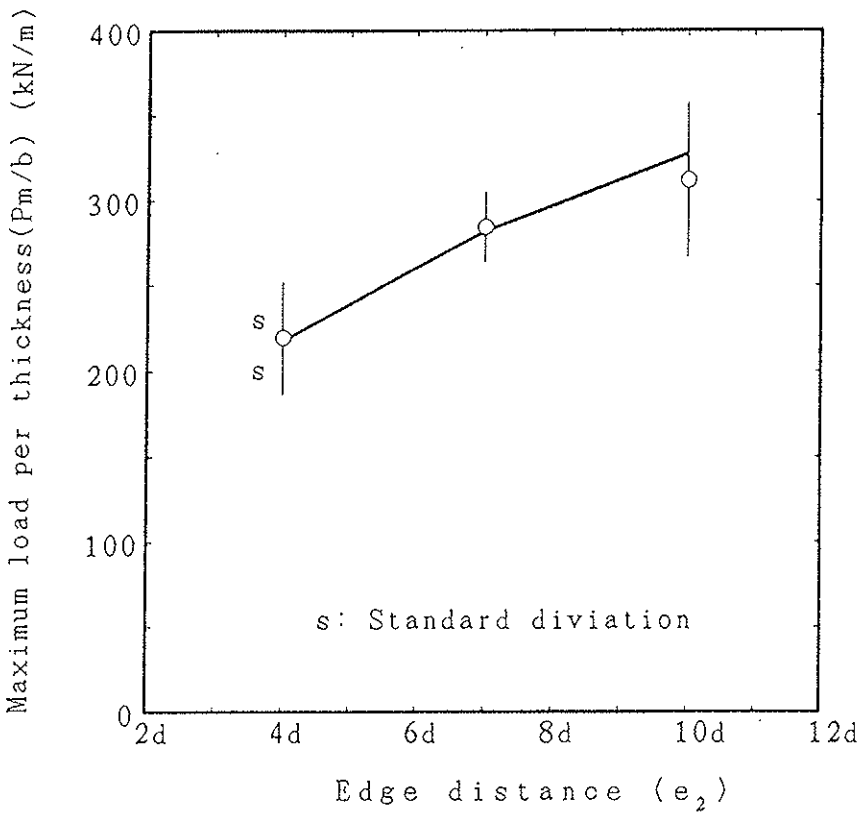

Fig.11 Maximum load and e_2(d=20mm).

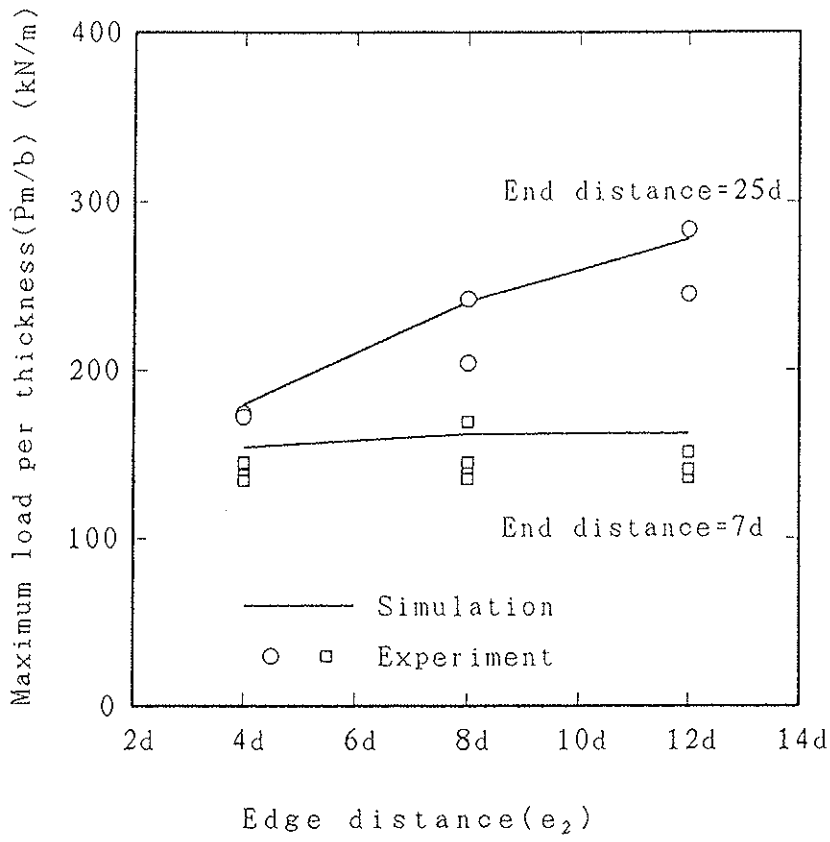

Fig.12 Maximum load and e_2(d=12mm).

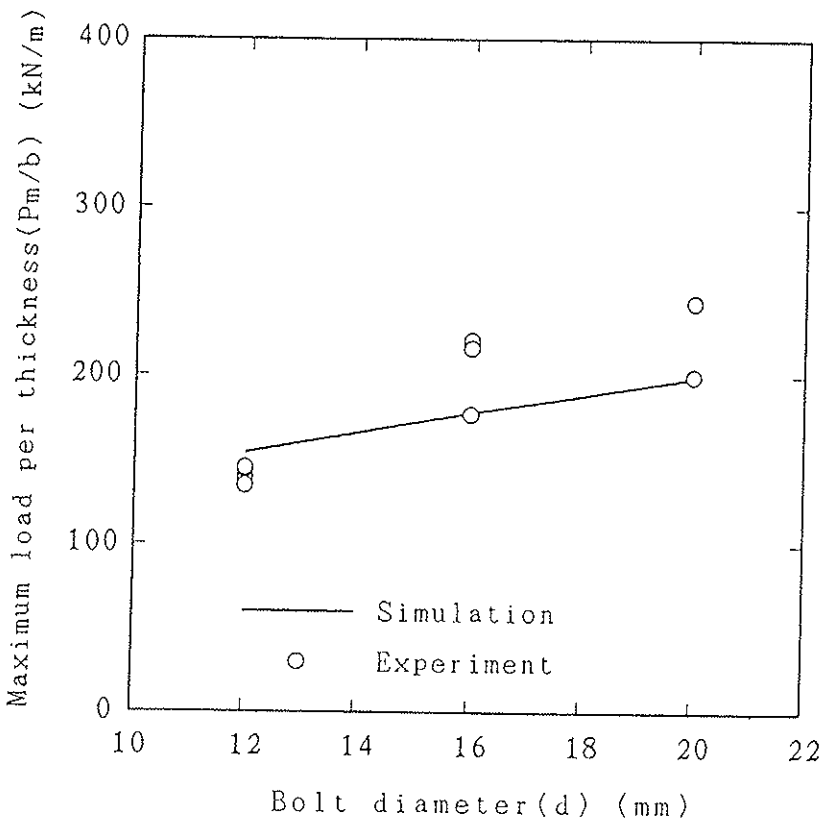

Fig.13 Maximum load and d(e_1=7d).

CIB-W18/28-7-6

INTERNATIONAL COUNCIL FOR BUILDING RESEARCH STUDIES AND DOCUMENTATION

WORKING COMMISSION W18 - TIMBER STRUCTURES

DESIGN PROCEDURE FOR LOCALLY REINFORCED JOINTS WITH DOWEL-TYPE FASTENERS

by

H Werner
University of Karlsruhe
Germany

MEETING TWENTY - EIGHT

COPENHAGEN

DENMARK

APRIL 1995

Design Procedure for Locally Reinforced Joints with Dowel-Type Fasteners

Hartmut Werner
University of Karlsruhe, Germany

1 Introduction

The load-carrying capacity of joints with dowel-type fasteners, such as nails, bolts and dowels frequently determines the size of the members. By gluing a wood-based panel on the surface of the timber members, member properties are improved and the spacings and distances of the fasteners can be reduced. The reinforcing material must be able to distribute concentrated loads uniformly while the glueline transfers the shear stresses into the timber.

The results of some preliminary tests with plywood reinforced joints made by BLASS and WERNER 1988 showed, that the danger of splitting was considerably reduced and the load-carrying capacity increased, because of the high embedding strength of the reinforcing material.

At the University of Karlsruhe locally reinforced joints with dowels and metric threaded rods were tested. A calculation model based on the modified "Johansen-theory" was used for evaluating the test data. The results invited to present a proposal for calculating the design load-carrying capacities of locally reinforced joints with dowel-type fasteners.

2 Material properties

2.1 Embedding strength of reinforced timber

The deformations beneath the fasteners were influenced by gluing a wood-based panel on the surface of the timber members. The lateral displacement of the timber is impeded. Tests with reinforced timber were carried out in line with EN 383. The hole in the timber was predrilled with the diameter of the fastener and the reinforcements have a longsized hole (see Fig. 1).

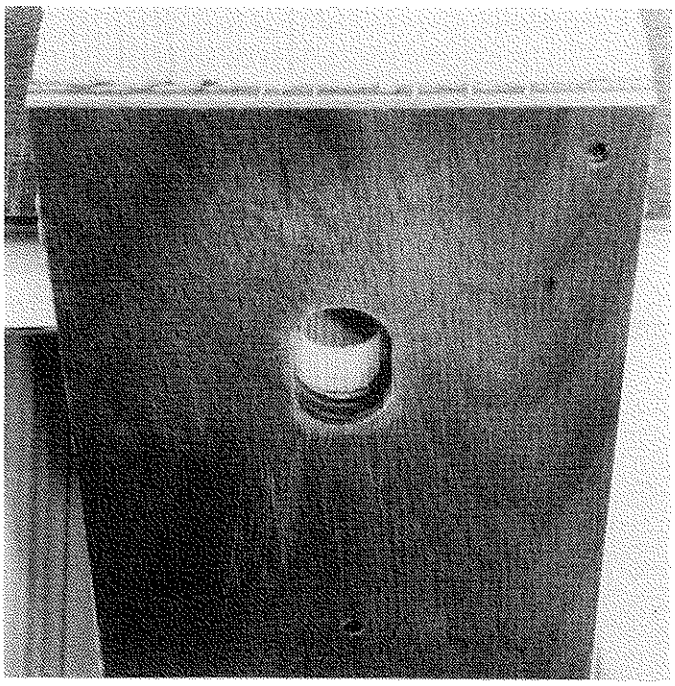

Figure 1: Embedding test piece of reinforced softwood

The evaluation of the test data gives the following expression for bolts and dowels in softwood:

$$f_{h,0,k} = 0{,}09 \cdot \rho \cdot (1 - 0{,}01 \cdot d) \quad (1)$$

with $f_{h,0,k}$ in N/mm^2, ρ in kg/m^3 and d in mm

The embedding strength values of reinforced softwoods are approximately 10% higher than those given in ENV 1995-1-1 Eq. 6.5.1.2 b.

2.2 Embedding strength of different reinforcements

Reinforcements with high embedding strengths such as plywood made of beech veneers or densified veneer wood (dvw) are appropriate for joints with high load-carrying capacities.

Embedding strength of plywood made of beech

The embedding strengths of plywood made of beech veneers were tested in line with EN 383. The test results were compared with 900 tests performed by DRÖGE and KRAMER 1989 who used a different test method. From the evaluation of the test data the following conclusions can be drawn:

- The embedding strength values at different angle with respect to the grain direction of the face ply do not show any significant difference.
- The thickness of the veneers and the diameter of the dowel-type fastener have influence on the embedding strength.
- For dowel-type fasteners between 8 and 30 mm diameter and veneer thicknesses between 1,4 and 3,0 mm the following characteristic embedding strength can be used:

$$f_{h,k} = \left(0{,}79 + \frac{3{,}8}{\sqrt{d}}\right) \cdot 30 \qquad (\mathrm{N/mm^2}) \qquad (2)$$

with d in mm

Embedding strength of densified veneer wood

The embedding strengths of densified veneer wood (dvw) made of beech, poplar and maritime pine compressed to different densities were tested by EHLBECK, WERNER 1992 and RODD 1993 in line with the main principles of EN 383. The test results were summarized by LEIJTEN 1994. From the test data the following may be argued:

- The embedding strength of dvw under compression load and under tension load turned out to be approximately the same.
- The embedding strength values at 0° and 45° angle with respect to the grain direction of the face ply do not show any significant difference.
- Any effect of veneer grades can be disregarded.
- For beech and maritime pine dvw neither the thickness of the test pieces nor the dowel diameter have any significant influence on the embedding strength.

- The embedding strength may be assumed to increase linearly with increasing density of the dvw independent of the wood species. The test results and the regression line for dvw made of beech veneers are shown in Fig. 2.

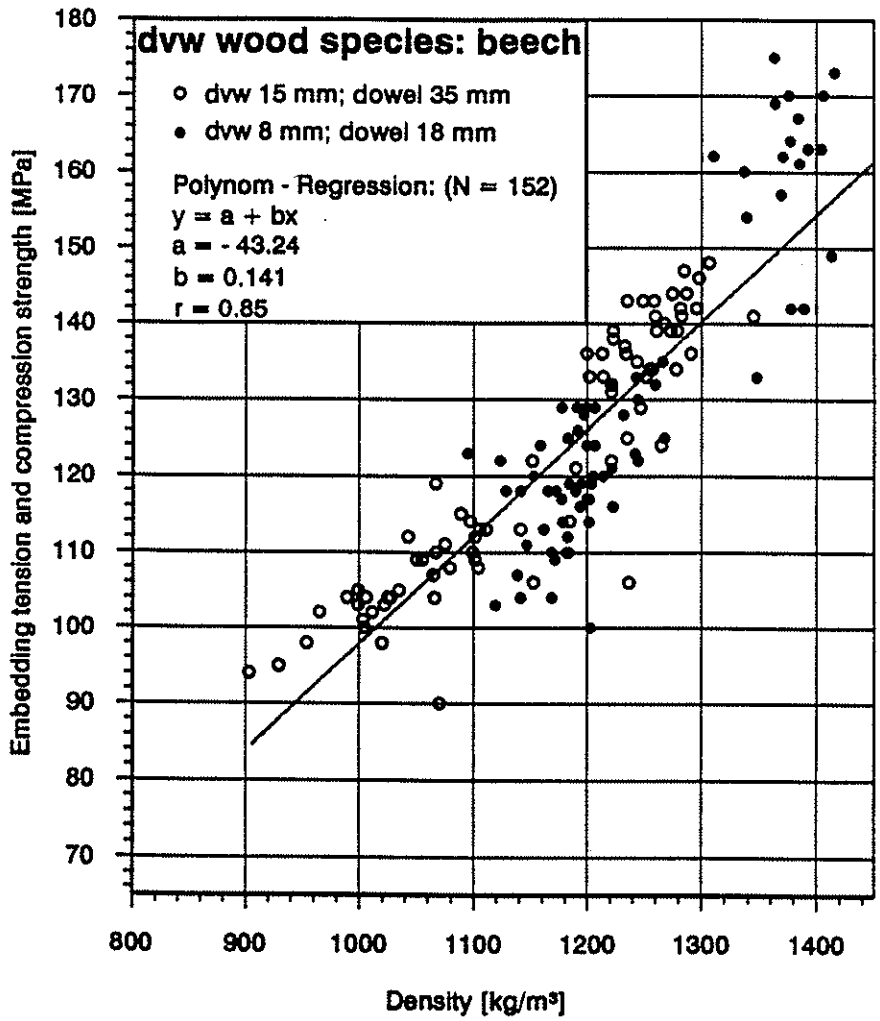

Figure 2: Density - embedding strength relation of beech dvw (LEIJTEN 1994)

3 Design procedure

The following proposal for a design procedure could to be used in an Annex of EUROCODE 5. The design method is based on a modified „Johansen-theory“ with the understanding that the embedding strength and the thickness of each reinforcing member used are the same.

3.1 Reinforced timber-to-timber joints

(1) The design load-carrying capacity per shear plane per fastener, for reinforced timber-to-timber joints made with dowel-type fasteners should be taken as the smallest value found from the following formulae:
Design load-carrying capacities for fasteners in single shear:

$$R_d = min \begin{cases} \left(f_{h,1,d} \cdot s_1 + f_{h,t,d} \cdot t\right) \cdot d & (3a) \\ \left(f_{h,2,d} \cdot s_2 + f_{h,t,d} \cdot t\right) \cdot d & (3b) \\ \dfrac{f_{h,1,d}\, s_1\, d}{1+\beta} \cdot \sqrt{\beta\left(1 - 4\eta\left(\dfrac{t}{s_1}\right)^2\right) + 2\beta^2\left(1 + \left(\dfrac{s_2}{s_1}\right) + \left(\dfrac{s_2}{s_1}\right)^2 + 4\left(\dfrac{t}{s_1}\right) + 8\left(\dfrac{t}{s_1}\right)^2 + 4\left(\dfrac{t}{s_1}\right)\left(\dfrac{s_2}{s_1}\right) - 2\eta\left(\dfrac{t}{s_1}\right)^2\right) + \beta^3\left(\dfrac{s_2}{s_1}\right)^2} & \\ \qquad - \dfrac{\beta\, f_{h,1,d}\, s_1\, d}{1+\beta} \cdot \left[1 + 4\left(\dfrac{t}{s_1}\right) + \left(\dfrac{s_2}{s_1}\right)\right] + f_{h,t,d} \cdot d \cdot t & (3c) \\ k_{sys} \cdot \dfrac{\beta \cdot f_{h,1,d} \cdot d}{2+\beta} \cdot \left[\sqrt{(s_1 + 4t)^2 + \dfrac{2+\beta}{\beta}\left(s_1^2 - 4\eta t^2 + \dfrac{4 M_{y,d}}{d \cdot f_{s1}}\right)} - (s_1 + 4t)\right] + f_{h,t,d} \cdot t \cdot d & (3d) \\ k_{sys} \cdot \dfrac{\beta \cdot f_{h,1,d} \cdot d}{1+2\beta} \cdot \left[\sqrt{(s_2 + 4t)^2 + (1+2\beta)\left(s_2^2 - 4\eta t^2 + \dfrac{4 M_{y,d}}{\beta \cdot d \cdot f_{s1}}\right)} - (s_2 + 4t)\right] + f_{h,t,d} \cdot t \cdot d & (3e) \\ k_{sys} \cdot \dfrac{2 \cdot \beta \cdot f_{h,1,d} \cdot d}{1+\beta} \cdot \left[\sqrt{t^2 - \dfrac{1+\beta}{2\beta}\left(\eta t^2 - \dfrac{2 M_{y,d}}{d \cdot f_{s1}}\right)} - t\right] + f_{h,t,d} \cdot t \cdot d & (3f) \end{cases}$$

Design load-carrying capacities for fasteners in double shear:

$$R_d = min \begin{cases} \left(f_{h,1,d} \cdot s_1 + f_{h,t,d} \cdot t\right) \cdot d & (3g) \\ \left(0{,}5 \cdot f_{h,2,d} \cdot s_2 + f_{h,t,d} \cdot t\right) \cdot d & (3h) \\ k_{sys} \cdot \dfrac{\beta \cdot f_{h,1,d} \cdot d}{2+\beta} \cdot \left[\sqrt{(s_1 + 4t)^2 + \dfrac{2+\beta}{\beta}\left(s_1^2 - 4\eta t^2 + \dfrac{4 M_{y,d}}{d \cdot f_{s1}}\right)} - (s_1 + 4t)\right] + f_{h,t,d} \cdot t \cdot d & (3j) \\ k_{sys} \cdot \dfrac{2 \cdot \beta \cdot f_{h,1,d} \cdot d}{1+\beta} \cdot \left[\sqrt{t^2 - \dfrac{1+\beta}{2\beta}\left(\eta t^2 - \dfrac{2 M_{y,d}}{d \cdot f_{s1}}\right)} - t\right] + f_{h,t,d} \cdot t \cdot d & (3k) \end{cases}$$

s_1 and s_2	timber thickness or penetration
t	thickness of the reinforcement
$f_{h,1}$ ($f_{h,2}$)	embedding strength in s_1 (s_2)
$f_{h,t}$	embedding strength of the reinforcement
M_y	fastener yield moment
d	fastener diameter
k_{sys}	system and correction factor
β	ratio $\dfrac{f_{h,2,d}}{f_{h,1,d}}$
η	ratio $\dfrac{f_{h,t,d}}{f_{h,1,d}}$

The value in the square brackets must be greater than zero. The various failure modes are illustrated in Fig. 3

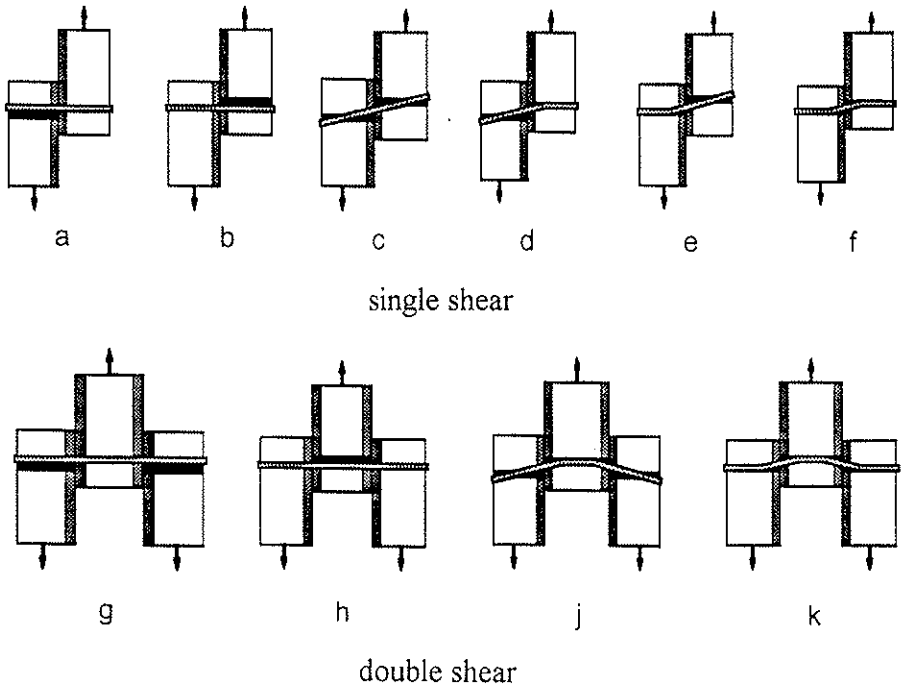

Figure 3: Failure modes for reinforced timber-to-timber joints

With the thickness t of the reinforcement approaching zero, equ. (3a-k) turn over to formulae 6.2.1 a-k in ENV 1995-1-1, with a system factor k_{sys} of 1,1.

3.2 Steel-to-timber joints

(1) The design load-carrying capacity per fastener for single shear reinforced steel-to-timber joints, for a thin steel plate (i.e. for $t_{steel} \leq 0{,}5d$ where t_{steel} is the steel plate thickness), should be taken as the smaller value found from the following formulae:

$$R_d = min \begin{cases} f_{h,1,d} \cdot d \cdot \left[\sqrt{2 s_1^2 + 2\,(2-\eta)\,t^2 + 4\,t\,s_1} - (s_1 + 2\,t) \right] + f_{h,t,d} \cdot t \cdot d & (4a) \\ k_{sys} \cdot f_{h,1,d} \cdot d \cdot \left[\sqrt{(4-\eta)\,t^2 + \dfrac{2\,M_{y,d}}{d \cdot f_{h,1,d}}} - 2\,t \right] + f_{h,t,d} \cdot t \cdot d & (4b) \end{cases}$$

For thick steel plate (i.e. for $t_{steel} \geq d$), the design load-carrying capacity should be taken as the smaller value found from the following formulae:

$$R_d = min \begin{cases} \left(f_{h,1,d} \cdot s_1 + f_{h,t,d} \cdot t\right) \cdot d & (4c) \\ k_{sys} \cdot f_{h,1,d} \cdot d \cdot \left[\sqrt{2\, s_1^2 + 2(2-\eta)t^2 + 4t\, s_1 + \frac{4\, M_{y,d}}{d \cdot f_{h,1,d}}} - (s_1 + 2t)\right] + f_{h,t,d} \cdot t \cdot d & (4d) \\ k_{sys} \cdot f_{h,1,d} \cdot d \cdot \left[\sqrt{(4-\eta)\, t^2 + \frac{4\, M_{y,d}}{d \cdot f_{h,1,d}}} - 2\, t\right] + f_{h,t,d} \cdot t \cdot d & (4e) \end{cases}$$

For $0{,}5d < t_{steel} < d$ linear interpolation is permitted. The symbols are as defined in chapter 3.1, and the failure modes are illustrated in Fig. 4a-e. The value in the square brackets must be greater than zero.

(2) The design load-carrying capacity per shear plane per fastener for double shear reinforced joints with the centre member of steel should be taken as the smallest value found from the following formulae:

$$R_d = min \begin{cases} \left(f_{h,1,d} \cdot s_1 + f_{h,t,d} \cdot t\right) \cdot d & (4f) \\ k_{sys} \cdot f_{h,1,d} \cdot d \cdot \left[\sqrt{2\, s_1^2 + 2(2-\eta)t^2 + 4t\, s_1 + \frac{4\, M_{y,d}}{d \cdot f_{h,1,d}}} - (s_1 + 2t)\right] + f_{h,t,d} \cdot t \cdot d & (4g) \\ k_{sys} \cdot f_{h,1,d} \cdot d \cdot \left[\sqrt{(4-\eta)\, t^2 + \frac{4\, M_{y,d}}{d \cdot f_{h,1,d}}} - 2\, t\right] + f_{h,t,d} \cdot t \cdot d & (4h) \end{cases}$$

The symbols are defined in chapter 3.1, and the failure modes are illustrated in Fig. 4f-h. The value in the square brackets must be greater than zero.

(3) The design load-carrying capacity per shear plane per fastener for double shear reinforced joints with both outer members of thin steel should be taken as the smaller value found from the following formulae:

$$R_d = min \begin{cases} 0{,}5 \cdot f_{h,2,d} \cdot s_2 \cdot d + f_{h,t,d} \cdot t \cdot d & (4j) \\ k_{sys} \cdot f_{h,2,d} \cdot d \cdot \left[\sqrt{(4 - \frac{f_{h,t,d}}{f_{h,2,d}})\, t^2 + \frac{2\, M_{y,d}}{d \cdot f_{h,2,d}}} - 2\, t\right] + f_{h,t,d} \cdot t \cdot d & (4k) \end{cases}$$

For thick steel plates (i.e. for $t_{steel} \geq d$), the design load-carrying capacity should be taken as the smaller value found from the following formulae:

$$R_d = min \begin{cases} 0{,}5 \cdot f_{h,2,d} \cdot s_2 \cdot d + f_{h,t,d} \cdot t \cdot d & (4l) \\ k_{sys} \cdot f_{h,2,d} \cdot d \cdot \left[\sqrt{(4 - \frac{f_{h,t,d}}{f_{h,2,d}})\, t^2 + \frac{4\, M_{y,d}}{d \cdot f_{h,2,d}}} - 2\, t\right] + f_{h,t,d} \cdot t \cdot d & (4m) \end{cases}$$

For $0{,}5d < t_{steel} < d$ linear interpolation is permitted. The symbols are defined in chapter 3.1, and the failure modes are illustrated in Fig. 4j-m. The value in the square brackets must be greater than zero.

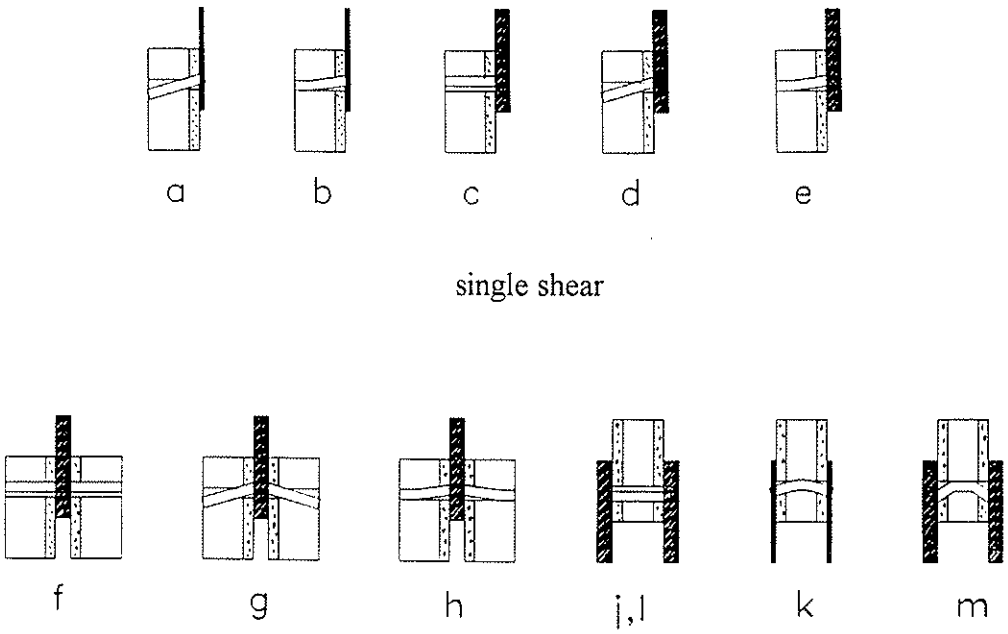

Figure 4: Failure modes for steel-to-timber reinforced joints

The requirement that the value in the square brackets must be greater than zero follows from the assumption that the yield points are not located in the thin reinforcements.

(4) A check should also be made on the strength of the steel plate.

(5) The glue area A_L on the surface of the joint members should satisfy the following condition:

$$A_L = \frac{f_{h,t,d}}{f_{v,d}} \cdot n \cdot t \cdot d \qquad (5)$$

where the symbols are defined as follows:

$f_{h,t,d}$	design embedding strength of the reinforcement
$f_{v,d}$	minimum design shear strength (smallest value of the glueline, the reinforcement or the timber)
n	number of fasteners
t	thickness of the reinforcement
d	diameter of the fastener

4 Test and calculation results

The load-carrying capacity and the load-deformation behaviour of double-shear reinforced joints with dowels and metric threaded rods up to 24 mm were investigated. The test results are published in EHLBECK and WERNER 1994. All test pieces were loaded in grain direction of the softwood and of the face ply of the reinforcement. As reinforcement plywood made of beech veneers (t = 6; 10 and 15 mm) was glued on the surface of the timber member. The test pieces for shear tests loaded in tension is shown in Fig. 5. The ratio of side member thickness, s_1, to middle member thickness, s_2, was constant, with s_1/s_2 = 0,5.

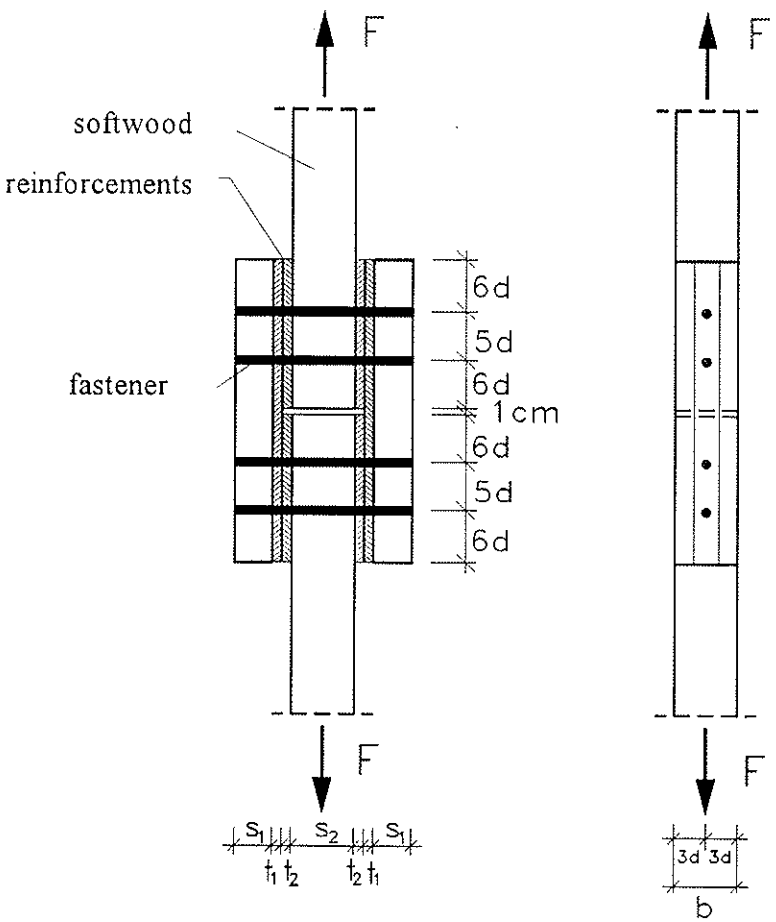

Figure 5: Test piece for shear tests loaded in tension

In **Table 1** the mean values of the tested maximum load R_{test} per fastener are compared with the calculated load-carrying capacities R_{cal}.

Table 1: Comparison between the tested maximum load R_{test} per fastener and the calculated load-carrying capacity R_{cal}

Mean values of the tests loaded in tension with plywood reinforced timber-to-timber joints (number of tests: n = 80; i.e. 5 per test series)

test series	thickness t (mm)	diameter d (mm)	slender-ness s_2/d	maximum load R_{test} (kN)	cal. load-carrying capacity R_{cal} (kN)	ratio $\frac{R_{test}}{R_{cal}}$
Fastener: dowels made of cold formed steel (St 37 K)						
S 8/4/6	6	8	4	10,4	10,9	0,95
S 8/6/6	6	8	6	12,6	12,5	1,00
S 8/8/6	6	8	8	16,3	14,6	1,12
S 16/2/6	6	16	2	25,6	27,0	0,95
S 16/4/6	6	16	4	34,1	36,3	0,94
S 16/6/6	6	16	6	38,7	39,2	0,99
S 16/6/10	10	16	6	41,8	43,2	0,97
S 16/6/15	15	16	6	51,5	49,1	1,05
S 24/4/10	10	24	4	68,8	72,5	0,95
S 24/6/10	10	24	6	80,7	79,1	1,02
Fastener: metric threaded rods (property class 8.8)						
M 8/6/6	6	8	6	15,2	14,5	1,05
M 8/8/6	6	8	8	17,9	15,8	1,13
M 12/4/6	6	12	4	25,4	25,4	1,00
M 12/6/6	6	12	6	28,5	26,7	1,06
M 12/8/6	6	12	8	31,7	30,3	1,05
M 20/6/10	10	20	6	62,9	62,8	1,00

With a computer program called "XJOINT" different dowelled joints were calculated and compared with test results. A good agreement between the test results and the calculated values can be stated.

A computer model for calculating the ultimate loads of joints with dowel-type fasteners was presented in WERNER 1993 and is used to determine characteristic values of the load-carrying capacities. The stochastic model of joints with dowel-type fasteners includes the statistic distribution functions of the influencing properties and their autocorrelation, i.e. embedding stress-strain relationship, yield moment of the fastener, thicknesses of the members and withdrawal resistance of the fastener. The diameter of the fastener is regarded as a deterministic variable.

The ultimate loads of dowelled reinforced joints with softwood loaded in grain direction under normal climate conditions were calculated. The following variations were investigated:

Fastener:	cold formed smooth round dowels (St 37 K)
reinforcement:	plywood made of beech veneers
Fastener diameter:	d = 8; 16 and 24 mm
Thickness of the reinforcement:	t = 6 mm
Slenderness:	$\lambda = s_2/d$ = 0; 2; 4; 6; 8 and 10
ratio s_1/s_2:	s_1/s_2 = 0,50 and 0,75

By way of example, the evaluation of the calculation for d = 16 mm and s_1/s_2 = 0,75 is shown in Fig. 6. In this diagram the load-carrying capacity curves of the mean values and the nonparametric values of the 5th percentile are presented.

The comparison between the simulation results and the design procedure (see Fig. 6) with

$$f_{h,1,k} = f_{h,2,k} = 0{,}09 \cdot \rho_k \cdot (1 - 0{,}01 \cdot d) \quad \text{(N/mm}^2\text{)}$$
$$f_{h,t,k} = (0{,}79 + 3{,}8/\sqrt{d}) \cdot 30 \quad \text{(N/mm}^2\text{)}$$
$$M_{y,k} = 82 \cdot d^3 \quad \text{(Nmm)}$$

and a system and correction factor k_{sys} = 1,06 gives a good agreement. The characteristic yield moment for the dowels made of cold formed steel (St 37 K according to DIN 1652) follows from bending tests in line with EN 409.

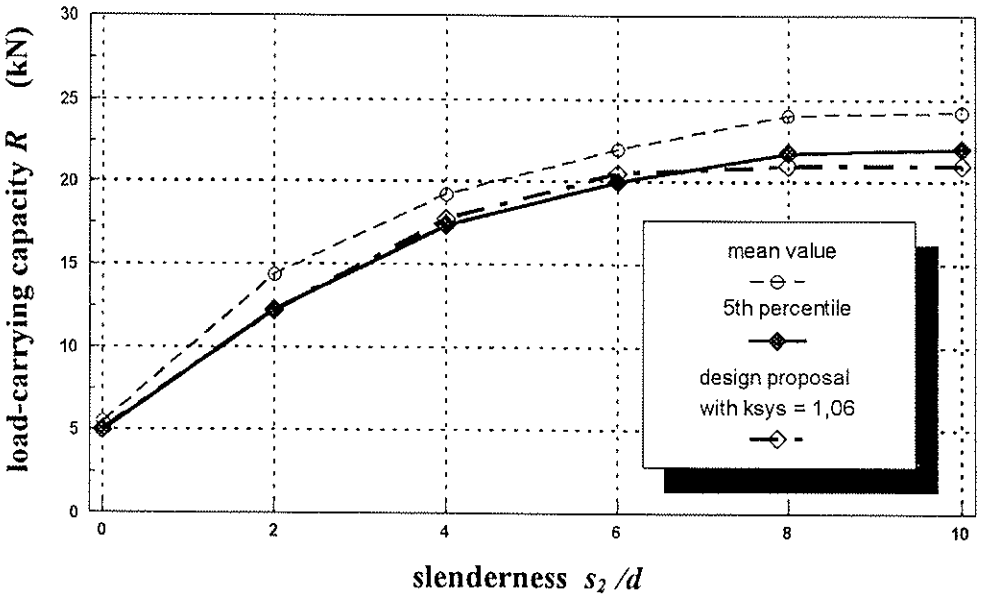

Figure 6: Load-carrying capacity R per shear plane per fastener over slenderness s_2/d
(Dowel St 37 K; d = 16 mm; s_1/s_2 = 0,75)

5 Conclusions

Locally reinforced joints with dowels and metric threaded rods and their influencing material properties were tested. A calculation model and a computer programme were used, taking into account the non-linear embedding stress-strain behaviour, the yield moment and the so-called "chain effect".

A design procedure for reinforced joints with dowel-type fasteners based on the modified "Johansen-theory" was presented. The results from the Monte Carlo simulation were compared with this design method.

Presuming that the embedding strengths and the yield moments are calculated as proposed in chapter 2 and 4, a system and correction factor k_{sys} = 1,06 for timber-to-timber joints in double shear can be added to the equations describing failure modes with fastener yield points. By using the M_y-values determined from the equation (6.5.1.2e) given in EC 5 the proposed system factor should be checked. Because of the low splitting tendency and the low variability of the load-carrying capacities a value for k_{sys} greater than 1,0 can be taken into account.

6 References

BLAß, H.J.; WERNER, H. 1988 : Stabdübelverbindungen mit verstärkten Anschlußbereichen. In: bauen mit holz 90(1988), S. 601-607

DRÖGE, G.; KRAMER, S. 1989 : Die Lochleibungsbruchspannungen von Bau - Furniersperrholz nach DIN 68705, T.5. In: Holzbau - Statik - Aktuell, 10/1989, S. 10 - 13

EHLBECK, J.; WERNER, H. 1992 : Embedding strength of densified veneer wood for dowel-type fastener. Karlsruhe: Versuchsanstalt für Stahl, Holz und Steine, Abt. Ingenieurholzbau, Universität Karlsruhe(TH). - Forschungsbericht

EHLBECK, J.; WERNER, H. 1994 : Möglichkeiten zur Leistungssteigerung von Anschlüssen mit stiftförmigen Verbindungsmitteln. Karlsruhe: Versuchsanstalt für Stahl, Holz und Steine, Abt. Ingenieurholzbau, Universität Karlsruhe(TH). -Forschungsbericht

LEIJTEN, A.J.M. 1994 : Analysis of embedding tests 17 mm and 35 mm dowel. Delft: University of Technology, Department of Civil Engineering, Timber Structures, Niederlanden.
-Report 25.4-94-08/HA-61

RODD, P.D. 1993 : Embedding strength of densified veneer wood with dowel-type fasteners. Brighton: Structural Timber Research Unit, Department of Civil Engineering, University of Brighton, UK

WERNER, H. 1993 : Tragfähigkeit von Holz-Verbindungen mit stiftförmigen Verbindungsmitteln unter Berücksichtigung streuender Einflußgrößen. Karlsruhe: Universität Karlsruhe. - Dissertation

CIB-W18/28-7-7

INTERNATIONAL COUNCIL FOR BUILDING RESEARCH STUDIES AND DOCUMENTATION

WORKING COMMISSION W18 - TIMBER STRUCTURES

VARIABILITY AND EFFECTS OF MOISTURE CONTENT ON THE WITHDRAWAL CHARACTERISTICS FOR LUMBER AS OPPOSED TO CLEAR WOOD

by

J D Dolan

J W Stelmokas

Virginia Polytechnic Institute and State University

USA

MEETING TWENTY - EIGHT

COPENHAGEN

DENMARK

APRIL 1995

SUMMARY

The axial withdrawal resistance of smooth, plain-shank nails in wood will be reduced when the wood is seasoned or subjected to cyclic moisture conditions. Due to the unavailability of Eurocode documents, all comparisons to design specification requirements are referenced to the National Design Specification for Wood Construction (NDS, AFPA 1993). This design specification provides a "wet service factor" to account for the wet service reduction. However, the specification assumes that all of this reduction occurs between the fiber saturation point and 19% moisture content, while as much shrinkage occurs above as below 19%. Therefore, the reduction in withdrawal resistance may also behave in the same fashion. The NDS does not recognize this possibility.

The objectives of this study were twofold: (1) Determine the effect of changes in moisture content on the axial withdrawal strength of smooth, plain-shank nails, and compare the results to NDS design values, and (2) Determine the variability of axial withdrawal strength within a single grade of lumber rather than small, clear specimens.

It was found that the design factors of safety, based on mean test results, were much lower than assumed for design values and a significant amount of variability of maximum load was observed within moisture conditions and along length of boards for a given moisture content.

It is recommended that the NDS allowable withdrawal loads for plain, smooth-shank nails be modified by either (a) reducing the nominal values by as much as 75%, (b) a second moisture adjustment factor be introduced for connections manufactured at 19% moisture content and subsequently dry to 12% or less, or (c) dry lumber to a maximum moisture content of 15% rather than the current 19%. As an alternative, the reduction associated with smooth shank nails in withdrawal could be avoided by requiring helix threaded or ring shank nails when withdrawal forces are present.

INTRODUCTION

The ability of a nail driven into a piece of wood to resist axial withdrawal forces depends on several parameters: physical dimensions of the nail, the type of nail-shank surface, depth of penetration into the fastening member, orientation of the wood fibers, wood moisture content, and the specific gravity of the wood. For a given nail and penetration depth, wood properties govern withdrawal resistance. For smooth, plain-shank nails, this resistance depends entirely on the frictional forces created during driving between the nail surface and the surrounding wood fibers. In general, nails driven into the side grain of dense, dry wood will provide the most resistance to axial forces. Withdrawal of the smooth, plain-shank nail occurs during axial loading when the frictional forces are exceeded (Ehlbeck, 1979). However, this friction is not constant over time, it will decrease. The relaxation of the wood fibers surrounding the nail and/or dimensional changes of wood during seasoning or cyclic moisture conditions cause a reduction of the frictional forces. The initial friction can be reduced by as much as four-fifths due to relaxation and/or seasoning (Stern et al., 1994). Therefore, smooth, plain-shank nails subjected to axial withdrawal forces immediately after driving will have a much higher resistance compared to nails pulled over time.

Because the axial withdrawal resistance of smooth, plain-shank nails is reduced due to seasoning or cyclic moisture conditions, the National Design Specification for Wood Construction (NDS, AFPA 1993) provides a 'wet service factor' (C_M). (The NDS is used as the reference design specification for this paper because other design codes such as the Eurocode were not available to the writers.) For smooth, plain-shank nails, a 75% reduction (C_M=0.25) is required for tabulated nominal withdrawal design values when green (moisture content (MC) $\geq$ 30%) or partially seasoned (19% < MC < 30%) lumber at the time of fabrication will dry (MC $\leq$ 19%) in-service, and when dry lumber will be subjected to cyclic moisture conditions (MC cycling between >19% and <19%). No reduction is necessary if wet lumber remains wet or dry lumber remains dry (i.e. C_M=1.0).

Even though the NDS recognizes a reduction in withdrawal resistance occurs due to shrinkage (i.e. decrease in moisture content), the specification assumes that all of this reduction occurs between the fiber saturation point and 19% MC. It is generally assumed that the dimensional change of wood as it progresses from a moisture content above the fiber saturation point to 0% follows a linear relationship. This relationship is displayed in Figure 1. As shown in Figure 1, as much shrinkage is assumed to occur above as below 19% MC. Therefore, the reduction in withdrawal resistance may also behave in the same fashion. The NDS does not recognize this possibility. Figure 2 illustrates the application of the NDS wet service factor to the tabulated nominal withdrawal design values for smooth, plain-shank nails. If a connection is fabricated with lumber above 19% and allowed to dry below 19% in-service, then a 75% reduction in allowable capacity must be taken. However, if a connection is assembled at 19% (which is the North American industry standard for kiln-dried lumber) and allowed to dry, no reduction is necessary (C_M=1.0). Most lumber for residential uses, especially roof systems, will achieve an in-service MC of approximately 6 - 12%. This is a significant reduction from 19% which is considered "dry". Thus, according to Figure 1, a significant dimensional change will also occur which should correspond to a significant loss in axial withdrawal resistance of smooth, plain-shank nails. As mentioned above, the NDS does not appear to recognize that such a reduction could take place at moisture contents below 19%.

OBJECTIVES

The purpose of this study was to provide experimental data on the relationship between variable moisture content and axial withdrawal resistance of smooth, plain-shank nails and compare this data to NDS design values. Also, the study is intended to provide data that simulates anticipated 'real-world' field conditions and provide data on the variability of smooth-shank nails when used in an "in-grade" condition. All previous experimental data concerning this subject (available to the writers) involved clear, straight-grained, matched specimens. Thus, the actual variability of nail withdrawal resistance values within a piece of lumber that contains knots, cross-grain, juvenile wood, and other associated wood growth irregularities is unknown. Therefore, the objectives of this experimental investigation were twofold:

(1) Determine the effect of changes in moisture content on the axial withdrawal strength of smooth, plain-shank nails, and compare the results to NDS design values, and

(2) Determine the variability of axial withdrawal strength within a single grade of lumber rather than small, clear specimens.

BACKGROUND

The subject of nails in wood connections and assemblies has been studied extensively. The ability of nails to resist axial withdrawal forces has been a large part of this research. Recently, Stern et al. (1994) summarized essentially all of the research conducted throughout the world during the past 50 years concerning this subject. This report includes information covering the physical, material, and mechanical properties of nails and staples, performance of nailed and stapled connections, methods for determining withdrawal resistance, influence of fabrication procedures, and proper fastening methods. The purpose of this section is to briefly summarize some of the results, conclusions, and recommendations made by Stern, et al. regarding smooth, plain-shank nails.

When a smooth, plain-shank nail is driven into a piece of wood, the friction created between the nail shank surface and surrounding wood fibers allows the connection to resist axial withdrawal forces. According to Stern et al.,

> "The ultimate axial withdrawal resistance of plain-shank nails is reached when the friction between the surface of these nails and the surrounding wood is exceeded by the axial withdrawal force. This results in fastener withdrawal and, during continued testing at a constant rate of withdrawal, in a slightly decreased withdrawal resistance when the friction is again overcome. This occurs again and again, as shown in [Figure 3], with the maximum withdrawal resistance decreasing with nail penetration decrease."

If the wood surrounding plain-shank nails experiences a reduction in moisture content or "seasons", the friction decreases significantly. "This loss may be as much as four-fifths of [the] initial withdrawal resistance .... if the fasteners were driven into green or only partially seasoned

wood. For this reason, plain-shank nails [and staples], designated to transmit structural forces, should never be loaded in withdrawal if driven into such wood. Yet, static axial load transmission by these fasteners is feasible if they are driven into dry wood which is not subject to shrinkage under service conditions." (Stern et al. 1994). Stern also mentions that cyclic changes in moisture content that cause repetitive shrinking and swelling of the wood will result in the backing out of plain-shank nails in-service. However, "driving such fasteners all the way through the fastening wood member, such as sheathing, can considerably reduce, if not eliminate, the occurrence of backing out of plain-shank fasteners." (Stern et al. 1994).

Stern et al. (1994) also discuss four methods for determining the withdrawal resistance design values of nails: (1) based on test data, (2) using empirically developed regression models, (3) using the NDS tabulated design values, and (4) using the ASME MH1.7M Standard fastener evaluation procedure. Because this report is primarily concerned with experimental data and the comparison of this data to NDS design values, only these methods will be discussed. Other international standards are available to make equivalent calculations.

NDS design values in capacity per inch penetration for nails resisting axial withdrawal forces are based on the following empirical formula that was developed by researchers at the US Forest Products Laboratory.

$$W = 1380\, G^{5/2}\, D$$

where, W is the normal (10 year) load duration nominal axial withdrawal design value in pounds per inch of penetration into the side grain of main member, G is the ovendry specific gravity of wood, and D is the fastener diameter (in.)

The method described above will provide the *nominal* withdrawal resistance design value for nails. Nominal values must be multiplied by all applicable adjustment factors to determine the allowable design value. These factors include: load duration (C_D), wet service (C_M), temperature (C_t), toe-nail (C_{tn}), preservatively-treated wood (C_p), and fire retardant-treated wood factor (C_r).

Stern et al. (1994) also provide several extensive experimental data sets for nails loaded in axial withdrawal. These data sets include information regarding fastener type, size, finish, and penetration depth and wood species, moisture content, specific gravity, and grain orientation. Also the mean ultimate axial withdrawal values for both immediate/delayed and constant/variable moisture contents are provided along with allowable design values for certain data sets. The data that is applicable and comparable to the data of this report is summarized and discussed below. However, all experimental data provided by Stern et al. (1994) and by all other previous researchers analyzing the axial withdrawal resistance of smooth, plain-shank nails is for clear, straight-grained matched specimens. As will be discussed below, this report tried to simulate anticipated field conditions and, therefore, may show some difference when compared to previous research.

EXPERIMENTAL METHODOLOGY

Design Parameters and Variables

The nails used for this experiment were 63.5 x 3.33 mm bright common purchased from a local hardware store. These are smooth, plain-shank nails with no applied surface coating.

The lumber was green (MC ≥ 30%), air-dry (19% < MC < 30%), or dry (MC ≤ 15%) #2 Southern pine 38 x 89 in either 2.4m or 3.0 m lengths, depending upon availability. The wood was

purchased from local saw mills which included all acceptable wood irregularities such as knots, wane, juvenile wood, etc. permitted by the grade designation "#2". All of the boards were visually graded as exclusively #2 by certified lumber graders, and no attempt was made to remove irregularities from the boards.

Six different moisture conditions were evaluated. The moisture content (%) at the time the nails were driven (fabricated) and at the time the nails were pulled (tested) were, respectively, as follows: (1) green → green, (2) green → 19, (3) green → 12, (4) 19 → 19, (5) 19 → 12, and (6) 12 → 12. To simulate anticipated field conditions, a relaxation and/or seasoning period of a minimum of 5 weeks was allowed between fabrication and testing. Previous test have shown that virtually all of the capacity loss due to fiber relaxation occurs within 5 weeks of manufacture.

The 'green' boards were maintained above the fiber saturation point between the time of purchase and time of fabrication by immersion in a water bath. To facilitate this procedure, the 2.4m boards were sawn into end-matched 1.2m lengths. After fabrication, boards requiring "seasoning" were allowed to air-dry in the laboratory to their respective MCs. Maintaining the 'green' and 19% MCs was accomplished by wrapping the boards in plastic with an occasional application of water mist. The 12% boards were placed in an environmental chamber that controls temperature and humidity corresponding to a constant MC of approximately 12%. All moisture contents were monitored daily between time of fabrication and testing with a Lignomat Lignomaster (model #G1000) electrical resistance moisture meter.

Samples of 10 boards per moisture condition (except green → green which had 9.5 boards) were used in the study. Nails were hand-driven to a penetration of two inches into the center of the narrow edge of the boards using a 50mm spacer block to simulate attaching 50mm plywood to the lumber. The nails were spaced 50mm from one end of the board and 100mm on center thereafter. No attempt was made to avoid growth characteristics such as knots, wane, etc.

The number of nails per board and per moisture condition along with the other variables mentioned above are summarized in Table 1.

Testing

Nail withdrawal tests were conducted in accordance with ASTM D 1761 requirements except for two aspects so that anticipated field conditions could be simulated. First, ASTM D 1761 requires that the wood be clear, straight-grained, and free of defects; as mentioned above this was not the case. Second, ASTM D 1761 also requires that the nails be cleaned in an alcohol or similar solution to remove any coatings or surface films as a result of manufacturing operations. Because this is highly unlikely to occur in the field, nails were used "straight-from-the-box". However, a comparison was performed between treated (rinsed in alcohol) and untreated (out-of-the-box) nails to quantify the difference, if any, that may occur in the maximum withdrawal resistance of such nails. The results of this comparison are discussed below.

Nails were pulled in tension using a MTS servo-hydraulic testing machine at a uniform rate of 2.5 mm/min. Maximum load was recorded directly from the testing machine.

Specific gravity (SG) and moisture content (MC) samples were obtained for each nail by machining an approximate 38 x 25 x 25 mm wood block adjacent to each nail hole. Ovendry specific gravity and moisture content were determined, respectively, in accordance with ASTM D 2016 and D 2395 procedures.

ANALYTICAL PROCEDURE

Censoring of Data

After testing was complete and moisture content determined, it was discovered that some of the ends of the 19% boards, especially the end-matched 1.2m lengths of the green → 19 condition, were significantly below 19% MC. This was deemed an "end-effect". Therefore, to minimize influence on the results, nails at the ends of such boards were censored from the data. In order to be consistent and symmetric, so variability along the length of one board could still be determined, nails were censored from both ends of the board even if one end was at an acceptable MC (19% ± 2%).

Summary Statistics

After censoring of the data due to the observed "end-effect", maximum load, moisture content, and specific gravity summary statistics were calculated for each board and each moisture condition. These statistics include: mean, median, mode, standard deviation, coefficient of variation (COV), skewness, minimum, maximum, and count. These are shown for each moisture condition in Table 2 and will be discussed below.

Comparing Means

In order to detect a difference between the maximum load means between each moisture condition, statistical two-sample t-tests assuming unequal variances were performed at a significance level = 0.05. The results are presented in Table 3 and discussed below. The P-values are reported for each test so the reader can make his/her own judgement if the results are significant. However, in general, if the P-value is less than the significance level, then the results are significant and a difference exists. And vice-versa, if the P-value is greater than the significance level, then the results are not significant and a difference may not exist.

NDS Design Values

The NDS design values shown in Table 4 were calculated using the empirical formula discussed above, the mean specific gravity for each moisture condition, nail diameter (D) of 3.33 mm, and a nail penetration depth = 50mm. A load duration factor of 1.6 was applied because maximum load was reached within five minutes, and depending on the moisture condition, the wet service factor was applied.

Factor-of-Safety of Allowable Design Values

A "factor-of-safety" was calculated by dividing the mean maximum test load data by the NDS allowable design value for each moisture condition. This "factor-of-safety" is a measure of the difference that exists between the results of this experiment and NDS design values. These results are shown in Table 4 and discussed below.

RESULTS and DISCUSSION

Effect of Variables on Withdrawal Resistance

Maximum load, moisture content, and specific gravity data for each moisture condition are summarized in Table 2. Mean maximum load comparisons for all possible moisture condition combinations were made using statistical two-sample t-tests for comparing means (assuming unequal variances, significance level = 0.05). The results of these comparisons are shown in Table 3. A significant difference between the mean maximum loads was found for every combination. This was expected because of the different moisture conditions being tested. However, it was expected that the 19 → 19 boards would have a higher mean maximum load than the green → green boards because the wood fibers are stiffer at 19% MC than above the fiber saturation point. Instead, green → green was significantly higher than 19 → 19. Corrosion of the nails was observed for the green → green boards and, thus, may have contributed to this unexpected difference. Stern (1969) discusses, "If the [smooth, plain-shank] nails should rust, however, their initial withdrawal resistance may be regained or even increased provided the wood around the nail shank is not chemically deteriorated by the rust in the presence of moisture."

For the boards tested at 19% MC (green → 19 and 19 → 19) it was generally observed that lower local MCs resulted in lower maximum loads while higher local MCs resulted in higher maximum loads. This trend was not observed for the green → green, green → 12, 19 → 12, and 12 → 12 boards. The possible reason that the boards tested at 12% MC did not show the same trend is the interaction of specific gravity, drying rates at knot location, and final moisture content. This trend should be expected because, as discussed above, when wood loses moisture it shrinks and this dimensional change causes a loss in withdrawal resistance for smooth, plain-shank nails. Therefore, increased moisture loss results in increased shrinkage which results in decreased withdrawal resistance. Because of the difficulty in maintaining 19% MC at all locations, this trend can be clearly seen in Figures 5 and 7. These figures show maximum load, moisture content, and specific gravity for each nail position along one representative board.

For all moisture conditions, there did not appear to be a significant relationship between maximum load and specific gravity. In general, a higher SG corresponds to a higher withdrawal resistance for clear wood. This was not always observed for this experiment as shown in Figures 4 - 9. The peaks in the SG graph usually correspond to location of knots. A higher SG occasionally corresponded to a higher P_{max} while at other times it did not; even if a nail was driven directly into a knot. The interaction of moisture content and seasoning with specific gravity and relaxation may have caused this unpredictable behavior.

Comparison of Mean Test Data to NDS Design Values

Mean maximum test load data were compared to NDS design values following the methods described above. As can be seen from Table 4, test data values are less conservative than the NDS design assumption of a factor of safety of 5.0 for every moisture condition tested. This data corresponds to the factor-of-safety (F.O.S.) calculations in Table 4. Every F.O.S. is less than the design code F.O.S. of five (1.2 / 6.0).

Currently, a 75% reduction is taken when green lumber at the time of fabrication will become dry (MC ≤ 19%) in-service. This reduction factor is slightly conservative as shown in Table 4 - only a 66% reduction was observed in this experiment. However, a 45% reduction was observed between the 19 → 19 and 19 → 12 moisture conditions. Also, because the F.O.S. for the 19 → 12 moisture condition is less than 1.0 this suggests failure will frequently occur. As mentioned above, the NDS does not require that the wet service factor be applied to the 19 → 12 moisture condition; the data in Table 4 suggest otherwise. The test results indicate that a moisture reduction factor of 0.50 is in order for nail connections fabricated at 19% MC and allowed to dry to less than 12% MC.

There are possible reasons for the observed discrepancy between test data and NDS design values. Corrosion of nails in the green → green boards and/or the difficulty in maintaining 19% MC may have played a small role. But these are factors that are likely to be seen in-service and which NDS design values should account for. However, the authors cannot be sure but have consulted with American Forest and Paper Association (AFPA) and Forest Products Laboratory (FPL) representatives to determine likely reasons for the difference (Line, 1995 and Winnistoipher, 1995). First, NDS design values are based on short-term tests, i. e.. the nails were pulled immediately after driving - no conditioning period to allow for relaxation. As mentioned above, smooth, plain-shank nails subjected to axial withdrawal forces immediately after driving will have a much higher resistance compared to nails pulled over time. A relaxation and/or seasoning period of a minimum of five weeks was allowed between fabrication and testing in this experiment. Second, the experiments in this study were performed using full-size, on-grade #2 lumber with nails spaced four inches on-center regardless of knots and other growth characteristics. NDS design values are based on experimental tests performed on small, clear, straight-grained specimens. Therefore, allowing for relaxation and/or seasoning, and using actual lumber may have caused the test data design values to be lower than the NDS design values. A third factor may have been that the tests used as the basis for the NDS allowable loads used alcohol washed nails while this investigation used untreated nails.

It is the writers' opinions that the tests performed in the study are more likely to represent actual field conditions versus tests which form the basis for the NDS. There are four approaches that could be taken to correct for the observed differences: (1) If the design code F.O.S. of five (1.2 / 6.0) and current method of handling MC change (i. e.. one reduction factor) are desirable, then the nominal axial withdrawal values for smooth, plain-shank nails must be lowered by the range of ratios shown in Table 4, (2) A second range of wet service factors could be introduced such that a 75% reduction is taken when green or unseasoned lumber dries below 19% MC (current method), a 50% reduction when 15 - 19% MC lumber dries below 12% MC in-service (proposed addition), and 0% reduction for when lumber initially is less than 15% MC and will remain below 15% MC, (3) The moisture content requirement for kiln-dried lumber could be lowered to 15% rather than 19% as it is today, or (4) helically threaded or ring shank nails could be required for situations governed by withdrawal resistance.

Variability of Maximum Load Data

Table 2 displays the overall maximum load COV for each moisture condition while Figures 4 - 9 display representative COVs for representative boards of each moisture condition. The effects of moisture content and specific gravity on maximum load have been discussed above. ASTM D 1761 mentions, "general experience indicates that the COV from tests of fasteners ranges from about 15 - 30%". As seen from Table 2, the overall maximum load COVs fall in this range.

Therefore, according to ASTM D 1761, the variability observed in this experiment for maximum load was in the expected range of values. However, one objective of this experiment was to determine and report the variability of withdrawal resistance along the length of one board or within an actual piece of lumber and within a given grade of lumber because no such data exists. This variability is displayed in Figures 4-9 and Table 2 for each moisture condition.

CONCLUSION

Experimental tests were performed to determine the effect of changes in moisture content on the axial withdrawal strength of smooth, plain-shank nails. The variability of axial withdrawal strength within a piece of lumber and within a specific grade was also determined. Tests were designed to simulate anticipated field conditions and to evaluate NDS design procedures. Based on the tests conducted, the following conclusions can be drawn:

- Design values based on test results are much lower than corresponding NDS design values; delayed testing, actual lumber, and untreated nails may partially explain this difference.

- A significant amount of variability of maximum load was observed within moisture conditions and along length of boards for given moisture content.

- Mean test capacities for each moisture condition were all significantly different from one another.

- No significant relationship was observed between maximum load and specific gravity.

- Difficulty in maintaining 19% moisture content and corrosion of nails in 'green' boards may have influenced the results.

It is recommended that the NDS allowable withdrawal loads for plain, smooth-shank nails be modified by either (a) reducing the nominal values by as much as 75%, (b) a second moisture adjustment factor be introduced for connections manufactured at 19% moisture content and subsequently dry to 12% or less, (c) dry lumber to a maximum moisture content of 15% rather than the current 19%, or (d) require helically threaded of ring shank nails be used for resisting withdrawal forces.

REFERENCES

American Forest and Paper Association (AFPA). 1993. "ANSI/NoPA NDS 1991. National Design Specification for Wood Construction." AFPA. Washington, D.C.

American Society for Testing and Materials (ASTM). 1993. "Standard Test Methods for

Mechanical Fasteners in Wood." ASTM D 1761. ASTM. Philadelphia, PA.

Ehlbeck, J. 1979. "Nailed Joints in Wood Structures." Virginia Polytechnic Institute and State University, Wood Research and Wood Construction Laboratory, Bulletin No. 166, VPI & SU, Blacksburg, VA.

Line, P. 1995. Personal communication with American Forest and Paper Association representative.

Stern, E.G. 1969. "Mechanical Fastening of Southern Pine - A Review." Virginia Polytechnic Institute and State University, Wood Research and Wood Construction Laboratory, Bulletin No. 87, VPI & SU, Blacksburg, VA.

Stern, E.G., Loferski, J.R., Dolan, J.D. 1994. "Performance of Nails and Staples in Resisting Axial Withdrawal Forces." Department of Wood Science and Forest Products, VPI & SU, Blacksburg, VA.

Winnistoipher, S. 1995. Personal communication with U.S. Forest Products Laboratory representative.

Table 1. Summary of test variables and design parameters.

MC % at fabrication	date of fabrication	MC % at test	days conditioned	# of boards	# of nails per board	total # of nails
* green	9/13/94	green	40	9.5	24	228
* green	9/14/94	19	45	10	24	240
* green	9/14/94	12	93	10	24	240
19	9/21/94	19	50	10	24	240
19	9/21/94	12	53	# 10	24 - 30	276
12	9/13/94	12	94	10	23	230
					TOTAL:	1454

* Cut into 1.2m end-matched lengths to facilitate conditioning.
\# Four 2.4m and six 3.0m boards

Other variables and design parameters:

- 63.5 x 3.33 mm common nails, bright
- #2 Southern Pine, 38 x 89 mm in either 2.4m or 3.0 m lengths
- nails were hand-driven 50 mm into the center of the narrow edge of board using a 50 mm spacer to simulate 50 mm plywood
- nails spaced 50 mm from end of board and every 100 mm thereafter

Table 2. Summary statistics of test data (after censoring).

	MOISTURE CONDITIONS								
	grn => grn			grn => 19			grn => 12		
	Pmax (N)	MC %	ovendry SG	Pmax (N)	MC %	ovendry SG	Pmax (N)	MC %	ovendry SG
mean	1108	95.3	0.53	621	19.2	0.56	378	13.8	0.51
std. error	12.3	1.901	0.005	8.5	0.093	0.005	5.5	0.043	0.004
median	1105	95.7	0.51	619	19.2	0.54	375	13.9	0.49
mode	1087	94.0	0.49	625	19.3	0.51	286	14.0	0.48
stand. dev.	184	28.3	0.08	117	1.3	0.07	86	0.7	0.07
COV %	16.6	29.7	15.30	18.9	6.7	12.70	22.7	4.9	13.66
skewness	0.155	-0.110	1.840	0.165	0.345	1.069	0.218	-1.065	2.183
minimum	533	25.2	0.39	335	15.4	0.44	153.8	11.1	0.41
maximum	1650	168.5	0.92	1109	22.5	0.91	685.1	15.2	0.85
count	222	222	222	190	190	190	240	240	240
	MOISTURE CONDITIONS								
	19 => 19			19 => 12			12 => 12		
	Pmax (N)	MC %	ovendry SG	Pmax (N)	MC %	ovendry SG	Pmax (N)	MC %	ovendry SG
mean	791	20.0	0.52	441	13.8	0.52	1009	12.5	0.52
std. error	18.1	0.178	0.006	7.9	0.036	0.005	15.1	0.092	0.004
median	800	20.8	0.51	421	13.8	0.51	1013	12.1	0.51
mode	926	20.8	0.54	343	13.7	0.54	965	11.6	0.49
stand. dev.	264	2.6	0.08	130	0.6	0.08	229	1.4	0.06
COV %	33.3	13.0	15.80	29.5	4.4	14.90	22.7	11.1	11.68
skewness	0.146	-0.850	2.100	0.876	-1.401	2.628	0.476	0.464	1.102
minimum	261	12.3	0.40	156	10.6	0.41	563	9.7	0.40
maximum	1569	23.7	0.94	901	15.2	1.01	1940	16.1	0.74
count	213	213	213	273	273	273	230	230	230

Table 3. Maximum load comparisons for all possible moisture condition combinations using statistical two-sample t-tests asssuming unequal variances. (all values in imperial units (lbs and inches))

significance level = 0.05

If the P-value is less than the significance level, then the results are significant and a difference exists.

	gm => gm	*gm => 19*
Mean	249.27	139.58
Variance	1705.14	693.87
Observations	222.00	190.00
Pooled Variance	2356.42	
df	411.00	
t	28.17	
P(T<=t) one-tail	***0.00***	
t Critical one-tail	1.65	
P(T<=t) two-tail	***0.00***	
t Critical two-tail	1.97	

	gm => 19	*12 => 12*
Mean	139.58	226.87
Variance	693.87	2659.57
Observations	190.00	230.00
Pooled Variance	1770.78	
df	354.00	
t	-22.38	
P(T<=t) one-tail	***0.00***	
t Critical one-tail	1.65	
P(T<=t) two-tail	***0.00***	
t Critical two-tail	1.97	

	gm => gm	*gm => 12*
Mean	249.27	85.09
Variance	1705.14	372.39
Observations	222.00	240.00
Pooled Variance	1012.69	
df	308.00	
t	54.04	
P(T<=t) one-tail	***0.00***	
t Critical one-tail	1.65	
P(T<=t) two-tail	***0.00***	
t Critical two-tail	1.97	

	gm => 12	*19 => 19*
Mean	85.09	177.89
Variance	372.39	3513.71
Observations	240.00	213.00
Pooled Variance	1849.02	
df	252.00	
t	-21.85	
P(T<=t) one-tail	***0.00***	
t Critical one-tail	1.65	
P(T<=t) two-tail	***0.00***	
t Critical two-tail	1.97	

	gm => gm	*19 => 19*
Mean	249.27	177.89
Variance	1705.14	3513.71
Observations	222.00	213.00
Pooled Variance	2590.63	
df	377.00	
t	14.52	
P(T<=t) one-tail	***0.00***	
t Critical one-tail	1.65	
P(T<=t) two-tail	***0.00***	
t Critical two-tail	1.97	

	gm => 12	*19 => 12*
Mean	85.09	99.13
Variance	372.39	857.71
Observations	240.00	273.00
Pooled Variance	630.72	
df	475.00	
t	-6.48	
P(T<=t) one-tail	***0.00***	
t Critical one-tail	1.65	
P(T<=t) two-tail	***0.00***	
t Critical two-tail	1.96	

	gm => gm	*19 => 12*
Mean	249.27	99.13
Variance	1705.14	857.71
Observations	222.00	273.00
Pooled Variance	1237.59	
df	386.00	
t	45.64	
P(T<=t) one-tail	***0.00***	
t Critical one-tail	1.65	
P(T<=t) two-tail	***0.00***	
t Critical two-tail	1.97	

	gm => 12	*12 => 12*
Mean	85.09	226.87
Variance	372.39	2659.57
Observations	240.00	230.00
Pooled Variance	1491.55	
df	290.00	
t	-39.15	
P(T<=t) one-tail	***0.00***	
t Critical one-tail	1.65	
P(T<=t) two-tail	***0.00***	
t Critical two-tail	1.97	

	gm => gm	12 => 12
Mean	249.27	226.87
Variance	1705.14	2659.57
Observations	222.00	230.00
Pooled Variance	2190.84	
df	435.00	
t	5.11	
P(T<=t) one-tail	***0.00***	
t Critical one-tail	1.65	
P(T<=t) two-tail	***0.00***	
t Critical two-tail	1.97	

	19 => 19	19 => 12
Mean	177.89	99.13
Variance	3513.71	857.71
Observations	213.00	273.00
Pooled Variance	2021.08	
df	292.00	
t	17.77	
P(T<=t) one-tail	***0.00***	
t Critical one-tail	1.65	
P(T<=t) two-tail	***0.00***	
t Critical two-tail	1.97	

	gm => 19	gm => 12
Mean	139.58	85.09
Variance	693.87	372.39
Observations	190.00	240.00
Pooled Variance	514.35	
df	336.00	
t	23.89	
P(T<=t) one-tail	***0.00***	
t Critical one-tail	1.65	
P(T<=t) two-tail	***0.00***	
t Critical two-tail	1.97	

	19 => 19	12 => 12
Mean	177.89	226.87
Variance	3513.71	2659.57
Observations	213.00	230.00
Pooled Variance	3070.18	
df	422.00	
t	-9.24	
P(T<=t) one-tail	***0.00***	
t Critical one-tail	1.65	
P(T<=t) two-tail	***0.00***	
t Critical two-tail	1.97	

	gm => 19	19 => 19
Mean	139.58	177.89
Variance	693.87	3513.71
Observations	190.00	213.00
Pooled Variance	2184.66	
df	300.00	
t	-8.54	
P(T<=t) one-tail	***0.00***	
t Critical one-tail	1.65	
P(T<=t) two-tail	***0.00***	
t Critical two-tail	1.97	

	19 => 12	12 => 12
Mean	99.13	226.87
Variance	857.71	2659.57
Observations	273.00	230.00
Pooled Variance	1681.32	
df	349.00	
t	-33.31	
P(T<=t) one-tail	***0.00***	
t Critical one-tail	1.65	
P(T<=t) two-tail	***0.00***	
t Critical two-tail	1.97	

	gm => 19	19 => 12
Mean	139.58	99.13
Variance	693.87	857.71
Observations	190.00	273.00
Pooled Variance	790.54	
df	432.00	
t	15.52	
P(T<=t) one-tail	***0.00***	
t Critical one-tail	1.65	
P(T<=t) two-tail	***0.00***	
t Critical two-tail	1.97	

Table 4. Ratios of mean test data vs. NDS (AFPA, 1993) allowable design values ("factor-of-safety", F.O.S.)

(1) moisture condition change (%)	(2) mean test data (N)	(3) NDS allowable design values (N)	(4) F.O.S. (2) / (3)
grn => grn	1107	525	2.1
grn => 19	622	151	4.1
grn => 12	378	120	3.1
19 => 19	791	498	1.6
19 => 12	440	498	0.9
12 => 12	1009	498	2.0

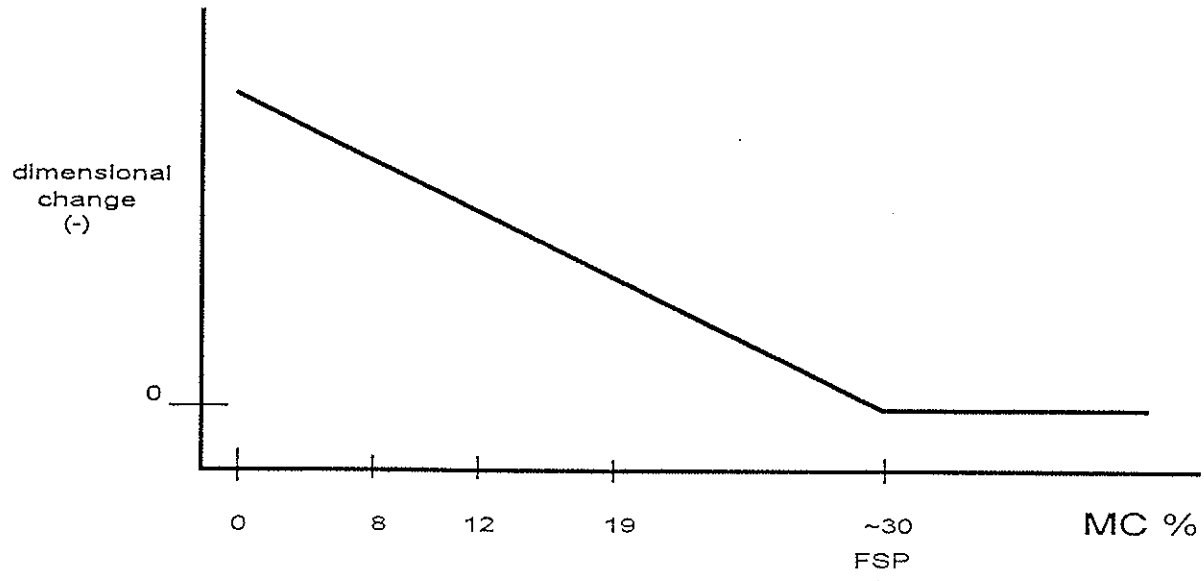

Figure 1. The assumed dimensional change (-) of wood as it progresses from a moisture content above the FSP to 0% moisture content.

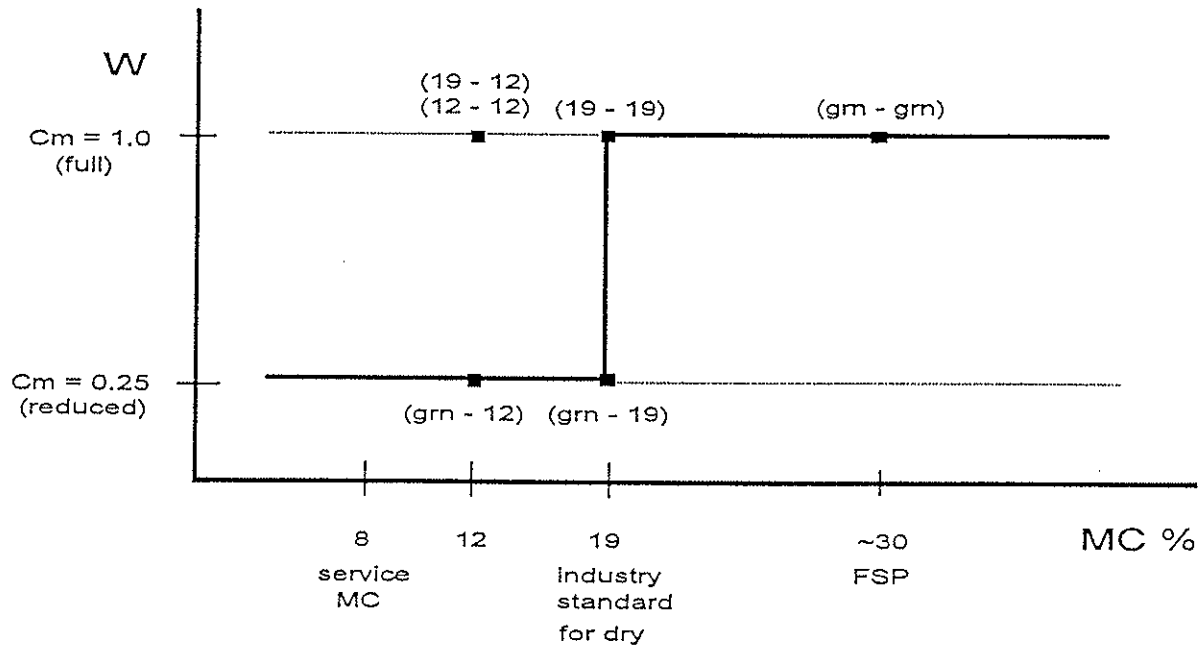

Figure 2. Application of the NDS (AFPA, 1993) "wet service factor (Cm)" to nominal withdrawal design values for plain-shank nails.

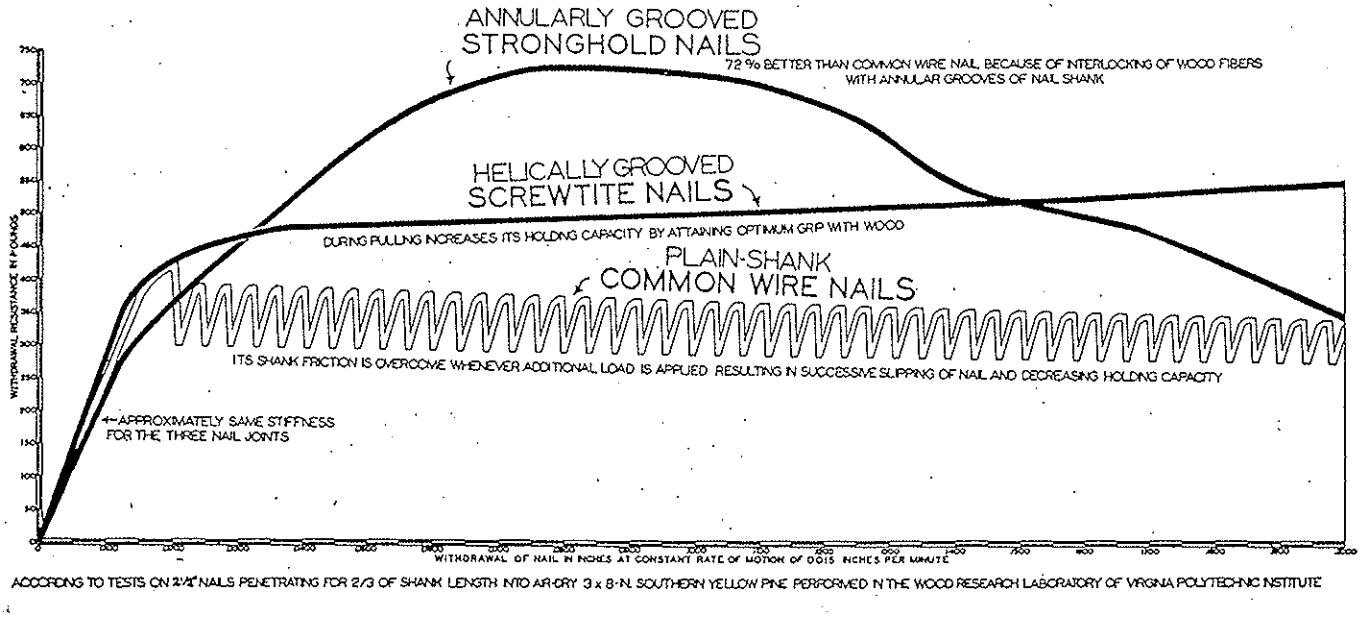

Figure 3. Relationship between withdrawal resistance and axial withdrawal of 2 1/2" x 0.135" low-carbon-steel plain-shank, helically grooved Screwtite, and annularly Stronghold nails (Stern et al. 1994).

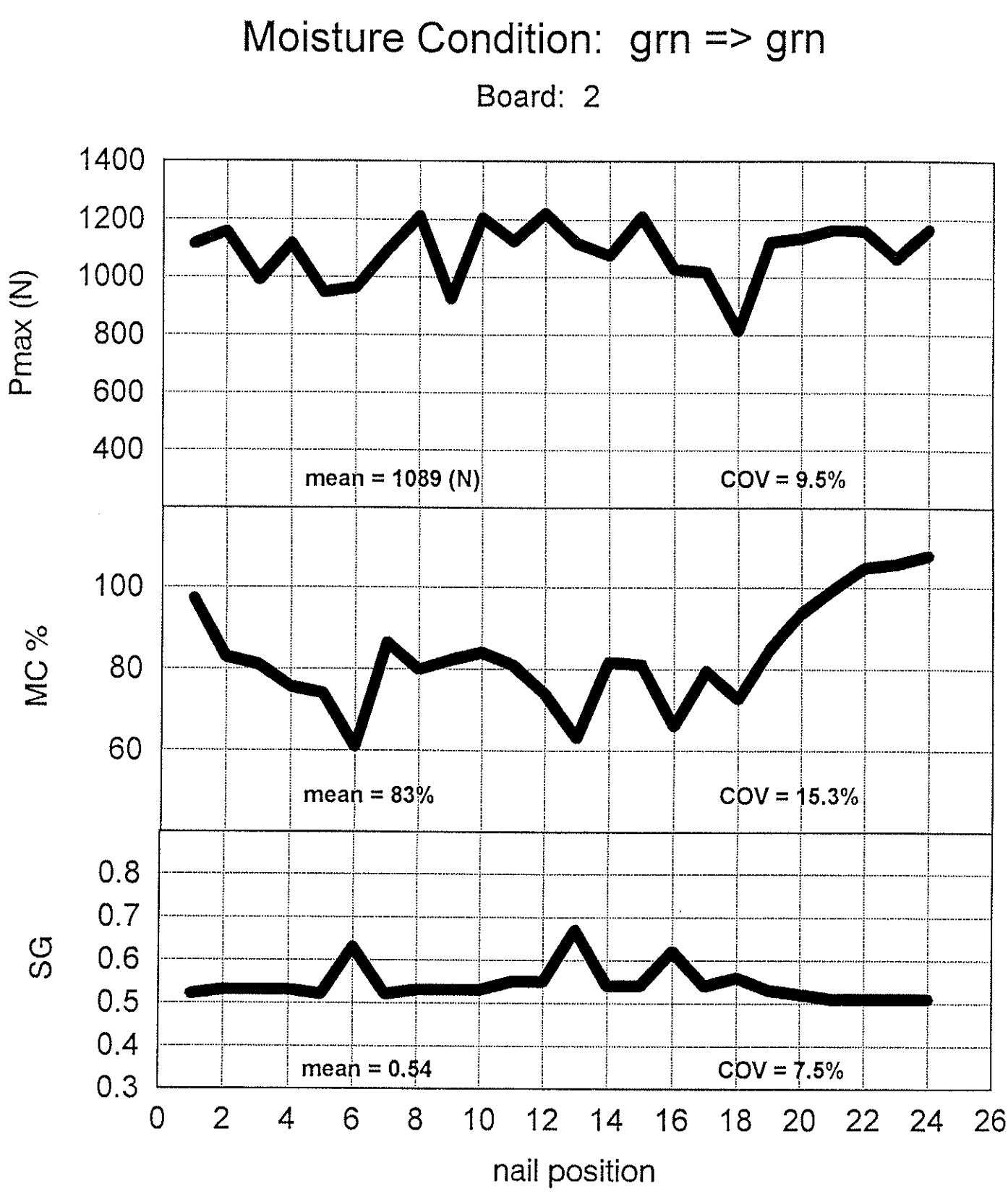

Figure 4. Representative board from the green - green moisture condition showing Pmax, MC, and SG relationship with respect to nail position along length of board.

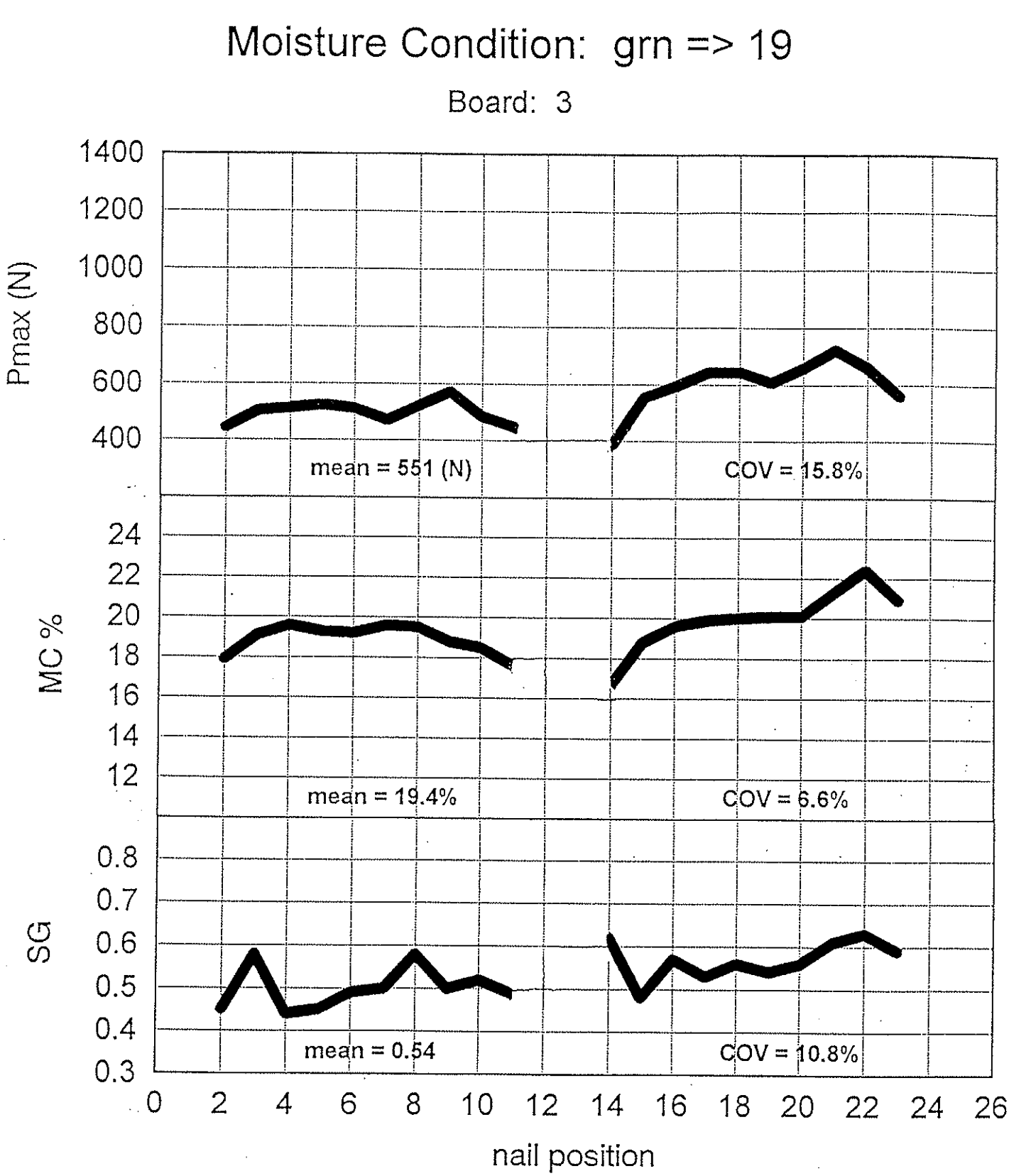

Figure 5. Representative board from the green - 19 moisture condition showing Pmax, MC, and SG relationship with respect to nail position along length of board.

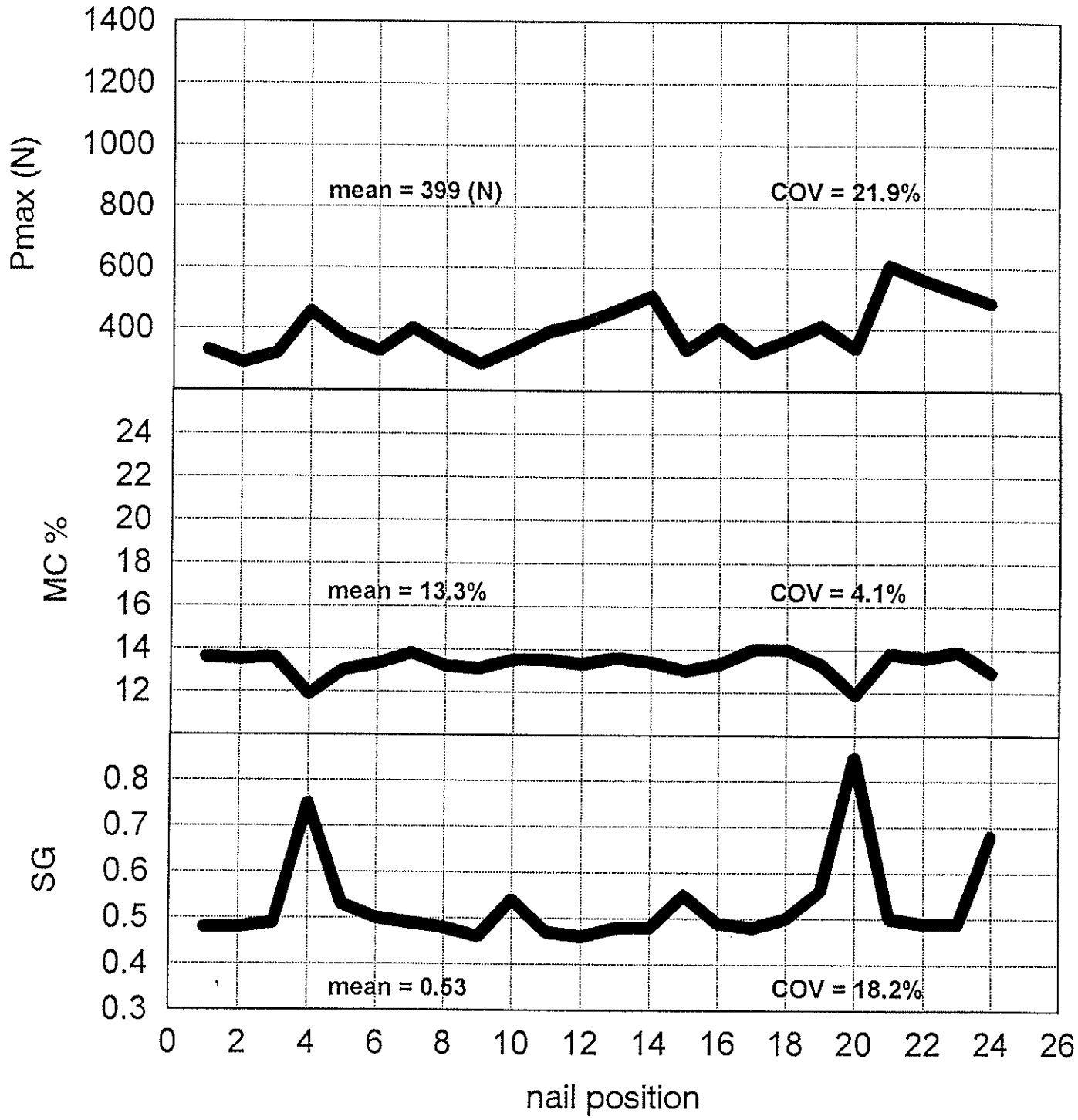

Figure 6. Representative board from the green - 12 moisture condition showing Pmax, MC, and SG relationship with respect to nail position along length of board.

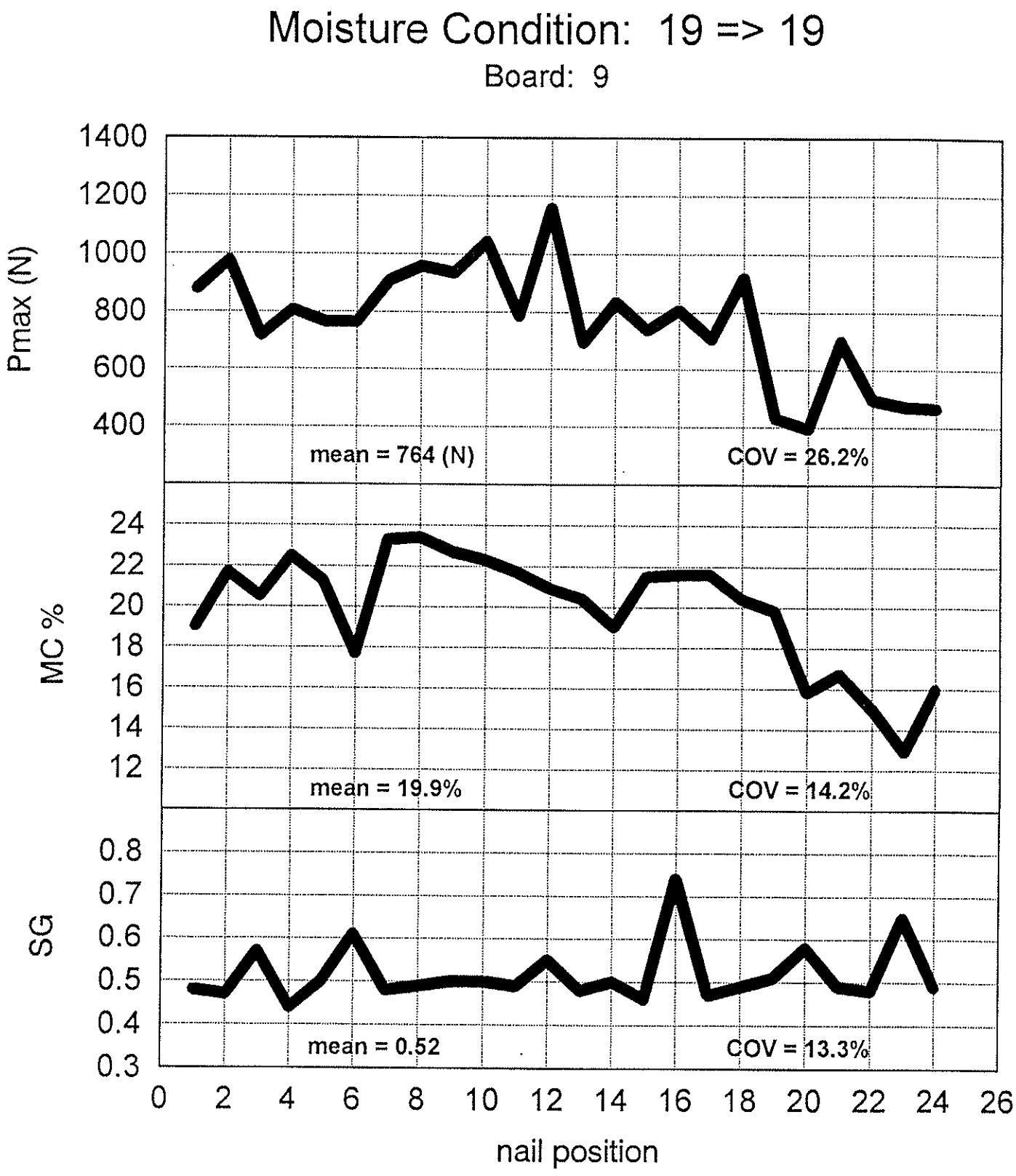

Figure 7. Representative board from the 19 - 19 moisture condition showing Pmax, MC, and SG relationship with respect to nail position along length of board.

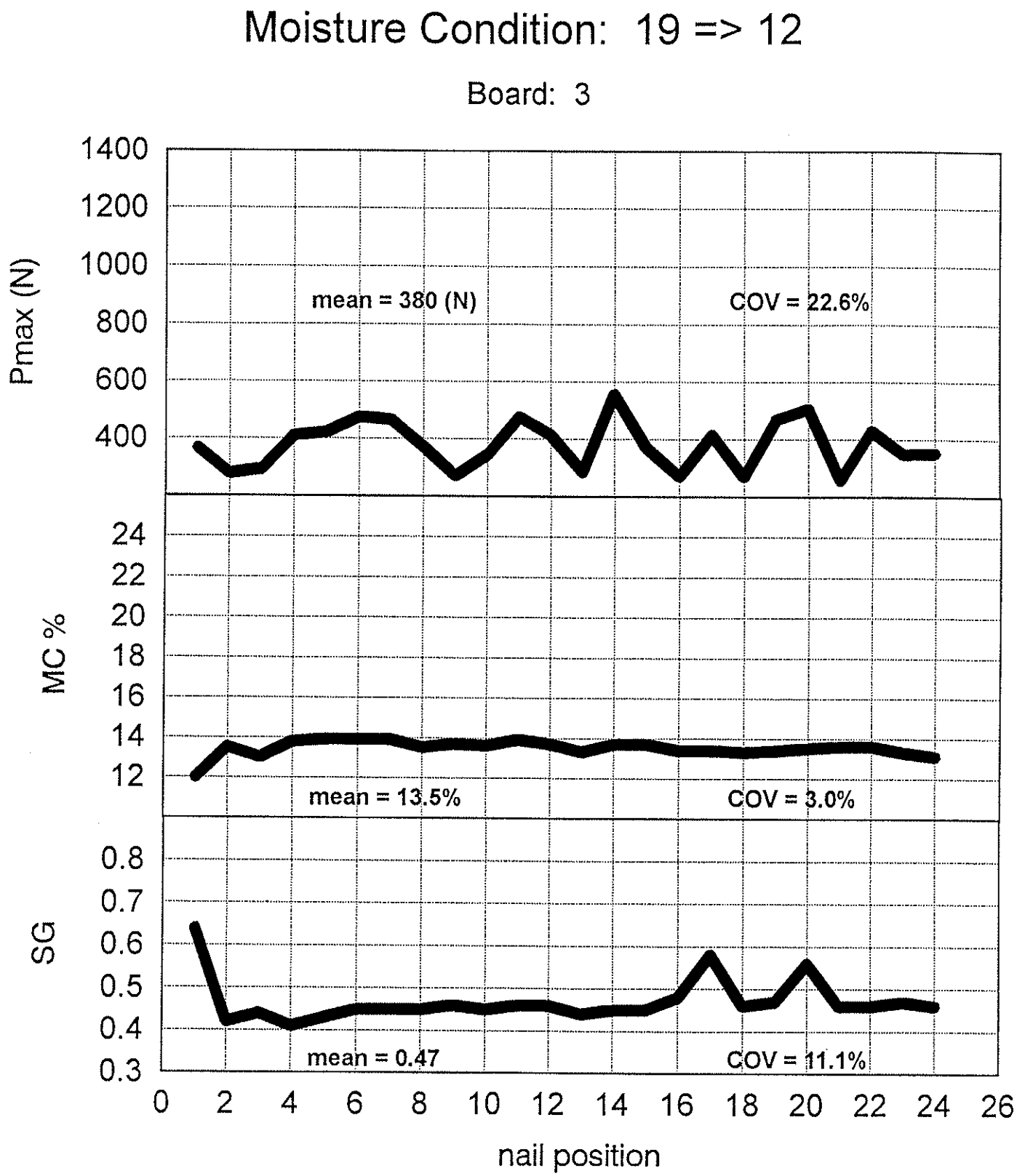

Figure 8. Representative board from the 19 - 12 moisture condition showing Pmax, MC, and SG relationship with respect to nail position along length of board.

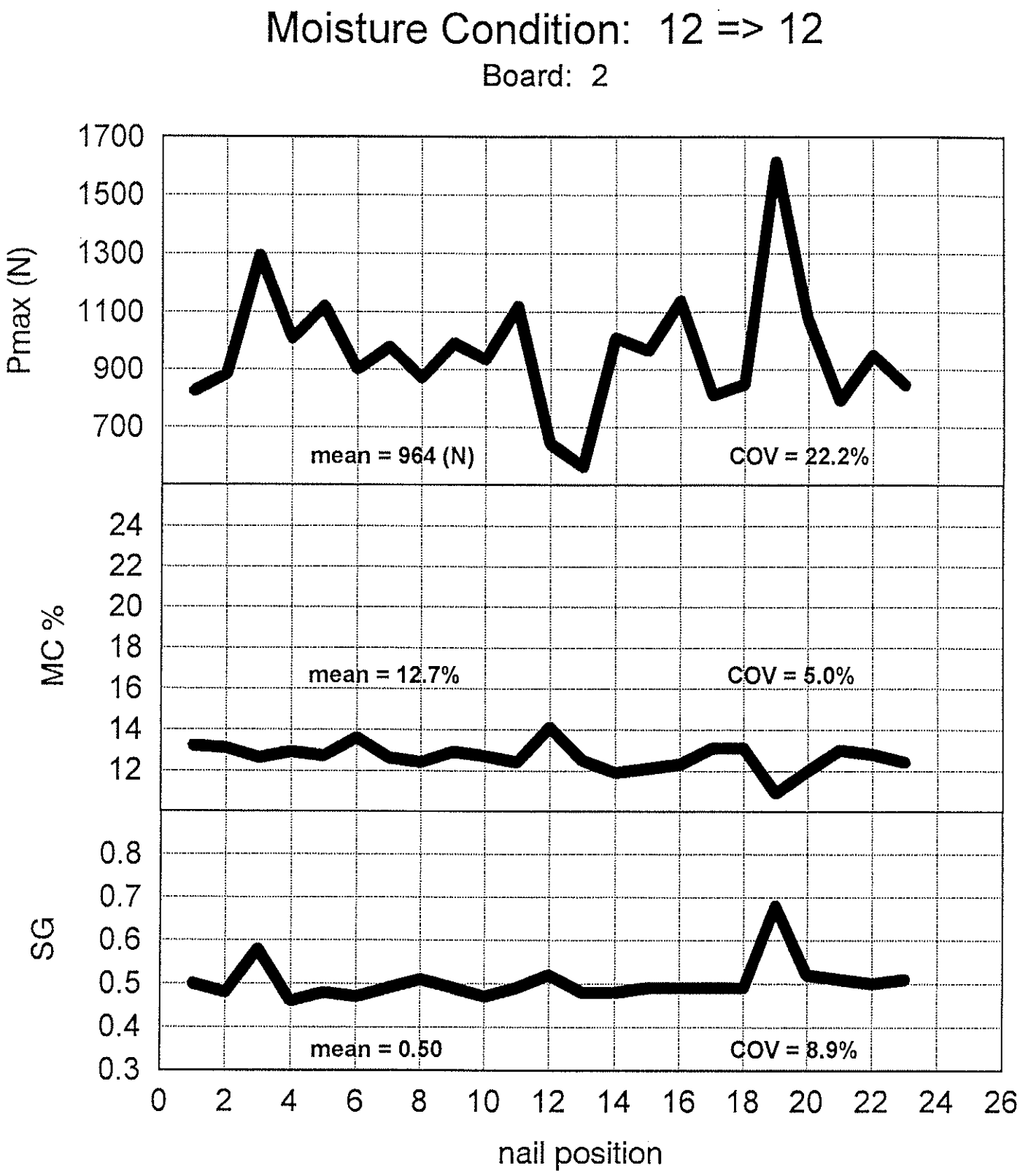

Figure 9. Representative board from the 12 - 12 moisture condition showing Pmax, MC, and SG relationship with respect to nail position along length of board.

INTERNATIONAL COUNCIL FOR BUILDING RESEARCH STUDIES AND DOCUMENTATION

WORKING COMMISSION W18 - TIMBER STRUCTURES

NAIL PLATE CAPACITY IN JOINT LINE

by

A Kevarinmäki
Helsinki University of Technology
J Kangas
Technical Research Centre of Finland
Finland

MEETING TWENTY - EIGHT

COPENHAGEN

DENMARK

APRIL 1995

1. INTRODUCTION

Eurocode 5 design method for the nail plate capacity of joint line is a translated version of the Norwegian design rules (AASHEIM & SOLLI 1990). The theory was first time presented by NORÈN (1981). BOVIM and AASHEIM presented a paper (1985) where they made comparisons between measured and calculated values of plate strength of nail plates. Their conclusion was that the design method presented gave a good prediction of the plate strength, but only a Gang Nail 18 plate was used in this comparison.

In order to elucidate if the design method can be used for any nail plate, the results from testing of 6 different nail plates were compared with the theory by KÄLLSNER and KANGAS (1991). Their conclusion was that the agreement between the measured and the theoretical capacity values in tension is mostly rather good but somewhat varying: the biggest difference was about 30 %. Also in shear the agreement was acceptable with the plate types where the nail holes were more or less in a staggered arrangement. In the case of plates, where the nail holes have been punched to straight lines also in y-direction, perpendicular to the main axes of the nail plate, the theory overestimates clearly the shear capacities, when the angle α is about 30 (tension-shear) or 135 (compression-shear) degrees. Otherwise the theory underestimates the shear capacities of this kind of plates in range $45° < \alpha < 75°$.

The reason for this quite poor agreement described above is in the big differences between the shear strength values in x- and y-directions of the actual type of nail plates and also in the nail plate buckling of certain shear loading directions. The double orthogonal punched ("diagonal") type plates have quite small difference between $f_{v,0}$ and $f_{v,90}$ values, while the plates with orthogonal location of nail lines have naturally a weak shear strength in $\alpha = 90°$ direction due to bending of the narrow strips between the nail holes over the joint line. Already small inclination between the plate and joint line increases clearly the shear capacity, when the joint line does not any more go through the same nail hole row. The calculation model is based on the theory of the orthotropic material, which assumption is not valid for the "single orthogonal" nail plate type, where especially the strength properties vary in the y-direction depending on the situation of the x-direction points.

2. EUROCODE 5 METHOD

The plate capacity has conventionally been designed using tabled strength values given separately for tension, compression and shear. So the loads have always had to be

distributed to components: one parallel to the joint line (shear), and other perpendicular to the joint line (normal force). The moment in the joint line or the combination effect of the shear and normal forces have not normally been taken into account in this separate strength verification. The plate design method of Eurocode 5 has been given by rather simple formulas, where simultaneously the stresses from the compression, tension, shear and moment are taken into account. The other benefit of EC5 method is that all strength distributions may be calculated by the strength values of main axes, so the number of required characteristic plate strength properties is much lower than with the conventional methods. However, the plate strength test results are needed also in other loading directions for verification of the theory and its remodifying.

In Eurocode 5 the plate forces are calculated in the two main directions for each straight part of the joint line:

$$F_x = F\cos\alpha \pm 2F_M \sin\gamma \tag{1}$$

$$F_y = F\sin\alpha \pm 2F_M \cos\gamma \tag{2}$$

where F is the resultant direct force per plate on the joint,

F_M is the force from the joint line moment M per plate according to the plastic theory ($F_M = 2M/l$) (*Figure 1*),

α is the angle between the x-direction and the force F,

γ is the angle between the x-direction and the joint line and

l is the length of the plate along the straight part of the joint line.

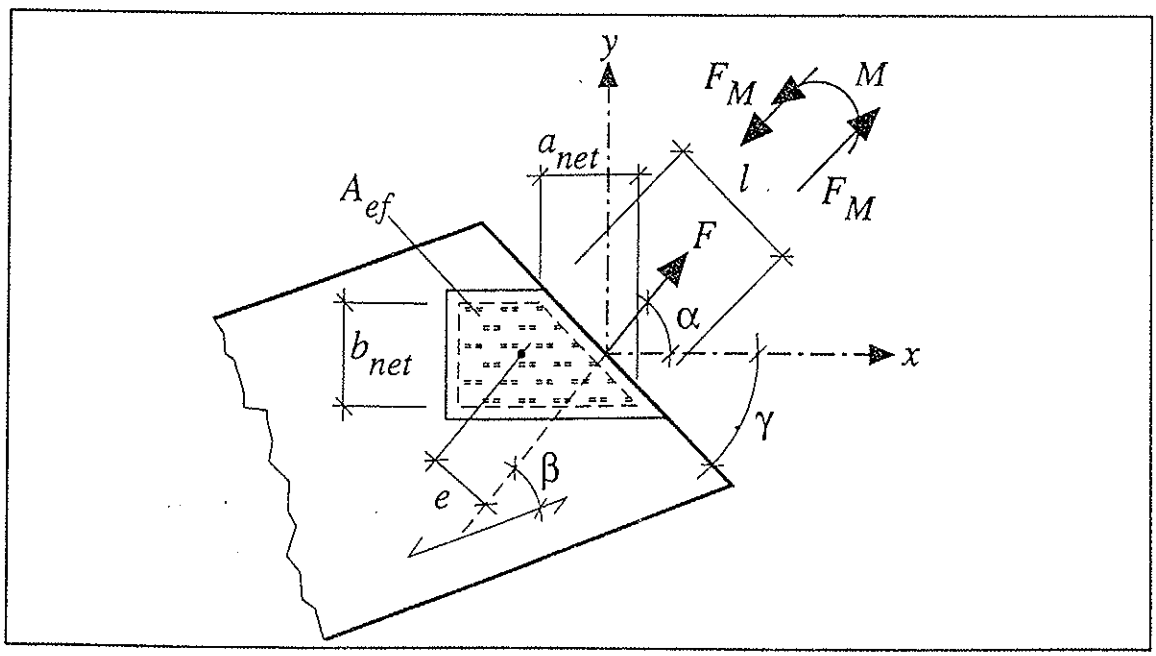

Figure 1. Punched metal plate fastener joint - Geometry and loading (WHALE, 1995).

In design the following condition should be satisfied:

$$\left(\frac{F_{x,d}}{R_{x,d}}\right)^2 + \left(\frac{F_{y,d}}{R_{y,d}}\right)^2 \leq 1 \qquad (3)$$

The design values of the plate capacity, $R_{x,d}$ and $R_{y,d}$ in the x- and y-directions, are calculated according to the following formulas:

$$R_{x,d} = \max \begin{cases} f_{n,0,d}\, \ell \sin\gamma : & f_{n,0,d} = \begin{cases} f_{t,0,d} & \text{if } F_x \text{ is tension} \\ f_{c,0,d} & \text{if } F_x \text{ is compression} \end{cases} \\ f_{v,0,d}\, \ell \cos\gamma \end{cases} \qquad (4)$$

$$R_{y,d} = \max \begin{cases} f_{n,90,d}\, \ell \cos\gamma : & f_{n,0,d} = \begin{cases} f_{t,90,d} & \text{if } F_y \text{ is tension} \\ f_{c,90,d} & \text{if } F_y \text{ is compression} \end{cases} \\ f_{v,90,d}\, \ell \sin\gamma \end{cases} \qquad (5)$$

where $f_{t,0,d}$ is the design tension capacity per unit width of the plate in the x-direction ($\alpha = 0°$),

$f_{c,0,d}$ is the design compression capacity per unit width of the plate in the x-direction ($\alpha = 0°$),

$f_{v,0,d}$ is the design shear capacity per unit width of the plate in the x-direction

$f_{t,90,d}$ is the design tension capacity per unit width of the plate in the y-direction ($\alpha = 90°$),

$f_{c,90,d}$ is the design compression capacity per unit width of the plate in the y-direction ($\alpha = 90°$) and

$f_{v,90,d}$ is the design shear capacity per unit width of the plate in the y-direction

This design method is based on the plastic behaviour of nail plate in the joint line. Finding out the most economical plastic stress distribution requires a separate calculation program for the cases, when the plate covers several joints so that equilibrium is fulfilled and the condition in equation (3) is satisfied in each straight part of the joint line.

All simplifications to determine the force F and moment M of each straight part are on the safe side, when the equilibrium condition is satisfied, because Eurocode 5 allows the fully plastic situation ($F_M = 2M/\ell$). One possibility is to calculate the joint line stresses according to the elastic theory, so that the joint line stiffnesses are directly proportional to the plate strength values of the actual loading direction. The using of elastic theory to the plate design has been presented by POUTANEN (1994). Anyhow the elastic theory leads to bigger nail plate sizes than the optimal use of the method of Eurocode 5.

3. PROPOSAL TO DIMINISH THE OVER- AND UNDERESTIMATION OF EC5 METHOD IN PLATE SHEAR CAPACITY

The comparisons between test results and EC5 method have shown that Eurocode 5 may not be solved in the case of the "orthogonal" nail plates, 1) without the clear overestimation of shear capacity on certain ranges of both tension and compression shear when the nail plate buckling is governing, and 2) otherwise without clear underestimation of shear capacity on the area $45° < \alpha < 90°$. One possible method to eliminate these over- and underestimation's is presented on the following. It has been made so that two additional terms, added to Eurocode equations, would effect on capacities only on needed ranges.

The overestimation is eliminated by equation (6), where the buckling has been taken into account by the axial strength reduction. For the determination of the reduction parameter γ_0 at least shear test series in the point $\alpha = 30°$ are needed.

The underestimated values may be increased to the acceptable level by the equation (7), where the plate shear capacity depending on the y-direction shear strength is increased between loading angles $45° < \alpha < 90°$ by the coefficient k_v. The value of coefficient k_v is determined for the actual type of nail plate by at least two shear test series between α angles 45° and 85°.

In the cases of the nail plates with orthogonal location of nail rows equations (4) and (5) are replaced by following equations:

$$R_{x,d} = \max \begin{cases} f_{n,0,d}\, l \sin(\gamma - \gamma_0 \sin(2\gamma)) : & f_{n,0,d} = \begin{cases} f_{t,0,d} & \text{if } F_x \text{ is tension} \\ f_{c,0,d} & \text{if } F_x \text{ is compression} \end{cases} \\ f_{v,0,d}\, l \cos\gamma \end{cases} \qquad (6)$$

$$R_{y,d} = \max \begin{cases} f_{n,90,d}\, l \cos\gamma : & f_{n,0,d} = \begin{cases} f_{t,90,d} & \text{if } F_y \text{ is tension} \\ f_{c,90,d} & \text{if } F_y \text{ is compression} \end{cases} \\ k\, f_{v,90,d}\, l \sin\gamma : & k = \begin{cases} 1 + k_v \sin(2\gamma) & \text{if } F_x \text{ is tension} \\ 1 & \text{if } F_x \text{ is compression or zero} \end{cases} \end{cases} \qquad (7)$$

where γ_0 and k_v are the constants determined for the actual type of nail plate by shear tests.

The value of constant $\gamma_0 \geq 0°$ is determined so that the plate strength, in case of pure shear in loading direction $\alpha = 30°$, calculated according to equations (6), (5) and (3) by

the mean strength values of the main axes, is equal with the test results in the corresponding case. The relative effect of equation (6) to the plate strength of EC5 is highest in the shear loading when the direction α is about 30 degrees. The reduction effect is significant and also in good agreement with the compression shear test results, when angle α is about 135°.

The changes to the tension or compression strength values are small. Better correspondence with the test results is achieved also in tension by equation (6) than by (4). The calculated capacities were, according to the comparison by KÄLLSNER (1991) in tension direction $\alpha = 60°$, systematically little higher than the respective tension test results, and just on that angle range the reduction from the tension capacities of EC5 is the biggest by equation (6).

The compression capacity will increase a little when $30° < \alpha < 60°$ and also the tension capacity on α values $\alpha < 40°$. Both changes are going to the right direction. According to the calculations of KÄLLSNER (1991) the tension capacities in $\alpha = 30°$ direction were systematically lower than the test results. As an example the comparisons between the test results and calculated mean values of shear, tension and compression capacities are shown in *Figures 2-5* for FIX and TOP-91 nail plates. The type of failure of presented test results was plate capacity, except in shear test series $\alpha = 45°$ and $\alpha = 60°$ of the both nail plates and $\alpha = 150°$ of FIX-plate, where the failure mode was anchorage. The presented shear test values are the maximum shear capacities up to a slip limit of 7.5 mm without timber contact.

The constant γ_0 would be 13.5° for FIX and 15° for TOP-91 nail plate, when the shear capacity in $\alpha = 30°$ direction is equal with the mean value of test results. The value of coefficient k_v is 0.42 for FIX and 1.25 for TOP-91 nail plate, when the increased shear capacities from EC5 values are according to the test results at the safe side.

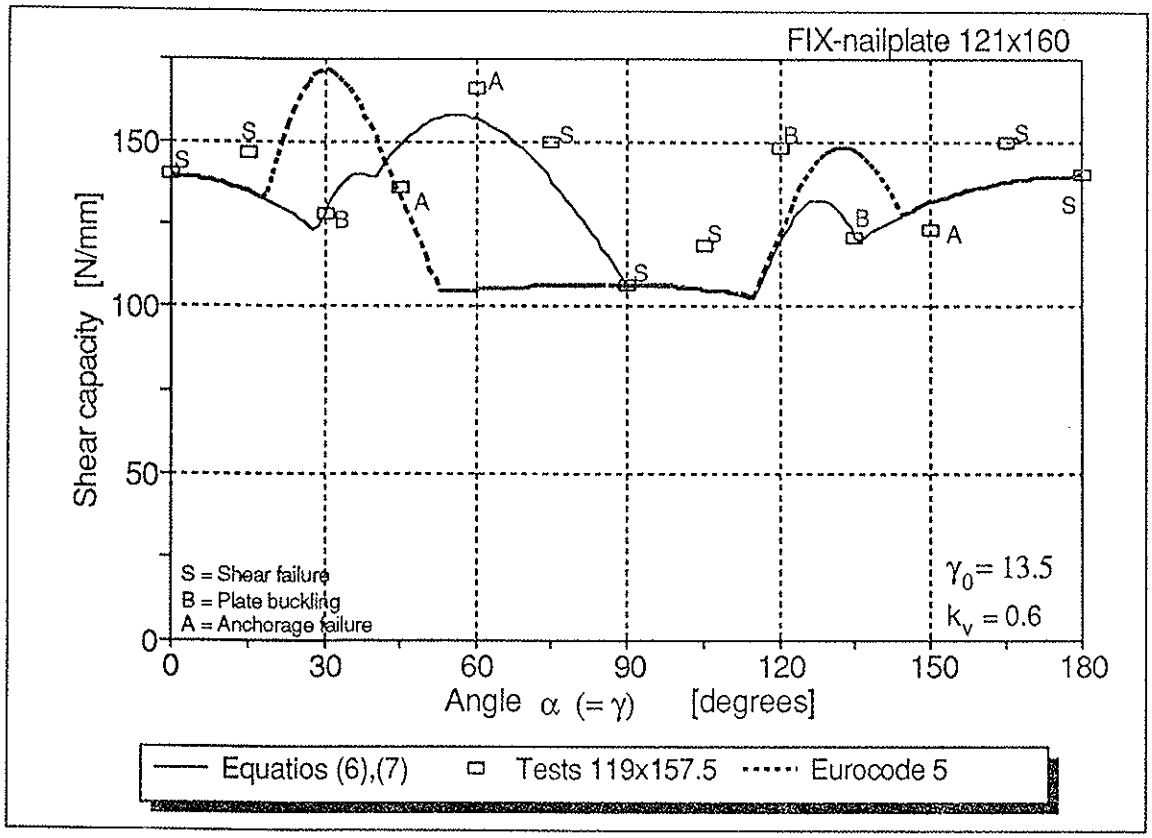

Figure 2. Results of shear test series of FIX nail plate and the calculated mean capacities.

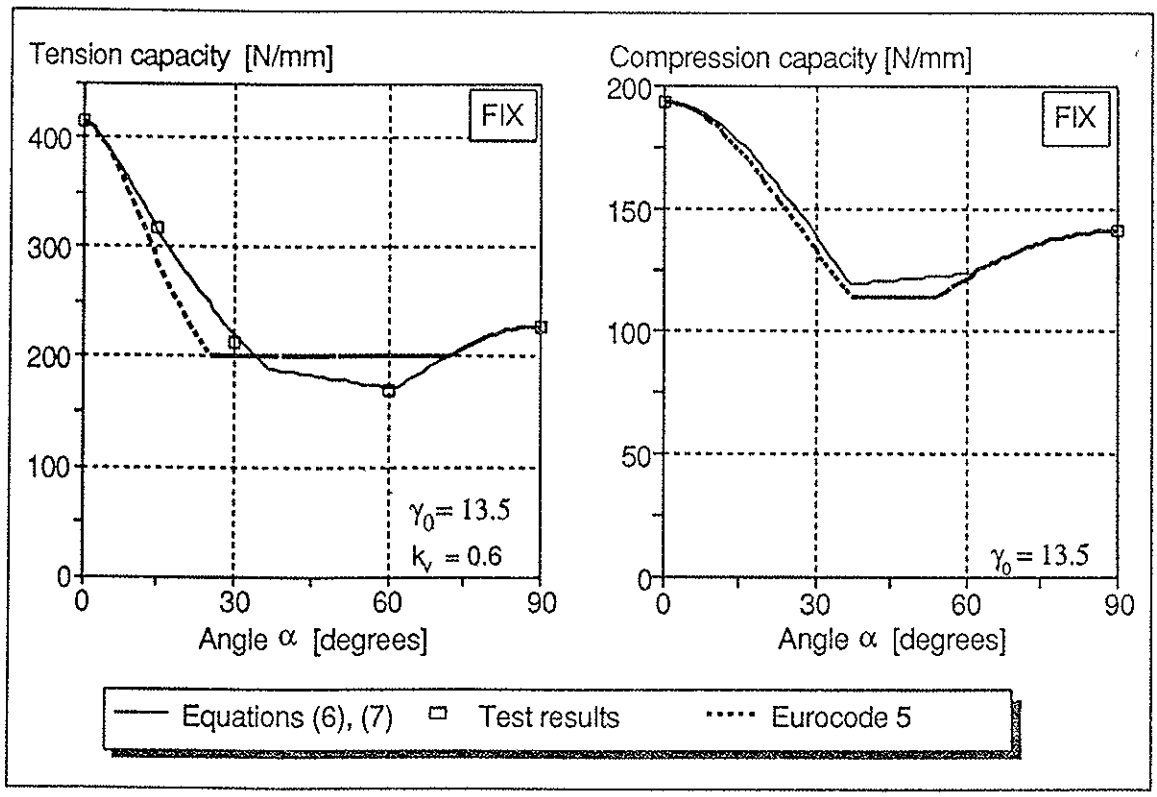

Figure 3. Results of tension and compression test series of FIX nail plate and the calculated mean capacities.

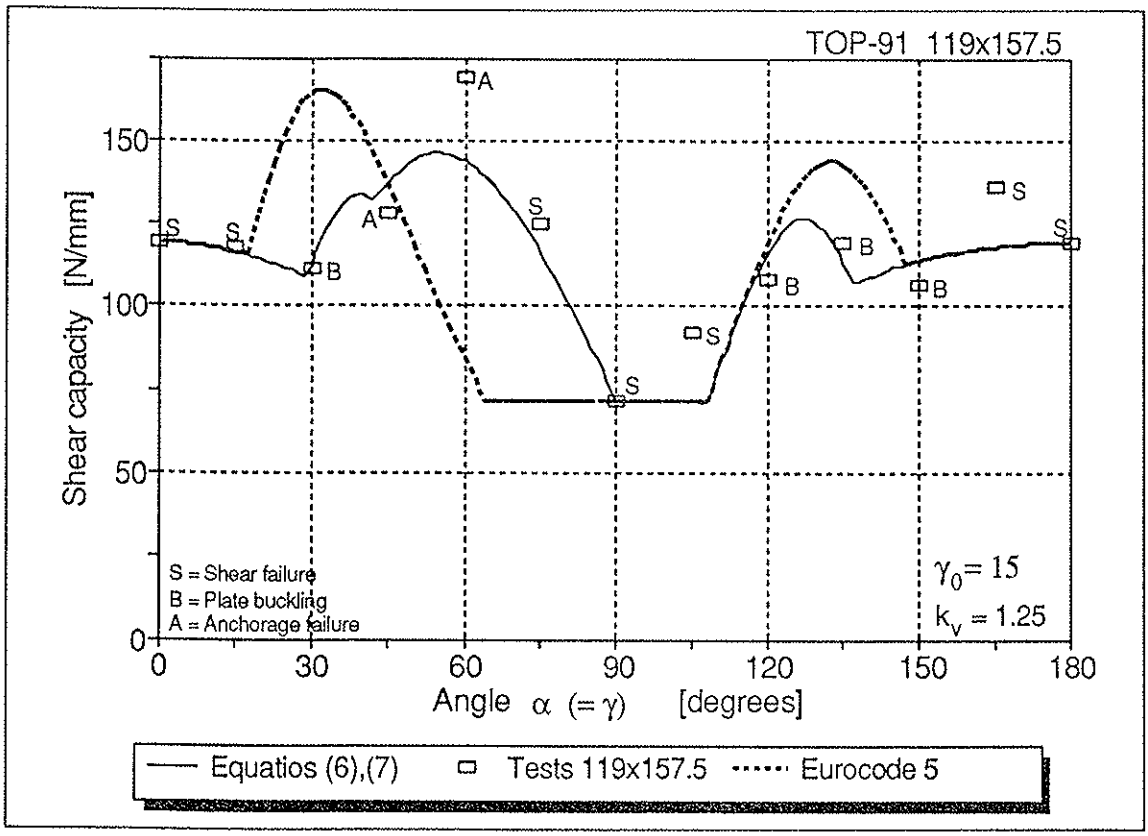

Figure 4. Results of shear test series of TOP-91 nail plate and the calculated mean capacities.

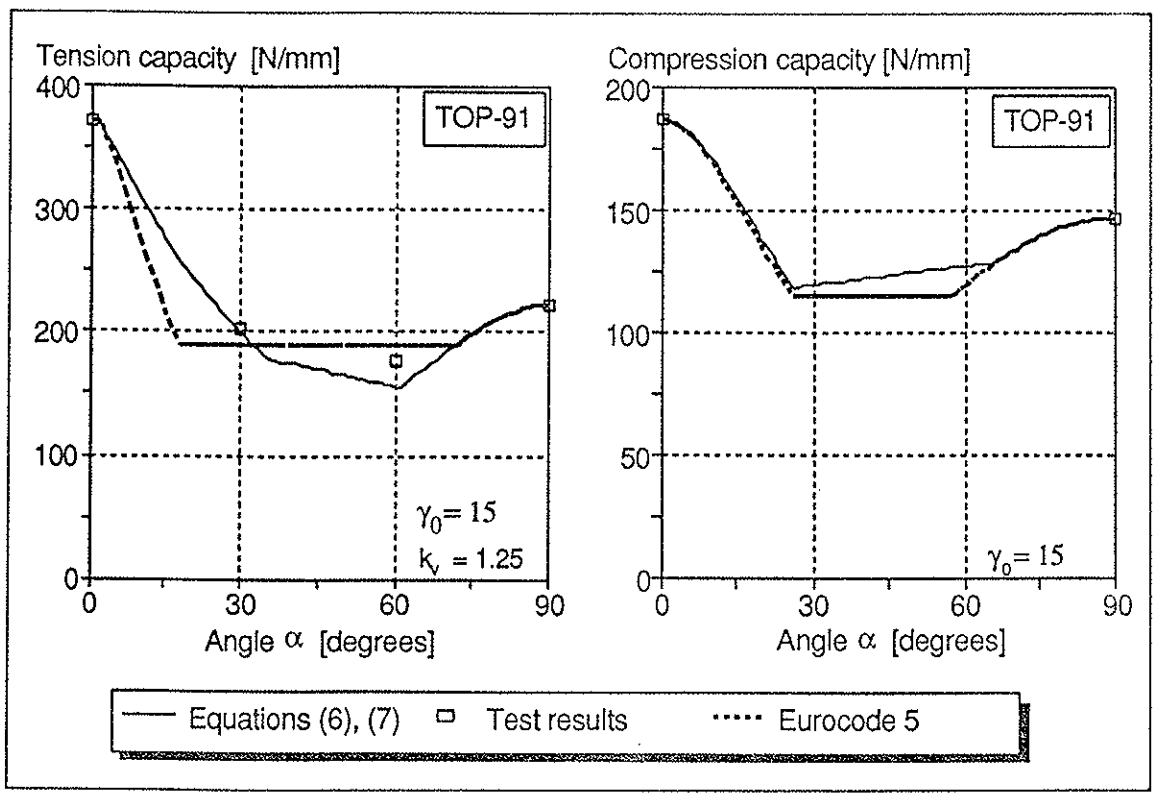

Figure 5. Results of tension and compression test series of TOP-91 nail plate and the calculated mean capacities.

REFERENCES

AASHEIM, E. & SOLLI, K.H., 1990, Proposal for Design Code for Nail Plates. Proceedings CIB-W18 Lissabon, Portugal.

BOVIM, N.I. & AASHEIM, E., 1985, The Strength of Nail Plates. Proc. CIB-W18 Beit Oren, Israel.

ENV 1995-1-1, 1993, Eurocode 5 - Design of Timber Structures - Part 1-1: General Rules for Buildings. CEN Brussels.

KÄLLSNER, B. & KANGAS, J., 1991, Theoretical and Experimental Tension and Shear Capacity of Nail Plate Connections. Proceedigns CIB-W18 Oxford, United Kingdom.

NORÈN, B., 1981, Design of Joints with Nail Plates. Proceedings CIB-W18 Warsaw, Poland.

POUTANEN, T., 1994, Steel failure Design in Truss Plate Joints. Paper 27-7-3, CIB-W18 meeting twenty-seven, Sydney, Australia.

WHALE, L., 1995, Punched metal plate fastener joints. STEP lecture C11, STEP/EUROFORTECH, Almere, The Netherlands.

CIB-W18/28-7-9

INTERNATIONAL COUNCIL FOR BUILDING RESEARCH STUDIES AND DOCUMENTATION

WORKING COMMISSION W18 - TIMBER STRUCTURES

AXIAL STRENGTH OF GLUED-IN BOLTS
CALCULATION MODEL BASED ON NON-LINEAR FRACTURE MECHANICS
A PRELIMINARY STUDY

by

C J Johansson

E Serrano

P J Gustafsson

B Enquist

Lunds Institute of Technology

Sweden

MEETING TWENTY - EIGHT

COPENHAGEN

DENMARK

APRIL 1995

Axial Strength of Glued-in Bolts
Calculation model based on non-linear fracture mechanics - A preliminary study

by

Carl-Johan Johansson, Erik Serrano, Per-Johan Gustafsson and Bertil Enquist
Division of Structural Mechanics
Lunds Institute of Technology, Box 118, S-221 00 Lund, Sweden

Abstract

Axially loaded bolts have been studied theoretically and experimentally. A theoretical model developed for lap joints in pure shear has been used. The model, which consists of an analytical expression, is based on a combination of Volkersen theory and non-linear fracture mechanics. Properties of the bond line, such as the fracture energy, the shear strength and the shape of the τ-δ curve are included in the model. The moduli of elasticity of the adherends is also considered. The bond line properties have been determined experimentally on very short threaded bolts, with a bond line length of only 5 mm. Both relatively ductile and brittle adhesives have been studied. Bolts have also been analysed by means of a finite element method. A good correspondence with the analytical model was obtained for different values of the fracture energy and the shear strength. An important prerequisite in the model is that the stresses perpendicular to the bond line are negligible. The finite element analysis showed that such stresses only occur locally at the ends of the bond line and that they are relatively small. The model allows simple analysis of how different factors affect the axial strength of glued-in bolts. It can for example be shown, that for short bolts the bond line shear strength is the decisive factor. For long bolts the fracture energy is the most import. Moreover, due to its simplicity and other characteristics, the model may be of great interest for future codes of practice.

Introduction

Glued-in bolts have been used in the Scandinavian countries and in Germany for more than 20 years. The major area of application has been in glulam structures. The bolts are used to prevent cracks in the apex zone of curved beams and in end notched beams or to transfer forces into a structure or part of a structure as in a column-foundation joint and in a frame corner. Advantages obtained by using glued-in bolts include: High local force transfer, very stiff connections when loaded in the axial direction and good fire properties.

Threaded bolts are preferred in order to obtain a mechanical bond between the bolt and the adhesive. Bolts with a diameter of between 12 and 24 mm are common. The bolts are glued-in either by injection of the glue or by screwing in the bolt. In the first case the holes are normally 1 mm larger than the outer diameter of the bolt to give sufficient clearance for the injection of glue. In the other case the hole is smaller than the bolt diameter, normally by an amount equal to the depth of the thread. Glue is poured into the hole and the bolt is screwed in. To allow for distribution of the glue the bolt has to have a channel cut along its length. The glue can also be applied along the depth of the hole and the length of the bolt with a brush and then it is not always necessary to use grooved bolts.

The strength of glued-in bolts have been studied by Riberholt (1986, 1988), Ehlbeck et al (1992) and Ehlbeck and Siebert (1987). Gerold (1992) gives a state-of-the-art report. Müller and von Roth (1991) and Hollinsky (1993) also studied glued-in concrete ribbed steel and glass fibre respectively.

The main activities in these investigations have been testing of the axial strength at different bolt length, bolt diameter, type of glue, angles between bolt and wood fibre direction etc. Elhbeck and Siebert (1987), Müller and von Roth (1991) and Hollinsky (1993) have also measured the strain distribution along bolts and from that calculated the shear stresses between bolt and wood at different axial load levels.

Müller and von Roth (1991) calculated the stresses perpendicular to the grain by means of finite element analysis.

Riberholt (1988) has presented the following useful expression for the axial strength:

$$F_{ax} = k\rho d\sqrt{l_g} \qquad (1)$$

where k is a constant which depends of the glue type, ρ is the wood density, d is the bolt diameter and l_g is the glued-in length. The expression has been obtained by fitting a function to test data and is now used in the design of bolt connections in Denmark (TOP, 1987).

In Sweden an even simpler expression is used, namely

$$F_{ax} = f_v l_g d\pi \qquad (2)$$

where f_v is the shear strength determined at an l_g/d ratio 15 - 20 (Boverket).

The purpose of the present study has primarily been to investigate the possibility to apply a model developed for single-lap joints to axially loaded bolts

New approach using non linear fracture mechanics

Gustafsson (1987) studied the strength of lap joints in pure shear theoretically using a theory developed for rivet connections by Volkersen (1938) and a non-linear fracture mechanics approach, taking account of the complete τ–δ curve of the bond line, see Figure 2. He presented a method of analysis, which makes it possible to study the significance of various parameters. The fracture energy defined as the area under the τ–δ curve was found to be an important factor. The maximum load that the joint can carry is expressed as

$$\frac{F_u}{f_v bl} = f\left[\frac{l^2 f_v^2}{t_1 E_1 G_f}, \alpha, g\right] \tag{3}$$

where l, E_1, E_2, b, t_1 and t_2 are defined in Figure 1 and

f_v is the shear strength

G_f is the fracture energy

$\alpha = \frac{E_1 t_1}{E_2 t_2}$

g is a function describing the shape of the τ-δ curve

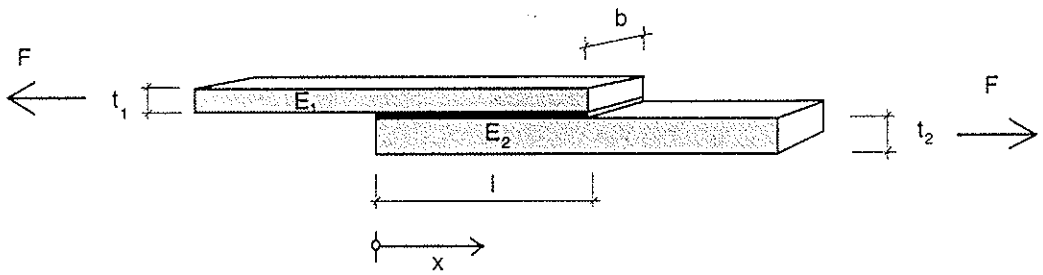

Figure 1 Geometry of single-lap joint.

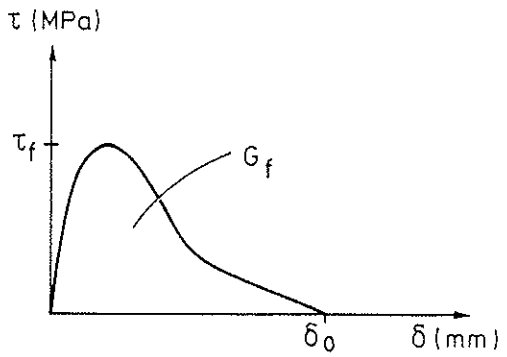

Figure 2 Constitutive relation of bond line.

Important assumptions are: The glueline is in a state of pure shear and the adherends are in a state of pure tension without any bending effects.

Assuming a τ-δ curve shape corresponding to curve I in Figure 3 Gustafsson developed the following expression for the maximum load:

$$\frac{F_u}{f_v bl} = \frac{(1+\alpha)\sinh\omega}{\omega(\alpha+\cosh\omega)} \qquad \text{for } \alpha \leq 1 \qquad (4)$$

where $\omega = \sqrt{\frac{1+\alpha}{2}}\sqrt{\frac{l^2 f_v^2}{t_1 E_1 G_f}}$

It can also be shown that

$$\frac{F_u}{f_v bl} = \frac{(1+\alpha)\sinh\omega}{\omega((\alpha+\cosh\omega)\cosh\omega-\sinh^2\omega)} \qquad \text{for } \alpha > 1 \qquad (5)$$

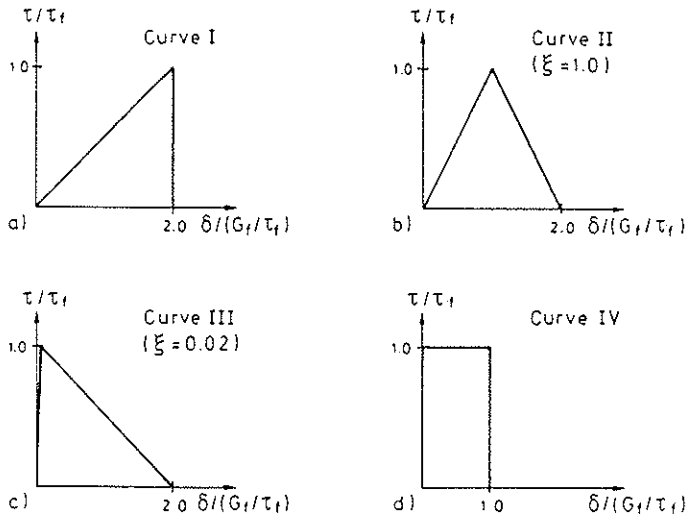

Figure 3 Different shapes of the τ–δ curve. From Gustafsson (1987).

A further step is to apply these expressions to the glued-in bolt connection described in Figure 4 and to exchange A_1 for A_{wood}, A_2 for A_{bolt}, E_1 for E_{wood}, E_2 for E_{bolt} and b for ϕ, the circumference of the glue line, which is equal to $d_{bolt}\pi$, where d_{bolt} is the outer diameter of the bolt. We then obtain:

$$\frac{F_u}{f_v d_{bolt}\pi l} = \frac{(1+\alpha)\sinh\omega}{\omega(\alpha+\cosh\omega)} \qquad \text{for } \alpha \leq 1 \qquad (6)$$

$$\frac{F_u}{f_v d_{bolt}\pi l} = \frac{(1+\alpha)\sinh\omega}{\omega((\alpha+\cosh\omega)\cosh\omega-\sinh^2\omega)} \qquad \text{for } \alpha > 1 \qquad (7)$$

where

$$\omega = \sqrt{\frac{1+\alpha}{2}}\sqrt{\frac{l^2 f_v^2 d_{bolt}\pi}{A_{wood} E_{wood} G_f}} \qquad (8)$$

and

$$\alpha = \frac{A_{wood}\, E_{wood}}{A_{bolt}\, E_{bolt}} \qquad (9)$$

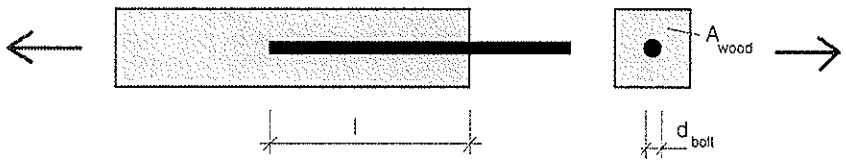

Figure 4 Glued-in bolt connection in tension.

Comparison with test results

Riberholt (1988) has presented own and other researcher's results from axial strength tests on glued-in bolts with different lengths, diameters and wood densities. In Figure 5 and 6 his results from 16 mm and 20 mm bolts are compared with Eq. 7 ($\alpha > 1$). The following values of the parameters were used:

A_{wood} = 10000 mm² (Assumed value. Not clear what cross section dimensions that were used in the different investigations.)

E_{wood} = 12500 N/mm² (The mean wood density, $\rho_{0,12}$, in Riberholt's tests was about 400 kg/m³, which roughly corresponds to a modulus of elasticity of 12500 N/mm².)

d_{bolt} = 15.7 mm and 19.8 mm respectively

E_{bolt} = 200 000 N/mm²

In Figure 5 Eq. 7 fits well with the data from 16 mm bolts glued with phenol-rescorcinol adhesive if the shear strength, f_v, is set to 7.0 N/mm² and the fracture energy, G_f, to 2.1 kNm/m². Correspondingly a good fit is obtained for 20 mm bolts glued with two component polyurethane adhesive if f_v is set to 8.0 N/mm² and G_f to 2.9 kNm/m². The fracture energies are much higher than the values presented by Wernersson (1990). The reason for this will be dealt with later in this paper. For bolts with polyurethane adhesive the fracture energy is higher than for bolts with phenol resorcinol, which is to be expected as the latter is the more brittle.

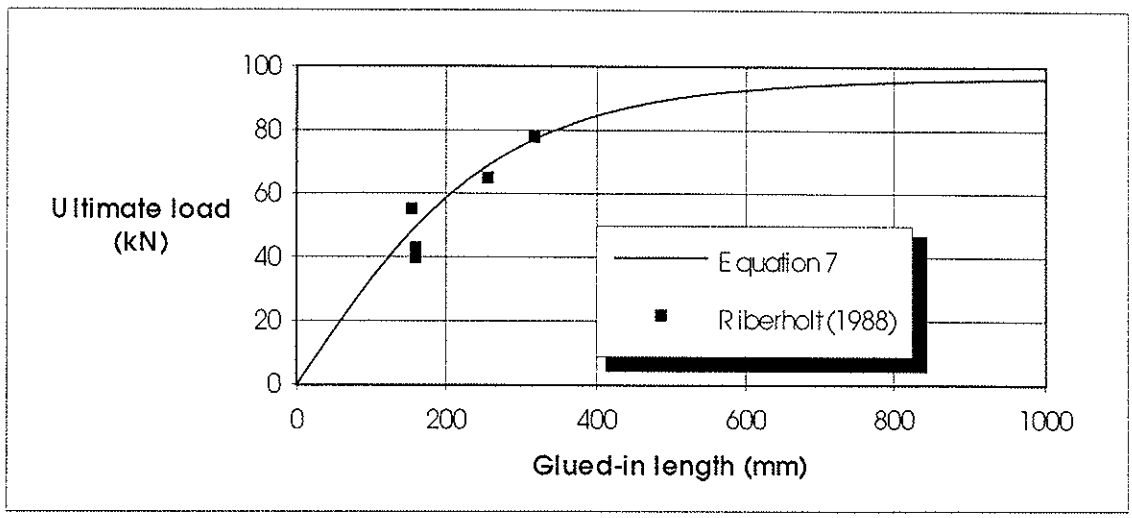

Figure 5 *Comparison between Riberholt's (1988) results for 16 mm bolts and Eq. 7, which is based on Gustavsson's (1987) non-linear fracture mechanics theory for lap joints. The bolts were glued with phenol-rescorcinol adhesive. The holes were about 1 mm smaller than the bolts.*

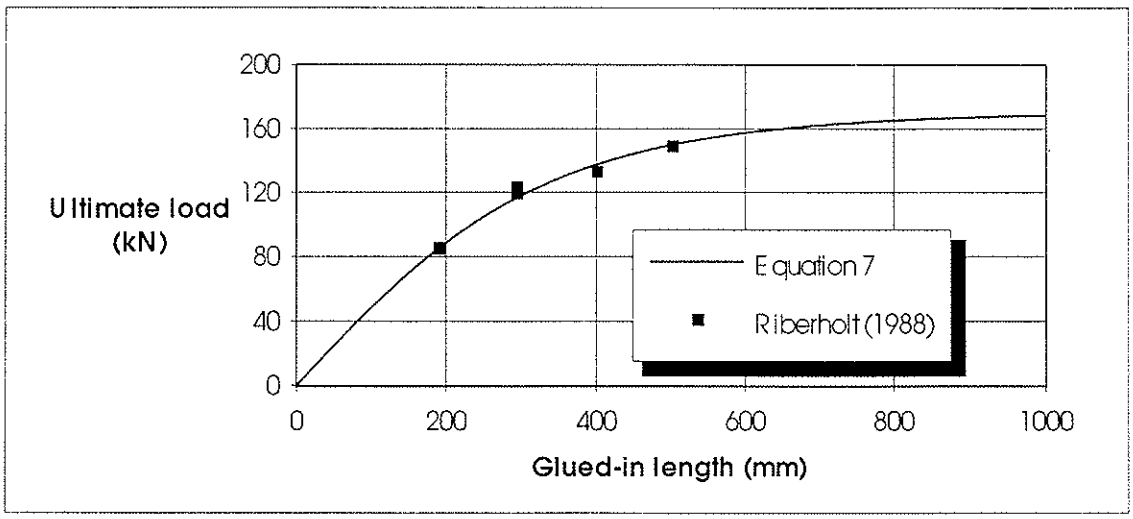

Figure 6 *Comparison between Riberholt's (1988) results for 20 mm bolts and Eq. 7. The bolts were glued with two component polyurethane adhesive. The holes were about 1 mm larger than the bolts.*

Non-linear FEM analysis

Description of studied glued-in bolt

Ehlbeck and Siebert (1987) have studied the bond shear stress distribution in a large number of glued-in bolts. The strain in the steel along the length of loaded bolts was measured and based on this the shear stresses were calculated.

A FEM analysis of one of these bolts (CIL 4.2) has been carried out. A comparison is made with results from Eq. 7 and with the measured shear stress distribution. The geometry of the specimen is described in Figure 7.

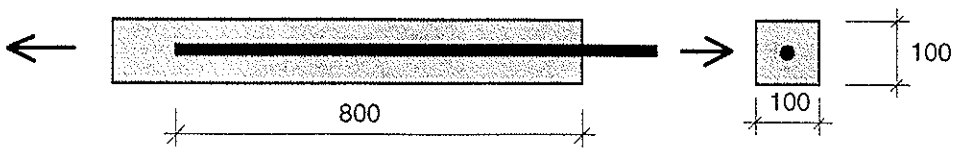

Figure 7 *Geometry of the analysed bolt specimen. The diameter of the bolt is 16 mm.*

The code ABAQUS has been used with axisymmetric modelling and with a mixed-mode constitutive model for the bond line behaviour according to Wernersson (1994). A total of 8 different calculations have been carried out. In all cases the bond line has had the following properties:

- $G_{f,shear}$ = 2 kNm/m² (fracture energy in shear)
- $G_{f,tension}$ = 1 kNm/m² (fracture energy in tension)
- τ–δ_s and σ–δ_n relations according to Figure 8 (two alternatives)

The wood has been modelled as an orthotropic material with

- E_L = 12000 N/mm²
- E_R = 600 N/mm²
- G_{RL} = 450 N/mm²

The FEM mesh is shown in Figure 9.

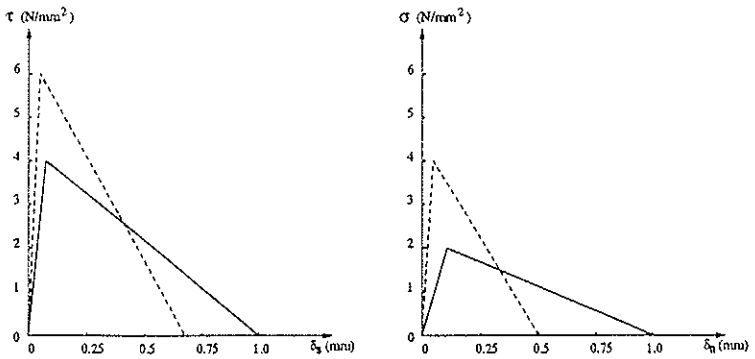

Figure 8 τ–δ_s *and* σ–δ_n *relations used in the calculations.*

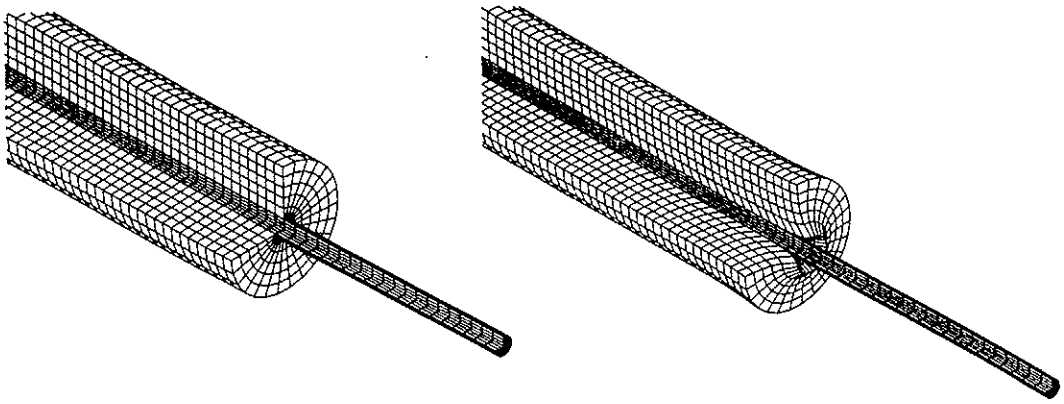

Figure 9 *FEM mesh and the bolt connection in a deformed state.*

Results and comparison with Eq. 7

Axial strength values from the FEM calculations are presented in Table 1 together with values obtained from Eq.7.

In the tested bolt the cross section area has been reduced due to a channel that was cut along the bolt for the wires from the strain gages. This has been handled in the calculations by reducing the modulus of elasticity of the bolt material.

In calculation C8 an elasto-plastic material model has been used for the steel with a yield stress of 640 N/mm².

Table 1 *Parameter values used in the calculations. The fracture energy in shear has been set to 2 kNm/m² and the fracture energy in tension perpendicular to the fibre direction has been set to 1 kNm/m².*

Calculation No	E_{bolt} (N/mm²)	f_v (N/mm²)	f_t (N/mm²)	F_u (kN)	
				FEM	Eq. 7
C1	100 000	6	4	64.3	66.2
C2	100 000	6	2	65.5	66.2
C3	100 000	4	4	63.9	64.7
C4	150 000	6	4	82.0	82.9
C5	150 000	4	4	80.3	79.0
C6	200 000	6	4	97.9	97.4
C7	200 000	4	4	95.2	90.2
C8	200 000/0	6	4	97.6	97.4

The following conclusions can be drawn:

- The axial strength is almost independent of the shear strength and the tensile strength. With a shorter glued-in length the effect of the shear strength will be more pronounced.

- The simple expression given by Eq.7 gives almost the same result as the non-linear FEM model.

- The axial strength is much affected by E_{bolt}. Hence, according to theory the axial strength is also much affected also by the glueline fracture energy.

The stress distribution along the bolt in the elastic stage is shown in Figure 10 (calculation C1). Tension stresses of any magnitude perpendicular to the bolt axis only occur at the entrance of the hole. The stress state along the bolt is principally one-dimensional, which is one important reason for the good agreement between the one-dimensional expression in Eq. 7 and the FEM analysis.

In Figure 11 the shear stress distribution from the FEM analysis (calculation C1) at different load level is shown. The measured shear stress distribution (calculation based on strain measurements) at one load level is also presented.

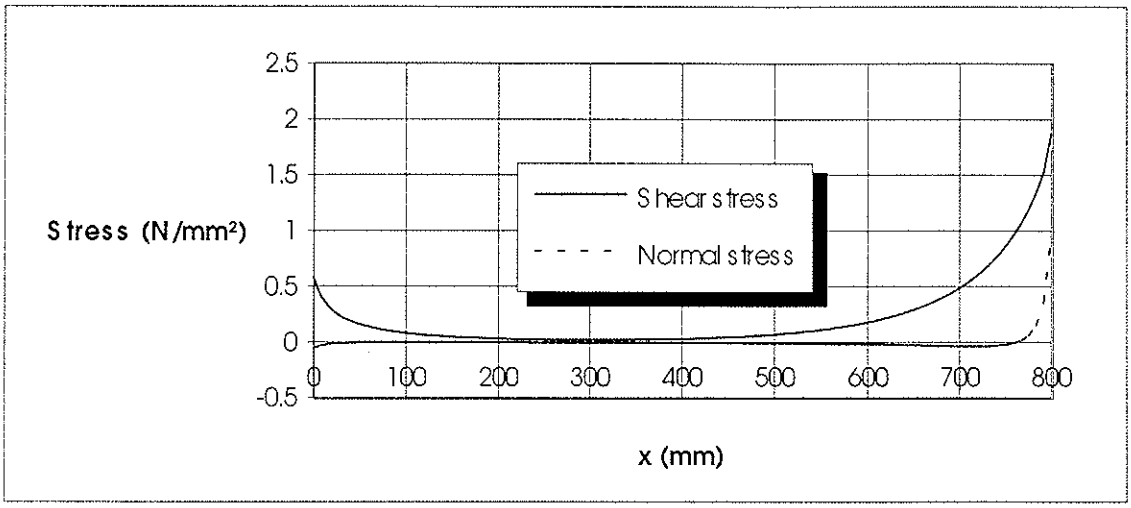

Figure 10 *Linear elastic shear stress distribution and normal stress perpendicular to the bolt axis distribution from the FEM analysis (calculation C1). x=800 mm is at the entrance of the hole.*

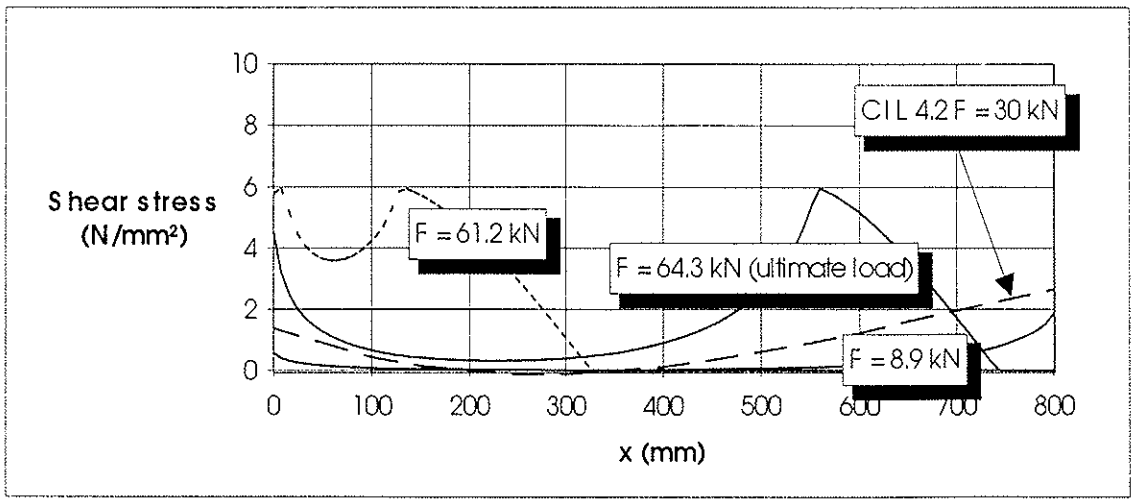

Figure 11 *Shear stress distribution according to the non-linear FEM analysis at different load levels (calculation C1) and measured stress distribution at one load level.*

Small specimen testing

In order to obtain the complete τ–δ curve a glued-in bolt specimen with a very short glued-in length was designed, see Figure 12. The diameter of the steel bolt was 15.7 mm (thread depth = 1.1 mm) and the hole diameter 17 mm, which gave a clearance of 0.65 mm. The glued length was 4.5 mm.

Spruce (*Picea Abies*) with a density ($\rho_{0,9}$) of 470 kg/m^3 was used. Two adhesives were studied; an epoxy adhesive, EP20/VP with hardener B20/1 which is rather brittle from Wevo-Chemie GmbH and a polyurethane adhesive, Casco 1959 with hardener 1821 which is more ductile from Akzo-Nobel A/S.

To avoid formation of CO_2 voids in the glueline, which easily occur in polyurethanes if the moisture content in the wood is too high, wood with a moisture content of 9 % was used. Testing was also carried out at this moisture content.

The setup for the test is shown in Figure 12. Load was applied at a constant rate of 0.5 mm/min. All tests were interrupted before zero load was reached.

The recorded deformation is the total deformation. To obtain the local shear slip in the bond line, δ, the elastic deformations outside the bond line must be subtracted. For the sake simplicity the deformations indicated in Figures 13 and 14 are, however, the total deformations. The evaluation of shear strength and fracture energy is not affected by this.

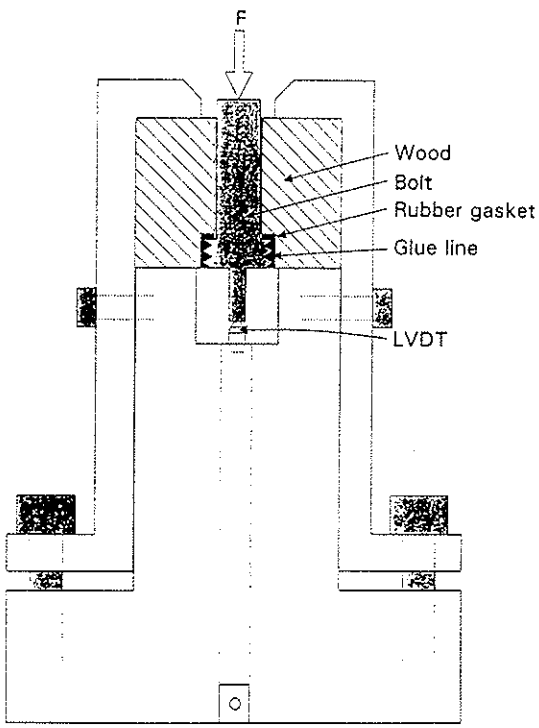

Figure 12 Small glued-in bolt specimen and test set-up.

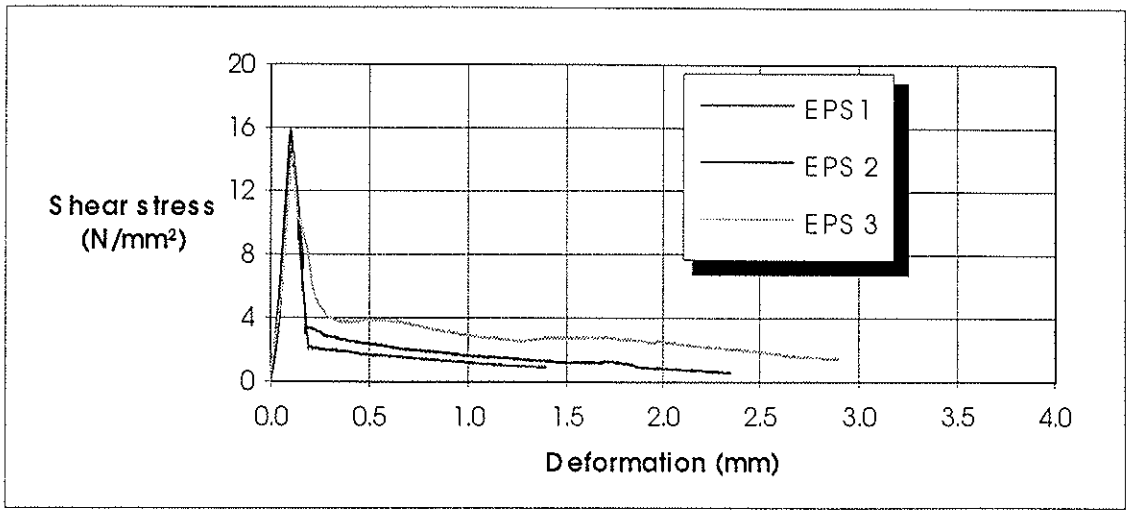

Figure 13 τ–δ *curves for specimens glued with epoxy adhesive.*

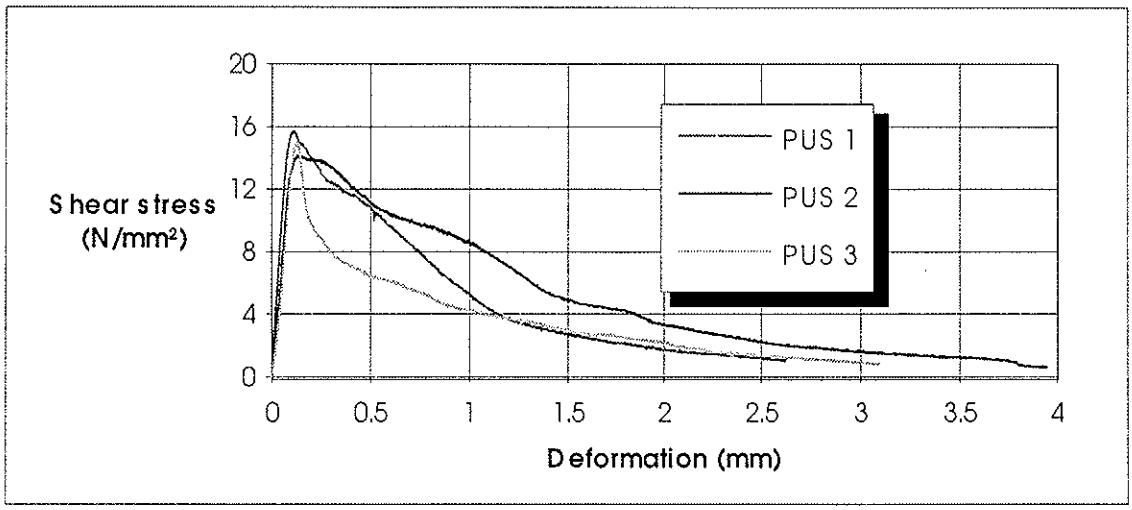

Figure 14 τ–δ *curves for specimens glued with polyurethane adhesive.*

Table 2 *Shear strength and fracture energy. (PUS: two component polyurethane adhesive , EPS: two component epoxy adhesive).*

Specimen No	Shear strength, f_v (N/mm²)	Fracture energy, G_f (kNm/m²)
PUS 1	15.7	12.5
PUS 2	14.2	17.7
PUS 3	15.0	10.4
EPS 1	15.2	2.7
EPS 2	15.8	5.1
EPS3	14.3	8.4

The shear strength, f_v, and the fracture energy, G_f, see Table 2, are considerably higher than the values found by Wernersson (1990), who tested phenol resorcinol and one-

component polyurethane adhesives. However, in his tests the adherends were free to move in the direction perpendicular to the glue surface. This is not the case in bolt, where displacement perpendicular to the bond line is prevented by the surrounding wood. Wernersson (1994) demonstrated the effect of keeping the displacements perpendicular to the glue line at zero during the shear test. For phenol resorcinol he found an increase of the shear strength by 30 % and of the fracture energy by 100%.

It is obvious from the curves in Figure 13 and 14, that after failure in the bondline there is considerable friction and as a consequence of that, the axial load is not at zero until the bolt is completely out of the hole.

The shear strength and fracture energy from the small test are higher than the values obtained from the curve fitting in Figure 5 and 6. One reason for this is that the wood density in the small specimens most likely was higher than in the test presented by Riberholt (1988).

Conclusions

- A simple model based on Volkersen theory and non-linear fracture mechanics can be used to predict the pull out strength of bolts glued in parallel to the fibre direction.

- The shear strength and the fracture energy required in the model can be obtained by curve fitting to pull out strength data from bolts with different lengths or possibly also by testing small glued-in bolt specimens and recording the complete τ–δ curve.

Acknowledgements

Financial support from the Swedish Council for Building Research (BFR) is gratefully acknowledged. Adhesives have been provided free of charge from Akzo Nobel A/S and Wevo-Chemie GmbH.

References

Boverket (1992) Typeapproval concerning glued-in bolts in gluam. TG1396/78, Swedish National Board for Physical Planning and Building, Karlskrona/Sweden.(in Swedish)

Ehlbeck, J. and Siebert, W. (1987) Praktikable Einleimmethoden und Wirkungsweise von eingeleimten Gewindestangen unter Axialbelastung bei Übertragung von Grossen Kräften und bei Aufnahme von Querzugkräften in Biegeträgern. Teil 1: Einleimmethoden/Messverfahren/Haftspannungsverlauf. Forschungsbericht: Versuchsanstalt für Stahl, Holz und Steine, Abteilung Ingenieurholzbau, Universität Karlsruhe/Germany.

Ehlbeck, J., Belchior-Gaspard, P. and Gerold, M. (1992) Praktikable Einleimmethoden und Wirkungsweise von eingeleimten Gewindestangen unter Axialbealstung bei Übertragung von grossen Kräften und bei Aufnahme von Querzugkräften von Klima-

einwirkung und Langzeitbeanspruchung. Forschungsbericht: Versuchsanstalt für Stahl, Holz und Steine, Abteilung Ingenieurholzbau, Universität Karlsruhe/Germany.

Gerold, M. (1992) Verbund von Holz Stahl und gewindestangen aus Stahl. Bautechnik 69, pp. 167-178.

Gustafsson, P.-J. (1987) Analysis of Generalized Volkersen-joints in Terms of Non-linear Fracture Mechanics, in: Verchery, G. and Cardon, A. H. (ed), Mechanical Behaviour of Adhesive Joints. Edtion Pluralis, Paris/France.

Hollinsky, K. H. (1993) In Brettschichtholz eingeleimten Stabelemente. Tteil 2: Haftspannungsverlauf unter axialer Stabzuglast für Buchenholzstab, Gewindestab, Betonstahl und Glasfaserstäbe. Holzforschung und Holzverwertung 1, pp. 5-11.

Müller, J. and Roth, von W. (1991) Untersuchungen zum Tragverhalten von parallel zur Faser in Nadelholz eingeleimten Stäben aus unterschiedlichen Materialien. Holz als Roh- unfd Werkstoff 49, pp. 85-90.

Riberholt, H. (1986) Glued bolts in glulam. Department of Structural Engineering., Technical University of Denmark. Report 210, Lyngby/Denmark.

Riberholt, H. (1988) Glued bolts in glulam - Proposal for CIB-Code. CIB.W18A/21-7-2, Parksville/Canada.

TOP (1987) Glued-in bolts. Traebranchens Oplysningsråd. (in Danish)

Wernersson, H. (1990) Wood Adhesive Bonds - Fracture Softening Properties in Shear and in Tension. Report TVSM - 3012, Lund Institute of technology. Division of Structural Mechanics, Lund/Sweden.

Wernersson, H. (1994) Fracture Characterization of Wood Adhesive Joints. Report TVSM-1006, Lund Institute of technology. Division of Structural Mechanics, Lund/Sweden.

Volkersen, O. (1938) Die Nietkraftverteilung in zugbeanspruchter Nietverbindungen mit konstanten Laschenquersnitten. Luftfahrtvorschung, Band 15, pp. 42-47.

CIB-W18/28-7-10

INTERNATIONAL COUNCIL FOR BUILDING RESEARCH STUDIES AND DOCUMENTATION

WORKING COMMISSION W18 - TIMBER STRUCTURES

CYCLIC LATERAL DOWEL CONNECTION TESTS FOR SEISMIC AND WIND EVALUATION

by

J D Dolan
Virginia Polytechnic Institute and State University
USA

MEETING TWENTY - EIGHT

COPENHAGEN

DENMARK

APRIL 1995

SUMMARY

Displacement-controlled monotonic, and load- and displacement-controlled cyclic tests were conducted on nail and bolt connections to determine their adequacy in resisting repetitive, reversing loads such as those experienced during seismic and high wind events. The specimen configurations were determined so that three of the four possible yield modes for the connections were obtained. Specimen configurations included solid wood to solid wood, plywood to solid wood, and light-gauge sheet steel to solid wood for nailed connections, and solid wood to solid wood (in two thicknesses) and 6 mm steel plate to solid wood for bolted connections.

The test protocol for the displacement-controlled cyclic tests followed the newly proposed ASTM test standard for mechanically fastened connections, which is a modification of the that is based on the Sequential Phased Displacement procedure used by the Joint Technical Coordinating Committee on Masonry Research (TCCMAR) for the United States-Japan Coordinated Earthquake Research Program (Porter, 1987). Parts of the test procedure were also influenced by test protocol proposals made by Polensek, A. (1988), and Reyer, E. and A.O. Oji, (1991).

Information obtained from these tests include, 1) monotonic yield load and displacement, capacity, and ductility, 2) indications of whether damage accumulation occurs at cyclic loads as high as 75 percent of capacity for nails and 54 percent of capacity for bolts, and 3) equivalent energy initial stiffness, yield load and displacement, and ductility, as well as absolute capacity, energy dissipation and stiffness degradation characteristics under cyclic loading. The cyclic response characteristics are based on a stabilized response rather than the initial response of the connection.

Findings include that there is no damage accumulation effects on connections for loads has high as 75 percent capacity for nails and 54 percent of capacity for bolts. The stabilized response of dowel connections in wood provide significant ductility for system response. Large values of hysteretic and equivalent viscous damping were determined due to the friction and yielding of the fasteners. Dowel connections must be designed to yield in order to obtain ductile response in wood structures since wood as a material fails in a brittle manner.

INTRODUCTION

An increase in the load duration factor, C_D, for wood construction under seismic and wind loading from 1.33 to 1.6 was included in the 1991 edition of the *National Design Specification® for Wood Construction* (NDS®). This change is based on long-term rationale that has been applied to wood construction. While this increase does not reflect any change in philosophy from previous design codes, it highlights an area of limited research support for connections. The lack of research data raises questions about the load duration increase and adequacy of dowel connections for seismic loading at historic magnitudes. The basis of the questioning relates to previous connection tests used to determine design values for the NDS which were performed with monotonic quasi-static and impact loading, while seismic events produce a reversing load effect on the connections.

To understand why $C_D = 1.6$ is proposed for short-term loads such as seismic actions, consider the method used to calculate 10 year nominal design values. Connection design values are based on experimental yield loads derived from monotonic tests with a rate of loading causing failure of specimens in 5-10 minutes. This short-term load is then indexed to a nominal design value based on a service duration of 10 years. (Normal or 10-year load duration considers that wood structures experience a cumulative design load effects of 10 years duration over the useful life of

the structure.) To adjust short-term values to nominal 10-year loads, values are divided by 1.6. Therefore, a load duration factor of 1.6 simply adjusts 10 year nominal values back to short-term (10-minute) design values for seismic loads. The 1.6 load duration factor is considered to be conservative since it adjusts nominal design values to a 10-minute design value, whereas an earthquake is a much shorter load event. In fact, if factor-of-safety values remain unchanged, a more accurate load duration factor for seismic design most likely will be higher than 1.6 if the capacities continue to be based on monotonic test results.

However, monotonic tests are not representative of cyclic loads such as earthquakes. Monotonic tests do not provide information on any effect of prior cyclic load history on connection capacity and/or ductility. There is concern that previous load history may affect connection reserve capacity and/or ductility in situations of cyclic loading.

Long-term static performance information is needed since there currently are no experimental results on which to directly base the expected long-term performance of connections. As stated earlier, current procedures for adjusting the short-term experimental results to a 10-year nominal value are based on long-term material strength tests of wood and engineering judgement. Therefore, while long-term connection tests will not address the effect of reversing load such as the cyclic loading associated with seismic events, they will provide information that will be useful in correctly setting 10-year duration, nominal capacities. This research project was necessary to determine the effects of cyclic load history on nail and bolt connections and determine apparent factors-of-safety and other performance characteristics needed to compare different materials for cyclic load conditions.

The specific information presented cannot determine directly whether the load duration factor of 1.6 is correct or not since long-term load tests of connections have not been performed. The long-tern connection tests are required for setting the nominal design values to which all of the other durations are calibrated. This report can only provide information concerning whether the seismic design values, calculated according to the 1991 NDS or other design specification, are conservative.

Related detailed and summary information on connection tests is presented in companion reports that are available from the Department of Wood Science and Forest Products, Timber Engineering Center, which is located in the Brooks Forest Products Research Center at Virginia Polytechnic Institute and State University. Summary and detailed data for each specimen tested to determine monotonic and load-controlled cyclic performance are presented in Virginia Polytechnic Institute and State University (VPI&SU) Timber Engineering Reports No. TE-1994-001 and TE-1994-002, respectively. The summary and detailed data for each specimen tested under the proposed ASTM standard, Sequential Phased Displacement (SPD), procedure are presented in VPI&SU Timber Engineering Reports No. TE-1994-003 and No. TE-1994-004 respectively.

TEST PROCEDURES

Specimen Configurations

Connection geometries were chosen to represent typical connection details found in wood construction, and include three of four yield modes that can occur in timber connections. Connections were in single shear with one dowel fastener each. Fifteen specimens of each nail connection type and ten specimens of each bolt connection type were tested in each sample. Table 1 summarizes the types and numbers of replications used for nail connections in displacement-control

cyclic tests. Table 2 summarizes the same information for bolt connections.

All lumber and plywood used for the tests was purchased at local lumber retailers. Specimens were constructed from southern pine, and were cut so as to avoid localized defects in the wood as much as possible. The wood was conditioned at a temperature of 20 $\pm 3^0$ C and relative humidity of 65±5% for a minimum of 14 days, or until the equilibrium moisture content was reached. Steel plate used in two connection geometries was also locally purchased and consisted of 6 mm, ASTM A36 mild carbon steel (ASTM 1989-a) and 1.4 mm A446 galvanized sheet steel (ASTM 1989-b). Nails used in the connection geometries were 3.7 x 76 mm and 4.1 x 89 mm brite common nails.

Table 1 shows that three types of nail connections were tested, and each type of connection was tested in two configurations (parallel-to-grain and perpendicular-to-grain). Two configurations used for these cyclic tests were included to investigate effects of grain orientation with respect to load. Since nailed connections are characterized by yielding of the nails as well as the wood, two yield modes that represent fastener yielding (modes III_s and IV) were included. Three types of commonly used connections were included, 1) plywood-to-lumber which is used in shear walls and diaphragms, 2) lumber-to-lumber which is typical of light framing connections, and 3) light-gauge sheet steel-to-lumber which is typical of joist hangers and other light-gauge metal connectors. Fifteen replicates were tested in each configuration to provide some information on the statistical variation in connection performance.

Summary information on type and number of replicates for bolt connection tests is presented in Table 2. Bolted connections were subjected to loading in the parallel- and perpendicular-to-grain orientations to investigate effects of grain orientation on connection performance, with each configuration being tested with 10 replicates.

The stationary member for all bolted connections was defined as the member that was clamped in a fixed position in the testing fixture, and was located on the nut side of all bolted connections. For all nailed connections, the stationary member was the penetrated or main member of the connection. The active member for all connections was defined as the member that was moved by the MTS hydraulic actuator in a cyclic manner during the tests. All bolted connections tested with the load acting perpendicular-to-grain to the stationary member required that the stationary members be wider than the active members in order to meet edge distance requirements for the full 1991 NDS design value.

Three types of bolted connection geometries were tested in an effort to include three of four yield modes possible for bolted connections. Connections were also chosen to simulate typical connections used in wood structures. The 38 mm-to- 38 mm lumber connection with a 19 mm bolt represents typical diaphragm chord connections. The 89 mm-to- 89 mm lumber connections with a 19 mm bolt represents the yield mode expected in a concrete to wood connection such as a ledger board for a roof attached to a tilt-up concrete wall. Finally, 89 mm -to- 6 mm steel plate connections represent typical connection hardware used in glulam and post-frame connections.

Specimen Fabrication

The full test program required five samples of matched specimens. Matched samples were obtained by cutting five replicates of each component from adjacent locations in a single board of southern pine lumber. This matching technique provided specimens in each sample with as close to identical physical characteristics as possible. Obvious local variations such as knots or splits were

avoided in choosing the locations of each set of four components. Matched components were then marked so that sets of five "identical" specimens produced five samples, each with 15 or 10 matched specimens depending on whether the fasteners were nails or bolts, respectively. Summary results of tests on three of the five matched samples are presented in a companion report (Dolan, et al., 1994a). Two matched samples were tested using the new ASTM procedure, and the results are presented in this report. Detailed results for each specimen tested are available in a companion report (Dolan and Gutshall, 1994b).

Nail Connections

Nailed connections were fabricated and then placed in an environmental chamber (at 20^0 C and 65% relative humidity) for a minimum of 14 days to allow for relaxation of wood fibers around the nail and to achieve approximate equilibrium moisture content. This conditioning time provided a more accurate representation of a nailed connection that has been in service for a period of time. Nailed connections usually have a higher initial stiffness immediately after assembly because wood fibers in contact with the nail shank have not relaxed.

Pre-drilled nail holes, meeting the guidelines established in the 1991 NDS, were used to guide the nails and prevent splitting of the wood members during driving with a hand-held hammer for all except a second sample of 38 mm-to- 38 mm lumber connections that was loaded parallel-to-grain. This second sample was tested with out pilot holes to determine the effect of pre-drilling on connection response. The 1991 NDS allows a pre-drilled hole no more than 75% of nail diameter for wood with a specific gravity less than 0.60. Therefore, connections using 3.7 mm common nails were pre-drilled with a 1.6 mm hole, or 42% of nail diameter, and connections using 4.1 mm common nails were pre-drilled with a 2.4 mm hole, or 58% of nail diameter. For 1.4 mm steel plate-to-38 x 89 mm connections, a 3.6 mm hole (95% of nail diameter) was pre-drilled in the steel plate. Members used in the testing had actual average specific gravities ranging from 0.48 to 0.62 depending upon the grade and size of lumber used.

Bolted Connections

Bolted connections were fabricated immediately prior to testing. A bolt hole that was 1.6 mm larger than the bolt was used for both wood and steel members of all bolted connections. This was in accordance with assembly tolerances given in the 1991 NDS and *1989 Manual of Steel Construction, Allowable Stress Design* published by the American Institute of Steel Construction. All bolt holes were centered between the edges of members and drilled with high speed steel drill bits to ensure smoothness and uniformity. In all connection configurations, end distances exceeded minimum requirements given in the 1991 NDS for use of full design values, and standard A307 mild carbon steel bolts or their equivalent were used.

Active members of connections were held by a gripping fixture attached to the testing machine. A high-strength bolt was inserted through the gripping fixture into a pre-drilled hole of the same diameter to prevent any slipping between the wood or steel member and the grip. Stationary members of the connections were blocked to prevent any movement.

Test Equipment

All tests were conducted in the Wood Engineering Laboratory of the Brooks Forest Products Research Center at Virginia Polytechnic Institute and State University. Two MTS servohydraulic

test machines were used to conduct displacement-controlled cyclic tests. Displacements and loads were measured using two linear variable differential transformers (LVDT) that were attached to the sides of specimens to measure connection slip, and load cells attached to the MTS actuators. Data was acquired using commercial data acquisition software on a micro computer in the engineering laboratory. Acquired data was analyzed using commercial spreadsheet software.

Test specimens were held in place and guided by a steel fixture to prevent rotation that would result in forces other than pure shear being applied to the specimen. Figure 1 shows a diagram of the test fixture. One important aspect of the fixture alignment is that the center of the load cell is in the connection shear plane. This minimizes any moment introduced into the specimen. Rollers are included in the fixture to minimize the effects of friction between the fixture and the moving side of the specimen.

Proposed ASTM Test Procedure

The method used in this study is a proposed new ASTM standard that is being considered by ASTM subcommittee E06.13, and is currently being revised for a third ballot in subcommittee. The standard is a modification of the "Sequential Phased Displacement" (SPD) procedure used by the Joint Technical Coordinating Committee on Masonry Research (TCCMAR) for the United States-Japan Coordinated Earthquake Research Program. This procedure is used by TCCMAR to serve as a uniform basis for comparing components not subjected to real-time earthquake loading during testing. The procedure entails reversed-cyclic displacements of progressively increasing magnitude until a first major event (FME) occurs. The loading is then followed by degradation and stabilization cycles before progressing to the next higher increment of displacements. This process is repeated until failure occurs. Details of the procedure are presented in Dolan (1993, 1994).

For this study, failure was defined as catastrophic failure, when the specimen was physically unable to carry any load, or when a connection slip of 25 mm was obtained. A maximum displacement of 25 mm was used as a failure criteria for two reasons. First, if a connection in a real structure were to slip as much as 25 mm, load would be most likely be transferred to other locations in the structure due to load sharing. Second, the 25 mm inch displacement was close to the maximum displacement that the test fixture could tolerate and continue to maintain the specimen's correct alignment.

The Sequential Phased Displacement (SPD) procedure followed in these tests more accurately represents an earthquake or high wind excitation pattern than does the usual monotonic or simple reverse cyclic loading patterns used for previous tests. Rationale behind this approach centers on two main concepts: degrading of displacements and defining a stabilized hysteresis system. The stabilized hysteresis system provides information for defining conservative estimates of performance and design, and is a more realistic expectation of the response of connections subjected to multiple loading cycles than provided by monotonic loading.

Moisture Content and Specific Gravity Tests

Small specimens were cut from each connection in the vicinity of the nail or bolt immediately after the SPD test was complete. Moisture content and specific gravity were then determined for the wood components of the connection following ASTM D-143, standard methods

of testing small clear specimens of timber (ASTM, 1993).

Property Definitions

All properties determined from the cyclic tests were based on stabilized connection response. In other words, the hysteresis for the last cycle of each phase was extracted from the load-displacement time-history and used for analysis. Three cyclic properties were determined directly from the load-displacement time history. These properties are **hysteretic damping, cyclic stiffness,** and **equivalent viscous damping**, and are defined by Dolan (1993, 1994). However, the results for these variables not included in this report. The reader can find the damping information in Dolan, et al. (1994b).

An additional five properties were determined based on an equivalent energy, elastic-plastic load-displacement curve. The equivalent energy, elastic-plastic curve was based on the envelope curve containing the hysteresis curves for stabilized connection response. These five properties are **elastic stiffness, yield load, yield displacement, stabilized capacity**, and **ductility**.

RESULTS AND DISCUSSION

Prior to presenting detailed results of the experimental investigation, a couple of general observations can be made. First, all of nails and bolts yielded in the predicted modes. This indicates that the yield model does indeed predict yielding of a wood connection properly. However, yield and failure modes can be quite different. For nails and connections governed almost completely by yielding of the fastener, yield and failure modes are typically the same. This is not true for connections that are effected more by crushing of the wood. When significant wood crushing occurred, failure of the connection typically was splitting of the side member of the connection.

A second observation is that connections loaded perpendicular-to-grain were loaded in compression perpendicular-to-grain not tension perpendicular-to-grain. This is one limitation of the specimen configuration used in the investigation, and the effect of tension perpendicular-to-grain should be investigated.

Rresults for monotonic tests of nailed connections are shown in Table 3. Most of the data shown in Table 3 can be found in other research, and the findings presented are not of significance by themselves. However, these tests were included in the investigation as control groups with which results of cyclic tests could be compared. One variable that is not typically determined in monotonic tests is the value of ductility, a measure of how far a connection can deform without failing. As shown, ductility of nail connections was very high (14.3 - 38.2). This is because yielding occurs primary by the nail,which is made of ductile steel wire, withdrawing and bending rather than the wood crushing. One results that was not expected is that lower ductilities were associated with light-gauge steel side plate specimens. This low ductility was due to the short length between the head of the nail and the wood. This produced more shear than bending moment in the nail and resulted in lower connection displacements. The typical failure mechanism for connections with light-gauge steel side plates was for the sheet steel to buckle locally around the nail head rather than the nail withdrawing from the wood. The highest ductilities were associated with the connections with plywood side plates which showed significant crushing in the local area of the nail. Only the two connections consisting of wood members showed a higher ductility in the parallel-to-grain direction due to more severe crushing of the wood around the nail. This crushing was located primarily in the less dense early-wood regions.

The effect of using pilot holes when fabricating the specimens was investigated using the lumber-to-lumber connection configuration with the loading in the parallel-to-grain direction. This configuration was chosen because it had the lowest factor of safety when compared to the 1991 NDS allowable design values. As shown in Table 3, using pilot holes had insignificant effect on capacity of connections, and when differences between the mean values were investigated with the statistical t-test, the hypothesis of the means being the same could not be rejected at the 95% confidence limit. This result validates the data for both connections with and without pilot holes.

Table 4 shows capacities and associated displacements for three nail configurations, both for monotonic and load-controlled cyclic loading. The cyclic loading protocol followed is described in detail by Dolan, et al. (1994a) and will not be presented in detail here. However, the final load level used in the cyclic tests was 75%, 55%, and 46% of capacity for lumber-to-lumber, plywood-to-lumber, and sheet steel-to-lumber connections respectively. If capacities of connections subjected to monotonic loading are compared to capacities of connections after having been cycled, the apparent trend is that prior cycling resulted in a small increase in connection capacities. However, a statistical t-test used to determine whether the means of the samples were different could not distinguish between the samples values at a 95% confidence limit. The same result was obtained when the mean values of the corresponding displacements were compared. This finding indicates that the load history of the connection does not affect the capacity nor the ductility of nailed connections, provided that the loads are kept below 75% of capacity.

Table 5 shows results of monotonic tests on bolted connections. Again, most of the results are similar to findings previously published by other researchers. However, ductilities for the three connections are not generally published, and indicate that bolted connections are less ductile than nails, as would be expected. However, ductilities are much higher than expected, and range from 5.4 to 7.5. This is significant and provides information useful in determining the ductility capacity of a structure constructed with these types of connections.

Table 6 shows capacities and associated displacements for monotonic and load-control cyclic tests of bolted connections. As was found for nail connections, there was no detrimental effect on capacity or ductility of bolted connections when subjected to prior cyclic loading at magnitudes as high as 38% of capacity in the parallel-to-grain direction. Load-control cyclic tests were not conducted for connections loaded perpendicular-to-grain.

Sequential Phased Displacement (SPD) test results for nailed connections are shown in Table 7. While direct comparisons between monotonic and SPD test results is not possible due to differences in variable definition, trends between variables can be seen. First, yield load and displacements are of similar magnitudes, indicting that initial stiffness and curvature of the load-deflection envelope curves from SPD tests are similar to those found with monotonic tests. The elastic stiffness from SPD tests is approximately the same for lumber-to lumber connections, slightly higher for plywood-to-lumber connections, and significantly higher for sheet steel-to-lumber connections when compared to their equivalent monotonic stiffnesses. Finally, stabilized capacities of connections is lower that equivalent monotonic test capcities, as would be expected. However, absolute SPD capacity was not statistically distinguishable from monotonic capacity, indicating again that load history of nail connections does not adversely affect capacity of the connection. This result is even more impressive when one considers that the SPD test subjects connections to over 60 reverse loading cycles before failure occurs, indicating that low cycle fatigue was not a significant problem for the nail connections tested.

If Table 7 is further investigated, the same trends found between the three connections subjected to monotonic loading is prevalent in the SPD test results. Plywood-to-lumber connections are weakest and least stiff, followed by lumber-to-lumber connection, with sheet steel-to-lumber connection being strongest and most stiff. However, ductility values show that lumber-to-lumber connections are the most ductile and sheet steel-to-lumber connections are the least ductile. Again, the ductility trend is a direct result of the nail not withdrawing from the wood in sheet steel-to-lumber connections, while nail withdrawal in the other two connections provided the ductility capacity. This indicates that restrictions on penetration length, such as used in New Zealand, are effective methods to ensure ductility in lateral resisting systems such as shear walls.

The slight difference between capacities of the nail connections constructed with pilot holes and those constructed with driven nails is insignificant. While there was a slight decrease in capacity, the magnitude of loss was small and would not have a significant effect on structural performance.

The only connection effected by grain orientation was the sheet steel-to-lumber connection. As shown in Table 7, when this connection is oriented so that the load is perpendicular-to-grain, stiffness and absolute capacity are higher. The remainder of the performance characteristics are not significantly affected by load orientation with respect to grain of the wood.

Ductility was affected by the SPD test due to the difference in definitions of failure and a small effect of fatigue failures. While low cycle fatigue was not a problem, connections did fail at lower displacement levels during SPD tests than during monotonic tests. This was a direct effect of strain hardening that resulted from repetitive yielding of nails at the hinge location.

Table 8 shows the results of SPD tests on bolted connections loaded parallel-to-grain. When these values are compared to similar values for monotonic tests, a trend becomes apparent. Yield load, stiffness, and stabilized capacity are lower that similar values for monotonic tests. However, absolute capacity of connections either increased when subjected to cyclic loads or remained approximately the same for both tests loads. Ductilities of all connections was lower when the connection was subjected to cyclic loads. This decrease in ductility was at least a 50% reduction from the monotonic values. However, when one considers that elastic stiffness from SPD tests was lower than initial stiffness from monotonic tests, one might assume that displacement at capacity might not be effected. When displacement at capacity is compared for the two tests, the data show that cyclic load history does have a significant effect on the ductility of bolted connection loaded parallel-to-grain. This indicates that while bolted connections retain their capacity during cyclic loading, they become more brittle in their failure mechanism. this result also shows why small dowel diameters are freferable to large dowels when cyclic loading is expected.

The performance characteristics of connections did not change as much when the loading was oriented perpendicular-to-grain. When results for SPD tests of bolts loaded perpendicular-to-grain, shown in Table 9, are compared to results for monotonic tests, shown in Table 5, there is not a significant change in any variable other than stiffness and ductility . This is probably because connections were loaded in compression not tension perpendicular-to-grain, and the primary response of the connections was to crush the wood and the bolt after initial yielding occured. Since displacement at capacity remained fairly constant between the two tests, differnces in ductility are due more to differences in variable definition than changes in performance.

Finally, as with all of SPD test results stabilized capacity of all connections is lower than either monotonic or absolute capacity found in SPD tests. This is due to the initial degrade in

strength associated with crushing of the wood in the local area surrounding nails or bolts. This degrading capacity is significant in many connections and should be considered when setting design values for wood connections. Whether a wood structure is subjected to wind or seismic loading is immaterial if the structure is to survive multiple loading events, stabilized response is the performance that should be assumed for design. This is because a designer does not know ahead of time how many moderate wind storms or earthquakes a structure will experience prior to the design event. Designing for stabilized response will ensure adequate performance.

CONCLUSIONS

The results of an experimental study of the cyclic response of nail and bolt connections were presented and conclucsions about their performance were made. In particular, performance characteristics related to wind and earhtquake loading were discussed. The following conclusions were made after analyzing the results:

- Cyclic load history does not affect the capacity or ductility of nail and bolt connections as long as the load magnitude is below 75% of capacity for nails and 38% of capacity for bolts loaded parallel-to-grain.
- Cyclic loads do reduce the ductilities of bolt connections at higher load levels, and shows why smaller diameter dowel connections provide superior performance when the connection is subjected to cyclic type loading.
- Cyclic loads reduce the stiffness of connections.
- Low cycle fatigue of nails and bolts does not affect the connection configurations tested. However, fastener fatigue did affect nails in that they failed at lower displacements under the SPD test protocol than under the monotonic test protocol.
- A slight difference was observed between the capacity of nail connections constructed with and without pilot holes. However, the magnitude of the difference was small and was not of practical significance.
- Maximum penetration restrictions, such as those used by the New Zealand design code, are benefitial in that they will guarenttee that the nail will withdraw from the wood when loaded lateraly, providing ductile response.

ACKNOWLEDGEMENTS

The author would like to acknowledge the support received from the American Forest and Paper Association for this work through research project number 230-11-110A-023-822663-1.

REFERENCES

AISC Manual of Steel Construction., 1989. American Institute of Steel Construction, Inc. (AISC), New York, NY.

American Society for Testing and Materials (ASTM), 1989. "ASTM A-36/A-36m-88c, Standard specification for structural steel." *Annual Book of ASTM Standards*, Vol 01.06, pp. 106-108. ASTM, Philadelphia, PA.

American Society for Testing and Materials (ASTM), 1992. "ASTM A-446/A-446M-89, Standard specification for steel sheet, zinc-coated (galvanized) by the hot-dip process, structural (physical) quality." *Annual Book of ASTM Standards*, Vol 01.09, pp. 37-78. ASTM, Philadelphia, PA.

American Society for Testing and Materials (ASTM), 1990. "ASTM D-143-83, Methods of Testing Small Clear Specimens of Timber." *Annual Book of ASTM Standards*, Vol. 04.09. ASTM, Philadelphia, PA.

Dolan, J.D., 1993. "Proposed Test Method for Dynamic Properties of Connections Assembled with Mechanical Fasteners." *Proceedings from the Meeting of the International Council for Building Research Studies and Documentation Working Commission W18 - Timber Structures,* August, 1993. 10 pp.

Dolan, J.D., 1994 "Proposed Test Method for Dynamic Properties of Connections Assembled with Mechanical Fasteners." *ASTM Journal of Testing and Evaluation.* 22(6):542-547.

Dolan, J.D. and S.T. Gutshall, 1994a. *Detailed Data for Monotonic and Load-Controlled Cyclic Tests of Nail and Bolt Connections.* Virginia Polytechnic Institute and State University, Timber Engineering Report No. TE-1994-002.

Dolan, J.D. and S.T. Gutshall, 1994b. *Detailed Data for Sequential Phased Displacement Tests of Nail and Bolt Connections.* Virginia Polytechnic Institute and State University, Timber Engineering Report No. TE-1994-004.

Dolan, J.D., S.T. Gutshall, and T.E. McLain, 1994a. *Monotonic and Cyclic Tests to Determine Short-Term Duration-of-Load Performance of Nail and Bolt Connections, Volume I: Summary Report.* Virginia Polytechnic Institute and State University, Timber Engineering Report No. TE-1994-001.

Dolan, J.D., S.T. Gutshall, and T.E. McLain, 1994b. *Cyclic Phased Displacement Tests to Determine Short-Trem Duration-of-Load Performance of Nail and Bolt Connections, Volume I: Summary Report.* Virginia Polytechnic Institute and State University, Timber Engineering Report No. TE-1994-003.

Federal Specification FF-W-92 for Washers, Metal, Flat (Plain), ANSI B18.6.1 American National Standard for Slotted and Recessed Head Wood Screws.

National Design Specification for Wood Construction, 1991. National Forest Products Association., Washington, D.C.

Polensek, A. (1988). Parts of this standard are taken from a draft proposal written by A. Polensek that was never submitted to the ASTM committee.

Porter, M.L., 1987. "Sequential Phased Displacement (SPD) Procedure for TCCMAR Testing" Proceedings of the Third Meeting of the Joint Technical Coordinating Committee on Masonry Research, U.S.-Japan Coordinated Earthquake Research Program, Tomamu, Japan.

Reyer, E. and A.O. Oji, 1991. "Timber Structures - Joints made with Mechanical Fasteners - A Proposed Test Procedure", Presentation at the Meeting of the RILEM TC 109 TSA Meeting in Watford, England.

Table 1: Summary of type and number of nail connection specimens tested under displacement-control cyclic loads.

Fastener Type mm	Main / Side Member Materials	Load Direction	Expected Yield Mode	Number of Replicates
3.7 x 76	Lumber / 12 mm Ply	Parallel-to-Grain	III_s	15
3.7 x 76	Lumber / 12 mm Ply	Perpendicular-to-Grain	III_s	15
4.1 x 89	Lumber / Lumber	Parallel-to-Grain	IV	15
4.1 x 89	Lumber / Lumber	Perpendicular-to-Grain	IV	15
3.7 x 76	Lumber / 1.4 mm Steel	Parallel-to-Grain	III_s	15
3.7 x 76	Lumber / 1.4 mm. Steel	Perpendicular-to-Grain	III_s	15

Table 2: Summary of type and number of bolt connection specimens tested under displacement-control cyclic loads.

Fastener Type	Main / Side Member Materials	Load Direction	Expected Yield Mode	Number of Replicates
19 mm Bolt	38 mm / 38 mm Nominal Lumber	Parallel-to-Grain	II	10
		Perpendicular-to-Grain	II	10
19 mm Bolt	89 mm / 89 mm Nominal Lumber	Parallel-to-Grain	IV	10
		Perpendicular-to-Grain	III_M	10
13 mm Bolt	6 mm Steel Plate / 89 mm Nominal Lumber	Parallel-to-Grain	III_S	11
		Perpendicular-to-Grain	III_S	10

Table 3: Averages and coefficients of variation (%) for monotonic tests of nailed connections.

	38 x 89 / 38 x 89 mm 4.1 x 89 mm Common Nail		12 mm Plywood/ 38 x 89 mm 3.7 x 76 mm Common Nail		1.4 mm steel Plate/ 38 x 89 mm 3.7 x 76 mm Common Nail	
Monotonic Parameters	Parallel-to-Grain	Perpendicular-to-Grain	Parallel-to-Grain	Perpendicular-to-Grain	Parallel-to-Grain	Perpendicular-to-Grain
Yield Load:	1.07 kN (16.4)	0.95 kN (8.8)	0.71 kN (22.4)	0.72 kN (11.1)	1.36 kN (28.0)	1.37 kN (14.6)
Yield Displacement:	0.53 mm (33.3)	0.5 mm (14.1)	0.48 mm (18.9)	0.5 mm (21.6)	0.38 mm (12.7)	0.35 mm (12.2)
Initial Stiffness:	3818 kN/m (42.9)	3363 kN/m (24.4)	2750 kN/m (39.7)	25219 kN/m (33.2)	7706 kN/m (36.8)	8109 kN/m (36.0)
Capacity:	1.82 kN (7) (14.6)	2.02 kN (0) (9.7)	1.64 kN (6) (12.2)	1.74 kN (0) (11.7)	2.34 kN (0) (11.5)	2.73 kN (0) (12.9)
Displacement at Capacity:	15.7 mm (60.5)	10.5 mm (23.9)	17.7 mm (42.6)	10.9 mm (29.4)	5.2 mm (30.8)	5.9 mm (19.6)
Capacity for Driven Nail	2.02 kN -16.8					
Ductility:	30.1 (66.8)	21.4 (25.0)	38.2 (45.5)	22.1 (27.3)	14.3 (30.8)	16.4 (30.6)
Yield Mode:	IV		III_s		III_s	

Note: Numbers in parenthesis to the right of the capacities are the number of specimens in which capacity was controlled by the limiting displacement.

Table 4: Capacity, associated displacement, and their associated COV (%) of nail connections with and without prior cyclic loading.

	38 x 89 mm/ 38 x89 mm 4.1x89 mm Common Nail		12 mm Plywood/2x4 3.7x76 mm Common Nail		1.4 mm Steel Plate/2x4 3.7x76 mm Common Nail	
Parameter	Not Cycled	Cycled	Not Cycled	Cycled	Not Cycled	Cycled
Capacity:	1.82 kN (7) (14.6)	1.95 kN (5) (10.9)	1.64 kN (6) (12.2)	1.66 kN (6) (11.2)	2.34 kN (0) (11.5)	2.37 kN (0) (9.5)
Displacement at Capacity:	15.9 mm (60.5)	12.9 mm (70.5)	17.7 mm (42.6)	18.6 mm (35.8)	5.23 mm (30.8)	6.6 mm -23.6

Note: Numbers in parenthesis to the right of the capacities are the number of specimens in which capacity was controlled by the limiting displacement.

Table 5: Average values and coefficients of variation (%) for monotonic properties of bolted connections without prior cyclic load history.

	38 x 89 / 23 x 89 mm (184 mm) 19 mm bolt		6 mm Steel/ 89 x 89 mm (140mm) 13 mm bolt		89 x 89 / 89 x 89 mm (184 mm) 19 mm bolt	
Monotonic Parameters	Parallel-to-Grain	Perpendicular-to-Grain	Parallel-to-Grain	Perpendicular-to-Grain	Parallel-to-Grain	Perpendicular-to-Grain
Yield Load:	12.5 kN (19.6)	11.3 kN (11.5)	13.0 kN (14.4)	10.7 kN (15.2)	15.4 kN (15.1)	11.2 kN (14.1)
Yield Displacement:	2.8 mm (12.2)	4.3 mm (13.0)	2.6 mm (21.6)	3.7 mm (18.1)	3.7 mm (16.8)	4.37 mm (22.4)
Initial Stiffness:	6585 kN/m (18.6)	3468 kN/m (14.1)	7601 kN/m (30.1)	3590 kN/m (14.4)	5762 kN/m (19.0)	3450 kN/m (26.9)
Capacity:	23.2 kN (3) (18.4)	22.8 kN (9) (7.6)	23.8 kN (4) (16.6)	29.0 kN (10) (5.0)	27.9 kN (10) (9.3)	22.2 kN (10) (11.9)
Displacement at Capacity:	18.7 mm (20.9)	23.1 mm (3.5)	18.4 mm (29.2)	23.4 mm (3.7)	22.7 mm (4.3)	22.5 mm (5.5)
Ductility:	6.5 (17.5)	5.5 (13.4)	7.5 (36.8)	6.5 (21.0)	6.3 (17.3)	5.4 (19.6)
Yield Mode:	II	II	IV	III_M	IV	III_S

Note: Numbers in parenthesis to the right of the capacities are the number of specimens in which capacity was controlled by the limiting displacement.

Table 6: Average capacity, associated displacement, and COV (%) for bolted connections loaded monotonically in the parallel-to-grain direction, with and without prior cyclic loading.

	38 x 89 / 23 x 89 mm (184 19 mm bolt		6 mmSteel/ 89 x 89 mm 13 mm bolt		89 x 89 / 89 x 89 mm (184 mm) 19 mm bolt	
Parameter	Not Cycled	Cycled	Not Cycled	Cycled	Not Cycled	Cycled
Capacity:	23.2 kN (3) (18.4)	26.4 kN (1) (8.6)	23.8 kN (4) (16.6)	25.0 kN (6) (14.0)	27.9 kN (10) (9.3)	27.8 kN (10) (7.9)
Displacement at Capacity:	18.7 mm (20.9)	21.0 mm (12.1)	18.4 mm (29.2)	21.0 mm (19.7)	22.7 mm (4.3)	23.8 mm (3.2)

Note: Numbers in parenthesis to the right of the capacites are the number of specimens in which capacity was controlled by the limiting displacement.

Table 7: Average property values and coefficients of variation for the equivalent energy elastic-plastic system determined in the sequential phased displacement testing.

	38 x 89 / 38 x 89 mm 4.1 x 89 mm Common		12 mm Plywood/38x89 mm 3.7 x 76 mm Common Nail		1.4mm Steel Plate/38x89 mm 3.7 x 76 mm Common Nail	
Parallel-to-grain	Mean	COV	Mean	COV	Mean	COV
Yield Load (Kn)	1.51	*12.4*	1.22	*11.3*	2.19	*10.1*
Yield Displacement (mm)	0.4	*29.2*	0.6	*29.2*	0.5	*28.3*
Elastic Stiffness (kN/m)	3815	*27.0*	2288	*48.9*	4479	*25.1*
Max. Displacement (mm)	6.5	*9.3*	5.6	*10.4*	3.9	*6.6*
Load at Max. Displacement (kN)	1.41	*16.6*	1.24	*12.6*	2.14	*11.7*
Stabilized Capacity (kN)	1.68	*13.9*	1.39	*12.6*	2.42	*9.8*
Displacement at Stabil Cap. (mm)	3.8	*30.7*	4.0	*15.5*	2.4	*11.7*
Yield Load/Stabilized Capacity	0.90	*3.2*	0.88	*3.1*	0.91	*1.8*
Absolute Capacity (kN)	2.1	*15.0*	1.73	*10.3*	2.94	*7.3*
Absolute Capacity Driven Nail kN	1.94	*14.6*				
Ductility Ratio	16.3	*23.3*	10.2	*40.4*	8.1	*27.0*
Yield Mode:	IV		III_s		III_s	
Perpendicular-to-grain	Mean	COV	Mean	COV	Mean	COV
Yield Load (kN)	1.56	*13.1*	1.25	*11.2*	2.22	*20.5*
Yield Displacement (mm)	0.6	*25.5*	0.6	*24.2*	0.5	*25.4*
Elastic Stiffness (kN/m)	3106	*23.6*	2219	*24.3*	4772	*30.2*
Max. Displacement (mm)	6.4	*12.5*	4.5	*11.5*	3.3	*8.9*
Load at Max. Displacement (kN)	1.62	*16.8*	1.27	*15.3*	2.22	*21.5*
Stabilized Capacity (kN)	1.79	*14.0*	1.37	*11.5*	2.42	*20.3*
Displacement at Capacity (mm)	3.9	*36.8*	3.4	*25.3*	2.2	*25.1*
Yield Load/Stabilized Capacity	0.91	*3.0*	0.91	*1.9*	0.92	*2.4*
Absolute Capacity (kN)	2.11	*14.3*	1.75	*10.0*	3.06	*16.7*
Ductility Ratio	12.3	*24.0*	8.1	*27.2*	7.0	*23.1*

Table 8: Averages and coefficients of variation for properties, and apparent factors-of-safety developed from stabilized hystereses in the sequential phased displacement tests for parallel-to-grain orientation.

	38 x 89 / 23 x 89 mm 19 mm bolt		6 mm Steel/ 89 x 89 13 mm bolt		89 x 89 / 89 x 89 mm 19 mm bolt	
Parallel-to-grain	Mean	COV	Mean	COV	Mean	COV
Yield Load (kN)	16.6	*10.8*	16.4	*16.6*	22.0	*12.1*
Yield Displacement (mm)	5.2	*29.1*	3.4	*17.8*	5.1	*17.0*
Elastic Stiffness (kN/m)	3424	*24.1*	4983	*27.4*	4417	*16.6*
Max. Displacement (mm)	11.8	*22.2*	10.3	*28.9*	19.2	*26.7*
Load at Max. displacement. (kN)	17.0	*14.1*	16.7	*15.0*	22.1	*16.1*
Stabilized Capacity (kN)	18.1	*11.3*	17.7	*16.4*	24.8	*12.5*
Displacement. at Stab. Capacity (mm)	10.2	*22.3*	8.4	*26.9*	14.1	*23.9*
Yield Load/Max. Load	0.92	*2.4*	0.93	*1.9*	0.89	*4.7*
Absolute Capacity (kN)	24.0	*10.6*	24.0	*7.0*	30.7	*10.9*
Ductility Ratio	2.4	*21.4*	3.1	*30.5*	3.8	*27.8*
Yield Mode	II		III_s		IV	

Table 9: Averages and coefficients of variation for properties, and apparent factors-of-safety developed from stabilized hystereses in the sequential phased displacement tests for perpendicular-to-grain orientation.

	38 x 89 / 23 x 89 mm 19 mm bolt		6 mm Steel/ 89 x 89 13 mm bolt		89x89 / 89x184 mm 19 mm bolt	
Perpendicular-to-grain	Mean	COV	Mean	COV	Mean	COV
Yield Load (kN)	16.1	*11.7*	20.7	*9.0*	19.1	*10.8*
Yield Displacement (mm)	6.7	*23.5*	6.7	*15.3*	6.1	*20.4*
Elastic Stiffness (kN/m)	2497	*17.4*	3191	*18.1*	3221	*20.8*
Max. Displacement (mm)	21.0	*17.5*	23.7	*7.9*	23.1	*16.7*
Load at Max. Displacement. (mm)	19.0	*11.9*	19.3	*10.5*	19.2	*17.7*
Stabilized Capacity (kN)	19.3	*10.8*	21.7	*10.5*	21.6	*11.0*
Displacement. at Stab. Cap. (mm)	20.1	*20.3*	16.7	*9.6*	16.3	*27.5*
Yield Load/Max. Load	0.83	*5.6*	0.95	*2.7*	0.89	*4.5*
Absolute Capacity (kN)	23.7	*8.6*	23.0	*15.8*	26.5	*8.3*
Ductility Ratio	3.3	*24.8*	3.7	*18.6*	3.8	*18.7*
Yield Mode	II		III_S		III_M	

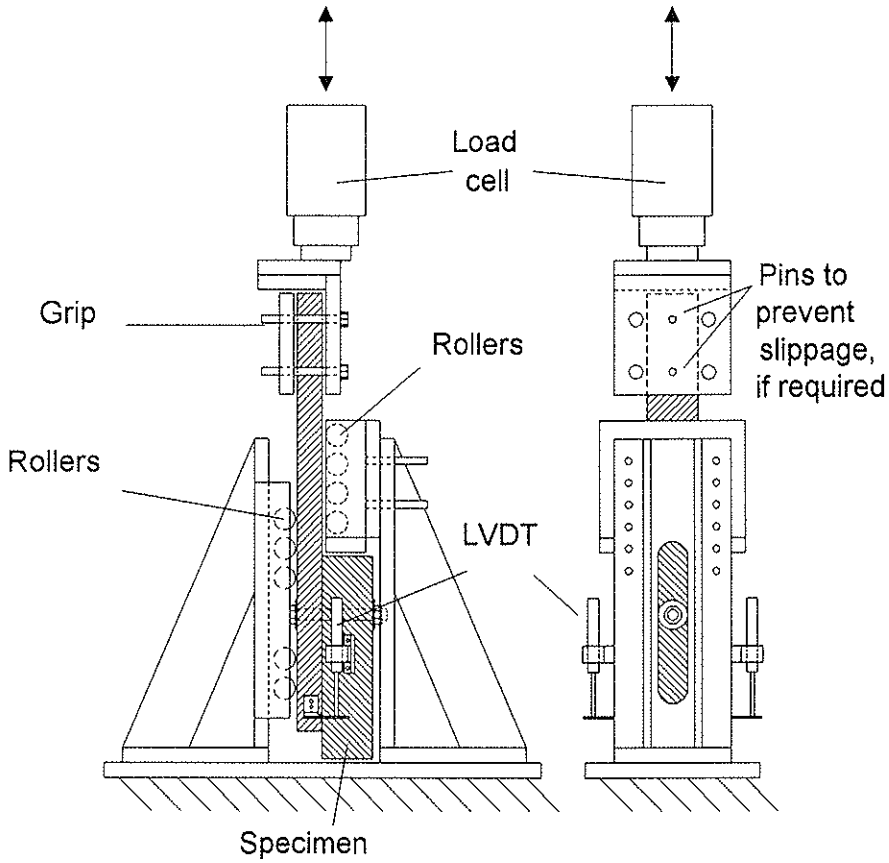

Figure 1: Test fixture used for connection lateral load tests.

INTERNATIONAL COUNCIL FOR BUILDING RESEARCH STUDIES AND DOCUMENTATION

WORKING COMMISSION W18 - TIMBER STRUCTURES

EVALUATION OF CREEP BEHAVIOR OF STRUCTURAL LUMBER IN NATURAL ENVIRONMENT

by

R Gupta

R Shen

Oregon State University

USA

MEETING TWENTY - EIGHT

COPENHAGEN

DENMARK

APRIL 1995

Abstract

In order to describe creep behavior of structural lumber in natural environment, a bending test with twenty Douglas-Fir beams subjected to a constant load was conducted under an open shed in the Forest Research Laboratory at Oregon State University. Deflections of the beams were measured along with daily fluctuations in temperature and relative humidity. An existing five-element creep model [3] was used to fit the experimental data. The five-element model did not describe creep behavior of structural lumber in natural environment. The general observations show that stiffness of the beams has strong influence on magnitude of creep strain, and the creep strain closely follows the fluctuations of air temperature. A four-element model, including the stiffness and air temperature effects, has been developed. The model fits the experimental data very well.

Introduction

Wood, as one of the most commonly used construction materials, exhibits notable creep behavior under sustained loads. It has been verified that creep behavior of wood has significant effects on the safety and serviceability of wood structures over their design life. Number of researchers in the world have been studying this time-dependent behavior of wood for decades.

In previous studies, most of the investigations on creep behavior have focused on small and clear wood samples subjected to the constant environmental conditions [1], [5], [8], [10]. However, wood in service, behaves differently from the small, clear samples, and also wood under constant environmental conditions behaves differently from wood under cyclic environmental conditions. It has been found that the properties of wood change with moisture content, which depends on the temperature and relative humidity of the ambient environment. Therefore, the results of the studies with the small, clear samples may not be directly used for full-size structural beams.

In order to describe creep behavior quantitatively, both empirical and mechanical creep models have been developed from the previous investigations. Fridley et al. [3] developed a five-element creep model using creep data of full-size structural beams subjected to step-constant loads in several constant environmental conditions. The model was capable of predicting creep behavior of wood in controlled cyclic environmental conditions. There are few studies on creep behavior of wood in natural environment [6], [7].

The main objective of this study is to evaluate creep behavior of structural lumber in natural environment. A creep experiment with full-size structural beams subjected to a constant load was set up in an open shed. A four-element model was finally developed to describe creep behavior of structural lumber in natural environment.

Materials and Methods

Twenty, No.2 grade, Douglas-Fir beams (1.5-in. by 3.5-in. by 8-ft.), specially selected from a local lumber mill, are used as specimens for creep test. The basic properties and characteristics (at 11% moisture content) of all specimens, such as dimensions, modulus of elasticity (MOE), specific gravity, and critical defects are listed in Table 1. The specimens were sorted into five test groups from A to E based on their modulus of elasticity (MOE) and specific gravity.

One extra specimen is used for determining moisture content. All specimens were initially conditioned (20°C and RH 69%) to 11% moisture content.

In order to observe long term creep behavior of wood under natural environment, the applied constant load is chosen at a lower level. The applied load for all the specimens is determined in terms of the deflection limits of 1/360 of the span. The load level is about 10% of ultimate strength for group A and 5% of ultimate strength for group E based on the values of modulus of rapture from the Wood Handbook [11]. Each specimen had two seventy-five pound weights two feet apart as shown in Figure 1.

Twenty deflection sensors were used to measure deflections for all the specimens. A load cell was used to monitor the change of weight of the moisture content sample beam. A temperature and relative humidity probe was used to detect the temperature and relative humidity of the ambient environment.

The experiment is set-up in an open shed outside the Forest Research Laboratory (FRL) at Oregon State University. The set-up is shown in Figure 1. A data logger is used to record all data taken by the sensors during the experimental period.

All twenty one specimens were weighted and assumed to have the same moisture content (11%) as the controlled room (20°C and RH 69%) before they were taken to the experimental spot. The experiment is still continuing, but this paper reports the results for about first 5000 hours.

Data Analysis

Creep behavior is usually described using strain in most previous publications. Deflections, in this case, were very small due to the low level of applied load, and were converted into strain using the geometric relationship. Four observations per day based on the corresponding daily maximum and minimum temperature, and the daily maximum and minimum measurements of deflection, were used to determine strain.

The elastic strain is determined using the deflection at three seconds after a specimen is loaded. The following power law was used to predict creep strain at the 5000th hour :

$$\varepsilon(t) = \varepsilon_e + bt^{n} \quad \ldots\ldots (1)$$

where $\varepsilon(t)$ = total creep strain at time t; ε_e = elastic strain; b, n = model constant.

The total creep deformation at the 5000th. hour for every specimen is listed in Table 2. The elastic experimental deformation and the theoretical deformation are also given in Table 2.

The data for one of the specimens was somehow misrecorded, and was excluded from the experiment.

It has been assumed that moisture content of all specimens is same as that of the moisture content sample beam. Moisture content of the sample beam is calculated using the weight of the sample beam at time t and its original moisture content, 11%.

Results and Discussion

Creep Behavior of Structural Lumber in Natural Environment

Temperature and relative humidity of the ambient environment, as well as moisture content of the sample beam are shown in Figure 2. Creep strains for specimens, one from each group, are shown in Figures 3. Figure 4 shows the comparison of air temperature with creep strain of one specimen.

Several characteristics have been observed from the analysis of the environmental data collected over six months. Figure 2 shows that moisture content of the sample beam changes little during the six months, although daily temperature and relative humidity fluctuates frequently. This can be explained by the fact that the wood beams responding to the variations in the environment is not as quick as that of the air. Besides, average temperature, 16° C, and average relative humidity, 69%, during the six months for the experiment, are close to the initial environmental conditions in the controlled room (20° C, RH 69%).

Table 2 shows the differences in deformations among the specimens in detail. Some trends about the elastic deformations and the creep deformations can be observed in this table. The value of elastic deformations decreases from group A (lowest MOE) to group E (highest MOE), and so does the value of the total creep deformations (the 5000th. deformations). The same trend for creep strain can also be observed from Figure 3. The total strain goes down from group A to group E. This is because the magnitude of MOE mirrors the stiffness or the capability of the material to resist against deformation in elastic region. Therefore, deformation is smaller for the specimen with higher MOE.
Creep strain for the specimens within each group are close to each other. However, specimen 04A5 has much higher creep strain than the others in group A, whereas, its MOE and specific gravity is close to the others. The defects within load span for each specimen in Table 1 shows that specimen 04A5 is the only one in group A having an edge knot, and the knot is located at the center of the beam, although in the compression zone. However, the grain distortion around the knot extends into the tension zone causing large deflections.

Since each specimen has similar shape of the creep strain curve, and it was observed from Figure 4 that creep strain of one of the specimens follows the fluctuations in air temperature, it is concluded that creep strain follows the fluctuations in air temperature for every specimen. This observation agrees with previous studies that the stiffness of wood decreases as temperature increases, based on constant moisture content [2], [4], [11]. Therefore, the air temperature may have more influence on creep behavior of full-size beams in natural environment.

Modelling

A five-element creep model

A five-element creep model was developed by Fridley et al. [3], to predict load and environmental effects, as well as mechano-sorptive effects to the primary and secondary creep behavior. For a constant load, the model is expressed as follows:

$$\varepsilon(t) = \frac{\sigma}{K_e} + \frac{\sigma}{K_k}\left[1 - \exp\left(-\frac{K_k t}{\mu_k}\right)\right] + \frac{\sigma t}{\mu_v} + \frac{\sigma}{\mu'_{ms}}|\Delta w|\left[1 - \exp\left(-B_w t\right)\right] \quad \ldots\ldots (2)$$

Where $\varepsilon(t)$ is total strain at time t for the applied stress σ. All other variables are explained in Fridley et al. [3]. The mechano-sorptive strain in the model mainly depends on the changes of moisture content, Δw, and the parameter, μ'_{ms}, for the mechano-sorptive element was developed under controlled environmental conditions [3].

The prediction for creep strain of structural lumber in natural environment using the five-element model are shown in Figure (5) and (6). The predicted result is close to the experimental data for group C (Figure 6), but far below for group A (Figure 5). This is probably due to the difference in MOE between the two groups.

Unlike this study, in Fridley's experiment for developing the five-element model, all groups of specimens had similar values of MOE [3]. Although MOE (K_e, the elastic spring constant) has been included in Fridley's model, it can only predict creep strain of the specimen which has similar MOE to those used in developing the five-element model.

It has previously been discussed that creep strain is also affected by MOE. As shown in Figure 5, predicted strain from Fridley's model is much lower than the actual strain. This is because the MOE for group A is much lower than that for those used to develop this model. On the other hand, the MOE for group C is close to that for Fridley's samples as shown in Figure 6. Therefore, the predicted creep curve is close to the experimental creep curve.

Based on the discussions above, a creep model should include a parameter, which takes MOE effects into account, so that, the model can describe creep behavior of beams with different MOE.

It has also been observed from Figure (5) and (6) that the five-element model does not describe the fluctuations in creep strain, like the experimental curves. It has been previously discussed that the fluctuations in creep strain is due to the air temperature, not the moisture content. Although the five-element model does include the temperature effects, its contribution to the creep strain is very small. However, in this study, as the recorded moisture content changed little during the six months, the relative change of moisture content is almost zero. Probably thanks to this reason, the predicted curves do not reflect the environmental fluctuations, as expected.

The mechano-sorptive element in Fridley's model has no effects on creep strain in our experiment. After the mechano-sorptive element is taken off from the five-element model, the predicted curve using the Burger model is exactly on the top of the predicted curve using the five-element model, showing no mechano-sorptive effects. This is because the mechano-sorptive element is dominated by the changes of moisture content, Δw. As it has been discussed, the moisture content during the six months has changed little. Therefore, the mechano-sorptive creep strain has contributed little to the total creep strain.

The model parameters in Fridley's study [3] were determined under either constant or controlled cyclic conditions with large changes of moisture content, which may not be suitable for creep behavior under natural environmental conditions. This is probably the other reason why the five-element model does not predict the creep behavior of structural lumber in natural environment.

Four-element model

The four-element model, developed in this study, includes MOE and temperature effects, based on the Burger model, shown as follows:

$$\varepsilon(t) = Q*\{\frac{\sigma}{K_e} + \frac{\sigma}{K_k}*[\,1-\exp\,(-\frac{K_k*t}{\mu_k})\,] + \frac{\sigma*t}{\mu_v}\}. \quad . \quad . \quad . \quad . \quad . \quad (3)$$

where $\varepsilon(t)$ = total strain at time t; Q = MOE factor (reference MOE, 1.35 x 10^6 psi (07D5) divided by actual edge-wise MOE, E_e in Table 1); σ = the applied stress; K_e =the Hookean spring constant associated with elastic deformation(i.e., modulus of elasticity); K_k and μ_k =the Hookean spring constant and viscosity of the Newtonian dash pot, respectively, of the Kelvin element; μ_v=the viscosity of the Newtonian dashpot associated with unrecoverable strain. However, if the four parameters, K_e, K_k, μ_k, and μ_v, are constant, the prediction will be a smooth exponential curve. Therefore, the temperature fluctuations were added into the model to adjust K_e, K_k, μ_k, and μ_v for the temperature effects.

Figure 7 shows the predicted creep curve using the four-element model, equation (3), and the experimental creep curve of the reference specimen, 07d5. Although the predicted curve is not on the top of the experimental curve, the predicted curve reflects the fluctuation trends of the experimental curve, and is quantitatively close to the experimental curve.

Figure (8) to (11) shows the predicted creep strain and experimental creep strain of specimens, one from each group other than group D. It can be observed that the predicted creep strain may quantitatively represent the experimental creep strain.

A computer program, Statgraphics [9], was used to statistically compare the predicted creep data with the experimental creep. The comparison results show that the predicted data using the four-element model is statistically equal to the experimental data. Therefore, The four-element model, equation (3), could be used to predict the creep behavior of structural lumber in natural environment.

Summary

Based on the analysis of the data from the creep experiment over six months, it may be concluded that creep deformation can be much larger than elastic deformation, and it depends upon the stiffness of the beams.

The Fridley's five-element creep model does not predict creep behavior of structural lumber in natural environment. Due to the little change in moisture content in the specimens, the mechano-sorptive element in the five-element model does not contribute creep strain of structural lumber subjected to the natural cyclic environmental conditions.

It was observed that the fluctuations of creep strain follow the variations of air temperature. Temperature fluctuations and edge-wise MOE are considered to be two major effects in modelling. A four-element model was developed to predict the creep strain of structural lumber in natural environment. The four-element model has fitted the experimental data very well. The four-element model has verified that MOE of the beams does affect the creep strain.

Literature cited

1. Christensen, G.N. 1962: *The use of small specimens for studying the effect of moisture content changes on the deformation of wood.* Aust. J. Appl. Sci., Vol. 13, No. 4:242-257.

2. Davidson, R.W. 1962: *The influence of temperature on creep in wood.* Forest Products Journal, August, 377-381.

3. Fridley, K.J., R.C. Tang and Lawrence A. Soltis 1992d: *Creep behavior model for structural lumber.* Journal of Structural Engineering. 118(8):2261-2277.

4. Fridley, K.J., R.C. Tang and L.A. Soltis 1990a: *Thermal effects on load-duration behavior of lumber. Part 1. Effect of constant temperature.* Wood and Fiber Sci. 21(4):420-431.

5. Grossman, P.U.A. and Kingston 1954: *Creep and strss relaxation in wood during bending.* Aust. J. Appl. Sci. 5(4):403-417.

6. Meierhofer U. and J. Sell 1979: *Physical phenomena in timber construction elements exposed to weathering, Part 2: Structural timber elements exposed to outdoor weathering under shelter.* Holz als Roh-und Werkstoff 37:227-234.

7. Pozgaj, A. 1982: *Deformation of wood during creep flexural load in an outdoor climate.* Holztechnologie, 23(1):36-40.

8. Senft, J.F. and S.K.Suddarth 1971: *An analysis of creep-inducing stress in Sitka spruce.* Wood Fiber 2(4):321-327.

9. Statgraphics, version 5 1991 STSC, Inc.

10. Szabo, T. and G. Ifju 1970: *Influence of stress on creep and moisture distribution in wooden beams under sorption conditions.* Wood Sci. 2(3):159-167.

11. Wood Handbook-wood as an engineering material 1987: USDA. Forest Service, Forest Products Lab. Agriculture handbook No.72.

TABLE 1. INITIAL PARAMETERS OF SPECIMENS

Group	Spec No.	Width (in.)	Depth (in.)	Length (ft.)	Modulus of Elasticity (10^6 psi) Ef.	Ee.	Ec.	Weight (lbs.)	MC (%)	Specific Gravity	Defect in Load Span
A	02A1	1.505	3.511	8.0	1.28	1.07	1.42	8.973	11	0.491	CK
	01A3	1.509	3.516	8.0	0.98	0.97	1.10	7.231	11	0.395	CK
	03A4	1.513	3.508	8.0	1.22	0.95	1.39	9.017	11	0.496	CK
	04A5	1.489	3.457	8.0	1.23	0.93	1.33	8.179	11	0.446	EK
B	17B2	1.513	3.538	8.0	1.32	0.98	1.50	8.708	11	0.481	EK
	19B3	1.506	3.519	8.0	1.43	1.19	1.51	9.237	11	0.506	EK
	18B4	1.502	3.511	8.0	1.38	1.21	1.45	8.620	11	0.468	CK
	20B5	1.519	3.520	8.0	1.46	1.30	1.51	8.267	11	0.444	CK
C	13C1	1.516	3.530	8.0	1.71	1.47	1.89	9.854	11	0.593	CK
	14C2	1.514	3.529	8.0	1.56	1.15	1.70	9.766	11	0.537	CK
	16C4	1.512	3.515	8.0	1.50	1.65	1.59	9.237	11	0.505	EK
	15C5	1.517	3.530	8.0	1.56	1.27	1.64	9.083	11	0.487	CK
D	05D2	1.512	3.515	8.0	1.90	1.89	1.96	9.877	11	0.528	EK
	06D3	1.505	3.517	8.0	1.83	1.42	1.98	10.317	11	0.566	EK
	07D5	1.518	3.537	8.0	1.79	1.35	2.08	10.163	11	0.557	EK
	08D8	1.521	3.510	8.0	1.81	1.68	2.10	9.832	11	0.536	CK
E	09E2	1.508	3.515	8.0	2.31	1.71	2.57	10.979	11	0.603	CK
	10E3	1.509	3.515	8.0	2.18	1.96	2.37	10.053	11	0.552	EK
	11E4	1.518	3.515	8.0	2.15	1.61	2.52	10.670	11	0.592	CK
	12E7	1.526	3.539	8.0	2.06	1.53	2.26	10.406	11	0.564	EK

MOE = Modulus of Elasticity; Ef = Flatwise MOE; Ee = Edgewise MOE;
Ec = Dynamic MOE; MC = Moisture Content;
CK = Centerline Knot; EK = Edge Knot.

TABLE 2. COMPARISON OF DEFORMATION

Group	Specime No.	Elastic Deform. (in.)	Equatio Deform. (in.)	Creep Deform. (in.)
A	02A1	0.212	0.214	0.430
	01A3	0.290	0.274	0.476
	03A4	0.261	0.218	0.493
	04A5	0.282	0.242	0.758
B	17B2	0.242	0.197	0.422
	19B3	0.218	0.199	0.415
	18B4	0.213	0.210	0.381
	20B5	0.187	0.198	0.277
C	13C1	0.137	0.157	0.241
	14C2	0.164	0.175	0.456
	16C4	0.174	0.189	0.262
	15C5	0.178	0.181	0.292
D	05D2	0.148	0.154	0.241
	06D3	0.154	0.152	*
	07D5	0.176	0.141	0.311
	08D8	0.128	0.143	0.178
E	09E2	0.116	0.117	0.207
	10E3	0.120	0.127	0.196
	11E4	0.125	0.119	0.208
	12E7	0.138	0.129	0.260

* Data lost

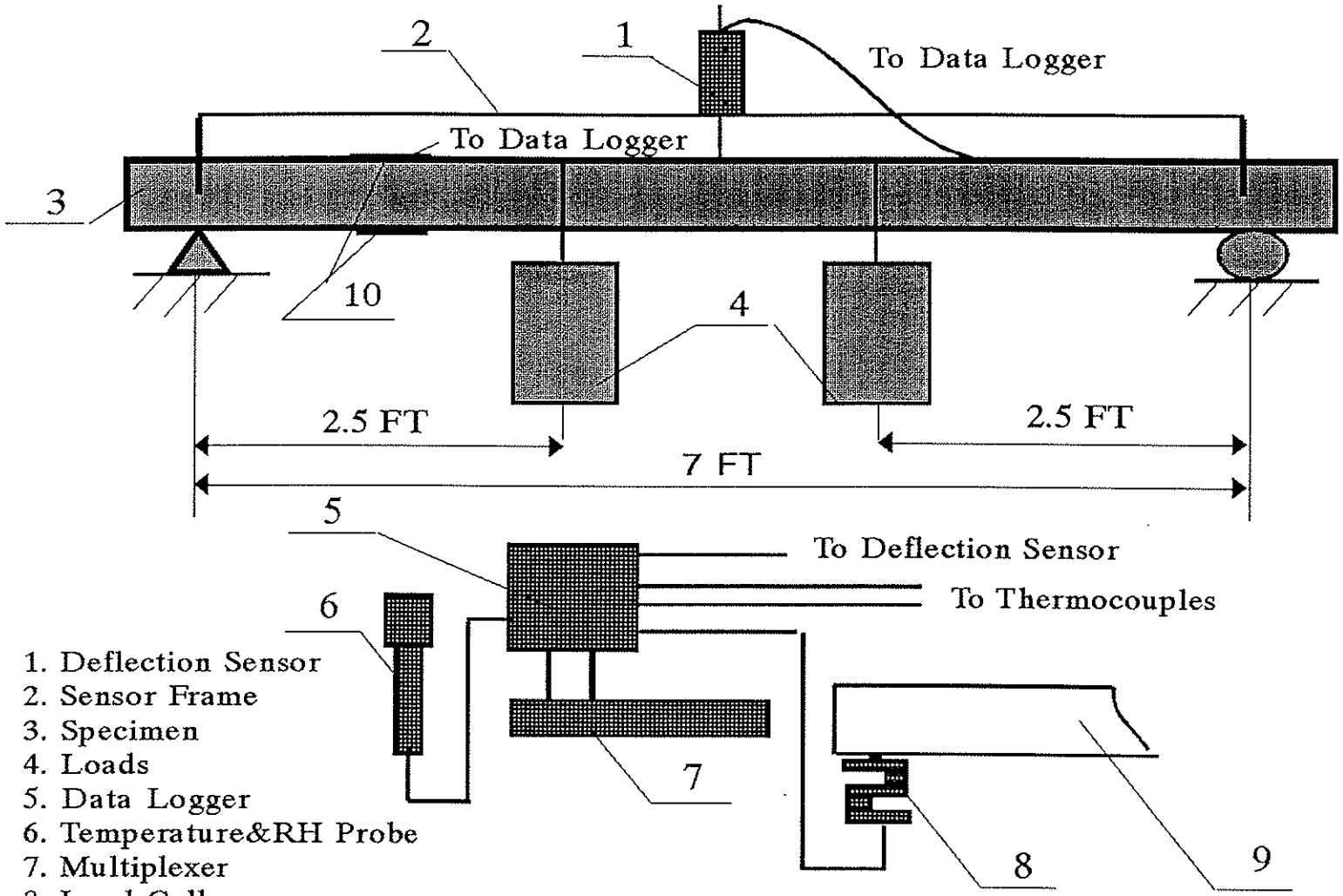

Figure 1 Set-Up of Experiment

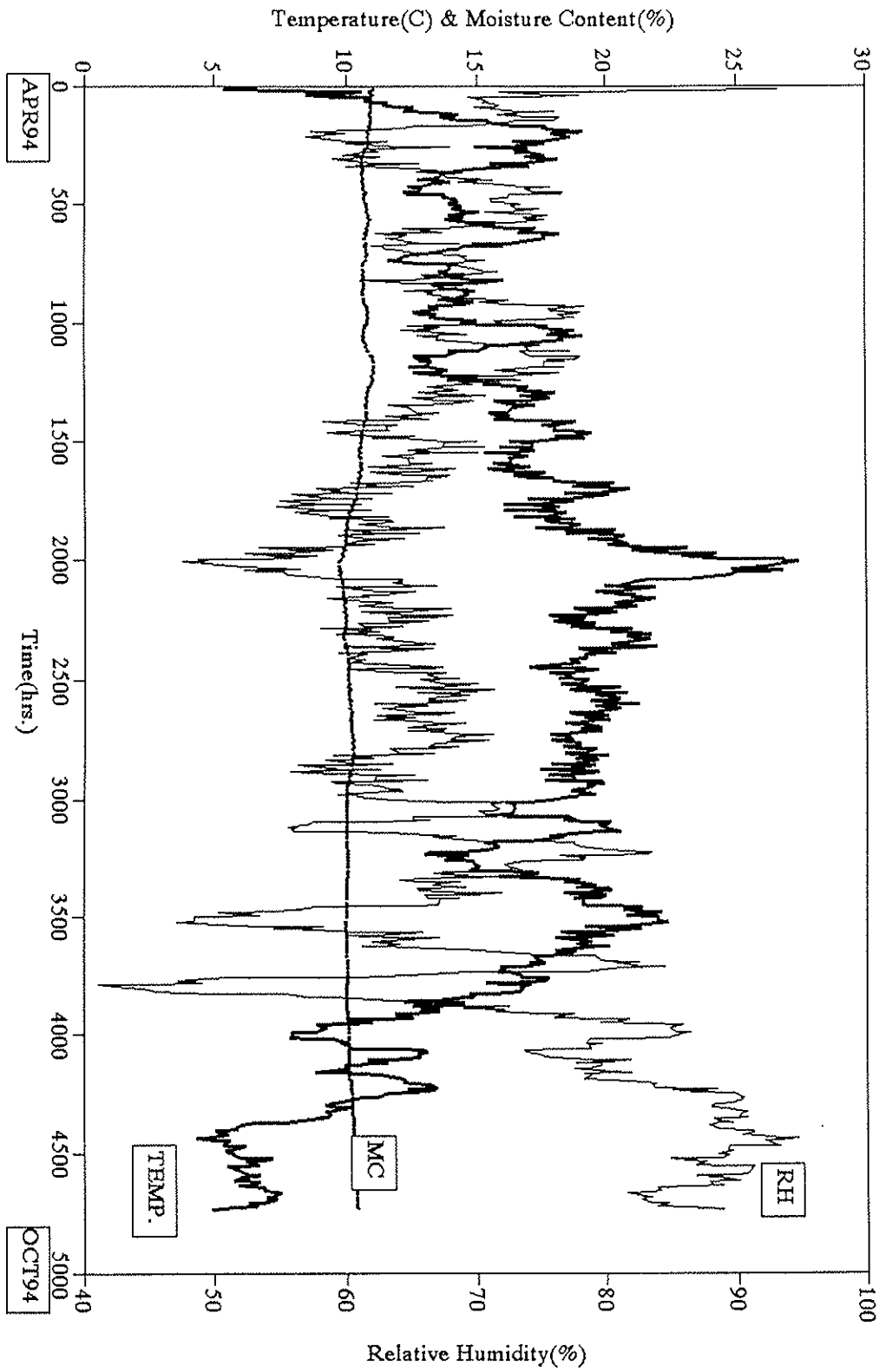

Figure 2 Environmental Characteristics and Moisture Content

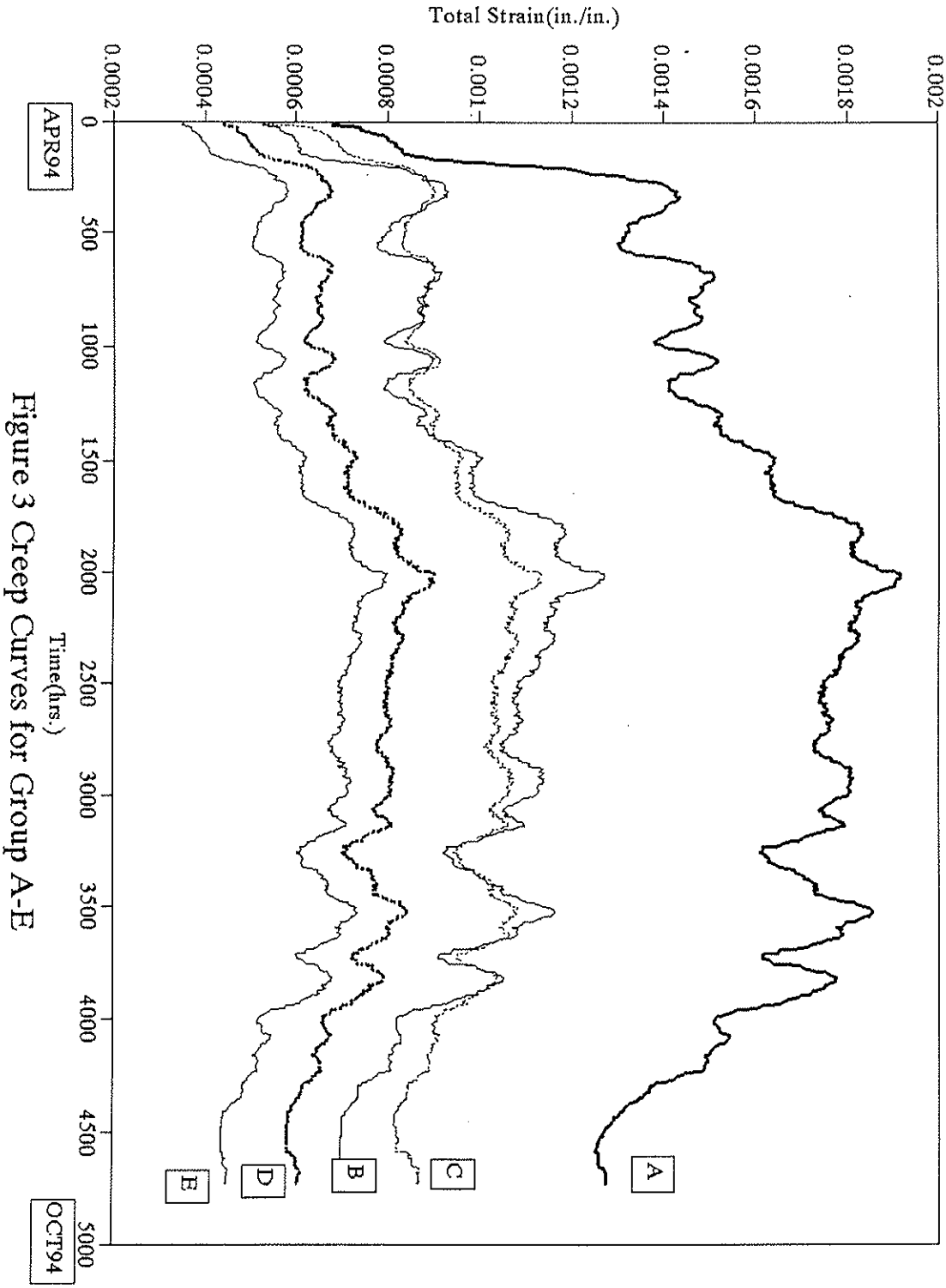

Figure 3 Creep Curves for Group A-E

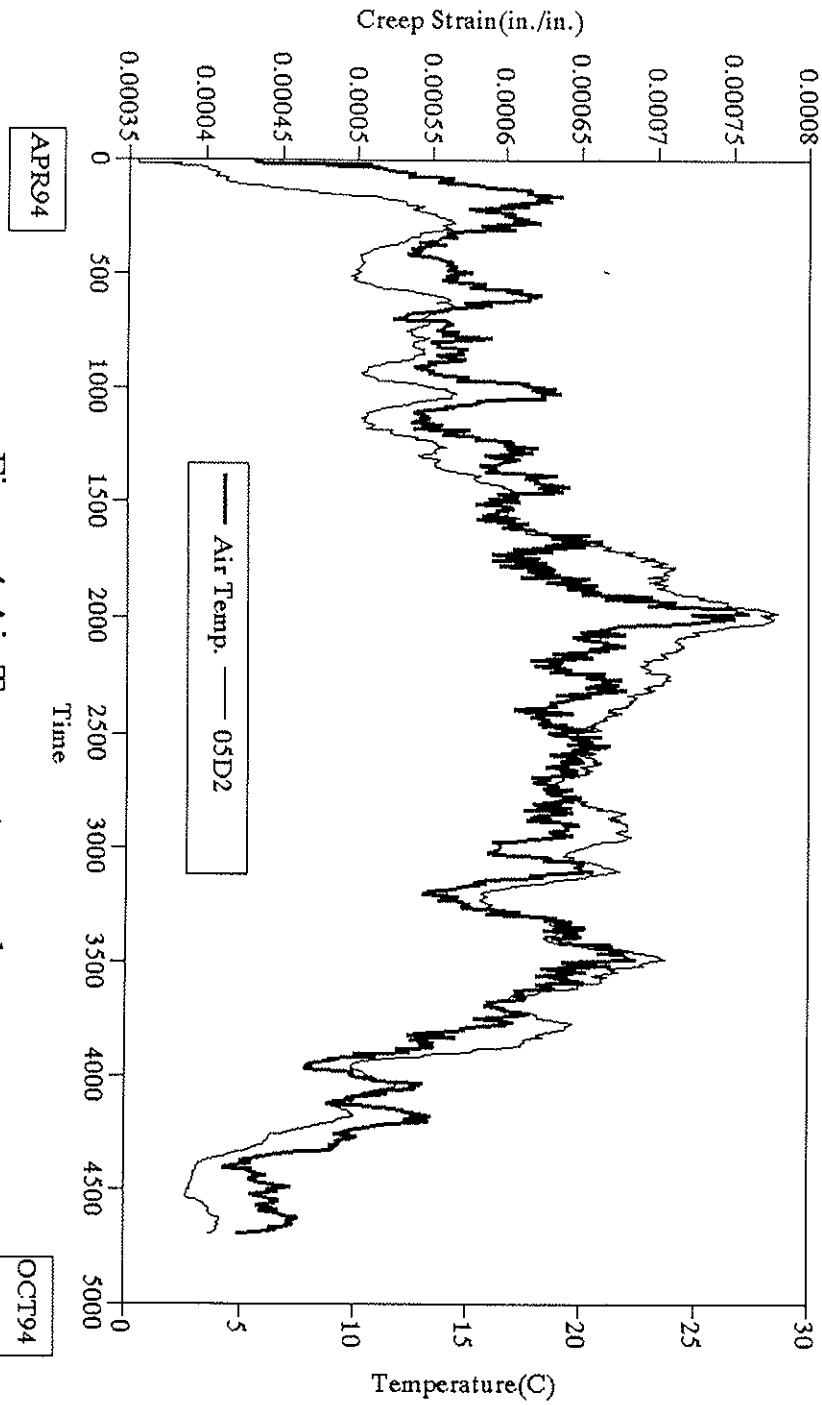

Figure 4 Air Temperature and Creep Strain

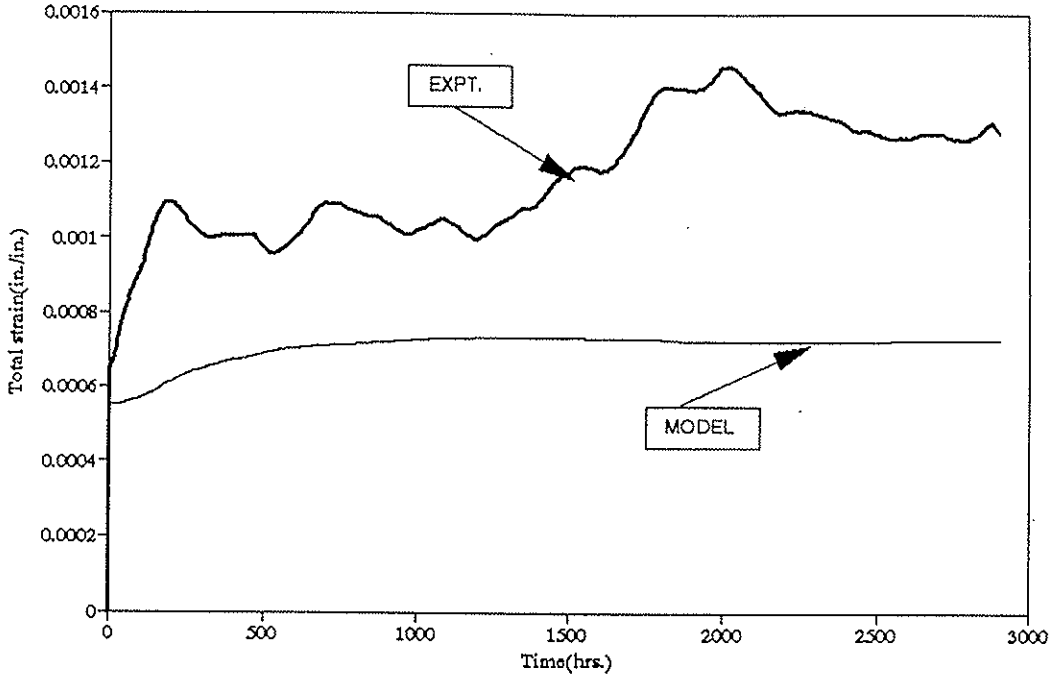

Figure 5 Strain(Group A) Predicted
Using Five-element Model(Fridley)

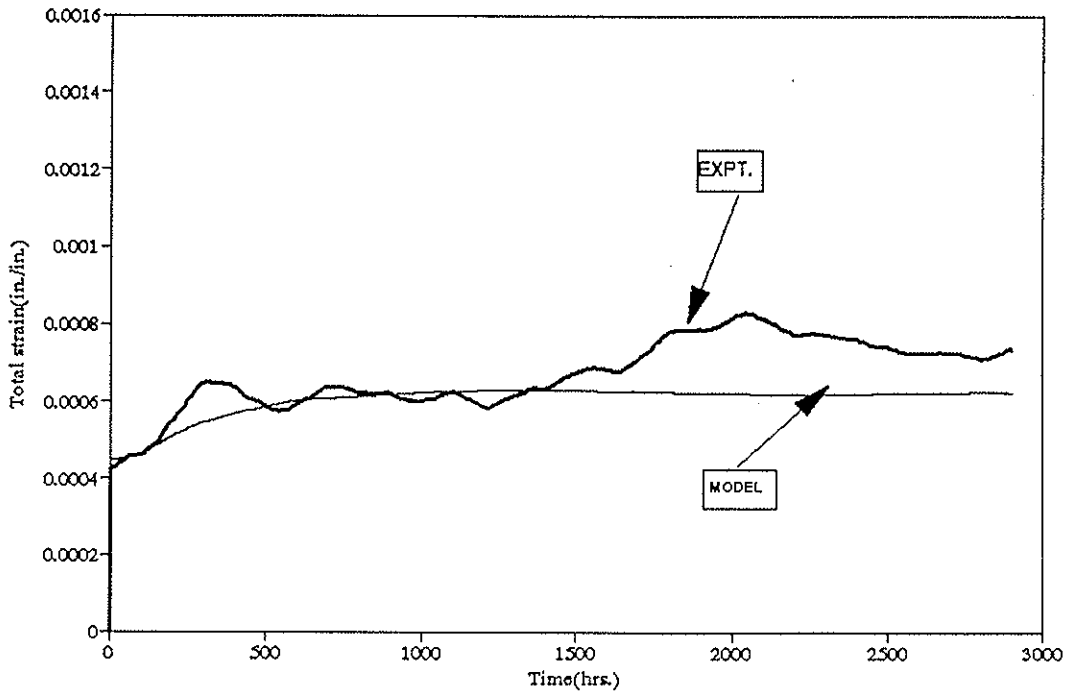

Figure 6 Strain(Group C) Predicted
Using Five-element Model(Fridley)

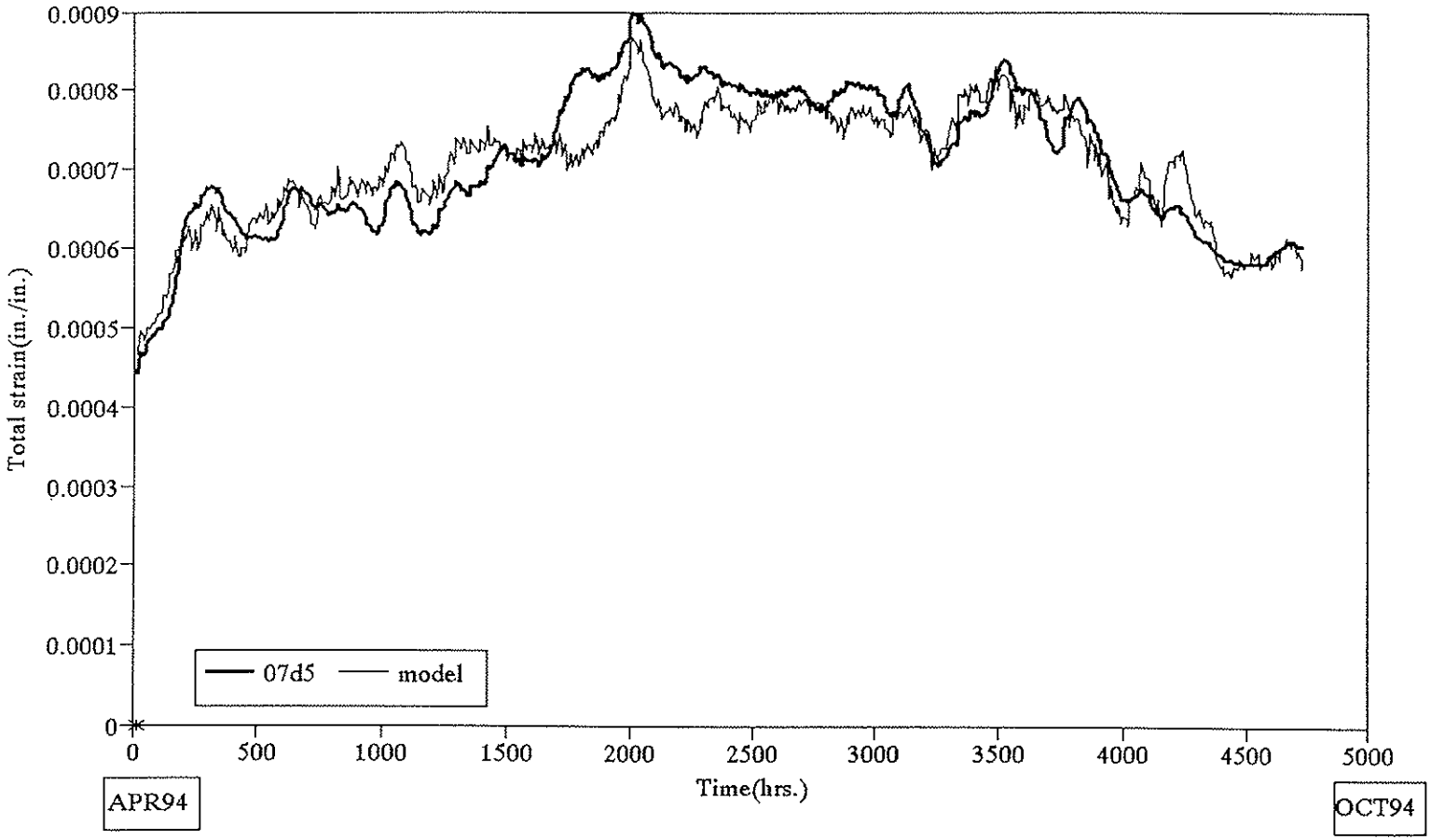

Figure 7 Four-Element Model
Prediction for Reference Beam 07d5

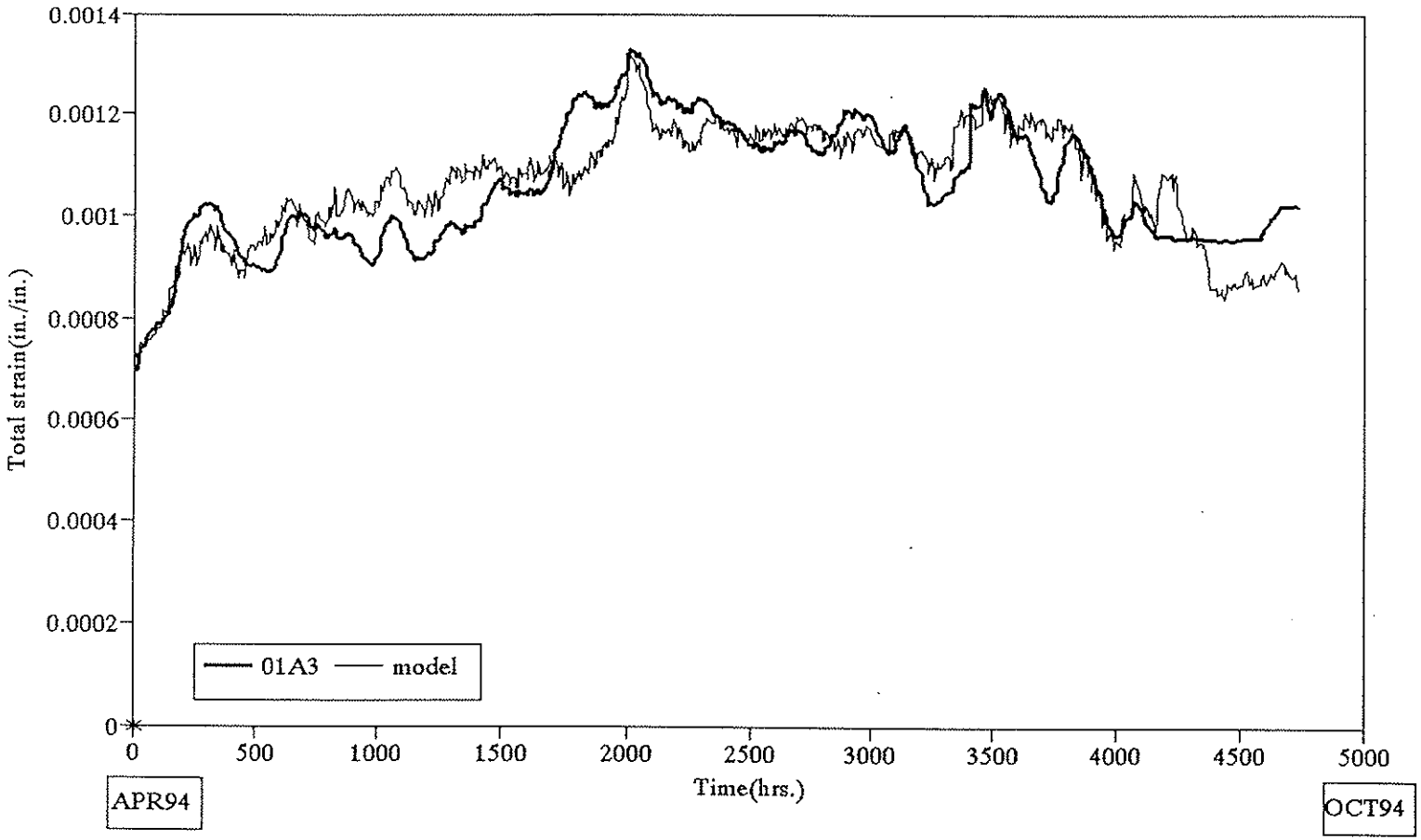

Figure 8 Four-Element Model
Prediction for 01A3

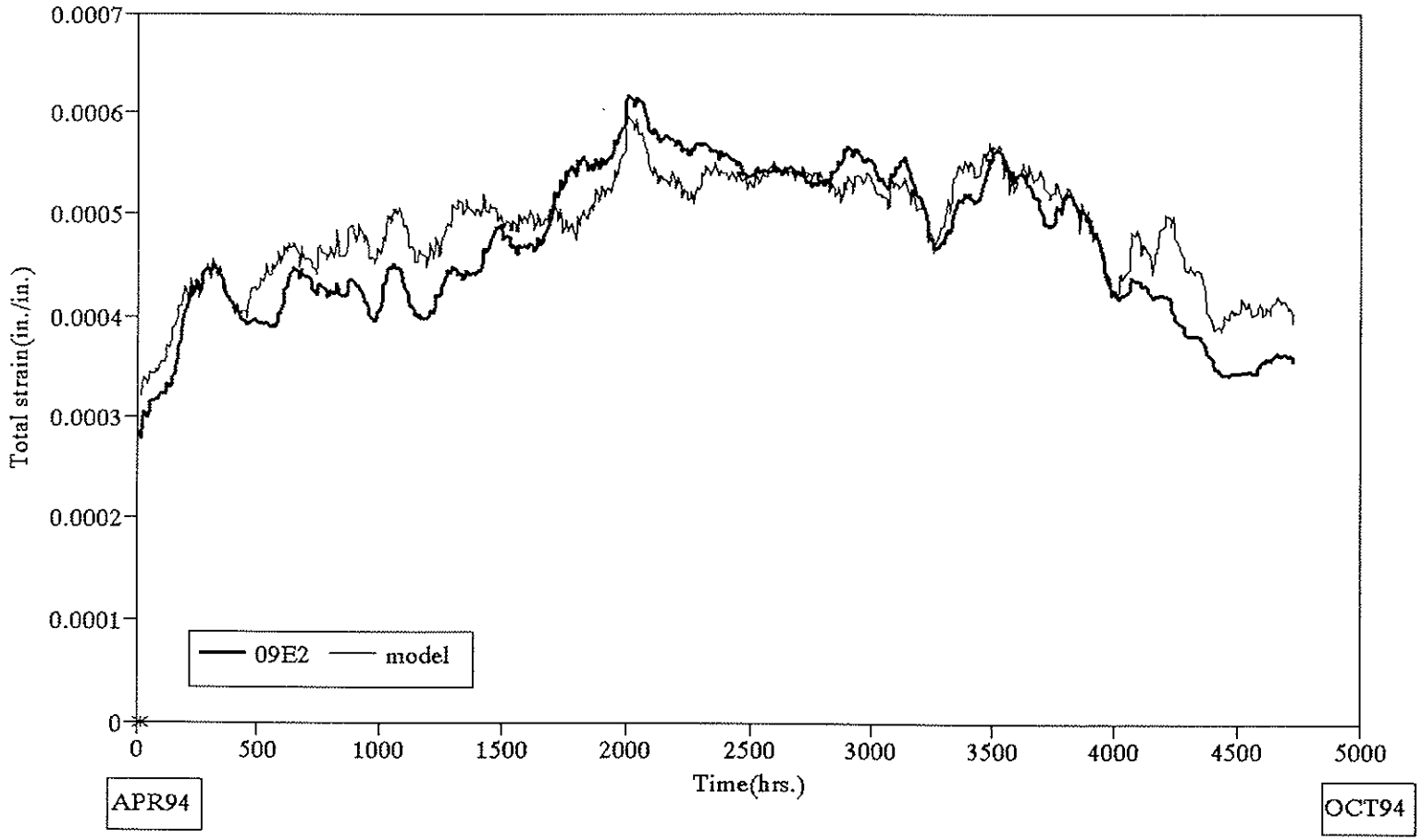

Figure 9 Four-Element Model
Prediction for 09E2

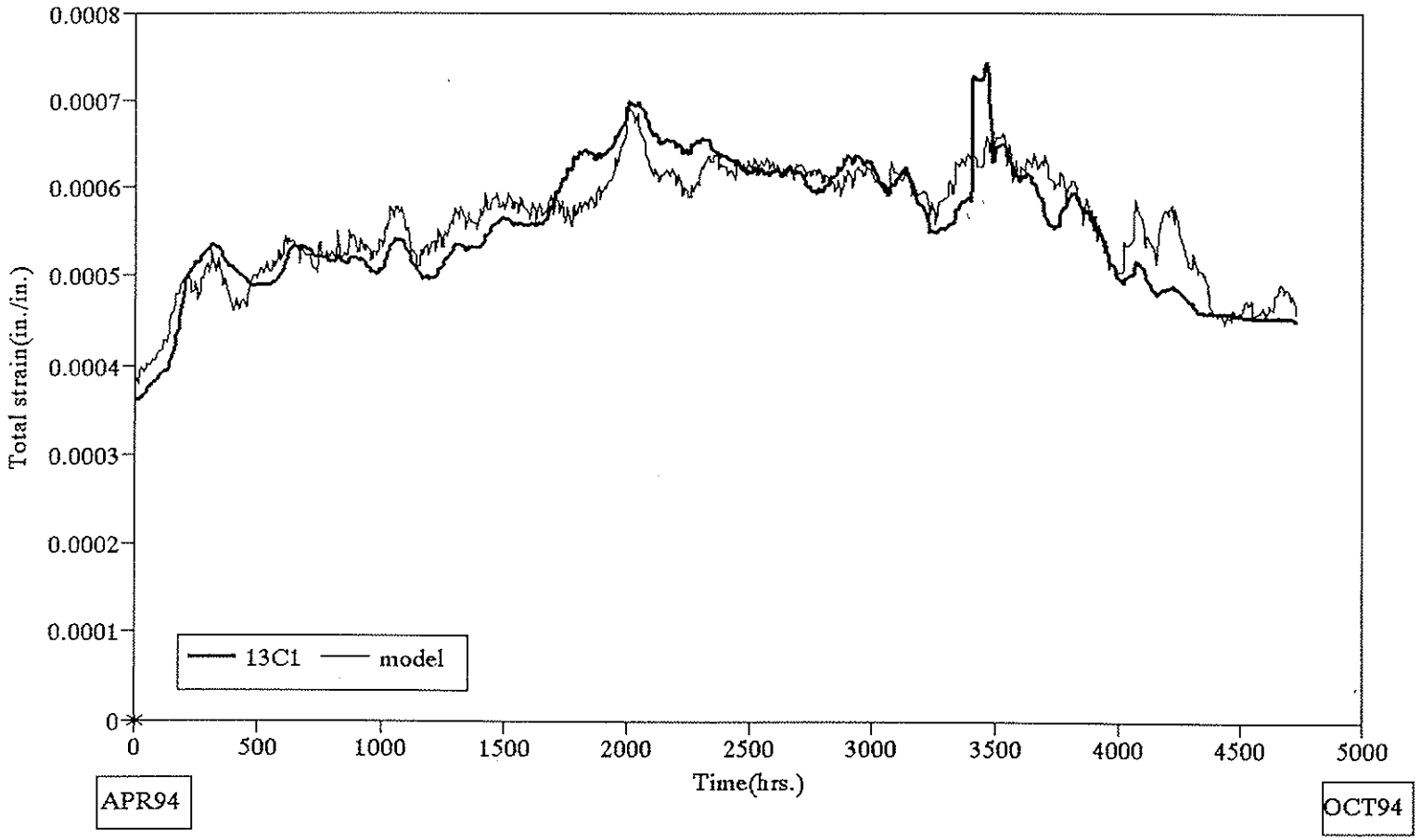

Figure 10 Four-Element Model
Prediction for 13C1

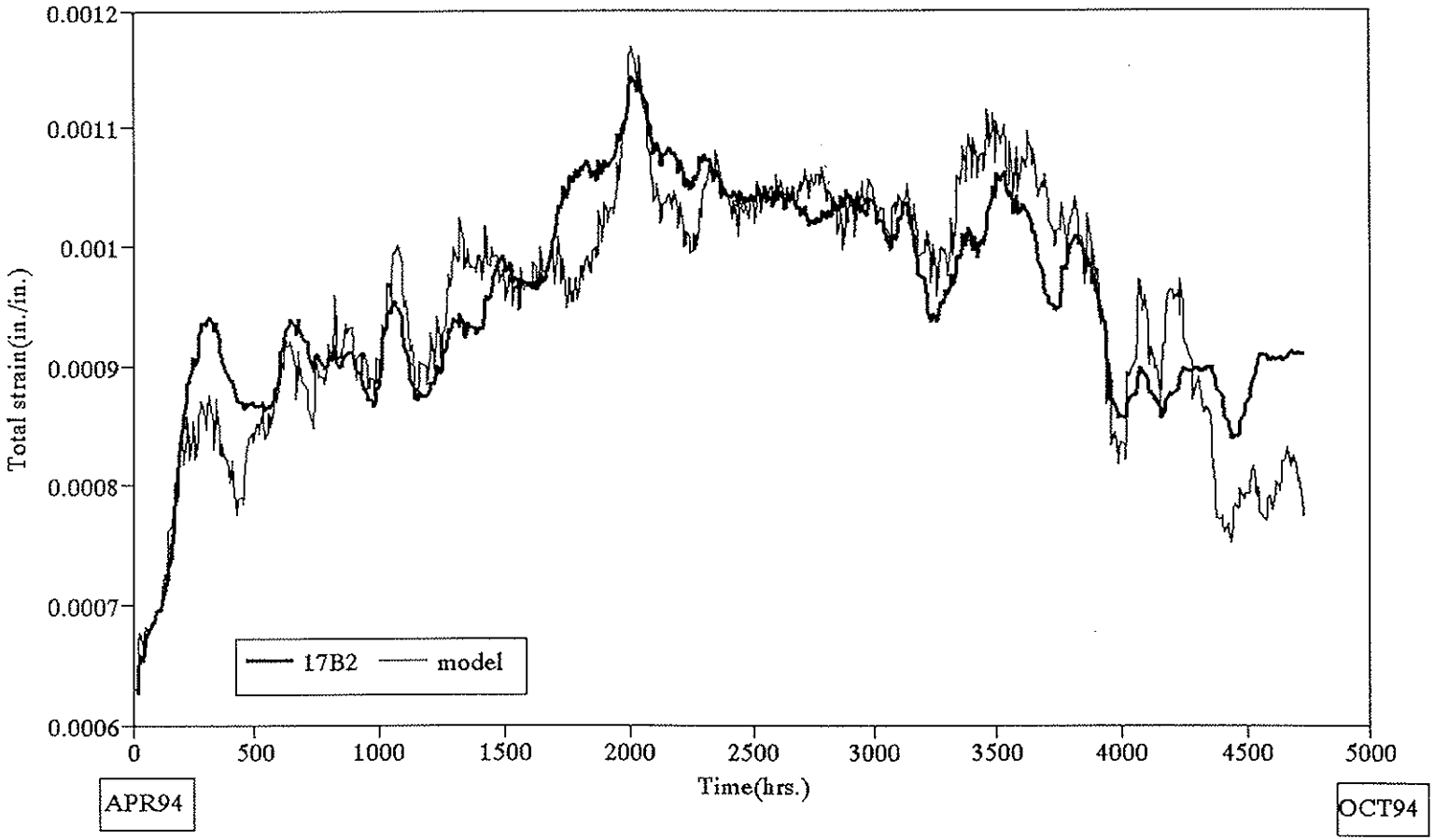

Figure 11 Four-Element Model
Prediction for 17B2

INTERNATIONAL COUNCIL FOR BUILDING RESEARCH STUDIES AND DOCUMENTATION

WORKING COMMISSION W18 - TIMBER STRUCTURES

DETERMINATION OF CHARACTERISTIC BENDING STRENGTH OF GLUED LAMINATED TIMBER

by

E Gehri
Federal Institute of Technology, Zurich
Switzerland

MEETING TWENTY - EIGHT

COPENHAGEN

DENMARK

APRIL 1995

1. Introduction

The situation up to 1992 has been described by Gehri (1992) where also the requirements for the finger-joint based on the tensile strength are given. Meanwhile new research by Falk / Solli / Aasheim (1992) and Colling (1994) allow a better understanding of the behaviour of glued laminated beams in reference to the lamination strength. The last draft of prEN 1194 (September 1994) takes partly in account the new findings.

It has to be recalled here that the strength model for bending is now based on a depth of h = 600 mm and a beam length of 16 to 18 times the depth (see figure 1).

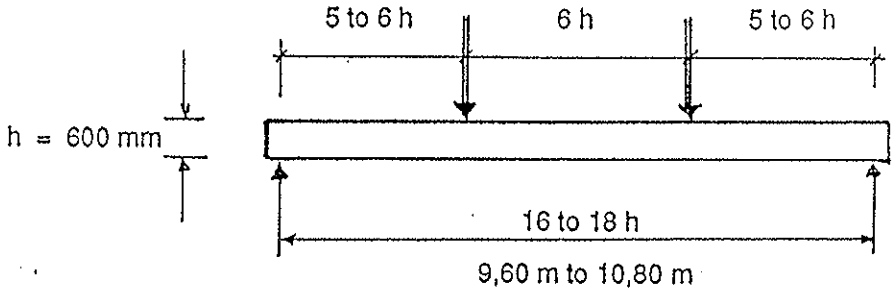

Figure 1: Geometry and load application for reference depth h = 600 mm

The width of the beam had not been considered in the bending strength model till now, although in all "european" strength models the tensile strength of the laminations has to be referred to a width of t = 150 mm, using adjusting factor of $(150/b)^{0,2}$. This seems not logical.

The strength model used in the USA takes in account for both, for tensile strength of the lamination and for bending strength of the glulam beam, a width factor (see AITC 117 – 93: Design Standard Specifications for Structural Glued Laminated Timber). This has to be reminded when analysing and comparing the results of different research works.

2. Strength models for bending based on wood strength

The european strength models for bending based on wood strength have the following form:

$$f_{m,g,k} = a_\ell + b_\ell \cdot f_{t,0,\ell,k}$$

The above model is valid for homogeneous girders. For combined sections, with outer laminations of depth h/6 and modulus of elasticity E_2 , the model has to be adjusted with the multiplication factor:

$$\left[1 - \left(\frac{2}{3}\right)^3 \left(1 - \frac{E_2}{E_1}\right)\right]$$

E_2 : outer laminations
E_1 : inner laminations

$E_2 > E_1$

For the constants a_ℓ and b_ℓ the following proposals were made:

- Gehri (1992) $a_\ell = 12$ N/mm^2 $b_\ell = 1.0$

  This proposal is a simple linearisation of an earlier proposal in prEN 1194:

  $$f_{m,g,k} = (2.35 - 0.035\, f_{t,0,\ell,k})\, f_{t,0,\ell,k}$$

  a formula proposed by Riberholt/Ehlbeck/Fewell (1990).

- Colling (1994) $a_\ell = 7$ N/mm^2 $b_\ell = 1.15$
- prEN 1194 (Sept. 94) $a_\ell = 9$ N/mm^2 $b_\ell = 1.20$

The proposal made by Colling (1994) gives a better approach of the available test results. The results of the different proposals are given in figure 2.

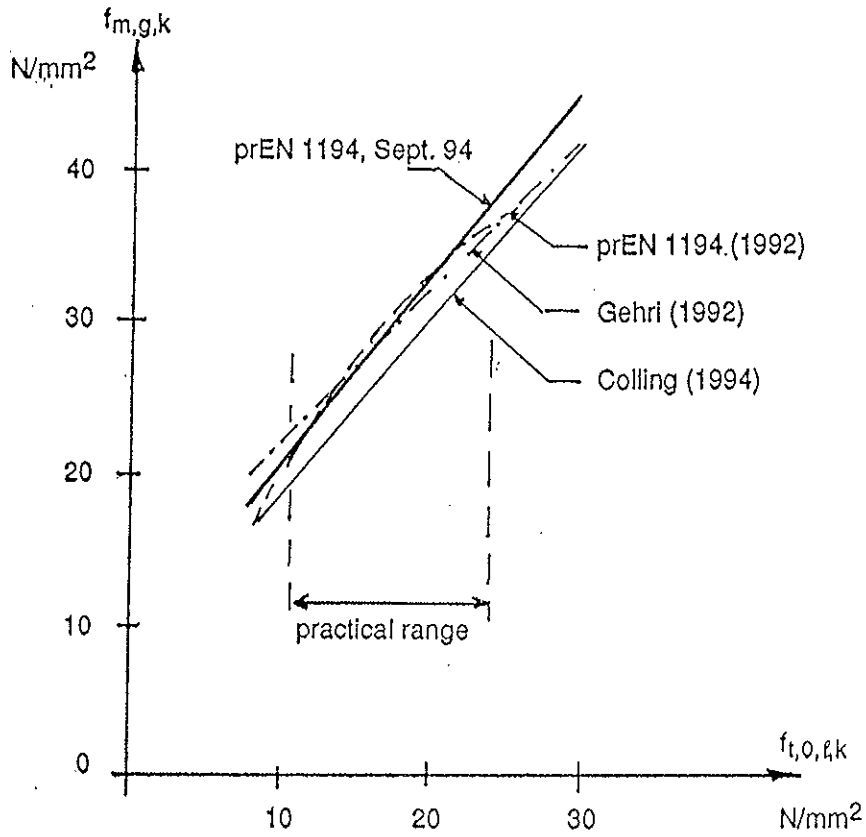

Figure 2: Comparison of the different strength models in function of the tensile strength of the lamination

3. Evaluation of new results

End of 1992 the results of a large research made in Norway by Falk/Solli/Aasheim on the bending performance of glued laminated beams were published. Colling (1994) used in his proposal those results for the calibration of the factors a_ℓ and b_ℓ.

The beams used in the above research had only a width of 90 mm. The measured values of tensile strength (based on 1 m free length) were adjusted to the reference width of 150 mm, that means the tensile strength was reduced by about 10 %, the bending strength of the beams remaining unadjusted.

A more logical approach would take in account that both strength values (tensile strength of the lamination and bending strength of the beam) have to be adjusted, in a first approach using for both the same relationship. Based on this the following formula is obtained (based on h = 600 mm):

$$f_{m,g,k} = 6\ N/mm^2 + 1{,}05 \cdot f_{t,0,\ell,k}$$

The actual proposal in prEN 1194 with

$$f_{m,g,k} = 9\ N/mm^2 + 1{,}2 \cdot f_{t,0,\ell,k}$$

overestimates the test values by more than 15 %.

4. Derivation of a more appropriate relationship

When calibrating the european strength model with test results, one must be aware about the importance of small variations relating to the coefficient of variation on the final result. Bearing in mind the small number of specimens, it seems therefore more indicated to derive the relationship between $f_{m,g,k}$ and $f_{t,0,\ell,k}$ using the middle values and corresponding coefficients of variations.

Based on the test results the following relationship may be found:

$$f_{m,g,50} = 4.5 + f_{t,0,\ell,50} \qquad [\text{in } N/mm^2]$$

Using machine graded laminations the coefficient of variation for the tensile strength varies between 0.18 and 0.24 . For a good grading quality the values lay near to 0.2 .

Tests on beams – with failure mode in the lamination – show for the bending strength a coefficient of variation of 0.12 to 0.16 , the lower values being valid for better graded material.

Based on this the above relationship may be rewritten on characteristic value basis to:

$$f_{m,g,k} = 3.5 + (1.15 \text{ to } 1.25)\, f_{t,0,\ell,k} \qquad [\text{in } N/mm^2]$$

low / high coefficient of variation

An easier approach valid for coefficient of variation < 0.3 on the tensile strength of the laminations, would be:

$$f_{m,g,k} = 4 + 0.75 \cdot f_{t,0,\ell,50}$$

Since in many cases the small number of specimens do not allow for a reliable estimation of the characteristic value, a better approach may be to use the middle values of the test results and an assumed or adjusted relationship between the coefficient of variations of both strengths.

5. Conclusions

Based on the approach given in section 4, the requirement in prEN 1194 should be changed. It is recommended the following:

(a) – Requirements concerning wood strength (for homogeneous sections and depth $h = 600$ mm) based on tensile strength of lamination:

$$f_{m,g,k} = 4 + 0.75 \cdot f_{t,0,\ell,50} \quad N/mm^2$$

For machine graded laminations with coefficient of variation for the tensile strength smaller than 0.3.

(b) – Requirements concerning end joint strength (for homogeneous sections and depth $h = 600$ mm) based on tensile strength of finger-joint:

$$f_{m,g,k} = 1.18 \cdot f_{t,j,k} \quad N/mm^2$$

The above requirements are valid for beam and lamination width of $b = 150$ mm. For other widths use an adjusting factor of $(150/b)^{0.1}$.

For combined sections, with outer laminations of depth $h/6$ and modulus of elasticity E_2, the following adjusting factor has to be used on both requirements:

$$\left[1 - \left(\frac{2}{3}\right)^3 \left(1 - \frac{E_2}{E_1}\right)\right]$$

E_2 : outer laminations
E_1 : inner laminations

$E_2 > E_1$

References

Colling, F.: Annexes to new draft of prEN 1194. July 1994.

Falk, R. / Solli, K. / Aasheim, E.: The performance of glued laminated beams manufactured from machine stress graded norwegian spruce. Norwegian Institute of Wood Technology, 1992, Publ. 77.

Gehri, E.: Determination of characteristic bending values of glued laminated timber – EN-approach and reality. CIB-W18 A/25-12-1, 1994, Ahus.

CIB-W18/28-12-2

INTERNATIONAL COUNCIL FOR BUILDING RESEARCH STUDIES AND DOCUMENTATION

WORKING COMMISSION W18 - TIMBER STRUCTURES

SIZE FACTOR OF NORWEGIAN GLUED LAMINATED BEAMS

by

E Aasheim

K H Solli

The Norwegian Institute of Wood Technology

Norway

MEETING TWENTY - EIGHT

COPENHAGEN

DENMARK

APRIL 1995

SIZE FACTOR OF NORWEGIAN GLUED LAMINATED BEAMS

Erik Aasheim and Kjell Helge Solli,
The Norwegian Institute of Wood Technology

April 1995

Background

A research project where the aim was to determine the size factor k_h of Norwegian glued laminated beams has been carried out by The Norwegian Institute of Wood Technology in co-operation with two Norwegian producers of glued laminated timber [1]. The purpose of this project was to compare the laboratory results with the corresponding values of k_h given in Eurocode 5 [2]:

$$k_h = \left(\frac{600}{h}\right)^{0,2}$$

with the following limits: $1,0 \le k_h \le 1,15$.

The limits correspond to $h = 600\ mm$ $(k_h = 1,0)$ and $h = 300\ mm$ $(k_h = 1,15)$.

Materials

It was decided to test beams with depths corresponding to the upper and lower value of k_h, i.e. depths of 300 mm and 600 mm.

The lamellae (38 mm x 90 mm) were machine strength graded to the Norwegian strength class T30 (characteristic bending strength of 30 N/mm²). They were planed to thickness 33,3 mm, finger jointed and glued together to beams in a normal industrial process.

The bending test program included 24 beams with a cross-section of 90 mm x 300 mm and 20 beams with a cross-section of 90 mm x 600 mm. In addition to this, 15 lamellae with finger joints were randomly selected from the production for determination of the finger joint tension strength.

Test methods

The procedure was according to ISO 8375 (1985) [3] and the test arrangements are described in Figure 1 and Figure 2.

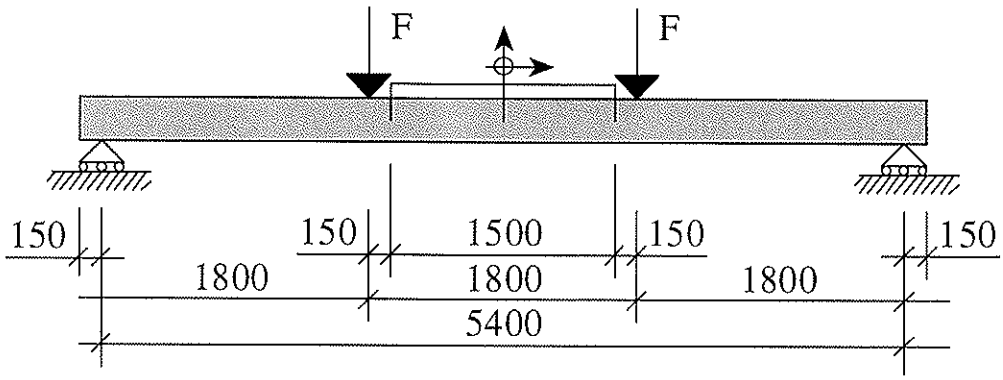

Figure 1. Test arrangement for beams with 300 mm depth.

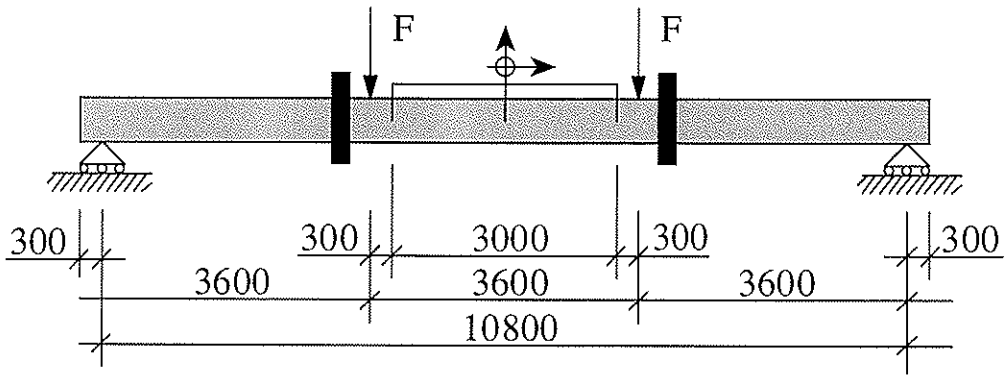

Figure 2. Test arrangement for beams with 600 mm depth.

The beams with depth 600 mm were supported to prevent lateral deflection and buckling.

The finger joint tension test was performed with a free span of ca. 1000 mm between the grips. The finger joints were located in the middle of the span.

Moisture content and density

The moisture contents (w) of the beams were measured in the lamellae where the failure occurred, as close to the failure as possible. The values are given in Table 1.

	300 mm (n = 24)	600 mm (n = 20)
w_{mean}	11,1	10,9
std	0,64	1,13
V (%)	5,8	10,4

Table 1. Moisture content in beams close to the failure.

The pieces for determination of density were cut out of the lamella where the failure occurred, as close to the failure as possible. If the failure occurred in a finger joint, a piece from both sides of the joint was cut out and the mean value was calculated. The density values are adjusted to 12 % moisture content according to prEN 384 [4]. The values of the adjusted density are given in Table 2.

	300 mm (n = 24)	600 mm (n = 20)
ρ_{mean}	440	436
std	53,6	35,8
V	12,2	8,2
$\rho_{0.05\text{-}n}$	338	365
$\rho_{0.05\text{-}w}$	374	368

Table 2. Density (kg/m³) in beams close to the failure.

$\rho_{0.05\text{-}n}$ = characteristic value based on the normal distribution.
$\rho_{0.05\text{-}w}$ = characteristic value based on the Weibull-3 parameter distribution.

Results from bending test

The bending tests included both bending strength and modulus of elasticity according to [1].

The results of modulus of elasticity are given in Table 3. The values are adjusted to a moisture content of 12 % according to [4].

	300 mm (n = 24)	600 mm (n = 20)
MOE_{mean}	13777	13682
std	1125	1235
V	8,17	9,03
$MOE_{0.05\text{-}n}$	11637	11239
$MOE_{0.05\text{-}w}$	11906	11498

Table 3. MOE (N/mm²).

$MOE_{0.05\text{-}n}$ = characteristic value based on the normal distribution.
$MOE_{0.05\text{-}w}$ = characteristic value based on the Weibull-3 parameter distribution.

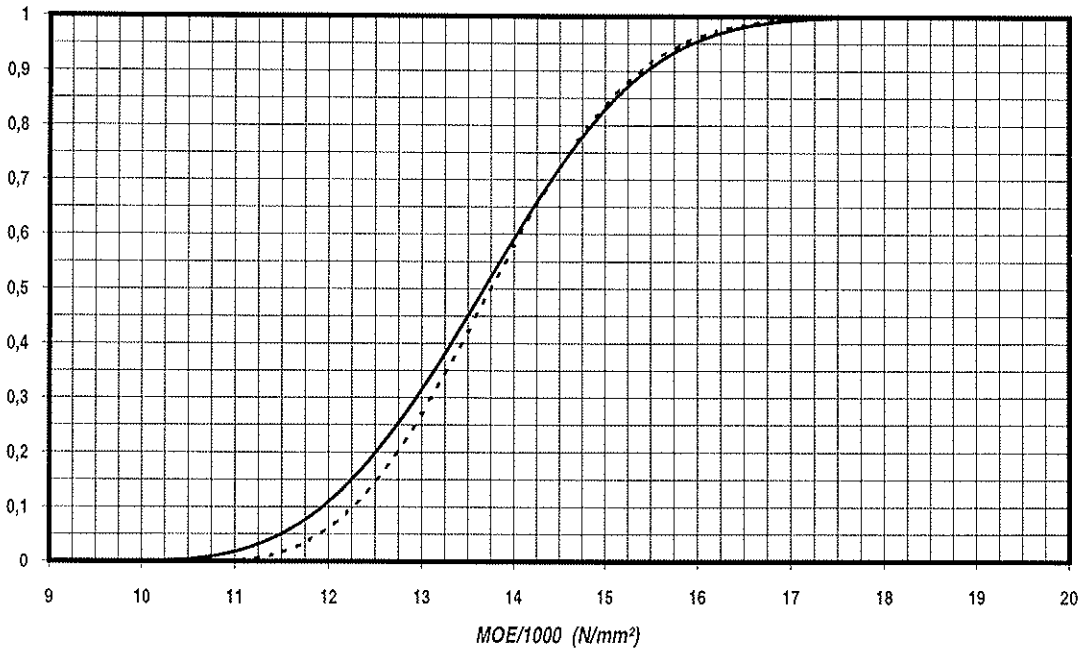

Figure 3. Distribution of the MOE (N/mm²).

In Figure 3 the continuous line refers to beams with depth h = 600 mm. The dotted line refers to beams with depth h = 300 mm. The curves are based on the Weibull-3 parameter distribution.

The results of bending strength are given in Table 4.

	300 mm (n = 24)	**600 mm (n = 20)**
$f_{m,mean}$	44,0	39,4
std	6,79	4,05
V	15,4	10,3
$f_{m,0.05-n}$	31,1	31,6
$f_{m,0.05-w}$	34,1	32,0

Table 4. Bending strength (N/mm²).

$f_{m,0.05-n}$ = characteristic bending strength based on the normal distribution.

$f_{m,0,05-w}$ = characteristic bending strength based on the Weibull-3 parameter distribution.

Compared to the results from a similar bending test of Norwegian glued laminated beams with depth of 300 mm [5] the results are approximately identical to the values of the 300 mm beams in Table 4.

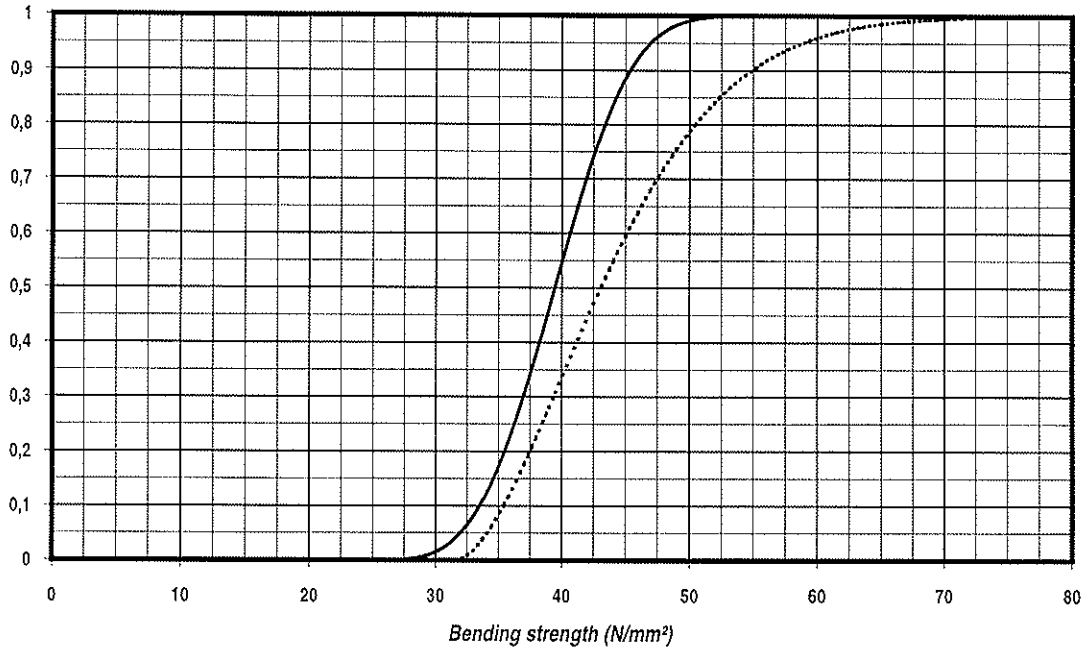

Figure 4. Distribution of the bending strength (N/mm²).

In Figure 4 the continuous line refers to beams with depth h = 600 mm. The dotted line refers to beams with depth h = 300 mm. The curves are based on the Weibull-3 parameter distribution.

For both beams with 300 mm and 600 mm depth 6 failures started at finger joints. The bending strength of those finger joint failures is given in Table 5.

	300 mm (n = 6)	**600 mm (n = 6)**
$f_{m,mean}$	46,6 (*44,0*)	38,3 (*39,4*)
std	5,95 (*6,79*)	4,10 (*4,05*)
V (%)	12,8 (*15,4*)	10,7 (*10,3*)

Table 5. Bending strength (N/mm²) of failures in finger joints.

The values in the parenthesis refer to the total sample of each depth, see Table 4. The finger joints did not represent any weaker points than what other "natural" defects did.

Results from finger joint tension test

15 lamellae with finger joints were tested in tension. The finger jointed lamellae were taken from the same basic sample as the beam lamellae.

The results of the finger joint tension test are given in Table 6.

$f_{t,fj,mean}$	38,6
std	6,61
V (%)	17,1
$f_{t,fj,0.05-n}$	25,5
$f_{t,fj,0.05-w}$	27,12

Table 6. Tension strength of finger joints (N/mm²).

$f_{t,fj,0.05-n}$ = characteristic value based on the normal distribution.
$f_{t,fj,0.05-w}$ = characteristic value based on the Weibull-3 parameter distribution.

Discussion

The mean value of the ultimate bending strength for the 300 mm beams was about 12 % higher than the mean value of 600 mm beams. The variation of the ultimate bending strength of 300 mm beams (V = 15,4 %) was also higher than the corresponding variation for 600 mm beams (V = 10,3 %). One important question to answer is why this difference appears when the lamellae to both depths were from the same sample and therefore theoretically should have the same properties. The difference of the mean densities was for example less than 1 %.

One reason might be the different geometry (different depth) and a different stress distribution. But the main reason is probably caused by the test method. This can easily be explained by assuming that the probability of the major defect occurring in a specific volume is constant for the same grade and grading method. By increasing the volume the probability of finding the major defect also increases.

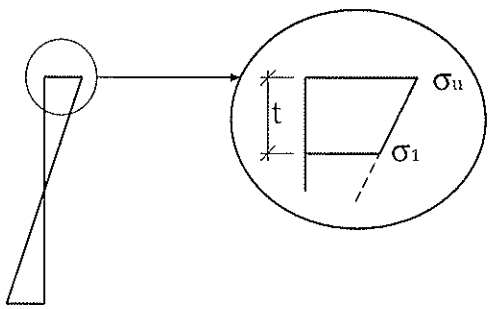

Figure 5. Bending stress distribution in a beam.

If t_{300} = 33,3 mm (depth of a lamella) for a 300 mm beam, the corresponding depth of a 600 mm beam is t_{600} = 66,6 mm (see Figure 5). Since the distance with constant bending moment is twice as long for a 600 mm beam than for a 300 mm beam the "stress volume" limited by t, σ_u and σ_1 is four times bigger

for a 600 mm beam. This gives a much higher probability of finding the major defect when testing a 600 mm beam than a 300 mm beam.

This was shown in practice during the testing of the 300 mm beams. It was observed that *some* of the beams had outer lamellae which consisted of almost clear wood in the area of constant maximum moment, i.e. no finger joints, no knots etc. In other 300 mm beams the outer lamella had one or more defects. When testing 600 mm beams no beams were observed without any defects in the two outer lamellae in the area of constant maximum moment.

The consequence of this was that both the mean value and the variation of ultimate stress for the 300 mm became higher (either "clear wood" or defects) than the corresponding values of the 600 mm beams ("all" had defects).

The effect of this must also be seen in connection with the grading accuracy. If the grading method manages to limit the strength variation of the sample to a narrow interval the effect of different "stress volumes" will become smaller. In the extreme consequence the size effect caused by the testing method will be approaching zero for lamellae with approximately identical properties. Then the resulting size effect will also decrease.

Conclusion

Based on Eurocode 5 it should be expected that $k_h = \frac{f_{m,k,300}}{f_{m,k,600}} = 1,15$.

The result from this project shows a lower value of k_h. By using the values from the Weibull-3 parameter distribution the following value of k_h was given for a depth of 300 mm:

$$k_h = \frac{f_{m,k,300}}{f_{m,k,600}} = \frac{34,1}{32,0} \approx 1,07$$

The corresponding size factor calculated from the mean values was $k_h \approx 1,12$. Based on observations of the lamellae and their distribution of defects it is assumed that much of the size effect can be explained by the test method and the grading accuracy.

If this assumption is correct, then the size factor k_h is not only a function of the depth, but also of the grading accuracy and the strength class.

References

[1] Solli, K. H.: Høydefaktor for norsk limtre. Arbeidsrapport nr. 536000, 1994. Norsk Treteknisk Institutt (The Norwegian Institute of Wood Technology), Oslo. (In Norwegian)

[2] ENV 1995-1-1 Eurocode 5 - Design of timber structures - Part 1 - 1: General rules and rules for buildings. December 1993.

[3] ISO 8375 Solid timber in structural sizes: Determination of some physical and mechanical properties. First edition - 1985-07-01.

[4] prEN 384 Structural timber - Determination of characteristic values of mechanical properties and density. Final draft, March 1994.

[5] Falk, R. H., Solli, K. H., Aasheim, E.: The performance of glued laminated beams manufactured from machine stress graded Norwegian spruce. Meddelelse 77, 1992. Norsk Treteknisk Institutt (The Norwegian Institute of Wood Technology), Oslo.

CIB-W18/28-12-3

INTERNATIONAL COUNCIL FOR BUILDING RESEARCH STUDIES AND DOCUMENTATION

WORKING COMMISSION W18 - TIMBER STRUCTURES

DESIGN OF GLULAM BEAMS WITH HOLES

by

K Riipola
Technical Research Centre of Finland
Finland

MEETING TWENTY - EIGHT

COPENHAGEN

DENMARK

APRIL 1995

Design of glulam beams with holes

Kirsti Riipola

This paper compares three design methods for glulam beams with holes. The compared methods are the German method, the method of the Swedish Glulam Handbook, and the linear elastic fracture mechanics method presented by the author in Bordeaux 1992. The linear elastic fracture mechanics method gives the best correspondance between the predicted and observed capacities. The density of the timber material is of importance for the prediction to be accurate.

The details of the method, material, and analyses are explained in Riipola 1995. The load configuration and the main symbols are presented in Fig. 1.

Experimental material

The experiments with known density reported by Penttala (1980), Johannesson (1983), and Pizio (1991) were analysed. The specimens used in these experiments were made of commercial glulam of spruce. Only the beams loaded so, that the hole was in the shear region, and broken by crack growth, were analysed. The total number of the glulam beams in this analysis was 67.

The German method

The German method is presented by Kolb and Frech (1977). The method itself is based on the allowable stresses, but it is here modified so, that instead of the allowable shear stress, the characteristic shear strength is used. Thus, the predicted load can be expressed as follows:

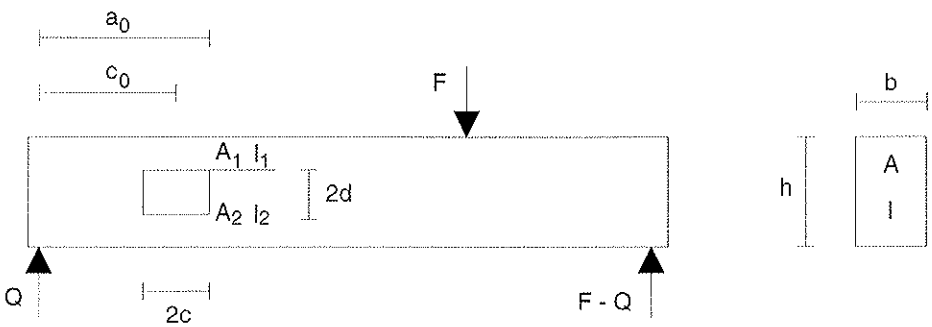

Figure 1. The beam with a hole.

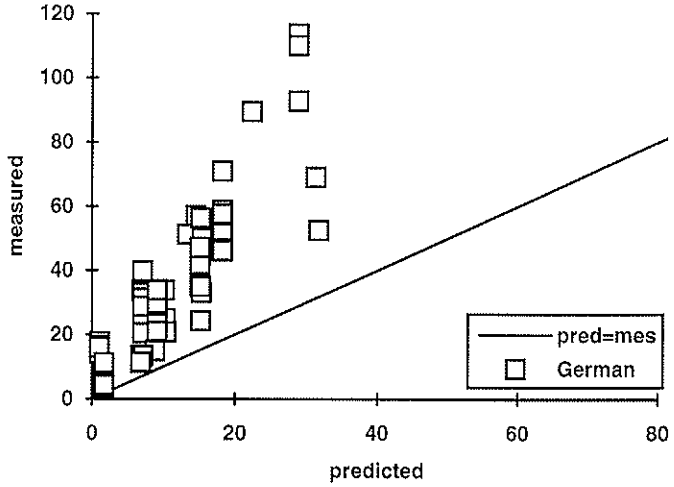

Figure 2. The measured load versus the predicted one according to the German method. Load values in kN.

$$Q_{pred} = \frac{b(h-2d)^2}{6h} f_v \qquad (1)$$

The interpretation of the method in the case of the circular hole is unclear. It has been assumed, that a circular hole is like a rectangular one with the same depth. This leads to underestimation of the capacity of the beam. In the evaluation, it has been assumed that the characteristic shear strength f_v = 3.8 MPa for C40 can be used, when the characteristic load capacity is predicted. The result is shown in Fig. 2. The correlation for the regression line through origin is 0.961 and the slope of the line is3,041. This means, that when the method is used, a considerable additional safety factor is included. The figure shows, that the method fails in differentiating the various cases and, e.g. the predicted value of 30 kN corresponds to measured values from 50 to 110 kN.

The Swedish method

According to the Swedish method presented in the Glulam Handbook, the characteristic load capacity is calculated according to Eq. 2.

$$Q_{pred} = \frac{2b(h-2d)}{3} \kappa_0 \kappa_{vol} f_v \qquad (2)$$

where the correction factors κ_0 and κ_{vol} are given by Eqs. 3 to 5.

$$\kappa_0 = 1 - 555(D/h)^3 \qquad \text{for D/h} \le 0{,}1 \qquad (3)$$

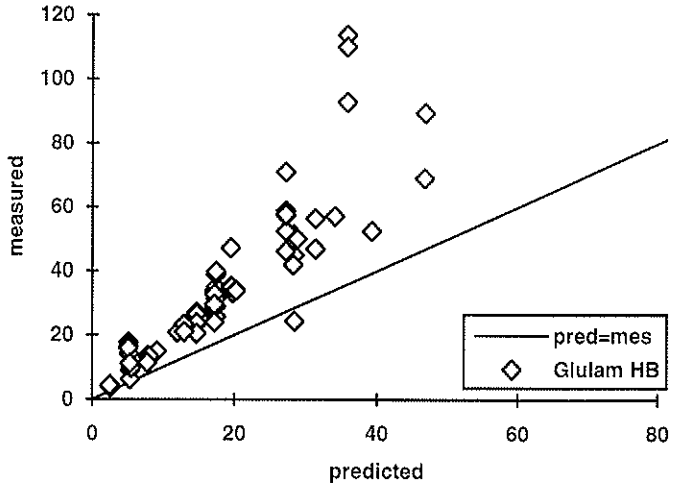

Figure 3. The measured load versus the predicted one according to the method in the Swedish Glulam handbook. Load values in kN.

$$\kappa_0 = 1.62/(1.8 + D/h)^2 \qquad \text{for D/h} > 0{,}1 \qquad (4)$$

$$\kappa_{vol} = (90/b)^{0.2} \qquad \text{for } 90 \le b \le 215 \qquad (5)$$

For a rectangular hole D is equal to the diagonal of the hole.

The result is shown in Fig. 3. The correlation for the regression line through origin is 0.965 and the slope of the line is 1.894. The method describes the results reasonably well, but especially for larger load values, the prediction lies considerably on the safe side. For one beam of the 67, the capacity of the beam is overestimated.

Fracture mechanics method

According to the linear elastic fracture mechanics method, the stress intensities K_I and K_{II} are the fundamental parameters (Eqs. 6 and 7). The critical load level is set by Wu´s fracture criterion (1967), where the stress intensities are compared with the appropriate fracture toughness values (Eq. 8). This criterion shall be considered as an approximation of an physically justifiable criterion presented by Charalambides et al. (1992).

$$K_I^2 = J_I E c_I^2 \qquad (6)$$

$$K_{II}^2 = J_{II} E c_{II}^2 \qquad (7)$$

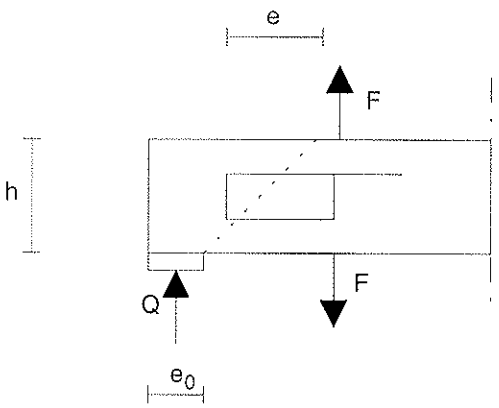

Figure 4. The opening component for holes near to the support.

$$\left(\frac{K_I}{K_{IC}}\right)^1 + \left(\frac{K_{II}}{K_{IIC}}\right)^2 \leq 1 \tag{8}$$

The values of the constants c_I and c_{II} are approximately 1/3 and 2/3, respectively. For a glulam beam with a rectangular cross section and a hole in the neutral axis, the simplified equations for the J-values are given by Eqs. 9 to 12 (Riipola 1995).

$$J_I = \frac{Q^2}{4bG}\frac{(I_2/A_2 - I_1/A_1)(A_2 - A_1)}{(I_1 + I_2)(A_1 + A_2)} \tag{9}$$

$$J_{II} = \frac{Q^2 a_0^{\,2}}{2bE}\left\{\left[1 - \frac{c_0 h}{a_0(h+2d)}\right]\left(\frac{k}{I_1 + I_2} - \frac{1}{I}\right) + \frac{c_0 h}{a_0(h+2d)}\left[\frac{4(A_1 + A_2)}{h^2 A_1 A_2} - \frac{1}{I}\right]\right\} + k_0 k \frac{Q^2 a_0 (a_0 - c_0)}{8bE}\left(\frac{1}{I_1} - \frac{1}{I_2}\right) - J_1 \tag{10}$$

$$k = 1 - \frac{c_0}{a_0}\left[1 - \frac{(h-2d)^2}{3(h+2d)^2}\right] \tag{11}$$

$$k_0 = 1 + \frac{c_0 r(2 - \sqrt{2})}{(a_0 - c_0)(h + 2r)} \tag{12}$$

In addition, a correction for holes near to the support has been done. In this case, a larger amount of the supoprt reaction is carried by the upper part of the beam, which results in an additional opening component at the hole corner (Fig. 4). This component is given by Eq. 13.

$$J_I = \left[\frac{eQ}{2(e_0 + 2h)}\right]^2 \frac{A_1 + A_2}{2bGA_1A_2} \qquad (13)$$

A circular hole is treated like a rectangular one, which has the same center and height. The width in the axis direction and the level of crack growth are defined by a radius, that makes the angle of 45° with the neutral axis.

The characteristic capacity can be predicted according to the fracture mechanics method, when the characteristic fracture toughness values 200 an 1200 $kNm^{-3/2}$ are used in mode I and II, respectively. The result is shown in Fig. 5. The correlation for the regression line through origin is 0.981 and the slope of the line is 1.526. The fracture mechanics method succeeds best in differentiating the various beams and the predicted capacities follow the x = y line most closely. For 3 beams of the 67, the capacity of the beam is overestimated.

Conclusions

Linear elastic fracture mechanics gives the best prediction also for such holes, that have a minor effect on the capacity of the beam.

The method should apply also to other kind of holes, that are not centered with the neutral axis. An application to holes not in the shear region is, in principle, also possible. About these, however, there are not

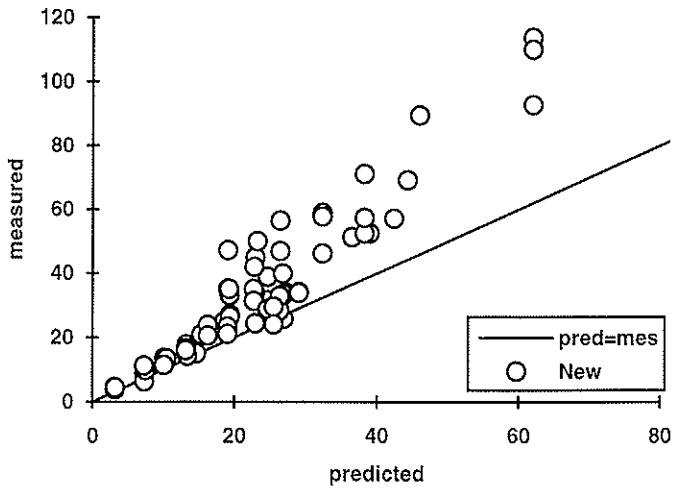

Figure 5. The measured load versus the predicted one according to the fracture mechanics method when characteristic fracture toughness values are used. Load values in kN.

sufficiently of experimental material, that the validity could be demonstrated.

Literature

Carling, O., Johannesson, B., 1988.
Limträhandboken [Glulam Handbook]. Svenskt Limträ, Stockholm. 110p. (In Swedish.)

Charalambides, M., Kinloch, A.J., Wang, Y., Williams, J.G., 1992.
On the analysis of mixed-mode failure. International Journal of Fracture 54:269-291.

Johannesson, B., 1983.
Design problems for glulam beams with holes. Chalmers University of Technology, Division of Steel and Timber Structures. Doktorsavhandlingar vid Chalmers Tekniska Högskola, Ny serie Nr 458. Göteborg. 73 p.

Kolb, H., Frech, P., 1977.
Untersuchungen an durchbrochenen Bindern aus Brettschichtholz. Holz als Roh- und Werkstoff 35:125-134. (In German).

Penttala, V., 1980.
Reiällinen liimapuupalkki. [Glulam beam with hole.] Helsinki University of Technology, Division of Structural Engineering, publication 33. Espoo. 101 p. (In Finnish).

Pizio, S., 1991.
Die Anwendung der Bruchmechanik zur Bemessung von Holzbauteilen, untersucht am durcbrochenen und am ausgeklinkten Träger. Publ. Nr. 91-1, Baustatik und Stahlbau, Eidg. Techn. Hochschule, Zürich. 142 p. (In German).

Riipola, K.1995.
Design of timber beams with holes. Fracture mechanics approach Journal of Structural Engineering, 121(2):225-239.

Wu, E.M., 1967.
Application of fracture mechanics to anisotropic plates. J. Appl. Mech. Trans. ASME E 34(4):967-974.

List of symbols

Roman numbers I and II are used as subindices to identify the fracture modes. I refers to the opening mode and II to the forward shear mode.

Indices 1 and 2 refer to the upper and lower part of the beam, respectively.

The following symbols are used in this paper:

A, A_i	Area for the beam or beam part.
a_0	Distance from the beam support to the crack initiation point
b	Width of the beam
c	Half the length of the hole
c_0	Location coordinate of the hole centre
c_I, c_{II}	Orthotropicity constants.
D	Hole diameter
d	Half the height of the hole
E	Modulus of elasticity in the direction of the grain
e	Length measure for the estimation of the location correction
e_0	Length of the support or the load
F	Concentrated load
G	Modulus of rigidity
h	Depth of the beam
I, I_i	Moment of inertia for the beam or beam part
J, J_I, J_{II}	Strain energy release rate
J_{corr}	Location correction term to J_I and J_{II} due to the opening or closing component
K_I, K_{II}	Stress intensity
K_{IC}, K_{IIC}	Fracture toughness
k, k_0	Parameters
L	Span width of the beam
Q	Shear force for the beam
Q_{pred}	Estimated shear force at the hole corresponding to the failure load
r	Radius of a circular hole
κ_0, κ_{vol},	Parameters needed in the Swedish method

CIB-W18/28-12-4

INTERNATIONAL COUNCIL FOR BUILDING RESEARCH STUDIES AND DOCUMENTATION

WORKING COMMISSION W18 - TIMBER STRUCTURES

COMPRESSION RESISTANCE OF GLUED LAMINATED TIMBER SHORT COLUMNS

by

U Korin
National Building Research Institute
Israel

MEETING TWENTY - EIGHT

COPENHAGEN

DENMARK

APRIL 1995

COMPRESSION RESISTANCE OF GLUED LAMINATED TIMBER SHORT COLUMNS

Dr. U. Korin

1. INTRODUCTION

According to Eurocode 5 rules[1], the ultimate limit state of timber columns loaded in compression parallel to the grain, should satisfy the condition:

$$\sigma_{c,o,d} \leq f_{c,o,d} \quad (1)$$

where: $\sigma_{c,o,d}$ - the design stress, and

$f_{c,o,d}$ - the design strength

A check shall also be made of the instability condition. It is necessary to take into account bending stresses due to initial curvature, eccentricities and induced deflection.

The design compression stress, $f_{c,o,d}$, may be derived for various slenderness of columns according to the following set of equations:

$$\lambda_{rel,y} = \sqrt{\frac{f_{c,o,k}}{\sigma_{c,crit,y}}} \quad (2)$$

$$\sigma_{c,cri,y} = \frac{\pi^2 E 0.05}{\lambda_y^2} \quad (3)$$

$$\sigma_{c,o,d} \leq k_{c,y} f_{c,o,d} \quad (4)$$

with

$$k_{c,y} = \frac{1}{k_y + \sqrt{k_y^2 - l_{rel,y}^2}} \quad (5)$$

$$k_y = 0.5[1 + \beta_c(\lambda_{rel,y} - 0.5) + \lambda_{rel,y}^2] \quad (6)$$

where β_c a factor related with the straightness of the lumber -

for solid timber β_c=0.2

for glulam β_c=0.1

The behaviour under axial compression load of some glued laminated timber columns, as well as some solids lumber columns supplied from various sources was investigated. The ultimate compression stresses at various slendernesses were compared with the Eurocode 5 recommended design method.

2. EXPERIMENTAL

The following groups of timber were used for the investigation:

square (67.5x67.5 mm) solid lumber from Finland (Pine)

square (67.5x67.5 mm) glued laminated timber from Finland (Pine)

square (67.5x67.5 mm) solid lumber from USA (Douglass fir)

square (67.5x67.5 mm) glued laminated timber from USA (Douglass fir)

square (65.0x65.0 mm) glued laminated timber prepared at the laboratory from Israeli grown Jerusalem Pine.

The material arrived at the laboratory in the form of 3000 mm long columns. Each column was cut to test specimens of the following lengths: 1500 mm, 750 mm, 375 mm and 187.5 mm.

Compression loading tests were performed by the use of the laboratory universal testing machines equipped with specially developed suitable pinned ends. Thus, fixation of the loaded ends was prevented.

The following records were prepared for each of the tested specimens: dimensions, weight, moisture content, knots count, and size of largest knot, axial deformation versus axial load during the loading test, and the ultimate resistance of the columns.

Due to the actual dimensions of the pinned ends, it was assumed that the rotation centers were located 42 mm outside the ends of the loaded columns, and thus 84 mm were added to the measured length of each specimen for the purpose of calculation of the slenderness λ.

3. TEST RESULTS AND DISCUSSION

The different test results of the various timbers are presented in tables 1-3. The ultimate strength of the 375 mm columns having a slenderness of about 24, was considered as the compression strength of the timber $f_{c,o}$. Due to the small number of the tested specimens no characteristic values of the timber were calculated, and the further analysis is based on the average values obtained and summarized hereafter:

Group 1 - source - Finland (Pine) - (Glulam)

Average modulus of elasticity in compression $E_{c,o}$ - 12,440 MPa

Average longitudinal ultimate compression strength, $f_{c,o}$ - 29.6 MPa.

Group 2 - source - USA (Douglass fir) - (Glulam)

Average modulus of elasticity in compression - 10,210 MPa

Average longitudinal ultimate compression strength, $f_{c,o}$ - 34.3 MPa

Group 3 - source - Israel (Jerusalem Pine) - (Glulam)

Average modulus of elasticity in compression - 11,350 MPa

Average longitudinal ultimate compression strength, $f_{c,o}$ - 39.5 MPa

The average ultimate strengths, $f_{c,o}$, of the tested specimens are presented in figures 1-3 against the relevant slendernesses of the same.

In addition to that, the drawings present also the calculated critical stresses, $\sigma_{c,crit}$, and the calculated design strengths, $f_{c,o,d}$.

Comparison of the calculated critical stresses, $\sigma_{c,crit}$ and the calculated design strengths, $f_{c,o,d}$ with the experimental values of the average ultimate strengths, $f_{c,o}$, shows generally that there is a good agreement between $f_{c,o,d}$ and $f_{c,o}$ up to slenderness of about 50. For larger slendernesses, the design strengths, $f_{c,o,d}$, shifts towards the critical stresses, $\sigma_{c,crit}$, curves, which intersects the ultimate strengths, $f_{c,o}$ curves at slenderness of about 60 to 70.

At slenderness of 80, for example, the calculated critical stresses and design strengths of all the three Glulams, are smaller than the relevant experimental ultimate strengths and the values of the first two, only account for about 65-80 percent of the last one.

REFERENCES

[1] Eurocode 5: Design of timber structures, part 1 [DD ENV 1955-1-1, 1994].

Table 1 - Compression test data for specimens made from solid lumber and glulam (Finland, Pine)

Specimen length (mm)	Slenderness	Source: Finland	Lumber (67.5x67.5 mm)				Glulam (67.5x67.5 mm)			
		Specimen	1	2	3	avg	4	5	6	avg
187.5	13.9	Density (kg/m^3)	477	486	512	492	559	591	603	584
		f_c (MPa)	32.3	38.4	39.6	36.8	40.8	46.6	46.4	44.6
		E (MPa)	12,050	11,840	12,510	12,130	11,880	12,330	15,200	13,140
375	23.6	Density (kg/m^3)	484	516	487	496	558	476	608	581
		f_c (MPa)	28.0	36.3	36.2	33.5	35.4	40.5	42.9	39.6
		E (MPa)	8,800	12,910	15,810	12,510	14,040	11,430	13,280	12,710
750	42.8	Density (kg/m^3)	497	508	544	516	593	556	600	583
		f_c (MPa)	16.9	16.8	40.2	313	39.5	39.7	36.8	38.7
		E (MPa)	8,880	8,450	12,550	9,960	12,950	10,530	11,330	11,600
1500	81.2	Density (kg/m^3)	505	520	594	540	595	607	590	597
		f_c (MPa)	20.4	27.6	25.0	24.3	16.5	34.4	20.9	23.9
		E (MPa)	7,630	12,090	13,060	10,930	11,840	13,600	11,510	12,320
Average $E_{c,o}$ (MPa)			11,380				12,440			
Average density (kg/m^3)			511				586			

Table 2 - Compression test data for specimens made from solid lumber and glulam (USA, Douglass fir)

Specimen length (mm)	Slenderness	Source: USA	Lumber (67.5x67.5 mm)				Glulam (67.5x67.5 mm)			
		Specimen	7	8	9	avg	10	11	12	avg
187.5	13.9	Density (kg/m^3)	470	430	433	444	507	449	445	484
		f_c (MPa)	37.2	28.1	31.8	32,4	40.1	45.3	37.8	41.1
		E (MPa)	11,290	8,620	10,350	10,090	10,210	13,530	11,640	11,790
375	23.6	Density (kg/m^3)	472	465	498	478	493	538	462	499
		f_c (MPa)	35.2	21.5	21.3	26.0	36.4	30.2	36.2	34.3
		E (MPa)	11,270	4,840	7,910	8,010	8,630	--	7,600	8,115
750	42.8	Density (kg/m^3)	493	466	470	476	497	523	463	494
		f_c (MPa)	33.4	19.5	19.5	24.1	33.9	31.5	30.3	31.6
		E (MPa)	10,660	8,550	6,065	8,425	7,290	12,460	11,200	9,875
1500	81.2	Density (kg/m^3)	484	448	463	465	484	509	454	482
		f_c (MPa)	13.4	12.8	13.9	13.4	30.9	13.5	24.5	23.0
		E (MPa)	11,130	10,400	10,300	10,610	10,090	11,040	12,090	11,070
Average $E_{c,o}$ (MPa)			9,280				10,210			
Average density (kg/m^3)			466				490			

Table 3 - Compression test data for specimens made from solid lumber and glulam (Israel, Jerusalem Pine)

Specimen length (mm)	Slenderness	Source: Israel	Lumber (67.5x67.5 mm)				Glulam (67.5x67.5 mm)		
		Specimen	13	14	15	16	17	18	avg
187.5	14.5	Density (kg/m^3)	625	679	634	672	647	664	654
		f_c (MPa)	41.6	40.2	40.6	44.7	39.1	40.0	41.1
		E (MPa)	10,890	12,140	11,180	14,990	11,580	11,280	12,010
375	24.5	Density (kg/m^3)	661	661	652	683	653	678	665
		f_c (MPa)	34.8	40.3	42.2	36.9	41.7	41.1	39.5
		E (MPa)	11,390	12,480	12,270	9,850	12,520	11,360	11,640
750	44.4	Density (kg/m^3)	644	686	652	629	681	682	662
		f_c (MPa)	33.2	32.6	35.7	38.8	37.4	37.7	35.9
		E (MPa)	10,010	11,860	11,210	11,180	10,340	10,690	10,880
1500	84.4	Density (kg/m^3)	689	--	679	697	656	690	682
		f_c (MPa)	16.7	--	16.8	26.2	12.1	16.2	19.6
		E (MPa)	11,470	--	11,400	12,010	9,810	9,630	10.860
Average $E_{c,o}$ (Mpa)			11,350						
Average density (kg/m^3)			666						

Fig. 1 - Source: Finland, Pine 67.5x67.5mm Columns

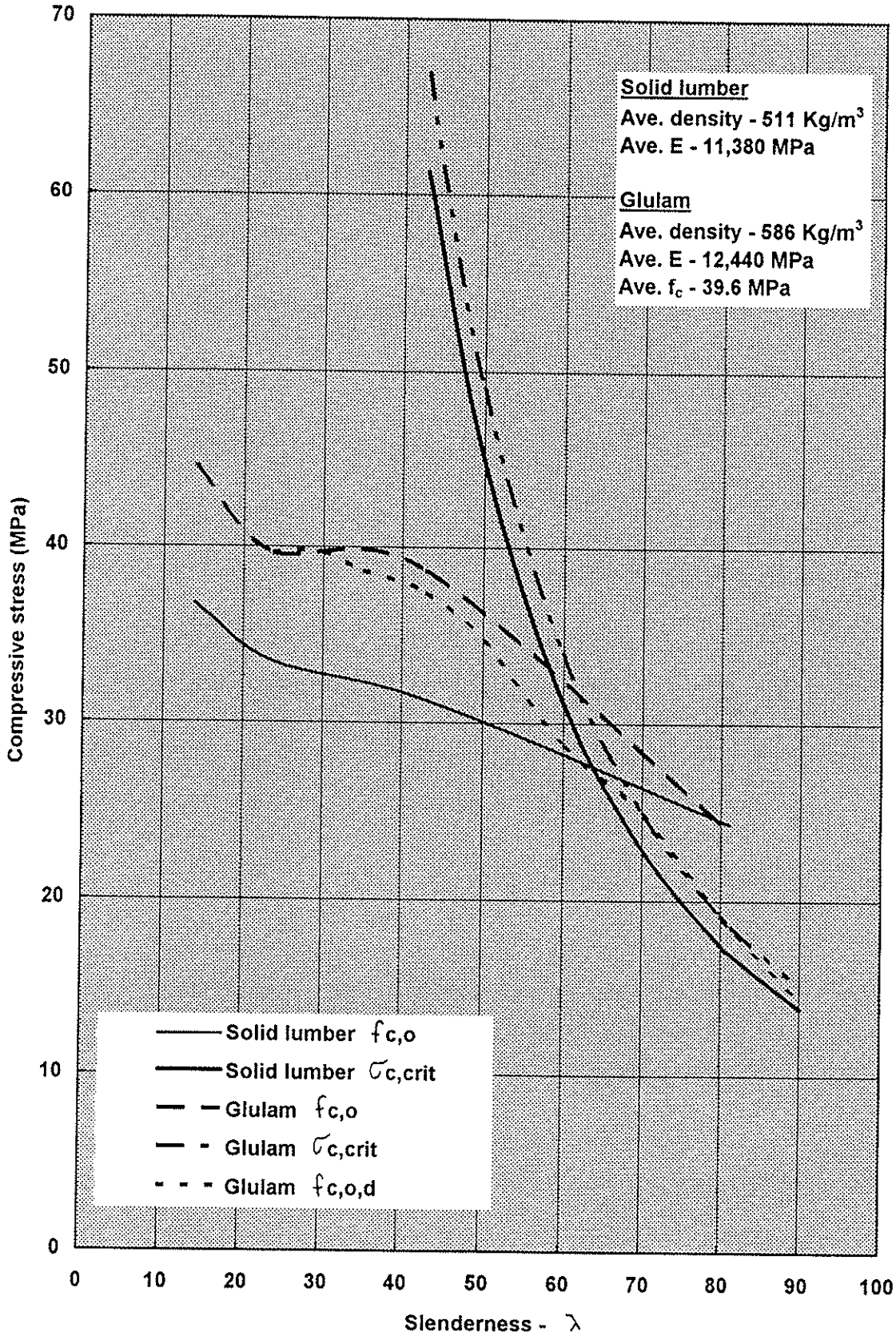

Fig. 2 - Source: USA, Douglass fir 67.5x67.5mm Columns

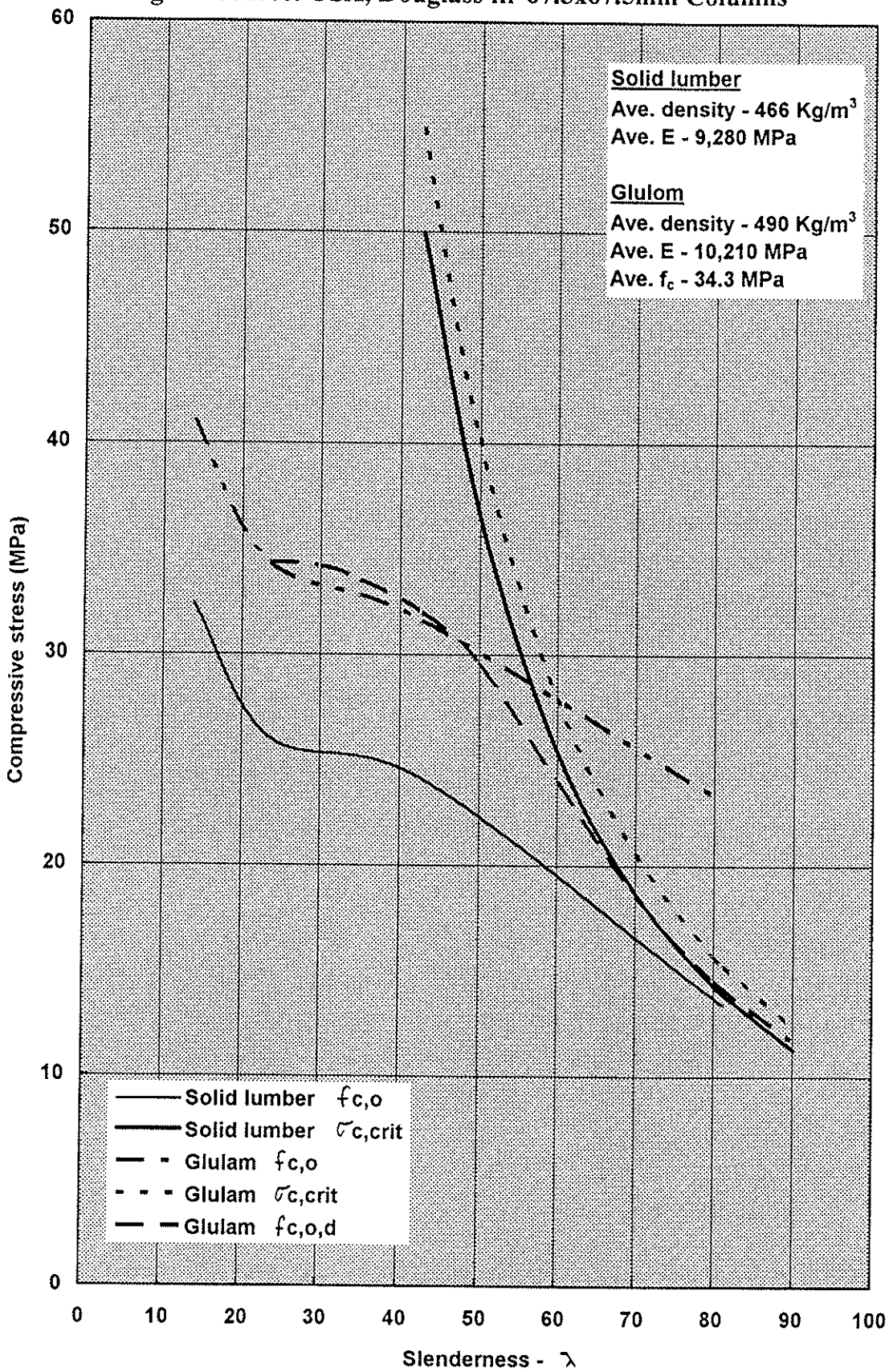

Fig. 3 - Source: Israel, Jerusalem Pine 65x65mm columns

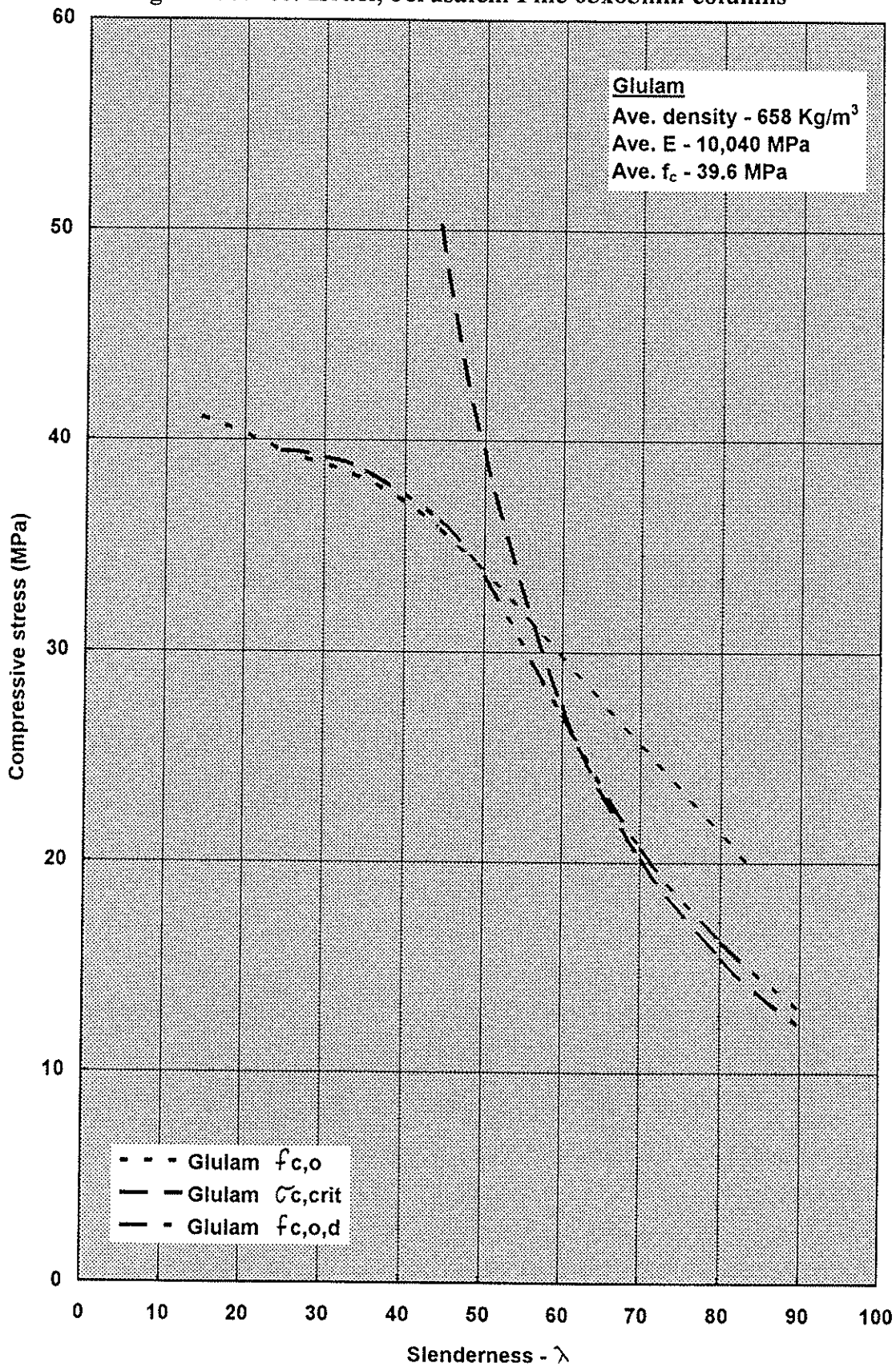

INTERNATIONAL COUNCIL FOR BUILDING RESEARCH STUDIES AND DOCUMENTATION

WORKING COMMISSION W18 - TIMBER STRUCTURES

BACKGROUND INFORMATION FOR "DESIGN RATED ORIENTED STRAND BOARD (OSB)" IN CSA STANDARDS - SUMMARY OF SHORT-TERM TEST RESULTS

by

E Karacabeyli

P Lau

W Deacon

Forintek Canada Corporation

C R Henderson

F V Meakes

Structural Board Association, Willowdale

Canada

MEETING TWENTY - EIGHT

COPENHAGEN

DENMARK

APRIL 1995

Background Information for "Design Rated Oriented Strand Board (OSB)" in CSA Standards - Summary of Short-term Test Results

EROL KARACABEYLI*, PETER LAU*, C.R. HENDERSON**,
F.V. MEAKES**, WILLIAM DEACON*

*Forintek Canada Corp., 2665 East Mall, Vancouver, B.C., Canada V6T 1W5
Tel: (604) 224-3221 Fax: (604) 222-5690

**Structural Board Association, 45 Sheppard Ave. East, Suite 412,
Willowdale, Ont. Canada M2N 5W9
Tel: (416) 730-9090 Fax: (416) 730-9013

January 24, 1995

Abstract

The 1994 edition of CSA (Canadian Standards Association) Standard O86.1, Engineering Design in Wood, includes, for the first time, specified strength and stiffness capacities for Design Rated OSB (Oriented Strand Board). Design Rated OSB panels are manufactured in accordance with a new CSA Standard O452. In this paper, the results of the short-term (1 to 10 minutes) test data which led to the establishment of the three rating grades of Design Rated OSB are presented. In addition, factors which may affect the classification such as panel thickness and orientation are discussed.

Key words: OSB, waferboard, structural panels, wood

Background

Waferboard has been utilized mainly as a construction sheathing material for over several decades; oriented strand board (OSB) for over the last decade. Waferboard typically consists of a single layer of randomly placed wood wafers. The OSB panels typically consist of three layers of wafers or strands; the two surface layers are approximately aligned with the major axis of the panel while the strands in the centre layer are either aligned perpendicular to the surface layers or laid randomly. This arrangement improves the stiffness and strength of the panels along the major axis.

OSB and waferboard in Canada are currently being manufactured according to CSA standard O437.0 (1993). This is a prescription standard which provides manufacturing requirements for two grades of OSB, O-1 and O-2, and one grade of waferboard, R-1. For the U.S. markets, OSB is manufactured according to PS2 (National Institute of Standards and Technology 1992) which is harmonized with CSA Standard O325.0 (1993). PS2 and CSA O325.0 are performance based standards which provide requirements for assessing performance based sheathing panels for use in wood-frame construction.

For small buildings (not exceeding 600 m^2 in building area and three storeys in height) as defined in Part 9 of the National Building Code of Canada (NBCC) (Associate Committee on the National Building Code, 1995), waferboard and OSB are permitted providing they comply with CSA Standards O325 or O437 (Canadian Standards Association 1993a,b). For buildings not covered by Part 9 (NBCC) and other structural applications such as I joists, box beams, gusset plates, and stress skin panels, engineers have had to rely on manufacturers to supply proprietary design values.

To make the engineering property values of OSB and waferboard readily available to professional designers, the Structural Board Association (SBA), formerly The Waferboard Association, launched a research program which involved the following events:

1) The structural properties needed for typical design were identified. (These structural properties, and the associated test standards which were followed in their determination, are given later in this paper.)

2) Under contract with the SBA, Forintek Canada Corp. (Forintek) conducted a comprehensive testing program to evaluate the structural properties of panels produced by all the mills of the Association. Results from these tests (Lau 1988, Lau and Lam 1990) revealed, that there were significant differences between waferboard and OSB, and also between panels of the same grade produced by different mills. This ruled out adopting a single set of industry wide design values for a particular panel grade, since the product with the lowest engineering properties would govern these design values, penalizing mills producing stronger and stiffer panels.

3) To solve this problem, Forintek staff proposed a standardised qualification, quality assurance and certification system. This approach (often called "mill specific") was approved in principal by code agencies and accepted by the industry. An industry standard embracing this approach was then developed. Subsequent industry trials confirmed the feasibility of this approach (Lucuik 1992).

4) Based on this industry standard, a new CSA standard O452 (CSA 1994b), which standardizes the qualification and certification procedures for "Design Rated OSB" was introduced. Furthermore, this standard includes the requirement of a quality control program specific to the mill, developed under the guidance of a qualified certification agency, to ensure that the product continues to conform to the

specifications as certified. The designation "Design Rated OSB" is used to distinguish this product from other OSB products.

CSA Standard O452 (CSA 1994b) specifies three rating grades (A, B and C) of each nominal thickness of Type 1 (Standard) Design Rated OSB and their associated minimum basic strength and stiffness capacities. In addition, this standard provides the avenue for manufacturers to produce a) Type 2 (Plus) Design Rated OSB, a product qualifying for a Type 1 rating, and with one or more properties certified as exceeding the minimum Type 1 grade values by ten percent or more; and b) Type 3 (Proprietary) Design Rated OSB, a product for which non standard proprietary design values have been determined and certified by the certifying agency.

5) The basic strength and stiffness capacities in CSA Standard O452 are based on short-term destructive tests which had a duration of 10 minutes or less (see Appendix I). These values are adjusted for load duration to arrive at the specified strength and stiffness capacities published in CSA Standard O86.1 (CSA 1994a) (see Table 1).

In this paper, the test results which led to the establishment of the minimum values for the three rating grades of Design Rated OSB are presented. Effects of thickness, orientation and loading mode (tension versus compression) on short-term engineering properties are discussed.

Test Programs - Materials and Methods

The following strength and stiffness test data on waferboard and OSB were used in this paper:

a) Data collected on 15.9 mm (5/8") thick panels (Lau 1988, Lau and Tardif 1990, Lau and Lam 1990). The panels were sampled from eight mills. The R-1 grade waferboard specimens were provided by six mills, and O-2 grade OSB specimens were provided by four mills;

b) Data collected on 9.5 mm (3/8") and 15.5 mm (5/8") thick O-2 grade panels from one mill (Stieda 1989);

c) Data collected on 11.0 mm (7/16") and 15.5 mm (5/8") thick panels for qualification and verification testing of the mill specific approach (Lucuik 1992). The OSB panels were sampled from two mills;

d) Data collected on 9.5 mm (3/8"), 11.0 mm (7/16"), 11.9 mm (15/32"), 12.7 mm (1/2"), 15.5 mm (5/8"), 18.3 mm (23/32"), 19.1 mm (3/4") thick proprietary panels provided by one mill (Lowood 1993).

The number of bending, tension and shear tests conducted for establishment of engineering properties are given in Tables 2 to 5[1]. Details about the sampling, cutting patterns and testing methods are given in the reports named above. Strength and stiffness capacities were determined using "large specimens" and procedures described in the following ASTM Standards:

a) Bending: D3043 Method C Pure Moment Test for Large Panels;

---

[1]Compression tests were also conducted, but data are not included in Tables 2 to 5. See section "Tension versus Compression" for explanation.

b) Axial: D3500 Method B Tension and D3501 Method B Compression;

c) Shear: D2718 Planar or Shear-In-Plane (SIP) and D2719 Method C Shear-through-the-thickness (STT).

All tests, except the verification tests in Lucuik (1992), were carried out after the sample material had been conditioned in a 20°C/65% RH (Relative Humidity) environment. Tests were carried out in two directions: parallel to the major axis of the full-size panel (0°orientation), and perpendicular to the major axis of the full-size panel (90°orientation). The major axis is the axis with the greater stiffness and strength in bending.

Bearing: test specimens used by Lau and Tardif (1990) were prepared and tested according to a test procedure used by the Council of Forest Industries of B.C. (COFI) for plywood. Bearing test data provided by Lowood (1993) were collected according to ASTM Standard D143.

In addition to the above tests, "small specimens" were tested using procedures described in CAN3-O437.0 for Bending (dry), Internal Bond (IB), Bond Durability (BD).

Conformance of the Test Samples to the Governing Standard

The conformance of the waferboard and OSB samples used in the test programs to the governing product standard (CSA Standard O437.0-1985) can be summarized as follows: 1) Lau (1988) and Lau and Lam (1990) reported that the sampled R-1 grade waferboard and O-2 grade OSB panels generally met the requirements; 2) Lucuik (1992) reported that the panels from mill 1 generally met the requirements for O-2 grade OSB, but some of the OSB properties from mill 2 were found to be below the requirements; 3) Stieda (1989) reported that panels conformed to the requirements of O-2 grade OSB; 4) The panels used in testing the proprietary product conformed to the requirements of O-2 grade OSB (Lowood 1993).

Test Results

The condensed test results are given in Tables 2 to 5 for, respectively, fifth percentile ultimate strength capacities, mean panel stiffness, fifth percentile ultimate stresses and mean moduli (E and G) for each data set. In calculation of ultimate stresses, Modulus of Elasticity (MOE or E) and Modulus of Rigidity (G), the assumption of homogeneity has been made, and actual specimen thickness has been used except with data from Lowood (1993) where nominal thickness has been used. The 75% lower tolerance limit of the fifth percentile of ultimate stresses and strength capacities of each sample was calculated assuming normal distribution. For moduli (E and G) and stiffness capacities (EI, EA and GTT as defined in Table 3), the 95% lower tolerance limit of the sample mean value was calculated.

Detailed statistics about strength and stiffness capacities, ultimate stresses, MOE, G, moisture content, thickness and relative density for each mill are presented in Karacabeyli and Deacon (1993) for each thickness, test orientation, and panel type. The mean moisture content of the OSB and waferboard panels in a data set which were conditioned in a 20°C/65% RH environment was found to be 9% and 7% respectively (versus 12% for wood). Generally, on average, the OSB and waferboard panels were found to be slightly thicker than the nominal thickness marked on the panel. The mean relative density of the sample panels in a data set ranged from 0.62 to 0.69.

Lau and Tardif (1990) reported that the mean proportional limit of the bearing stress of waferboard varied from 4.4 to 7.0 MPa. Test results provided by Lowood (1993) showed that the mean compression strength (corresponding to a 2.5 mm deflection) perpendicular to surface of OSB varied between 4.2 and 4.8 MPa. Although the results from these investigations are not directly comparable, using the lowest mean value, a basic bearing strength of 4.2 MPa was assigned for Design Rated OSB.

Interpretation of the Test Data and Development of "Design Rated OSB"

Variability

Lau (1988), and Lau and Lam (1990) observed a significant difference between mills in almost all the properties tested, which in effect excludes the possibility of having acceptable design values for grades defined in CSA Standard O437. On the other hand, the within-mill variances were small i.e., coefficient of variation for most engineering properties was generally 17% or less (Tables 2 to 5), suggesting individual mills can effectively control their production to achieve a reasonable level of uniformity. This makes the mill specific procedure described earlier practical.

Tension versus Compression

In tests of axial (tension and compression) strength and stiffness, the ultimate compression stress values were found to be consistently greater than the tension values (Lau and Lam 1990). The MOE values in tension and compression, on the other hand, were found to be close to each other (Karacabeyli and Deacon 1993). Based on these findings, for simplicity tension values were adopted for both tension and compression.

Thickness

In Table 6, the characteristic values of ultimate stress and moduli (E and G) are given for OSB from three mills which sampled more than one panel thickness for testing, and for all waferboard data. Generally, there does not seem to be a pronounced effect of thickness on ultimate stress and moduli (E and G), with the exception of ultimate planar shear (or shear-in plane, SIP) stress which was found to be generally greater --up to 25 %-- for smaller thicknesses. This finding suggested that the stress and moduli data for several thicknesses could be combined. Subsequently one ultimate stress and one E or G value (Table 7) were used with geometric properties for each thickness to establish basic (short-term) capacities for Design Rated OSB.

Orientation

Also shown in Table 6, the ultimate stress and MOE values in bending in the 0° orientation were found to be consistently greater than those found for the 90° orientation. Thus different design values are necessary for the two orientations for Design Rated OSB. A similar difference was also observed for the tension and planar (or shear-in-plane, SIP) loading modes, but on a smaller scale. While different design values are assigned for the two orientations in the tension loading mode, for simplicity, one conservatively chosen value (0.80 MPa) is assigned for SIP properties in both orientations. The differences between the two orientations in shear-through-thickness (STT) properties were not significant, consequently one design value for Design Rated OSB is assigned for both orientations.

MOR/MOE Correlations

For OSB, a strong correlation ($R^2=0.7$ for large specimens in both orientations, and for small specimens in the 0°orientation) was observed between mean bending MOR (Modulus of Rupture) and mean bending MOE properties when the MOR-MOE relationship was represented by a linear relationship (Karacabeyli and Deacon 1993). (Note that this strong correlation was obtained by lumping mean values of all thicknesses together. The R^2 value for an individual thickness category would be lower.) This finding implies that procedures similar to those used in the production of MSR (Machine Stress Rated) lumber may be employed, depending on the correlation, to produce MSR OSB.

Rating Grades for Type 1 (Standard) Design Rated OSB in CSA O452

There are three rating grades (A,B,C) of Type 1 (Standard) Design Rated OSB for which the requirements are given in CSA Standard O452 (1994b). The minimum levels for the A and C grades were set based on groups of the highest and the lowest test values of O-2 grade OSB. Since the requirements of O-2 grade OSB in CSA O437 (CSA 1993b) are set as prerequisites for Design Rated OSB, the R-1 grade waferboard and O-1 grade OSB have been excluded. The minimum levels for the B was set at an approximate mid-way between A and C. The basic (short-term) capacities for these grades are given in Appendix I. The corresponding ultimate stresses and moduli (E and G) for these levels are given in Table 7. It is stipulated in CSA O452 that a rating grade for a product is assigned on the basis of the lowest property in terms of minimum levels. In setting the levels for these rating grades, a deliberate decision was made to make the bending strength in the 0° orientation the governing property. The other property levels were set conservatively. In other words, if the bending strength complies with the requirement of a particular grade, then the other properties would likely qualify for that grade.

The rating grade is specific to a product not to a property. However, to facilitate the understanding of the process, the conformance of a particular property to a rating grade is shown in the "R" column in Tables 2 and 3 in terms of strength and stiffness capacities, and in Tables 4 and 5 in terms of ultimate stresses and moduli (E and G). Results show that test data fall mostly into the A and C grades. The differences in the "R" R values in Tables 2 and 4 (strength capacities versus stresses) and Tables 3 and 5 (stiffness capacities versus E and G) may be attributed to the fact that in calculation of stresses, actual specimen thicknesses were used (with one exception).

The CSA Standard O452 requires that qualification test data be obtained at standard conditions (20°C/65% RH), and a mill specific moisture conditioning factor, established by the certification agency, be used to convert test values to 20°C/80% RH. Note that, with one exception, the test results presented in this paper (from which the grade levels were developed) were obtained in an environment of 20°C/65% RH. Adjustments on these test results (from 20°C and 65% RH to 20°C and 80% RH) could result in some reductions in the capacities which would ultimately reduce the property rating for some data sets in Tables 2 to 5. Such adjustments, however, were not made here.

Figures 1 to 4 show the fifth percentile values of ultimate stresses and Figure 5 the mean values of MOE for the 0° orientation. The values collected for different thicknesses of OSB and waferboard were combined and ranked on the basis of ultimate stress in bending (MOR) which is considered the most important design property. Therefore, the vertical axis in these figures shows the rank based on bending MOR. All other properties are shown based on this rank. These figures indicate that a positive correlation exists between the bending MOR and ultimate tensile stress, and also between bending MOR

and MOE in the direction parallel to the major axis of the panel. The correlation between bending MOR and ultimate shear (STT or SIP) stresses was found to be almost non-existent. Also shown in these figures are the minimum levels for the three grades (A, B and C) of Design Rated OSB.

Specified Strength and Stiffness Capacities of Type 1 Design Rated OSB in CSA O86.1

The CSA Standard O86.1 includes specified strength and stiffness capacities for Design Rated OSB (Table 1). These capacities are only applicable to dry service conditions. The specified strength capacities in CSA Standard O86.1 (which are influential on strength limit states) were based on 80% of the strength capacities (except bearing) in CSA Standard O452. This adjustment was made to account for load duration effects as the specified strength capacities in CSA Standard O86.1 are published for "Standard Term" loading which includes snow and occupancy load combinations. The specified stiffness and bearing capacities in CSA Standard O86.1 are the same as those in CSA Standard O452 without modification as these properties are considered to be influential only on the serviceability limit states.

Code Implementation and Implications

In its November 1993 meeting, the Canadian Standards Association Technical Committee on Engineering Design in Wood approved the inclusion of the engineering properties for "Design Rated OSB (Oriented Strand Board)" in CSA Standard O86.1 (CSA 1994a), "Engineering Design in Wood". These design properties are for OSB panels complying with the requirements of the new standard CSA O452 (CSA 1994b), "Design Rated OSB". With the publication of specified capacities for "Design Rated OSB" in CSA Standard O86.1, structural engineers can specify Design Rated OSB as a construction sheathing material in large structures and as structural components covered by the Part 4 of the NBCC (Associate Committee on the National Building Code 1995).

Acknowledgements

The authors gratefully acknowledge the financial support of the Canadian Forest Service, as well as the considerable expenditure on the part of the Structural Board Association in support of the testing programs reported here. The authors also wish to thank Mr. J. Lowood of the SBA and Mr. H.P. Vokey, consultant to the SBA, and Dr. C.K.A. Stieda, Mr. J.C. Havard and Mr. J. Shields of Forintek for their comments. Finally the authors acknowledge the contribution made by Mr. H.P. Vokey (then of Forintek) in developing the "mill specific approach".

References

Associate Committee on the National Building Code. 1995. National Building Code of Canada. National Research Council of Canada. Ottawa, Ont., Canada. In print.

Canadian Standards Association. 1985. CSA Standard O437.0. "Waferboard and Strandboard". CSA, Rexdale, Ontario, Canada.

Canadian Standards Association. 1993a. CSA Standard O325.0. "Construction Sheathing". CSA, Rexdale, Ontario, Canada.

Canadian Standards Association. 1993b. CSA Standard O437.0. "OSB and Waferboard". CSA, Rexdale, Ontario, Canada.

Canadian Standards Association. 1994a. CSA Standard O86.1. Engineering Design in Wood (limit States Design). CSA, Rexdale, Ontario, Canada. In print.

Canadian Standards Association. 1994b. CSA Standard O452. Design Rated OSB: Specifications, Test Methods, Quality Assurance. CSA, Rexdale, Ontario, Canada. In print.

Karacabeyli, E. and Deacon, W. 1993. Summary of short-term test results for waferboard and oriented strand board. Report (No. 15) prepared for Canadian Forest Service. Forintek Canada Corp., Vancouver, B.C., Canada.

Lau, P.W.C. 1988. Structural performance of waferboard (5/8") for floor systems. Contract report prepared for The Waferboard Association (now Structural Board Association). Forintek Canada Corp. Ottawa, Ont., Canada.

Lau, P.W.C. and Lam F. 1990. Mechanical properties of 15.9 mm (5/8") waferboard and OSB. Contract report prepared for Structural Board Association. Forintek Canada Corp. Ottawa, Ont., Canada.

Lau, P.W.C. and Tardif Y. 1990. Bearing resistance of 15.9 mm (5/8") waferboard and OSB. Prepared for Structural Board Association. Forintek Canada Corp. Ottawa, Ont., Canada.

Lowood, J.D. 1993. Proprietary information provided by Structural Board Association (SBA)., Willowdale, Ont., Canada.

Lucuik, M. 1992. Engineering properties of OSB - Phase 2. Verification of draft industry standard. Contract report prepared for Structural Board Association. Forintek Canada Corp. Ottawa, Ont., Canada.

National Institute of Standards and Technology, 1992. Performance Standard for Wood-based Structural-use Panels. Voluntary Product Standard PS 2-92. U.S. Dept. of Commerce, USA.

Stieda, C.K.A. 1989. Summary of short-term engineering properties of O-2 grade strandboard (OSB) at dry service conditions. Contract report prepared for Jager Industries Inc. Forintek Canada Corp. Vancouver, B.C., Canada.

Table 1. Specified Capacities for Type 1 (Standard) Design Rated OSB (CSA Standard O86.1)

DESIGN RATING			Strength Capacities					Stiffness and Rigidity Capacities				
			Bending m_p[1]		Axial (Tension/ Compression) t_p[2], p_p[2]		Shear-Through-Thickness v_p[3]	Bending B_b[4] = EI		Axial (Tension/ Compression) B_a[5] = EA		Shear-Through-Thickness Rigidity B_v[6] = GTT
NOMINAL THICKNESS	RATING GRADE		Orientation of applied forces relative to major axis					Orientation of applied forces relative to major axis				
			0°	90°	0°	90°	0° & 90°	0°	90°	0°	90°	0° & 90°
mm			N•mm/mm	N•mm/mm	N/mm	N/mm	N/mm	N•mm²/mm	N•mm²/mm	N/mm	N/mm	N/mm
9.5	- A		290	90	79	38	30	590,000	170,000	46,000	19,000	9,500
9.5	- B		240	90	63	38	30	490,000	170,000	39,000	19,000	9,500
9.5	- C		190	90	47	38	30	390,000	170,000	33,000	19,000	9,500
11.0	- A		390	120	91	44	35	920,000	270,000	53,000	22,000	11,000
11.0	- B		320	120	73	44	35	760,000	270,000	46,000	22,000	11,000
11.0	- C		260	120	55	44	35	610,000	270,000	38,000	22,000	11,000
12.5	- A		500	160	100	50	40	1,300,000	390,000	60,000	25,000	12,000
12.5	- B		420	160	83	50	40	1,100,000	390,000	52,000	25,000	12,000
12.5	- C		330	160	62	50	40	900,000	390,000	43,000	25,000	12,000
15.5	- A		770	240	130	62	50	2,600,000	740,000	75,000	31,000	15,000
15.5	- B		640	240	100	62	50	2,100,000	740,000	64,000	31,000	15,000
15.5	- C		510	240	77	62	50	1,700,000	740,000	53,000	31,000	15,000
18.5	- A		1100	340	150	74	59	4,400,000	1,300,000	89,000	37,000	18,000
18.5	- B		910	340	120	74	59	3,600,000	1,300,000	77,000	37,000	18,000
18.5	- C		720	340	92	74	59	2,900,000	1,300,000	64,000	37,000	18,000
22.0	- A		1600	480	180	88	70	7,300,000	2,100,000	110,000	44,000	22,000
22.0	- B		1300	480	150	88	70	6,100,000	2,100,000	91,000	44,000	22,000
22.0	- C		1000	480	110	88	70	4,900,000	2,100,000	76,000	44,000	22,000
28.5	- A		2600	810	240	110	91	16,000,000	4,600,000	140,000	57,000	28,000
28.5	- B		2200	810	190	110	91	13,000,000	4,600,000	120,000	57,000	28,000
28.5	- C		1700	810	140	110	91	11,000,000	4,600,000	98,000	57,000	28,000

Notes:

a) All Type 1 Design Rated OSB panels:
- Planar (shear-in-plane or SIP in Table 2) strength V_{pl} (0° and 90°) = 0.64 MPa
- Planar shear strength in bending v_{pb} (0° and 90°)= 2/3 $v_{pl}t_1$ where t= nominal thickness
- Specified Strength in bearing (normal to the plane), q_p = 4.2 MPa

b) Tabulated values are based on the following standard conditions: a) dry service conditions b) standard term duration of load

c) For Type 2 Design Rated OSB panels add the designated percentage increase for the Plus property to the Type 1 specified capacity listed for that property.

[1] m_p: Bending strength capacity per mm. width (MS in Table 2)
[2] t_p, p_p: Axial strength capacity per mm. width (TA in Table 2)
[3] v_p: Shear-through-thick strength capacity per mm shear resisting panel length (STT in Table 2)
[4] B_b: Bending stiffness capacity per mm. width (EI in Table 3)
[5] B_a: Axial stiffness capacity per mm. width (EA in Table 3)
[6] B_v: Shear-through-thick rigidity per mm. panel depth (i.e. G times nominal thickness, GTT in Table 3)

Table 2. 5th Percentile Values of Short-term Ultimate Strength Capacities for Waferboard and Oriented Strand Board (OSB)

Panel Type	Nominal Thickness	Orient-ation	Mill	Bending				Tension				Shear-Through-Thickness				Planar Shear			
				N[1]	MS[2]	CV[3]	R[4]	N	TA[5]	CV	R	N	STT[6]	CV	R	N	SIP[7]	CV	R
	mm	degrees			N•mm/mm	%			N/mm	%			N/mm	%			MPa	%	
OSB	9.5	0	3	100	356	15	B	100	108	12	A	100	77	8	A	100	1.2	10	A
OSB	9.5	0	3	30	389	9	A	28	113	10	A	.	.	.		31	1.4	10	A
OSB	11.1	0	3	5	476	8	B	8	137	10	A	.	.	.		8	1.5	4	A
OSB	11.1	0	2	30	345	12	C	.	.	.		.	.	.		30	0.8	17	A
OSB	11.1	0	2	30	365	12	C	.	.	.		.	.	.		.	.	.	
OSB	11.1	0	1	30	397	14	C	.	.	.		.	.	.		30	1.0	10	A
OSB	11.1	0	1	30	376	14	C	.	.	.		.	.	.		.	.	.	
OSB	11.9	0	3	30	638	8	A	28	133	10	A	.	.	.		32	1.2	9	A
OSB	12.7	0	3	5	663	6	A	8	140	10	A	.	.	.		8	1.1	13	A
OSB	15.5	0	3	100	1023	12	A	100	181	9	A	100	129	6	A	100	0.9	13	A
OSB	15.9	0	3	5	1302	4	A	8	174	9	A	.	.	.		8	0.8	14	A
OSB	15.9	0	2	30	638	15	C	.	.	.		.	.	.		29	0.7	23	-
OSB	15.9	0	1	30	800	12	B	.	.	.		.	.	.		30	0.9	14	A
OSB	15.9	0	1	30	775	12	C	.	.	.		.	.	.		.	.	.	
OSB	15.9	0	-1	20	858	11	B	20	147	11	B	20	119	7	A	20	1.2	7	A
OSB	15.9	0	-5	20	774	17	C	20	174	10	A	20	103	10	A	20	1.0	15	A
OSB	15.9	0	-10	20	885	9	B	20	163	9	A	20	141	6	A	20	1.2	11	A
OSB	15.9	0	-13	20	832	13	B	20	152	14	B	20	124	9	A	20	1.6	8	A
OSB	18.3	0	3	12	1410	9	A	.	.	.		.	.	.		.	.	.	
OSB	19.1	0	3	18	1682	6	A	28	221	11	A	.	.	.		30	1.0	10	A
OSB	9.5	90	3	100	232	12	A	100	103	9	A	100	82	8	A	100	1.5	9	A
OSB	9.5	90	3	30	272	7	A	28	112	10	A	30	88	6	A	32	1.8	12	A
OSB	11.1	90	3	5	390	4	A	8	130	10	A	5	98	5	A	8	1.7	11	A
OSB	11.1	90	2	30	183	19	A	.	.	.		.	.	.		.	.	.	
OSB	11.1	90	2	30	215	14	A	.	.	.		.	.	.		.	.	.	
OSB	11.1	90	1	30	272	10	A	.	.	.		.	.	.		.	.	.	
OSB	11.1	90	1	30	259	12	A	.	.	.		.	.	.		.	.	.	
OSB	11.9	90	3	30	401	9	A	28	145	9	A	30	103	7	A	30	1.6	11	A
OSB	12.7	90	3	5	470	4	A	8	161	7	A	5	109	4	A	8	1.2	20	A
OSB	15.5	90	3	100	610	12	A	100	161	9	A	100	134	6	A	100	1.1	14	A
OSB	15.9	90	3	5	707	8	A	8	154	14	A	5	129	5	A	8	1.4	12	A
OSB	15.9	90	2	29	431	14	A	.	.	.		.	.	.		.	.	.	
OSB	15.9	90	1	30	533	10	A	.	.	.		.	.	.		.	.	.	
OSB	15.9	90	1	30	551	7	A	.	.	.		.	.	.		.	.	.	
OSB	15.9	90	-1	19	603	10	A	19	134	15	A	19	105	9	A	19	1.1	18	A
OSB	15.9	90	-5	20	404	17	A	20	100	12	A	20	126	7	A	20	1.0	11	A
OSB	15.9	90	-10	20	861	7	A	20	206	9	A	20	129	9	A	20	1.3	14	A
OSB	15.9	90	-13	20	585	9	A	20	126	11	A	20	147	6	A	20	1.3	10	A
OSB	18.3	90	3	12	870	9	A	.	.	.		12	154	6	A	.	.	.	
OSB	19.1	90	3	18	1101	6	A	27	231	9	A	18	166	5	A	30	1.3	12	A
WAF[8]	15.9	0	-5	17	719	10	C	17	135	10	B	17	110	9	A	17	1.1	9	A
WAF	15.9	0	-8	20	792	8	C	20	153	10	B	20	129	6	A	20	1.5	14	A
WAF	15.9	0	-9	19	564	13	-	19	118	10	C	19	96	9	A	19	1.2	12	A
WAF	15.9	0	-11	20	660	8	C	20	156	9	B	20	126	6	A	20	1.4	9	A
WAF	15.9	0	-12	20	741	6	C	20	142	12	B	20	130	6	A	20	1.3	10	A
WAF	15.9	0	-13	18	686	12	C	18	136	16	B	18	116	8	A	18	1.2	13	A
WAF	15.9	90	-5	20	701	8	A	20	133	10	A	20	117	7	A	20	1.0	10	A
WAF	15.9	90	-8	20	647	7	A	20	145	10	A	20	129	7	A	20	1.3	16	A
WAF	15.9	90	-9	20	508	13	A	20	104	11	A	20	102	6	A	20	1.1	11	A
WAF	15.9	90	-11	20	670	6	A	20	139	8	A	20	133	4	A	20	1.3	8	A
WAF	15.9	90	-12	20	639	10	A	20	133	12	A	20	122	8	A	20	1.1	17	A
WAF	15.9	90	-13	19	752	8	A	19	127	13	A	19	124	8	A	19	1.1	13	A

[1]N: Number of replicates
[2]MS: Bending Strength Capacity per mm width (m_p in Table 1)
[3]CV: Coefficient of Variation
[4]R: Conformance of a particular property to a Rating Grade.
[5]TA: Axial Strength Capacity per mm width (t_p or p_p in Table 1)
[6]STT: Shear-through-thick strength capacity per mm shear resisting panel length (v_p in Table1)
[7]SIP: Shear-in-plane strength capacity (v_{pi} in Table 1)
[8]WAF: Waferboard

Table 3. Mean Values of Panel Stiffness for Waferboard and Oriented Strand Board (OSB)

Panel Type	Nominal Thickness	Orient-ation	Mill	Bending				Tension				Shear-Through-Thickness			
				N[1]	EI[2]	CV[3]	R[4]	N	EA[5]	CV	R	N	GTT[6]	CV	R
	mm	degrees			MN•mm²/mm	%			kN/mm	%			kN/mm	%	
OSB	9.5	0	3	100	0.68	10	A	100	48.3	11	A	100	12.4	14	A
OSB	9.5	0	3	30	0.62	10	A	.	.	.		.	.	.	
OSB	11.1	0	3	5	0.81	7	B	.	.	.		.	.	.	
OSB	11.1	0	2	30	0.74	21	C	.	.	.		.	.	.	
OSB	11.1	0	2	30	0.81	14	B	.	.	.		.	.	.	
OSB	11.1	0	1	30	0.96	16	A	.	.	.		.	.	.	
OSB	11.1	0	1	30	0.91	12	B	.	.	.		.	.	.	
OSB	11.9	0	3	30	1.23	8	B	.	.	.		.	.	.	
OSB	12.7	0	3	5	1.33	4	B	.	.	.		.	.	.	
OSB	15.5	0	3	100	3.08	10	A	100	81.5	9	A	100	20.5	10	A
OSB	15.9	0	3	5	2.69	4	A	.	.	.		.	.	.	
OSB	15.9	0	2	30	1.96	15	C	.	.	.		.	.	.	
OSB	15.9	0	1	30	2.67	13	A	.	.	.		.	.	.	
OSB	15.9	0	1	30	2.55	7	B	.	.	.		.	.	.	
OSB	15.9	0	-1	20	2.94	12	A	20	85.8	12	A	20	25.1	7	A
OSB	15.9	0	-5	20	2.89	20	A	20	102.4	14	A	20	23.3	9	A
OSB	15.9	0	-10	20	2.44	8	B	20	87.6	14	A	20	24.7	7	A
OSB	15.9	0	-13	20	2.82	6	A	20	112.2	20	A	20	26.1	6	A
OSB	18.3	0	3	12	4.79	4	A	.	.	.		.	.	.	
OSB	19.1	0	3	18	4.77	6	A	.	.	.		.	.	.	
OSB	9.5	90	3	100	0.23	10	A	100	97.2	10	A	100	12.8	10	A
OSB	9.5	90	3	30	0.25	9	A	.	.	.		.	.	.	
OSB	11.1	90	3	5	0.37	4	A	.	.	.		.	.	.	
OSB	11.1	90	2	30	0.37	19	A	.	.	.		.	.	.	
OSB	11.1	90	2	30	0.38	23	A	.	.	.		.	.	.	
OSB	11.1	90	1	30	0.34	17	A	.	.	.		.	.	.	
OSB	11.1	90	1	30	0.34	18	A	.	.	.		.	.	.	
OSB	11.9	90	3	30	0.47	14	A	.	.	.		.	.	.	
OSB	12.7	90	3	5	0.47	13	A	.	.	.		.	.	.	
OSB	15.5	90	3	100	1.07	9	A	100	67.2	8	A	100	20.7	9	A
OSB	15.9	90	3	5	1.22	7	A	.	.	.		.	.	.	
OSB	15.9	90	2	29	1.00	14	A	.	.	.		.	.	.	
OSB	15.9	90	1	30	0.97	11	A	.	.	.		.	.	.	
OSB	15.9	90	1	30	0.91	8	A	.	.	.		.	.	.	
OSB	15.9	90	-1	19	1.21	10	A	19	88.7	11	A	19	24.8	8	A
OSB	15.9	90	-5	20	0.99	14	A	20	50.4	13	A	20	25.9	7	A
OSB	15.9	90	-10	20	1.35	8	A	20	103.2	14	A	20	25.0	7	A
OSB	15.9	90	-13	20	1.02	10	A	20	53.4	8	A	20	25.9	10	A
OSB	18.3	90	3	12	1.95	12	A	.	.	.		.	.	.	
OSB	19.1	90	3	18	2.17	6	A	.	.	.		.	.	.	
WAF[7]	15.9	0	-5	17	1.83	10	C	17	71.4	10	B	17	25.1	8	A
WAF	15.9	0	-8	20	1.84	9	C	20	87.0	13	A	20	26.8	4	A
WAF	15.9	0	-9	19	1.63	11	-	19	70.5	14	B	19	22.2	8	A
WAF	15.9	0	-11	20	1.67	6	-	20	82.7	13	A	20	27.6	7	A
WAF	15.9	0	-12	20	1.83	5	C	20	75.7	10	A	20	28.1	8	A
WAF	15.9	0	-13	18	1.85	6	C	18	73.4	17	B	18	25.3	8	A
WAF	15.9	90	-5	20	1.87	7	A	20	68.2	15	A	20	24.9	7	A
WAF	15.9	90	-8	20	1.26	9	A	20	65.8	10	A	20	24.4	8	A
WAF	15.9	90	-9	20	1.42	15	A	20	55.7	15	A	20	21.4	7	A
WAF	15.9	90	-11	20	1.48	5	A	20	68.6	14	A	20	24.7	7	A
WAF	15.9	90	-12	20	1.51	9	A	20	75.2	15	A	20	28.0	9	A
WAF	15.9	90	-13	19	1.78	6	A	19	68.0	12	A	19	27.5	8	A

[1]N: Number of replicates
[2]EI: Bending Stiffness Capacity per mm width (B_b in Table 1)
[3]CV: Coefficient of Variation
[4]R: Conformance of a particular property to a Rating Grade.
[5]EA: Axial Stiffness Capacity per mm width (B_a in Table 1)
[6]GTT: Shear-through-thick rigidity per mm panel depth,G times nominal thickness (B_v in Table1)
[7]WAF: Waferboard

Table 4. 5th Percentile Values of Short-term Ultimate Stress (f) for Waferboard and Oriented Strand Board (OSB)

Panel Type	Nominal Thickness	Orient-ation	Mill	Bending				Tension				Shear-Through-Thickness				Planar Shear			
				N[1]	f	CV[2]	R[3]	N	f	CV	R	N	f	CV	R	N	f	CV	R
	mm	degrees			MPa	%			MPa	%			MPa	%			MPa	%	
OSB	9.5	0	3	100	19.3	15	C	100	11.1	11	A	100	7.4	8	A	100	1.2	10	A
OSB	9.5	0	3	30	25.9	9	A	28	11.9	10	A	.	.	.		31	1.4	10	A
OSB	11.1	0	3	5	23.2	8	B	8	12.3	10	A					8	1.5	4	A
OSB	11.1	0	2	30	14.6	10	-	30	8.5	12	B	30	4.2	11	A	30	0.8	17	A
OSB	11.1	0	2	30	14.2	14	-												
OSB	11.1	0	1	30	18.6	11	C	30	8.4	11	B	30	5.5	10	A	30	1.0	10	A
OSB	11.1	0	1	30	17.8	12	C												
OSB	11.9	0	3	30	27.0	8	A	28	11.2	10	A	.	.	.		32	1.2	9	A
OSB	12.7	0	3	5	24.6	6	A	8	11.0	10	A					8	1.1	13	A
OSB	15.5	0	3	100	22.6	12	B	100	11.1	11	A	100	7.6	7	A	100	0.9	13	A
OSB	15.9	0	3	5	30.9	4	A	8	11.0	9	A					8	0.8	14	A
OSB	15.9	0	2	30	13.6	17	-	30	7.2	17	C	20	4.8	14	A	29	0.7	23	-
OSB	15.9	0	1	30	17.8	12	C	30	8.5	11	B	30	5.5	6	A	30	0.9	14	A
OSB	15.9	0	1	30	16.2	14	C												
OSB	15.9	0	-1	20	19.1	11	C	20	8.9	11	B	20	7.4	7	A	20	1.2	7	A
OSB	15.9	0	-5	20	19.0	15	C	20	10.8	10	A	20	6.4	9	A	20	1.0	15	A
OSB	15.9	0	-10	20	19.4	9	C	20	9.8	10	B	20	8.5	6	A	20	1.2	11	A
OSB	15.9	0	-13	20	18.0	14	C	20	9.2	14	B	20	7.5	9	A	20	1.6	8	A
OSB	18.3	0	3	12	25.3	9	A												
OSB	19.1	0	3	18	27.7	6	A	28	11.6	11	A	.	.	.		30	1.0	10	A
OSB	9.5	90	3	100	12.8	12	A	100	10.5	8	A	100	7.8	8	A	100	1.5	9	A
OSB	9.5	90	3	30	18.1	7	A	28	11.8	10	A	30	9.3	6	A	32	1.8	12	A
OSB	11.1	90	3	5	19.0	4	A	8	11.7	10	A	5	8.8	5	A	8	1.7	11	A
OSB	11.1	90	2	30	8.0	16	A	30	5.0	18	A	.	.	.		.	.	.	
OSB	11.1	90	2	30	9.0	12	A					.	.	.		.	.	.	
OSB	11.1	90	1	30	12.2	10	A	30	7.8	10	A	.	.	.		.	.	.	
OSB	11.1	90	1	30	12.4	10	A												
OSB	11.9	90	3	30	17.0	9	A	28	12.2	9	A	30	8.6	7	A	30	1.6	11	A
OSB	12.7	90	3	5	17.5	4	A	8	12.7	7	A	5	8.6	4	A	8	1.2	20	A
OSB	15.5	90	3	100	13.4	12	A	100	10.0	9	A	100	7.9	7	A	100	1.1	14	A
OSB	15.9	90	3	5	16.8	8	A	8	9.7	14	A	5	8.1	5	A	8	1.4	12	A
OSB	15.9	90	2	29	9.5	14	A	29	5.7	14	A	9	4.8	7	A	.	.	.	
OSB	15.9	90	1	30	12.1	8	A	30	7.6	14	A	.	.	.		.	.	.	
OSB	15.9	90	1	30	11.5	11	A												
OSB	15.9	90	-1	19	13.1	11	A	19	8.0	15	A	19	6.4	8	A	19	1.1	18	A
OSB	15.9	90	-5	20	9.3	17	A	20	6.2	12	A	20	7.9	6	A	20	1.0	11	A
OSB	15.9	90	-10	20	18.7	8	A	20	12.4	10	A	20	7.7	10	A	20	1.3	14	A
OSB	15.9	90	-13	20	13.2	9	A	20	7.5	12	A	20	8.7	6	A	20	1.3	10	A
OSB	18.3	90	3	12	15.6	9	A					12	8.4	6	A				
OSB	19.1	90	3	18	18.1	6	A	27	12.1	9	A	18	8.7	5	A	30	1.3	12	A
WAF[4]	15.9	0	-5	17	17.3	8	C	17	8.4	10	B	17	6.8	10	A	17	1.1	9	A
WAF	15.9	0	-8	20	19.1	7	C	20	9.5	11	B	20	8.1	7	A	20	1.5	14	A
WAF	15.9	0	-9	19	13.5	11	-	19	7.5	9	C	19	6.0	8	A	19	1.2	12	A
WAF	15.9	0	-11	20	15.2	8	-	20	9.7	9	B	20	7.9	6	A	20	1.4	9	A
WAF	15.9	0	-12	20	17.0	6	C	20	8.7	12	B	20	8.0	6	A	20	1.3	10	A
WAF	15.9	0	-13	18	14.7	11	-	18	8.2	16	C	18	7.0	8	A	18	1.2	13	A
WAF	15.9	90	-5	20	16.2	8	A	20	8.2	10	A	20	7.2	7	A	20	1.0	10	A
WAF	15.9	90	-8	20	14.5	9	A	20	8.7	11	A	20	7.6	10	A	20	1.3	16	A
WAF	15.9	90	-9	20	12.4	10	A	20	6.5	10	A	20	6.2	7	A	20	1.1	11	A
WAF	15.9	90	-11	20	15.4	7	A	20	8.5	9	A	20	8.3	5	A	20	1.3	8	A
WAF	15.9	90	-12	20	14.5	10	A	20	8.2	12	A	20	7.5	8	A	20	1.1	17	A
WAF	15.9	90	-13	19	16.3	8	A	19	7.6	13	A	19	7.4	8	A	19	1.1	13	A

[1]N: Number of replicates
[2]CV: Coefficient of Variation
[3]R: Conformance of a particular property to a Rating Grade.
[4]WAF: Waferboard

Table 5. Mean Values of Modulus of Elasticity (E) and Rigidity (G) for Waferboard and Oriented Strand Board (OSB)

Panel Type	Nominal Thickness	Orient-ation	Mill	Bending				Tension				Shear-Through-Thickness			
				N[1]	E	CV[2]	R[3]	N	E	CV	R	N	G	CV	R
	mm	degrees			MPa	%			MPa	%			MPa	%	
OSB	9.5	0	3	100	7425	10	B	100	4859	10	A	100	1194	13	A
OSB	9.5	0	3	30	8731	10	A	.	.	.		.	.	.	
OSB	11.1	0	3	5	7123	7	B	.	.	.		.	.	.	
OSB	11.1	0	2	30	4940	15	-	30	3601	26	C	30	978	9	A
OSB	11.1	0	2	30	5336	11	-	.	.	.		.	.	.	
OSB	11.1	0	1	30	7129	8	B	30	3837	17	C	30	1056	12	A
OSB	11.1	0	1	30	7134	9	B	.	.	.		.	.	.	
OSB	11.9	0	3	30	8755	8	A	.	.	.		.	.	.	
OSB	12.7	0	3	5	7800	4	B	.	.	.		.	.	.	
OSB	15.5	0	3	100	8736	10	A	100	5106	10	A	100	1229	10	A
OSB	15.9	0	3	5	8045	4	B	.	.	.		.	.	.	
OSB	15.9	0	2	30	5195	17	-	30	3361	23	-	20	620	12	-
OSB	15.9	0	1	30	7242	9	B	30	3769	20	C	30	1116	8	A
OSB	15.9	0	1	30	6946	9	B	.	.	.		.	.	.	
OSB	15.9	0	-1	20	8076	12	B	20	5247	12	A	20	1529	8	A
OSB	15.9	0	-5	20	8319	15	A	20	6354	13	A	20	1447	8	A
OSB	15.9	0	-10	20	6474	8	C	20	5296	14	A	20	1491	7	A
OSB	15.9	0	-13	20	7578	7	B	20	6807	20	A	20	1585	7	A
OSB	18.3	0	3	12	9373	4	A	.	.	.		.	.	.	
OSB	19.1	0	3	18	8215	6	B	.	.	.		.	.	.	
OSB	9.5	90	3	100	2520	10	A	100	3848	10	A	100	1211	9	A
OSB	9.5	90	3	30	3517	9	A	.	.	.		.	.	.	
OSB	11.1	90	3	5	3284	4	A	.	.	.		.	.	.	
OSB	11.1	90	2	30	2465	13	A	30	2173	21	A	.	.	.	
OSB	11.1	90	2	30	2493	8	A	.	.	.		.	.	.	
OSB	11.1	90	1	30	2674	9	A	30	2773	34	A	.	.	.	
OSB	11.1	90	1	30	2709	15	A	.	.	.		.	.	.	
OSB	11.9	90	3	30	3358	14	A	.	.	.		.	.	.	
OSB	12.7	90	3	5	2775	13	A	.	.	.		.	.	.	
OSB	15.5	90	3	100	3023	9	A	100	4219	9	A	100	1242	9	A
OSB	15.9	90	3	5	3635	7	A	.	.	.		.	.	.	
OSB	15.9	90	2	29	2717	14	A	29	2370	24	A	9	517	14	-
OSB	15.9	90	1	30	2553	9	A	30	3163	30	A	.	.	.	
OSB	15.9	90	1	30	2480	10	A	.	.	.		.	.	.	
OSB	15.9	90	-1	19	3249	11	A	19	5363	12	A	19	1506	8	A
OSB	15.9	90	-5	20	2821	13	A	20	3121	13	A	20	1608	6	A
OSB	15.9	90	-10	20	3610	8	A	20	6255	14	A	20	1513	7	A
OSB	15.9	90	-13	20	2735	10	A	20	3243	8	A	20	1575	10	A
OSB	18.3	90	3	12	3821	12	A	.	.	.		.	.	.	
OSB	19.1	90	3	18	3738	6	A	.	.	.		.	.	.	
WAF[4]	15.9	0	-5	17	5356	8	-	17	4440	11	B	17	1562	8	A
WAF	15.9	0	-8	20	5564	7	C	20	5480	13	A	20	1681	5	A
WAF	15.9	0	-9	19	4771	6	-	19	4399	13	B	19	1382	7	A
WAF	15.9	0	-11	20	4841	8	-	20	5161	13	A	20	1724	7	A
WAF	15.9	0	-12	20	5138	5	-	20	4666	10	B	20	1729	8	A
WAF	15.9	0	-13	18	4724	7	-	18	4386	17	B	18	1513	8	A
WAF	15.9	90	-5	20	5251	6	A	20	4194	15	A	20	1532	7	A
WAF	15.9	90	-8	20	3715	9	A	20	4113	11	A	20	1516	10	A
WAF	15.9	90	-9	20	4142	9	A	20	3462	14	A	20	1330	7	A
WAF	15.9	90	-11	20	4330	6	A	20	4284	15	A	20	1541	7	A
WAF	15.9	90	-12	20	4238	10	A	20	4636	15	A	20	1726	8	A
WAF	15.9	90	-13	19	4621	6	A	19	4077	12	A	19	1645	9	A

[1]N: Number of replicates
[2]CV: Coefficient of Variation
[3]R: Conformance of a particular property to a Rating Grade.
[4]WAF: Waferboard

Table 6. Short-Term Ultimate Stresses (f) and Modulus of Elasticity (E) and Rigidity (G)

Panel Type		OSB									WAF[1]
Mill No.		Mill #1		Mill #2		Mill #3-JAG		Mill #3-SBA3			All Mills
Nominal Thickness (mm)		11.0	15.5	11.0	15.5	9.5	15.5	9.5	11.9	19.1	15.5
ULTIMATE STRESS (5th Percentile)	(MPa)										
Bending	0	18.2	17.0	14.4	13.6	19.3	22.6	25.9	27.0	27.7	16.1
	90	12.3	11.8	8.5	9.5	12.8	13.4	18.1	17.0	18.1	14.9
Tension	0	8.4	8.5	8.5	7.2	11.1	11.1	11.9	11.2	11.6	8.7
	90	7.8	7.6	5.0	5.7	10.5	10.0	11.8	12.2	12.1	7.9
Shear-through-thickness	0	5.5	5.5	4.2	4.8	7.4	7.6	-	-	-	7.3
	90	-	-	-	4.8	7.8	7.9	9.3	8.6	8.7	7.4
Planar Shear	0	1.0	0.9	0.8	0.7	1.2	0.9	1.4	1.2	1.0	1.3
	90	-	-	-	-	1.5	1.1	1.8	1.6	1.3	1.2
E or G (Mean)	(MPa)										
Bending	0	7130	7090	5140	5200	7430	8740	8730	8760	8820	5070
	90	2690	2520	2480	2720	2520	3020	3520	3360	3740	4380
Tension	0	3840	3770	3600	3360	4860	5110	-	-	-	4760
	90	2770	3160	2170	2370	3850	4220	-	-	-	4130
Shear-through- thickness	0	1060	1120	980	620	1190	1230	-	-	-	1600
	90	-	-	-	520	1210	1240	-	-	-	1550
Planar Shear	0	-	-	-	-	180	160	-	-	-	160
	90	-	-	-	-	200	210	-	-	-	130

[1]WAF: Waferboard

Table 7. Levels of the short-term ultimate stresses and Moduli (E and G) for the Three Rating Grades of Design Rated OSB

Nominal Thickness	GRADE	ULTIMATE STRESSES (MPa)						E AND G (MPa)				
		Bending		Tension/C[1]		STT[2]	SIP[3]	Bending		Tension/C		STT
		0[4]	90[5]	0	90	0 & 90	0 & 90	0	90	0	90	0&90
All	A	24.1	7.5	10.3	5.0	4.0	0.8	8300	2400	4800	2000	1000
All	B	20.0	7.5	8.3	5.0	4.0	0.8	6900	2400	4100	2000	1000
All	C	15.9	7.5	6.2	5.0	4.0	0.8	5500	2400	3400	2000	1000

Note:
Bearing Strength (Normal to the plane) for all grades: 4.2 MPa.

[1]Tension/C: Tension and Compression
[2]STT: Shear Through Thickness
[3]SIP: Planar Shear or shear-in-plane
[4]0: Orientation, 0°
[5]90: Orientation, 90°

List of Figures

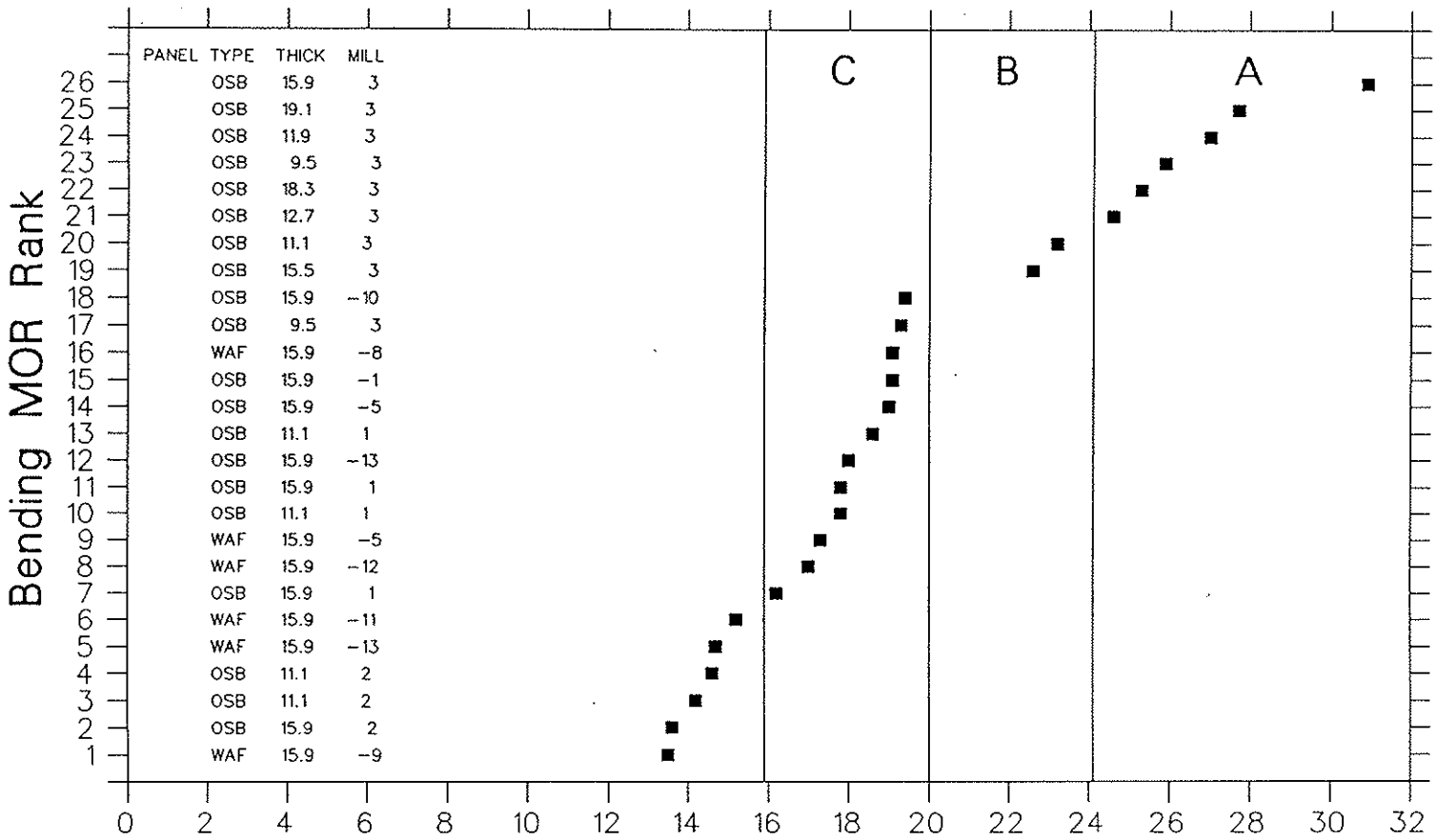

Figure 1 Fifth Percentile of Ultimate Bending Stress (MPa) Measured Parallel to the Major Axis of the Panel

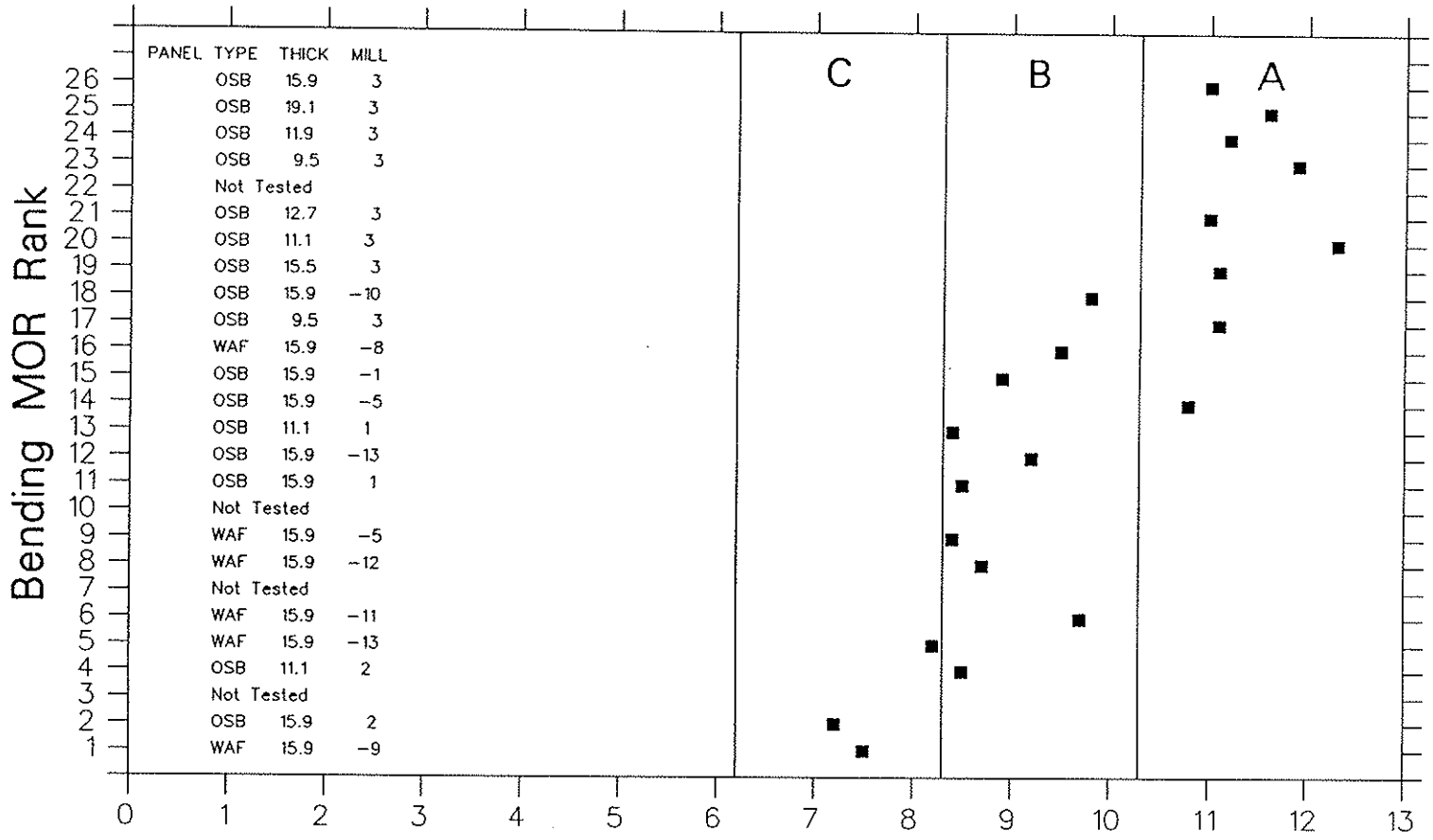

Figure 2 Fifth Percentile of Ultimate Tensile Stress (MPa) Measured Parallel to the Major Axis of the Panel

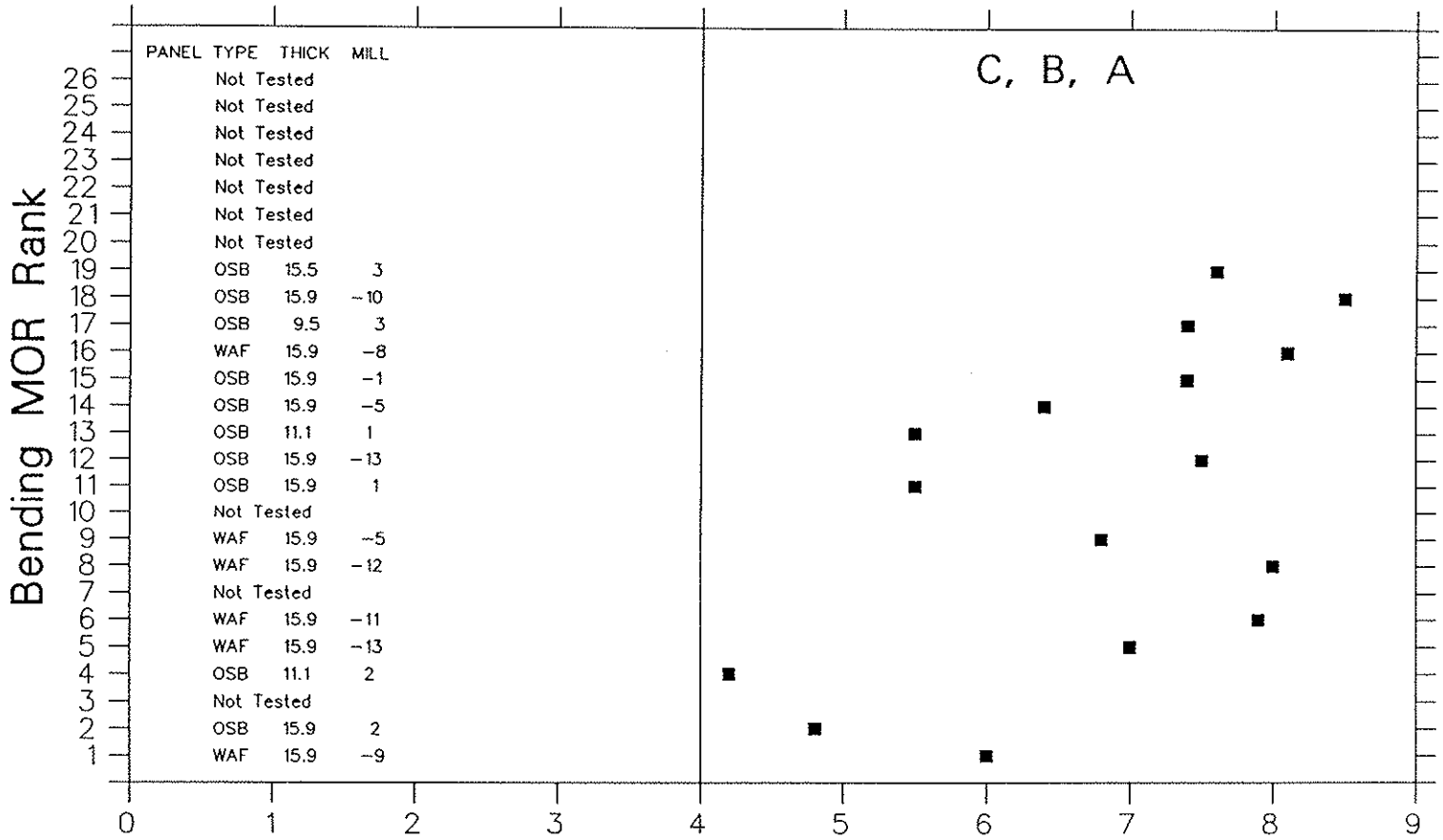

Figure 3 Fifth Percentile of Ultimate STT Stress (MPa) Measured Parallel to the Major Axis of the Panel

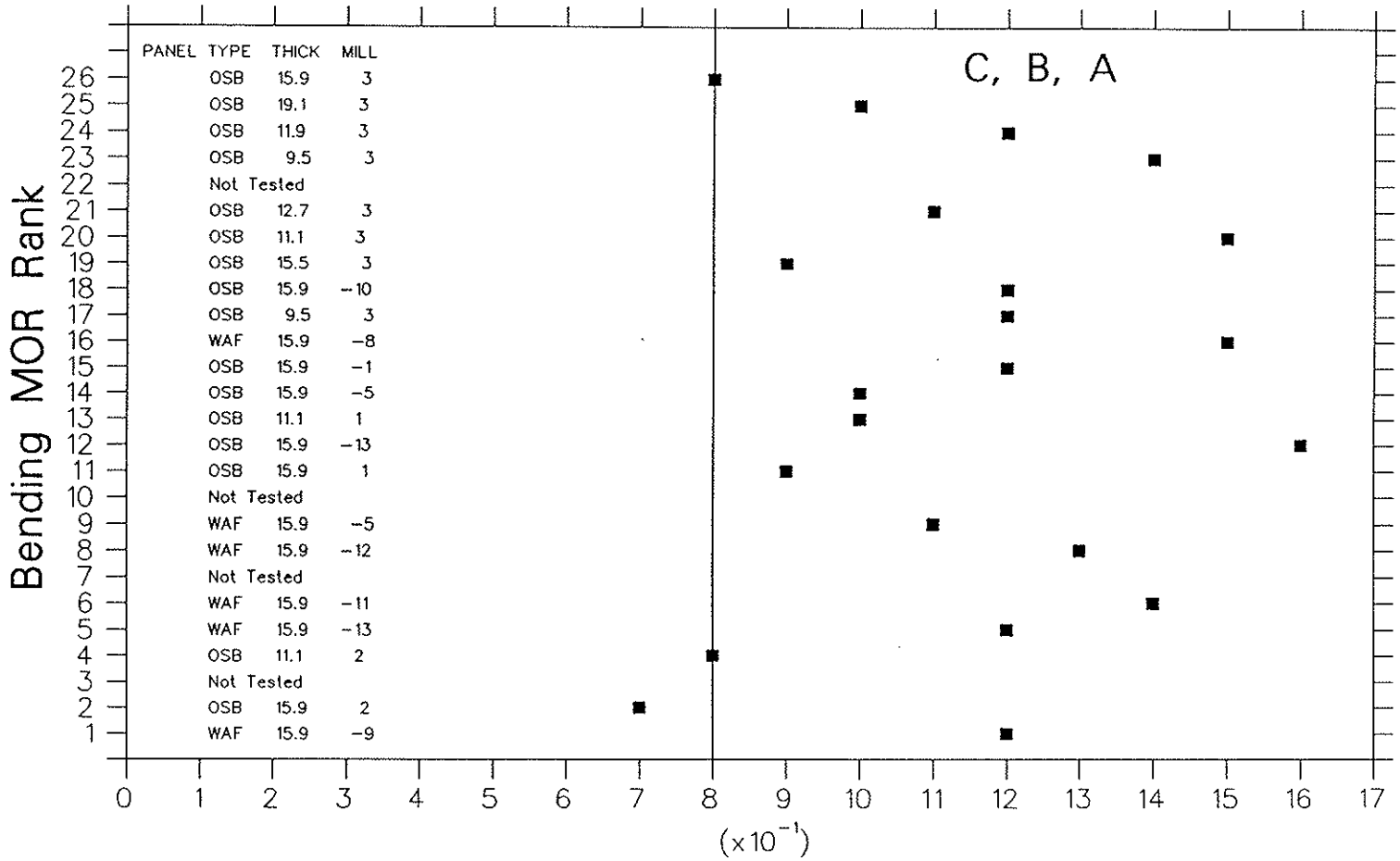

Figure 4 Fifth Percentile of Ultimate Planar Shear Stress (MPa) Measured Parallel to the Major Axis of the Panel

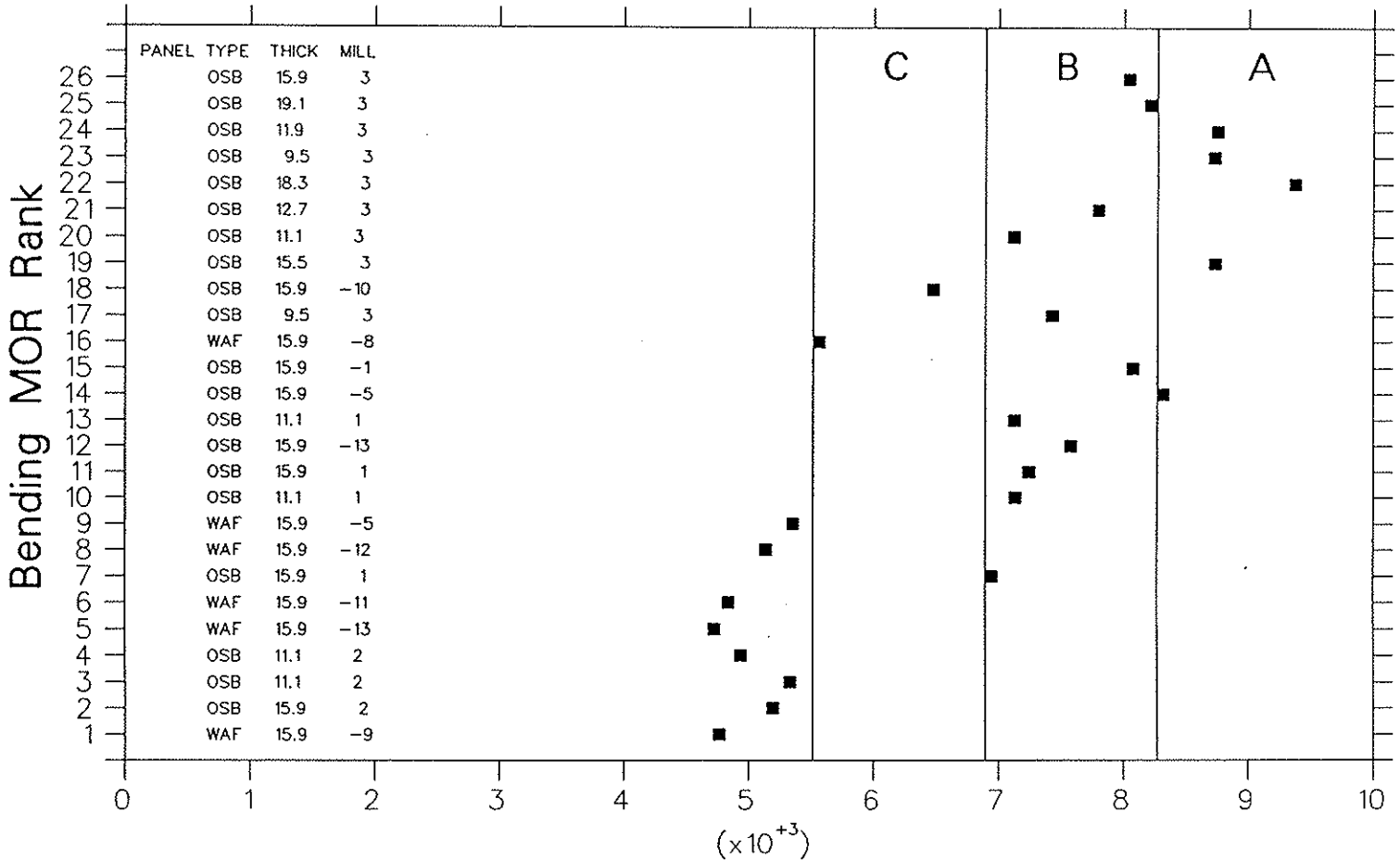

Figure 5 Mean Bending MOE (MPa)
Measured Parallel to the Major Axis of the Panel

Appendix 1. Minimum Basic Structural Capacities for Qualification of Type 1 (Standard) Design Rated OSB (CSA Standard O452)

Property		Strength Capacities					Stiffness and Rigidity Capacities				
Design Rating		Bending MS		Axial (Tension/Compression) TA		Shear Through Thickness STT	Bending EI		Axial (Tension/Compression) EA		Shear Through Thickness Rigidity GTT
NOMINAL THICK	GRADE	Orientation of applied forces relative to major axis					Orientation of applied forces relative to major axis				
		0°	90°	0°	90°	0° & 90°	0°	90°	0°	90°	0° & 90°
(mm)		Nmm/mm	Nmm/mm	N/mm	N/mm	N/mm	Nmm²/mm	Nmm²/mm	N/mm	N/mm	N/mm
9.5	- A	365	115	100	45	40	590,000	170,000	46,000	19,000	9,500
9.5	- B	300	115	80	45	40	490,000	170,000	39,000	19,000	9,500
9.5	- C	240	115	60	45	40	390,000	170,000	33,000	19,000	9,500
11.0	- A	485	150	115	55	45	920,000	270,000	53,000	22,000	11,000
11.0	- B	405	150	90	55	45	760,000	270,000	46,000	22,000	11,000
11.0	- C	320	150	70	55	45	610,000	270,000	38,000	22,000	11,000
12.5	- A	630	195	130	60	50	1,350,000	390,000	60,000	25,000	12,500
12.5	- B	520	195	105	60	50	1,120,000	390,000	52,000	25,000	12,500
12.5	- C	415	195	80	60	50	900,000	390,000	43,000	25,000	12,500
15.5	- A	965	300	160	75	60	2,570,000	740,000	75,000	31,000	15,500
15.5	- B	800	300	130	75	60	2,140,000	740,000	64,000	31,000	15,500
15.5	- C	635	300	95	75	60	1,710,000	740,000	53,000	31,000	15,500
18.5	- A	1380	430	190	90	75	4,370,000	1,270,000	89,000	37,000	18,500
18.5	- B	1140	430	155	90	75	3,640,000	1,270,000	77,000	37,000	18,500
18.5	- C	905	430	115	90	75	2,910,000	1,270,000	64,000	37,000	18,500
22.0	- A	1950	605	230	110	90	7,340,000	2,130,000	106,000	44,000	22,000
22.0	- B	1610	605	180	110	90	6,120,000	2,130,000	91,000	44,000	22,000
22.0	- C	1280	605	135	110	90	4,890,000	2,130,000	76,000	44,000	22,000
28.5	- A	3270	1020	295	140	115	16,000,000	4,630,000	138,000	57,000	28,500
28.5	- B	2710	1020	235	140	115	13,300,000	4,630,000	118,000	57,000	28,500
28.5	- C	2150	1020	175	140	115	10,600,000	4,630,000	98,000	57,000	28,500

Notes: (1) The minimum basic shear-in-plane (planar shear) strength, 0° and 90°, shall be 0.80 MPa.

(2) The minimum capacities specified above are based on short term tests (less than 10 min) adjusted to 80% RH/20°C and shall not be used directly for structural design. Specified design capacities shall be determined in accordance with CSA Standard O86.1 from the above values.

(3) The basic bearing strength perpendicular to the plane of all Design Rated OSB panels shall be taken as 4.2 MPa.

CIB-W18/28-13-2

INTERNATIONAL COUNCIL FOR BUILDING RESEARCH STUDIES AND DOCUMENTATION

WORKING COMMISSION W18 - TIMBER STRUCTURES

TORSIONAL STIFFNESS OF WOOD-HARDBOARD COMPOSED I-BEAM

by

P Olejniczak
Agricultural University of Poznan
Poland

MEETING TWENTY - EIGHT

COPENHAGEN

DENMARK

APRIL 1995

Torsional Stiffness of Wood-Hardboard Composed I-Beam

Piotr Olejniczak, M.Sc. Eng.
Faculty of Wood Technology
Agricultural University of Poznań, Poland

1. Introduction

One of the major factors determining a free supported beam stability is a torsional stiffness. According to the classic theory of stability (Timoshenko, 1936) the share of torsional stiffness in total buckling resistance is considerable. It means, the torsional stiffness of a beam section has low value in relation to bending stiffness in plane perpendicular to the beam plane. Moreover, the torsional stiffness of composed wooden cross-section is determined not in simply way. Wood has a low value elastic properties in direction perpendicular to the grain and shear modulus of elasticity in longitudinal – transverse direction. It cause that the fastening in any support system, web-flanges connection and the act of the stiffeners glued into the beam are characterized as the flexible areas. The wood base, composed I-beam cross-section never remains undeformed in the elastic torsional post-buckling deflection. This deformation causes that the total buckling resistance is lower than possible to suppose, even if the elastic properties of beam composing materials are well known. The balance of the torsional rigidity of wood – hardboard I-beam is considered in this report.

2. Experimental investigations

The eight 1 meter long samples of I-beam, made of spruce or pine flanges 45 × 45 mm section and hardboard web 6.4 and 10.0 mm thick, in two size series were examined in the experiment. The flanges were made of solid wood and the webs – two hardboard wet formed sheets glued smooth to smooth face in thickness. Each element of beam was examined before testing finally formed sample of I-beam. Samples of I-beam examined series are shown on Figure 2.1.

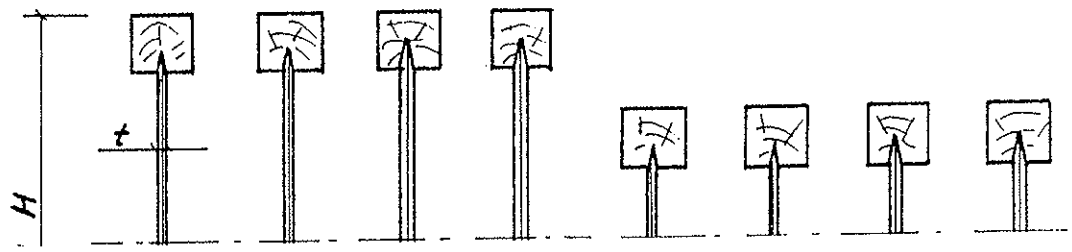

Beam:	B1	B2	B3	B4	B5	B6	B7	B8
Flange wood	pine	spruce	pine	spruce	pine	spruce	pine	spruce
H, mm	360	360	360	360	220	220	220	220
t, mm	6,4	6,4	10,0	10,0	6,4	6,4	10,0	10,0

Fig. 2-1. I-beams series examined in experiment (nominal dimensions)

All experimental tests were carried out on specially prepared equipment allowing to apply the twisting moment to the examined element or beam sample. Twisting

equipment consists two pairs of grips fastened one to rigid, the second to turning steel plate. The twisting moment was applied as a force acting on the cantilever end of the turning plate. The end of cantilever was displaced with controlled rate and the force was measured by the testing machine. Each examination was carried on under similar conditions: the twisting rate was equal approximately 1 °/m per minute and the final twisting angle per unit length equal to 3.5 °/m. All tests were carried out in laboratory without controlled climate.

2.1. The examination of torsional rigidity of wood flanges

Each flange approximately 1 m long was four time tested in twisting equipment, each time turned 90° to previous position. The flanges were relaxed approximately hours between the test sequences. High repeatability was obtained. The rotation magnitude of two flange sections was measured by mean of the additional levers fastened directly to the wood and the displacement gauges (Fig. 2-2). The distance between gauges was equal about 0.9 m. The applied twist produced the shear stress in wood approximately 1.4 MPa.

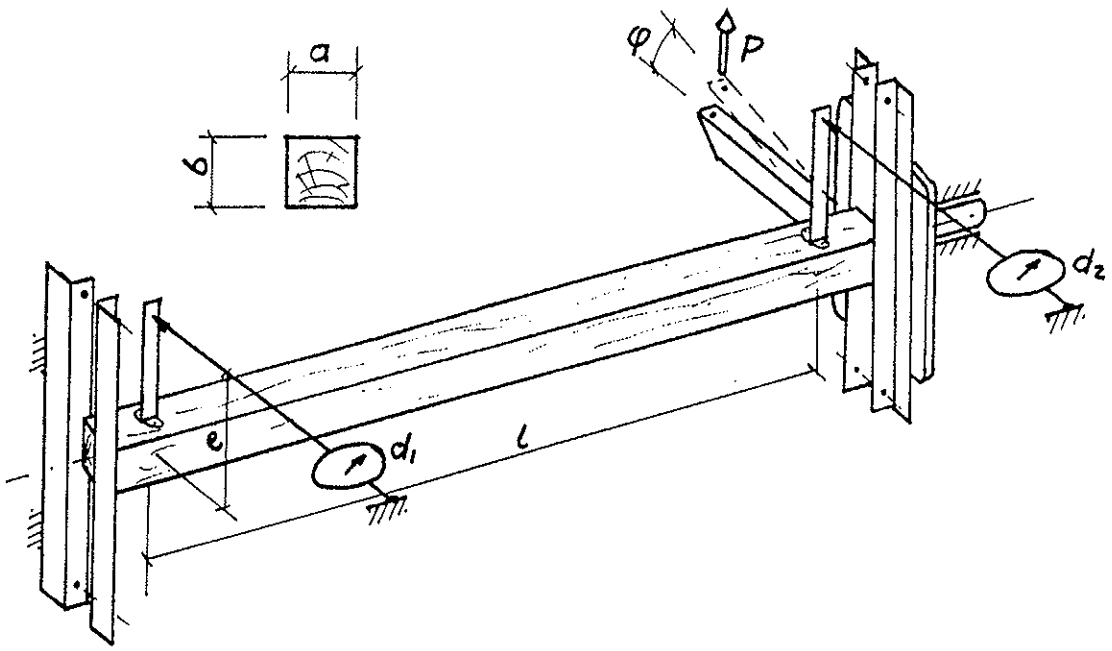

Fig. 2-2. The examination of torsional of flanges

The actual twisting angle per unit length was evaluated from the formula:

$$\theta = \frac{d_1 - d_2}{e \cdot l}$$

and flange torsional rigidity as:

$$C_f = \frac{M_f}{\theta} = P \cdot \frac{r}{\theta}$$

In addition, the shear modulus of elasticity of wood was evaluated as for quadrilateral section with assumption that its dimension is equal to average of actual dimensions:

$$G_f = \frac{C_f}{\left(\frac{a+b}{2}\right)^4 \cdot 0.141}$$

The statistical representation of results is exposed in Table 2-1.

Table 2-1. Torsional rigidity and shear modulus of flanges

	Spruce		Pine	
	Tors. rigidity C_f Nm^2	Shear modulus G_f MPa	Tors. rigidity C_f Nm^2	Shear modulus G_f MPa
average	506	865	461	754
max	563	966	545	886
min	441	747	386	639
standard deviation	39.9	73.9	39.3	79.1
variation coefficient	7.3%	8.5%	8.5%	10.5%

2.2. Web plates torsional rigidity examination

Web plates formed from two sheets of hardboard were fastened in grips and twisted similarly to flanges (Fig. 2-3). The angel of twist was measured by the displacement of the cantilever end of testing equipment. Each plate was examined two times: turned up-down and relaxed approximately 2 hours between repetition. As the single element the webs were tested in height with surplus for forming the wedged joints. The twisting

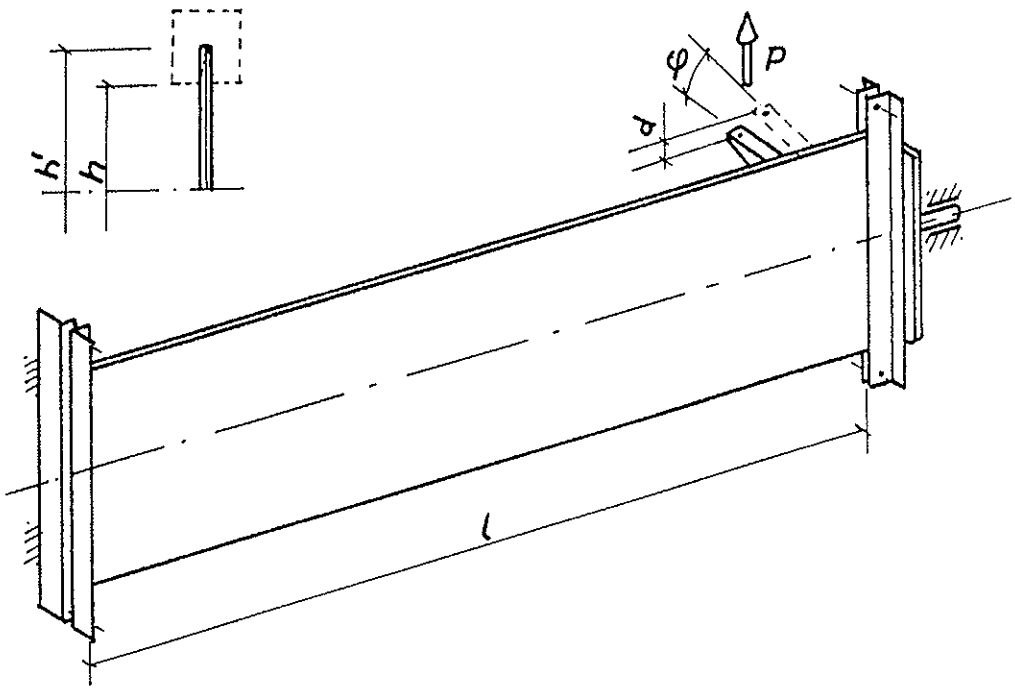

Fig. 2-3. Twisting of the web plates

angle per length unit was assumed as:

$$\theta = \frac{d}{r \cdot l}$$

The web plates torsional rigidity was evaluated from the formula:

$$C'_w = \frac{M_w}{\theta} = \frac{P \cdot r}{\theta}$$

and corrected for height equal to the distance between flanges:

$$C_w = C'_w \frac{h}{h'}$$

The shear modulus was calculated as for thin-walled open section:

$$G'_w = \frac{3C'_w}{h' \cdot t^3}$$

The thickness measured in ten points for each plate and for particular samples was relatively varied. The results of torsional rigidity of web plates exposes Table 2-2.

Table 2-2. Torsional rigidity and shear modulus of web plates

Web sample	Height h mm	Thickness t mm	Torsional rigidity C_w Nm^2	Shear modulus G_w MPa
1	265	6.79	50.0	1811
2	264	6.69	48.0	1618
3	270	9.85	157.5	1831
4	268	9.80	149.3	1777
5	129	6.78	22.5	1680
6	130	6.63	16.4	1299
7	136	10.31	74.9	1486
8	132	10.37	57.0	1161

2.3. I-beam torsional rigidity examination

After forming the wedged cuts along the flanges and moulding the edges of web plates the beam samples 1 meter long were assembled. The flanges, respectively made of pine and spruce, were selected in order to choose for each beam sample the pair of flanges of similar rigidity and the same material. Testing of beam samples were performed in the same conditions as before their elements (Fig. 2-4). The ends of beams were fastened in testing instumentation thus to keep the ends of flanges the same grip pair. It means that the end sections of beam samples were braced with grip elements. Each samples were twisted three times in interval as in former examinations.

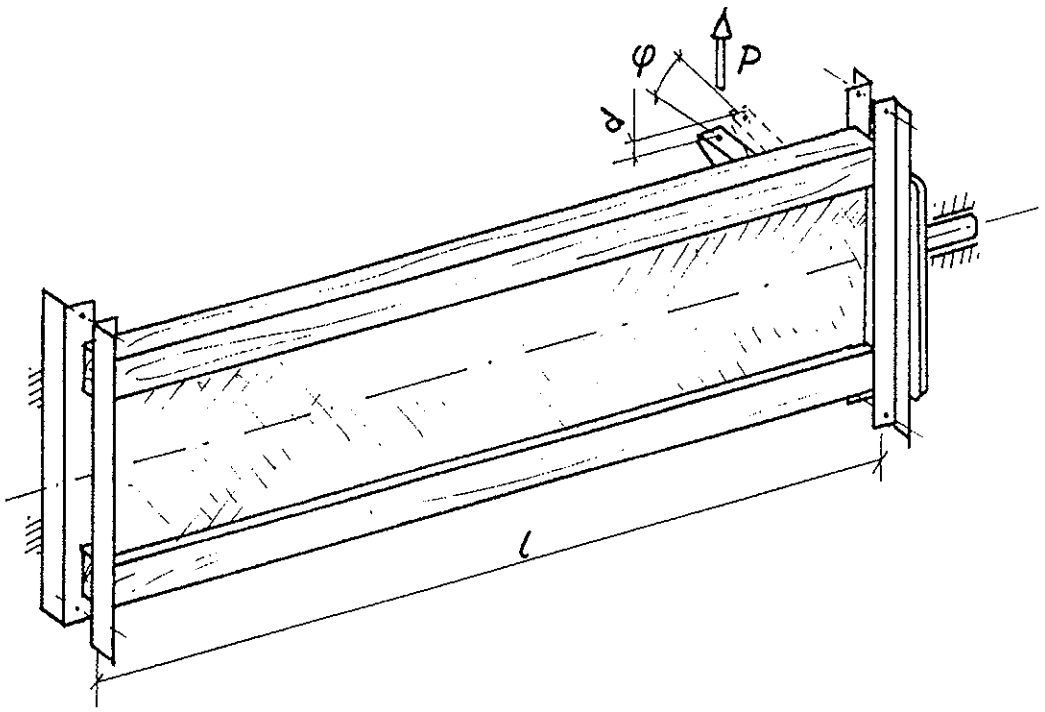

Fig. 2-4. Torsional rigidity examination of I-beam samples

The resuls are exposed in Table 2-3. The torsional rigidity was evaluated from the formula:

$$C_b = \frac{M_b}{\theta}$$

Table 2-3. Torsional rigidity of beam samples and total rigidity of their elements

Beam sample	Height/web thickness H/t mm/mm	Tors. rigidity C_b Nm^2	Total tors. rigidity $\sum C_e$ Nm^2	Relative difference $(C_b - \sum C_e)/C_b$ %
B1	355/6.79	798	1143	−43.2
B2	355/6.96	675	852	−26.2
B3	361/9.85	919	1074	−16.9
B4	359/9.80	932	1183	−26.9
B5	220/6.78	666	1028	−54.4
B6	222/6.63	618	889	−43.9
B7	226/10.31	830	1109	−33.6
B8	223/10.37	626	981	−56.7

The torsional rigidity of beams was compared with the particular summ of the element rigidities. The deficite of rigidity was obserwed in each cause. The comparision of rigidities is performed on Figure 2-5.

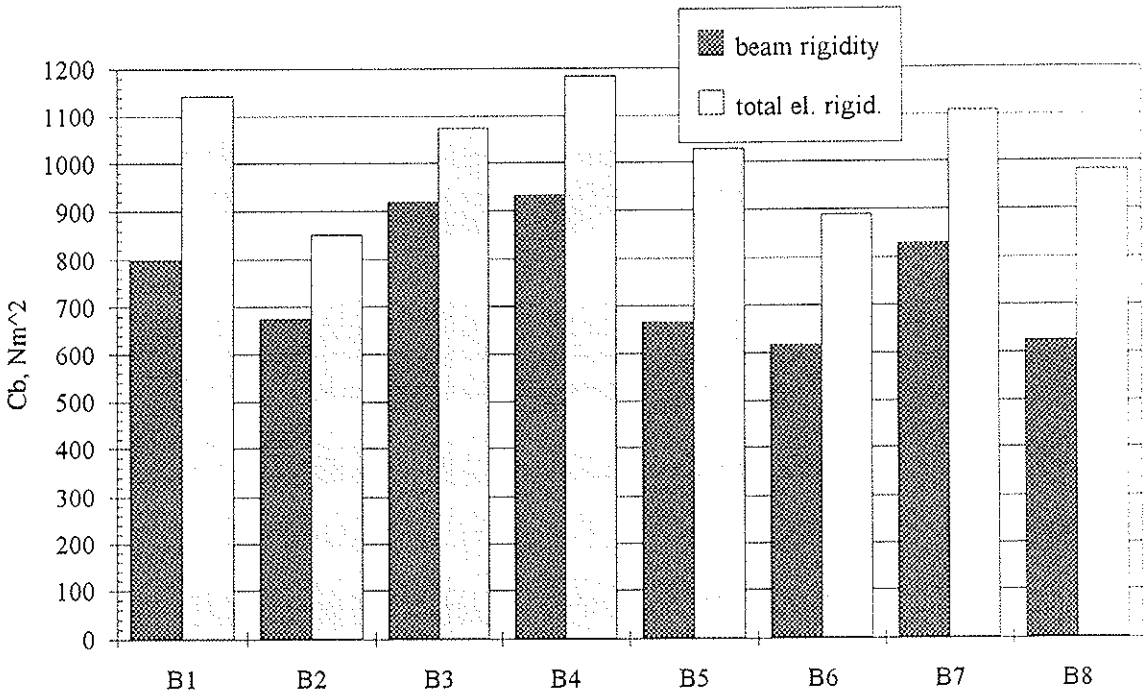

Fig. 2-5. Torsional rigidity of beam samples and total rigidity of the elements

The deficit of torsional rigidity confirms that well known formula for evaluation total torsional rigidity of composed open sections (Timoshenko 1936, Kollbrunner, Basler 1969):

$$K = \sum K_e = \sum (J_\omega \cdot G_e)$$

is not valid for baems made of wood and wood-base materials.

2.4 Additional experiment on torsional flexibility of wood – flange joint

For examonation of beam in finite element method symulation the supplementary experiment was carried out. The fragments of beams containing the piece of web and flange were examined as shown on Figure 2-6. The joint flexibility was tested for two kinds of wedge: for web 6.4 mm and 10 mm thick, four samples of each size.

a) b)

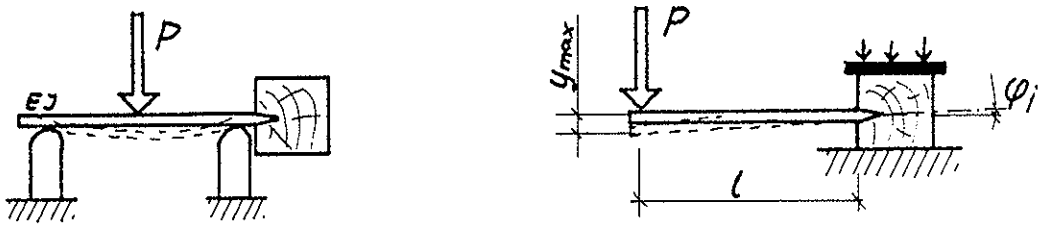

Fig. 2-6. Torsional flexibility of web – flange joint examination: a) modulus of elesticity of web plate; b) torsional flexibility

The flexibility was evaluatued from increment of the free end deflection in consequence of web rotation in flange:

$$y_{max} = \frac{P \cdot l^3}{(3 \cdot E \cdot J)} + \varphi_j \cdot l,$$

where the angel of twist was calculated as:

$$\varphi_j = \frac{M_s}{K_j} = \frac{P \cdot l}{K_j}.$$

and the torsional flexibility per unit length:

$$K_j = \frac{1}{\left(\frac{y_{max}}{P \cdot l^2} - \frac{4 \cdot l}{E \cdot b \cdot t^3}\right) \cdot b}$$

Table 2-4 contains the average values of torsional flexibility of web-flange joint.

Table 2-4. Web-flange joint flexibility

Wedged joint h_j/b mm/mm	Torsional rigidity average Nm/m	Standard deviation Nm/m
11.5/6.4	6840	1285
21.0/10.0	10840	2290

3. Finite element method balance of torsional rigidity of I-beam

In the analysis the action of single elements on each other was considered together with their torsional rigidity. There were examined a few variants of siple model. The best one is described below. This model contains also the elements representing the testing instrumentation parts. The flanges were represented, in phisical meaning, by straight bar under pure torsion, and in model as a twisting spring element. For particular beam model examination were taken mean value of actual torsional stiffness of real flange pair from experiment reduced by the rigidity of web surplus applied in model as a distance from real web height to the flange longitudinal axis:

$$K_f = \frac{C_f}{l} - \frac{C_w}{l} = \frac{C_f - G_w \cdot b \cdot \frac{t^3}{6}}{l}.$$

The fastening flexibility of flanges in grips was represented as a twisting spring. The magnitude was assumed as mean value calculated from deficite of angel of twist between grips and wood rotation from examinatin of flanges. Assumed values are exposed in Table 3-1.

Table 3-1. Torsional flexibility of flanges in grips

	Torsional flexibility of flanges in grips	
	Spruce	Pine
	Nm	Nm
average	3200	2260
max	4180	3630
min	2140	1550
standard deviation	530	485
variation coefficient	16.6%	18.5%

The web plate was represented by eight plates elements for which the modulus of elasticity was evaluated on a base of shear modules for particular beams and Poisson's ratio equal to 0.25 - from experimental investigation on hardboard properties (Ganowicz et al. 1984).

The torsional flexibility of web - flange joint were assumed in analytic model as one-dimension spring elements, which spring quantity was evaluated for half of sample length on the base of results of supplementary experiment. The idea of analytic model is shown on Figure 3-1.

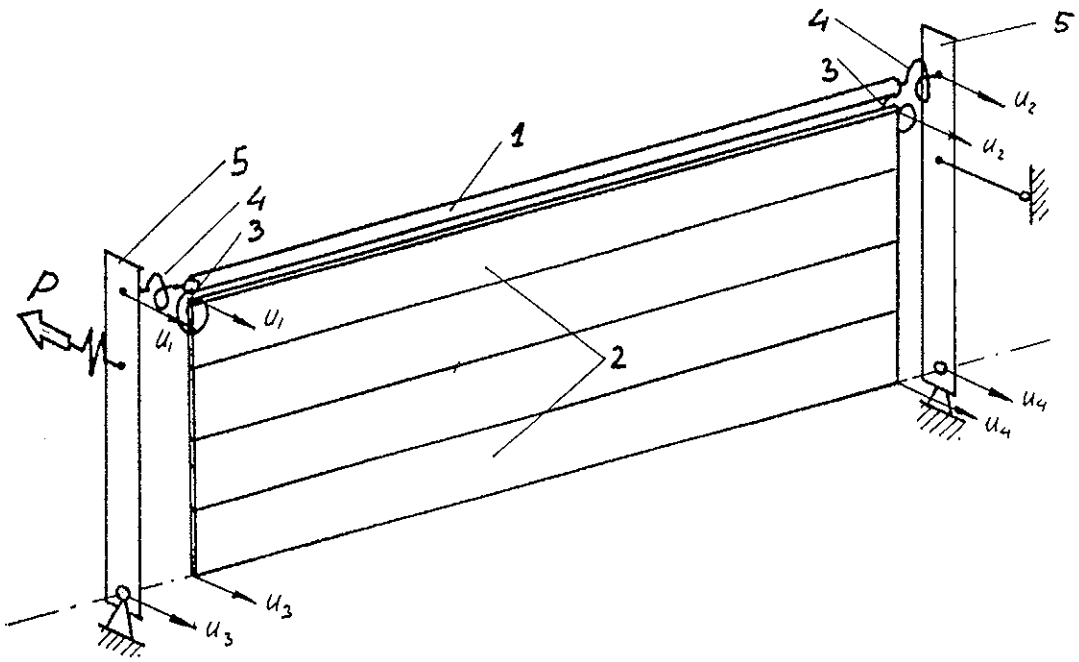

Fig. 3-1. Analytic model for examination the torsional rigidity of I-beam samples
1 – K_f, flange torsional stiffness, 2– web plate elements, 3 – web-flange joint flexibility, 4 – flange fastening flexibility, 5 – instrumentation elements

Results of the examination of particular beams models are exposed in Table 3-2 and pictured on Figure 3-2.

Table 3-2. Torsional rigidity results of beams from experiment and FEM evaluation

Beam sample	Height/web thickness H/t mm/mm	FEM torsional rigidity C_{bMES} Nm^2	Experimental torsional rigidity C_b Nm^2	Relative difference $(C_{bMES} - C_b)/C_b$ %
B1	355/6.79	821	798	+2.9
B2	355/6.96	663	675	−1.8
B3	361/9.85	872	919	−5.1
B4	359/9.80	931	932	+0.1
B5	220/6.78	766	666	+15.0
B6	222/6.63	678	618	+9.7
B7	226/10.31	886	830	+6.7
B8	223/10.37	755	626	+20.6

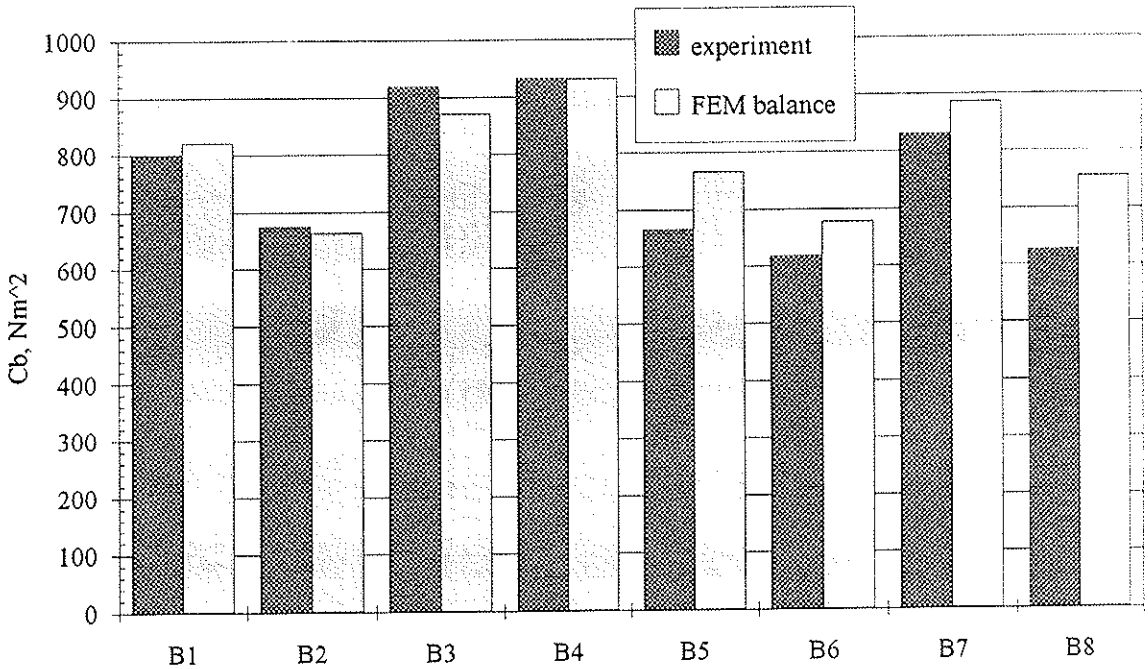

Fig. 3-2. Torsional rigidity of I-beam samples compared with examined models

4. Conclusions

Evaluation of the torsional stiffness of composed wood-base I-beam should not be performed as for open sections elements made of isotropic material. In opposition it will tend the over estimation of the torsional stiffness. The results obtained from experiment and FEM investigation prove that for calculation of torsional rigidity is necessary to consider torsional flexibility of flanges in support braces, web – flange joint flexibility; the web elements as working under torsion and bending, and stiffness of bracing elements. In I-beam with wood flanges the torsional stiffness is limited mostly by low elastic properties in direction perpendicularly to the grain.

References

1. Timoshenko S.: "Theory of Elastic Stability", Mc Graw-Hill Book Company Inc., New York, 1936.
2. Kallbrunner C.F., Basler K.: "Torsion in structures", Springer-Verlag, Berlin/Heidelberg, 1969.
3. Ganowicz R., Dziuba T., Kwiatkowski K., Kostka W.: "Elementy konstrukcyjne z drewna i płyty pilśniowej", Akademia Rolnicza w Poznaniu, 1984.
4. Dahlblom O., Peterson A., Petersson H.: "Manual for CALFEM", Lund Institute of Technology, Lund 1986.

CIB-W18/28-19-1

INTERNATIONAL COUNCIL FOR BUILDING RESEARCH STUDIES AND DOCUMENTATION

WORKING COMMISSION W18 - TIMBER STRUCTURES

FRACTURE OF WOOD IN TENSION PERPENDICULAR TO THE GRAIN: EXPERIMENT AND NUMERICAL SIMULATION BY DAMAGE MECHANICS

by

L Daudeville
Laboratoire de Mécanique et Technologie, Cachan
France
M Yasumura
Building Research Institute, Ibaraki
Japan
J D Lanvin
Centre Technique du Bois et de l'Ameublement, Paris
France

MEETING TWENTY - EIGHT

COPENHAGEN

DENMARK

APRIL 1995

INTRODUCTION

The major presentations in that paper are in one hand a Damage Mechanics approach for the fracture analysis in wood and in another hand an experimental program for the determination of the fracture energy in mode I of spruce and fir.

Modeling damage phenomena in wood for a structural analysis is very complex. This is due to the anisotropy property of this material that exhibits different kinds of damage: cracking parallel to the grain under tearing (mode I) or shearing (mode II and III), failure under tension or compression along the grain direction. Some damage mechanisms are brittle, others are more progressive. The complexity of modeling is also due to the influence of random defects that may introduce a scatter and a scale effect on the response to a mechanical loading.

Normally, timber structures are designed with the intent of avoiding failure modes associated with crack growth parallel to the grain. Nevertheless, the study of cracking, that may be responsible of the timber structure failure in a large number of cases, is necessary to evaluate the load-bearing capacity of a structure or of a sub-structure (e.g. a mechanical joint).

In classical Linear Elastic Fracture Mechanics (LEFM), a theory which is commonly used for the fracture analysis of metals or brittle materials such as ceramics, all damage phenomena are assumed to be concentrated at the crack tip. Non Linear Fracture Mechanics (NLFM) introduces the notion of planar process zone where cohesive stresses are assumed to occur (Hillerborg et al. 1976; Bazant and Kazemi 1990; Jenq and Shah 1985; Nallathambi and Karihaloo 1986) for concrete and (Gustafsson 1985; Boström 1988) for wood.

A simplified approach based upon Damage Mechanics (DM) for the analysis of cracking is presented. Like in NLFM, all damage phenomena are assumed to occur on a surface (or on a line in a 2D problem). NLFM and DM have been developed to treat the problem of fracture in materials that exhibit a softening behavior i.e. for non brittle materials. In such materials, fracture is preceded of localisation phenomena. In the proposed approach, an interface is used for the modelling of damage. The interface model relates tractions to relative displacement jumps in the localised zone.

NLFM has been essentially applied to the problem of fracture in concrete. In such an isotropic material, the first mode of fracture (tension) is predominant. Because of the orthotropic behavior of wood, the crack may propagate along the grain under mixed mode conditions. The interface model allows the analysis of cracking along an expected crack path under pure or mixed fracture modes. Continuous interface elements have been used for civil-engineering applications (Ngo and Scordelis 1967; Hohberg and Bachmann 1988; Gens et al.; Rots and Schellekens 1990; Garcia-Alavarez et al. 1994). The proposed interface model has been applied to study the delamination of composite laminates (Allix and Ladevèze 1992; Daudeville and Ladevèze 1993; Allix et al. 1995).

In DM models, damage is described by means of the relative variations of stiffness that may be significant in the case of a fatigue loading. An important limitation of LEFM is due to the necessity of assuming the existence of a crack. Both NLFM and DM concepts can be applied to treat the problem

of crack initiation in originally uncracked structures. In this paper the problem of propagation of an already cracked area is studied.

The so-called size effect may be significant in problems of cracking in concrete (Bazant 1984) or in wood (Aicher 1992; Aicher et al. 1993). In the analysis of that phenomenon, one may separate this effect into the "volume effect" and the "structural effect".

- The "volume effect" is due to the existence of defects in the material and the amount of defects is a function of the volume. It may be handled by a probabilistic description of mechanical properties. In this study, we analyse the deterministic feature of fracture only which involves to choose sound timber in an experimental program.
- The process zone size depends on the micro heterogeneity size of wood. The process zone concerns a relatively important region for small specimens and is negligible for large specimens. In the latter case, LEFM concepts are then valid. The process zone influence produces an effect that is called a "structural effect". DM and NLFM approaches that include the notion of process zone may reproduce the "structural effect".

The proposed damage modeling and fracture mechanics have the same kind of application and the link between the two approaches is possible. We give relations between the fracture energy and characteristic parameters of the DM modeling.

The interface model allows the analysis of cracking under pure or mixed mode conditions. In order to compare computational and experimental results, we focus on the simulation of fracture in wood under static tension perpendicular to the grain. An experimental program has been performed for the fracture analysis of spruce and fir species. The standard three point bending (TPB) test proposed by Larsen and Gustafsson (1989) was carried out at specimens of the CIB-type. The experimental data concern the fracture energies with respect to the wood orientation. The influences of the density, of the growth ring width, of the pattern orientation are also presented.

In order to minimise the number of tests, the specimen size is constant. Thus, the size-effect has not been examined. A further analysis of propagation under mixed conditions will be carried out.

The TPB test was first analysed by means of LEFM concepts. The critical energy release rate G_c is defined for the maximum load (onset of propagation of the initial crack). G_c was computed by the Finite Element (FE) method. The fracture propagation was analysed by LEFM and with the identified G_c value. That G_c value does not seem to allow the prediction of the post-peak load-displacement curve.

Breaking with the assumption of a constant value for G_c allows the load-displacement curve prediction. It is then defined the critical energy release rate G_p for a steady state of propagation.

In a second step, the TPB test was analysed by the DM approach. The only identified parameter is the fracture energy per unit cracked area G_f that is a material parameter of the modeling and that depends on the wood orientation. G_f was identified with the maximum load.

Load-displacement curves are correctly described by the DM approach. An interesting result is that for each wood orientation, the experimental fracture energy value is very close of the fracture energy G_f we identified in the modeling.

That value corresponds to the critical energy release rate for a steady state of propagation. The previous result confirms that the fracture energy is the parameter that governs fracture propagation.

This study shows that the experimental fracture energy obtained with the CIB standard TPB test can be considered as a material parameter for the analysis of fracture.

ANALYSIS OF FRACTURE BY DAMAGE MECHANICS

Damage phenomena are assumed to be concentrated on a zero-thickness interface. The interface modeling allows the crack propagation study under pure or mixed mode conditions. Classically, the experimental analysis of fracture is carried out in the framework of LEFM. Therefore, the proposed modeling of crack propagation is compared with LEFM.

Interface modeling in elasticity

The interface Γ connects the two parts of a solid Ω^+ and Ω^-.

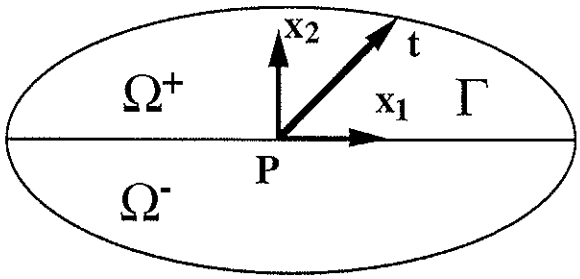

Fig. 1: Interface Γ connecting two parts of a solid

To simplify, let us consider a plane stress problem in the plane $\mathbf{x_1x_2}$ ($\mathbf{x_1}$ is the grain direction). The relative displacement vector $[\mathbf{u}]$ (jump of displacement between the Ω^+ and Ω^- regions) at point P is:

$$[\mathbf{u}] = \mathbf{u}^+ - \mathbf{u}^- = [u_1]\,\mathbf{x_1} + [u_2]\,\mathbf{x_2} \qquad (1)$$

Which satisfies the contact condition:

$$[u_2] \geq 0 \qquad (2)$$

The elastic traction vector is:

$$\mathbf{t} = \sigma_{12}\,\mathbf{x_1} + \sigma_{22}\,\mathbf{x_2} = k_1\,[u_1]\,\mathbf{x_1} + k_2\,[u_2]\,\mathbf{x_2} \qquad (3)$$

Note the interface model is presented with the assumption of a plane stress state. In the case of a three-dimensional problem, a direction $\mathbf{x_3}$ perpendicular to grain and a stiffness k_3 are introduced. In this case, because of wood orthotropy the interface behavior may be orthotropic ($k_1 \neq k_2 \neq k_3$).

Modeling of damage

The main features and assumptions of the damage model are listed below:

- Damage is described through the damage variables d_1 and d_2 that are relative to the stiffness decrease.
- There is no damage under compression (unilateral effect).

• There are no irreversible displacement discontinuities.

• During the elastic stage of the loading process, no significant relative displacement occurs. Therefore the stiffness values have to be high.

The traction-relative displacement curve in mode I is given in Fig. 2.

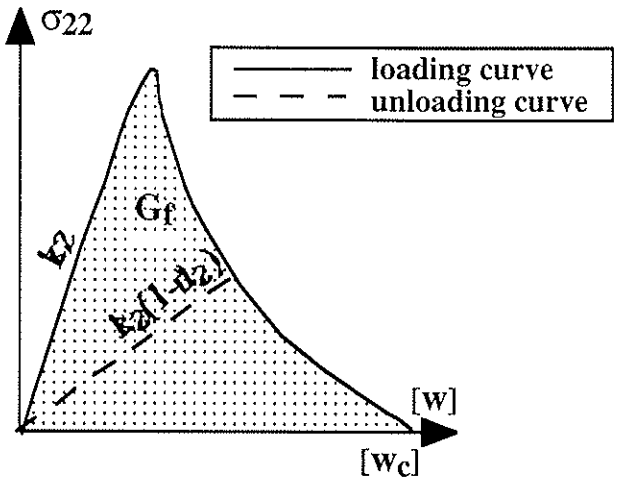

Fig. 2: Traction-relative displacement curve in mode I

The thermodynamical potential is the strain energy, its expression under a plane stress state is:

$$E_D = \frac{1}{2}\left\{\frac{\langle -\sigma_{22}\rangle_+^2}{k_2} + \frac{\langle \sigma_{22}\rangle_+^2}{k_2(1-d_2)} + \frac{\sigma_{12}^2}{k_1(1-d_1)}\right\} \tag{4}$$

$\langle\cdot\rangle_+$ denotes the positive part. There is no contribution of σ_{11} because the interface is a zero-thickness medium. The variables Y_{di}, that are similar to the energy release rate introduced in Fracture Mechanics, are conjugated to d_i:

$$Y_{d1} = \frac{1}{2}\frac{\sigma_{12}^2}{k_1(1-d_1)^2} \quad \text{and} \quad Y_{d2} = \frac{1}{2}\frac{\langle \sigma_{22}\rangle_+^2}{k_2(1-d_2)^2} \tag{5}$$

Mode II Mode I

The damage evolution equations are relations between d_1, d_2 and Y_{d1}, Y_{d2}. A particular choice of the damage evolution law is presented below (a justification is given further).

Damage evolution is assumed to be governed by:

$$\underline{Y} = \sup_{\tau \le t} \frac{n}{n+1}\left(Y_{d2} + \gamma Y_{d1}\right) \tag{6}$$

γ is a coupling factor between modes I and II and:

$$d = d_1 = d_2 = w(\underline{Y}) \quad \text{and} \quad d \le 1 \tag{7}$$

with:

$$w(\underline{Y}) = \frac{\langle \underline{Y} - n\,Y_0 \rangle_+^n}{(Y_c - n\,Y_0)^n} \qquad (8)$$

Y_c, Y_0 and n characteristic parameters of the damage evolution law of the interface. The term nY_0 corresponds to a threshold energy and Y_c to a critical energy. These parameters can be identified by the analyse of fracture tests.

A link with Linear Elastic Fracture Mechanics

Interface models are introduced for the simulation of the decohesion between two solids or between two parts of a solid. Classical fracture tests may be used for the identification of fracture models. A link between Damage Mechanics and Fracture Mechanics is presented. It has already been presented in (Allix et al. 1994).

Fracture tests (Valentin et al. 1989) allow to obtain the three inter-laminar fracture toughnesses G_{Ic}, G_{IIc} and G_{IIIc} relative to the modes I, II and III. G_{ic} values (i=I, II, III) are different because of the interface orthotropy. G_{ic} are defined in the framework of LEFM.

An other parameter of fracture for non-brittle materials is the fracture energy G_f (e.g. in mode I). G_f is defined in the framework of NLFM. The fracture energy G_f is the dissipated energy per unit crack area during complete cracking of a specimen.

Analysis of fracture propagation

The dissipative phenomena are assumed to occur on the interface Γ only. The necessary work for a fracture propagation of length Δa during Δt is:

$$\int_{\Delta t} P_d \, dt = G(a)\, b\, \Delta a \qquad (9)$$

Where b is the specimen width and P_d is the dissipated power.

Within the framework of Damage Mechanics. We get for a plane stress problem:

$$G(a)\, b\, \Delta a = \int_{\Delta t} \int_{\Gamma} (Y_{d2} + Y_{d1})\, \dot{d}\, d\Gamma\, dt \qquad (10)$$

Let us consider a steady state of fracture propagation. It means that during crack propagation the process-zone has a constant size l_p and translates without modification.

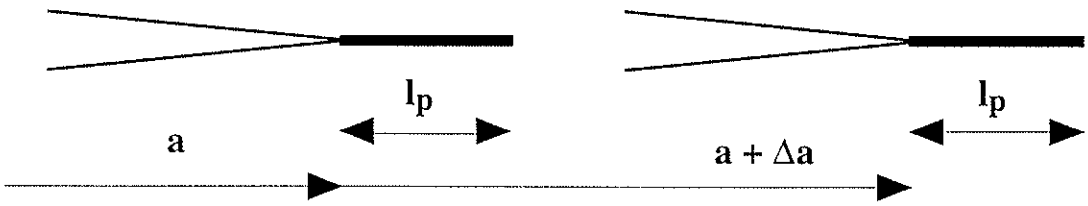

Fig. 3: Steady state of propagation

This distinction between the fracture onset and the steady state of propagation is classical for non brittle materials that exhibit a R-curve effect. Rather than the critical energy release rate G_c that is defined at the onset of cracking according to LEFM, the critical energy release rate G_p defined for a steady state of fracture propagation is considered. G_p is difficult to obtain experimentally because of the difficulty to measure the crack length.

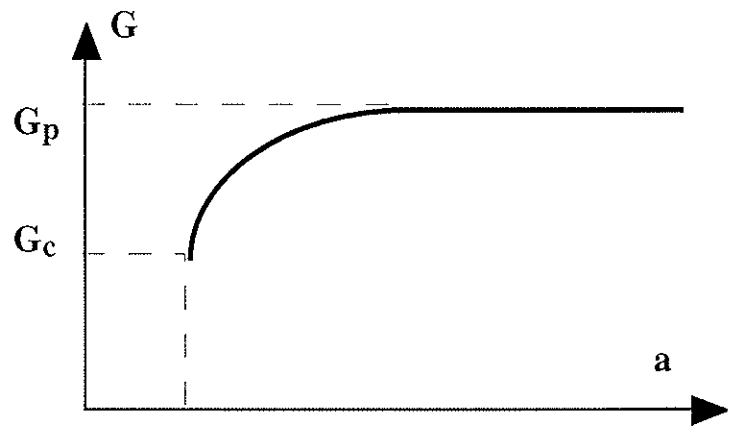

Fig. 4: Distinction between onset and steady state of propagation for the definition of the energy release rate

Let us define the crack tip by d=1. A steady state of fracture propagation means that the decohesion process is the same at each point of Γ thus G(a) has reached its stabilized value G_p. Then (10) becomes:

$$G_p = \int_{d=0}^{d=1} (Y_{d2} + Y_{d1})\, \delta d \qquad (11)$$

A mixed mode of fracture is considered. (11) cannot be used as a fracture criterion because G_p is not an intrinsic parameter. Pure modes have to be considered to introduce the intrinsic toughnesses G_{pI} and G_{pII}. (11) can be written as:

$$G_p = G_I + G_{II} = \int_{d=0}^{d=1} Y_{d2}\, \delta d + \int_{d=0}^{d=1} Y_{d1}\, \delta d \qquad (12)$$

Let us define the ratio c such that:

$$c = \frac{Y_{d1}}{Y_{d2}} = \frac{G_{II}}{G_I} \quad \text{then} \quad G_p = \int_{d=0}^{d=1} (1 + c)\, Y_{d2}\, \delta d \qquad (13)$$

By considering the constitutive equations (6)-(8), it becomes:

$$G_p = \frac{(1 + c)\,(Y_c - Y_0)}{1 + \gamma\, c} \qquad (14)$$

In particular, under pure modes of fracture we have the following relations:

$$G_{pI} = Y_c - Y_0 \quad ; \quad G_{pII} = \frac{Y_c - Y_0}{\gamma} \tag{15}$$

The previous equations give some relations between the Fracture Mechanics and the Damage Mechanics parameters. An other interesting result is obtained under mixed mode conditions. Using (15) and (12) the criterion for fracture propagation under mixed mode conditions is:

$$\frac{G_I}{G_{pI}} + \frac{G_{II}}{G_{pII}} = 1 \tag{16}$$

This condition is classically proposed in the available analyses of fracture in orthotropic materials such as wood. It is expressed in terms of stress intensity factors or in terms of critical energy release rates (Hunt and Croager 1957; Lum and Foschi 1988; Murphy 1986; Patton-Mallory and Cramer 1987; Triboulot et al. 1984; Valentin et al.1991). The second term of equation (16) can be written with an exponent (generally equal to 2) as proposed by some authors (Wu 1967; Mall et al. 1983) by modifying the proposed damage evolution law (6)-(8).
Note that critical energy release rates are not sufficient data because they only give information about the area under the stress-displacement curves but not on their shapes. This point will be discussed later.

Fracture energy

We are now considering the fracture energy G_f dissipated during complete cracking of a specimen (e.g. in mode I). Note h the ligament length and b the specimen width. The fracture energy G_f can be obtained by the integration of the load-displacement curve (see Fig. 2). By simplification the work due to the weight is not considered in the following formula:

$$G_f = \frac{1}{b\ h} \int_0^\infty F\ du \tag{17}$$

Assuming the decohesion process is the same at each point of Γ during complete cracking is equivalent to neglect the transient state of propagation and then:

$$G_f \simeq G_p \tag{18}$$

Note that in the case of a perfectly brittle material there is no process zone and then:

$$G_f = G_p = G_c \tag{19}$$

Thus, the ratio $\frac{G_c}{G_p}$ can be considered as an indicator of LEFM applicability.

Finite element strategies

Due to damage on interfaces, a instability point may appear (e.g. a snap-back in a force-displacement diagram). That critical point cannot be passed with a Newton-Raphson method that

pilots the computation in term of "force" (see Fig. 5). A Riks like method (Riks 1979; Crisfield 1983) allows to control the computation and pass such a limit point.
In a FE scheme, the iterative procedure is (see Fig. 5):

$$\begin{cases} \mathbb{K}\ \delta_i = \lambda_{i+1}\ \mathbf{F} - \mathbf{f}(\mathbf{U}_i) \\ \lambda_{i+1} = \lambda_i + \delta\lambda_i \\ \text{constraint: } g(\delta\lambda_i) = 0 \end{cases} \tag{20}$$

By the Newton-Raphson method ($\delta\lambda_i = 0$); by a Riks-like method the load factor is released, it is then necessary to impose a constraint ($g(\delta\lambda_i) = 0$).

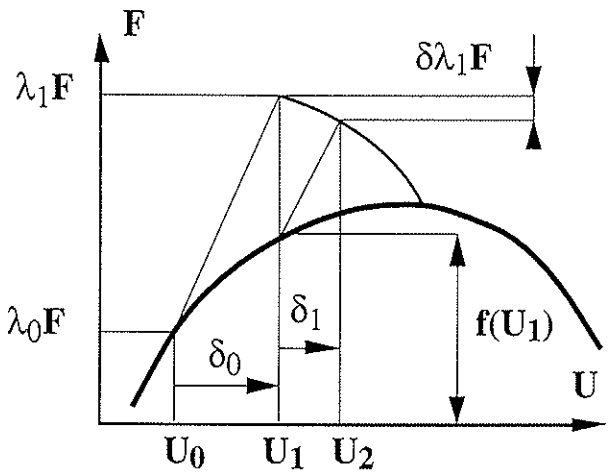

Fig. 5: Iterative strategy

Riks and Crisfield propose a constraint that concerns the norm of the global vector δ_i. Such a global constraint may lead to a non-convergence when damage is localised on an interface. To ensure a good convergence we propose to use of a local constraint that considers only the more significant degrees of freedom in the increase of damage.
The interface is modelled by joint elements. Note α and β the two closer nodes of the Gauss point where the increase of damage has been the more important at the initial step.

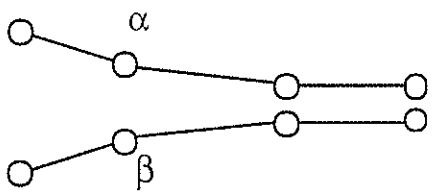

Fig. 6: Joint elements

The local constraint consists in imposing a constant value for the jump of displacement between α and β along the direction n (n = 1, 2 is the mode of principal damage).

$$(\delta_i)_n^{\alpha} - (\delta_i)_n^{\beta} = 0 \quad \text{for} \quad i \geq 1 \tag{21}$$

Equation (21) gives $\delta\lambda_i$.

LINEAR AND NON-LINEAR ANALYSES OF THE CIB TEST

An experimental program has been carried out for the determination of the fracture energy in tension perpendicular to grain for spruce and fir species. The three point bending test recommended by Larsen and Gustafsson (1989) is used. Main experimental results are given.
Then, the Finite Element analysis of two typical tests that differ by the wood orientation (RL and TL) has been performed by use of LEFM and of the proposed DM approach. The comparison between experimental and computational results concerns two TPB tests only in order to examine the ability of both approaches to predict the load deflection response.
Tentative conclusions are given about the use of the fracture energy for the fracture design analysis of wooden structures.

Experimental program

Presentation

About eighty specimens were tested at the Centre Technique du Bois et de l'Ameublement (C.T.B.A.) Paris in order to measure the fracture energy. The Larsen and Gustafsson (1989) CIB recommendation have been chosen to measure the fracture energy rather than the French standard (NF B 51-011 1985) because the latter standard only defines the ultimate splitting strength F_{end} by the following formula:

$$F_{end} = \frac{P_{max}}{b} \qquad (22)$$

P_{max} is the maximum load (N) and b is the specimen width (20 mm). The tested area is 20×20 mm^2.

The CIB-type specimens and the wood orientations are given in Fig. 7. From full size boards (50×150×3000 mm) of spruce and fir tested in a research program about the mechanical properties of French structural timber, cubic specimens (45×45×45 mm) were manufactured and conditioned at the following climate conditions: 20±2°C and 65±5% RH.
During first experiments the notch geometry proposed by Larsen and Gustafsson (1989) was tested. In such conditions, the crack propagation direction did not remain constant because the cut cannot be made correctly by the blade. So, a V-notch was chosen (like CHARPY specimens of fracture mechanics) directly cut by a specific saw blade. With such a notch geometry, the crack propagated straight ahead. In add, the notch length was chosen equal to 0.6×b (see Fig. 7) to ensure a stable load deflection response (Larsen and Gustafsson 1990). The tested area is h_0×b = 18×45 mm^2.
Specimens were tested to failure in stroke displacement control with a constant head speed during the test. A load cell of 500 daN was used. The fracture energy is (Larsen and Gustafsson 1989):

$$G_f = \frac{W + mgu_0}{h_0\, b} \qquad (23)$$

W is the area under the load deflection curve, u_0 is the deflection at failure, m is the mass of the beam (see Fig. 8).

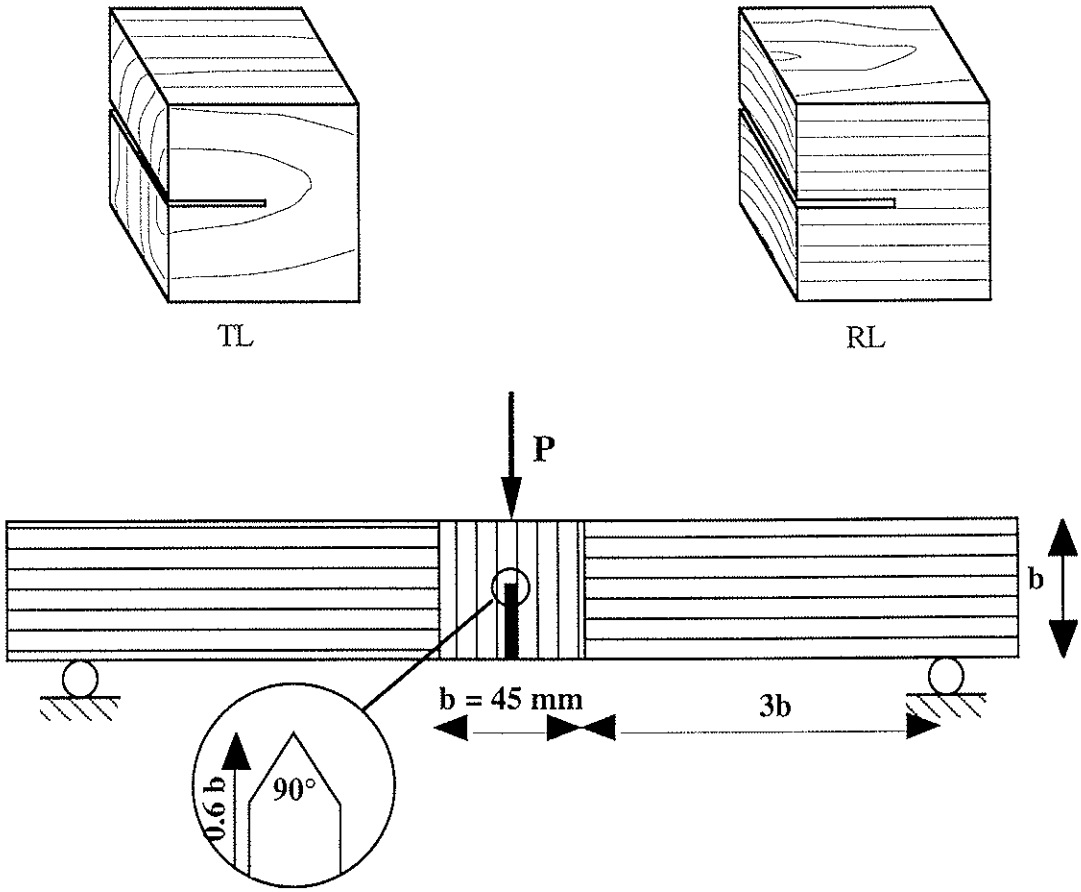

Fig. 7: Three point bending test and CIB-type specimen

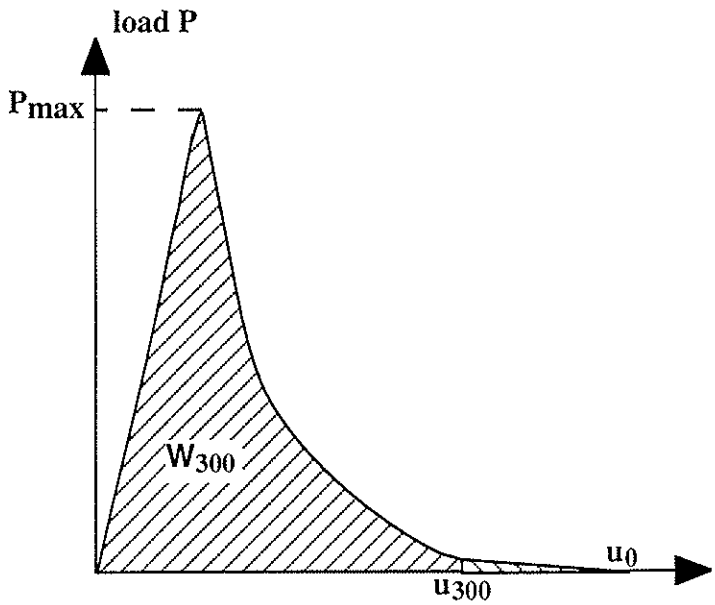

Fig. 8: Typical load deflection curve

Results

Twenty-six specimens were first broken with a head speed of 0.75 mm/mn (see Table 1). The mean time of failure is close to 300s as recommended by the CIB. With such a head speed, some tests presented a unstable crack propagation just after the maximum load. Therefore fivty-six specimens were tested with a head speed of 0.50 mm/mn (see Table 2).

Table 1: Fracture energy G_f (Nm/m^2) for a head speed of 0.75 mm/mn

Species		Mean	Standard deviation	C.V.	Min	Max	Nb
Spruce (Picea excelsa)	RL	189.8	26.5	13.9	159	229.4	5
	TL	144.1	39	27.1	99.8	194.8	6
FIR (Abies pectinata)	RL	189.4	43.2	22.8	126.8	296.9	14
	TL	96.8			96.8	96.8	1
All results		175.5	44.9	25.6	96.8	296.9	26
Failure time (s)		276	71	16.3	170	464	26

Table 2: Fracture energy G_f (Nm/m^2) for a head speed of 0.50 mm/mn

Species		Mean	Standard deviation	C.V. (%)	Min	Max	Nb
Spruce (Picea excelsa)	RL	274	65.2	23.8	169.6	438.8	27
	TL	222.2	80.4	36.2	136	294.9	4
FIR (Abies pectinata)	RL	271.1	100.7	37.1	127.5	526.3	21
	TL	188.9	56.2	29.8	130.3	255.7	4
All results		263.1	82.6	31.4	127.5	526.3	56
Failure time (s)		661	16.9	25.6	336	1032	51

With such a head speed of 0.50 mm/mn, the time to failure is then much greater than 300s. So, the fracture energy obtained with the deflection at failure u_0 may be a non significant parameter because an important time is spent to crack a very small ligament with a load value close to zero (see Fig. 8). It was then decided to calculate G_{f300} (see Table 3) which is defined with the deflection at 300s u_{300} and the corresponding area under the curve W_{300} as follows:

$$G_{f300} = \frac{W_{300} + mgu_{300}}{h_0\ b} \qquad (24)$$

Table 3: Fracture energy G_{f300} (Nm/m^2) for a head speed of 0.50 mm/mn

Species		Mean	Standard deviation	C.V. (%)	Min	Max	Nb
Spruce (Picea excelsa)	RL	225.9	42.3	18.7	164.8	344.9	27
	TL	184.7	51.3	27.8	131.4	246.4	4
FIR (Abies pectinata)	RL	225.3	59.8	26.6	126.2	367	21
	TL	171.8	42.1	24.5	114.2	196.6	4
All results		218.9	52.4	23.9	114.2	367	56

Note the coefficient of variation in Table 3 is less than in Table 2.

Because the time to failure was close to 300s with a head speed of 0.75 mm/mn (see Table 1), all the results are mixed and presented in Table 4.

Table 4: Fracture energy G_{f300} (Nm/m^2)

Species		Mean	Standard deviation	C.V. (%)	Min	Max	Nb
Spruce (Picea excelsa)	RL	220.1	42	19.1	159	344.9	32
	TL	159.6	46	28.8	99.8	246.4	10
FIR (Abies pectinata)	RL	210.2	55.3	26.3	126.2	367	35
	TL	156.8	58.3	37.2	96.8	236.2	5
All results		204.6	53.5	26.2	96.8	367	82

Note the presented result for spruce and for the orientation RL is close to the fracture energy value proposed in (Aicher 1992)

Other parameters such as the growth ring width, the orientation of pattern and the density have been measured for each specimen. The results are given in Table 5, 6 and 7 to be compared with the fracture energy.

Fig. 9 shows the ratio between the fracture energy G_{f300} and the mean fracture energy $(G_{f300})_{mean}$ versus the orientation of pattern.

Table 5: Annual growth ring width (mm)

Species		Mean	Standard deviation	C.V. (%)	Min	Max	Nb
Spruce (Picea excelsa)	RL	2.9	1.3	46.9	1	6.2	32
	TL	2.5	1.2	49.9	1.6	4.8	10
FIR (Abies pectinata)	RL	1.9	0.7	39.2	0.6	4.5	35
	TL	2.5	1	39.1	1.4	3.7	5
All results		2.4	1.2	48.7	0.6	6.2	82

Table 6: Orientation of pattern (deg.)

Species		Mean	Standard deviation	C.V. (%)	Min	Max	Nb
Spruce (Picea excelsa)	RL	8.3	8	95.9	0	27.1	32
	TL	82.6	6.7	8.1	70.4	90	10
FIR (Abies pectinata)	RL	6.4	8.2	127.6	0	30	35
	TL	82.3	7.5	9.1	73	90	5

Table 6: Density (kg/m^3)

Species		Mean	Standard deviation	C.V. (%)	Min	Max	Nb
Spruce (Picea excelsa)	RL	428	50.1	11.7	361.7	520.7	32
	TL	438.6	37.5	8.5	378.4	489.6	10
FIR (Abies pectinata)	RL	436.3	39.8	9.1	378.9	520.9	35
	TL	451.3	71.1	15.8	393.8	575.1	5
All results		434.3	45.5	10.5	361.7	575.1	82

Conclusion of the experimental program

The CIB recommendation is a simple method to estimate the fracture energy G_f of wood in tension perpendicular to the grain. The French standard could change in the future.

A V-notch was cut on specimens to correctly initiate the crack propagation. Different head speeds were tested but for each of them, the fracture energy was defined at the same time 300s. These results should be confirmed by new tests.

The mean fracture energy of French white wood (for both spruce and fir) is close to 200 Nm/m^2. This value could be introduced into design codes.

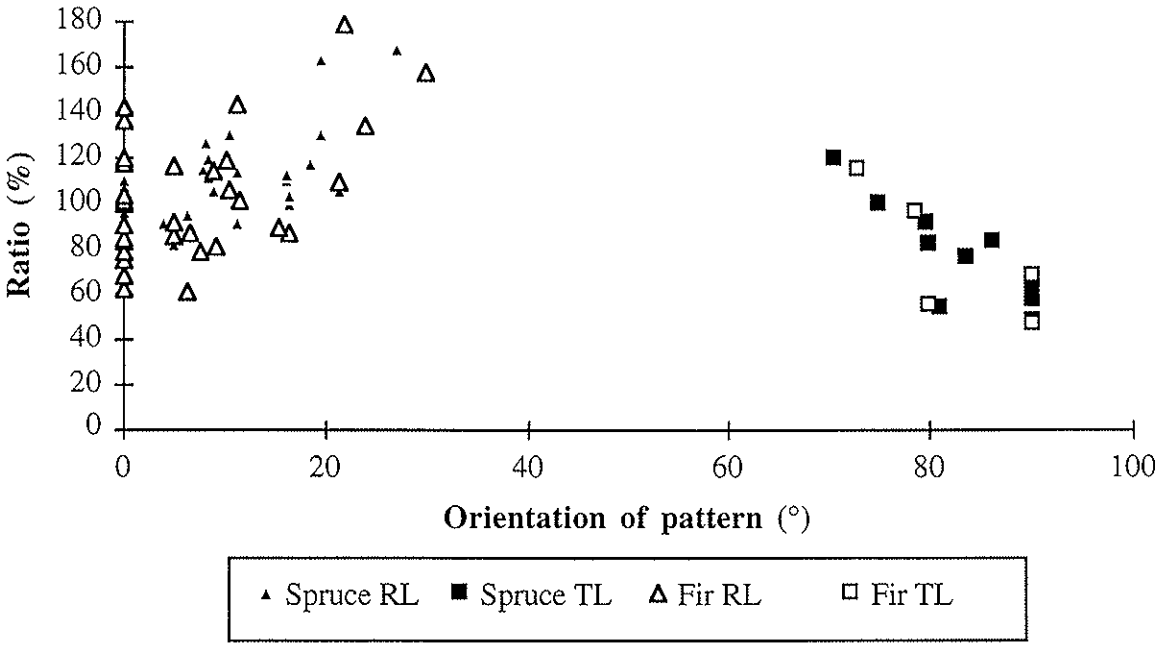

Fig. 9: Ratio $G_{f300}/(G_{f300})_{mean}$ versus orientation of pattern

Linear Elastic Fracture Mechanics analysis

Classical analysis

Model wood behaviour depends on the treated application. The actual behaviour of wood includes viscous, plastic and damage phenomena. However, for most engineering calculations wood can be modelled as a orthotropic, homogeneous and linear-elastic material. For a fracture study, the modeling of crack tip phenomena defines the framework analysis. LEFM is based upon the assumption that damage phenomena are concentrated at the crack tip. Then, in the case of a pure mode of fracture, the analysis consists in the comparison of the energy release rate G that is a global variable or the local stress intensity factor K with a critical value.

The analysis of the TPB test is now conducted in the framework of LEFM by using the energy release rate G. A Griffith criterion for the mode I crack propagation condition is chosen (Griffith 1920):

$$\begin{array}{ll} G(P,a) < G_c & \text{No crack propagation} \\ G(P,a) = G_c & \text{Possible crack propagation} \end{array} \qquad (25)$$

G_c is the critical energy release rate for a mode I cracking. Different types of specimen can be used for the identification of G_c but a common point is the impossibility to measure directly G_c. According to the theory G_c does not depend on the structure. The critical energy release rate is therefore independent of the specimen and of the crack length. The initial crack length seems to have no influence for DCB (Valentin and Morlier 1982) and SEN (Ewing and Williams 1979) specimens. A key point of the theory is the assumption of no dependence of G_c with the crack length during crack

propagation. The experimental checking of this assumption is difficult experimentally because it needs to measure the crack length.

G(P,a) is computed by the compliance method. The elastic stiffness for given loading and crack length is calculated by the FE method (code CASTEM 2000). The crack propagation is modelled by separating two connected lines. The mesh refinement at the crack tip is constant during the crack propagation.

The energy release rate is:

$$G = -\frac{1}{b}\frac{\partial W}{\partial A} = \frac{P^2}{2b}\frac{\partial (1/k)}{\partial a} \tag{26}$$

with
- W: Potential energy
- a: Crack length
- k: Elastic stiffness
- b: Specimen width

Thus for two FE computations 1 and 2:

$$\frac{G}{P^2} \simeq \frac{1}{2b}\frac{1}{\Delta a}\left(\frac{1}{k_2} - \frac{1}{k_1}\right) \tag{27}$$

with $\Delta a = a_2 - a_1$ and $\Delta a << a$

As said before, the comparisons between computational and experimental results concern only two tests carried out on spruce for the RL and TL orientations. The density is about 400 kg/m^3, the maximum loads and the fracture energies for the RL and TL orientations were found equal to:

$$\begin{cases} P_{max} = 148 \text{ N} , G_{fRL} = 175 \text{ Nm/m}^2 \\ P_{max} = 86 \text{ N} , G_{fTL} = 90 \text{ Nm/m}^2 \end{cases} \tag{28}$$

The elastic moduli were chosen in a first step by extrapolation of results given by Guitard (1987) with respect to the actual density. Nevertheless these values did not allow the correct stiffness (load/deflection) prediction. It was then decided to decrease the elastic moduli in the same proportion to obtain the correct stiffness. Therefore, the chosen elastic constants were:

$$\begin{cases} E_L = 11000 \text{ MPa} , E_R = 530 \text{ MPa} , E_T = 300 \text{ MPa} \\ G_{RL} = G_{LT} = 400 \text{ MPa} , \nu_{RL} = \nu_{TL} = 0.5 \end{cases} \tag{29}$$

G_c is calculated with the maximum load $P = P_{max}$ and for the initial crack length $a = a_0$. The crack propagation is then analyzed with the identified value of G_c by increasing the crack length and by applying the criterion (25) that allows the computation of the load P for a given crack length a with the equation (27). Results are given in Fig. 11 and Fig. 12. By comparing computational and experimental results, it appears that the LEFM approach cannot predict the load-displacement curve. LEFM predicts a snap-back that has not been experimentally observed.

By assuming that the chosen elastic constants (29) are correct, the G_c values (see Fig. 11 and Fig. 12) are low compared with the G_f values (28). That result is not very surprising because G_c is

related to the onset of propagation of a manufactured notch (with no process zone at the notch tip) and G_f is related to all the fracture process i.e. essentially to the propagation of a "natural" crack.

Steady state of propagation

The analysis of cracking was analyzed in a second step with the LEFM approach and by assuming the critical energy release rate is not constant during the crack propagation. The critical energy release rate $G_c(a)$ was calculated with the experimental load value and with the assumption that the stiffness obtained by the elastic FE computation (27) was valid.

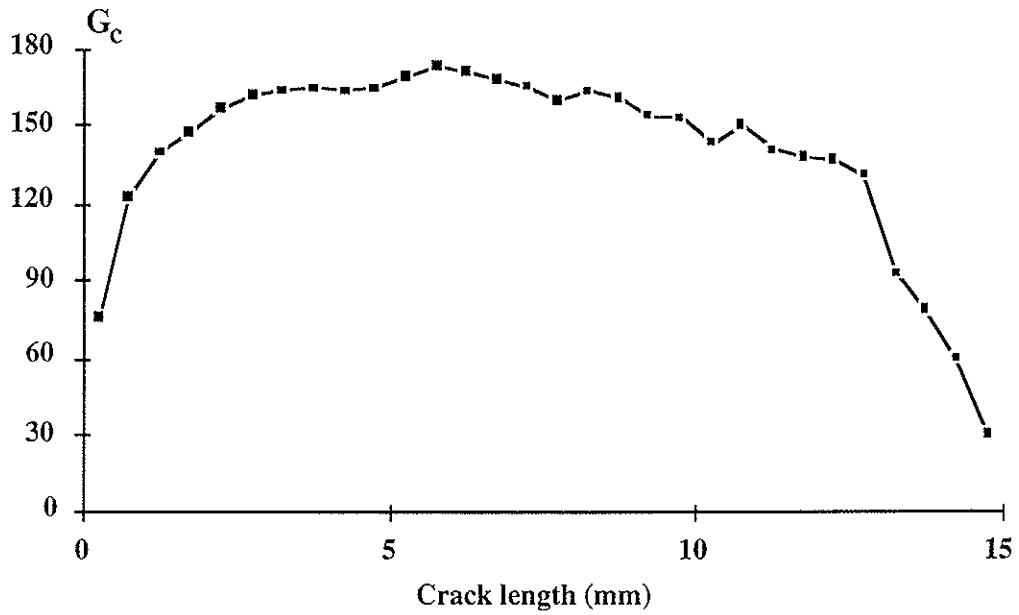

Fig. 10: Critical energy release rate (Nm/m^2) with respect to the crack length for the RL orientation

It appears that the hypothesis of a constant value for G_c is not valid and that a steady state of propagation is obtained for a short range of crack lengths (i.e. with no dependence of G_c with the crack length). Note the edge effect when the crack tip is near the end of the ligament.
For a fracture analysis of a structure with the LEFM approach, it is necessary to use the G_p value i.e. the critical energy release rate value corresponding to a steady state of propagation. According to the FE analysis, that value is about 170 Nm/m^2 for the RL orientation which is very close to the G_f value (28). This result seems to confirm that equation (18) is valid for the TPB test and that G_f can be considered as a material parameter that can be used for engineering calculations.

Damage Mechanics analysis

The fracture analysis of the two typical tests (28) is now performed by use of the proposed Damage Mechanics approach. The elastic constants are given in (29). The identification of characteristic parameters of the damage model (6)-(8) is quite easy because this is a mode I of fracture.

The interface model is used for the analysis of the crack propagation of an already cracked structure. In such a case, the major parameter that governs fracture is the critical energy release rate. Thus, the major condition to verify is equation (15).

(15) gives one relation for the four unknown parameters that are the critical energy Y_c, the threshold energy nY_0, the damage evolution exponent n and the interface stiffness k. If equation (15) is verified, the influence of the three free parameters is minor. It means that the shape of the traction-relative displacement curve of the DM modeling has a very little influence (see Fig. 2).

The last remark is no longer valid if there is no crack i.e. in the case of the onset of cracking analysis. These results have been shown in (Daudeville and Ladevèze 1994).

Therefore the following parameters have been chosen a priori:

$$Y_0 = 0 \ ; \ k = 10^3 \text{ N/mm}^3 \quad \text{and} \quad n = 1 \tag{30}$$

The only unknown parameter is then Y_c for each wood orientation. Those values have been identified in order to obtain a maximum load equal to the experimental maximum load. Then by using equations (15) and (18) the fracture energy can be calculated ($G_f = Y_c$). Results are given in Fig. 11 and Fig. 12.

Load-displacement curves are correctly described by the DM approach. The major point of that study is that for each wood orientation, the experimental fracture energy G_f value (28) is very close of the fracture energy value we used in the modeling.

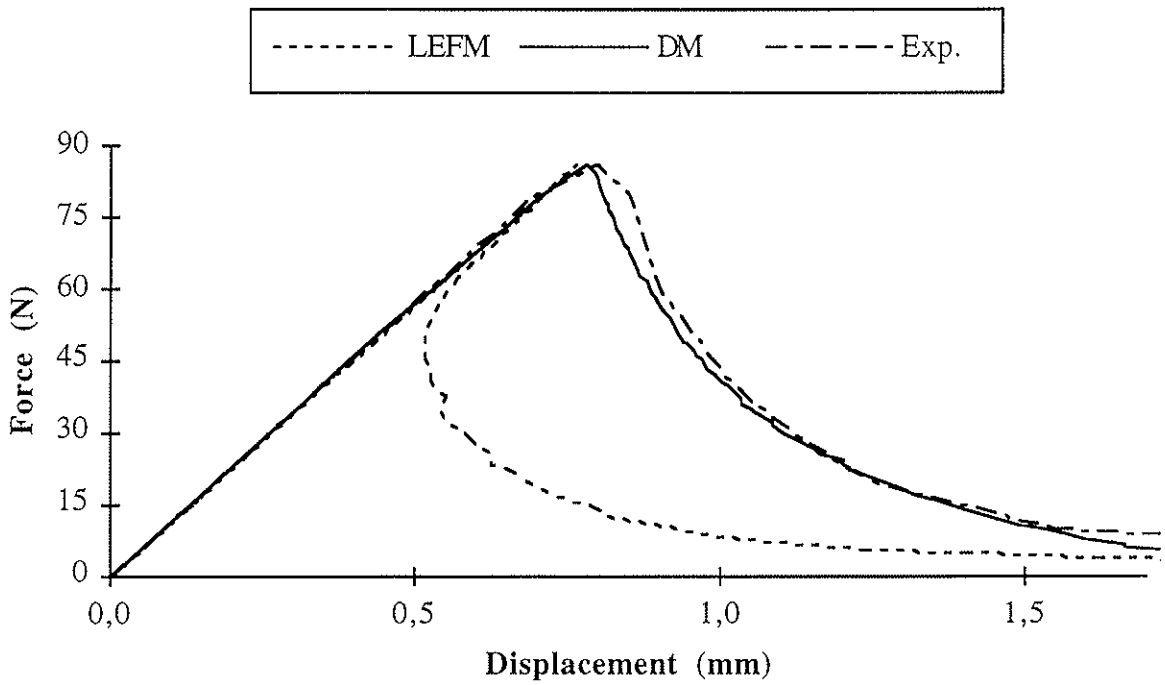

Fig. 11: Load-displacement curve for the TL orientation
$G_f = 80$ Nm/m^2, $G_c = 30$ Nm/m^2

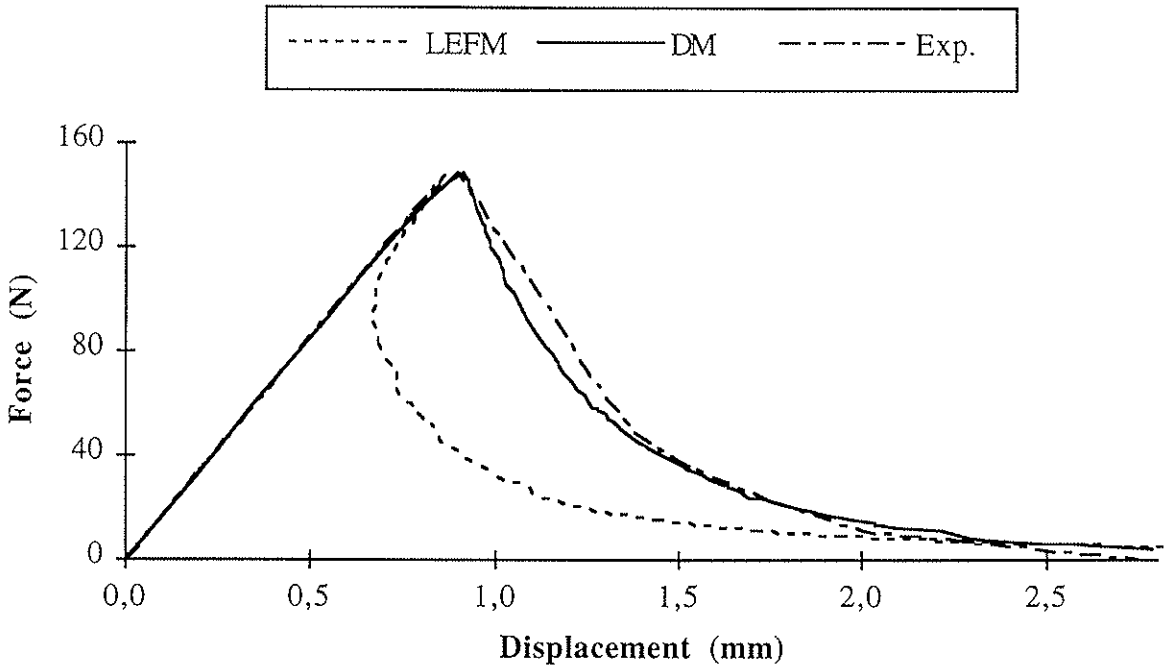

Fig. 12: Load-displacement curve for the RL orientation
G_f = 173 Nm/m^2, G_c = 75 Nm/m^2

CONCLUSION

An interface model has been presented for the analysis of cracking under pure or mixed mode conditions in an orthotropic medium such as wood. It is based upon Damage Mechanics that uses the decrease of stiffness as a damage indicator. A link between DM parameters and LEFM parameters allows a clear identification of the parameters of the model. The use of joint elements to simulate the crack propagation is easy to implement in a FE code.

An experimental program has been carried out on spruce and fir for the determination of the fracture energy in tension perpendicular to the grain by use of CIB standard TPB. The influence of wood parameters such as the wood orientation or the density has been examined.

Comparisons between simulation results of the classical LEFM and experimental results of the TPB test have shown that LEFM could not predict the post peak load displacement curve. This is due to non linear phenomena that occur in the process zone that can not be neglected in such a structure. The TPB test allows the determination of the critical energy release rate for a steady state of propagation G_p. Nevertheless, that value is difficult to calculate because it supposes to measure the crack length during the test or to compute its value through a FE analysis.

The computational results show that the fracture energy G_f value is quite equal to the G_p value. The latter result is interesting because it seems to prove that the fracture energy obtained with the TPB test can be considered as a material parameter that can be used for engineering calculations. The authors used the experimental fracture energy for the prediction of the load-bearing capacity of mechanical joints by means of LEFM concepts (Daudeville and Yasumura 1995). In such a problem, the size of

the process zone can be neglected, so the authors considered that the critical energy release rate was equal to the fracture energy. A good concordance was obtained between experimental and computational results.

The load-deflection curve is correctly predicted by the DM model. In add, it was shown the fracture energy was the major parameter that governs fracture propagation.

ACKNOWLEDGEMENTS

The authors would like to thank F. Dubois and A. Bengougam who carried out some experiments in Master's courses of ENS Cachan and M. Khebibeche for his advice.

REFERENCES

Aicher, S., Reinhardt, H.W. and Klöck, W., (1993), "Nichtlineares bruchmechanik-maßstabsgesetz für fichte bei zugbeanspruchung senkrecht zur faserrichtung", *Holz als Roh- und Werstoff*, 51, 385-394 (in German).

Aicher, S., (1992), "Fracture energies and size effect laws for spruce and oak in mode I", Determination of fracture properties of wood especially in mode II and mixed modes I and II, Proceedings of the RILEM TC 133 Meeting, Bordeaux France

Allix, O. and Ladevèze, P., (1992), "Interlaminar interface modeling for the prediction of delamination", *Composite Structures*, 22, 235-242.

Allix, O., Daudeville, L., Neau, J.L. and Ladevèze, P., (1995), "Necessity of using damage mechanics for the analysis of delamination specimens", 4th Int. Conf. on Computational Plasticity COMPLAS IV, Barcelona Spain.

Bazant, Z.P. and Kazemi, M.T., (1990), "Determination of fracture energy, process zone, length and brittleness number from size effect, with application to rock and concrete", *Int. J. of Fracture*, 44(2), 111-131.

Bazant, Z.P., (1984), "Size effect in blunt fracture: concrete, rock, metal", J. of Eng. Mechanics, ASCE, 104, 518-535.

Bengougam, A. and Dubois, F., (1994), "Simulation de la rupture d'un assemblage en bois boulonné", Mémoire de D.E.A. de l'E.N.S. de Cachan (in French).

Boström, L., (1988), "The fictitious crack model - A fracture mechanics approach applied on wood", International Conference on Timber Engineering, Seattle DC, 2, 559-565.

Crisfield, M.A., (1983), "An arc-length method including line searches and accelerations", *Int.Journal for Num.Methods in Eng*, 19, 1269-1289.

Daudeville, L. and Ladevèze, P., (1993), "A damage mechanics tool for laminate delamination", *Composite Structures*, 25(4), 547-555.

Daudeville, L. and Ladevèze, P., (1994), "Une méthode simplifiée pour l'analyse du délaminage auprès d'un bord droit", *Revue Européenne des Éléments Finis*, 3(1), 127-150.

Daudeville, L.and Yasumura, M., (to appear in 1995), "Failure analysis of timber bolted joints by fracture mechanics.", *Materials and Structures.*

Ewing, P.D. and Williams, J.G., (1979), "Thickness and moisture content effect in the fracture toughness of Scots Pine", *J. of Mat. Sc.*, 14-12, 2959-2966.

Garcia-Alvarez, V.O., Carol, I. and Gettu, R., (1994), "Numerical simulation of fracture in concrete using joint elements", *Anales de Mecanica de la Fractura*, 11, 75-80.

Gens, A., Carol, I. and Alonso, E.E., (1988), "An interface element formulation for the analysis of soil-reinforcement interaction", *Comp. and Geotechnics*, 7, 133-151.

Griffith, A., (1920), "The phenomena of rupture and flow in solids", Philosophical Transactions of the Royal Society of London, Series A, 221, 163-198.

Guitard, D., (1987), "Mécanique du matériau bois et composites", Cépadues-Editions, ISBN 2.85428.152.7 (in French).

Gustafsson, P.J., (1985), "Fracture mechanics studies of non-yielding materials like concrete", Technical Report TVBM-1007, Lund Institute of Technology.

Hillerborg, A., Modeer, M. and Petersson, P.E., (1976), "Analysis of crack formation and crack growth in concrete by means of fracture mechanics and finite elements", *Cement and Concrete Research*, 6, 773-782.

Hohberg, J.M. and Bachmann, H., (1988), "A macro joint element for non-linear arch dam analysis", Numerical Methods in Geomechanics, Ed. Swoboda G., Balkema, Rotterdam, 829-834.

Hunt, D.G. and Croager, W.P., (1982), "Mode II fracture toughness of wood measured by a mixed mode test method", *J. of Mat. Sc. Letters*, 1, 77-79.

Jenq, Y.S. and Shah, S.P., (1985), "A two parameter fracture model for concrete", *J. Eng. Mech.*, 111(4), 1227-1241.

Larsen, H.J.and Gustafsson, P.J., (1989), "Design of end-notched beams", CIB-W18A/22-10-1, Berlin DDR.

Larsen, H.J.and Gustafsson, P.J., (1990), "The fracture energy of wood in tension perpendicular to the grain", CIB-W18A/23-19-2, Lisbon Portugal.

Lum, C. and Foschi, O., (1988), "Arbitrary V-notches in orthotropic plates", *ASCE J. of Eng. Mech.*, 114(4), 638-655.

Mall, S., Murphy, J.F. and Shottafer, J.E., (1983), "Criterion for mixed mode fracture in wood", *ASCE J. of Eng. Mech.*, 109(3), 680-690.

Murphy, J.F., (1986), "Strength and stiffness reduction of large notched beams", *ASCE J. of Struct. Eng.*, 112(9), 1989-2000.

Nallathambi, P. and Karihaloo, B.L., (1986), "Determination of specimen-size independent fracture toughness of plain concrete", *Magazine of Concrete Research*, 38(135), 67-76.

Ngo, D. and Scordelis, A.C., (1967), "Finite element analysis of reinforced concrete beams", J. of the American Concrete Institute, 64(14), 152-163.

Patton-Mallory, M. and Cramer, S.M., (1987), "Fracture mechanics: a tool for predicting wood component strength", *Forest Products Journal*, 37(7-8), 39-47.

Riks, E., (1979), "An incremental approach to the solution of snapping and buckling problems", *International Journal of Solids and Structures*, 15, 524-551.

Rots, J.G. and Schellekens, J.C.J., (1990), "Interface elements in concrete mechanics", 2nd Int. Conf. on Computer Aided Analysis and Design of Concrete Structures, SCI-C, Volume 2.

Triboulot, P., Jodin, P. and Pluvinage, G., (1984), "Validity of fracture mechanics concepts applied to wood and finite element calculation", *Wood Sc. and Tech.*, 18(61), 11-24.

Valentin, G., Boström, L., Gustafsson, P.J., Ranta-Maunus, A. and Gowda, S., (1991), "Application of fracture mechanics to timber structures", RILEM state-of-art Report, Technical Research Centre of Finland, Espoo Finland, Research Notes 1262, ISBN 951.38.3891.1.

Valentin, G. and Morlier, P., (1982), "A Criterion of crack propagation in timber", Materials and Structures, 15, 88.

Wu, E.M., (1967), "Application of fracture mechanics to anisotropic plates", *ASME J. of Applied Mech. Series E*, 34(4), 967-974.

Yasumura, M. and Daudeville, L., (1995), "Failure of timber bolted joints subjected to lateral load perpendicular to grain", CIB-W18A/28-7-5, Copenhagen Denmark.

CIB-W18/28-19-2

INTERNATIONAL COUNCIL FOR BUILDING RESEARCH STUDIES AND DOCUMENTATION

WORKING COMMISSION W18 - TIMBER STRUCTURES

A NEW METHOD OF DETERMINING FRACTURE ENERGY IN FORWARD SHEAR ALONG THE GRAIN

by

H D Mansfield-Williams
Departement of Timber and Construction
Buckinghamshire College
United Kingdom

MEETING TWENTY - EIGHT

COPENHAGEN

DENMARK

APRIL 1995

Summary

A draft standard for determining the fracture energy of wood in forward shear (mode II) along the grain is to be proposed. The standard contains a new specimen, the Tapered End-Notched Flexural (TENF) specimen, and this paper describes its development and the accompanying testing programme.

The specimen promotes stable crack growth in pure shear and has been used successfully with a number of different species, but principally with *Picea abies*.

The fracture energy for *Picea abies* was determined as 760 Nm^{-1}.

Introduction

The RILEM Technical Committee TC 133 "Fracture in Wood" has considered mode II fracture in solid wood. This paper reports the development of a proposal for a new standard by the test sub-group of the committee. Some of the work of the design sub-group, which was a joint grouop of RILEM TC 133 and CIB W18A, is reported in CIB-W18/28-19-3 (Petersson, 1995) and CIB-W18/28-19-4 (Aicher *et al*, 1995).

Specimens previously used to determine mode II fracture parameters may be divided into two groups; compact shear specimens and beam specimens (Valentin, 1992). In general compact shear specimens are very sensitive to orthotropic parameters while end-notched beams have normal forces ahead of the crack. Murphy (1988) and Kretschmann and Green (1992) measured K_{IIC} in beams with centre splits, but crack propagation was unstable, which precludes the calculation of the fracture energy.

The committee aimed to design and test a robust mode II specimen that would promote stable crack growth in forward shear and be easy to manufacture and test.

Design of Specimen

The first design of specimen examined by the committee was an adaptation of the mode I specimen described in Nordtest Method NT BUILD 422 (1993). The dimensions of the mode I specimen were retained, but the loading conditions were altered to create a shear stress ahead of the notch (Figure 1). Although the specimen did fail in shear it was not possible to produce stable crack growth and so this specimen was abandoned.

The Tapered End-Notched Flexural (TENF) specimen proposed by Racois and Valentin (1993) (Figure 2) is a beam with a taper designed to promote stable cracking in pure shear along the grain. The tapered part has a constant breadth and a linear taper in the depth. The hammerhead at the end of the taper allows the supports to be in the same plane. A narrow cut forms an initial crack; the crack front is cut to a chevron so that there is a high stress at the tip of the chevron. Teflon plates are fitted tightly into the mouth of the crack above the support to prevent the crack closing under load. Initial tests with this specimen exhibited stable crack growth and it was adopted by the committee.

The linear taper of the original specimen (hereafter LTENF) was refined through finite element analysis by Aicher and Gierl (1994) (Figure 3). This showed that although the specimen was stable in practice, the stress intensity (K_{II}) increased slightly with crack length. To maintain stable crack growth the test machine must decrease the applied load in the moment that the crack propagates, but any stored energy in the machine, and the time taken for the control mechanism to react, work against stability even in stroke control. The K_I values are around zero so there is no separation of the fracture surfaces as the crack grows.

The design was modified by changing the function governing the taper in the depth to a parabolic function and by introducing a linear taper in the breadth (Figure 3). The modified specimen (PTENF) showed a slightly decreasing stress intensity (K_{II}) (Figure 4) with increasing crack length. A further modification was to offset the initial crack towards the tension edge of the specimen as a result of which the mode I stress intensity (K_I) is positive (Figure 5), but only about 2.5 % of the K_{II} value. This was intended to reduce friction at the crack tip.

An immediate disadvantage of the modifications was that the specimen became difficult to manufacture.

Testing Programme

Both specimens were tested; the specimen and loading arrangement for LTENF is shown in Figure 2 and for PTENF in Figure 6.

The specimens were conditioned at 20°C and 65 % relative humidity till they reached equilibrium. Moisture content and density were calculated (density was calculated with the oven-dry mass and the volume at test). The orientation of the crack was recorded as RL or TL, although some laboratories were more exact and either photocopied the end-grain, or noted the angle of the growth ring to the crack, where TL = 90° and RL = 0°.

Tests were conducted in stroke control at a speed of 1 mm per minute. The specimen was loaded until the crack had extended by about 40 - 70 mm, then was unloaded at the same speed. The crack extension was estimated either from the displacement of parallel lines drawn across the crack path or by colouring the side of the specimen black. The complete load-displacement curve was recorded. The displacement was measured by a device, such as a linear voltage displacement transducer (LVDT), mounted in a cradle that rested on the top of the specimen above the supports (Figure 6). Sample curves are shown in Figure 7.

After the test the notch of the failed specimen was forced open till the specimen separated in cleavage. The length of the crack extension was observed by holding the fracture surface at an angle to the light; the different modes of failure, shear and cleavage, formed a crack front that could be clearly distinguished. Invariably the crack grew from the top of the chevron notch; since the initial crack was

2 mm wide and offset by 1 mm crack growth began at the centre of the specimen and the K_I values may have been closer to zero than the finite element model suggested.

The above describes the procedure adopted for the standard. Other configurations were examined, for instance Aicher and Gierl (1994) found that a faster loading speed increased the fracture energy values and Kretschmann (1994) did not find a size effect in the LTENF specimen. In tests at Buckinghamshire College the coefficient of variation without a cradle for the transducer was high at 40%; with a cradle this decreased to 22%.

Results

The number of tests reported from each laboratory and included in this report is shown in Table I.

Laboratory	LTENF	PTENF
Bucks College, High Wycombe	-	11
FMPA, Stuttgart	25	34
FPL, Madison	7	8
LRBB, Bordeaux	7	-
SP, Borås	-	19
Totals	**39**	**72**

Table 1. Number of tests by each laboratory.

The test species was *Picea abies* except for FPL, Madison which tested *Picea sitchensis*. Tests were carried out on different species, principally *Fagus sylvatica* and *Quercus robur*, but these are not covered here.

Complete load-deflection curves were recorded for each test. Initially the fracture energy was calculated as

$$G_{II,F} = \frac{W}{A} \qquad [1]$$

where: $G_{II,F}$ = fracture energy in mode II; in N/m

W = work done by the midpoint force i.e. the area under the load deflection curve; in Nm

A = the area of the fracture surface created by the crack extension measured on one half of the specimen; in m^2

In all cases the load-deflection curve did not return to the origin, rather there was a residual deflection of about 0.2 - 0.3 mm that is probably due to friction and plastic deformation. Four methods were proposed to identify the mode II part of the curve (Figure 7). The hatched part of the curve was used to calculate W in [1].

The values were statistically evaluated following the method of Job (1995). The two specimen types were considered separately, but the data were not sub-divided further. There appeared to be some

systematic deviation between data series from different laboratories, but no adjustment was made as the cause of the deviation was not clear.

The data were ranked in ascending order then reduced by

$$x_i' = \frac{x_i - L}{s} \qquad [2]$$

where: x_i' = reduced individual toughness values

x_i = individual toughness values

L = location parameter of the distribution (threshold value)

s = sample standard deviation

Weibull and gamma distributions were fitted to the data. Shape parameters α and β and the location parameter L were fitted by minimizing the residual sum of squares. The goodness of fit is measured as the mean adjusted difference

$$\frac{\Sigma (\hat{x}_i - x_i')^2}{\Sigma x_i'} \qquad [3]$$

where: $\hat{x}_i$ = expected value from the distribution function

In the following tables the α and β shape parameters are shown as calculated from the reduced values.

Method	Distribution	α	β	Threshold Value	Mean adjusted difference	Mean of the distribution	Standard Deviation	CoV
1	Weibull	1.017	1.099	825.0	2.05%	1156.4	303.59	26.25%
2	Weibull	2.156	2.381	203.4	0.83%	512.7	146.69	28.61%
3	Weibull	1.932	2.162	336.6	0.57%	661.6	169.48	25.62%
4	Weibull	1.200	1.344	646.0	1.00%	946.8	237.93	25.13%

Table 2. Summary of statistical treatment of data for LTENF specimen.

Method	Distribution	α	β	Threshold Value	Mean adjusted difference	Mean of the distribution	Standard Deviation	CoV
1	Gamma	3.119	0.578	583.0	0.98%	1360.4	430.99	31.68%
2	Weibull	1.423	1.602	327.8	0.74%	592.4	181.66	30.67%
3	Gamma	3.864	0.528	275.7	1.74%	757.1	236.18	31.19%
4	Weibull	1.207	1.352	601.0	1.87%	1049.1	352.93	33.64%

Table 3. Summary of statistical treatment of data for PTENF specimen.

The cumulative distribution functions, probability density functions and residual plots for LTENF and PTENF are presented in Figure 8 and Figure 9 respectively.

Discussion

With the exception of methods 1 and 3 for PTENF a Weibull distribution could be fitted with greater accuracy than a gamma distribution. Methods 1 and 4 have high threshold values and probably over-estimate the fracture energy; method 1 for PTENF has a relatively wide spread. Method 2 provides a good fit and low variability, but at the expense of both discarding a large part of the data points collected during steady crack growth, and of accepting low mean values. Method 3 makes the assumption that the specimen behaves as a linear elastic material and would recover all the deflection were it not for the friction between the fracture surfaces. There is good agreement between observed and expected values for LTENF; for PTENF the agreement is less good. However, the residuals for PTENF are positive in the critical lower part of the curve, which means that the observed values are on the safe side of the distribution.

Method 3 was chosen and is included in the standard.

The coefficient of variation for LTENF is lower than for PTENF for all the methods. However PTENF was chosen because of the theoretical considerations arising from the finite element analysis detailed above. A large proportion of the LTENF specimens were tested in the one laboratory, which may partly explain the lower variation.

The dependencies of the fracture energy values determined by method 3 on density and crack orientation are shown in Figure 10 and Figure 11 respectively. The r-squared values show that there is little dependence in all cases, although the relationship with crack orientation is consistently positive. The exact values for crack orientation were used where they were available, otherwise TL was taken as 88°, R/TL as 45° and RL as 2°. Most laboratories only tested TL; only FMPA tested RL.

Conclusions

The proposed specimen allows the determination of fracture energy in forward shear. The mean value from the distribution curve for *Picea abies* is 757 Nm^{-1}; the arithmetic mean is 755 Nm^{-1}. The committee hope that it will prove useful in establishing a database of values for all structural timbers.

References

Aicher, S. and Gierl, M. (1994) Investigations on differently tapered end-notched flexure beams for G_{IIF} determination. Paper presented to RILEM TC-133 meeting, High Wycombe, December 1994.

Aicher S., Schmidt, J. and Brunold, S. (1995) Design of timber beams with holes and notches by means of fracture mechanics. Paper 28-19-4 presented at the 28th meeting of working Commission CIB-W18 of the International Council for Building Research Studies and Documentation. April 1995, Copenhagen.

Boström, L. (1993) Tests of tapered shear beam. Paper presented to RILEM TC-133 meeting, Stuttgart, December 1993.

Boström, L. (1994) Different methods to evaluate the TENF tests. Paper submitted to RILEM TC-133.

Boström, L. (1995) Draft standard proposal for: fracture energy in forward shear along the grain. Submitted to RILEM TC-133.

Job, L. (1995) Statistical evaluation of different methods for fracture energy evaluation in mode II. Submitted to RILEM TC-133.

Kretschmann, D.E. (1994) Effect of varying the dimensions of the RILEM TC-133 shear specimen for determination of fracture mechanics properties in wood. Paper presented to RILEM TC-133 meeting, Espoo, May 1994.

Kretschmann, D.E. and Green, D.W. (1992) Center-split beam as a method for determining mode II fracture properties. *in* Workshop on determination of fracture properties of wood especially in mode II and mixed mode I and II. RILEM TC-133 meeting, April 1992, Bordeaux.

Murphy, J.F (1988) Mode II wood specimen: Beam with center split. Journal of Testing and Evaluation, 16 (4) 364-368.

Nordtest Method NT BUILD 422 (1993) Wood: fracture energy in tension perpendicular to grain. Nordtest, Espoo.

Petersson, H. (1995) Fracture design analysis of wooden beams with holes and notches. Finite element analysis based on energy release rate approach. Paper 28-19-3 presented at the 28th meeting of working Commission CIB-W18 of the International Council for Building Research Studies and Documentation. April 1995, Copenhagen.

Racois, P. and Valentin, G.H. (1994) Proposal of a shear specimen for determination of fracture mechanics properties in wood (2nd draft, submitted to RILEM TC-133). LRBB, Bordeaux.

Valentin, G. (1992) Short presentation of mode II specimens. *in* Workshop on determination of fracture properties of wood especially in mode II and mixed mode I and II. RILEM TC-133 meeting, April 1992, Bordeaux.

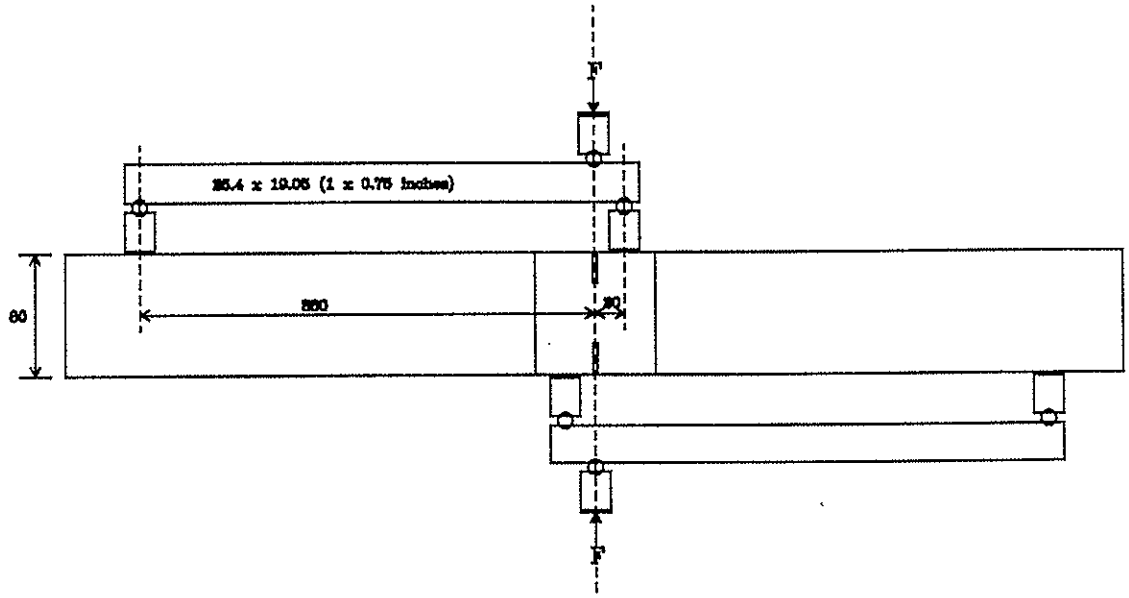

Figure 1. Test arrangement to cause shear failure in mode I beam specimen .

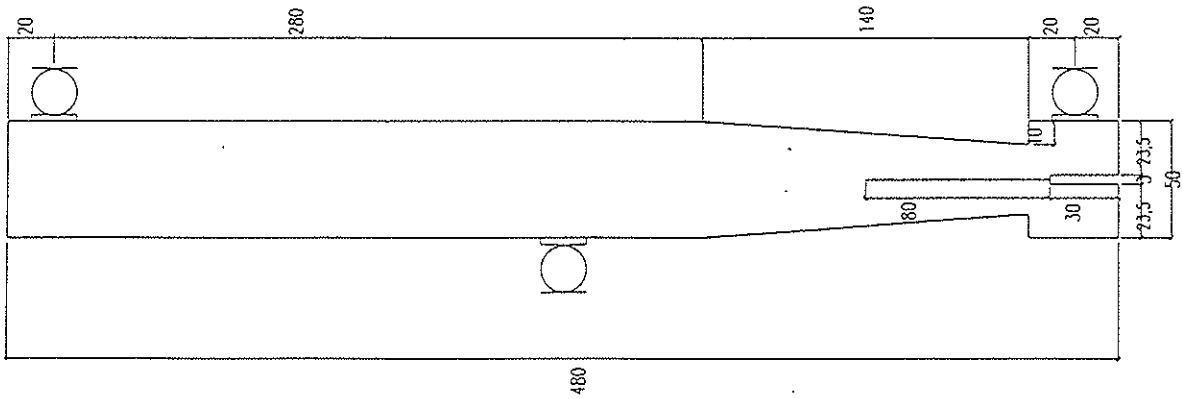

Figure 2. Geometry of LTENF specimen with dimensions as tested by Boström (1993).

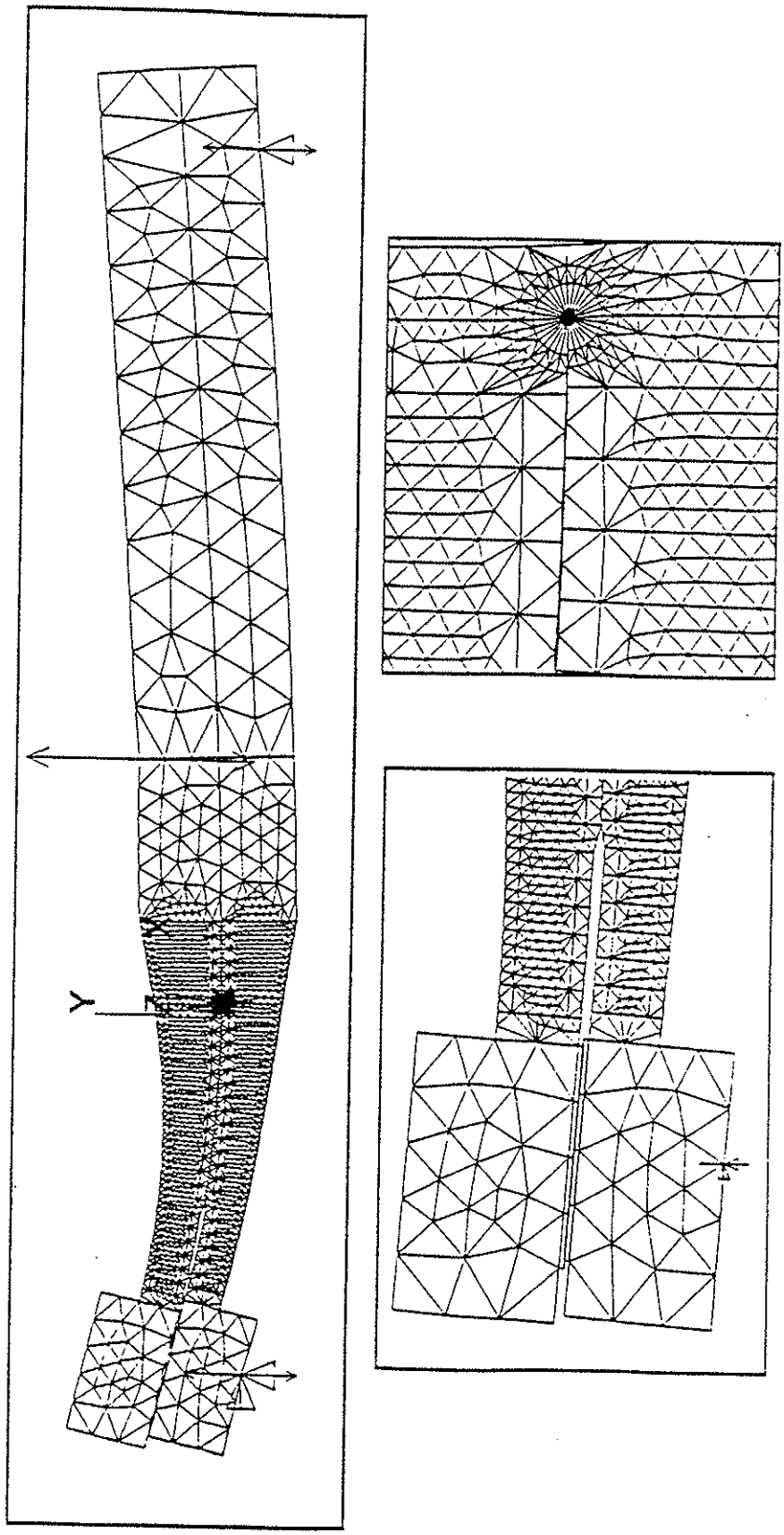

Figure 3. 2D finite element model of PTENF specimen with details of the deformed notch and crack tip. The deflections are magnified (Aicher and Gierl, 1994).

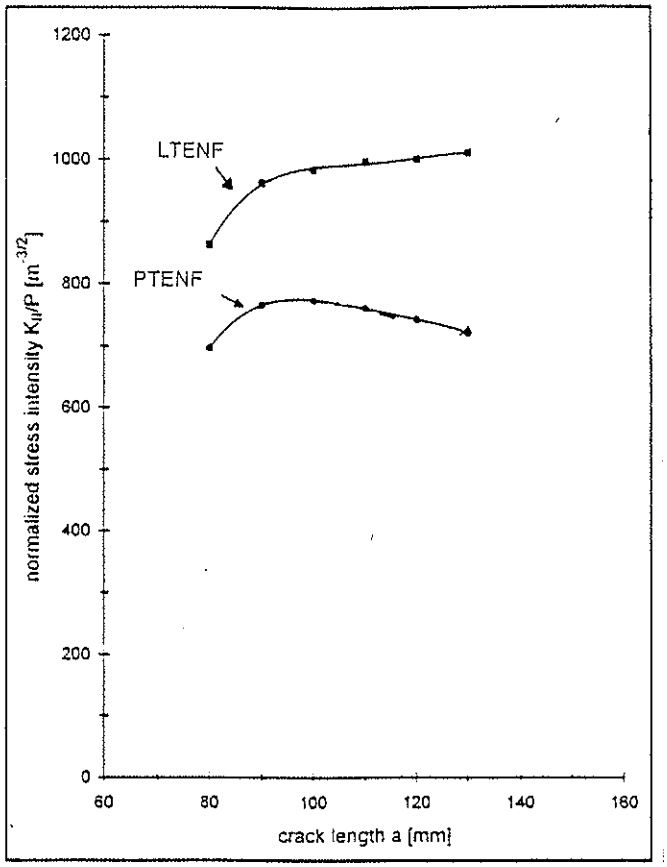

Figure 4. Stress intensity factor K_{II}/P and crack length for LTENF and PTENF (Aicher and Gierl, 1994).

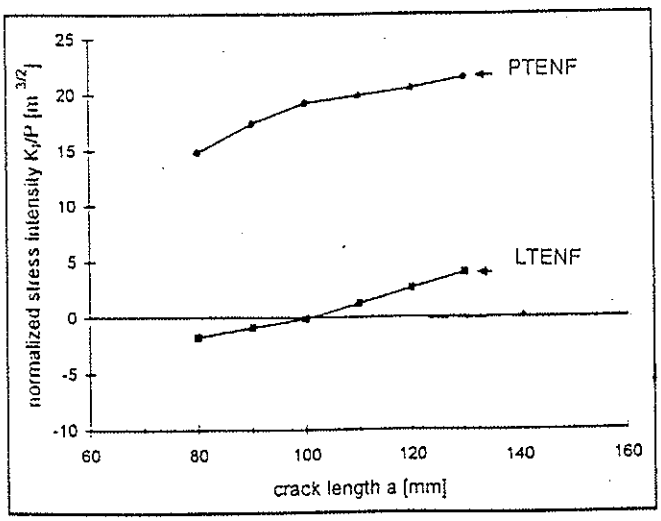

Figure 5. Stress intensity factor K_I/P and crack length for LTENF and PTENF (Aicher and Gierl, 1994).

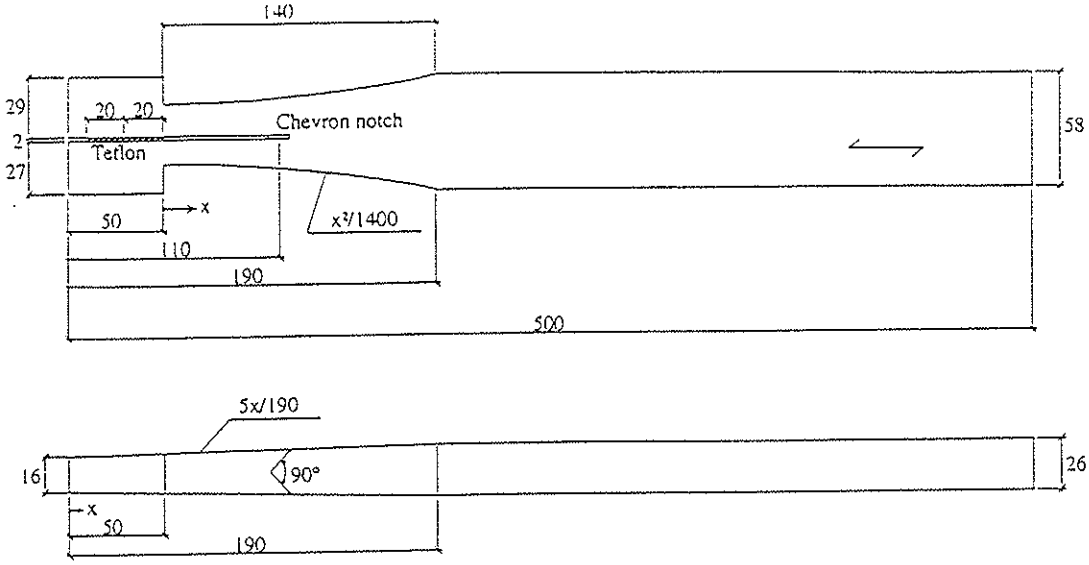

Geometry of the tapered end-notched flexure (TENF) beam. All values in mm.

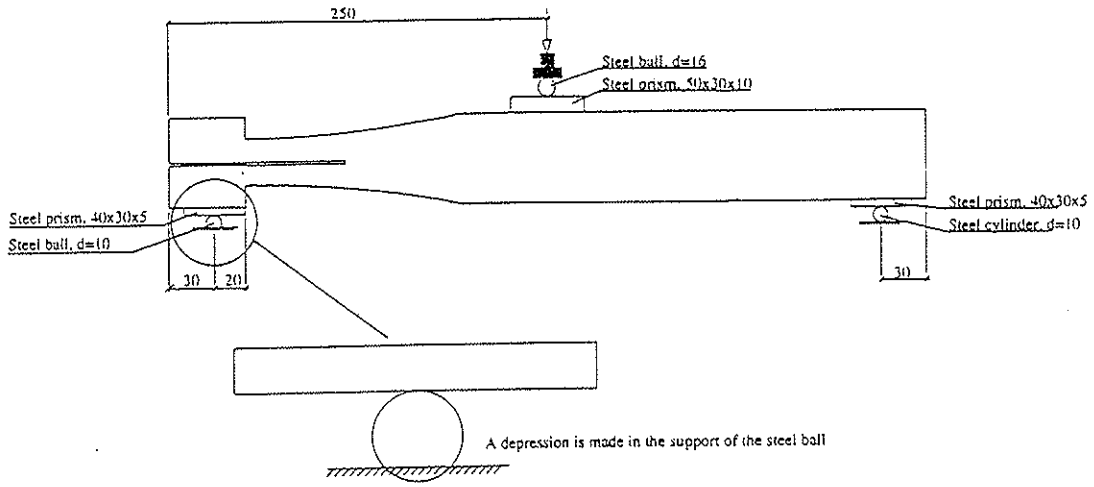

The simply supported test specimen is loaded at the midpoint.

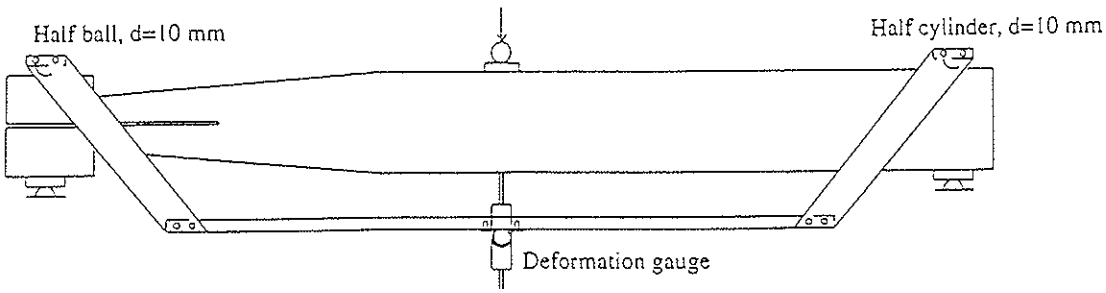

Cradle with deformation gauge for measurement of mid span deflection.

Figure 6. Geometry and loading arrangement for PTENF specimen (Boström, 1995).

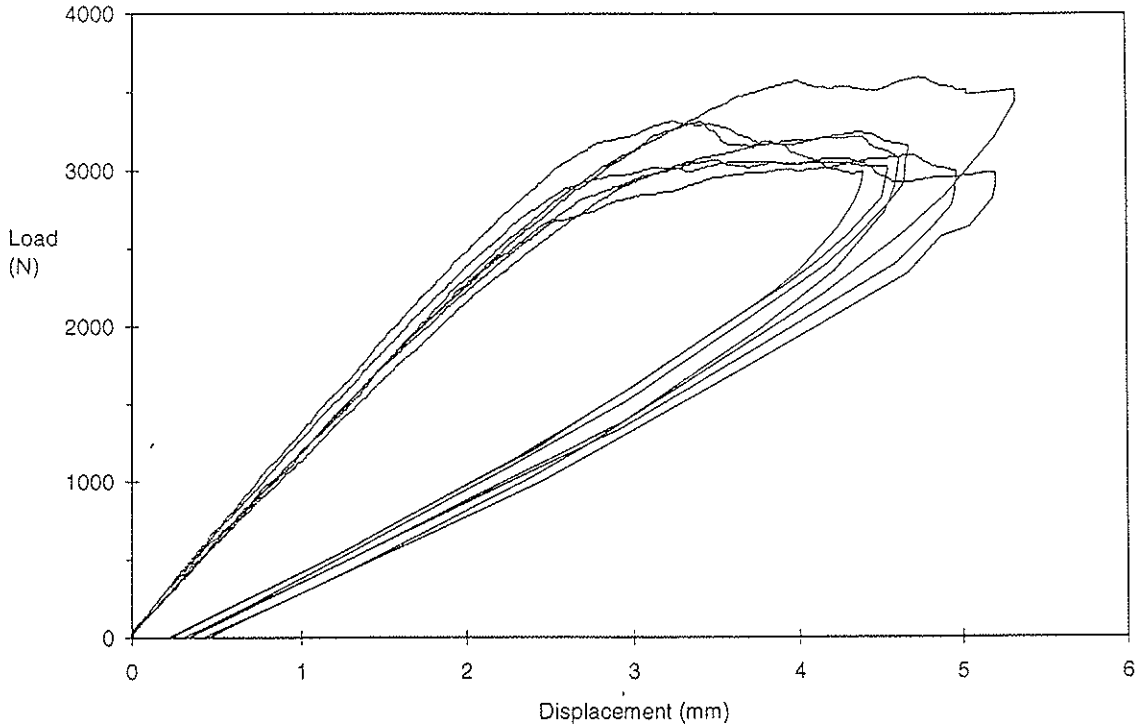

LTENF load-displacement curves from LRBB

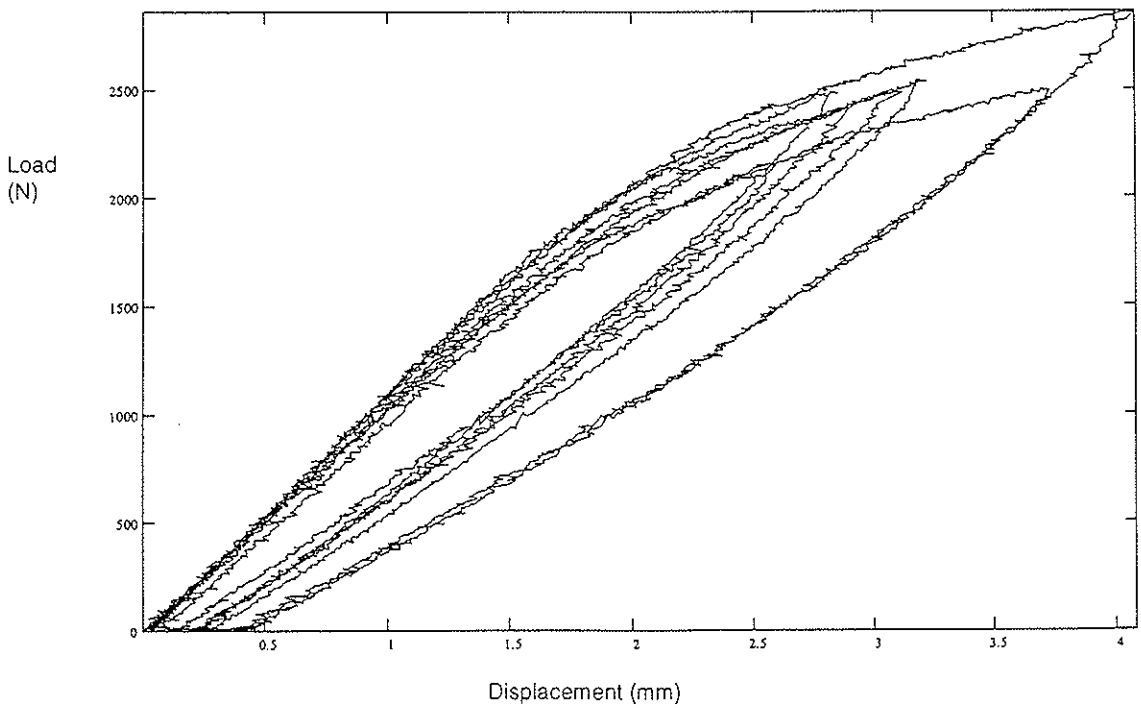

PTENF load-displacement curves from Bucks College

Figure 7. Examples of load-displacement curves.

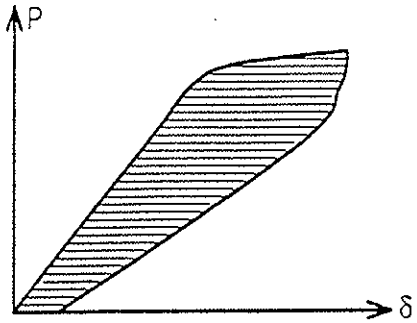

1 - Whole curve, G_F

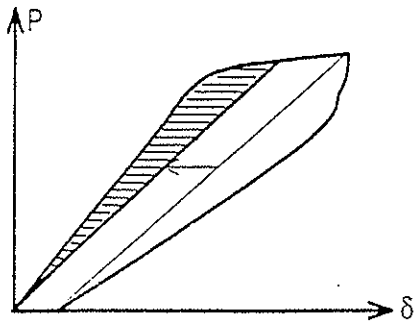

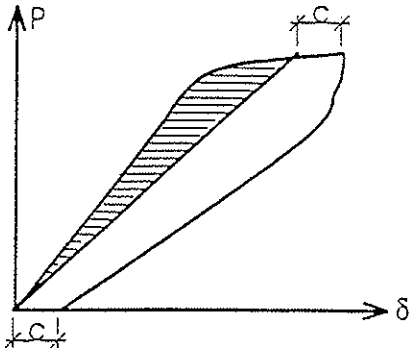

2 - Parallel movement of assumed second loading, G_F

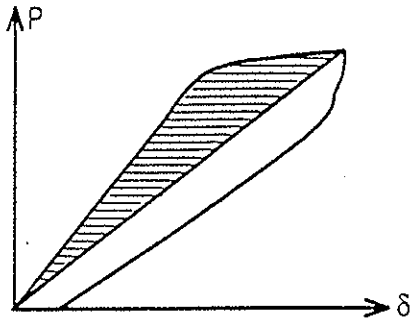

3 - Straight line from origin to maximum load, G_F

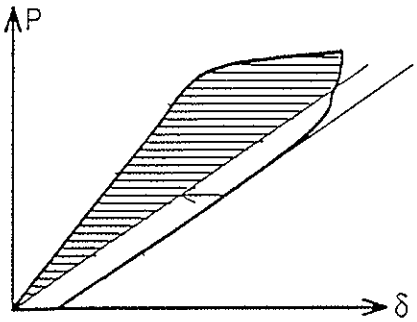

4 - Move slope from unloading branch, G_F

Figure 8. Methods to calculate fracture energy from the load-deflection curve (Boström, 1994).

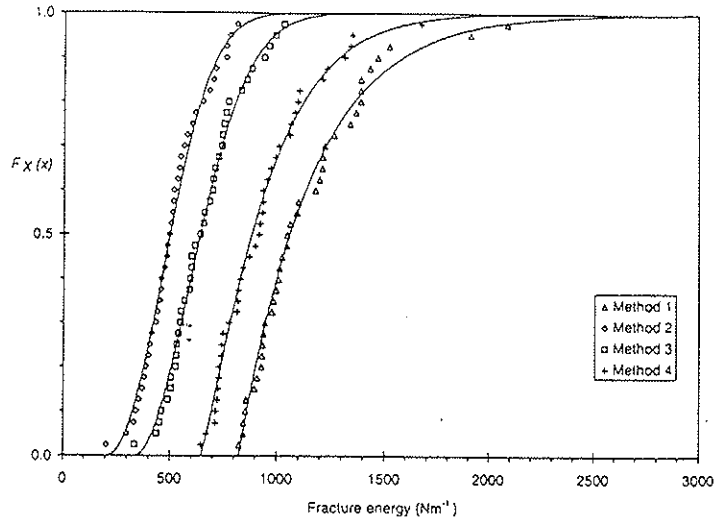

Cumulative Distribution Functions for LTENF

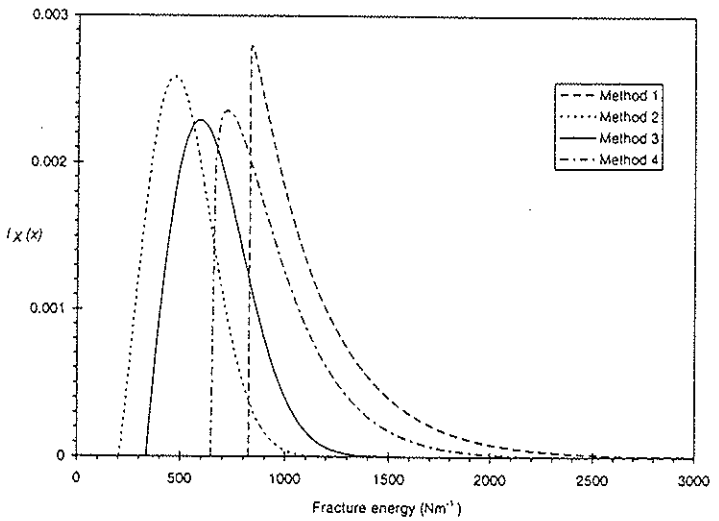

Probability Density Functions for LTENF

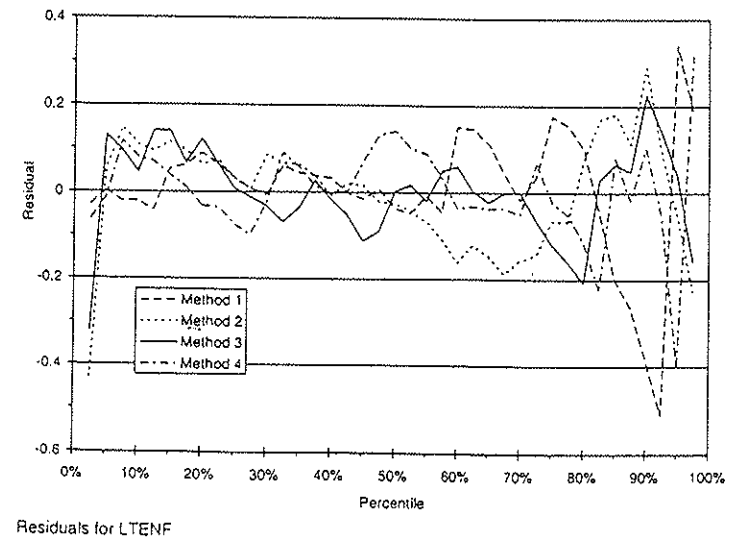

Residuals for LTENF

Figure 9. Cumulative distribution functions, probability density functions and residual plots for LTENF.

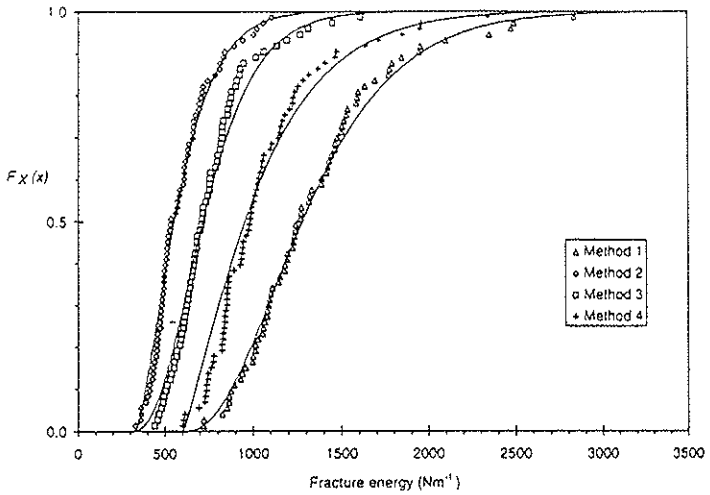

Cumulative Distribution Functions for PTENF

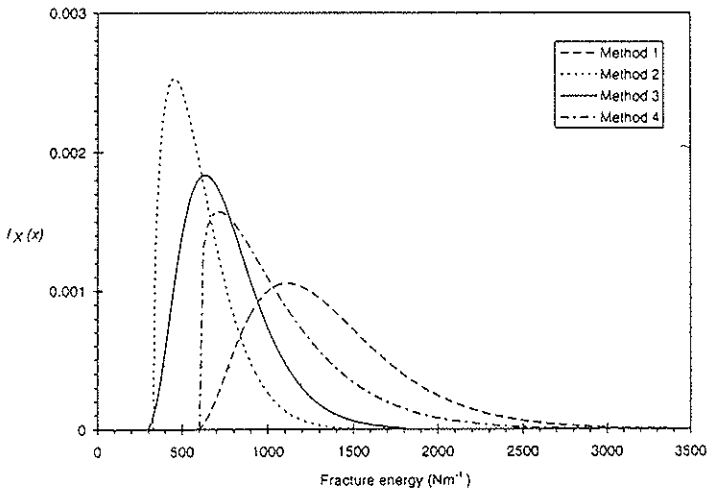

Probability Density Functions for PTENF

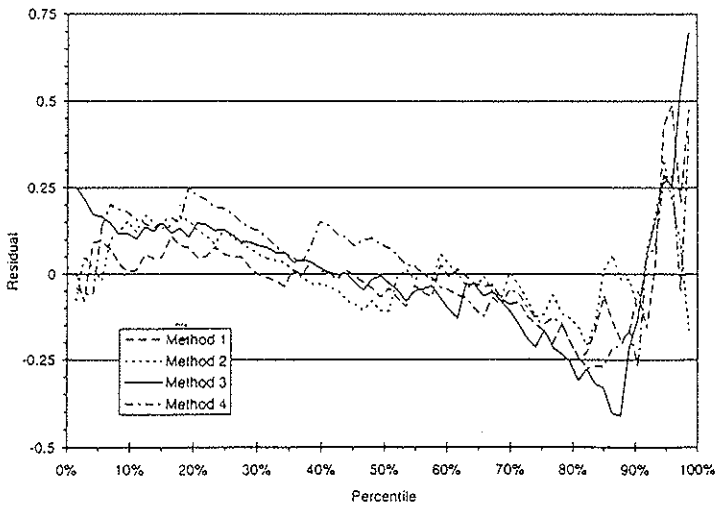

Residuals for PTENF

Figure 10. Cumulative distribution functions, probability density functions and residual plots for PTENF.

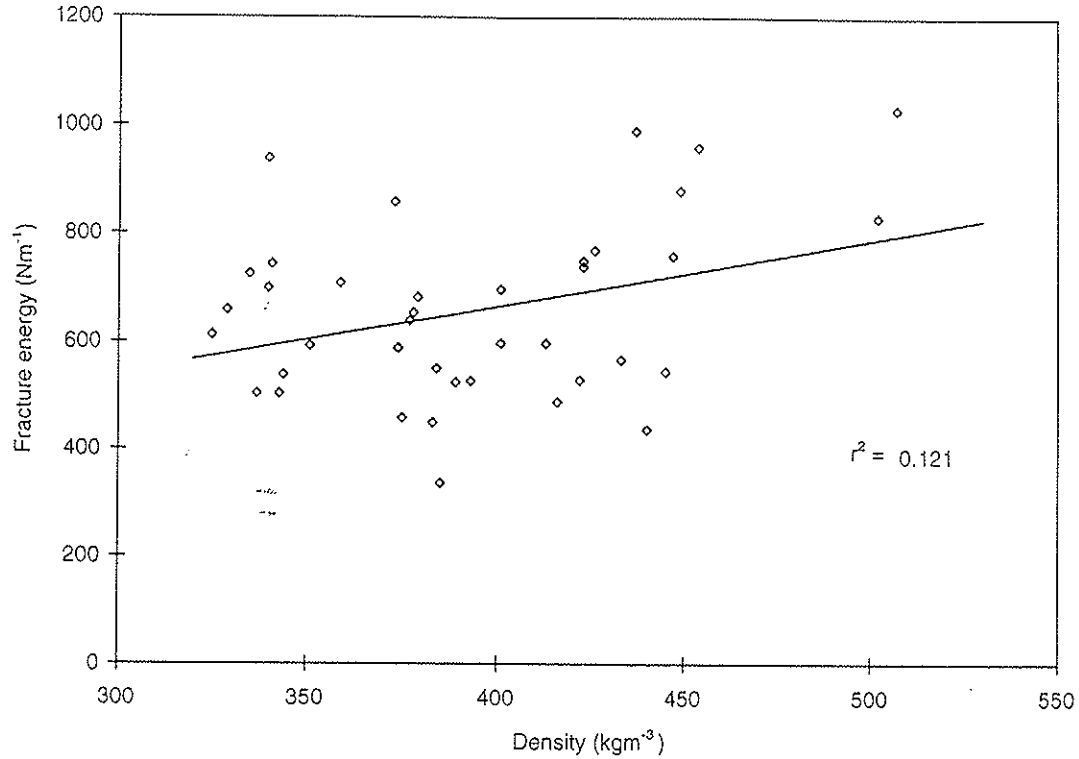

Density and Fracture Energy for LTENF

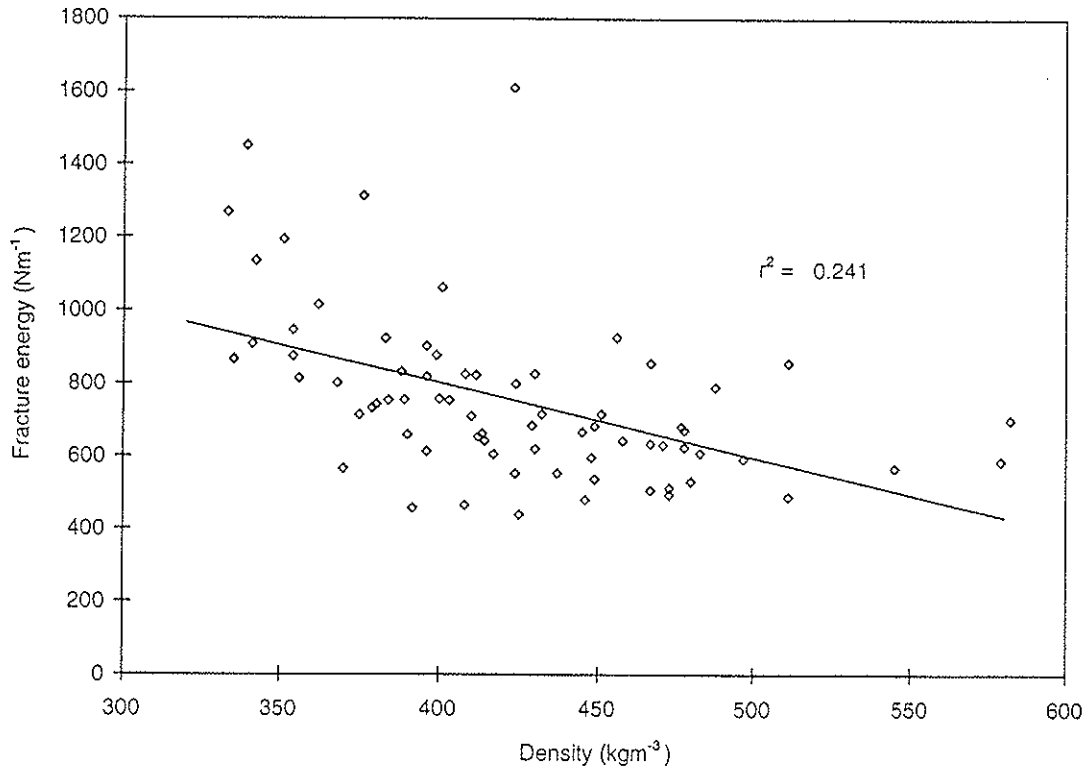

Density and Fracture Energy for PTENF

Figure 11. Dependence of fracture energy on density.

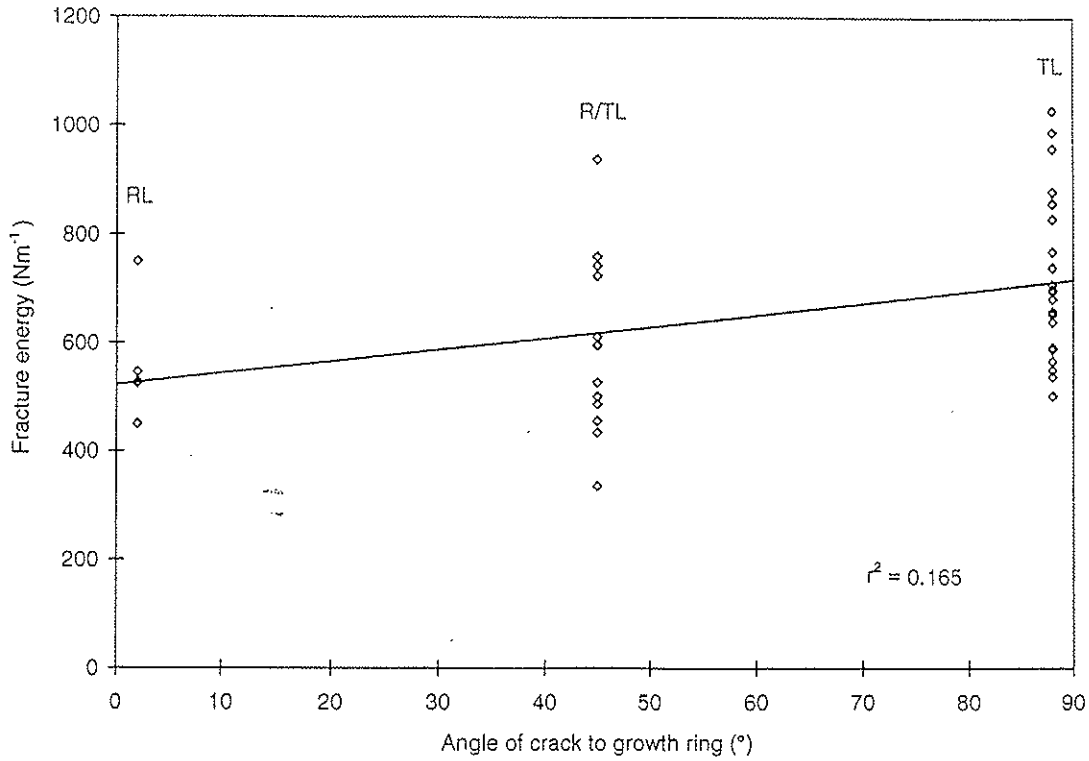

Crack Orientation and Fracture Energy for LTENF

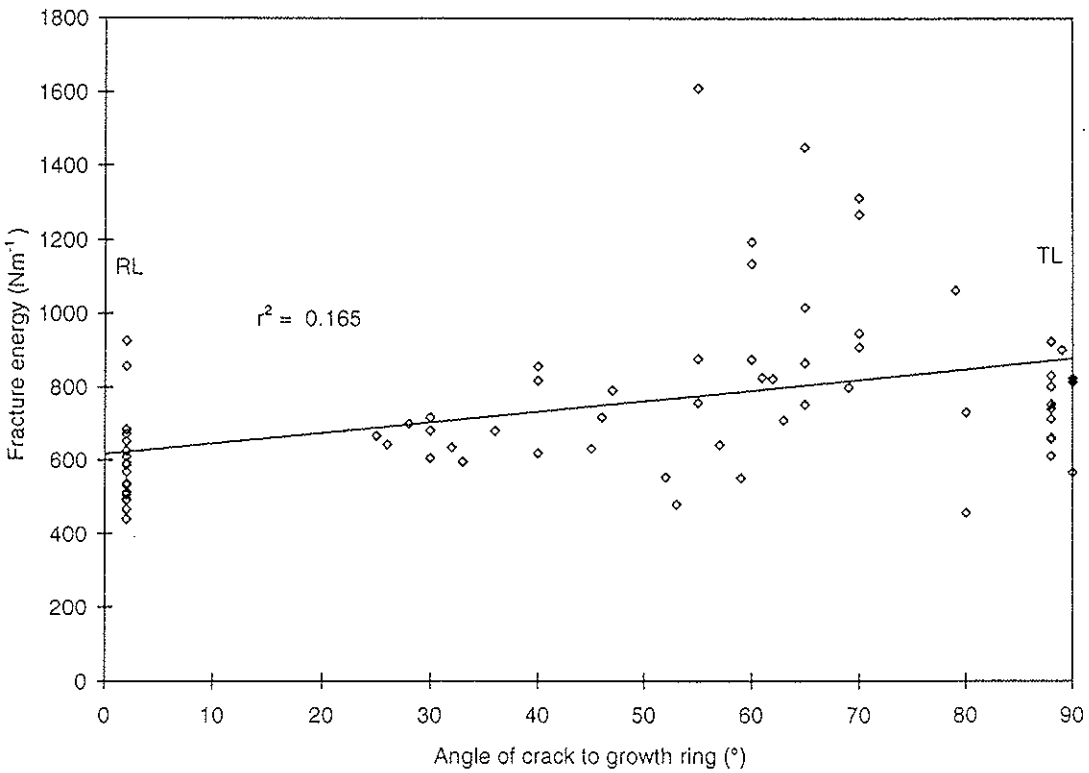

Crack Orientation and Fracture Energy for PTENF

Figure 12. Dependence of fracture energy on crack orientation.

CIB-W18/28-19-3

INTERNATIONAL COUNCIL FOR BUILDING RESEARCH STUDIES AND DOCUMENTATION

WORKING COMMISSION W18 - TIMBER STRUCTURES

FRACTURE DESIGN ANALYSIS OF WOODEN BEAMS WITH HOLES AND NOTCHES. FINITE ELEMENT ANALYSIS BASED ON ENERGY RELEASE RATE APPROACH

by

H Petersson
Lund Institute of Technology
Sweden

MEETING TWENTY - EIGHT

COPENHAGEN

DENMARK

APRIL 1995

Fracture design analysis of wooden beams with holes and notches

Finite element analysis based on energy release rate approach

Hans Petersson
Division of Structural Mechanics
Lund Institute of Technology/LUND UNIVERSITY
Box 118, S-221 00 Lund, Sweden

1 Introduction

One of the key issues dealing with structural design of timber structures is whether stress or fracture criteria should be used. It is obvious that in a number of cases a fracture design approach is to prefer, especially dealing with cracking caused by tensioning perpendicular to grain. In order to make the fracture mechanics approach to a realistic alternative for practical design in a broader sense, both simple hand calculation formulae [1] and standard procedures for robust finite element methods must be available. The basic idea is that the loadbearing capacity of the structure is traced by extending one or several hypothetical cracks. One of the benefits of such an approach is that the engineer better can estimate the influence of initial cracks in order to obtain a more reliable prediction of the failure load.

Different models may be used in design for fracture analysis of wooden structures, see [2] and [3]. One of the most promising models is based on an energy approach, and will be treated and applied in the following subsections [3]. It is often called the energy release rate approach, the compliance method or the virtual crack extension method. In the present study only linear elastic approximations are used for the material behaviour, and dynamic and nonlinear geometrical effects are not considered.

The prime material parameter to be used in the analysis is the fracture energy of wood in tension perpendicular to grain [4]. The influence of combined shear and tension on the fracture energy is considered by an empirical expression.

The wooden beam structures with notches and holes analysed are summarised in Figure 1 and more thoroughly described later on. Results from the analysis are given after description of the energy approach for crack analysis.

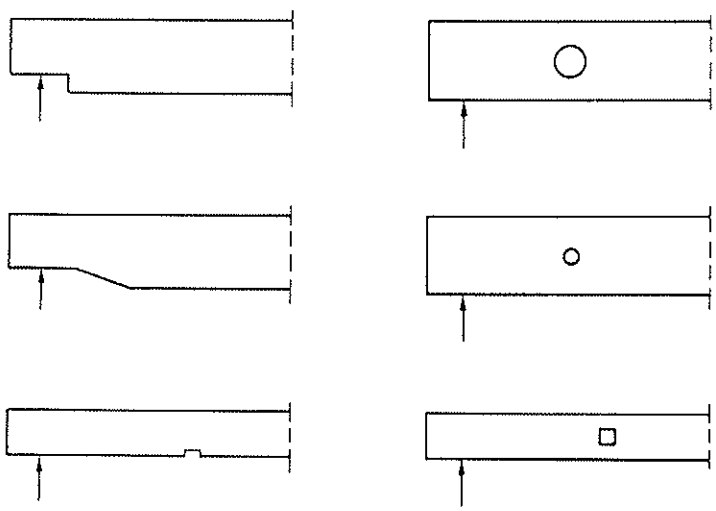

Figure 1 Types of beam structures studied [3]

2 Applied theory

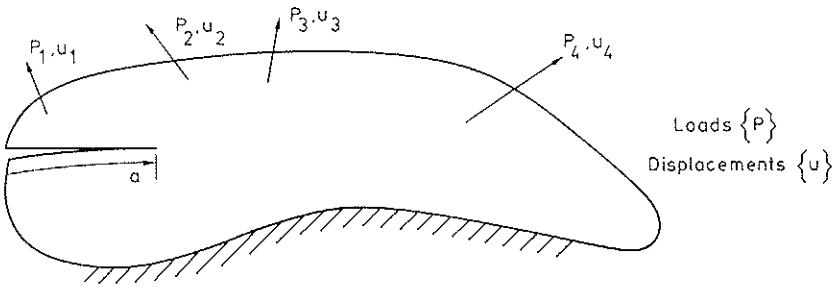

Figure 2 Two-dimensional body with a crack

Let us study the two-dimensional structure in Figure 2 with a set of constant reference loads $\{P\}$. Assume that the material is linear elastic and denote the associated displacements with $\{u\}$, where

$$\{P\} = \begin{bmatrix} P_1 \\ P_2 \\ \vdots \\ P_n \end{bmatrix} \quad \{u\} = \begin{bmatrix} u_1 \\ u_2 \\ \vdots \\ u_n \end{bmatrix} \tag{1}$$

Denote the crack length with a and the fracture energy per unit length with $b_c G_c$ where G_c is a material parameter. Then assume that the loads are increased proportionally, i.e. the actual loads are $\alpha\{P\}$ where α is gradually increased up to the value α_c, corresponding to stable or unstable crack growth. As the structure is linear elastic the corresponding displacements are $\alpha\{u\}$.

Let us now assume that the reference load $\{P\}$ and the load multiplication factor α are kept constant with respect to a variation of the crack length a. This gives us, for the critical value of $\alpha = \alpha_c$, that

$$\{P_c\} = \alpha_c\{P\} \tag{2}$$

$$\{u_c\} = \alpha_c\{u\} \tag{3}$$

According to [1] or [3], we may write

$$\alpha_c^2\{P\}^T \left\{\frac{du}{da}\right\} = 2\ b_c G_c \tag{4}$$

or

$$\alpha_c = \sqrt{\frac{2b_c G_c}{\{P\}^T \left\{\frac{du}{da}\right\}}} \tag{5}$$

This expression can be straightforwardly applied in finite element analysis.

In the numerical analysis the crack length a is gradually increased and for each value $a = a_i$ the corresponding displacements $\{u\}_i$ are calculated (for $i = 0, 1, 2, ...$). We introduce the notation

$$\Delta a_i = a_{i+1} - a_i \tag{6}$$

and obtain by a simple approximation

$$\alpha_{ci} = \sqrt{\frac{2b_c \Delta a_i G_c}{\{P\}^T(\{u\}_{i+1} - \{u\}_i)}} \qquad \text{for } a \approx \frac{a_{i+1} + a_i}{2} \tag{7}$$

In the finite element analysis presented in the following, low order elements were used in order to determine $\{u_i\}$. Only two-dimensional computations have been performed and where possible rectangular four-node elements were used. Plane stress state was assumed.

One difficulty in the analysis is that G_c is dependent on the mode of cracking. One suggestion for which value to choose for G_c is to estimate some average value of the ratio $\bar{\sigma}_\perp/\bar{\tau}$ between the normal and shear stresses (with respect to the crack plane in the cracking process zone), see Figure 3. In a finite element analysis an evaluation of the nodal forces from the individual elements close to the crack tip can give a reasonable estimate of the mixed mode state. An illustration is given by Figure 4, where the summations for elements ⓘ,ⓙ and ⓚ and elements ⓛ, ⓜ and ⓝ give identical results except for the sign. By this approach we may write

$$\frac{\sigma_\perp}{\tau} \approx \frac{\sum\limits_s P_{ys}}{\sum\limits_s P_{xs}} \tag{8}$$

after a summation over, for example, elements ⓛ, ⓜ and ⓝ.

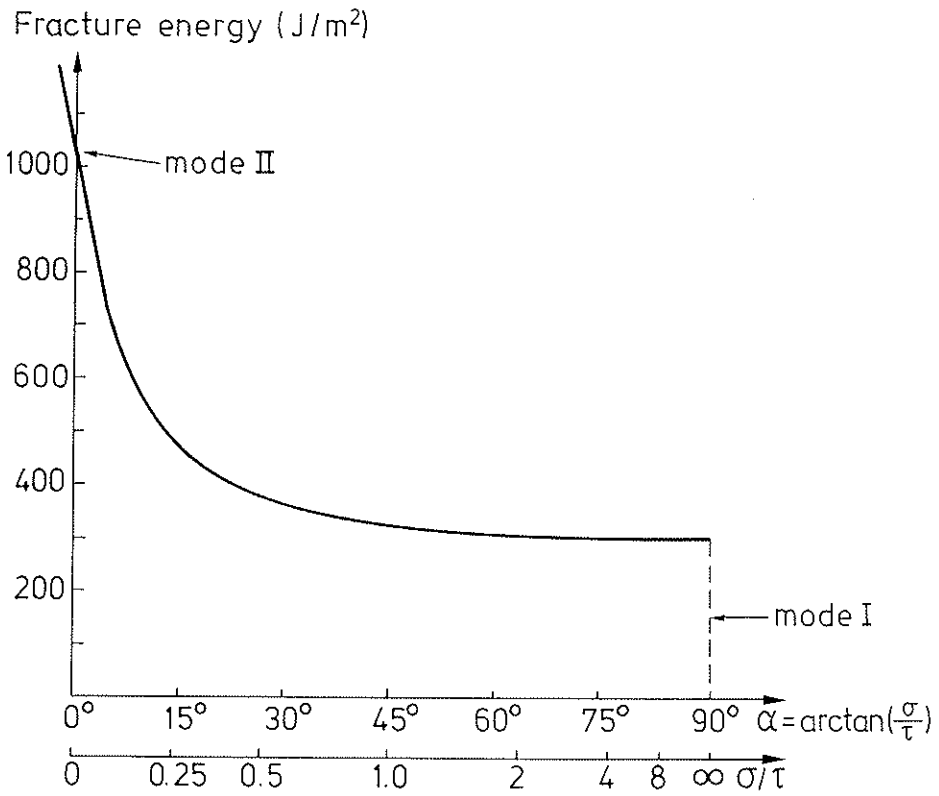

Figure 3 Fracture criterion for mixed mode

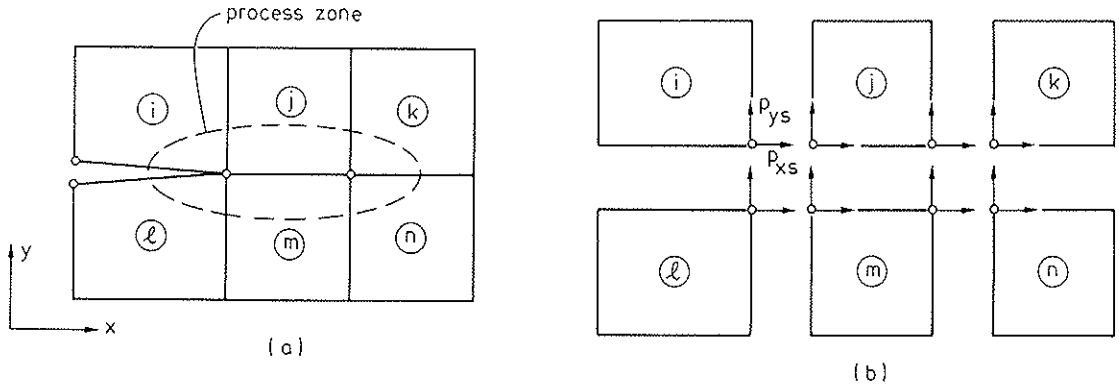

Figure 4 Nodal element forces close to cracking process zone.
(a) assembly of elements
(b) individual elements

A reasonable suggestion for the relation between G_c and $\bar{\sigma}_\perp/\bar{\tau}$ is derived in [3] and shown in Figure 3. The relation is somewhat complex,

$$G_c = \frac{1}{a}\left[1 + \frac{b^2}{2a}(1 - \sqrt{1 + \frac{4a}{b^2}})\right] \tag{9}$$

where

$$a = \frac{1-\kappa^2}{G_{IIc}} \tag{10}$$

$$b^2 = \frac{\kappa}{G_{Ic}} \tag{11}$$

and

$$\kappa^2 = \frac{1}{1 + \sqrt{\frac{E_\perp}{E_\parallel}}\left(\frac{\bar{\tau}}{\bar{\sigma}}\right)^2} \tag{12}$$

3 Numerical results

The material data used in the analysis are given in Figure 5 except for the value of G_c in mixed mode, where the expressions according to Eqs. (9) and (12) are applied.

Stiffness	
$E_\parallel = 12000$ MPa	$E_\perp = \frac{1}{30}E_\parallel$
	$G = \frac{1}{16}E_\parallel$
	$\nu_{\perp,\parallel} = 0.015$ (0.0)
Fracture energy	
G_{Ic} =300 J/m^2	G_{IIc} =3.5 G_{Ic}

Figure 5. Material data used in analysis

Six different geometries are analysed, see Figure 6. The results from the finite element calculations are based on meshes with about 100 elements in the depth direction for beam parts with the finest subdivision.

Calculations have been performed for different values of the fracture energy. G_c is set to G_{Ic}, G_{c6mm}, G_{c12mm} ..., respectively, where for example G_{c6mm} means that the ratio $\bar{\sigma}/\bar{\tau}$ in Eq. (8) is based on a summation over a length of 6 mm.

Results are presented in Figures 7 to 12. In each figure the finite element mesh used is shown at the top. Then the relation between the crack load V_f at support and the initial crack length are given for the beam depth $h = 0.095$m and $h = 0.6$m.

The problem in design will often be to choose a proper initial crack when determining the load-bearing capacity, see especially Figure 8.

The much higher values of V_f obtained for very small initial crack lengths is of minor interest to study as longer initial crack lengths must be considered in practice. Further, the assumptions applied in linear elastic fracture mechanics will probably lead to crude approximations in the studied examples when the initial crack lengths are very small.

The influence of mixed mode seems to be modest in almost all of the cases studied, at least for reasonable design values of the initial crack length (say between 6mm and 50mm for the examples studied).

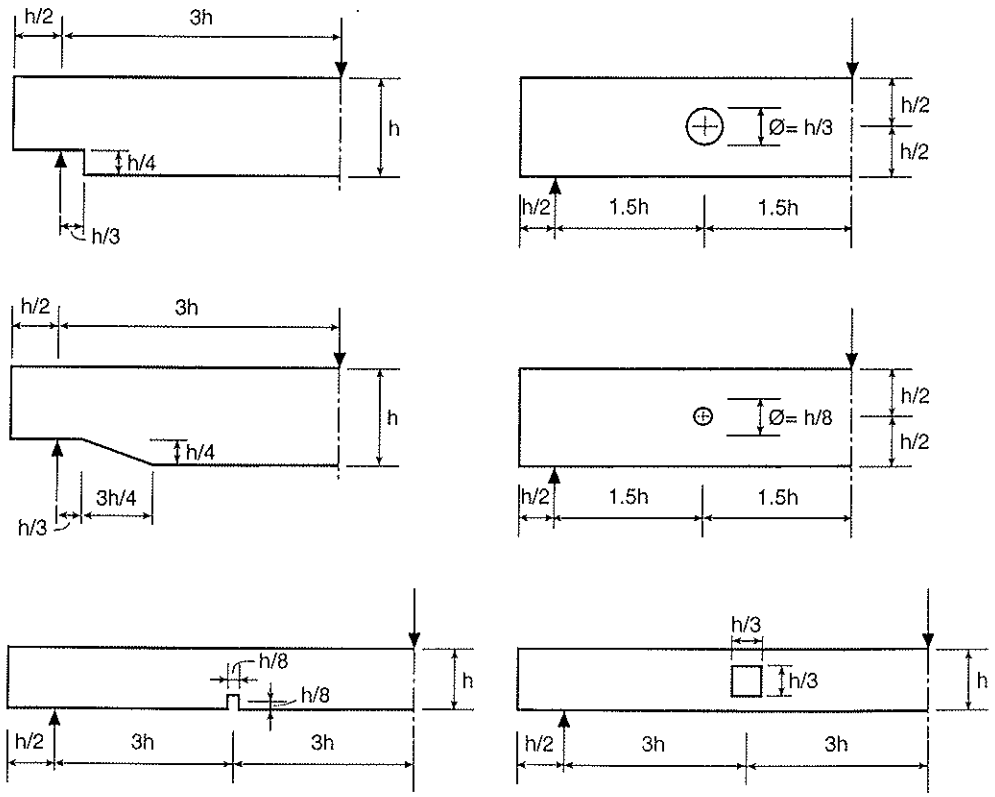

Figure 6 Beams with holes and notches [3]
Two different dimensions are treated
Alternative 1: $h = 0.095$ m and $b = 0.045$ m
Alternative 2: $h = 0.600$ m and $b = 0.120$ m

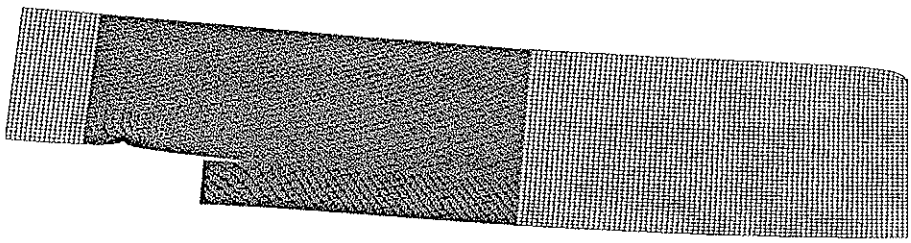

Deformed finite element mesh

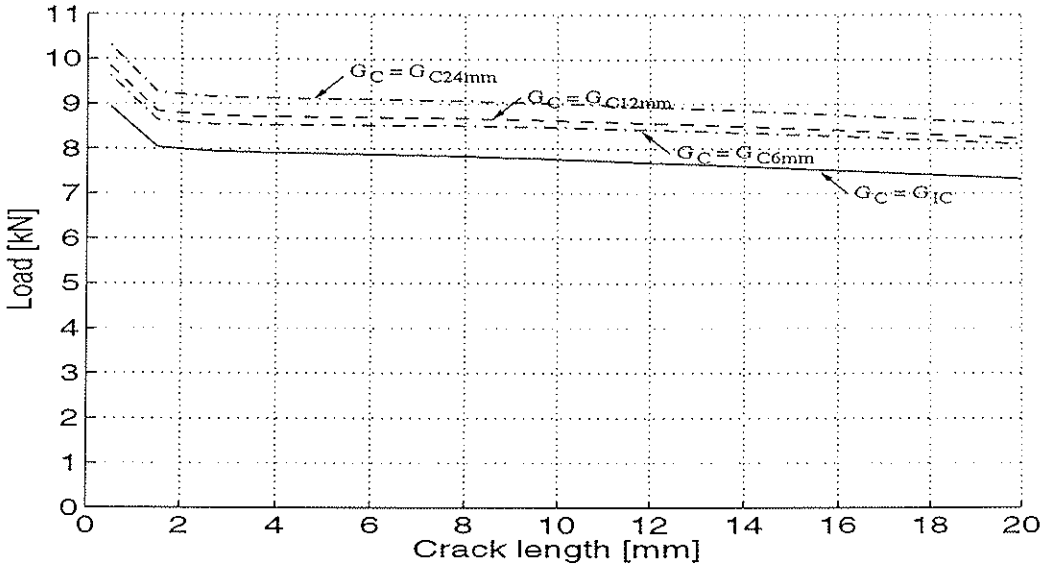

Notched beam with h=95 mm

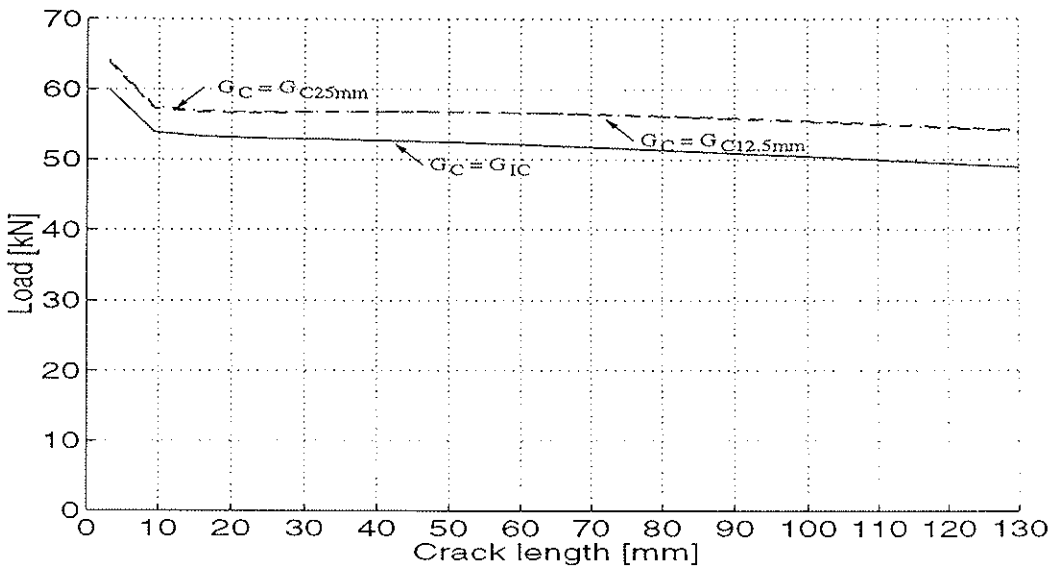

Notched beam with h=600 mm

Figure 7 Relation between crack load and crack length.

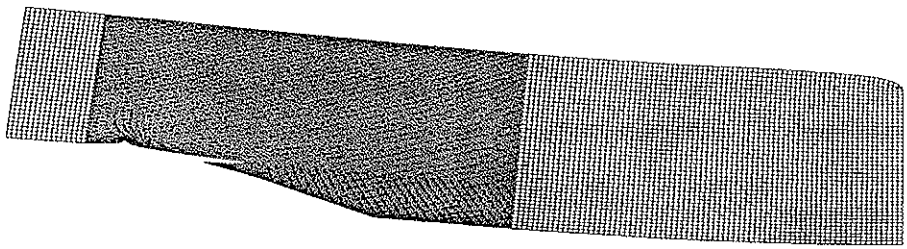

Deformed finite element mesh

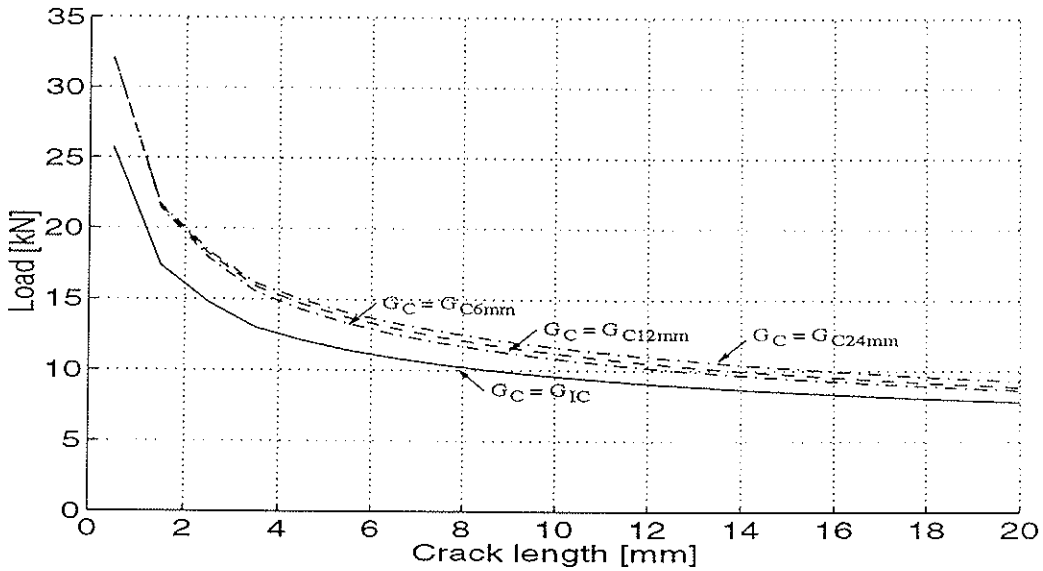

Notched beam with h=95 mm

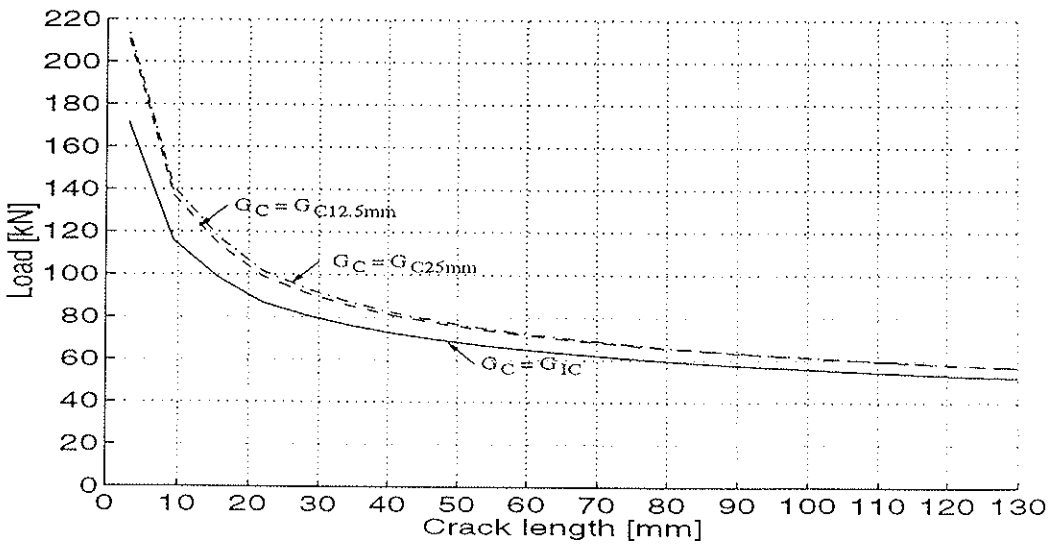

Notched beam with h=600 mm

Figure 8 Relation between crack load and crack length.

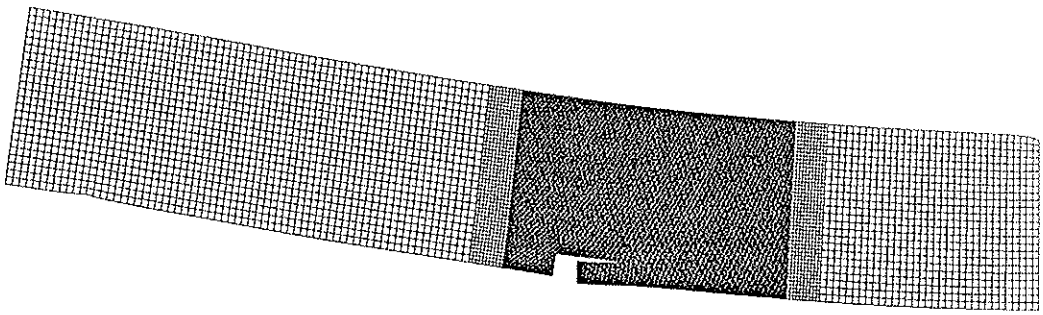

Deformed finite element mesh

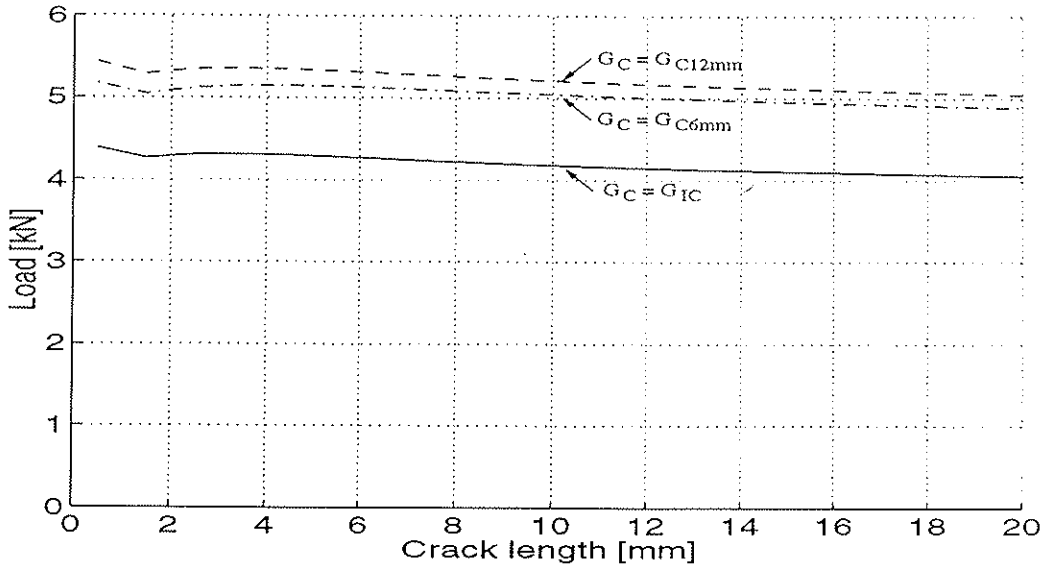

Notched beam with h=95 mm

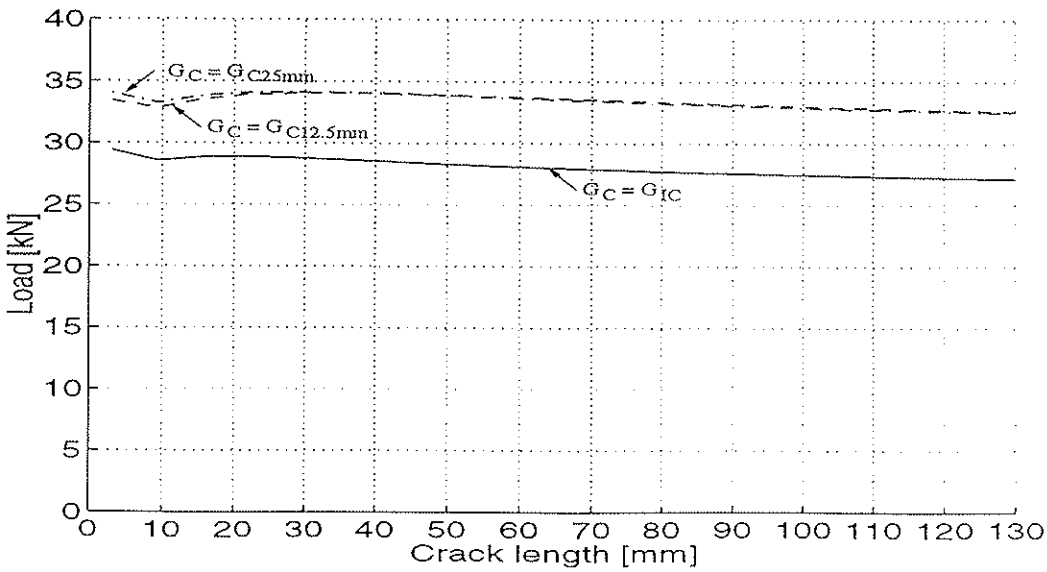

Notched beam with h=600 mm

Figure 9 Relation between crack load and crack length.

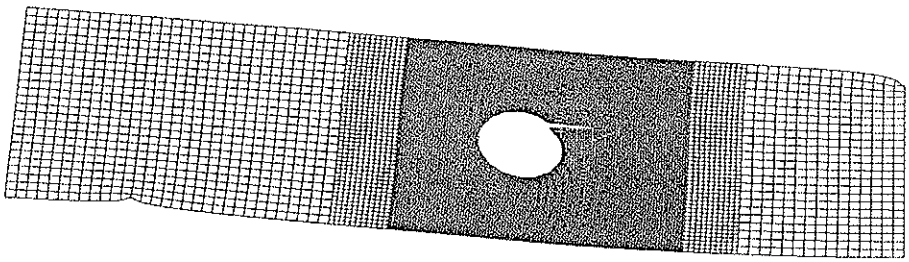

Deformed finite element mesh

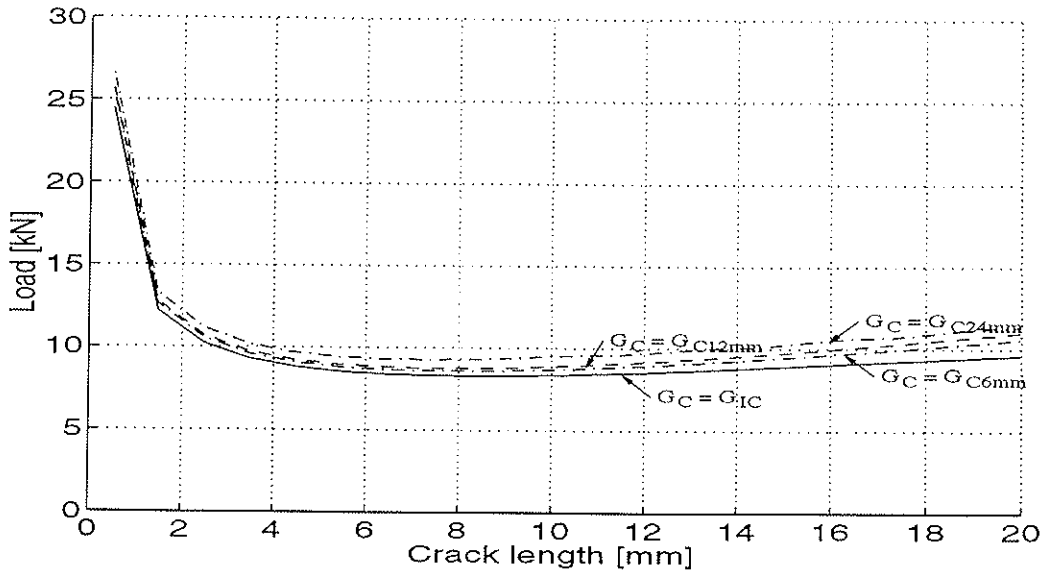

Beam with circular hole, h=95 mm, Ø=h/3

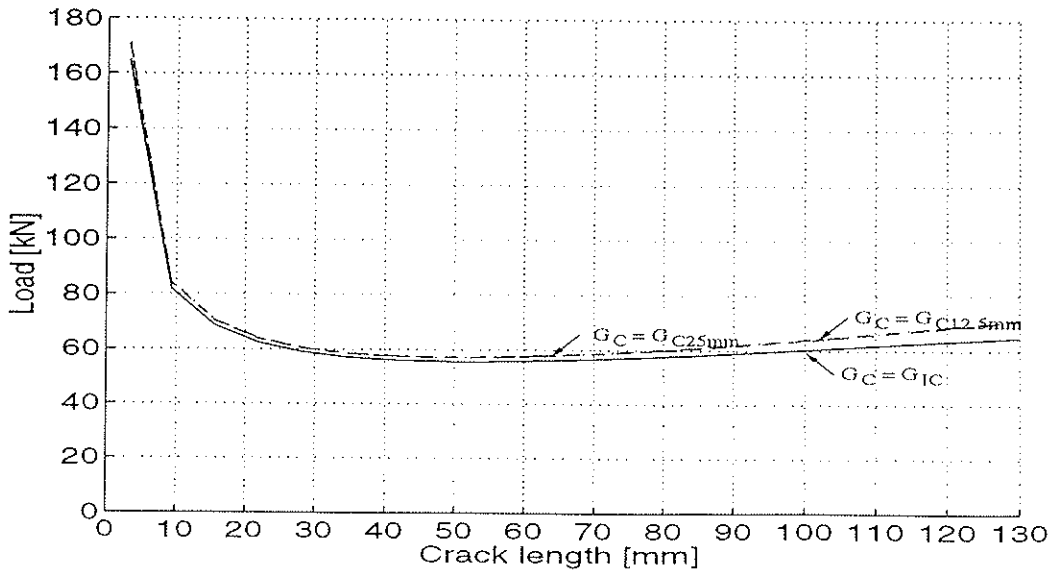

Beam with circular hole, h=600 mm, Ø=h/3

Figure 10 Relation between crack load and crack length.

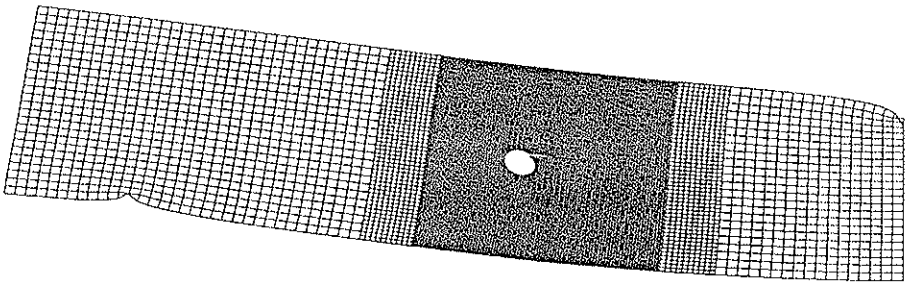

Deformed finite element mesh

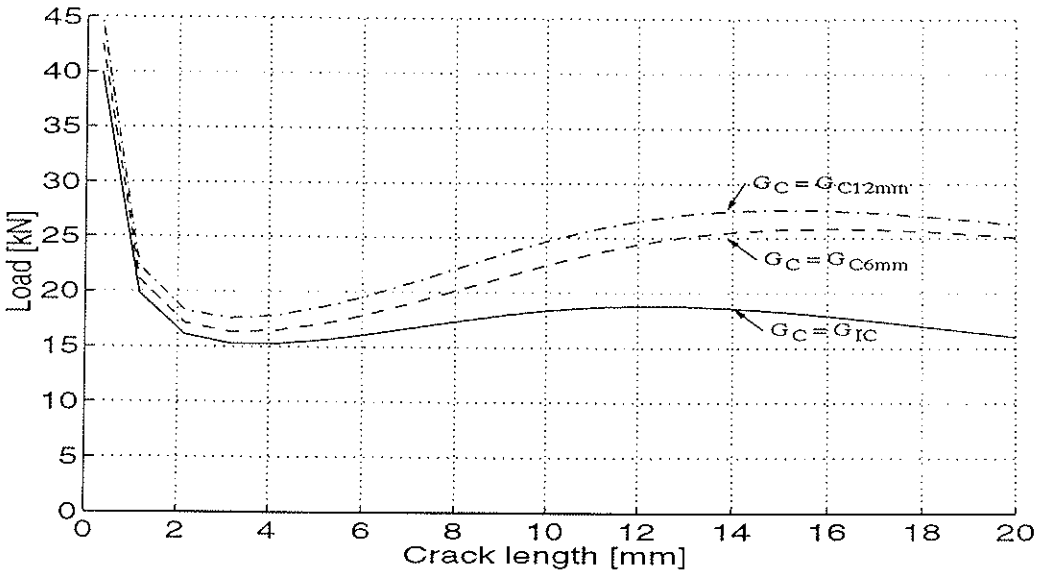

Beam with circular hole, h=95 mm, Ø=h/8

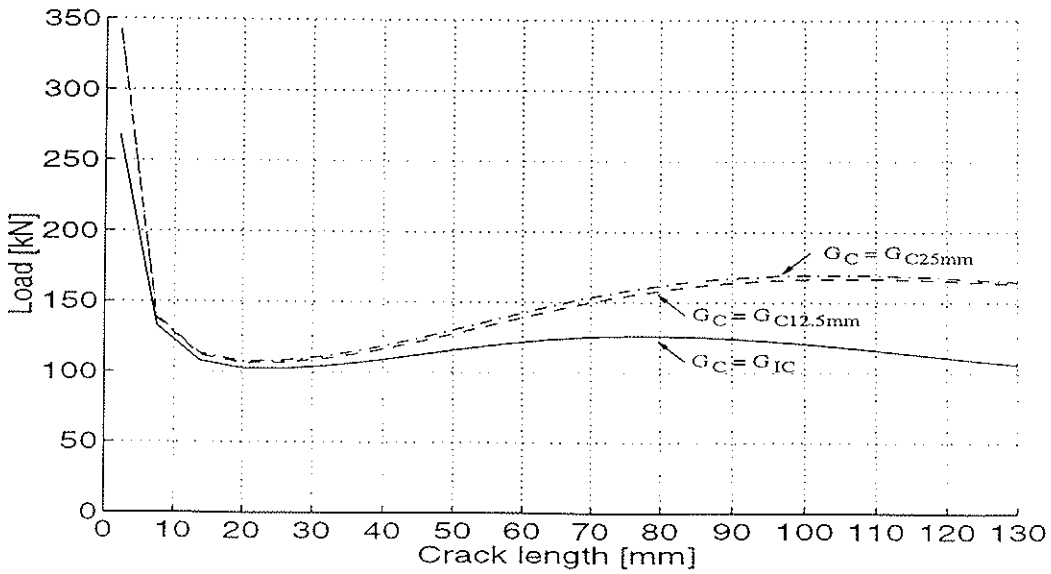

Beam with circular hole, h=600 mm, Ø=h/8

Figure 11 Relation between crack load and crack length.

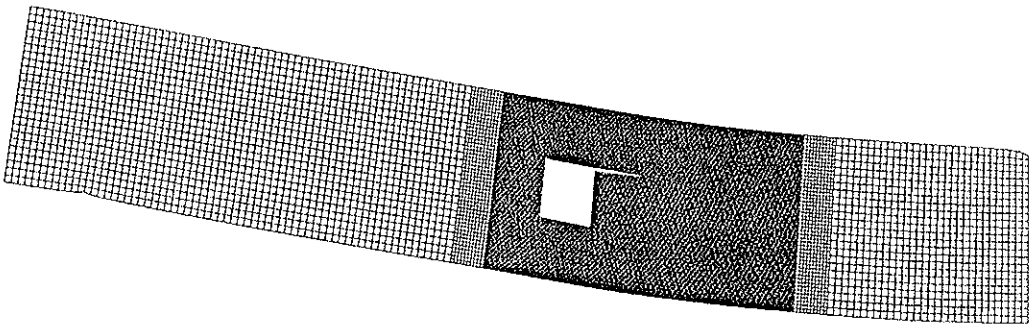

Deformed finite element mesh

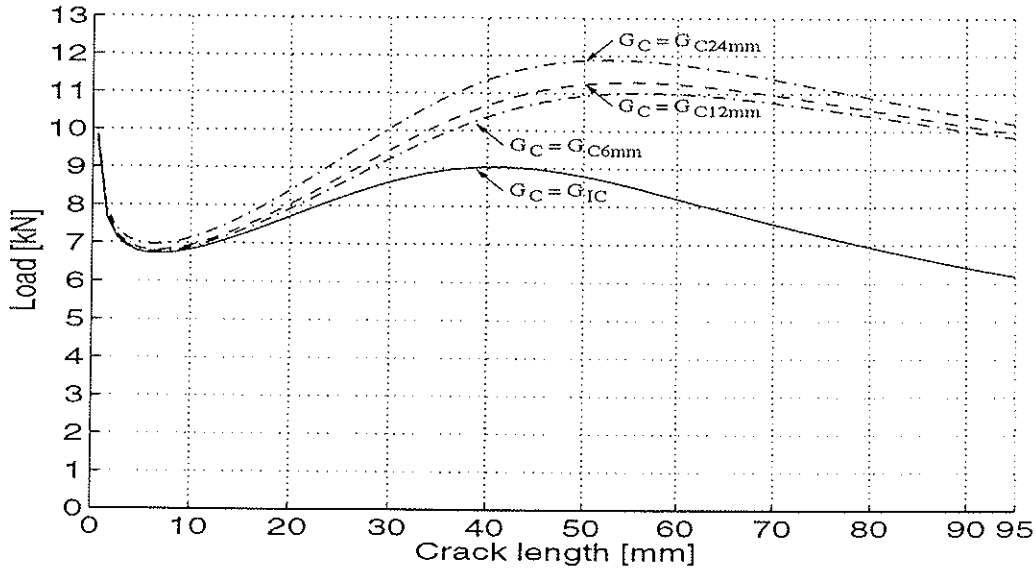

Beam with quadratic hole, h=95 mm

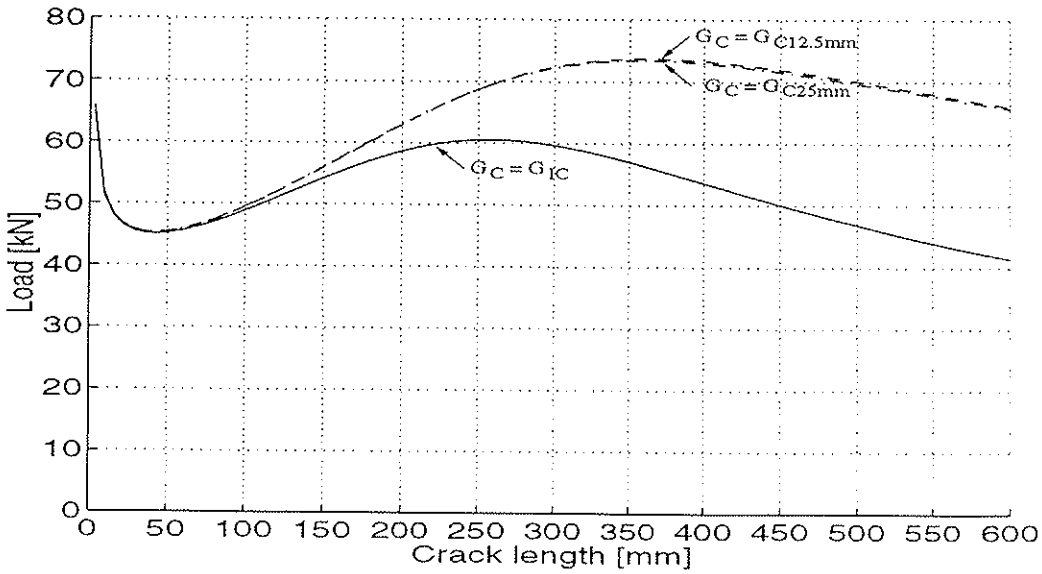

Beam with quadratic hole, h=600 mm

Figure 12 Relation between crack load and crack length.

4 Concluding remarks

It is obvious that the choice of a proper initial crack length at a notch or a hole is of importance in practical design. Such cracks must be considered unless some kind of reinforcement is provided. It seems reasonable to choose the design value for the initial crack length in different ways depending on the curve shape of the calculated relation between the crack load and the crack length, see Figures 7 to 12.

In Table 1 an attempt is made to estimate a reasonable value of the initial crack length a_o to be used for determining the support load V_f in the studied examples. It is interesting to observe that the differences of V_f based on $G_c = G_{Ic}$ and $G_c = G_{c12mm}$ are small, which clearly indicate that G_{Ic} is the prime fracture material parameter to be used in design.

From a computation point of view it is of interest to compare the results for relative coarse meshes with those for much finer meshes. As shown in [3] the results are quite mesh-independent. Thus, by use of an energy release rate approach reasonable good results will normally be obtained even with a relatively coarse mesh in the finite element analysis.

A interesting observation from a design point of view is that the load-bearing capacity according to Table 1 is almost proportional to $b\sqrt{h}$ instead of the cross sectional area bh normally expected. The load ratio relating to $h = 0.095$ m and $h = 0.600$ m

$$\frac{120}{45}\sqrt{\frac{600}{95}} = 6.70$$

is thus in good agreement with the corresponding ratios that can be obtained from the results shown in Table 1.

Geometry	h (mm)	a_0 (mm) FEM	V_f (kN) $G_c = G_{Ic}$	V_f (kN) $G_c = G_{c12mm}$
	95	6	7.9	8.7
	600	10	53.9	57.2
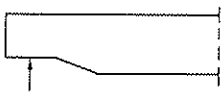	95	6	11.1	13.4
	600	30	79.5	89.6
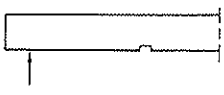	95	6	4.3	5.3
	600	10	28.6	32.9
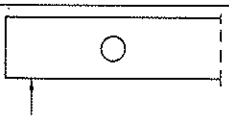	95	6	8.4	8.9
	600	40	56.2	57.6
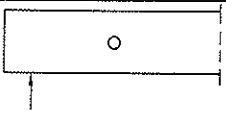	95	4	15.3	17.8
	600	20	102.5	106.3
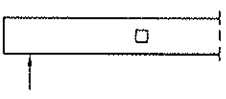	95	6	6.7	6.8
	600	40	45.1	45.3

Table 1. Estimated values for design of initial crack length a_0 and crack load V_f based on Figures 7 to 12

5 References

[1] Petersson, H: On design criteria for tension perpendicular to grain, CIB-W18/ 25-6-4, Åhus, Sweden 1992.

[2] Valentin, G.H. et al.: Application of fracture mechanics to timber structures. RILEM state-of-the-art report, Technical Research Centre of Finland, Research Notes No. 1262, Espoo Finland 1991.

[3] Gustafsson, P.J. (editor): RILEM (TC 133–TF) technical report - Timber fracture mechanics model for strength analysis of beams (in preparation)

[4] Larsen, H.J. and Gustafsson, P.J.: Fracture energy of wood in tension perpendicular to the grain. CIB-W18/23, Lisbon 1990.

Acknowledgements

Johan Gullander's assistance in carrying out a substantial part of the numerical calculations is gratefully acknowledged.

CIB-W18/28-19-4

INTERNATIONAL COUNCIL FOR BUILDING RESEARCH STUDIES AND DOCUMENTATION

WORKING COMMISSION W18 - TIMBER STRUCTURES

DESIGN OF TIMBER BEAMS WITH HOLES BY MEANS OF FRACTURE MECHANICS

by

S Aicher

J Schmidt

S Brunold

FMPA Baden-Württemberg

Germany

MEETING TWENTY - EIGHT

COPENHAGEN

DENMARK

Design of timber beams with holes by means of fracture mechanics

Aicher, S., Schmidt, J., Brunold, S.

FMPA Baden-Württemberg, – Otto-Graf-Institute –, Pfaffenwaldring 4, Stuttgart

1 Introduction

The incorporation of holes with varying geometries and sizes in timber beams especially in glulam members in order to provide space for electrical, sanitary or heating tubes is a often occurring demand in building practice. At present there are no design guide rules for holes in EC 5 what must be overcome to ensure competitiveness of timber structures in some important fields.

At the contour of rectangular or round holes stress singularities resp. stress concentrations occur which can impose considerable design problems depending strongly on the material used. A ductile material, such as steel, is rather intensitive to notches or other geometric discontinuities as stress concentrations are smoothed by plastic strains where a large amount of energy is consumed. Brittle materials however, such as wood especially in tension perpendicular and shear parallel to grain, have only very little possibility for strain energy redistribution. Such a material resp. structure in general will fail due to a fracture mechanics governed process of crack initiation and propagation.

There has been quite a lot of investigations in the past dealing with holes in timber beams; the results have led to several design recommendation in different countries. Important works, both theoretically, based on strength of materials design approches, and experimentally have been contributed i.a. by [1], [2], [3]. Recently, application of fracture mechanics to the problem was studied by several authors [4], [5], [6]. This paper reports on some of the work conducted within the framework of a recently finished Technical Committee of RILEM "Fracture of timber" (TC 133), where one part of the work was dedicated to strength analysis of timber beams with holes by means of different fracture mechanics models.

2 Fracture mechanics concept

2.1 Design crack approach

Structures suitably designed by means of fracture mechanics incorporate stress singularities and are built of a brittle material. Obviously easy to handle are structures with distinct single or multiple cracks of defined dimension. However, in many real structures no singularities exist in the perfect state, so in case of beams with round holes or with rectangular openings which in general have rounded corners. The singularities here are confined to the imperfect state of the structures where existing micro cracks in the material develop to minor or medium size cracks due to local stress concentrations from exterior loads and climate caused eigenstresses. The sizes and to a lesser extent the locations of the cracks are unknown what founds the probabilistic nature of the problem.

A suitable way to examine and design such structures is the design crack approach where the load carrying capacity is traced depending on one or several extending hypothetic cracks. Then, considerations based on sound engineering sense or better probability have to be applied to the judgement of the crack length in order to find a reliable design load. Obviously these considerations depend largely on the function of the generalized stress intensity factor or strain energy release rate $\overline{K}$, $\overline{G}$ vs. crack length. The expressions »generalized K or G values« mean that the mixed mode quantities K_i, G_i (i = I, II, III) are summarized in one idealized term $\overline{K}$, $\overline{G}$, which is compared to the equally idealized material resistances $\overline{K_c}$, $\overline{G_c}$.

2.2 Structure response vs. crack elongation

Structures can show completely different functions of $\overline{K}$ (or $\overline{G}$) and corresponding ultimate loads with increasing crack lengths (dead load conditions). Fig. 1 gives a typical example of a simple structure with steadily increasing $\overline{K}$-values and hence generally steeply decreasing ultimate loads, as conditions for instable crack growth

$$G(a) = \overline{G_c} \quad , \qquad \frac{\partial G(a)}{\partial a} > 0 \quad . \tag{1a, b}$$

are fulfilled.

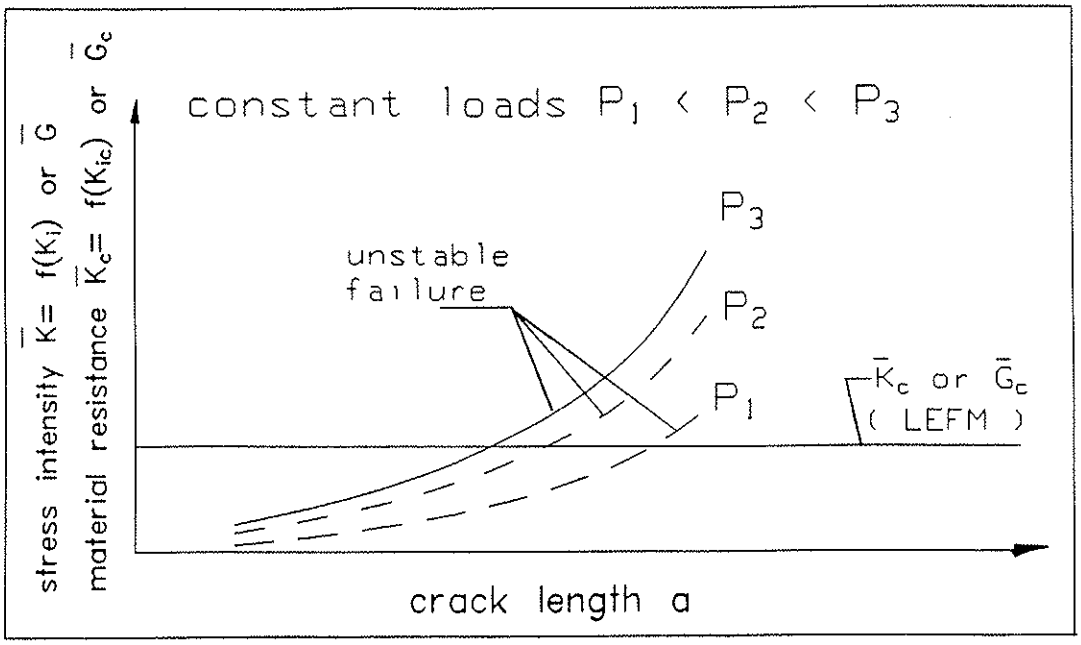

Fig. 1 Structure with steadily increasing generalized stress intensity $\bar{K} = f(K_i)$ vs. crack length *a* at constant loads and hence unstable failures with steepy decreasing ultimate loads P_u

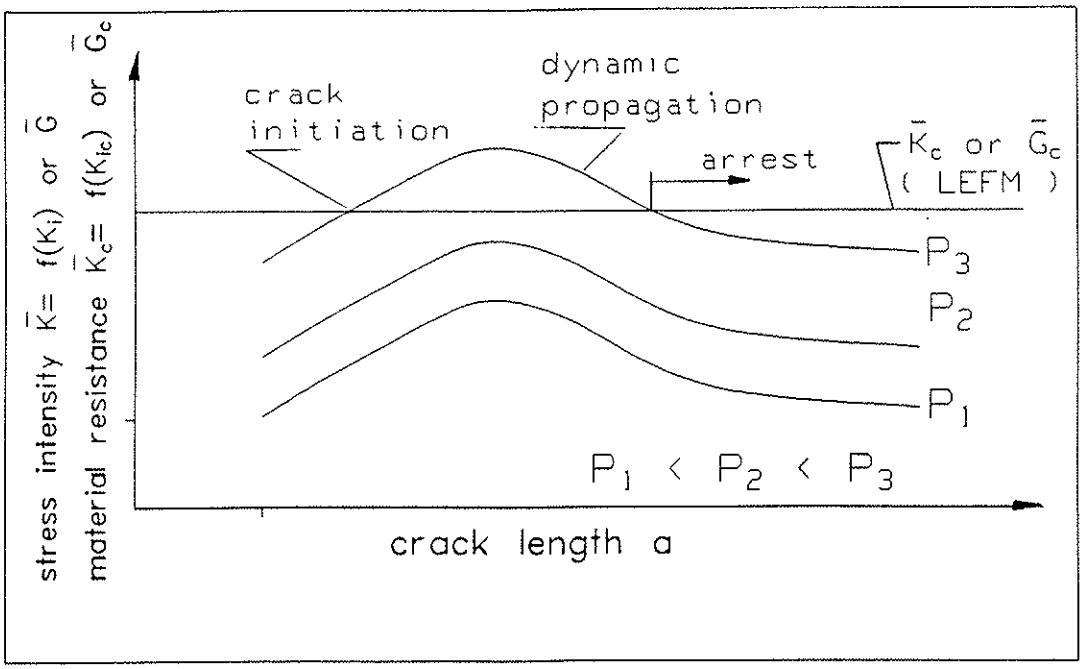

Fig. 2 Structure where crack arrest occurs at constant load condition due to decreasing generalized stress intensity factor $\bar{K} = f(K_i)$ after maximum $\bar{K}$ resp. minimum ultimate load P_u

In more complex structures non monotonic $\mathcal{K}$-functions are encountered which may first increase with crack length and after having reached a maximum, $\mathcal{K}$ remains constant or decreases (Fig. 2). In the latter case the critical load has a stable minimum and crack arrest can occur after initiation and unstable propagation.

Crack arrest may also occur when the material shows a (non)linear increase in crack resistance with crack elongation. This case shall not be considered here, as all problems due to relative structure sizes and wood brittleness will be considered in a conservative approximation to behave acc. to linear elastic fracture mechanics (LEFM).

3 Determination of stress intensity factors resp. strain energy release rates

In case of mixed mode situations some different approaches are known for separation of the interacting single mode stress intensities K_i resp. of the linear elastic equivalent strain energy release rates G_i (i = I, II, III). Following, only mixed mode I and II, thus 2D structures with inplane loading shall be regarded.

For numerical determination of K_i- resp. G_i-values – and thereof deduced ultimate loads – two methods suitable for commercial finite element programs have been used and are outlined briefly, following. For both methods i), ii) only one finite element run is necessary.

(i) method based on the singular displacement resp. stress field in the crack tip vicinity [7], [8]. The K_I, K_{II}-values are determined from FE computed displacements u, v at the crack faces, which are then extrapolated towards the crack tip and equated with the closed form expressions [9].

(ii) method based on virtual crack closure integral [10]. The two crack closure integrals G_I, G_{II} are derived from FE-computed nodal forces F_x, F_y and displacements u, v at the ligament resp. at the crack faces [10], [11], [12].

In case of linear elastic fracture mechanics and a crack resp. its extension parallel to a primary material axis (here: x-direction) stress intensity factors and strain energy release rates can be easily transformed into the related quantities

$$K_I = \sqrt{E_I^* \, G_I} \,, \qquad K_{II} = \sqrt{E_{II}^* \, G_{II}} \tag{2a, b}$$

where E_I^* , E_{II}^* are substitute E-moduli which in case of plane stress condition are given by

$$E_I^* = \sqrt{2\, E_x\, E_y}\ \rho\ , \qquad E_{II}^* = \sqrt{2}\, E_x\, \rho\ , \tag{3a, b}$$

$$\rho = \left[\left[\frac{E_x}{E_y}\right]^{0,5} + \frac{E_x}{2\, G_{xy}} - \nu_{yx} \right]^{-0,5} , \quad \frac{\nu_{yx}}{\nu_{xy}} = \frac{E_x}{E_y} .$$

3.1 K-factors from crack face displacements

The stress intensity factors acc. to method i) can be determined by means of finite element computed displacements at the crack faces ($\vartheta = 180°$) as decoupled quantities in a simple manner by (for details see, [8], [9])

$$K_I = c_I b_I\ , \quad K_{II} = c_{II} b_{II}\ , \tag{4a, b}$$

where b_I, b_{II} are the displacement extrapolations towards the crack tip $r \rightarrow 0$ as sketched in Fig. 3 ($\Delta\bar{v}$, $\Delta\bar{u}$ ≙ total opening resp. sliding displacements)

$$b_I = \lim_{r \to 0} \frac{\Delta \bar{v}(r)}{\sqrt{r}} , \qquad b_{II} = \lim_{r \to 0} \frac{\Delta \bar{u}(r)}{\sqrt{r}} . \tag{5a, b}$$

Quantities c_I, c_{II} are scalars depending in case of $\vartheta = 180°$ solely on the elastic properties of the material and by assumption that the extending crack is located parallel to grain (x-direction) are

$$c_I = 1 \,/\, \left[\mathrm{Re}\ (a_{21})\ 2 \sqrt{\frac{2}{\pi}} \right] , \qquad c_{II} = 1 \,/\, \left[\mathrm{Re}\ (a_{21})\ 2 \sqrt{\frac{2}{\pi}} \right] \tag{6a, b}$$

where

$$a_{12} = \frac{i}{\mu_1 - \mu_2} \left[p_2 - p_1 \right] , \qquad a_{21} = \frac{i}{\mu_1 - \mu_2} \left[\mu_1 q_2 - \mu_2 q_1 \right] , \tag{7a, b}$$

$$p_j = \frac{\mu_j^2}{E_x} - \frac{\nu_{yx}}{E_x} , \qquad q_j = \frac{1}{E_y\, \mu_j} - \frac{\nu_{yx}\, \mu_j}{E_x} , \quad \mathbf{(j = 1,2)} \tag{8a-d}$$

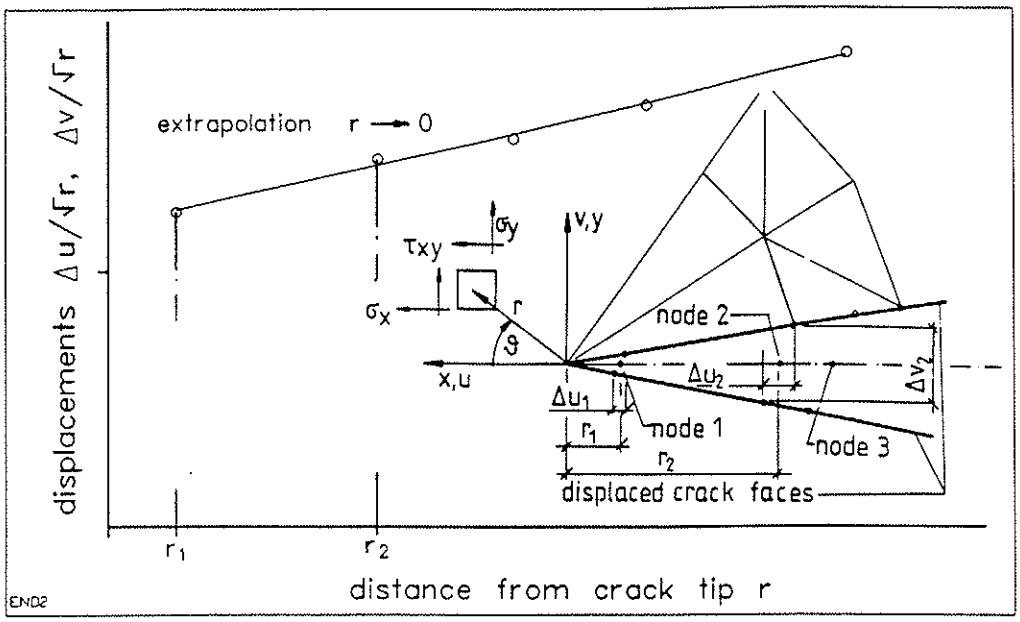

Fig. 3 Definition of displacement resp. stress field in crack tip vicinity and illustration of extrapolation of finite element computed crack face displacements for derivation of mixed mode stress intensities K_I, K_{II}

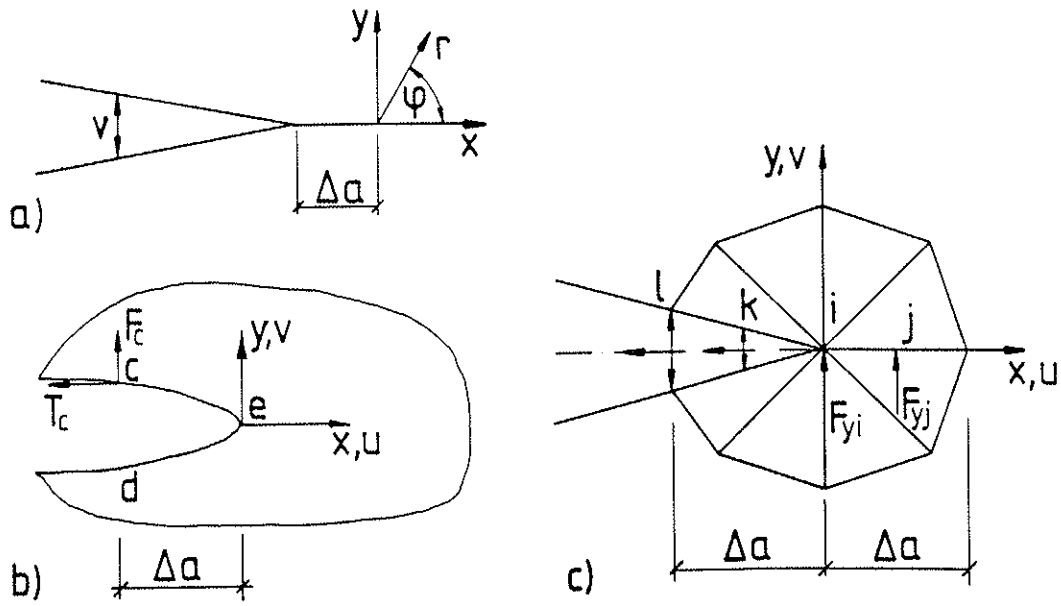

Figs. 4a – c Illustrations for virtual crack closure integral determination
a) symbols for analytical solution acc. to eqs. (10)
b) finite discretization
c) symbols of dimensions in FE-computations related to eqs. (12)

$$\mu_{1,2} = \left[\nu_{yx}^2 - \frac{E_x}{2\,G_{xy}} \pm \left(\nu_{yx}^2 - \frac{\nu_{yx}\,E_x}{G_{xy}} + \frac{E_x^2}{4\,G_{xy}^2} - \frac{E_x}{E_y} \right)^{\frac{1}{2}} \right]^{\frac{1}{2}} . \qquad (9a, b)$$

The letter i in eqs. (7a, b) is the imaginary unit $(i = \sqrt{-1})$.

3.2 Energy release rates by virtual crack closure integral

For engineering purposes an even more suitable method is based on the virtual crack closure integral [10] which in case of LEFM is equal to energy release rate. The integral is defined as that energy amount necessary to close a crack which has propagated by a distance Δa and can be written as

$$G_I = \frac{1}{b} \lim_{\Delta a \to 0} \frac{1}{2\Delta a} \int_0^{\Delta a} \sigma_y\,(\Delta a - r, 0°)\; v\,(r, 180°)\; dr \;, \qquad (10a)$$

$$G_{II} = \frac{1}{b} \lim_{\Delta a \to 0} \frac{1}{2\Delta a} \int_0^{\Delta a} \tau_{xy}\,(\Delta a - r, 0°)\; u\,(r, 180°)\; dr \;. \qquad (10b)$$

The stresses σ_y, τ_{xy} act at the crack ligament just before the crack tip (Fig. 4a) and displacements v, u are opening resp. slip of the crack faces immediately behind the crack tip. For determination of the closure integral via finite elements, stresses and displacements of eqs. (10) are discretized at nodes (Fig. 4b) resulting in [11]:

$$G_I = \frac{1}{b} \lim_{\Delta a \to 0} \frac{1}{2\Delta a}\, F_c\,(v_c - v_d) \;, \quad G_{II} = \frac{1}{b} \lim_{\Delta a \to 0} \frac{1}{2\Delta a}\, T_c\,(u_c - u_d) \;. \qquad (11a, b)$$

For practical computation the forces at node c have to be replaced by those at node e as the first show zero values because of crack opening what finally results in allmost simple and transparent equations for determination of the mixed mode energy release rates

$$G_I = \frac{1}{2b\Delta a}\,(F_{yi}\; v_\ell + F_{yj} v_k) \;, \qquad G_{II} = \frac{1}{2b\Delta a}\,(F_{xi}\; u_\ell + F_{xj} u_k) \;. \qquad (12a, b)$$

Prerequisite for application of above eqs. (12) is, that the elements immediately before and after the crack tip have equal edge length, suitably but not necessarily equal to crack elongation Δa. Comparative computations showed that crack elongations Δa in the range of a/20 to a/40 give similar good results. The use of regular

elements adjoining to the crack tip delivers more precise results compared to singular elements. It may also be stated that a literature known procedure to increase the result accuracy by performing two computation with crack lengths $a_1 = a - \Delta a/2$, $a_2 = a + \Delta a/2$ and using the forces associated to a_1 resp. the displacements of a_2 in eqs. (12) gives only marginal improvements for engineering purposes.

4 Interaction criterion

Out of a number of fracture mechanics interaction criteria discussed in literature the empiric Wu criterion [13] at the time seems to be the most appropriate one:

$$\frac{K_I}{K_{Ic}} + \left(\frac{K_{II}}{K_{IIc}}\right)^2 \leq 1 \qquad \text{or} \qquad \sqrt{\frac{G_I}{G_{Ic}} + \frac{G_{II}}{G_{IIc}}} \leq 1 \ . \tag{13a, b}$$

The analogous criteria for K of G quantities resemble formally and qualitatively the usual normal and shear stress interaction.

5 Stress intensity factors and ultimate loads of beams with holes

Following the course of K-factors and ultimate shear force capacities depending on a propagating crack is shown for different types of holes.

5.1 Examples

Four different hole geometries, see Table 1, all located in a simply supported beam with a single mid-span force were subject to a comparative study with the solutions given by other authors, too. The openings considered acc. to a proposal by Gustafsson were two round holes (structures d, e) with strongly different sizes relative to beam depth (d/h = 1/8 resp. 1/3) and two types of square holes, one with sharp corners and one with rounded corners (structures g and h respectively). In order to reveal the size effect, all geometries were investigated with two significantly different sizes: a small size 1 (h = 95 mm, b = 45 mm) and a large size 2 (h = 600 mm, b = 120 mm).

geometry	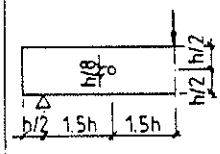		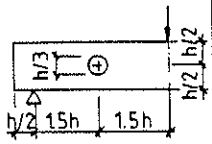		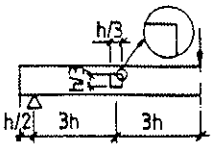		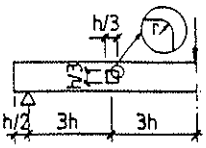	
No. of structure	d1	d2	e1	e2	g1	g2	h1	h2
depth h [mm]	95	600	95	600	95	600	95	600
width b [mm]	45	120	45	120	45	120	45	120

Table 1: Investigated structures with round resp. square holes

5.2 Modelling, crack location

There are two corners or locations at the hole contour stressed in tension perpendicular to grain; one of these is located towards the tension fiber edge and support (here termed lower left corner) and the other is diagonally opposite (upper right corner). Figs. 5 reveal the course of stress σ_y along hole contour, as well as the disturbance of the stress distribution due to cracks of different lengths and onsets. The load capacity vs. crack elongation behaviour was studied in detail for the lower left corner, whereas only distinct crack lengths were investigated at upper right corner. Hereby it has to be stated that theoretical load capacities resulting from cracking at the lower left corner are generally somewhat higher compared to fracture loads at upper right corner where mostly in experiments the primary crack starts. The crack onset at the contour of the round hole and at the rounded corners of the square holes was located throughout at $\vartheta = 45°$ (Figs. 5). The fact that the peak stress perpendicular to grain actually occurs at a lower angle of about 37° coincides well with experimentally measured crack onsets in [1]. There for round holes in average $\vartheta = 36°$ was obtained for the lower left corner whereas at the upper right corner the mean onset location was at 28° + 180°. Above modelling deficiency nevertheless has only a minor impact on the general trend of the results.

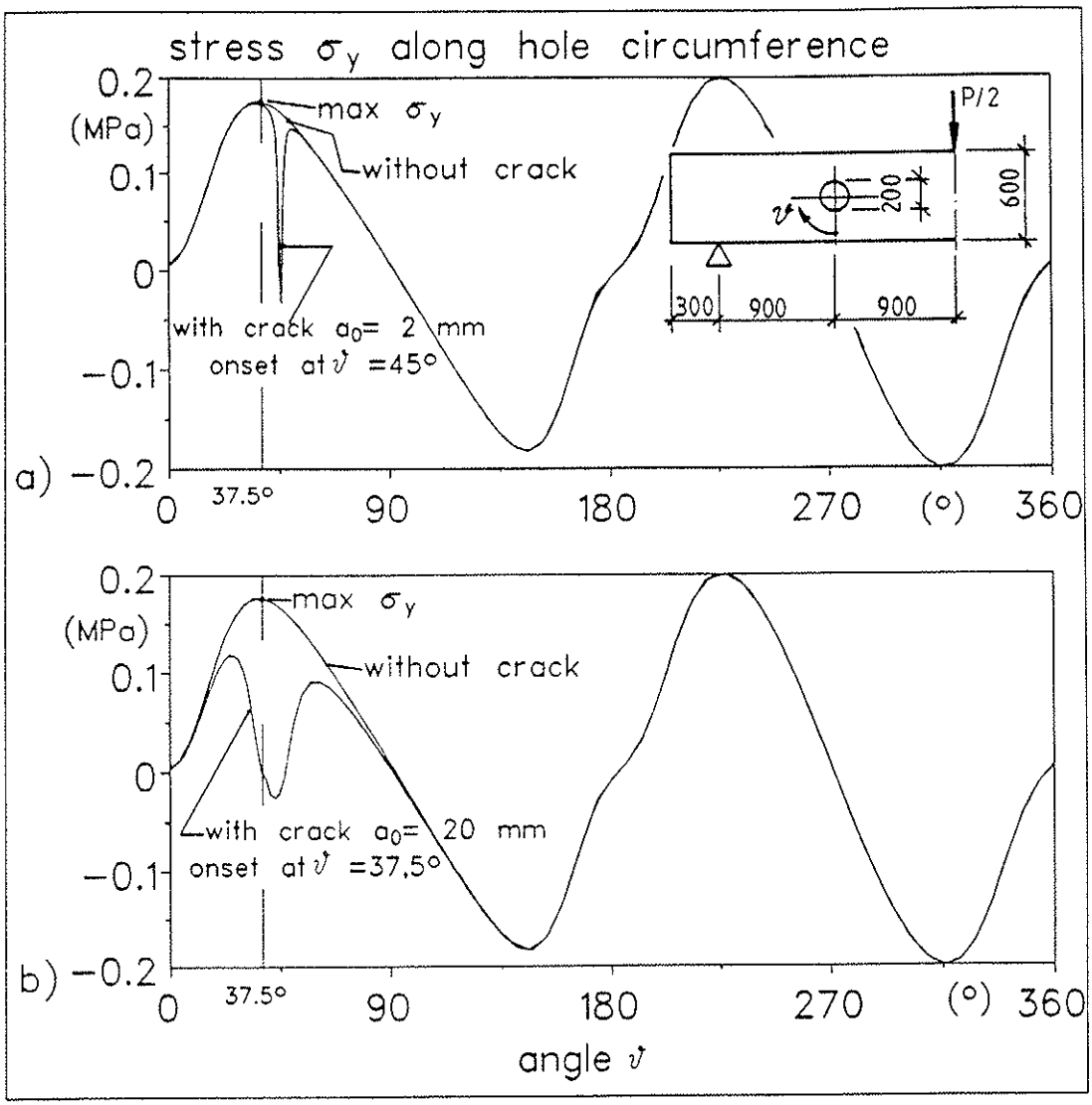

Fig. 5a, b Course of stress σ_y perpendicular to grain along hole circumference for a beam with a round hole with and without crack at lower left corner

a) crack length a_0 = 2 mm, crack onset at ϑ = 45°

b) crack length a_0 = 20 mm, crack onset at ϑ = 37,5°

All finite element models were generated automatically with specifications of fine element meshing in the hole and especially crack vicinity. Throughout triangular six-node isoparametric elements were used. For displacement determination acc. to method i) the midside nodes of the elements resp. of element edges adjoining to the crack tip node were shifted in quarter position of edge length to create a strain singularity. For evaluation with method ii) only regular elements were used. The edge length of the elements connected to the crack tip were mostly 1/8 of the design crack length **a.** The x-axis of the plane stress computations was located parallel to grain.

Figs. 6a, b reveal modelling details of the structures with differently sized round holes (large beams). Given are contour plots of the deformed and undeformed structures and close-ups of the finite element meshing of the hole area and immediate crack tip vicinity. Figs. 7a, b show the same for the large structures with square holes having sharp resp. rounded corners.

5.3 Material properties

The computations where performed with elasticity values of strength class C30 acc. to prEN 338:

$$E_x = 12 \text{ GPa}, \quad E_y = 0.4 \text{ GPa}, \quad G_{xy} = 0.75 \text{ GPa}, \; \nu_{yx} = \nu_{xy} \; E_x/E_y = 0.45.$$

In case of stress intensity factor determination only the orthotropic elasticity ratios are of influence on the results, whereas energy release rates also depend on the absolute elasticity quantities.

For fracture energy properties – in case of LEFM better termed critical energy release rates – the quantities

$$G_{Ic} = 300 \text{ Nm/m}^2, \quad G_{IIc} = 3.5 \; G_{Ic} = 1050 \text{ Nm/m}^2$$

were employed. Consistent with assumptions of linear fracture mechanics the related fracture toughnesses by means of eqs. (2), (3) and above elasticity values are

$$K_{Ic} = 0.5074 \text{ MPa} \sqrt{\text{m}}, \quad K_{IIc} = 2.2217 \text{ MPa} \sqrt{\text{m}} \; .$$

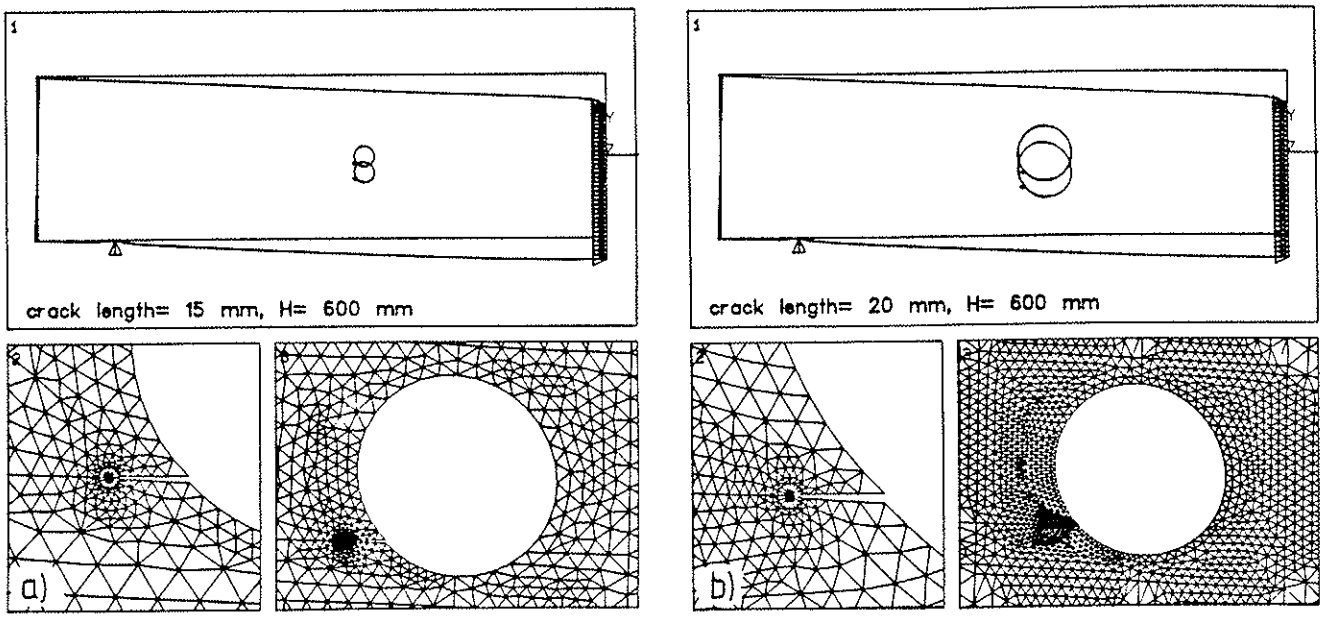

Figs. 6a, b Beams with round holes; contour plots of undeformed and deformed structures and finite element meshing of crack areas resp. crack tips
a) small hole d = h/8 (large structure d2)
b) large hole d = h/3 (large structure e2)

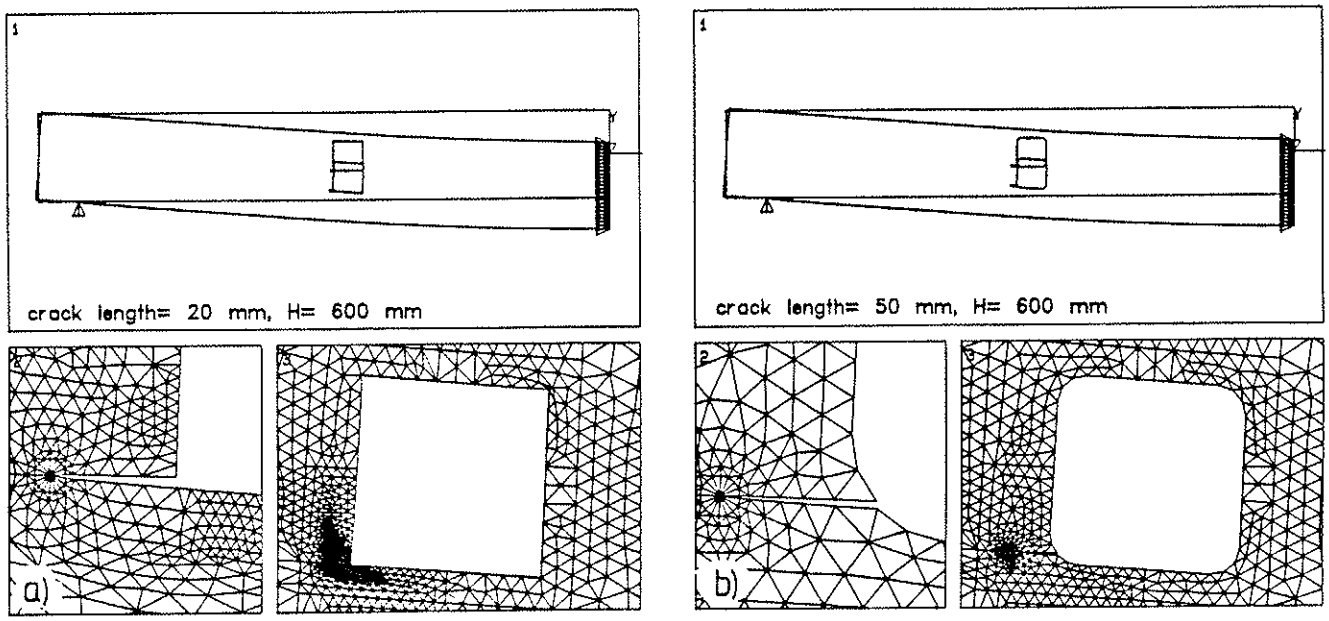

Figs. 7a, b Beams with square holes; contour plots of undeformed and deformed structures and finite element meshing of crack areas resp. crack tips
a) hole with sharp corners (large structure g2)
b) hole with rounded corners (large structure h2)

As fracture mechanics material data of wood are not so well established up to now, it should be mentioned that the considered values are not just grasped, but are at least partially, well empiric. G_{Ic} results from the experimental relationship [14a, b]

$$G_{Ic} = 0.65\ \rho_{12} \tag{14}$$

when a density of $\rho = 460$ kg/m^3 (strength class C30) is inserted. Eq. (14) has been verified as a quite reliable guess for the mean G_{Ic}-value in [15], too. In comparison thereto the ratio $G_{IIc}/G_{IC} = 3.5$ probably marks the upper edge acc. to recent investigations with a new fracture energy specimen type for mode II [16], [17]. With reference to this specimen the chosen ratio of 3.5 is correct when G_{IIc} is determined from the complete experimental loading and unloading curve; however when the G_{IIc} evaluation is based on another more plausible unloading compliance, the ratio G_{IIc}/G_{Ic} drops to roughly 2.

5.4 Results

Figs. 8 to 11 show for all geometries (only large sizes) the course of the stress intensity factors and the course of the resultant shear force capacities acc. to eqs. (13) as a function of a crack of length **a** propagating from lower left corner towards support. Figs. 8 and 9 refer to the small (d = h/8) resp. large (d = h/3) round holes and Figs. 10 and 11 depict the situation for the square holes with sharp resp. rounded corners. The two different computational approches – K-determination from displacements extrapolations in combination with closed form solutions resp. G-evaluation from crack closure integral and transformation to K-values via eqs. (2), (3) – gave a very good agreement in all examples investigated; the deviations were mostly within 1 %. The computational effort for crack closure integral is less. Condensed the following results are noteworthy:

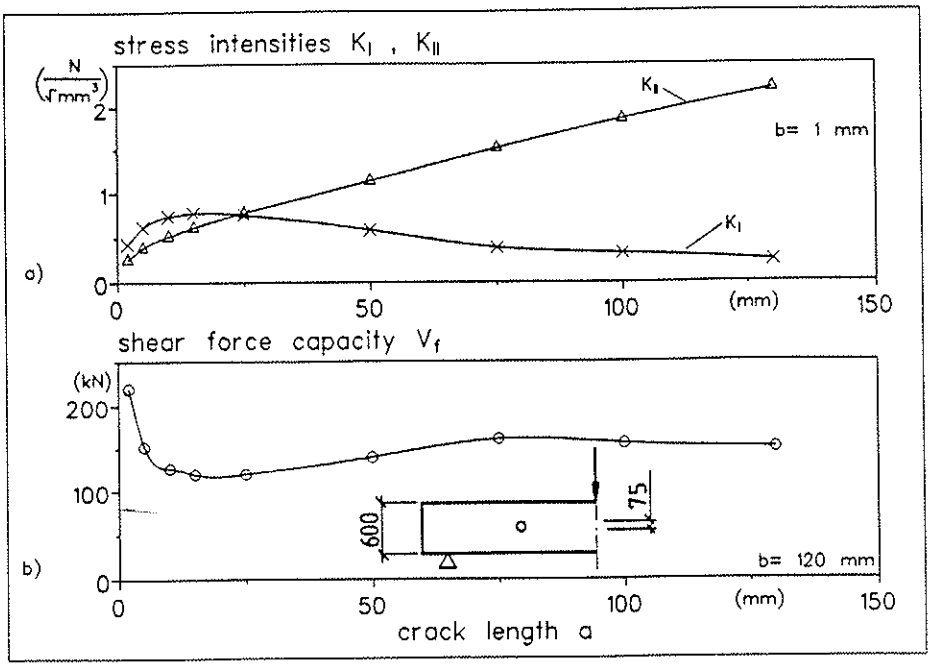

Fig. 8 Stress intensities K_I, K_{II} and resultant shear force capacities V_f vs. design crack length **a** in case of the beam with a relatively small hole d = h/8 (large structure d2)

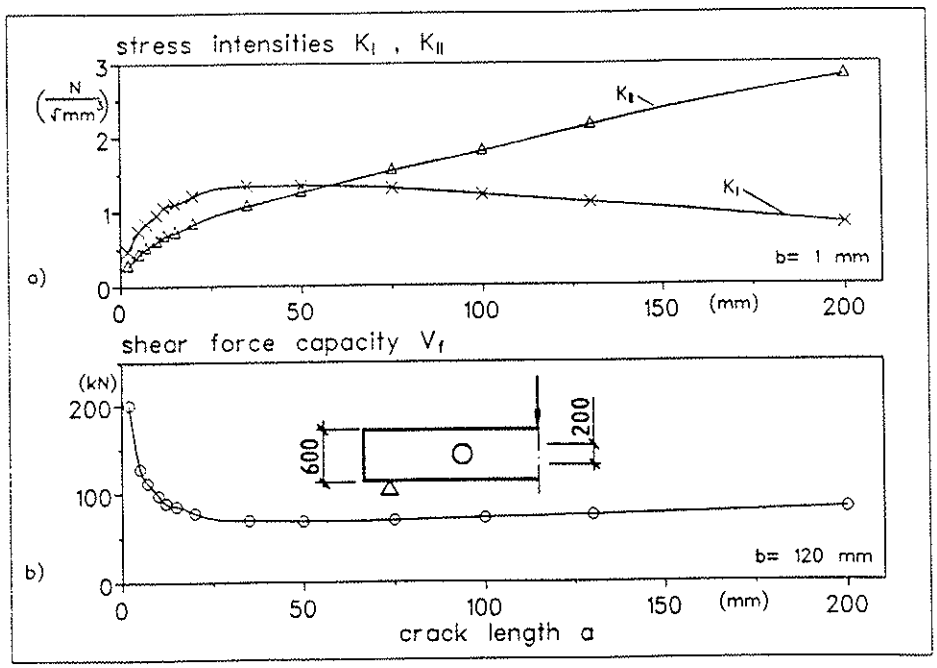

Fig. 9 Stress intensities K_I, K_{II} and resultant shear force capacities V_f vs. design crack length **a** in case of the beam with a relatively large hole d = h/3 (large structure e2)

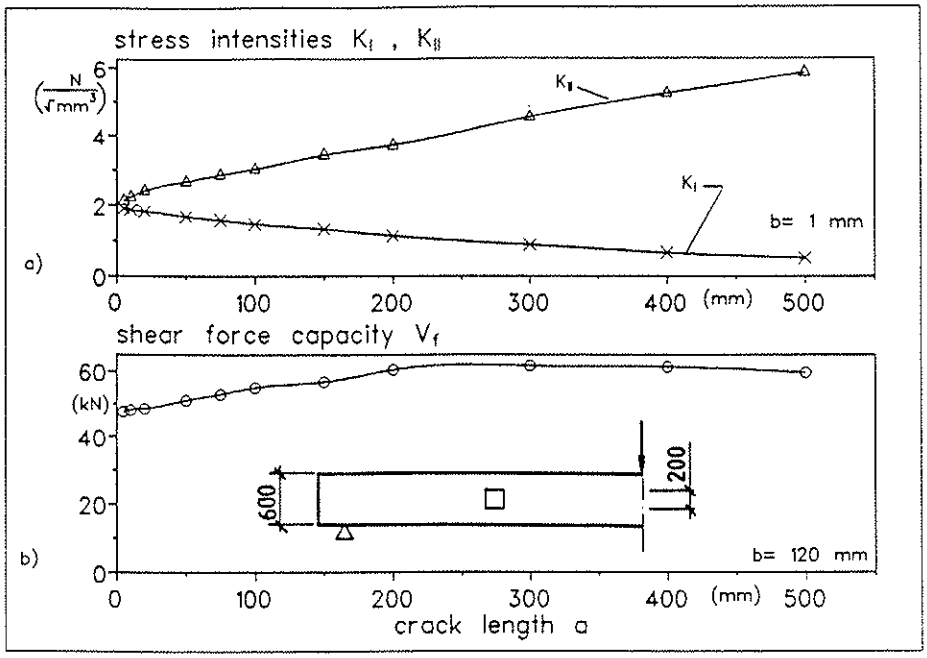

Fig. 10 Stress intensities K_I, K_{II} and resultant shear force capacities V_f vs. design crack length **a** in case of the beam with a square hole with sharp corners (large structure g2)

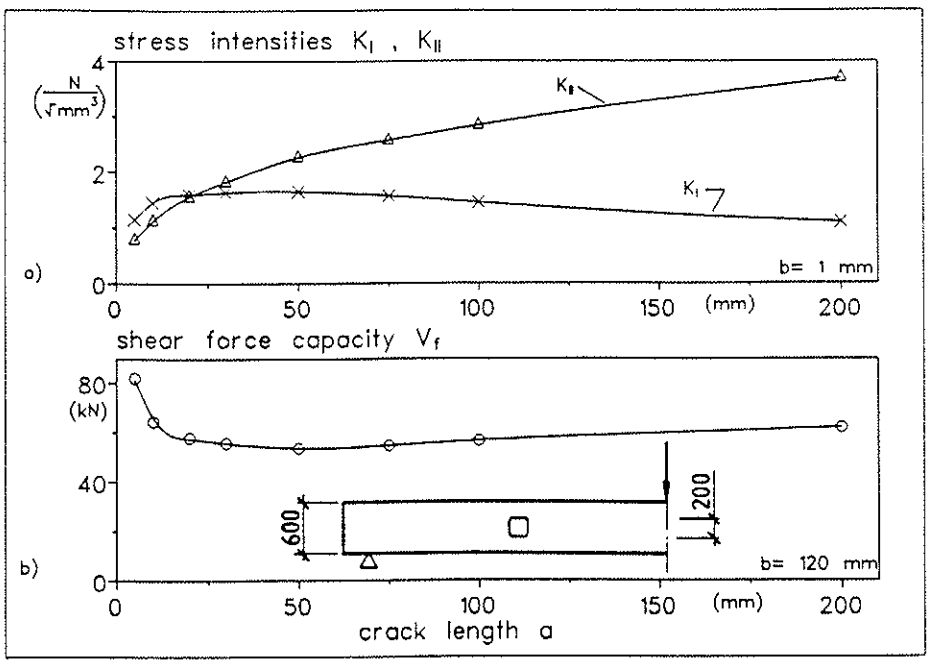

Fig. 11 Stress intensities K_I, K_{II} and resultant shear force capacities V_f vs. design crack length **a** in case of the beam with a square hole with rounded corners (large structure h2)

- In all cases of round holes or square holes with rounded corners, i. e., when no singularity exists in the perfect state of the structure, an exponential decrease of load capacity occurs within the first centimeters of crack propagation. The crack length a_0 associated to minimum load value varies slightly for the different geometries and depends on the size of the structure, too. For the large structures and large holes (e2, h2) a_0 is about 25–50 mm and in case of large structure and small hole (d2) a_0 is about 20 mm. In case of the small structures with depths of 95 mm, a_0 is in the range of 2–7 mm for the small and large holes, respectively. After minimum capacity is reached, further crack propagation throughout results in a capacity increase of roughly 10 to 35 % depending on geometry and size, which then is followed by the anticipated final load decrease.

- In case of a square hole with sharp corners a somewhat different situation occurs. Here the minimum capacity is associated to a very small crack length approaching zero length. This is bound to the fact that the singularity at zero crack length is not vanishing, as in case of the round holes, but is for a rectangular notch already very close ($r^{-0.45}$) to that of the sharp crack ($r^{-0.5}$), as shown by [18]. With increasing crack length a capacity increase similar to that sketched for the round holes takes place. In case of the large structure the maximum capacity increase is about 30 % and associated to a crack length of roughly 200 mm. It has to be mentioned that the load capacities at crack lengths of 25–50 mm where minimum load for round holes (large structures) occurred, do not differ strongly from minimum value; the alike is true for the small structure at crack lengths of 2–7 mm.

- smaller relative hole sizes obviously result in higher loading capacities. Quite similar for the beams with small (d1, e1) resp. large (d2, e2) dimensions the hole size of h/8 gives a roughly 60 % higher load capacity compared to hole sizes of h/3.

- a comparison of capacities of geometrically similar beams (structures 1 resp. 2) delivers throughout, as anticipated, ratios of

  $$V_2/V_1 \approx (b_2/b_1)\sqrt{h_2/h_1}$$

  i.e. the size effect law $1/\sqrt{h}$ of linear elastic fracture mechanics (similar geometry also includes relative crack length in a due range).

Table 2 summarizes the minimum capacities and the respective crack length as received predominantly for the lower left corner. In case of one structure (g2) a

comparison of capacities resulting from lower left resp. upper right corner is given for an explicit crack length (a_0 = 50 mm). Table 2 also includes results of other authors [19], [20] working on the same structures and elasticity values, however with different fracture mechanics approaches. The results given by [20] are also minimum values of load vs. crack length computations; the data refer throughout to a crack propagation from upper right corner giving minor to considerable lower loads depending on structure type. Contrary the capacities given by [19] refer to computations with only one crack length in each case, which – approach inherent – is assumed to deliver the minimum load. Without deepened discussion of individual results, in general are very good agreement between the different methods can be stated.

6 Comparison of fracture mechanics predictions and test results

In order to validate the theoretical load capacities derived by the design crack concept some experiments performed by [1], [2] on glulam beams with round and square holes were investigated. Four different configurations (three round holes, one square hole) are considered, differentiated by relative and absolute hole dimensions and position of hole vs. support. Table 3 denotes the geometries and dimensions of the examples investigated altogether with the experimental resp. theoretical results; Figs. 12 specify the geometry notations.

All tests referred to, were performed with single span beams and a mid-span load. The quality of the timber, spruce in both test series, was seemingly comparable (apart from beam No 8); in [2] it conformed to swedish grade L40 whereas a mean density ρ_{12} of about 460 kg/m^3 is specified in [1]. The experimental load capacities given in Table 3 are, whenever specified in the references, loads at first crack visible and then marked with an asterisk; all other loads given are ultimate loads.

In all tests cracks developed at both tensioned corners, however throughout [1] or predominantly [2] first at the upper right corner. The load carrying behaviour of the beams with square holes (corner radius 25 mm) was alike in both test series, i.e. after crack initiation the load could be increased in most cases by further 10 to 50 % until ultimate failure occurred suddenly. In case of the round holes a similar behavior was endeavored in [2], whereas in [1] all beams with round holes, except one, failed suddenly without visible preceeding crack propagation.

Geometry	No. of structure	shear force capacities V_f and associated crack lengths a_0								
		authors' results			Petersson's results [1]		Gustafssons' results			
		lower left corner		upper right corner			initial crack method		mean stress method	
		a_0	V_f	V_f	a_0	V_f	a_0	V_f	a_0	V_f
		mm	kN	–	mm	kN	mm	kN	mm	kN
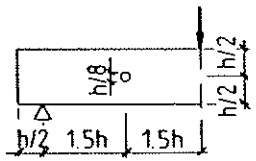	d1	2	18,1	–	4	17,8	12,9	27,70	22	22,60
	d2	18	117,3	–	20	106,3	9,2	135,6	19	152,3
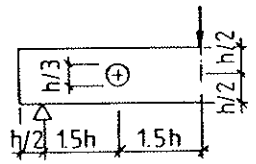	e1	7	10,1	–	6	8,9	9,2	8,2	19	10,3
	e2	35	68,1	–	40	57,6	9,2	75,6	19	90,3
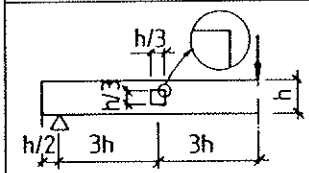	g1	1	7,0	–	6	6,8	9,1	6,0	18	7,2
	g2	1 50	46,8 51,2	45,7	40	45,3	9,1	45,5	18	48,3
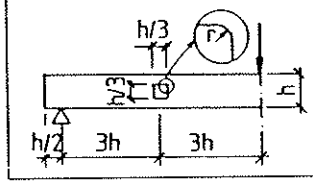	h1	7	8,2	–	–	–	9,1	6,2	18	7,6
	h2	52	53,5	–	–	–	9,1	52,6	18	61,8

Table 2: Theoretical shear force capacities V_f and associated crack lengths a_0 acc. to different fracture mechanics approaches
Authors' results: K resp. G determination from crack opening displacements resp. crack closure integral
Petersson's results: energy release rate analysis [20]; fine mesh, $G_c = G_{c12}$
Gustafsson's results: initial crack resp. mean stress method [19]

current No.	reference	specimen No. in [1], [2]	hole type	glulam beam dimensions depth h	glulam beam dimensions width b	slenderness ratio ℓ/h	mean density ϱ_{12} resp. grade	hole dimensions $h_h = a$	hole position ℓ_a	hole position ℓ_m	normalized hole dimensions resp. positions ℓ_a/h	normalized hole dimensions resp. positions h_h/h	normalized hole dimensions resp. positions $\ell/_m h$	shear force capacity V_f experimental	shear force capacity $\frac{V_f}{b\sqrt{h}}$ theoretical upper right corner	shear force capacity $\frac{V_f}{b\sqrt{h}}$ theoretical lower left corner	$\frac{V_{f,theor.}}{V_{f,exp.}} - 1$ upper right corner	$\frac{V_{f,theor.}}{V_{f,exp.}} - 1$ lower left corner
				mm		–	kg/m³ / –	mm	mm		–			kN	N/mm$^{3/2}$		%	
1	[2]	L1a	rd.	500	90	10	L40	250	525	650	1,05	0,50	1,3	25,7*	12,8			
2	[2]	L1b	rd.	500	90	10	L40	250	525	650	1,05	0,50	1,3	33,4	15,6			
3	[1]	P1	rd.	500	90	8	460	256	472	600	0,94	0,51	1,2	33,8	16,8	14,8	18,3	
4	[1]	P4	rd.	800	115	6,25	471	400	618	818	0,77	0,50	1,0	57,1*	17,6			
5–7	–	–	rd.	–	–	8,6	–	–	–	–	0,95	0,50	1,2	–	15,7	14,8	18,3	
5	[1]	P2	rd.	500	90	8	453	256	922	1050	1,84	0,51	2,1	31,6	16,7	14,0	20,1	
6	[2]	L3a	rd.	500	90	10	L40	250	1275	1400	2,55	0,50	2,8	35,0	17,4			
7	[2]	L3b	rd.	500	90	10	L40	250	1275	1400	2,55	0,50	2,8	31,3*	15,6			
5–7	–	–	rd	–	–	9,3	–	–	–	–	2,30	0,50	2,6	–	16,6	14,0	20,1	
8	[1]	P3	rd.	500	90	8	429	153	371	447	0,74	0,30	0,9	51,3	25,5	22,5	25,7	
9	[1]	P6	sq.	500	90	8	483	202	699	800	1,40	0,40	1,6	33,8	16,8	13,7	15,0	

Table 3: Geometries, dimensions and experimental shear force capacities of glulam beams with round and square holes investigated by [1], [2] and comparisson with theoretical load capacities acc. to the fracture mechanics design crack concept with $a_0 = 25$ mm; for dimension symbols, see Figs. 12

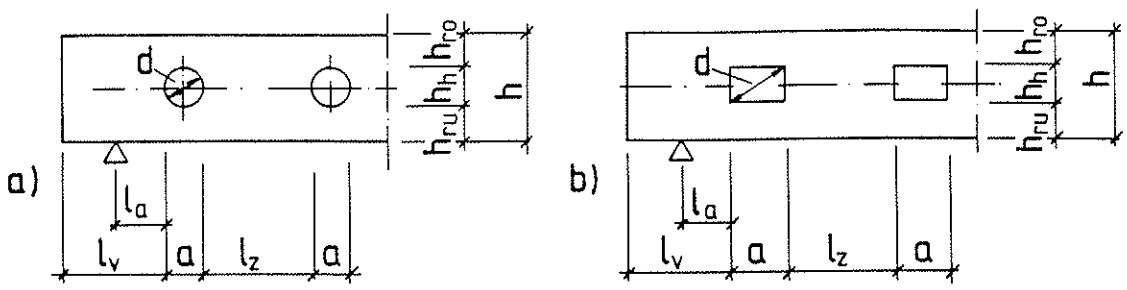

Fig. 12a, b Definition of symbols for beams with holes
a) round hole(s) b) rectangular hole(s)

The theoretical shear capacities of all configurations were computed with a design crack length of a_0 = 25 mm starting at an angle of ϑ = 45°. The loads are given for crack onset at the lower left and the higher stressed upper right corner. The elasticity and fracture mechanics material parameters used were those specified in chap. 5.3 for solid timber class C30. It should be mentioned that variations of the material parameters (elasticity and fracture mechanics properties) in a due range do not change the results significantly; this is similarly right for the design crack length which was chosen slightly shorter than probably associated to minimum capacity acc. to chap. 5.4.

The agreement of the theoretical and experimental results has to be termed good in general. As supposed, the theoretical failure loads resulting from crack propagation at lower left corner overestimate load capacity nearly throughout, in average by about 12 %. Contrary, the computed failure loads for upper right corner give a lower boundary (one exception) for the load capacity, in average 14 % beneath experimental results. When the mean theoretical failure loads for both diagonal corners are compared to test results, in most cases a very good agreement within 5–10 % error is received.

7 Design proposal

A simple and transparent design can be proposed on the basis of the interaction criterion (13), being:

$$\frac{K_{I,d}}{K_{Ic,d}} + \left(\frac{K_{II,d}}{K_{IIc,d}}\right)^2 \le 1\,, \quad K_{Ic,d} = \frac{K_{Ic,k} \cdot k_{mod}}{\gamma_M}\,, \quad K_{IIc,d} = \frac{K_{IIc,k} \cdot k_{mod}}{\gamma_M} \qquad (15a, b, c)$$

where $K_{I,d}$, $K_{II,d}$ are stress intensities at design load F_d; $K_{Ic,k}$, $K_{IIc,k}$ are characteristic values of the fracture toughnesses K_{Ic}, K_{IIc} in specific strength classes and γ_M is the EC 5 partial material safety factor.

7.1 Design stress intensities

Based on agreed design crack lengths a_0, say in the range of 25–50 mm, the design stress intensities should be provided for the most relevant geometry and load case situations by means of dimensionless stress intensities k_I, k_{II}, normalized with respect to cross-sectional dimensions b, h and load. The design values are then derived from

$$K_{I,d} = \frac{k_I}{b\sqrt{h}} F_d\,, \qquad K_{II,d} = \frac{k_{II}}{b\sqrt{h}} F_d\,. \qquad (16a, b)$$

The maximum design load F_d acc. to eqs. (15), (16) is then given by

$$\max F_d = -0.5\, s/r + \sqrt{(s/2r)^2 + 1/r}\,, \qquad (17)$$

$$r = \left[k_{II}/(b\sqrt{h} \cdot K_{IIc})\right]^2\,, \qquad s = k_I/\left(b\sqrt{h}\, K_{Ic}\right)\,.$$

The most important parameters to influence normalized k_I, k_{II}-values, apart from hole geometry (round resp. square or rectangular, incl. corner radius) are relative hole depth h_d/h, relative location of hole centroid ℓ_m/h or begin of hole ℓ_a/h and beam slenderness ℓ/h.

7.2 Characteristic fracture toughnesses , k_{mod}-factors

On the material side, the derivation of characteristic K-values could probably be resolved reasonable with already existing data, in a way outlined hereinafter.

Table 4 contains the mean fracture toughness values K_{Ic}, K_{IIc} for relevant strength classes derived from the empiric mode I fracture energy equation (14) and ratio $G_{IIc} = 3.5\ G_{Ic}$ via eqs. (3). A good fit for the data within the density range of about 420 to 480 kg/m^3 is then

$$\mathbf{K_I = 0.00111}\ \rho_{12}\ , \qquad \mathbf{K_{II} = 0.00487}\ \rho_{12}\ . \tag{18a, b}$$

In a rough approximation characteristic K_c-values may be derived analogous to those $G_{Ic,k}$-values used implicitly in the EC 5 equation for end-notched beams. There assumption was made that the characteristic G_c-values are similarly proportional to the characteristic densities as the mean energies vs. the mean densities.

Application of the ratio $\rho_k/\rho = 0.83$ as defined in EN 338 probably results in quite an underestimation of the effective scatter of the fracture mechanics properties as shown in [15]. By assumption of normal distribution within the strength classes and a very moderate C.O.V. of 15 %, the characteristic values would be a 3/4 fraction of eqs. (18), i.e.

$$\mathbf{K_{Ic,k} = 0.000833}\ \rho_{12}\ , \qquad \mathbf{K_{IIc,k} = 0.00365}\ \rho_{12}\ . \tag{19a, b}$$

Clearly, the given relationships for $K_{Ic,k}$, also being plausible, represent a first approach in view of lacking consisting data and should be experimentally verified closer. Hereby it has to be beared in mind that the material properties chosen, may it be K- or G-values, should reflect in a proper way the basic linear elastic fracture mechanics relationships of colinear crack extension (3), in order that the theoretically equivalent energy release and stress intensity approaches provide similar load capacity predictions.

A further item is, whether the k_{mod} factors as specified now in EC 5 for classic strength values can be merely adopted. The assessment of duration of load impact in different climate environments can be based only a few investigations so far, i.a. [21].

strength class	mean density	elasticity values				fracture mechanics substitute E-moduli		fracture energies resp. critical energy release rates		fracture toughnesses			
										K_{Ic}		K_{IIc}	
	ρ_{12}	E_x	E_y	G_{xy}	ν_{yx}	E_I^*	E_{II}^*	G_{Ic}	G_{IIc}				
	kg/m³	GPa			–	GPa		Nm/m²		MPa$\sqrt{m}$	N/mm$^{\frac{3}{2}}$	MPa$\sqrt{m}$	N/mm$^{\frac{3}{2}}$
C18	380	9	0,30	0,56	0,45	0,643	3,522	247	865	0,398	12,6	1,75	55,2
C22	410	10	0,33	0,63		0,713	3,924	267	935	0,436	13,8	1,92	60,6
C24	420	11	0,37	0,68		0,788	4,299	273	956	0,464	14,7	2,03	64,1
C27	450	12	0,40	0,75		0,858	4,702	299	1047	0,507	16,0	2,22	70,2
C30	460	12	0,40	0,75		0,858	4,702	299	1047	0,507	16,0	2,22	70,2
C35	480	13	0,43	0,81		0,925	5,085	312	1092	0,537	17,0	2,36	74,5
C40	500	14	0,47	0,88		1,008	5,499	325	1138	0,572	18,1	2,50	79,1

Table 4: Mean values for fracture energies resp. critical energy release rates for specific strength classes acc. to test results by [14] resp. assumed ration $G_{IIc}/G_{Ic} = 3,5$ and hereof deduced theoretically equivalent fracture toughnesses

7.3 Constructive details

With respect to constructive details some specifications, as given in DIN 1052, which have proven good in construction practice, should be adopted at least similarly. So, the maximum relative dimensions of holes symmetric to neutral axis (Fig. 12) should be restricted to ratios of about

$$\mathbf{h_d / h \leq 0.4, \quad a/h \leq 1}$$

and should not be increased strongly without accumulated construction field experience. For the minimum distances towards support resp. beam end and between possible successive holes, the ratios

$$\mathbf{\ell_A/h \geq 0.5 , \quad \ell_v/h \quad and \quad \ell_z/h \geq 1}$$

could be adopted.

8 Reinforcement of holes with plywood sheets

As the load bearing capacities of beams with medium to larger sized holes with depths of about 0.2 to 0.5 of cross-sectional height are very low, say roughly 0.15 to 0.4 times compared to beams without holes, reinforcement in most cases is economically inevitable.

Following, a crude design method for reinforcement with laterally glued on plywood sheets is given. Hereby, first the admissible shear capacity V, of the beam with an unreinforced hole is determined, say with the shown fracture mechanics approach. Then the design of the reinforcement with respect to an extra shear force V (limited by full beam cross-section) could be performed by a method similar to plywood reinforcements of end-notched beams in the German timber design code DIN 1052, and discussed for hole reinforcements by [3].

Only reinforcements of round and rectangular holes located symmetrically to neutral beam axis are regarded; for notations of the reinforcement symbols see Fig. 13a.

The design of the reinforcement is based on the elementary statics assumption that the shear stress equilibrium close to the sections I-I at either end of the hole is distorted as no shear stresses can be transferred along the free hole edge (Fig. 13b). The resultant non equilibrated shear forces are then assumed to act either as a tension force V_t at lower left and upper right corner resp. as a compression force V_c

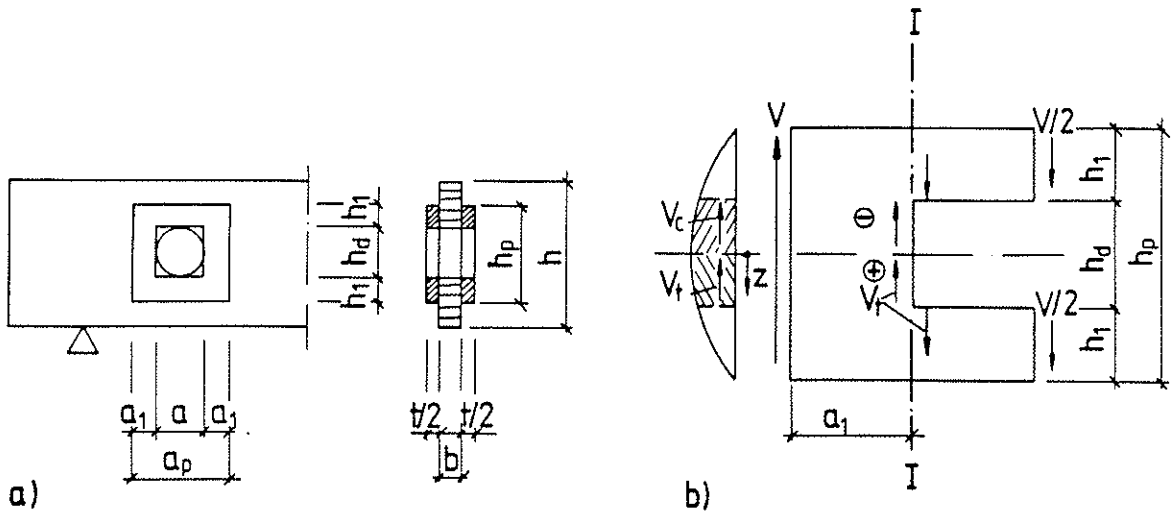

Fig. 13a, b Laterally glued on plywood reinforcement of round resp. rectangular holes
a) definition of symbols
b) illustration to crude determination of resultant tension resp. compression forces at hole corners

at the opposite corners. The resultant tension force in case of rectangular opening resp. reinforcement evolves as

$$V_t = \int_{z=0}^{h_d/2} \tau_{zx}\, dz = V\left[\frac{3}{4}\frac{h_d}{h_p} - \frac{1}{4}\left(\frac{h_d}{h_p}\right)^3\right] . \qquad (20)$$

The shear force V in eq. (20) holds for the extra shear force which shall be transferred solely by the reinforcement additionally to the capacity of the unreinforced beam. In case of the round hole, due to shifted location of maximum stress, the upper integration boundary may be taken as $z = h_d/2\sqrt{2}$ then resulting in

$$V_t = V\left[\frac{3}{4\sqrt{2}}\frac{h_d}{h_p} - \frac{1}{4\sqrt{2}^3}\left(\frac{h_d}{h_p}\right)^3\right] . \qquad (21)$$

The area of the plywood strip $a_1 \cdot t$ (t ≙ total thickness) to transfer the tension force V_t may then be determined by assumption of a triangular stress distribution in the

panels along length a_1 by consideration of some minimum requirements for a_1 and t (see below):

$$t\, a_1 = 2\, V_t / f_{t,\,\parallel,\,d,\,\text{plywood}} \quad . \tag{22}$$

The tension force V_t in the board has to be transferred by glue line shear stresses τ_{gl} within the area $A = a_1\, h_d/2$ (rectangular hole) resp. $a_1\, h_d/2\sqrt{2}$ (round hole) which then again by assumption of triangular distribution are

$$\tau_{gl} = V_t / 2A \quad . \tag{23}$$

With respect to constructive details the following minimum requirements for reinforcement dimensions acc. to DIN 1052 which are primarily based on tests have proven good in construction practice and could be adopted similarly (Fig. 13a):

$$\mathbf{h_1 \geq 0.25\, h_d \text{ and } \geq 0.1\, h\ ,} \qquad \mathbf{a_1 \geq 0.25\, a \text{ and } \geq h_1\ .}$$

The thickness t/2 of the individual plywood sheet consisting in minimum of 5 plies should not be much less than 20 mm, say 15 mm. The grain direction of the plywood in the glue line must be parallel to beam axis in order to reduce stress gradients.

9 Literature

[1] Penttala, V. (1980): Reiällinen Liimapuupalkki, report 33, Div. Structural Engineering, Helsinki University of Technology, Otaniemi

[2] Johannesson, B. (1983): Design problems for glulam beams with holes. Thesis, Div. Steel and Timber structures, Chalmers University of Technology, Göteborg

[3] Kolb, H., Epple, A. (1985): Verstärkung von durchbrochenen Brettschichtbindern. Schlußbericht Forschungsvorhaben I.4 – 34810, FMPA BW, Stuttgart

[4] Logemann, M. (1991): Abschätzung der Tragfähigkeit von Holzbauteilen mit Ausklinkungen und Durchbrüchen. Thesis, University of Hannover

[5] Pizio, S. (1991): Die Anwendung der Bruchmechanik zur Bemessung von Holzbauteilen, untersucht am durchbrochenen und am ausgeklinkten Träger. Thesis Nr. 9433, University of Zürich

[6] Riipola, K. (1995): Timber beams with holes: fracture mechanics approach. Journal Structural Engineering, Vol. 121, No. 2, pp. 225–239

[7] Sih, G. C., Paris, P. C., Irwin, G. R. (1965): On cracks in rectilinearly anisotropic bodies. Int. Journ. of Fracture Mech. 1, pp. 189–203

[8] Foschi, R. O., Barrett, J. D. (1976): Stress intensity factors in anisotropic plates using singular isoparametric elements. Int. Journ. for Numerical Methods in Eng., Vol. 10, pp. 1281–1287

[9] Aicher, S. (1995): Stress intensity factor approach. in: Fracture mechanics models for strength analysis of timber beams with a hole or a notch. RILEM TC 133 study report, in press, Lund

[10] Irwin, G. R. (1957): Analysis of stresses and strains near the end of a crack traversing a plate. Journ. of Applied Mechanics. Vol. 24, pp. 361–364

[11] Rybicki, E. F., Kanninen, M. F. (1977): A finite element calculation of stress intensity factors by a modified crack closure integral. Engineering Fracture mechanics, Vol. 9, pp. 931–938

[12] Shivakumar, K. N. et al. (1988): A virtual crack closure technique for calculating stress intensity factors for cracked three dimensional bodies. Int. Journ. of Fracture, Vol. 36, pp. R43–R50

[13] Wu, E. M. (1967): Application of fracture machanics to anisotropic plates. ASME Journ. Appl. Mechanics Series E 34, No. 4, pp. 967 – 974

[14a] Larsen, H. J., Gustafsson, P. J. (1990): The fracture energy of wood in tension perpendicular to the grain. Proceed. of CIB W 18A, meeting 23, paper 23-19-2, Lisbon

[14b] Larsen, H. J., Riberholt, H., Gustafsson, P. J. (1992): Note on Eurocode 5 – Design of notched beams. Paper dated 13.01.1992

[15] Aicher, S. (1994): Bruchenergien, kritische Energiefreisetzungsraten und Bruchzähigkeiten von Fichte bei Zugbeanspruchung senkrecht zur Faserrichtung. Holz als Roh- und Werkstoff 52, pp. 361–370

[16] Aicher, S., Gierl, M., Klöck, W. (1994): A study on mode II specimens for wood with emphasis on fracture energy determination. Otto-Graf-Journal, Vol. 5, pp. 11 – 40, Stuttgart

[17] Boström, L. et al. (1995): Fracture energy in forward shear along the grain. A draft standard proposal. Materials and Structures (to be submitted)

[18] Leicester, R. H. (1971): Some aspects of stress fields at sharp notches in orthotropic materials. I. Paper 57, Div. Forest Products Technology paper, CSIRO, Melbourne

[19] Gustafsson, P. J. (1995): Mean stress approach and initial crack approach. in: Fracture mechanics models for strength analysis of timber beams with a hole or a notch. RILEM TC 133 study report, in press, Lund

[20] Petersson, H. (1995): Energy release rate analysis. in: Fracture mechanics models for strength analysis of timber beams with a hole or a notch. RILEM TC 133 study report, in press, Lund

[21] Fonselius, M. (1991): Long-term fracture toughness of wood. Research Report 718, Technical Research Center of Finland, Espoo

INTERNATIONAL COUNCIL FOR BUILDING RESEARCH STUDIES AND DOCUMENTATION

WORKING COMMISSION W18 - TIMBER STRUCTURES

EUROCODE 5 - DESIGN OF TIMBER STRUCTURES - PART 2: BRIDGES

by

D Bajolet

E Gehri

J König

H Kreuzinger

H J Larsen

R Mäkipuro

C Mettem

MEETING TWENTY - EIGHT

COPENHAGEN

DENMARK

APRIL 1995

Eurocode 5 - Design of timber structures - Part 2: Bridges

Draft April 1995

Prepared by:

D Bajolet
E Gehri
J König
H Kreuzinger
H J Larsen
R Mäkipuro
C Mettem

Contents

Foreword

Objectives of the Eurocodes

(1) The "Structural Eurocodes" comprise a group of standards for the structural and geotechnical design of buildings and civil engineering works.

(2) They cover execution and control only to the extent that it is necessary to indicate the quality of the construction products, and the standard of workmanship needed to comply with the assumptions of the design rules.

(3) Until the necessary set of harmonised technical specifications for products and methods for the testing their performance are available, some of the Structural Eurocodes cover some of these aspects in informative Annexes.

Background to the Eurocode Programme

(4) The Commission of the European Communities (CEC) initiated the work of establishing a set of harmonised technical rules for the design of building and civil engineering works which would initially serve as an alternative to the differing rules in force in the various Member States and would ultimately replace them. These technical rules became known as the "Structural Eurocodes".

(5) In 1990, after consulting their respective Member States, the CEC transferred the work of further development, issue and updating of the Structural Eurocodes to CEN, and the EFTA Secretariat agreed to support the CEN work.

(6) CEN Technical Committee CEN/TC 250 is responsible for all Structural Eurocodes.

Eurocode Programme

(7) Work is in hand on the following Eurocodes, each generally consisting of a number of parts:

EN 1991 Eurocode 1	Basis of design and actions on structures
EN 1992 Eurocode 2	Design of concrete structures
EN 1993 Eurocode 3	Design of steel structures
EN 1994 Eurocode 4	Design of composite steel and concrete structures
EN 1995 Eurocode 5	Design of timber structures
EN 1996 Eurocode 6	Design of masonry structures
EN 1997 Eurocode 7	Geotechnical design
EN 1998 Eurocode 8	Design provisions for earthquake resistance of structures
EN 1999 Eurocode 9	Design of aluminium alloy structures

(8) Separate sub-committees have been formed by CEN/TC 250 for the various Eurocodes listed above.

(9) This part 1.1 of Eurocode 5 is being published as a European Prestandard (ENV) with an initial life of three years.

(10) This Prestandard is intended for experimental application and for the submission of

comments.

(11) After approximately two years CEN members will be invited to submit formal comments to be taken into account in determining future actions.

(12) Meanwhile feedback and comments on this Prestandard should be sent to the Secretariat of CEN/TC 250/SC 5 at the following address:

Secretariat of CEN TC 250/SC 5
BST
Box 5630
S-114 86 STOCKHOLM

or to your national standards organization.

National Application Documents (NAD's)

(13) In view of the responsibilities of authorities in member countries for safety, health and other matters covered by the essential requirements of the Construction Products Directive (CPD), certain safety elements in this ENV have been assigned indicative values which are identified as "boxed" or by [ ]. The authorities in each member state are expected to review the "boxed values" and may substitute alternative definitive values for these safety elements for use in national application.

(14) Some of the supporting European or International standards may not be available by the time this Prestandard is issued. It is therefore anticipated that a National Application Document (NAD) giving any substitute definitive values for safety elements, referencing compatible supporting standards and providing guidance on the national application of this Prestandard, will be issued by each member state or its Standards Organization.

(15) It is intended that this Prestandard is used in conjunction with the National Application Document valid in the country where the building or civil engineering work is located.

Matters specific to this Prestandard

Drafting note: To be completed

Section 1 General

1.1 Scope

(1)P Part 2 of Eurocode 5 deals with the structural design of bridges made of timber and other suitable wood based materials, either singly or composite with concrete, steel or other materials.

(2)P This Part does not cover the special rules of seismic design of timber bridges, for which Part 2 of Eurocode 8 (ENV 1998-2) is relevant.

1.2 Relationship to other Eurocodes

(1)P The relevant, general rules and rules for buildings given in Eurocode 5, Part 1 (ENV 1995-1-1) also apply to bridges, unless otherwise specified in 1.2(3)P or in the text.

(2)P In case of disagreement between Part 2 and Part 1-1, the rules of Part 2 apply.

(3)P The following clauses of Part 1-1 do not apply to bridges:

- 2.4 3(2) Examples of minimum corrosion protection
- 5.4.1.3 Simplified analysis of trusses
- 5.4.1.4(3)
- 5.4.1.5 Trusses with punched metal plate fasteners
- 5.4.2 Roof and floor diaphragms
- 5.4.3 Wall diaphragms

(4)P For concrete components their and the reinforcing bars, the relevant provisions of Eurocode 2, especially Part 1-1 and Part 2 apply.

(5)P For steel components, the relevant provisions of Eurocode 3, especially Part 1-1 and Part 2 apply.

(6)P For the basis of design, see section 2.

1.3 Distinction between Principles and Application rules, and indicative values

(1)P Depending on the character of the individual clauses, distinction is made in this Eurocode between Pinciples and Application Rules.

(2)P The Principles comprise:

- general and definitive statements for which there is no alternative, as well as
- requirements and analytical models for which no alternative is permitted unless specifically stated.

(3)P The Principles are preceded by the letter P.

(4)P The Application Rules are generally recognised rules which follow the Principles and satisfy their requirements.

(5)P It is permissible to use alternative design rules which differ from the Application Rules given in this Eurocode, provided that it is shown that the alternative rules accord with the relevant Principles and are at least equivalent with regard to the mechanical resistance, serviceability and durability achieved for the structure with the present Eurocode.

(6)P Numerical values identified by [ ] are given as indications. Other values may be specified by the member states.

1.4 Definitions

In addition to the definitions given in ENV 1995-1-1 the following definitions are applicable

Glued laminated deck: Deck made of individual laminations glued together. The individual laminations may be glued laminated members

Nail-laminated deck: Deck made of individual boards or planks nailed together

Prestressing: The result of controlled deformations on a structural element or parts of a structure. An examples is the prestressing of timber decks by means of bars or tendons.

Stress-laminated deck: Deck made of individual laminations held together by a permanent lateral pressure high enough to guarantee friction, such that no inter-lamination slip occurs. The laminations may be boards, planks or glued laminated members.

1.5 Notations

Drafting note: To be completed

1.6 Normative references

This European Standard incorporates by dated or undated normative reference, provisions from other publications. These normative references are cited at the appropriate places in the text and the publications are listed hereafter. For dated references, subsequent amendments to or revisions of any of these publications apply to this European Standard only when incorporated in it by amendment or revision. For undated references the latest edition of the publication referred to applies.

European Standards:

prEN 912	Timber fasteners - Specifications for connectors for timber
ENV 1991-1:1994	Eurocode 1: Basis of design and actions on structures Part 1: Basis of design
ENV 1991-2-4	Eurocode 1: Basis of design and actions on structures Part 2-4: Wind actions
ENV 1991-3	Eurocode 1: Basis of design and actions on structures Part 3: Traffic loads on bridges
ENV 1992-1-1	Eurocode 2: Design of concrete structures Part 1-1: General rules - General rules and rules for buildings
ENV 1992-2	Eurocode 2: Design of concrete structures Part 2: Bridges
ENV 1993-1-1	Eurocode 3: Design of steel structures

	Part 1-1: General rules - General rules and rules for buildings
ENV 1993-2	Eurocode 3: Design of steel structures
	Part 2: Bridges
ENV 1995-1-1:1993	Eurocode 5: Design of timber structures
	Part 1-1: General rules - General rules and rules for buildings

Section 2 Basis of design

2.1 General

(1)P Eurocode 1, Part 1 (ENV 1991-1) applies.

(2)P In case of a disagreement between ENV 1995-1-1 and ENV 1991-1, ENV 1991-1 applies, unless specified below.

2.2 Fundamental requirements

(1) Consideration should be given to the possibility of permanent damage to a superstructure by a group of pedestrians deliberately causing resonant oscillations of the superstructure.

(2) As a general precaution therefore, the bearings should be of robust construction with adequate provision to resist upward or lateral movement.

2.3 Fatigue

(1)P Limit states related to fatigue are classified as ultimate limit states, and are treated in section 8.

2.4 Partial safety factors for materials

(1)P Partial safety factors for material properties for ultimate limit states, fundamental combinations (γ_M) are given in Table 1.1.

2.5 Durability

2.5.1 Constructional protective measures

(1) Direct weathering of timber parts by rain and solar radiation should be avoided or reduced by constructional protective measures.

(2) Where a partial or complete covering of the main structural elements is not possible, one or more of the following measures should be considered:

- avoidance of standing water on timber parts through appropriate inclination
- avoidance of openings, slots, etc., where water may accumulate or infiltrate
- avoidance of direct absorption of water (e.g. capillary absorption from concrete foundation) through use of appropriate barriers
- avoidance of fissures and delaminations, especially in all positions where the end grain would be exposed, by appropriate sealing and/or cover plates
- avoidance of swelling and shrinking movements by ensuring an appropriate initial moisture content and by reducing moisture changes through adequate surface protection.

Table 1.1: Partial safety factors for material properties for ultimate limit states, fundamental combinations

Timber and wood based materials - normal verification - fatigue verification	 γ_M = [1,3] $\gamma_{M,fat}$ = [ ]
Steel used in joints - normal verification - fatigue verification	 γ_M = [1,1] $\gamma_{M,fa}$ = [ ]
Steel (no prestressing elements) used in composite members	$\gamma_{M,s}$ = [1,1]
Concrete used in composite members	$\gamma_{M,c}$ = [1,5]
Shear connectors in composite members - normal verification - fatigue verification	 $\gamma_{M,s}$ = [1,1] $\gamma_{M,s,fat}$ = [ ]
Prestressing steel elements - cables or bars, based on ultimate strength - cables or bars, based on 0,2 % proof stress - other structural elements	 $\gamma_{M,s}$ = [1,8] $\gamma_{M,s}$ = [1,4] $\gamma_{M,s}$ = [1,1]

2.5.2 Protection of metal parts

(1)P Metal parts such as steel-to-timber joints or prestressing bars which become inaccessible once the bridge is complete, shall be designed and adequately protected for the intended design working life.

(2)P All metal parts shall have an adequate protection against corrosion, e.g. hot dip zinc coating.

(3) Under severe conditions (e.g. when the use of corrosive de-icing agents cannot be excluded), stainless steel of adequate composition or special extra coatings (e.g. epoxy) should be used.

(4) For joints exposed to fatigue loads the possibility of stress corrosion should be considered.

(5) Steel parts encased in concrete, like reinforcing bars and prestressing cables, should be protected according to the relevant clauses in ENV 1992-1-1.

2.5 Distribution of concentrated loads

(1) The distribution of concentrated loads (wheel loads) on bridge decks should be determined by elastic analysis.

(2) The distribution through to the middle plane of the deck plate of wheel loads and other concentrated loads, follow the indications in table 2.3 and figure 2.1.

(3) The effective width b_{ef} for a rectangular contact area may be as indicated in table 2.4. The

distances a and b are defined in figure 2.2.

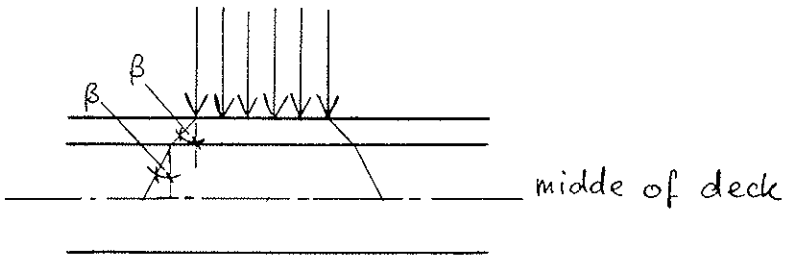

Figure 2.1: Distribution of concentrated loads.

Table 2.3: Angle of distribution of concentrated loads

	Angle β
Through the pavement	45 °
Through timber decks - in the direction of the laminations - perpendicular to the laminations	 45 ° 15 °
Through plywood decks	30 °

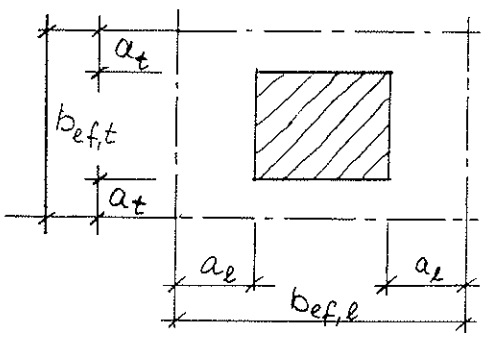

Figure 2.2: Effective width

Table 2.4: Contribution to effective width in metres

	a_l	a_t
Nail-laminated deck	0,15	0,10
Stress-laminated or glued laminated	0,60	0,20
Composite action timber/concrete	0,50	

Section 3 Material

3.1 General

3.1.1 Service classes

(1)P Bridges or bridge parts that are protected from direct weathering, e.g. covered bridges, shall be assigned to service class 2; other bridges or bridge parts to service class 3.

3.1.2 Load duration classes

(1) Variable actions due to the passage of traffic should be regarded as short-term *(or medium-term, still under discussion)* actions.

Section 4 Serviceability Limit States

4.1 General

(1) In the following certain serviceability limit states are describeded for bridges; they may be refered to when no other specifications are given by the competent authority.

(2) In general, serviceability limit states refer to the following aspects:

- to guarantee elastic behaviour in order to exclude
  - deviations from the intended geometry

- to limit deflections and curvature in order to exclude
  - unwanted dynamic impacts due to traffic

- to limit fundamental natural frequencies in order to exclude
  - vibrations due to traffic or wind annoying to pedestrians or passengers in cars
  - fatigue damage caused by resonance phenomena

- to achieve sufficient durability by
  - appropriate detailing to reduce moisture changes and biological attack

- to facilitate maintenance and repair by
  - accessibility of structural parts to permit maintenance, inspection and renewal
  - exchangeability of bearings, anchors, individual cables, transition joints etc. that may have a limited service life

(3) Some serviceability limit states may be verified by numerical assessments. Others may be dealt with by an appropriate design concept, or appropriate detailing.

4.2 Vibrations of pedestrian bridges

4.2.1 Vertical vibrations

(1)P For bridges where the fundamental natural frequency f_v of vibration in the vertical direction is greater than 5 Hz, no verification is required.

(2)P For bridges with a fundamental natural frequency f_v less than or equal to 5 Hz, the vertical acceleration a_v due to pedestrian traffic shall be 0,7 m/s^2 or less.

(3) For single span structures, the vertical acceleration may be taken as the greater value calculated from the following expressions, where equation (4.1) refers to excitation by a small group of pedestrians, while equation (4.2) refers to excitation by a stream of pedestrians:

$$a_v = 1200\ k_{f,v}\ k_a\ \frac{1 - e^{-n\,\delta}}{M\ \delta} \qquad (4.1)$$

$$a_v = 30\ k_{f,v}\ k_a\ \frac{1 - e^{-n\,\delta}}{m\ \delta} \qquad (4.2)$$

where:

l is the length of the bridge in m

b is the width of the bridge in m

m is the mass per unit area (self-weight) of the bridge in kg/m^2

$M = m\ l\ b$ is the mass of the bridge in kg

$\zeta = \frac{\delta}{2\ \pi}$ is the damping ratio

$n = \frac{l}{0{,}75}$ is the number of footsteps required to cross the bridge

k_a is a configuration factor

Note: Normally equation (4.2) is decisive for $l\ b \geq 40$ m^2

(4) The configuration factor k_a may be taken from table 4.1.

(5) For δ the value should be taken as:

$\delta = 0{,}06$ for structures without mechanical joints
$\delta = 0{,}10$ for structures with mechanical joints.

(6) The factor $k_{f,v}$ should be taken from figure 4.1.

Note: This simplified method is based on the assumption that the walking frequency corresponds to the fundamental natural frequency of the structure or to one half of it.

Table 4.1: Configuration factor k_a

Bridge configuration	k_a
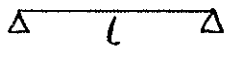	1,0
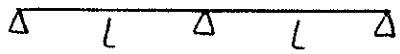	0,7
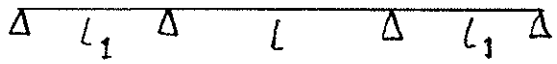	for $l_1/l = 1{,}0$ 0,6 for $l_1/l = 0{,}8$ 0,8 for $l_1/l \leq 0{,}6$ 0,9

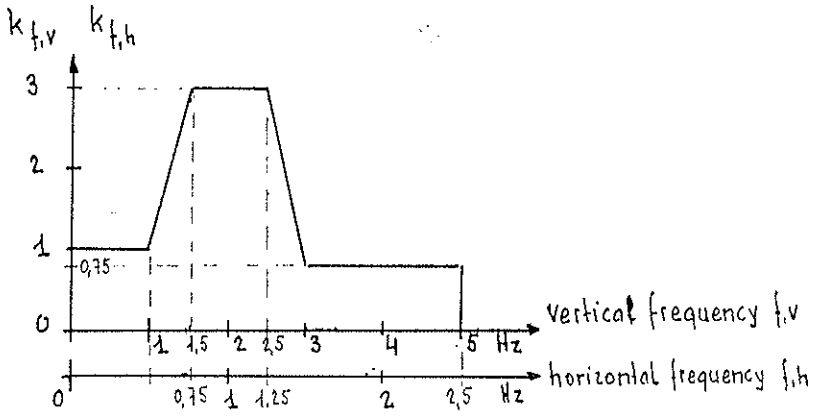

Figure 4.1: Relationship between coefficients $k_{f,v}$ and $k_{f,h}$ and natural frequencies

4.2.2 Horizontal vibrations

(1)P For bridges where the fundamental natural frequency f_h of vibration in the horizontal direction is greater than 2,5 Hz, no verification is required.

(2)P For bridges with a fundamental natural frequency f_h less than or equal to 2,5 Hz, the vertical acceleration a_v from pedestrian traffic shall not exceed 0,1 m/s^2.

(3) For single span structures, the horizontal acceleration may be taken as the greater value calculated from the following expressions, where equation (4.3) refers to excitation by a small group of pedestrians, while equation (4.4) refers to excitation by a stream of pedestrians:

$$a_h = 300\ k_{f,v}\ k_a\ \frac{1 - e^{-n\,\delta}}{M\ \delta} \tag{4.3}$$

$$a_h = 7{,}5\ k_{f,v}\ k_a\ \frac{1 - e^{-n\,\delta}}{m\ \delta} \tag{4.4}$$

The symbols are defined in 4.2.1(3).

Note: Normally equation (4.4) is decisive for $l\ b \geq 40\ m^2$

(4) The configuration factor k_a may be taken from table 4.1.

(5) For δ the values should be taken as given in 4.2.1(5).

(6) The factor $k_{f,h}$ should be taken from figure 4.1.

4.2 Vibrations caused by wind

(1)P No verification for the aerodynamic excitation of main bridge girders is required for
- road bridges having an effective span not greater than 50 m;
- pedestrian/cycle track bridges having no effective span greater than 30 m.

(2) The effective span should be taken as the maximum actual span or the half wave length for the fundamental flexural or torsional natural frequency, whichever is the greater.

(3)P Where the maximum effective span of a bridge is greater than given in 4.2(1)P, appropriate checks shall be carried out, according to the procedures given in ENV 1991-2-4.

(4)P Vibrations of members induced by vortex excitation shall be limited to avoid fatigue damage.

Note: Guidelines on the calculation of the stresses induced by vortex excitation is given in ENV 1993-2, Annex 5.9

4.3 Dynamic effects due to traffic

(1) The natural frequencies and deflections of highway bridge structures should be limited such, that the maximum deflection due to any frequent lorry according to ENV 1991-3, section 4, table 4.6 should not exceed the limits given in figure 4.2.

(2) In order to ensure that the provisions for impact included in the traffic loads given in ENV 1991 Part 3 apply, the roadway should be designed such that it exhibits an equal deflection behaviour along the length with no abrupt changes in stiffness or smoothness of surface giving rise to particular impact.

(3) Sudden changes in the slope of the deck or changes of level at expansion joints should be avoided.

(4) Supporting elements at the end of the bridge deck should be designed such that the deflection limit specified for the correct functioning of the expansion joint are not exceeded. A deflection of 5 mm should not be exceeded.

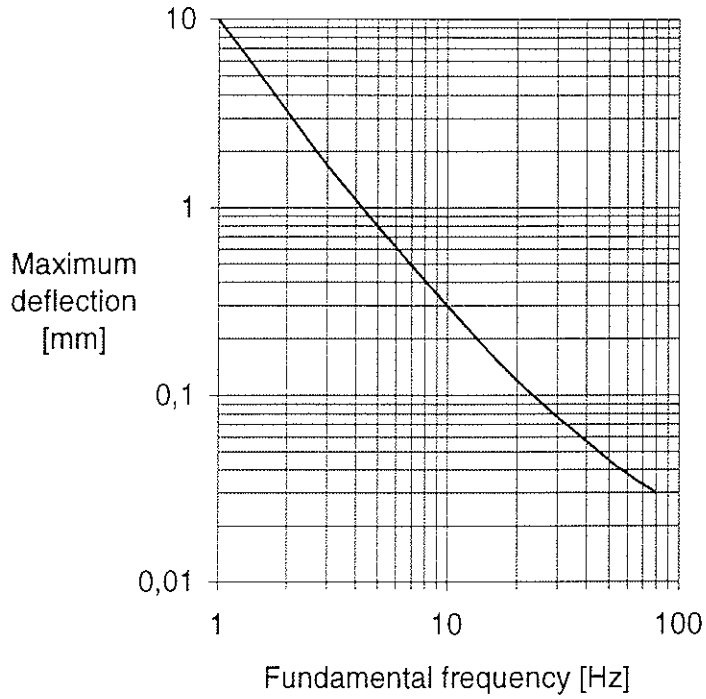

Figure 4.2: Maximum deflection due to frequent lorry load as a function of the fundamental natural frequency

Section 5 Ultimate limit states

5.1 Reinforced members

5.1.1 General

(1) This clause deals with timber members reinforced with other materials, e.g. by wood of other species, wood-based materials, glass- or carbon fibre or by steel, continuously glued to the timber. Herein are only considered reacting reinforcements; additional prestressing is dealt with in 5.2.4 and 5.3.

(2) The design models for the different limit states should, where necessary, take into account the following:

- different material properties (e.g. modulus of elasticity, strength and failure mode)
- different long-term behaviour of the materials (creep, relaxation)
- different climatic behaviour of the materials (temperature, moisture variations)
- different design situations (stages of construction, change of support conditions).

5.1.2 Longitudinal reinforced timber

(1)P In the analysis of longitudinally reinforced timber the assumptions shall be made of

- elastic behaviour until failure

- linear strain distribution over the cross section.

5.1.3 Transversally reinforced timber

(1)P Subclause 5.1.2(1)P applies.

(2)P Tensile strength perpendicular to grain shall be disregarded.

(3) The resistance of transversally reinforced timber with indirect load transfer as shown in figure 5.1 is limited by glued-in action, see Annex A.

5.1.4 Shear reinforcement

(1) The following rules deal with shear reinforcements of steel bars, see figure 5.2

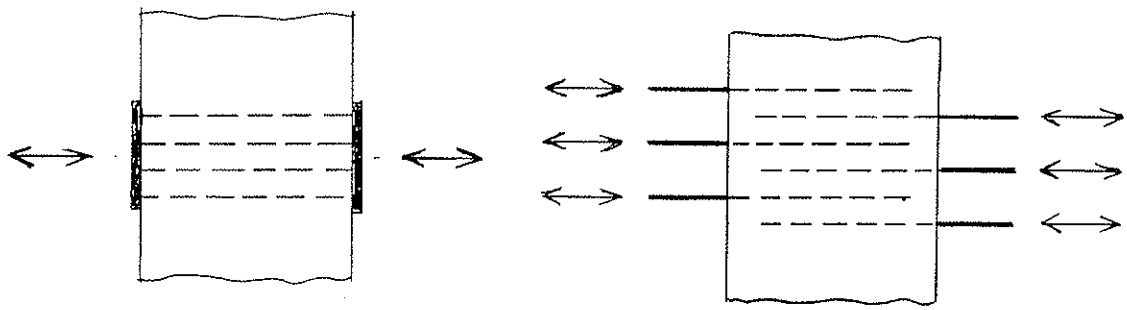

a) b)

Figure 5.1: Examples of load transfer by transversally reinforced timber: a) direct load transfer, b) indirect load transfer

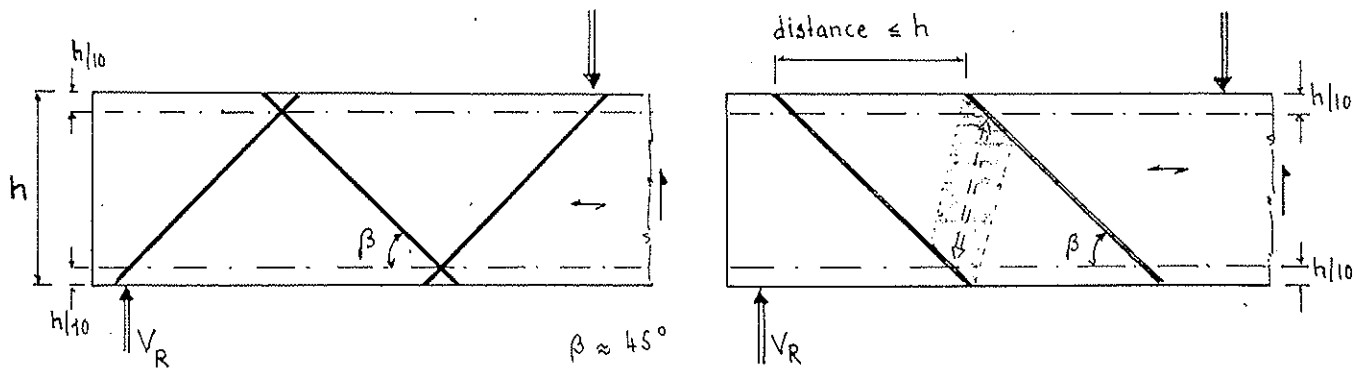

a) b)

Figure 5.2: Examples of shear reinforcement and geometric requirements

(2) The shear resistance should be taken as the greater of

$V_{R,\,timber} + 0{,}5\ V_{R,\,steel}$

or

$$V_{R,\,steel} + 0{,}5\ V_{R,\,timber}$$

where

$V_{R,\,steel}$ is the shear resistance in N of the reinforcement, determined using a truss model, see (3) and (4)
$V_{R,\,timber}$ is the shear resistance of the timber in N

(3) When the inclination of the steel bars is approximately 45 ° the shear resistance of the reinforcement may be taken as

$$V_{R,\,steel} = 0{,}7\ f_y\ A_{steel} \tag{5.1}$$

where

A_{steel} is the area of the reinforcing bar acting at one cross section
f_y is the yield strength of the steel bar.

(4) For the case shown in figure 5.7 b, the value of $V_{R,\,steel}$ should be limited to

$$V_{R,\,steel} \leq 0{,}4\ f_{v,\,k}\ b\ h \tag{5.2}$$

(4) The diameter of the steel bars should be limited by

$$d \leq \frac{h}{50}$$

where

h is the depth of the member.

(8) Unless a more detailed analysis is made, the shear stiffness of the reinforced member may be assumed to be increased in the same proportion as the shear resistance.

5.2 Decks

5.2.1 General

(1) The following rules are related to slabs used as deck systems as shown in figure 5.3

(2) Slabs may be analysed using a grid analogy or an orthotropic plate theory.

(3) For nail-laminated, stress-laminated and glued-laminated decks made of softwood laminations the relationships for the properties perpendicular to the laminations, the Poisson ratio μ may be taken from table 5.1.

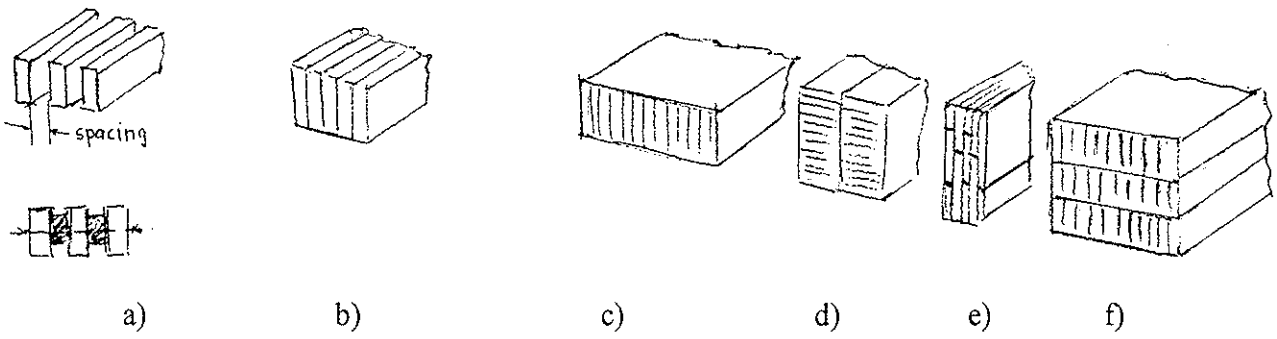

Figure 5.3: Types of deck systems: a) stringer deck, individual laminations cross-linked by connectors, b) nail-laminated or stress-laminated sawn timber deck, c) glued laminated deck, d) glued and stress-laminated, e) glued laminated and steel reinforced, f) glued and stress-laminated and steel reinforced

Table 5.1: Material properties of laminated decks perpendicular to the laminations

Type of deck	E_{90}/E_0	G/E_0	μ
Nail-laminated	- [1)]	0,03	-
Stress-laminated	0,015	0,03	0,3 to 0,4
Glued-laminated	0,030	0,06	0,3 to 0,4

[1)] Negligeable flexural stiffness in transverse direction

(4) For transversally steel reinforced glued-laminated decks, the ratio G/E_0 may be taken as $G/E_0 = 0{,}06$.

Note: The ratio E_{90}/E_0 depends largely on the level and the position of the reinforcement.

(5)P For decks made of wood-based materials such as plywood and particleboard, composite action of the deck and the supporting elements shall take into account the behaviour of the connections.

5.3.2 Load sharing

(1) The system strength factor k_{ls} in timber decks depends on the number of members that are considered to mutually support the load and on the coefficient of variation of the strength of the member involved.

(2) Unless a more detailed analysis is made, the values of k_{ls} given in figure 5.4 may be used for the bending and shear strength of laminated decks (nail / stressed / glued) provided the following requirements are fulfilled:

- the load-distribution system is designed to support the applied permanent and variable loads
- each element of the load-distribution system is continuous, i.e. without butt joints or mechanical joints.

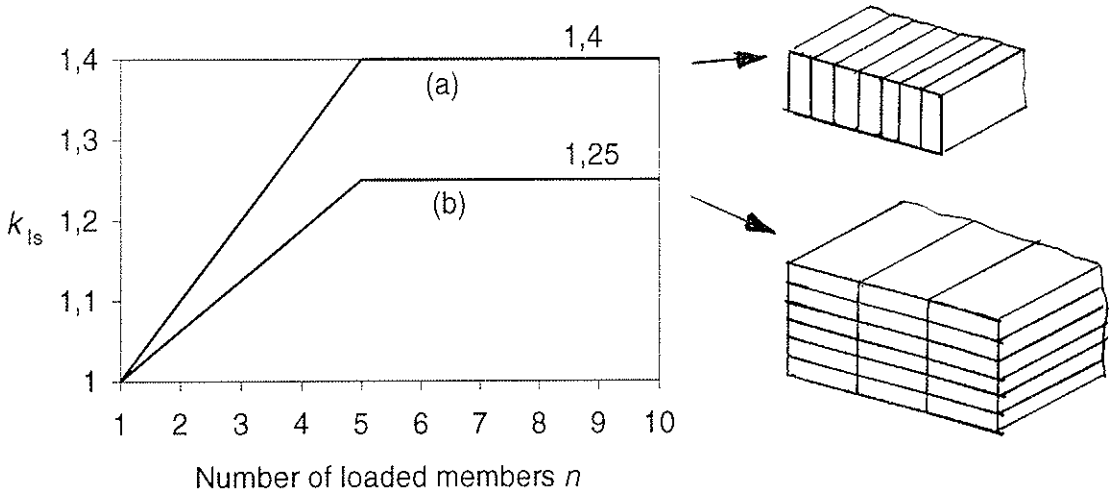

Figure 5.4: System strength factor k_{ls} for a) sawn or glued laminations, b) glued laminated beams

5.2.3 Reinforced decks

(1)P The relevant parts of 5.2 apply.

5.2.4 Stress-laminated decks

(1) Typical examples of stress-laminated decks are given in figure 5.5

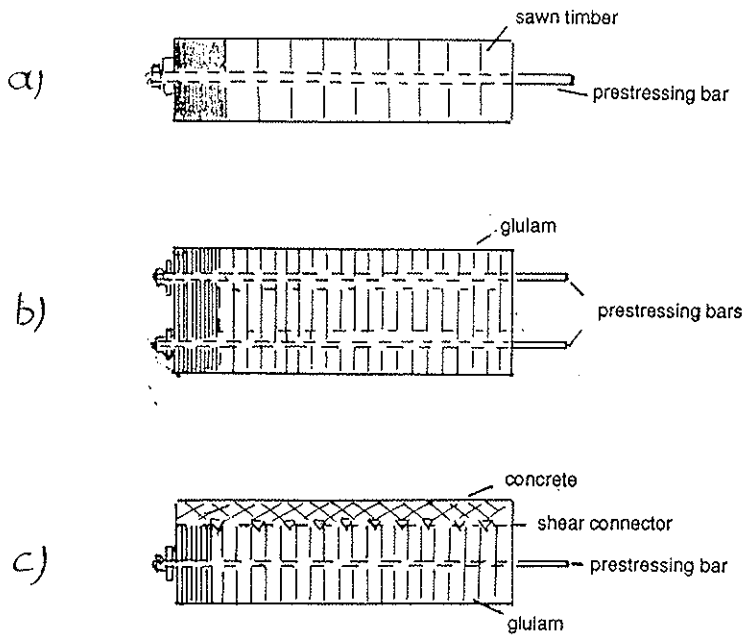

Figure 5.5: Typical examples of stress laminated decks: a) stress-laminated, b) glued and stress-laminated, c) stress-laminated and composite

2(P) The prestressing forces shall be such that no inter-laminar slip occurs.

Note: The prestressing forces required to achieve continuum behaviour depend on the friction between the laminations. The coefficient of friction is a function of wood species, roughness of contact surface, treatment of the timber and residual stress level between laminations. Creep and drying shrinkage may affect the residual stress level between the laminations.

(3) The minimum residual normal pressure between laminations of softwood should not be less than 0,35 N/mm^2.

(4) Uniform normal pressure may be assumed, provided that the following conditions according to (5), (6), (7) and (8) are observed, see figure 5.6.

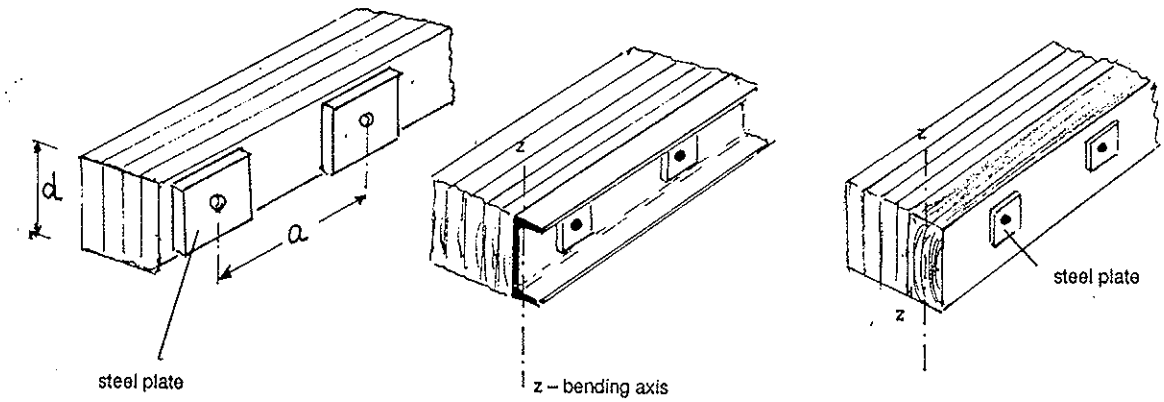

a) b) c)

Figure 5.6: Examples of anchorage details. (a) steel anchorage plates, (b) steel u-shaped bulkhead, (c) wood bulkhead

(5) For individual steel anchorage plates the contact area should fulfill the following condition:

$$A_s \geq \frac{a\ h}{2{,}5}$$

where

A_s is the contact area of the steel plate
a is the distance between prestressing bars
h is the depth of the deck

(6) For bulkheads of steel or timber which may be integral parts of the deck, the flexural stiffness should fulfill the following condition:

$$\frac{E\ I_z}{h} \geq 1{,}0 \times 10^9 \quad [\text{Nmm}] \qquad \text{for bulkheads of steel} \qquad (5.4)$$

$$\frac{E\ I_z}{h} \geq 3{,}0 \times 10^9 \quad [\text{Nmm}] \qquad \text{for bulkheads of timber} \qquad (5.5)$$

where

h is the depth of the deck

(7) The distance a between prestressing bars should fulfill the following condition:

$$a \leq \frac{b}{6}$$

where

b is the width of the deck

(8) The stiffness ratio of steel to timber should the following condition:

$$\frac{A_{\text{steel}}\ E_{\text{steel}}}{A_{\text{timber}}\ E_{90}} \leq 2{,}2 \qquad (5.6)$$

where

A_{steel} is the cross sectional area of the prestressing bar
E_{steel} is the modulus of elasticity of steel
$A_{\text{timber}} = a\ d$
E_{90} is the modulus of elasticity of timber perpendicular to grain

Note: Residual compressive force depends partly on the stiffness ratio of steel to timber. A lower value of the stiffness ratio is more favourable. Therefore the use of high-strength steel bars is indicated.

(9)P Maximum butt joint frequency shall be limited to 1 in 4.

(10)P In the calculation stiffness and strength of stress-laminated deck shall be reduced correspondingly to the number of butt joints.

(11)P For road and railway bridges, butt joints shall be supported at each joint to ensure the integrity of the deck due to moving loads.

Note: An example is given in figure 5.7.

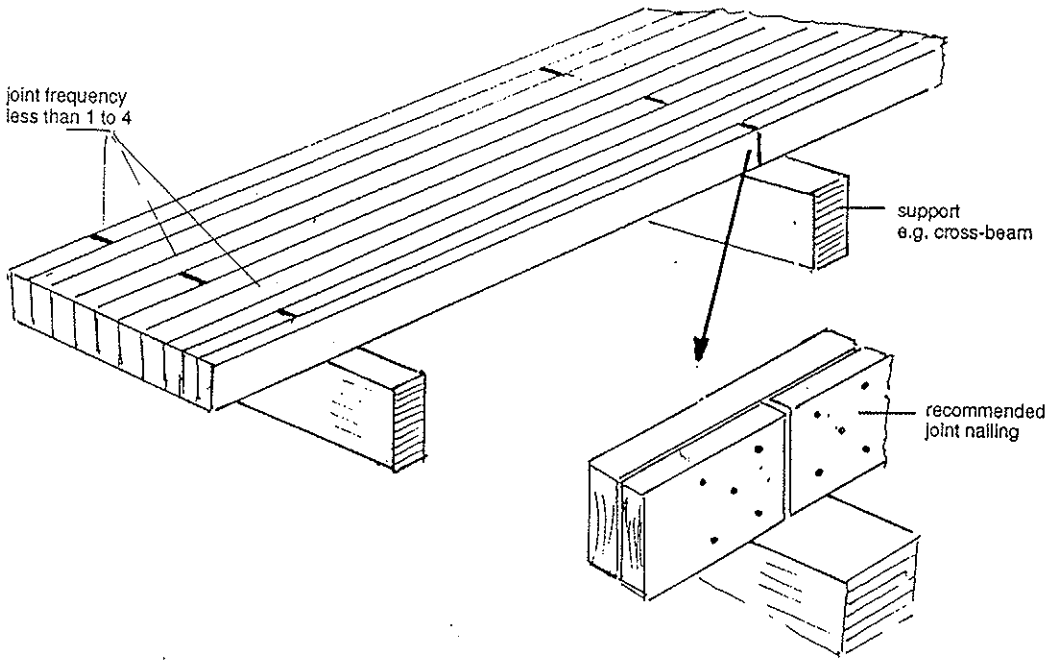

Figure 5.7: Example of butt-joint layout for road or railway bridge decks with a butt joint frequency of 1 in 4

5.3 Longitudinally prestressed members

(1) Subclause 5.1.1(2) applies

5.4 Timber and concrete composite members

5.4.1 General

(1) This clause deals with the following types of timber-concrete composite elements, which are mainly subjected to bending:

- timber-girder concrete composite deck (see figure 5.8 a)
- timber-deck concrete composite (see figure 5.8 b)

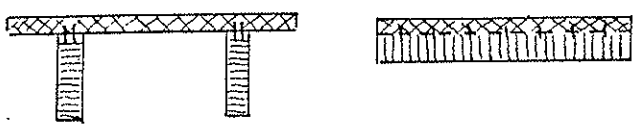

a) b)

Figure 5.8: Cross section of timber concrete composite decks: a) timber-girder concrete composite, b) timber-deck concrete composite

(3) The effective width of timber-girder concrete composite decks should be determined as for a concrete T-section.

(4)P The connectors shall be designed to transmit all forces due to the composite action, i.e. any adhesive bond between the timber and concrete surfaces shall be disregarded.

(5)P For fatigue verification of connectors, the effect of actions on the connectors shall be taken to remain in the elastic range.

(6)P For other ultimate limit states, elastic-plastic behaviour of the connector may be taken into account.

(7) In addition to 5.3.3 - 5.3.4 of ENV 1995-1-1 the provisions given in the following apply.

(8) Displacements between timber and concrete parts of the cross section affect the strain distribution. For the individual parts (timber and concrete) a linear strain distribution may be assumed (see figure 5.9).

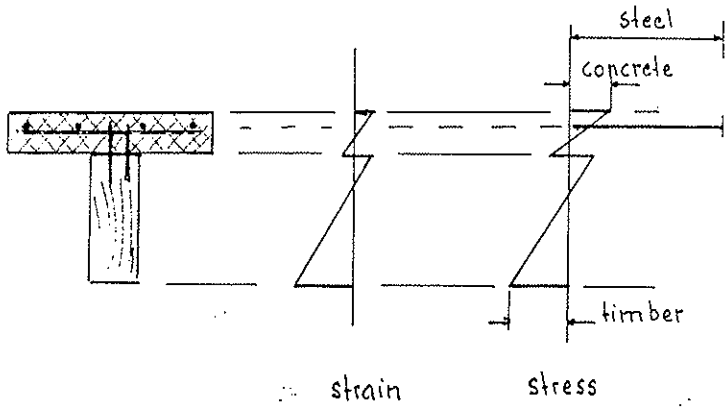

Figure 5.9: Strain and stress distribution over a composite cross section due to bending

(8) P The tensile strength of the concrete shall be disregarded.

(9) Stress concentrations due to
- abrupt changes of section modulus
- notches
- discontinuities in the connecting devices (by arrangement or/and different stiffness)
- concentrated introduction of forces

should be taken into account.

5.4.2 Composite beams in bending

(1) When the size factor is used according to 3.3.2(4) of ENV 1995-1-1 it should be related to an effective depth of the beam calculated as (see figure 5.10)

$$h_{ef} = 2\ a_u \tag{5.7}$$

(2) For the calculation of the strain distribution in the timber, the concrete within the section should be assumed uncracked. The tensile forces acting on the steel should then be derived from the equilibirum condition based on this assumption.

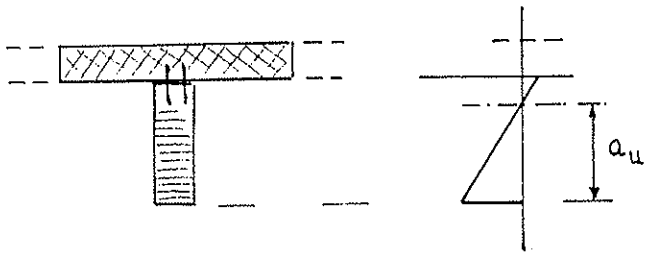

Figure 5.10: Definition of a_u

5.4.3 Connectors

5.4.3.1 General

(1) Figure 5.11 shows a range of suitable shear connectors. These have a range of force-displacement characteristics and failure modes,

(2) Connectors should be capable of transmitting tensile forces between the timber and concrete perpendicular to the shear plane.

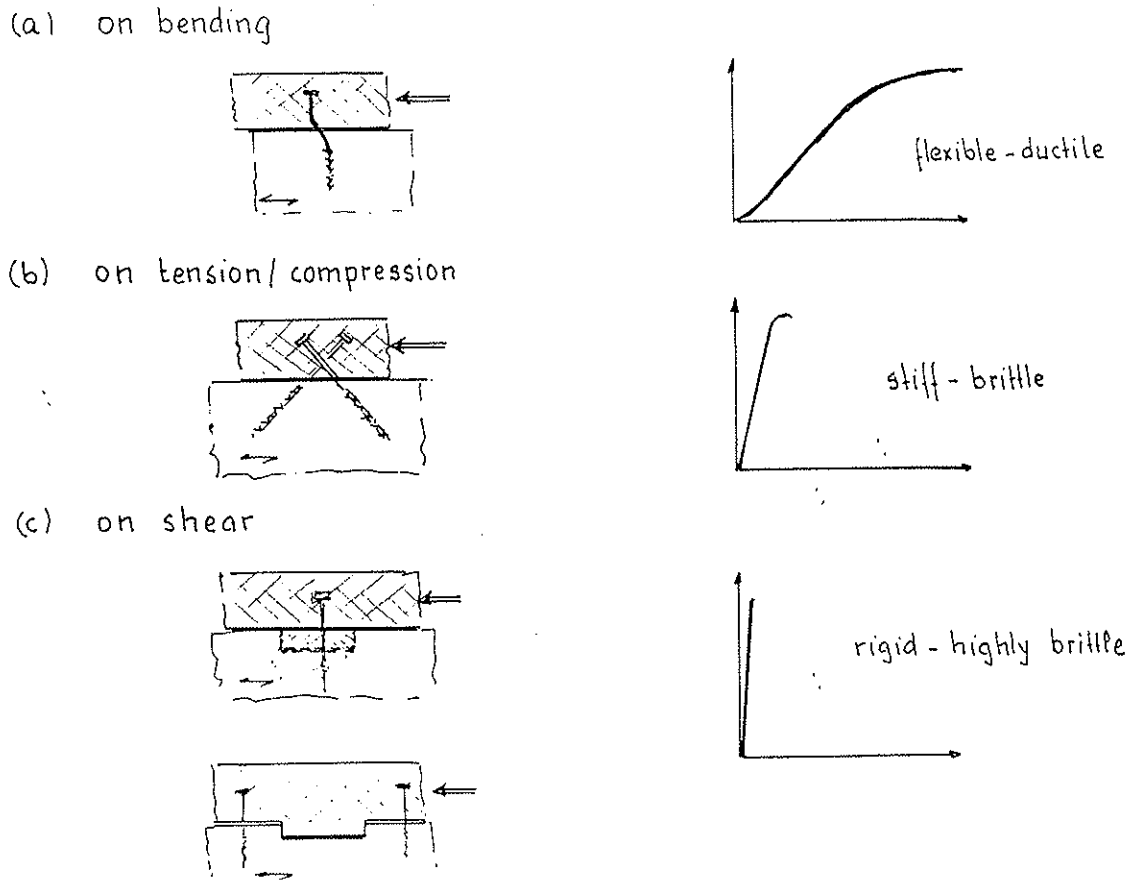

Figure 5.11: Different connector types and force-displacement characteristics

(3)P The lengthwise distribution of shear forces between the timber and the concrete shall be determined with regard to the assumed distribution of the normal stresses. The condition of equilibirum shall be fulfilled for any part of the composite beam.

(4)P For repeated actions such as those arising from traffic, it shall be ensured that effects on connectors shall remain in the elastic range.

(5) Where shear connectors are concentrated locally, each connector should be designed for bending moment in addition to shear force. The risk of splitting in timber and cracking in concrete should also be taken into account.

5.4.3.2 Flexible and ductile connectors

(1) Screws, dowels and annular ringed shank and threaded nails, inserted perpendicular to the shear plane, should be designed in accordance with the rules for timber-to-timber joints according to section 6 of ENV 1995-1-1.

(2) For screws, dowels and annular ringed shank and threaded nails, inserted perpendicular to the shear plane, the stiffness values given in 4.2 of ENV 1995-1-1 may be increased by 50 %, see figure 5.10 a.

(3)P In the case of an intermediate non-structural layer between the timber and the concrete (e.g. for formwork), see figure 5.12, the strength and stiffness parameters shall be determined by tests.

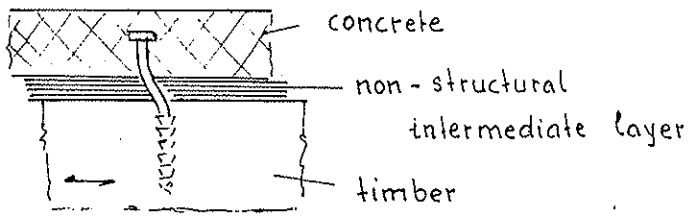

Figure 5.12: Formwork as an intermediate layer

5.4.3.3 Truss type connectors

(1) In the case of uni-directional inclined connectors the forces should be assumed to be transmitted as tensile forces as shown in figure 5.13.

(2) In the case of two-directional truss-like inclined connectors the shear force should be taken as tensile and compression forces as shown in figure 5.14.

(3) For repeated actions, truss-like connectors should be used. For fatigue resistance see 6.1(4)P and section 8.

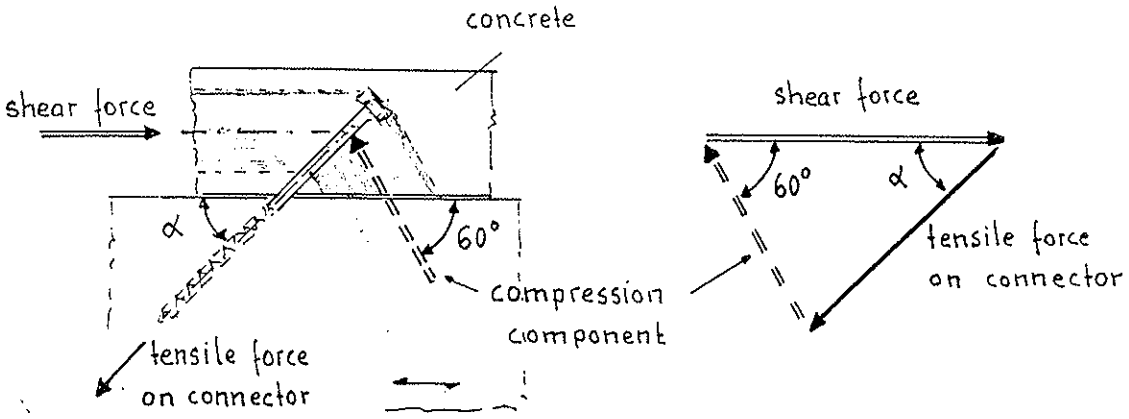

Figure 5.13: Analytical model for inclined connectors transmitting tensile and shear forces

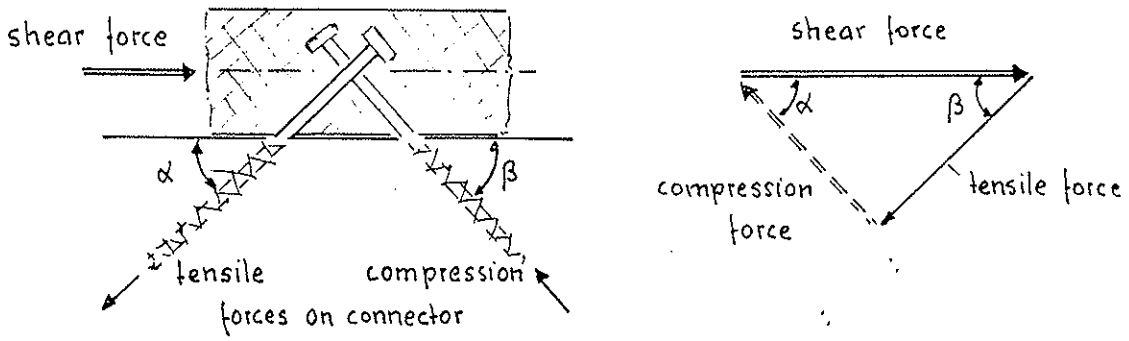

5.14: Transmission of forces for truss-like orientation of connectors

5.4.3.4 Grooved connectors

(1) For longitudinally or cylindrically grooved connectors, see figure 5.10 c, the shear force should be taken by direct contact pressure between the wood and the concrete cast in the groove.

(2) The connection may be assumed to be completely stiff.

Section 6 Joints

6.1 General

(1)P In bridges where frequently varying actions due to traffic may be expected to occur, the following provisions shall apply, in addition to those given in section 6 of ENV 1995-1-1.

6.2 Fatigue verification

(1)P The effect of fatigue shall be taken into account according to section 8.

6.3 Single-shear joints

(1)P In situations where repetitive loading occurs, dowelled single shear timber-to-timber and steel-to-timber joints shall be secured by the addition of bolts, fastened with suitable nuts and washers.

(3)P Nails or punched metal fasteners shall not be used.

6.4 Lateral load-carrying capacity of dowel-type fasteners

6.4.1 Timber-to timber and panel-to-timber joints

(1) The expressions given in 6.2.1 of ENV 1995-1-1 to determine the design load-carrying capacity for fasteners are only valid for a single fastener.

(2) In the expressions according to (1) the factor of 1,1 should be replaced by 1,0.

6.4.2 Steel-to timber joints

(1) The expressions given in 6.2.2 of ENV 1995-1-1 for the design load-carrying capacities are only valid for a single fastener.

(2) In the expressions according to (1) the factor of 1,1 should be replaced by 1,0 and the factor of 1,5 by 1,4.

6.5 Dowelled joints

(1) The load-carrying capacity of n dowels parallel to grain may be based on the effective number n_{ef} given by

$$n_{ef} = 2 \left(\frac{n}{2} \right)^{k_j \beta_r} \qquad (6.1)$$

with

$$\lambda_r = \frac{\lambda_{ef}}{\lambda_y} \quad \text{but} \quad \lambda_r \leq 1$$

$$\lambda_{ef} = \frac{t_2}{d} \qquad (6.3)$$

where

k_j is a factor taking into account the joint geometry and fabrication tolerances
λ_r is the slenderness ratio of the fastener
t_2 is the thickness of the middle member
d is the diameter of the dowel

provided that

$$t_1 f_{h,1,k} \geq 0{,}5\ t_2 f_{h,2,k} \tag{6.4}$$

where

t_1 is the thickness if the side member
$f_{h,1,k}$ characteristic is the embedding strength of the side member
$f_{h,2,k}$ characteristic is the embedding strength of the middle member.

(2) The definition of the slenderness ratio λ_y is given in figure 6.1 where the load-carrying

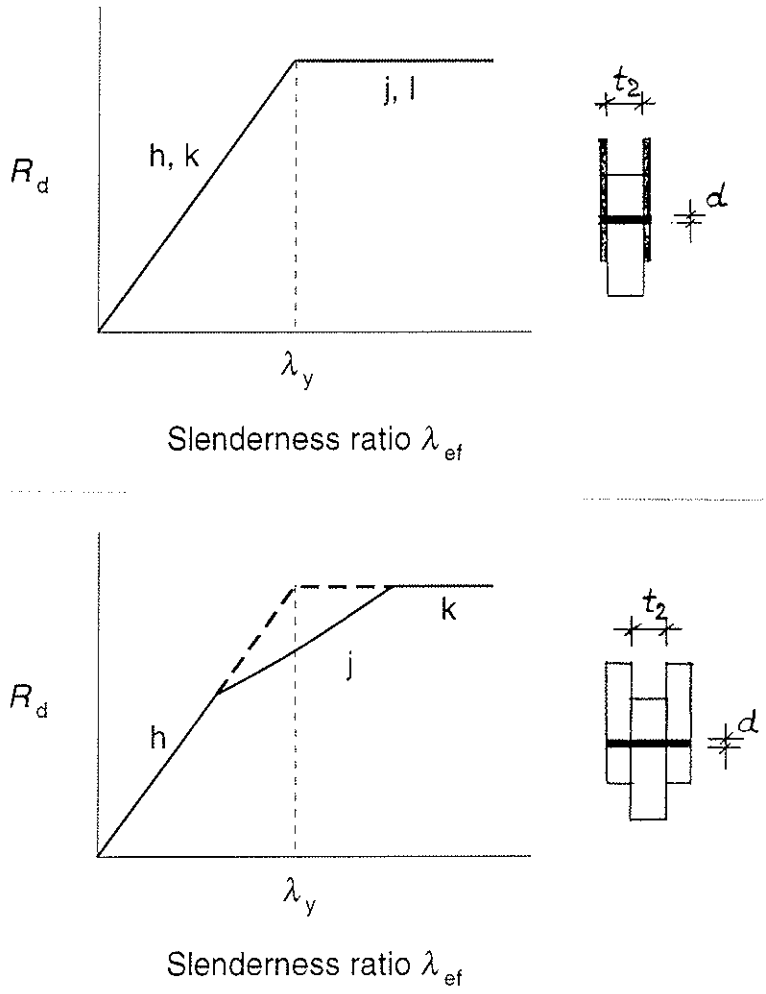

Figure 6.1: Load-carrying capacity as a function of the slenderness ratio λ_{ef}: a) steel-to-timber joint, b) timber-to-timber joint

capacity is shown as a function of the slenderness ratio λ_{ef}. The slenderness ratio λ_y is the ratio t_2/d where, for steel-to-timber joints, either failure mode (h/k) or failure modes (j,k) are possible according to Figure 6.2.2 in ENV 1995-1-1. For timber-to-timber joints the slenderness ratio λ_y is obtained from the intersection of the curves for failure modes (h) and (k) according to figure 6.1.2 in ENV 1995-1-1.

(3) Unless a better performance can be verified, the factor k_j may be taken as $k_j = 0,8$.

Section 7. Fabrication and erection

(1)P In stress-laminated decks, the effective normal pressure shall be controlled.

(2) When prestressing is applied the moisture content of the laminations should not deviate from the moisture content in the final stage.

Section 8 Fatigue verification

(1)P For structures or structural parts that are subjected to frequent stress variations from traffic load or wind it shall be verified that no failure or major damage will occur due to fatigue during the intended life.

(2)P The fatigue calculations shall be related to the stress range $\Delta\sigma$

$$\Delta\sigma = |\sigma_{max} - \sigma_{min}| \tag{8.1}$$

where

σ_{max} is the characteristic maximum stress from the fatigue action
σ_{min} is the characteristic minimum stress from the fatigue action

(3)P The stress shall be determined by an elastic analysis under the specified action.

(4)P The stresses shall include stresses in stiff or semi-rigid connections and secondary effects from deformations and distortions.

(5)P A fatigue verification is not required if $\Delta\sigma$ is less than 10 % of the corresponding normal design strength.

(6)P For a periodic loading with n cycles, it shall be verified that

$$\Delta\sigma = \frac{f_{fat,k}}{\gamma_{M,fat}} \tag{8.2}$$

where

$f_{fat,k}$ is the characteristic fatigue strength
$\gamma_{M,fat}$ is the partial safety factor for fatigue, see 2.3

(7) The characteristic fatigue strength may be calculated as

$$f_{fat,k} = k_{fat}\, f_k \tag{8.3}$$

where f_k is the characteristic strength for static load and k_{fat} is given in figure 8.1.

(8) In figure 8.1, m may be taken as m = 3 and the value $k_{fat,\infty}$ may be taken from table 8.1.

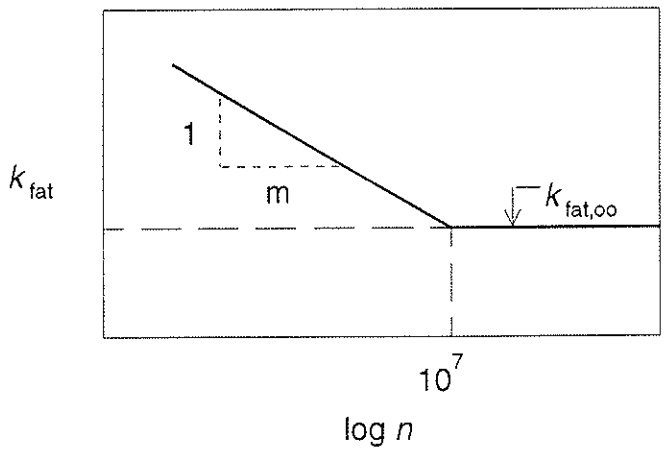

Figure 8.1: Relationship between $k_{fat,\infty}$ and the number of cycles n

Table 8.1: Values of $k_{fat,\infty}$

	$k_{fat,\infty}$
Members in - compression perpendicular and parallel to the grain	[0,6]
- bending, tension tension/compression	[0,3]
- shear	[0,25]
Joints with - dowels	[0,3]
- split-ring connectors according to prEN 912	[0,15]

(10)P In the case of loading in the form of a spectrum with n_i cycles corresponding to a stress range $\Delta\sigma_i$ an equivalent periodical stress range $\Delta\sigma_{eq}$ with n cycles shall be calculated according to the Palmgren-Miner rule as

$$\Delta\sigma_{eq} = \left[\frac{\left(\sum n_i \times \Delta\sigma_i\right)^m}{n}\right]^{\frac{1}{m}} \tag{8.4}$$

with

$$n = \sum n_i \tag{8.5}$$

Annex A (informative)
Glued-in rods

A.1 Scope

(1) This annex gives information on the design of glued-in steel rods which may be used as load introduction device in timber elements, especially in glued laminated timber.

(2) the design methods described in this annex may also be used for screw type rods, when a reliable mechanical load transfer is possible.

(3) The use of glued-in rods shall be limited to structures assigned to service classes 1 and 2, and to conditions of use which will remain in a temperature range between -20 °C and +50 °C.

A.2 General

(1) The resistance of connections using glued-in rods is limited by the following :
- (a) the strength of the steel rod
- (b) the load transfer capacity between the rod and the timber
- (c) the strength of the timber element

(2) Brittle failure modes should be avoided. The design should be such that failure of the rod is liable to occur according to indent (a) in (1).

(3) It should be taken into account that the characteristic load-carrying capacity of a multiple-fastener joint (i.e. several glued-in rods are acting together) will frequently be less than the sum of the individual glued-in rods. This effect is normally caused by brittle failure modes.

(4) In the case of rods in compression, consideration should be given to the possibility of buckling. This may be prevented by suitable restraints.

(5) The buckling length should be taken as

$$l_{cr} = 0{,}7\ l_a \qquad \text{(A.1)}$$

where

l_a is the anchorage length of the rod

(6) The resistance of the joints involving glued-in rods normally depends upon adequate strength within the timber itself. Attention should be given to the state of stress, especially in zones with tension perpendicular to grain or with shear stresses.

(7) Where anchorage forces occur which are parallel to grain and concentrated to a limited zone of the timber member, the tensile stresses should be calculated in relation to the effective area, see figure A.1.

(8) The spacing of rods and the hole diameters should satisfy the following conditions:

$$a_1 \leq 6\ d_h \tag{A.2}$$

$$d_h \leq 1{,}25\ d \tag{A.3}$$

where

h, b are the depth and width of the timber member
a_1 is the spacing of the rods
d_h is the diameter of the hole
d is the diameter of the rod

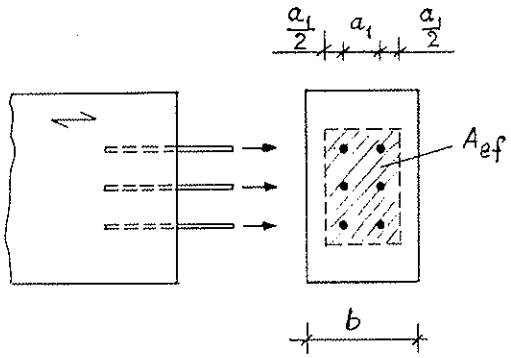

Figure A.1: Definition of effective area A_{ef}

(9) For softwoods, the design load-carrying capacity in tension per glued-in rod may be taken as, see figure A.2:

$$F_{t,\alpha,d} = \frac{0{,}15\ \rho_k}{\sin\alpha}\ \frac{k_{mod}}{\gamma_M}\ h_e^{0,7}\ b_e^{0,7}\left(\frac{h_e}{h}\right)^{0,2} \tag{A.3}$$

where

$F_{t,\alpha,d}$ is the design load-carrying capacity in Newtons
α is the angle between the rod and the direction of grain
ρ_k is the characteristic density of the timber member in kg/m^3
h_e is the anchorage depth of the rod perpendicular to grain in mm
$b_e = 6\ d_h$ is the effective width per rod in mm with $b_e \leq b$
d_h is the diameter of the hole in mm

(10) When the zone between rods is subjected to shear forces, see figure A.3, additionally to A.2(9) the shear resistance of the timber should be taken into account. For $h_e / h \leq 0{,}9$ the design load-carrying capacity should be taken as

$$F_{v,d} = f_{v,d}\ b_e\ h_e \tag{A.4}$$

where

$F_{v,d}$ is the design shear load-carrying capacity of the timber

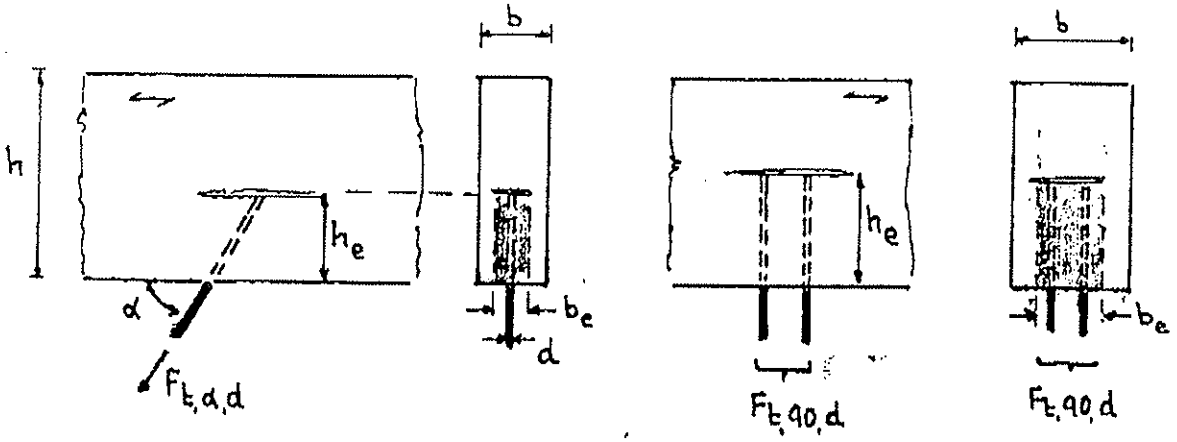

Figure A.2: Anchorage tensile force acting at an angle to grain

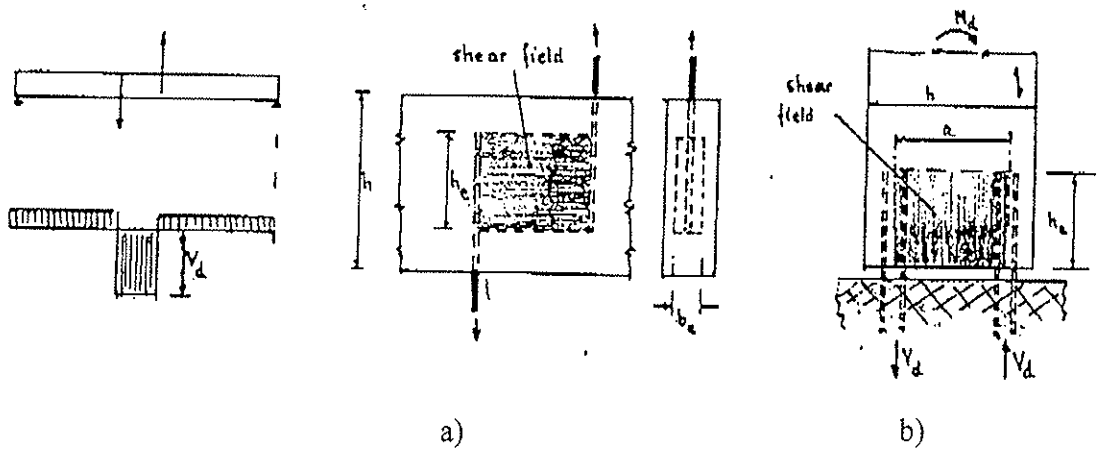

a) b)

Figure A.3: Shear zone between glued-in rods: a) Shear zone in a beam, b) shear zone at column base

A.3. Load transfer between steel rod and timber

(1) The load may be transferred from the steel rod to the timber in various ways, see figure A.4:

(a) mechanically, e.g. by screw-type rods
(b) glued connection, e.g.
(c) both mechanically and glued connection.

(2) The design load-carrying capacity should be taken as the smallest value determined for the following failure modes:

(a) local shear strength of timber around the hole surface
(b) adhesion strength glue-to-timber
(c) shear and tension strength of the adhesive
(d) adhesion strength glue-to-steel

Failure mode (a) depends also on the angle between the rod and the grain. Failure modes (b) to (d) are mainly dependent on the glue properties and in the case of failure mode (d) also on the surface properties and degree of mechanical anchorage.

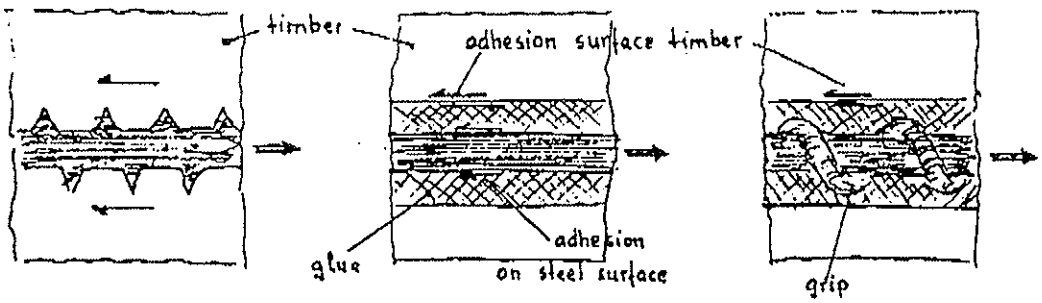

Figure A.4: Load transfer between steel rod and timber: a) mechanical, b) glued, mechanical and glued

(3) Failure mode (a) according to (2) shall be decisive

(4) The local characteristic shear strength of timber should be taken as

$$f_{v,k} = 1{,}2 \times 10^{-3}\, d^{-0{,}2}\, \rho_k^{1{,}5} \qquad \text{(A.5)}$$

where

$f_{v,k}$ is in N/mm^2
d is the rod diameter in mm
ρ_k is the characteristic density of timber in kg/m^3

This relationship may be used for any angle between the rod and the grain. When the strength of the adhesive is not critical, the rod diameter may be replaced by the hole diameter.

(5) Tests to determine the adhesion capacity and strength of the adhesive shall take account of the effect of moisture and temperature. The load may be transmitted mechanically, in which the adhesion strength need not be determined.

(6) For service class 2 the values of k_{mod} according to ENV 1995-1-1 should be reduced by 20 %.

(7) For screw-type rods the load-carrying capacity per rod should be taken as the smallest value resulting from the following failure modes:

(a) local shear strength of timber around the hole surface
(b) local strength of timber due to crushing
(c) local resistance of screw flanks (shear and bending)

(8) Failure mode (c) shall not be decisive.

(9) For the local shear strength of timber A.3.3 applies where in d is included the thread of the screw .

(10) The shape of the thread is important with respect to density and wood species. Since large friction may cause local shear damage of the timber in the hole, the surfaces should be

smooth and the diameter of the pre-drilled holes appropriate.

(11) For screw-type rods only the threaded part of the penetration length shall be used in the analysis.

(12) The minimum spacings and distances should be taken as

$$a_1 \geq 4\,d$$

$$a_2 \geq 2{,}5\,d$$

where a_1 and a_2 are defined in figure A.5.

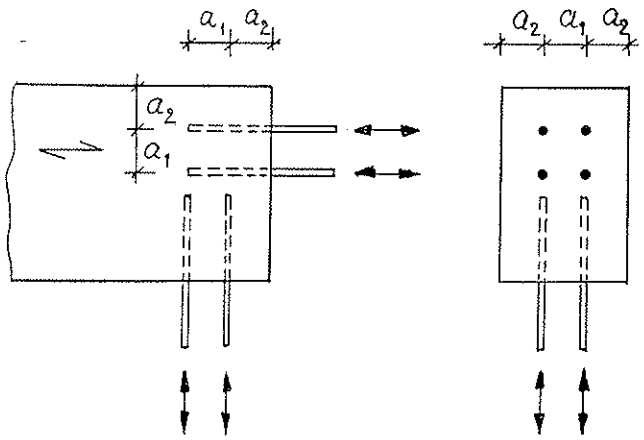

Figure A.5: Definition of spacings a_1 and distances a_2

(13) For the anchorage length l_a the following requirements according to table A.1 should be observed, see figure A.6

Table A.1: Requirements for anchorage length

Glued-in rods	$l_a \geq 0{,}4\,d^2$ $l_a \geq 8\,d$
Screw-type rods	$l_a \geq 0{,}3\,d^2$ $l_a \geq 6\,d$

(13) For load introduction parallel to grain small rod diameters are preferable, in order to reduce the risk of splitting.

(14) For load introduction perpendicular to grain the following should be observed

$$\frac{l_a}{d} \leq 30 \qquad \text{(A.6)}$$

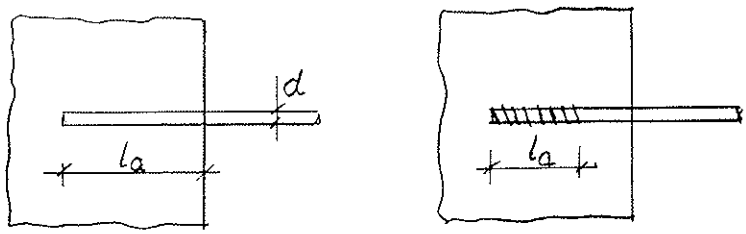

Figure A.6: Definition of anchorage length

A.4 Ultimate limit state

A.4.1 Lateral load-carrying capacity

(1) Glued-in rods inserted perpendicular to grain should be treated as dowels.

(2) The design load-carrying capacity of glued-in rods inserted parallel to grain and loaded laterally should be based on the embedding strength for perpendicular to grain reduced by 10 %.

(3) For glued-in rods inserted at an angle α to grain, linear interpolation may be used between the values according to A.4(1) and (2).

A.4.2 Combined laterally and axially loaded glued-in rods

(1) For combined laterally and axially loaded glued-in rods the following condition should be satisfied:

$$\left(\frac{F_{ax,d}}{R_{ax,d}}\right)^2 + \left(\frac{F_{la,d}}{R_{la,d}}\right)^2 \leq 1 \qquad \text{(A.7)}$$

where $R_{ax,d}$ and $R_{la,d}$ are the load-carrying capacities of the glued-in rod with axial load or lateral load alone.

A.5 Serviceability limit state

(1) For axially loaded glued-in rods, the instantaneous slip modulus K_{ser} per rod should be taken as

$$K_{ser} = 0{,}05\ \rho_k^{1,5}\ d^{1,8} \qquad \text{(A.8)}$$

where

K_{ser} is in N/mm
ρ_k is in kg/m^3
d is in mm.

This may be assumed to apply at all angles to the grain.

(2) For laterally loaded dowel-type glued-in rods, the instantaneous slip modulus K_{ser} per rod should be taken as

- for rod inserted perpendicular to grain:

$$K_{ser} = 0{,}05\ \rho_k^{1,5}\ d \tag{A.9}$$

- for rod inserted parallel to grain:

$$K_{ser} = 0{,}01\ \rho_k^{1,5}\ d \tag{A.10}$$

where the dimensions are as given in (1).

(3) For other angles to grain, linear interpolation may be applied.

CIB-W18/28-102-2

INTERNATIONAL COUNCIL FOR BUILDING RESEARCH STUDIES AND DOCUMENTATION

WORKING COMMISSION W18 - TIMBER STRUCTURES

RACKING STRENGTH OF WALL DIAPHRAGMS - DISCUSSION OF THE EUROCODE 5 APPROACH

by

B Källsner
Swedish Institute for Wood Technology Research
Sweden

MEETING TWENTY - EIGHT

COPENHAGEN

DENMARK

APRIL 1995

ABSTRACT

The design of wall diaphragms, according to Eurocode 5, is in some respects conservative and in other respects unsafe. To clarify the structural behaviour of wall diaphragms, a theoretical background is given. The design rules in Eurocode 5 are discussed and improvements of the code text are suggested. It is shown that the capacity of shear walls is influenced by different factors like boundary conditions and edge distances of the fasteners.

1 INTRODUCTION

A common way of stabilizing timber framed buildings against lateral load is to use the diaphragm action of roofs, floors and walls. In Eurocode 5 (ENV 1995-1-1:1993) two methods are presented in order to determine the racking strength of cantilevered wall diaphragms. The first method is to calculate according to a simplified procedure. The second one is to determine the racking strength by testing of prototype structures in accordance with prEN 594. The presentation of the two methods in Eurocode 5 is a compromise and not obvious in all details. The purpose of this paper is to give a brief theoretical background and suggest improvements of the code text.

2 BASIC THEORY FOR A SHEET ON A TIMBER FRAME

2.1 Elastic model

A typical example of a sheet on a timber frame is shown in Figure 1. This fundamental unit, consisting of a sheet fastened to a timber frame, will henceforth be called a wall unit. Källsner (1984) and Åkerlund (1984) proposed a calculation model for wall units based on the following assumptions:

- The frame members are rigid and hinged to each other. See Figure 2.
- The sheets are rigid and there is no direct contact between adjacent sheets or between a sheet and the adjacent structure.
- The load-displacement relationships of the joints between the sheet and the frame members are linear elastic until failure
- The displacements are small compared with the width and height of the sheets.

In order to determine the structural behaviour of a wall unit, different methods can be used. One way is to use equilibrium equations, see Åkerlund (1984). An alternative way is to use a method based on finding the minimum of the potential energy, see Källsner (1984) or Källsner and Lam (1995). In the right-hand part of Figure 2, the wall unit is shown in the loaded state. The vertical frame members (studs) have been given the rotation γ and the sheet the rotation φ in relation to their original positions. If the origin of the coordinates x and y is placed in the centre of gravity of the fasteners then the angles φ and γ are obtained as:

$$\varphi = \frac{1}{K} Hh \frac{1}{\sum_{i=1}^{N} x_i^2} \qquad (1)$$

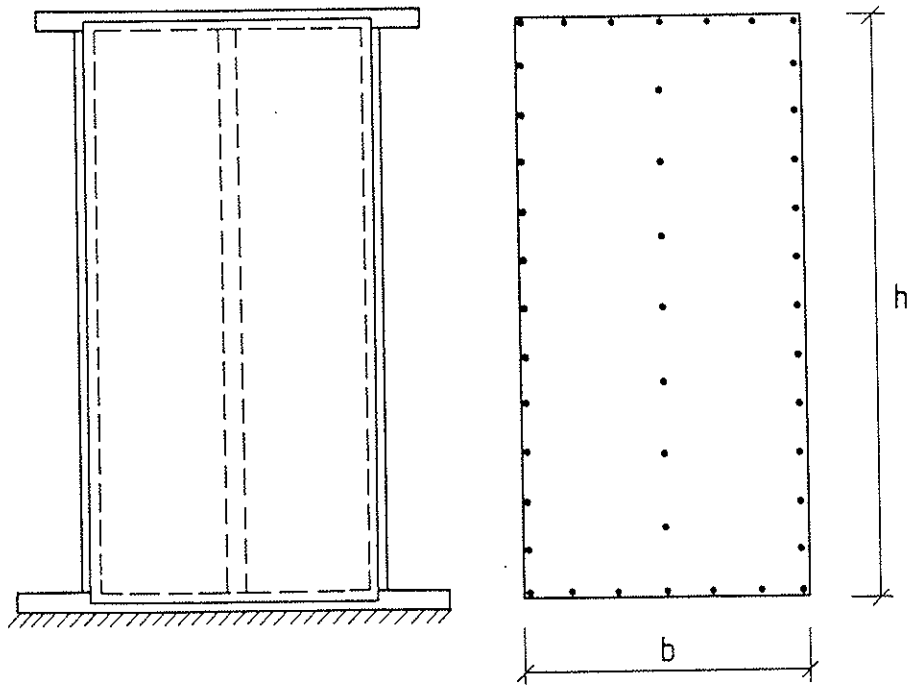

Figure 1. Wall unit consisting of a sheet fastened to a vertical timber frame.

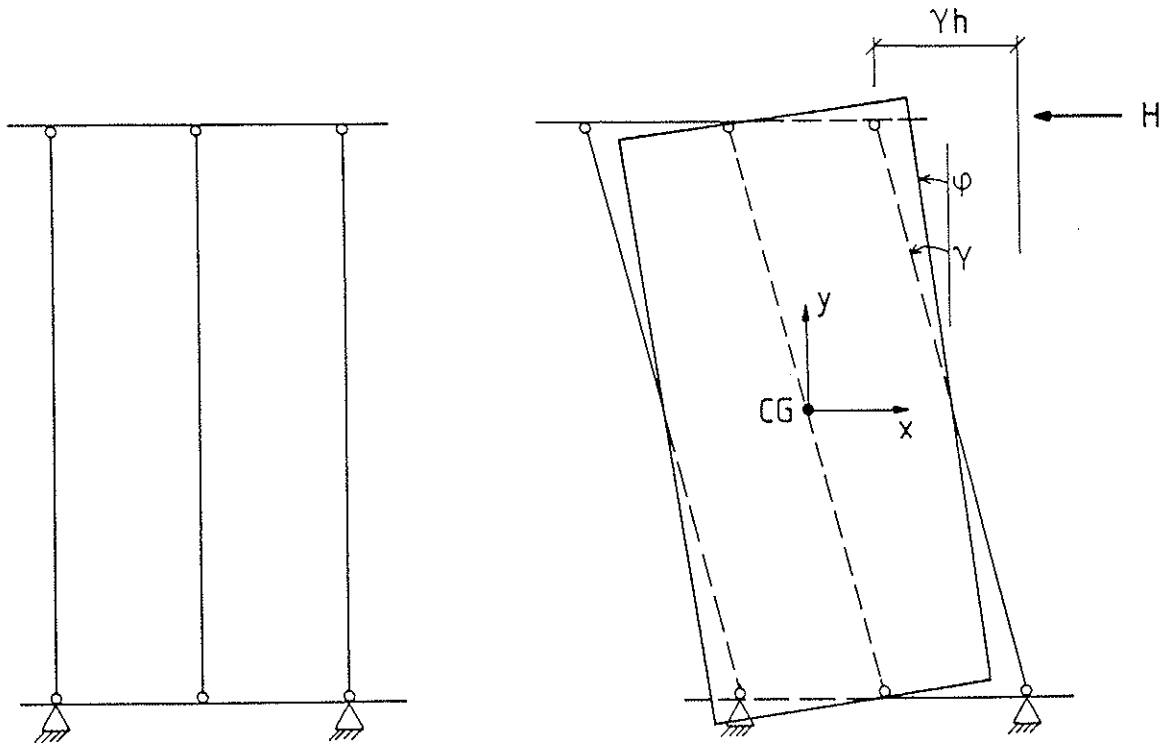

Figure 2. Static model of a wall unit in the unloaded and loaded state.

$$\gamma = \frac{1}{K} Hh \left(\frac{1}{\sum_{i=1}^{N} x_i^2} + \frac{1}{\sum_{i=1}^{N} y_i^2} \right) \tag{2}$$

where H = external horizontal force acting on the wall unit
h = height of the sheet
i = No. of fastener
K = displacement modulus for the fastener
N = total number o fasteners in the wall unit
x_i = x-coordinate of fastener No. i
y_i = y-coordinate of fastener No. i

The x- and y-components of the fastener forces are given as:

$$F_{xi} = - Hh \frac{y_i}{\sum_{i=1}^{N} y_i^2} \tag{3}$$

$$F_{yi} = - Hh \frac{x_i}{\sum_{i=1}^{N} x_i^2} \tag{4}$$

Maximum fastener force F_{max} occurs in that fastener which is most remote from the centre of gravity of the fasteners. Denoting the coordinates of this fastener by (x_{max}, y_{max}), it follows that

$$F_{max} = \sqrt{F_{xi}^2 + F_{xi}^2} = Hh \sqrt{\left(\frac{x_{max}}{\sum_{i=1}^{N} x_i^2} \right)^2 + \left(\frac{y_{max}}{\sum_{i=1}^{N} y_i^2} \right)^2} \tag{5}$$

Denoting the design capacity per fastener by F_d, the design racking load-carrying capacity H_d of the wall unit can be written as

$$H_d = \frac{F_d}{h \sqrt{\left(\frac{x_{max}}{\sum_{i=1}^{N} x_i^2} \right)^2 + \left(\frac{y_{max}}{\sum_{i=1}^{N} y_i^2} \right)^2}} \tag{6}$$

An example of how the fastener forces are distributed according to the elastic theory is shown in Figure 3.

The displacement of the upper horizontal timber frame member in relation to its original position is given by:

$$u_{frame} = \gamma h = \frac{1}{K} Hh^2 \left(\frac{1}{\sum_{i=1}^{N} x_i^2} + \frac{1}{\sum_{i=1}^{N} y_i^2} \right) \tag{7}$$

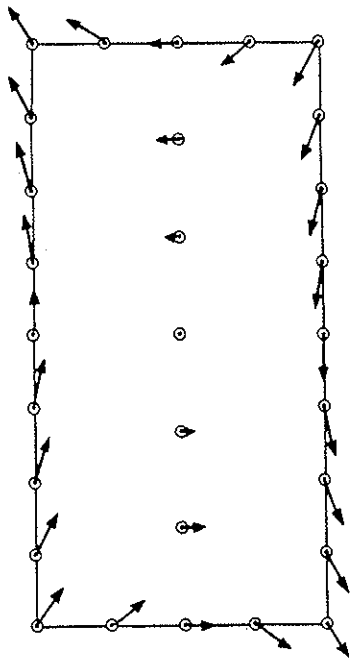

Figure 3. Force distribution on the sheet according to the linear elastic theory.

2.2 Plastic lower bound model

From tests of joints with nails and screws it is well-known that the load-displacement curves are often characterized by plastic deformations. A lower bound of the plastic load-carrying capacity of a wall unit can be obtained by assuming a force distribution that fulfils the conditions of force and moment equilibrium and where the force acting on each fastener is at the most equal to the plastic capacity of the fastener.

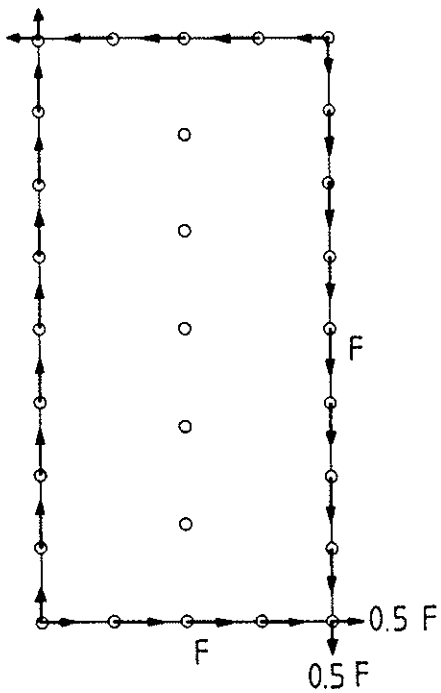

Figure 4. Force distribution on the sheet according to the plastic lower bound method assuming a pure shear flow.

For a wall unit as in Figure 1, where the distance between the fasteners along the edges of the sheet is constant, it is possible to find a force distribution that meets the requirements of force and moment equilibrium. See Figure 4. Each edge fastener except those in the corners may be assumed to carry the same load F_d parallel to the edge. Each corner fastener is assumed to carry one load component $F_d/2$ parallel to each of the associated sides of the sheet. The fasteners in the centre stud are assumed not to carry any load. With the chosen force distribution, which corresponds to a pure shear flow along the edges of the sheet, the load-carrying capacity H_d is

$$H_d = n F_d \tag{8}$$

where n denotes the number of fastener spacings along the upper horizontal timber member.

2.3 Comparison with test results

Full-scale testing of wall panels with different combinations of sheet materials and fasteners, Källsner (1984), shows that the elastic model in general somewhat underestimates the capacity.

The influence of different fastener patterns on the capacity H_d, determined according to the elastic theory, is illustrated in Figure 5. In this case it is assumed that h/b=2 and that the fastener spacing is constant along all the timber members. Wall unit 4 in Figure 5 is built up of crossing timber members where the sheet is fastened to the horizontal members.

For a wall unit built up as in Figure 1, the capacity H_d determined by Equation (8) is very close to the solution obtained by the elastic theory. See wall type 1 in Figure 5. Since the difference in capacity obtained by the two methods is small and the difference in the force distributions is moderate it seems reasonable to recommend the use of the simple force distribution according to Figure 4 for this type of wall unit.

3 DISCUSSION OF THE EUROCODE 5 APPROACH

3.1 Influence of different boundary conditions

In Eurocode 5, two different methods are given for the determination of the racking resistance of wall diaphragms: by calculation or by testing of prototype structures. There is, however, a fundamental difference in the two methods, namely the vertical anchoring of the stud on the tension side of the wall unit.

When the calculation method is used, it is clearly said that the tensile stud should be directly anchored to the substrate. This means that the boundary conditions on the tension side are very similar to those used for the models in section 2, where it was assumed that the frame members are connected by hinges to each other.

When the racking resistance of wall diaphragms is determined by testing prototype structures, the boundary conditions are somewhat different. In the relevant test standard prEN 594 it is said: "In this test method the bottom rail of the panel is bolted to the test rig and uplift is resisted by the sheeting fixings and also by the vertical loads on the top rail of the panel". The principal loading arrangements and the manner of fixing the wall panel to the test rig are shown in Figure 6. Since the stud on the tension side of the wall panel is not directly anchored to the base of the test rig, this stud will normally be subjected to substantial vertical displacement. Consequently, the structural behaviour will deviate

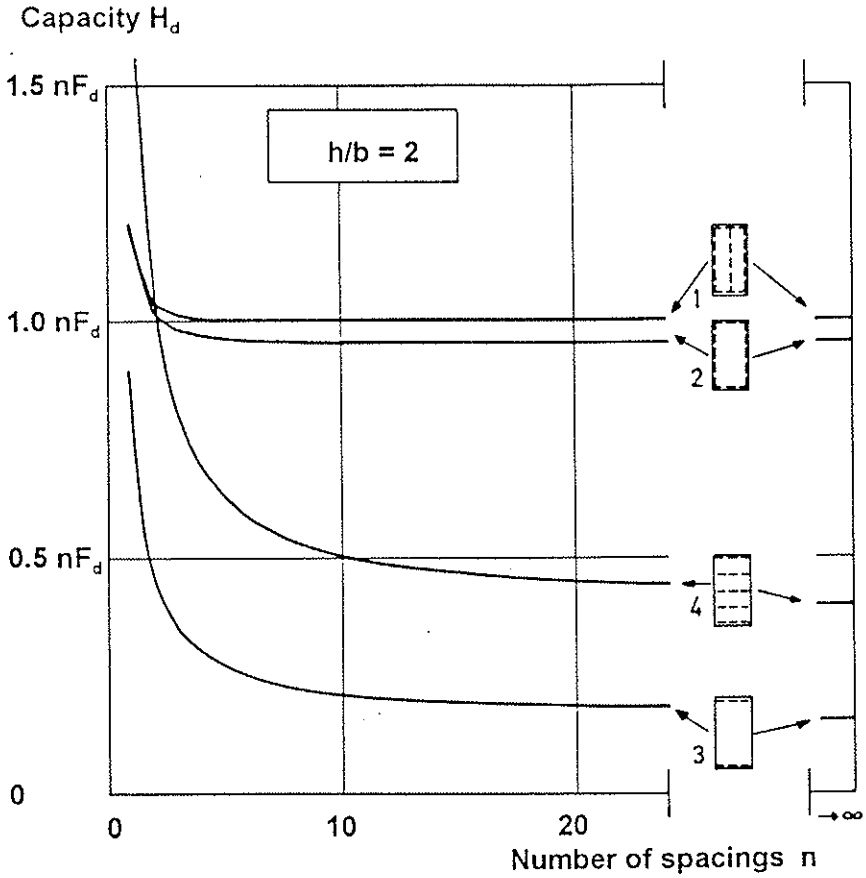

Figure 5. Load-carrying capacity H_d as a function of the number of fastener spacings n along the upper horizontal timber member. The relation is illustrated for four different fastener patterns assuming a constant fastener spacing along all timber members.

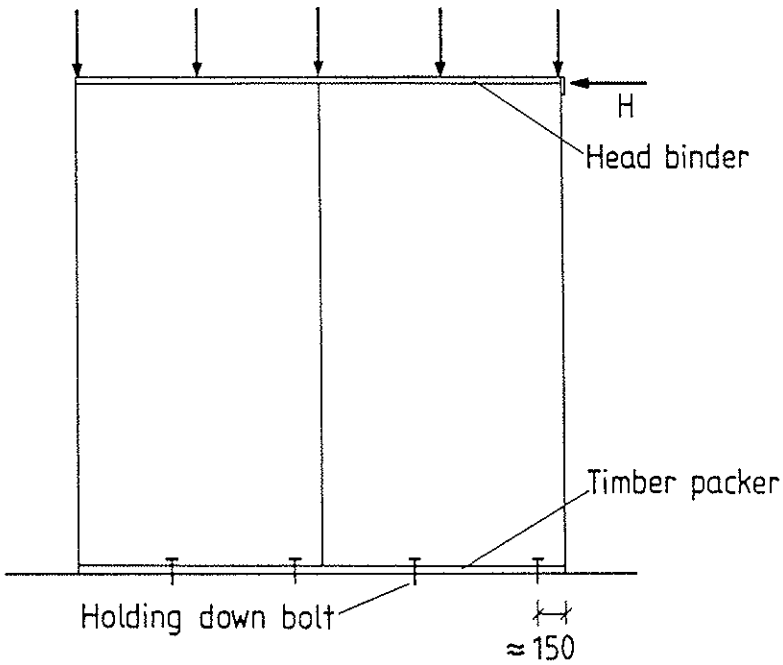

Figure 6. Principal loading arrangements and support conditions according to the test standard prEN 594.

considerably from what is assumed in the calculation procedure. This means that the fasteners located along the bottom rail on the tension side of the test panel will be subjected to vertical tension forces which strive to draw the sheet apart from the bottom rail. This redistribution of the fastener forces will result in a lower racking capacity for the wall panel. An additional effect is that the tensile forces will act almost perpendicularly to the edge of the sheet. From the testing of joints, it is well known that the strength is often considerably lower when the fastener forces act perpendicularly to the edge of the sheet than when they act parallel to the edge. This is especially the case when the fasteners are located close to the edges of the sheet material.

3.2 Influence of edge distance

In Eurocode 5, the minimum edge distance for nails depends on whether the fastener force acts towards the edge of the timber or away from it (i.e. if the edge is loaded or unloaded). For an unloaded edge, the minimum edge distance is 5d, where d denotes the diameter of the nail. For a loaded edge, the minimum edge distance is $5d(1+\sin\alpha)$, where α denotes the angle between the force and the grain direction. These edge distances can be used for the timber as well as for the sheet material.

The elastic model, used in section 2.1, shows that the fastener forces act at an angle to the edge. This angle is the largest for the corner fasteners where a minimum edge distance of almost 10d is often required. For a sheet splice over a stud, this implies a stud thickness of 40d, which means that with a nail diameter of 20 mm the minimum thickness of the stud is 80 mm. In most parts of the world where timber-framed buildings are used, the thickness of the timber members is between 38 and 50 mm. It has been shown in tests that wall panels work satisfactorily even if the edge distance is far below the minimum value given in Eurocode 5. For example in the tests reported by Källsner (1984) the dimension of the studs was 45x95 mm. It is obvious that the required minimum edge distances that are given in Eurocode 5 should be reduced in connection with the design of wall panels.

3.3 Wall panels consisting of more than one wall unit

For a wall panel consisting of only one sheet fixed to one side of a timber frame, according to Eurocode 5 the design racking load-carrying capacity is given by:

$$H_d = F_d \frac{b_i}{s} \tag{9}$$

where s is the spacing of the fasteners and b_i is the width of the sheet. Except for the symbols used, Equation (9) is identical to Equation (8), i.e. the capacity is identical to capacity determined with the plastic lower bound method in section 2.2 assuming a pure shear flow.

An example of a wall diaphragm built up of more than one wall unit is shown in Figure 7. To illustrate the structural behaviour of the wall, the structure is divided into two parts, the timber frame and the sheets. If we accept the model based on a pure shear flow in the sheets, we obtain the force distribution shown in the lower part of the figure, where all timber members and sheets are in equilibrium. The design racking capacity for this wall is obtained as the sum of the capacities of the individual wall units and is according to Eurocode 5 calculated as

$$H_{tot,d} = \sum F_d \frac{b_i}{s} \tag{10}$$

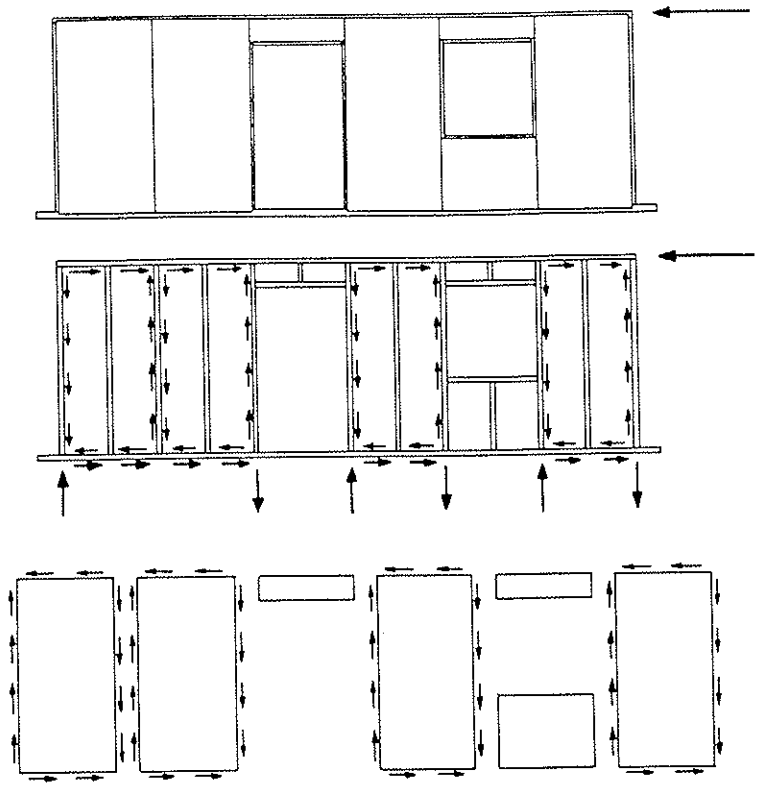

Figure 7. Example of wall panel that consists of more than one wall unit. Force distribution on the sheets and the timber frame according to the plastic lower bound method.

If the width of a wall unit is less than that corresponding to a sheet of full size, the capacity of this wall unit is reduced to

$$H_d = F_d \frac{b_i}{s} \frac{b_i}{b_{max}} \tag{11}$$

where b_{max} is the width of the widest sheet. This means that the capacity of a wall unit with a sheet of half the width is equal to 1/4 instead of 1/2 of the capacity of that corresponding to a full-sized sheet. The reason for this reduction is that wall units with different sheet widths will reach their maximum loads at different displacements. The proposed reduction is supported by test results and is in agreement with the elastic theory in section 2.1. The reduction is also justified by keeping the deformations in the serviceability limit state within appropriate limits. If the plastic theory had been fully accepted, the capacity would have been proportional to the width of the wall unit.

3.4 Sheets on both sides of the wall panel

If there are sheets of the same type and thickness, on both sides of the wall panel, according to Eurocode 5 the load-carrying capacity may be taken as the sum of the calculated contributions. Further it is said that, if the sheets or the fasteners are of different types, only half the load-carrying capacity of the weaker side should be taken. This reduction of weaker side seems to be far too high. Comparison of load-displacements curves for wall panels consisting of normally used combinations of interior and exterior sheet materials in Sweden shows that the maximum load is obtained at about the same displacement. It is only if we would like to mix fastener sheet combinations with completely different slip properties that a reduction of 50% could be justified. A more reasonable reduction of the load-carrying capacity of the weaker side should be 20%.

3.5 Force distribution between the studs

According to Eurocode 5, for sheets on both sides of a wall panel, compression studs should be designed for a force given by

$$V_{c,d} = 0.67\, H_{tot,d}\, \frac{h}{b_{tot}} \tag{12}$$

and for sheets on one side of a wall panel, compression studs should be designed for a force given by

$$V_{c,d} = 0.75\, H_{tot,d}\, \frac{h}{b_{tot}} \tag{13}$$

Coefficients 0.67 and 0.75 are in agreement with the German DIN 1052 where these values are used for wall panels built up of 1 or 2 wall units. In the German code, the compression force $V_{c,d}$ is the internal contact force between the vertical stud and the bottom rail. In Eurocode 5, it is not made completely clear what force $V_{c,d}$ represents.

The proposed values given here should be compared with the values obtained from the elastic model in section 2.1. For a wall unit with three vertical frame members, such as in Figure 1, and assuming the fasteners to be uniformly distributed along the frame members, the vertical force component between the stud and the bottom rail can be derived as

$$V_{c,d} = \frac{1 + 6\frac{h}{b}}{2\left(1 + 3\frac{h}{b}\right)}\, H_d\, \frac{h}{b} \tag{14}$$

For a wall unit with a height-to-width ratio of 2, Equation (14) can be simplified to

$$V_{c,d} = 0.93\, H_d\, \frac{h}{b} \tag{15}$$

This means that 93% of the overturning moment is taken as a force couple in the vertical frame members, while the remaining 7% of the moment is taken as fastener forces between the sheet itself and the bottom rail. It is obvious that there is a large risk that the vertical compression force $V_{c,d}$ will be underestimated if Equations (12) and (13) are used. A more reasonable proposal is to neglect the moment directly transferred from the sheet to the bottom rail and instead to design the compression stud for the force

$$V_{c,d} = H_d\, \frac{h}{b} \tag{16}$$

and the tensile stud for the force

$$V_{t,d} = H_d\, \frac{h}{b} \tag{17}$$

These expressions are also in agreement with the solution obtained from the plastic method in section

2.2, where a pure shear flow along the edges of the sheet was assumed. Compare the assumed force distribution for the wall diaphragm in Figure 7.

3.6 Anchoring of the tensile stud

When the elastic solution in section 2.1 was developed, one of the basic assumptions was that the members of the timber frame were hinged to each other. The most critical joint in this respect is the connection between the vertical stud and the bottom rail on the tension side of the wall unit. If large displacements are accepted in this joint, a different stress distribution occurs where high stresses are introduced between the sheet and the bottom rail. To avoid this problem it is necessary not only to take care of the vertical force according to Equation (17) but also to limit the displacements in the joint. One way of handling the problem is to give some limiting value for the displacements in this joint which should not be exceeded before the maximum racking load is reached. An alternative way is to design the joint for a somewhat higher force than that given by Equation (17).

A proper anchoring of the tensile stud is also very important, in order to limit the horizontal displacements of the wall in the serviceability limit state.

3.7 Buckling of wall panels

In Eurocode 5 no rules are given with respect to different modes of buckling of wall diaphragms. This is a very important issue that should be dealt with in the code.

If the sheets are very thin, there is a risk for local buckling of the sheets. Based on the elastic model in section 2.1 the distribution of the forces acting upon a sheet was shown in Figure 3. To determine the critical load for this force distribution is not easy. If we instead consider the force distribution according to the plastic lower bound method, see Figure 4, where all fasteners along the edges except those in the corners carry the same load, it is reasonable to determine the critical stress as if the sheet is subjected to a constant shear stress. For a sheet field with dimensions according to Figure 8, assuming homogeneous, isotropic and elastic material, the critical stress is obtained as

$$\tau_{cr} = k \frac{\pi^2 E}{12 (1-\nu)^2} \left(\frac{t}{b} \right)^2 \tag{18}$$

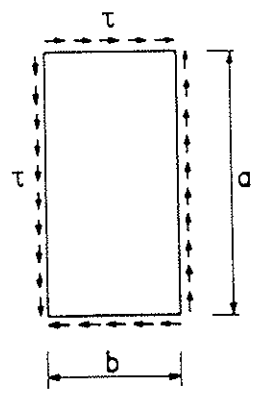

Figure 8. Sheet field loaded with a constant shear stress along the edges

where t is the thickness of the sheet and ν is Poisson's ratio. The value of the coefficient k depends on the length-to-width ratio of the sheet and on the boundary conditions. For a sheet simply supported along all four edges, an approximate expression for the coefficient k is given by

$$k = 5.35 + 4\left(\frac{b}{a}\right)^2 \tag{19}$$

For a sheet clamped along all four edges the corresponding expression for the coefficient k is changed to

$$k = 8.98 + 5.6\left(\frac{b}{a}\right)^2 \tag{20}$$

For a wall unit as shown in Figure 1, b should be taken as half the width of the sheet since the sheet is also supported along the centre stud. It should be pointed out that the boundary conditions in practice should give a coefficient k with a value somewhere between those given by Equations (19) and (20).

Another stability problem that has to be checked is the column buckling of the vertical studs. Shear stresses acting along the edges of the sheets introduce compression and bending stresses in the studs. Additional axial stresses are introduced by any vertical load.

3.8 Extrapolation of results from testing of prototype structures

If the capacity of a wall panel has been determined by testing according to prEN 594, Eurocode 5 gives formulae for the calculation of the capacity of similar constructions but with different height and width. From the discussion in section 3.1 we learn that the racking resistance of a wall diaphragm is very sensitive to different boundary conditions. Since the test standard also allows testing of wall panels with different boundary conditions than those given in Figure 6 and with different vertical loads, the formulae given in Eurocode 5 should consider these effects. At least there should be given some limits within which the formulae are valid.

REFERENCES

ENV 1995-1-1:1993 Eurocode 5 - Design of timber structures - Part 1-1: General rules and rules for buildings.

prEN 594 Timber structures - Test methods - Racking strength and stiffness of timber frame wall panels. - Draft document CEN/TC124/WG1 N252.

Källsner, B. (1984) Panels as wind-bracing elements in timber-framed walls. Report 56. Swedish Institute for Wood Technology Research, Stockholm, Sweden.

Källsner, B. and Lam, F. (1995) Diaphragms and shear walls. To be published.

Åkerlund, S. (1984) Enkel beräkningsmodell för skivor på regelstomme (Simple calculation model for sheets on a timber frame). Bygg & Teknik, No.1.